NASA TECHNICAL MEMORANDUM

NASA TM X-3431

NASA TM X-3431

TRANSONIC AERODYNAMIC CHARACTERISTICS OF A SUPERCRITICAL-WING TRANSPORT MODEL WITH TRAILING-EDGE CONTROLS

Michael J. Mann and Richard A. Langhans

Langley Research Center
Hampton, Va. 23665

NATIONAL AERONAUTICS AND SPACE ADMINISTRATION • WASHINGTON, D. C. • OCTOBER 1977

1. Report No.	2. Government Accession No.	3. Recipient's Catalog No.
NASA TM X-3431		

4. Title and Subtitle	5. Report Date
TRANSONIC AERODYNAMIC CHARACTERISTICS OF A SUPERCRITICAL-WING TRANSPORT MODEL WITH TRAILING-EDGE CONTROLS	October 1977
	6. Performing Organization Code
7. Author(s)	8. Performing Organization Report No.
Michael J. Mann and Richard A. Langhans	L-10871
	10. Work Unit No.
9. Performing Organization Name and Address	754-62-01-06
NASA Langley Research Center Hampton, VA 23665	11. Contract or Grant No.
	13. Type of Report and Period Covered
12. Sponsoring Agency Name and Address	Technical Memorandum
National Aeronautics and Space Administration Washington, DC 20546	14. Sponsoring Agency Code

15. Supplementary Notes

16. Abstract

A study has been conducted to determine the effects of wing trailing-edge control surfaces on the static transonic aerodynamic characteristics of a transport configuration with a supercritical wing. The configuration was tested with both an area-ruled fuselage and a cylindrical fuselage. The Mach number range was from 0.80 to 0.96 and the angle-of-attack range was from about -1° to 12°. The Reynolds number was 1.58×10^{6} based on the mean aerodynamic chord.

17. Key Words (Suggested by Author(s))	18. Distribution Statement
Transonic flow; Controls Supercritical wing; Control surfaces Transport; Advanced transport technology Transonic aircraft Trailing-edge controls	Unclassified – Unlimited Subject Category 02

19. Security Classif. (of this report)	20. Security Classif. (of this page)	21. No. of Pages	22. Price*
Unclassified	Unclassified	334	$10.00

*For sale by the National Technical Information Service, Springfield, Virginia 22161

TRANSONIC AERODYNAMIC CHARACTERISTICS OF A SUPERCRITICAL-WING TRANSPORT MODEL WITH TRAILING-EDGE CONTROLS

Michael J. Mann and Richard A. Langhans
Langley Research Center

SUMMARY

A study has been conducted to determine the effects of wing trailing-edge control surfaces on the static transonic aerodynamic characteristics of a transport configuration with a supercritical wing. The configuration was tested with both an area-ruled fuselage and a cylindrical fuselage. The Mach number range was from 0.80 to 0.96 and the angle-of-attack range was from about -1° to 12°. The Reynolds number was 1.58×10^6 based on the mean aerodynamic chord. It was found that the most outboard control was superior in maintaining rolling-moment effectiveness. All controls showed a decrease in roll effectiveness near drag-divergence conditions. The farther inboard the control was located, the more effective it was in generating changes in lift. The negative control deflections (trailing edge up) were generally superior to the positive deflections. As the Mach number was increased, the drag due to control deflection generally did not show a large increase prior to the drag-divergence Mach number. With the controls undeflected, the area-ruled fuselage resulted in an increase in drag-divergence Mach number of 0.02. Up to the drag-divergence Mach number (0.896) of the configuration with the cylindrical fuselage, the rolling moments and drag increments due to control deflection are in reasonably good agreement for both fuselages; however, beyond this Mach number there are significant differences.

INTRODUCTION

The NASA supercritical airfoil has been under development for a number of years and is designed to delay shock-induced boundary-layer separation to Mach numbers and lift coefficients significantly higher than for conventional airfoil sections. (See refs. 1 to 4 for properties of both slotted and integral airfoil sections.) Airplane configurations employing this concept have demonstrated significant increases in drag-divergence Mach number.

The success of wind-tunnel and flight investigations of configurations with sweptback supercritical wings (refs. 5 to 8) provided a strong impetus to the establishment of an

Advanced Transport Technology Program by the National Aeronautics and Space Administration (ref. 9). This program was continued in order to study the application of supercritical technology to transport airplanes. (See refs. 10 to 16.)

As part of this program, the present study[1] was made of wing trailing-edge control effects on a transport configuration designed to cruise near a Mach number of 0.90. The wing of the present configuration has supercritical airfoil sections and 33° of sweep at the quarter-chord line.

The purposes of this study were as follows:

(1) To determine the effects of trailing-edge control surfaces on the static aerodynamic characteristics of a transport with a supercritical wing when the flow is transonic and shock waves are present

(2) To determine to what extent the effects of control deflections on rolling moment, drag, and spanwise load distribution can be determined for the present configuration at transonic speeds by use of a cylindrical fuselage instead of an area-ruled fuselage

Experimental results were obtained at Mach numbers from 0.80 to 0.96, angles of attack from about -1° to 12°, and a Reynolds number of 1.58×10^6 based on the mean aerodynamic chord. Plots of the data have been used to show the effect of the controls on the longitudinal and lateral static aerodynamic characteristics and on the wing and fuselage pressure distributions.

Tabulations of the force data, wing and fuselage pressure data, and free-stream dynamic pressure and oil-flow photographs of the models with zero control deflection are included in a "Supplement to NASA TM X-3431," which is available upon request. A request form is included at the back of this paper.

SYMBOLS

The results presented herein are referred to the stability-axis system with the origin at the projection on the model centerline of the quarter-chord point of the mean aerodynamic chord. (See figs. 1(a) and 1(b) and table I.) All coefficients are based on the geometry of the basic trapezoidal wing which does not include the leading-edge glove or the trailing-edge extension but does include the fuselage intercept. (See fig. 1(b).)

The data presented herein were plotted and tabulated by machine, and the limitations of the machine as to available typeface necessitated some differences between these

[1]Because of the heavy work load in the Langley facilities, these tests were made in the Calspan 8-Foot Transonic Wind Tunnel. The tests were supervised by Linwood W. McKinney of NASA Langley Research Center assisted by Joseph F. Herman of Vought Corporation Hampton Technical Center.

notations and conventional symbols. The symbols are given in the conventional form with the machine notation included in parentheses where applicable. Values are given in the International System of Units (SI), except for the tabulation of dynamic pressure which is presented in lbf/ft^2 (1 lbf/ft^2 = 47.88 Pa). The measurements and calculations were made in U.S. Customary Units.

b — wing span, cm

c — streamwise local chord of total wing planform, which includes leading-edge glove and trailing-edge extension, cm

$\bar{c}$ — mean aerodynamic chord of basic trapezoidal wing panel, cm

c_{av} — average chord, S/b, cm

C_D (CD) — total drag coefficient, $\frac{\text{Drag}}{q_\infty S}$

ΔC_D — incremental total drag coefficient, defined to be total drag coefficient with controls deflected minus total drag coefficient with controls undeflected

C_L (CL) — total lift coefficient, $\frac{\text{Lift}}{q_\infty S}$

C_l (Cl) — rolling-moment coefficient, $\frac{\text{Rolling moment}}{q_\infty Sb}$

ΔC_l — rolling-moment coefficient corrected for model flexibility, defined to be rolling-moment coefficient with controls deflected minus rolling-moment coefficient with controls undeflected

$\Delta C_l'$ — estimated differential rolling moment, defined to be ΔC_l for a given control and negative deflection angle minus ΔC_l for the same control with a positive deflection angle of the same magnitude

C_m (CM) — total pitching-moment coefficient, $\frac{\text{Pitching moment}}{q_\infty S\bar{c}}$

c_n — section normal-force coefficient, $\int_0^1 \left(C_{p,l} - C_{p,u}\right) d\frac{x}{c}$

C_p (CP) pressure coefficient, $\frac{p - p_\infty}{q_\infty}$

$C_{p,l}$ (CPL) pressure coefficient on wing lower surface

$C_{p,u}$ (CPU) pressure coefficient on wing upper surface

F_i wing trailing-edge control surface; subscript i denotes surface location (see fig. 1(c))

L length of fuselage, cm

M_∞ (MINF) free-stream Mach number

p local static pressure, Pa

p_∞ free-stream static pressure, Pa

q_∞ (Q) free-stream dynamic pressure, Pa (lbf/ft^2 in computer tabulation)

S wing area of trapezoidal wing planform including fuselage intercept, cm^2

x' distance from model nose in plane of symmetry and parallel to WL, cm

x/c (X/C) distance from wing leading edge divided by streamwise local chord

x'/L (X/L) distance from model nose divided by fuselage length

y distance measured spanwise from plane of symmetry, cm

z distance measured parallel to plane of symmetry and perpendicular to x and y, zero at WL = -1.55 cm

z_u, z_l upper and lower airfoil z-coordinates

α (ALPHA) angle of attack, referenced to fuselage reference line (WL = 0.00), deg

δ_{Fi} deflection of wing control surface F_i (positive when trailing edge is down), deg

η = y/(b/2)

η_j (ETA) η at jth spanwise location of pressure orifices

θ circumferential location of pressure orifices on fuselage, deg

$\Lambda_{c/4}$ sweep of quarter-chord line of wing and vertical tail (see fig. 1(b))

Abbreviations:

FS fuselage station (distance from nose) of local wing leading edge, cm

WL water line (WL = 0.00 is the fuselage horizontal reference line through the moment reference center; see fig. 1(b))

APPARATUS AND PROCEDURES

Tunnel Description

The investigation was conducted in the Calspan 8-Foot Transonic Wind Tunnel. This is a continuous-flow, single-return tunnel with a rectangular, porous-wall test section. A description of the tunnel is given in reference 17.

Model Description

Details of the wind-tunnel model are given in figures 1(b) to 1(f), and a sketch of the model support system and test section is given in figure 1(g). Several model photographs are shown in figure 2. The model had an NASA supercritical wing with a quarter-chord sweep of 33°, trailing-edge controls on the right wing,[2] either a partially area-ruled fuselage or a cylindrical fuselage, and a vertical tail. The wing of the present configuration was obtained by unsweeping the wing used on the Mach 1 transport configuration of reference 6. General geometric characteristics of the model are given in table I.

The wing was mounted in a low position (fig. 1(b)) with a root incidence of approximately 2° (leading edge up with respect to WL = 0.00) and with 5° of twist (washout) between the root chord and the tip chord (fig. 3). The wing airfoil coordinates are presented in table II[3] and the planform coordinates are given in table III. The aerodynamic

[2]Controls were installed in one wing only in order to simplify model construction and testing. It was anticipated that a reasonable estimate of the effects of differential control deflection on both wings could be obtained by combining the effects of opposite deflections on the same wing.

[3]Subsequent to the initial model design, experimental evidence obtained in other test programs indicated that the wing should be tested with 0.5° more incidence than originally anticipated. Thus, the twist angles that would be calculated from the airfoil coordinates in table II are 0.5° less than the values presented in figure 3 which is for the tested configuration.

force coefficients have been based on preliminary measurements of the wing geometry; table I gives these preliminary or reference geometric properties and the true geometric properties. The true values were computed by using the coordinates in table II. It should be noted that the reference values are not necessarily compatible with each other.

The wing had four trailing-edge control surfaces on the right wing. These control surfaces are shown in figure 1(c) and their geometric characteristics are presented in table I.

The area-ruled fuselage was experimentally shaped at the design Mach number by use of pressure measurements on the wing root and on the fuselage top and sides (refs. 6 and 18). This technique essentially depended upon shaping the fuselage to control the pressure distribution at the wing root and maintain attached flow in that region of the wing. Normal cross sections for the area-ruled fuselage and the cylindrical fuselage are presented in figure 4, and the normal cross-sectional area distributions for the complete models are presented in figure 1(d).

Boundary-Layer Transition

Figure 1(f) shows the location and size of all transition strips. The strips were 0.127 cm wide and consisted of carborundum grit attached to the model with a plastic adhesive. The techniques of references 19 to 21 were used to size and locate the transition strips on the wing in an effort to simulate the full-scale Reynolds number boundary-layer characteristics at the wing trailing edge.

The transition strips were applied to the wing lower surface along a straight line that intersects the 20-percent-chord station at the wing tip and the 45-percent-chord station at $\eta = 0.4667$ and extends to the fuselage centerline. The transition strips were initially applied to the wing upper surface along the 40-percent-chord line; however, observation of the boundary-layer flow by using the technique of reference 22 indicated laminar separation ahead of the transition strip inboard of $\eta = 0.6889$. Since this separation would not occur at flight conditions, the transition strip inboard of $\eta = 0.6889$ was modified as shown in figure 1(f).

The transition strip on the fuselage was applied 3.810 cm aft of the model nose, and the transition strips on the vertical tail were located on the 31-percent-chord line.

Test Conditions

The tests were conducted at Mach numbers from 0.80 to 0.96 at a Reynolds number of 1.58×10^6 based on the mean aerodynamic chord. The stagnation temperature and the tunnel air humidity were maintained at values such that the dewpoint in the test section was reduced sufficiently to avoid shock condensation.

Measurements and Corrections

Aerodynamic forces and moments were measured by means of a six-component electrical strain-gage balance housed in the fuselage cavity. A thermocouple was attached to the nonmetric end of the balance to measure balance temperature. Two balance-cavity pressure orifices were installed on the sting just behind the balance and the cavity pressures were measured by an automanometer. The balance data were corrected for balance interactions, static tares, and changes in the modulus of elasticity of the gage section caused by differences between calibration and operational temperatures. The average cavity pressure was used to correct the measured drag to a condition of free-stream static pressure acting over an area of 19.32 cm^2.

Model angle of attack was measured with the Calspan strut-pod system. Corrections were made to the measured angle of attack for sting and balance deflection due to aerodynamic loads and for tunnel flow angularity. The sting and balance deflections were determined from static load calibrations. The tunnel-flow-angularity correction was determined from tests of the model in the upright and inverted positions and varied from 0.135° to 0.175° over the Mach number range of the investigation. No corrections have been applied to the data to account for wind-tunnel wall interference.

The model was instrumented with 111 pressure orifices on the upper and lower surfaces of the right wing. (See fig. 1(e) and table IV(a).) The area-ruled fuselage had a row of 23 orifices on the top centerline and right side, and the cylindrical fuselage had a row of 23 orifices on the top centerline. (See table IV(b).) The pressures were measured by an electrically actuated differential-pressure scanning valve located in the forward section of the fuselage.

The plots of the force and pressure data include a cubic spline curve fit of the data points. Although the data were carefully obtained and are believed to reflect a high degree of accuracy, no attempt was made to remove possibly bad pressure data points since the results of instrumentation checks necessary to do this were not available. Therefore, it has been left to the judgment of the reader to delete any possibly erroneous pressure data points. The pressure transducers were calibrated to an accuracy of 95.76 Pa (2 lb/ft^2).

PRESENTATION OF RESULTS

The longitudinal-force and rolling-moment data are presented in figures 5 to 56. The rolling moment is not zero with the controls undeflected, apparently due to model asymmetric flexibility. Thus, a rolling-moment coefficient ΔC_l has also been plotted, where ΔC_l is the rolling-moment coefficient with controls deflected minus the rolling-moment coefficient with controls undeflected. Plots have also been made of the wing and fuselage pressure distributions. When only one control was deflected, the pressure plots

are given for only the maximum, minimum, and zero deflection angles. When several controls were deflected simultaneously, the pressure plots are given for every control configuration. The pressure plots are at the angle of attack closest to the design lift condition $(C_L \approx 0.50)$.

The results for deflections of a given control on a given fuselage are grouped. The results of various control spanwise locations and spanwise lengths for a given deflection angle are also grouped (area-ruled configuration). These groups of figures are each arranged in order of increasing Mach number. Summary figures are given of the rolling moment and drag due to control deflection at the design lift as a function of Mach number, spanwise load distributions, drag-rise characteristics, and longitudinal-force characteristics.

	Figure
Results for single trailing-edge control deflection:	
F_1 control with area-ruled fuselage, $\delta_{F1} = 0^\circ$ and 10°	5 to 7
F_2 control with area-ruled fuselage, $\delta_{F2} = 0^\circ, \pm4^\circ, \pm10^\circ$, and $\pm15^\circ$	8 to 12
F_2 control with cylindrical fuselage, $\delta_{F2} = 0^\circ$ and $\pm15^\circ$	13 to 16
F_3 control with area-ruled fuselage, $\delta_{F3} = 0^\circ, \pm4^\circ$, and $\pm8^\circ$	17 to 22
F_3 control with area-ruled fuselage, $\delta_{F3} = 0^\circ, \pm10^\circ, \pm15^\circ$, and $\pm20^\circ$	23 to 29
F_3 control with cylindrical fuselage, $\delta_{F3} = 0^\circ, \pm4^\circ, \pm10^\circ$, and $\pm15^\circ$	30 to 33
F_4 control with area-ruled fuselage, $\delta_{F4} = 0^\circ, \pm4^\circ$, and $\pm10^\circ$	34 to 37
F_4 control with cylindrical fuselage, $\delta_{F4} = 0^\circ$ and $\pm10^\circ$	38 to 40
Effects of control spanwise location and control span:	
Spanwise-location effects of controls with area-ruled fuselage, $\delta_{Fi} = \pm4^\circ$	41 to 44
Spanwise-location effects of control with area-ruled fuselage, $\delta_{Fi} = \pm10^\circ$	45 to 48
Control-span effects with area-ruled fuselage, $\delta_{Fi} = \pm4^\circ$	49 to 51
Summary figures:	
Rolling moment due to control deflection as a function of Mach number at $\alpha = 3.5^\circ$	52
Drag due to control deflection as a function of Mach number at $C_L = 0.50$	53

Figure

Spanwise load distributions near design lift coefficient $(C_L \approx 0.50)$ with various control surface deflections 54

Variation of drag coefficient with Mach number at $C_L = 0.50$ for area-ruled and cylindrical configurations. Zero control surface deflections 55

Comparison of longitudinal force characteristics of area-ruled and cylindrical configurations with zero control surface deflections 56

DISCUSSION OF EXPERIMENTAL RESULTS

Although the control-surface effects were highly nonlinear for certain conditions, some general trends can be observed in the data. In general, as the Mach number increases, the effectiveness in producing ΔC_l and $\Delta C_l'$ at the higher angles of attack is reduced for controls F_1, F_2, and F_3 (figs. 5 to 33). In comparison, control F_4 is superior with regard to the magnitude and constancy of $\Delta C_l'$ (figs. 34 to 48). A direct comparison is made between controls F_2, F_3, and F_4 in figures 41 to 48. It can be seen that the effectiveness in generating changes in lift increases from control F_4 to F_3 and from F_3 to F_2 (and, in some cases, from F_2 to F_1, as seen by comparison of figs. 45 to 47 with figs. 5 to 7). The pitching moment is generally insensitive to the spanwise location of the control.

In addition to the effects of the spanwise location of a trailing-edge control, the influence of the spanwise length of the control is also important. Figures 49 to 51 show the progressive effects of increasing the span of a control deflected to $\pm 4^\circ$.

The negative control deflections generally maintained more rolling-moment effectiveness over the angle-of-attack range than the positive deflections. This difference was especially true at the higher Mach numbers where the effectiveness of the positive deflections decreased. (See figs. 11 and 28, for example.) The negative control deflections also produced larger increments in pitching moment and lift (and more drag, as will be discussed subsequently) than the corresponding positive control deflections.

The reason for the greater effectiveness of the negative control deflections was investigated by calculating the transonic flow over the wing airfoil section at $\eta = 0.2674$. The flow was assumed to be two-dimensional and the calculations were made by using the method of reference 23. A Mach number of 0.80 and an angle of attack corresponding to a wing angle of attack of 0° were selected and the control F_2 was deflected $\pm 10^\circ$. Assuming inviscid flow, it was found that the negative control deflection produced an increment in C_L about 50 percent larger than that produced by the positive deflection. When

the viscous effects were included in the calculations, it was found that the positive deflection caused significant boundary-layer separation which would further explain a reduction in control effectiveness for the positive deflection. These effects help to explain the occurrence of the larger changes in chordwise pressure distribution and model forces for the negative deflections. (See $\eta = 0.2929$ in fig. 11(d) and $\eta = 0.3809$ in fig. 28(d), for example.)

The deflection of any of the control surfaces generally affects the chordwise location, the spanwise extent, and the strength of the shock wave on the outboard region of the wing. The changes in the location of the outboard shock wave can be seen in the pressure distributions. These changes are also a factor in making negative control deflections more effective than positive deflections. Chordwise movement of the shock wave with control deflection either increases or decreases the lift locally and therefore either aids or retards the intended effect of the control deflection on the rolling moment. If a positive control deflection moved the shock wave forward, thereby decreasing lift, the rolling effect of the control would be reduced; if a negative control deflection moved the shock wave forward, the reduced lift would aid the rolling effect of the control. Such movements of the shock wave can be seen in figures 24(d) for $\eta = 0.5556$ and 0.7111, 26(d) for $\eta = 0.7111$, 27(d) for $\eta = 0.3809$ and 0.7111, and 28(d) for $\eta = 0.3809$ and 0.5556. Of course, cases do also occur where movement of the shock wave aids the rolling effect of a positive control deflection, as seen, for example, in figure 25(d) for $\eta = 0.7111$.

At the design lift, the outboard control F_4 had practically no effect on the shock wave on the area-ruled configuration, but did affect the shock location on the cylindrical configuration.

With the angle of attack fixed, the fuselage pressure distribution remained relatively insensitive to changes in control deflections; however, in some cases the entire fuselage pressure level was altered. (See figs. 38(e) and 51(g), for example.) The relatively minor effect of control deflections on the fuselage pressure distributions provides some justification for the assumption that the effects of differential control deflection on both wings can be obtained by combining the effects of opposite deflections on the same wing (negligible interaction between controls on opposite wings).

The fuselage and wing pressure distributions can also be used to understand the effect of the area rule on the drag when the controls are undeflected. The design lift coefficient is approximately 0.50 based on two-dimensional airfoil characteristics and sweep effects. The variation of drag coefficient with Mach number and a comparison of the longitudinal aerodynamic force characteristics for the cylindrical and area-ruled configurations are presented in figures 55 and 56, respectively. At the design C_L of 0.50, the drag-divergence Mach number $\left(\text{based on } \partial C_D/\partial M_\infty = 0.1\right)$ increased from 0.896 to 0.916 as a result of the application of the area rule. At Mach numbers below 0.896,

the drag levels are essentially the same for the two configurations; however, at Mach numbers above 0.896, the drag of the area-ruled configuration is considerably lower. At $M_\infty = 0.92$, for example, the difference in drag coefficient is 0.0042. Examination of the fuselage pressure distributions shows that the cylindrical fuselage has a region of acceleration followed by a strong compression wave, whereas the area-ruled fuselage does not have these. (Compare figs. 10(e) and 16(e).) The appearance of the acceleration region may be a function of the sweep of the isobars near the fuselage (ref. 24). The compression wave is caused by the straight sides of the cylindrical fuselage which straighten the streamlines and turn them outward, thereby generating a compression wave. This compression wave coalesces into a shock wave which affects the flow on the wing and apparently causes the earlier drag rise for the cylindrical fuselage configuration. (Compare wing pressure distribution at $\eta = 0.1902$ in figs. 10(d) and 16(d).)

The variations of corrected rolling-moment coefficient ΔC_l with Mach number and incremental drag coefficient ΔC_D with Mach number are summarized in figures 52 and 53. Figure 54 shows the spanwise load distributions for several control surface deflections. The drag data summarized in figure 53 more clearly present the drag results than was possible in the preceding data figures. Figures 52 to 54 also include a comparison between the area-ruled and cylindrical configurations in order to demonstrate the degree to which meaningful control data can be obtained on a configuration which is not area-ruled.

The ΔC_l curves were obtained from the curve fits of the data in the preceding data figures at an angle of attack of 3.5° (which is close to the design lift condition). The ΔC_D values were determined by second-order interpolations of the drag data at $C_L = 0.50$.

From figures 52(a), (b), and (c) it is seen that the control effectiveness near the design lift generally drops off above a Mach number of 0.90. This Mach number is close to the drag-divergence Mach number of 0.916 for the area-ruled configuration with zero control deflection. Figures 52(d) and (e) again show that, with regard to the magnitude and constancy of the rolling moment generated, control F_4 is generally somewhat superior. Figure 52(f) shows the progressive effects of increasing the span of the control. Figures 52(g), (h), (i), (j), and (k) give a direct comparison between the results for the cylindrical and area-ruled configurations. The results for the cylindrical and area-ruled configurations are in generally good agreement up to the drag-divergence Mach number ($M_\infty = 0.896$) for the cylindrical configuration. Beyond this point, however, there are significant differences in the results for the two configurations.

Figures 53(a), (b), and (c) show that negative control deflections generally produce more drag than the corresponding positive deflections. As the Mach number increases,

the drag due to control deflection generally does not show a large increase at or before the drag-divergence Mach number.

As the controls were deflected from the undeflected position to some given angle, the drag increased; however, frequently a further increase in control deflection caused a decrease in drag increment due to control deflection (fig. 53(b), for example).

The effects of control-surface spanwise location and span length are shown in figures 53(d), (e), and (f). Figures 53(g), (h), (i), (j), and (k) compare the results for the area-ruled and cylindrical configurations. Up to the Mach number 0.896, the values of ΔC_D for the cylindrical configuration agree within 0.0005 to 0.0009 with those for the area-ruled configuration.

The conclusion can be drawn that the rolling moment due to control deflections on the present transonic transport can be determined to a reasonably good approximation by use of a configuration which has not been area-ruled. Similarly, the drag increments due to control deflection can be estimated to within 0.0005 to 0.0009 by use of a non-area-ruled configuration. These results are valid for the design lift condition and up to the drag-divergence Mach number of the non-area-ruled configuration.

The spanwise load distributions of figure 54 were obtained by integrating the section pressure distributions near the design C_L and at a Mach number of 0.90. The effects of deflecting controls F_2, F_3, and F_4 are shown. These effects are very nearly the same on the cylindrical configuration as on the area-ruled configuration. The larger effect of the negative deflections compared with the positive deflections is also apparent in most cases.

The deflection of control F_4 on the cylindrical configuration removes the large dip in the spanwise load which may result in less induced drag. This change in the spanwise load may, therefore, be a factor in the reduction of the drag increment due to control deflection mentioned previously. Likewise, with zero control deflections, the area-ruled configuration has a more favorable spanwise load distribution than the cylindrical configuration. This result correlates with the lower drag of the area-ruled configuration at $M_\infty = 0.90$ and $C_L = 0.50$. (See figs. 55 and 56.)

It should be noted that the present configurations with undeflected controls do not, of course, have an optimum spanwise load distribution. Since the present wing was derived from another configuration designed for a higher Mach number ($M_\infty \approx 1.00$) by simply unsweeping the wing, the glove region does not appear to be compatible with the outboard part of the wing at the lower sweep angle. It can be seen that the dip in the spanwise load distribution occurs near the intersection of the wing and the glove. The application of the area rule to the fuselage did help to alleviate the problem somewhat, but the spanwise load distribution for the area-ruled configuration is still significantly different from an elliptic span load.

SUMMARY OF RESULTS

An experimental study has been made to determine the effects of wing trailing-edge controls on the static transonic aerodynamic characteristics of a transport configuration with a supercritical wing. The configuration was designed to cruise near a Mach number of 0.90. The results are summarized as follows.

The inboard controls decreased in rolling-moment effectiveness at the higher angles of attack as the Mach number was increased. The most outboard control was superior in maintaining roll effectiveness over the angle-of-attack range at the various Mach numbers. Near the design lift condition, all controls showed a decrease in roll effectiveness near the drag-divergence Mach number of the configuration with zero control deflection.

It was found that, in general, the farther inboard the control, the more effective the control was in generating changes in lift. The spanwise location of the control had a negligible effect on the pitching moment.

The negative control deflections generally maintained more rolling-moment effectiveness over the angle-of-attack range than the positive deflections, especially at the higher Mach numbers. The negative control deflections also produced more drag and larger increments in the lift and pitching moment than the corresponding positive control deflections.

As the Mach number was increased, the drag due to control deflection generally did not show a large increase prior to the drag-divergence Mach number. In some cases, as the deflection angle increased, the drag increment due to control deflection actually decreased.

The deflection of the controls affected the location of the shock wave which in turn acted to increase or decrease the rolling moment due to control deflection. The effect of the controls on the fuselage pressure distribution was usually minor and therefore provided some justification for assuming that the effects of differential control deflection on both wings can be obtained by combining the effects of opposite deflections on the same wing.

For Mach numbers above the drag-divergence condition of the configuration with the cylindrical fuselage, the cylindrical configuration had a higher drag than the area-ruled configuration. This higher drag was correlated with the existence of a shock wave on the cylindrical fuselage in the vicinity of the junction of the wing trailing edge and the fuselage.

The rolling moment due to control deflections on the present transonic transport can be determined to a reasonably good approximation by use of a configuration which has not been area-ruled. Also, the drag increments due to control deflection can be

estimated to within 0.0005 to 0.0009 by use of a non-area-ruled configuration. This procedure was determined to be valid for the design lift condition and up to the drag-divergence Mach number of the non-area-ruled configuration (with zero control deflections).

The effects of control deflections on the spanwise load distribution are very similar for the area-ruled and cylindrical configurations at the design lift and the drag-divergence Mach number of the cylindrical configuration. The deflection of the outboard control removed a large dip in the spanwise load of the cylindrical configuration.

Langley Research Center
National Aeronautics and Space Administration
Hampton, VA 23665
April 27, 1977

REFERENCES

1. Whitcomb, Richard T.; and Clark, Larry R.: An Airfoil Shape for Efficient Flight at Supercritical Mach Numbers. NASA TM X-1109, 1965.

2. Whitcomb, Richard T.; and Blackwell, James A., Jr.: Status on Research on a Supercritical Wing. Conference on Aircraft Aerodynamics, NASA SP-124, 1966, pp. 367-381.

3. Harris, Charles D.: Wind-Tunnel Investigation of Effects of Trailing-Edge Geometry on a NASA Supercritical Airfoil Section. NASA TM X-2336, 1971.

4. Harris, Charles D.; and Blackwell, James A., Jr.: Wind-Tunnel Investigation of Effects of Rear Upper Surface Modification on an NASA Supercritical Airfoil. NASA TM X-2454, 1972.

5. Bartlett, Dennis W.; and Re, Richard J.: Wind-Tunnel Investigation of Basic Aerodynamic Characteristics of a Supercritical-Wing Research Airplane Configuration. NASA TM X-2470, 1972.

6. Langhans, Richard A.; and Flechner, Stuart G.: Wind-Tunnel Investigation at Mach Numbers From 0.25 to 1.01 of a Transport Configuration Designed To Cruise at Near-Sonic Speeds. NASA TM X-2622, 1972.

7. Supercritical Wing Technology – A Progress Report on Flight Evaluations. NASA SP-301, 1972.

8. Whitcomb, Richard T.: Review of NASA Supercritical Airfoils. ICAS Paper No. 74-10, Aug. 1974.

9. Advanced Subsonic Transport Technology Assessment. Astronaut. & Aeronaut., vol. 10, no. 8, Aug. 1972, pp. 26-55.

10. McKinney, Linwood W.; Herman, Joseph F.; and Bodin, Lawrence A.: Effect of Wing-Mounted Nacelles on a 42° Swept Supercritical Wing Configuration at Near-Sonic Speeds. NASA TM X-2954, 1974.

11. General Dynamics: Experimental Investigation of Parametric Models in Support of a NASA Advanced Transport Technology Program. Volume 1: Data Summary. NASA CR-112130, 1972.

12. General Dynamics: Experimental Investigation of Parametric Models in Support of a NASA Advanced Transport Technology Program. Volume 2: Baseline Study – Basic Data and Test Description. NASA CR-112131, 1972.

13. General Dynamics: Experimental Investigation of Parametric Models in Support of a NASA Advanced Transport Technology Program. Volume 3: Wing Study – Basic Data and Test Description. NASA CR-112132, 1972.

14. General Dynamics: Experimental Investigation of Parametric Models in Support of a NASA Advanced Transport Technology Program. Volume 4: Nacelle Study – Basic Data and Test Description. NASA CR-112133, 1972.

15. General Dynamics: Experimental Investigation of Parametric Models in Support of a NASA Advanced Transport Technology Program. Volume 5: Empennage Study – Basic Data and Test Description. NASA CR-112134, 1972.

16. Little, D. R.; Eiswerth, J. E.; Hancock, J. P.; and Blackwell, J. A.: Wind Tunnel Test of a Series of Wing Mounted Nacelle Installations on a 0.02 Scale Model Near Sonic Four Engine Transport. Tech. Inform. Ser. No. R73AEG162, General Electric Co., July 1973.

17. 8-Foot Transonic Wind Tunnel. Rep. No. WTO-300, Calspan Corporation, Oct. 1971.

18. Bartlett, Dennis W.; and Harris, Charles D.: Aerodynamic Characteristics of an NASA Supercritical-Wing Research Airplane Model With and Without Fuselage Area-Rule Additions at Mach 0.25 to 1.00. NASA TM X-2633, 1972.

19. Loving, Donald L.: Wind-Tunnel—Flight Correlation of Shock-Induced Separated Flow. NASA TN D-3580, 1966.

20. Blackwell, James A., Jr.: Preliminary Study of Effects of Reynolds Number and Boundary-Layer Transition Location on Shock-Induced Separation. NASA TN D-5003, 1969.

21. Braslow, Albert L.; and Knox, Eugene C.: Simplified Method for Determination of Critical Height of Distributed Roughness Particles for Boundary-Layer Transition at Mach Numbers From 0 to 5. NACA TN 4363, 1958.

22. Loving, Donald L.; and Katzoff, S.: The Fluorescent-Oil Film Method and Other Techniques for Boundary-Layer Flow Visualization. NASA MEMO 3-17-59L, 1959.

23. Bauer, Frances; Garabedian, Paul; Korn, David; and Jameson, Antony: Supercritical Wing Sections II. Volume 108 of Lecture Notes in Economics and Mathematical Systems, Springer-Verlag, 1975.

24. Bagley, J. A.: Some Aerodynamic Principles for the Design of Swept Wings. Volume 3 of Progress in Aeronautical Sciences, Antonio Ferri, D. Küchemann, and L. H. G. Sterne, eds., Macmillan Co., 1962, pp. 1-83.

TABLE I.- GENERAL GEOMETRIC CHARACTERISTICS OF MODEL

	True values	Reference values
Wing:		
Sweep, $\Lambda_{c/4}$, deg	33	33
Aspect ratio	7.498	7.496
Taper ratio	0.418	0.376
Area, cm^2	1742.324	1742.861
Span, cm	114.3	114.3
Mean aerodynamic chord, cm	16.100	16.111
Root chord, cm	21.501	21.499
Tip chord, cm	8.986	8.072
Dihedral, deg	0	0
Twist (overall), deg	5.25	5.25
Incidence (root), deg	2.00	2.00
Origin of model stability axes, measured from nose, cm	73.075	73.594

Control surface:	F_1	F_2	F_3	F_4
Control-surface area/Wing area	0.016	0.015	0.010	0.015
Span, cm	5.868	5.867	4.191	12.700
Root chord, cm	4.623	4.623	4.318	2.286
Tip chord, cm	4.623	4.318	4.064	1.727

Vertical tail:	
Sweep, $\Lambda_{c/4}$, deg	45
Aspect ratio	1.354
Taper ratio	0.302
Tail area/Wing area	0.290

TABLE II.- WING AIRFOIL COORDINATES

[z = 0 at WL = -1.55 cm]

η	0.1043		0.1932	
c, cm	45.895		31.0713	
FS, cm	32.512		48.2056	
x/c	z_u/c	z_l/c	z_u/c	z_l/c
0	-0.0225	-0.0225	-0.0502	-0.0502
.0025	-.0153	-.0296	-.0417	-.0574
.0050	-.0119	-.0331	-.0386	-.0607
.0100	-.0075	-.0376	-.0338	-.0660
.0150	-.0043	-.0410	-.0305	-.0698
.0250	.0003	-.0465	-.0252	-.0754
.0500	.0078	-.0555	-.0162	-.0852
.0750	.0140	-.0618	-.0110	-.0910
.1000	.0182	-.0664	-.0074	-.0949
.1500	.0242	-.0728	-.0040	-.1000
.2000	.0283	-.0776	-.0023	-.1030
.2500	.0305	-.0808	-.0021	-.1046
.3000	.0307	-.0828	-.0027	-.1052
.4000	.0263	-.0834	-.0045	-.1033
.5000	.0173	-.0797	-.0083	-.0988
.5500	.0124	-.0751	-.0110	-.0954
.6000	.0074	-.0700	-.0144	-.0908
.6500	.0024	-.0642	-.0189	-.0853
.7000	-.0031	-.0584	-.0243	-.0787
.7500	-.0086	-.0525	-.0290	-.0727
.8000	-.0146	-.0468	-.0332	-.0675
.8500	-.0212	-.0434	-.0384	-.0631
.9000	-.0279	-.0424	-.0440	-.0611
.9500	-.0343	-.0435	-.0505	-.0611
1.0000	-.0424	-.0448	-.0585	-.0630

TABLE II.- Continued

η	0.2578		0.3111	
c, cm	21.7658		18.5000	
FS, cm	58.6616		63.2478	
x/c	z_u/c	z_l/c	z_u/c	z_l/c
0	-0.0880	-0.0880	-0.1135	-0.1135
.0025	-.0788	-.0959	-.1056	-.1208
.0050	-.0752	-.0995	-.1021	-.1243
.0100	-.0705	-.1046	-.0978	-.1290
.0150	-.0672	-.1082	-.0947	-.1324
.0250	-.0629	-.1133	-.0896	-.1372
.0500	-.0557	-.1213	-.0821	-.1440
.0750	-.0511	-.1263	-.0772	-.1482
.1000	-.0478	-.1297	-.0734	-.1514
.1500	-.0434	-.1332	-.0685	-.1552
.2000	-.0404	-.1354	-.0651	-.1571
.2500	-.0386	-.1363	-.0632	-.1576
.3000	-.0375	-.1364	-.0617	-.1573
.4000	-.0375	-.1342	-.0612	-.1554
.5000	-.0398	-.1296	-.0625	-.1504
.5500	-.0420	-.1261	-.0638	-.1457
.6000	-.0446	-.1214	-.0652	-.1410
.6500	-.0479	-.1153	-.0678	-.1341
.7000	-.0522	-.1074	-.0709	-.1251
.7500	-.0555	-.1000	-.0735	-.1164
.8000	-.0586	-.0935	-.0758	-.1089
.8500	-.0624	-.0882	-.0791	-.1032
.9000	-.0672	-.0857	-.0836	-.1007
.9500	-.0739	-.0862	-.0900	-.1021
1.0000	-.0832	-.0885	-.0997	-.1049

TABLE II.- Continued

η	0.3516		0.3864	
c, cm	17.2712		16.6657	
FS, cm	65.6140		67.1977	
x/c	z_u/c	z_l/c	z_u/c	z_l/c
0	-0.1282	-0.1282	-0.1399	-0.1399
.0025	-.1203	-.1364	-.1296	-.1494
.0050	-.1165	-.1401	-.1258	-.1532
.0100	-.1115	-.1448	-.1219	-.1579
.0150	-.1083	-.1481	-.1179	-.1612
.0250	-.1035	-.1524	-.1137	-.1658
.0500	-.0960	-.1591	-.1069	-.1729
.0750	-.0908	-.1635	-.1024	-.1773
.1000	-.0870	-.1668	-.0990	-.1804
.1500	-.0820	-.1702	-.0941	-.1841
.2000	-.0785	-.1718	-.0907	-.1858
.2500	-.0763	-.1722	-.0883	-.1863
.3000	-.0749	-.1720	-.0866	-.1860
.4000	-.0737	-.1695	-.0846	-.1832
.5000	-.0738	-.1641	-.0841	-.1777
.5500	-.0746	-.1592	-.0843	-.1736
.6000	-.0756	-.1545	-.0850	-.1678
.6500	-.0775	-.1465	-.0860	-.1593
.7000	-.0808	-.1369	-.0875	-.1476
.7500	-.0830	-.1274	-.0895	-.1370
.8000	-.0853	-.1191	-.0922	-.1284
.8500	-.0887	-.1125	-.0959	-.1221
.9000	-.0933	-.1097	-.1008	-.1188
.9500	-.0999	-.1112	-.1075	-.1201
1.0000	-.1100	-.1161	-.1164	-.1285

TABLE II.- Continued

η	0.4297		0.4730	
c, cm	16.1229		15.5811	
FS, cm	68.9531		70.7106	
x/c	z_u/c	z_l/c	z_u/c	z_l/c
0	-0.1490	-0.1490	-0.1586	-0.1586
.0025	-.1386	-.1581	-.1482	-.1675
.0050	-.1349	-.1618	-.1445	-.1711
.0100	-.1301	-.1665	-.1399	-.1757
.0150	-.1271	-.1696	-.1369	-.1788
.0250	-.1228	-.1741	-.1326	-.1831
.0500	-.1158	-.1808	-.1257	-.1897
.0750	-.1111	-.1849	-.1209	-.1936
.1000	-.1074	-.1876	-.1172	-.1961
.1500	-.1020	-.1906	-.1115	-.1989
.2000	-.0980	-.1917	-.1073	-.1997
.2500	-.0949	-.1916	-.1040	-.1993
.3000	-.0926	-.1905	-.1014	-.1980
.4000	-.0892	-.1865	-.0976	-.1934
.5000	-.0874	-.1798	-.0952	-.1863
.5500	-.0870	-.1751	-.0945	-.1814
.6000	-.0869	-.1688	-.0941	-.1749
.6500	-.0872	-.1598	-.0941	-.1658
.7000	-.0880	-.1477	-.0946	-.1535
.7500	-.0894	-.1367	-.0958	-.1424
.8000	-.0916	-.1278	-.0977	-.1335
.8500	-.0947	-.1212	-.1007	-.1270
.9000	-.0993	-.1178	-.1053	-.1237
.9500	-.1058	-.1190	-.1120	-.1251
1.0000	-.1148	-.1275	-.1216	-.1341

TABLE II.- Continued

η	0.5162		0.5595	
c, cm	15.0406		14.4988	
FS, cm	72.4637		74.2213	
x/c	z_u/c	z_l/c	z_u/c	z_l/c
0	-0.1687	-0.1687	-0.1795	-0.1795
.0025	-.1584	-.1774	-.1692	-.1880
.0050	-.1548	-.1810	-.1657	-.1915
.0100	-.1502	-.1855	-.1612	-.1959
.0150	-.1472	-.1885	-.1583	-.1988
.0250	-.1430	-.1927	-.1541	-.2030
.0500	-.1361	-.1991	-.1472	-.2092
.0750	-.1313	-.2028	-.1423	-.2127
.1000	-.1275	-.2052	-.1385	-.2150
.1500	-.1217	-.2077	-.1325	-.2172
.2000	-.1173	-.2082	-.1279	-.2174
.2500	-.1137	-.2075	-.1242	-.2165
.3000	-.1109	-.2060	-.1211	-.2147
.4000	-.1065	-.2010	-.1162	-.2092
.5000	-.1036	-.1934	-.1127	-.2013
.5500	-.1026	-.1883	-.1115	-.1960
.6000	-.1019	-.1816	-.1105	-.1892
.6500	-.1017	-.1725	-.1100	-.1799
.7000	-.1019	-.1601	-.1100	-.1674
.7500	-.1028	-.1489	-.1106	-.1562
.8000	-.1045	-.1399	-.1121	-.1472
.8500	-.1074	-.1334	-.1149	-.1407
.9000	-.1120	-.1302	-.1194	-.1376
.9500	-.1189	-.1319	-.1265	-.1394
1.0000	-.1289	-.1412	-.1369	-.1490

TABLE II.- Continued

η	0.6027		0.6460	
c, cm	13.9583		13.4165	
FS, cm	75.9742		77.7319	
x/c	z_u/c	z_l/c	z_u/c	z_l/c
0	-0.1910	-0.1910	-0.2036	-0.2036
.0025	-.1808	-.1993	-.1935	-.2118
.0050	-.1773	-.2028	-.1900	-.2152
.0100	-.1729	-.2070	-.1857	-.2193
.0150	-.1700	-.2099	-.1829	-.2222
.0250	-.1659	-.2140	-.1788	-.2261
.0500	-.1590	-.2200	-.1720	-.2319
.0750	-.1541	-.2234	-.1671	-.2352
.1000	-.1502	-.2255	-.1631	-.2371
.1500	-.1441	-.2274	-.1568	-.2388
.2000	-.1393	-.2274	-.1518	-.2386
.2500	-.1353	-.2262	-.1477	-.2371
.3000	-.1320	-.2242	-.1441	-.2349
.4000	-.1267	-.2183	-.1383	-.2285
.5000	-.1227	-.2099	-.1338	-.2198
.5500	-.1211	-.2044	-.1320	-.2141
.6000	-.1199	-.1975	-.1306	-.2071
.6500	-.1191	-.1881	-.1295	-.1976
.7000	-.1188	-.1756	-.1290	-.1851
.7500	-.1192	-.1643	-.1291	-.1738
.8000	-.1205	-.1553	-.1302	-.1647
.8500	-.1231	-.1488	-.1327	-.1583
.9000	-.1277	-.1458	-.1371	-.1553
.9500	-.1348	-.1478	-.1444	-.1573
1.0000	-.1456	-.1576	-.1554	-.1672

TABLE II.- Continued

η	0.6892		0.7279	
c, cm	12.8758		12.3914	
FS, cm	79.4850		81.0562	
x/c	z_u/c	z_l/c	z_u/c	z_l/c
0	-0.2169	-0.2169	-0.2297	-0.2297
.0025	-.2069	-.2249	-.2196	-.2375
.0050	-.2034	-.2282	-.2163	-.2407
.0100	-.1992	-.2323	-.2121	-.2447
.0150	-.1965	-.2350	-.2094	-.2474
.0250	-.1924	-.2389	-.2055	-.2512
.0500	-.1856	-.2445	-.1986	-.2567
.0750	-.1807	-.2476	-.1937	-.2597
.1000	-.1766	-.2495	-.1896	-.2613
.1500	-.1702	-.2508	-.1831	-.2625
.2000	-.1650	-.2504	-.1778	-.2619
.2500	-.1607	-.2488	-.1733	-.2600
.3000	-.1570	-.2463	-.1694	-.2574
.4000	-.1507	-.2395	-.1627	-.2503
.5000	-.1458	-.2304	-.1574	-.2408
.5500	-.1437	-.2246	-.1551	-.2349
.6000	-.1420	-.2174	-.1532	-.2276
.6500	-.1407	-.2079	-.1517	-.2181
.7000	-.1399	-.1954	-.1506	-.2055
.7500	-.1398	-.1840	-.1503	-.1942
.8000	-.1407	-.1750	-.1510	-.1851
.8500	-.1430	-.1685	-.1532	-.1787
.9000	-.1474	-.1655	-.1575	-.1757
.9500	-.1547	-.1676	-.1648	-.1778
1.0000	-.1659	-.1776	-.1762	-.1877

TABLE II.- Continued

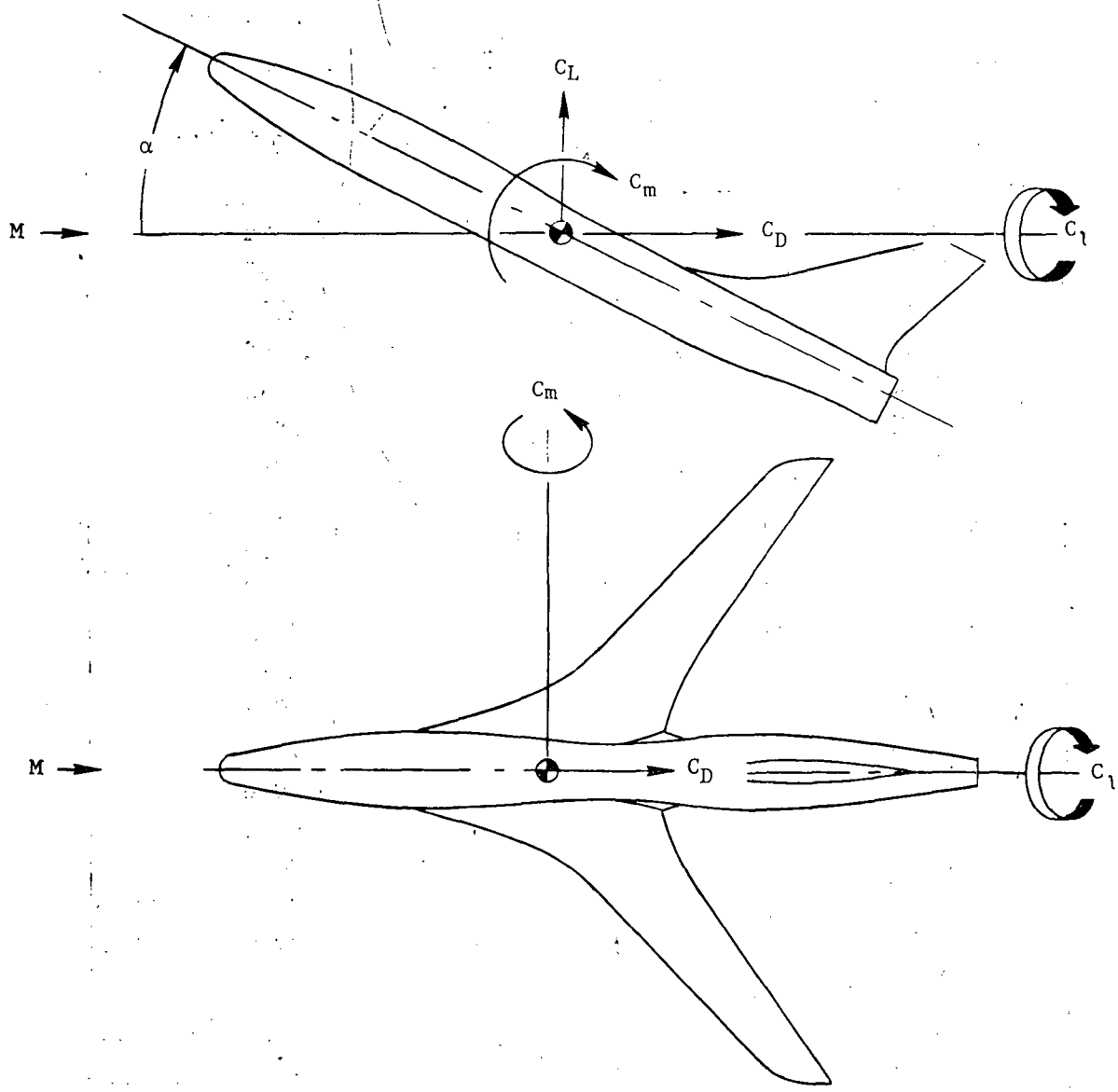
η	0.7757		0.8189	
c, cm	11.7932		11.2527	
FS, cm	82.9955		84.7486	
x/c	z_u/c	z_l/c	z_u/c	z_l/c
0	-0.2462	-0.2462	-0.2621	-0.2621
.0025	-.2363	-.2538	-.2523	-.2696
.0050	-.2330	-.2570	-.2491	-.2727
.0100	-.2290	-.2609	-.2451	-.2765
.0150	-.2263	-.2636	-.2425	-.2791
.0250	-.2224	-.2672	-.2386	-.2827
.0500	-.2156	-.2725	-.2319	-.2878
.0750	-.2106	-.2753	-.2269	-.2905
.1000	-.2065	-.2769	-.2228	-.2919
.1500	-.1998	-.2778	-.2160	-.2926
.2000	-.1944	-.2769	-.2104	-.2915
.2500	-.1897	-.2749	-.2055	-.2893
.3000	-.1856	-.2720	-.2013	-.2863
.4000	-.1785	-.2645	-.1938	-.2784
.5000	-.1727	-.2547	-.1876	-.2683
.5500	-.1702	-.2486	-.1849	-.2621
.6000	-.1680	-.2412	-.1825	-.2546
.6500	-.1662	-.2317	-.1805	-.2450
.7000	-.1649	-.2191	-.1790	-.2325
.7500	-.1644	-.2078	-.1782	-.2212
.8000	-.1649	-.1976	-.1785	-.2121
.8500	-.1669	-.1923	-.1803	-.2056
.9000	-.1710	-.1892	-.1843	-.2025
.9500	-.1783	-.1913	-.1915	-.2045
1.0000	-.1897	-.2012	-.2029	-.2142

TABLE II.- Concluded

η	0.8622		0.9054	
c, cm	10.7107		10.1702	
FS, cm	86.5063		88.2592	
x/c	z_u/c	z_l/c	z_u/c	z_l/c
0	-0.2793	-0.2793	-0.2981	-0.2981
.0025	-.2696	-.2866	-.2885	-.3032
.0050	-.2664	-.2896	-.2854	-.3083
.0100	-.2625	-.2934	-.2816	-.3119
.0150	-.2600	-.2959	-.2791	-.3144
.0250	-.2562	-.2994	-.2754	-.3178
.0500	-.2495	-.3044	-.2687	-.3226
.0750	-.2445	-.3069	-.2637	-.3251
.1000	-.2403	-.3082	-.2596	-.3263
.1500	-.2334	-.3087	-.2526	-.3266
.2000	-.2277	-.3075	-.2468	-.3251
.2500	-.2227	-.3051	-.2417	-.3226
.3000	-.2183	-.3019	-.2371	-.3192
.4000	-.2105	-.2937	-.2290	-.3107
.5000	-.2039	-.2833	-.2220	-.3001
.5500	-.2010	-.2770	-.2190	-.2937
.6000	-.1984	-.2694	-.2162	-.2861
.6500	-.1962	-.2598	-.2138	-.2765
.7000	-.1945	-.2474	-.2118	-.2641
.7500	-.1935	-.2360	-.2107	-.2528
.8000	-.1936	-.2270	-.2105	-.2437
.8500	-.1952	-.2204	-.2119	-.2371
.9000	-.1990	-.2173	-.2156	-.2338
.9500	-.2061	-.2191	-.2224	-.2355
1.0000	-.2174	-.2286	-.2336	-.2447

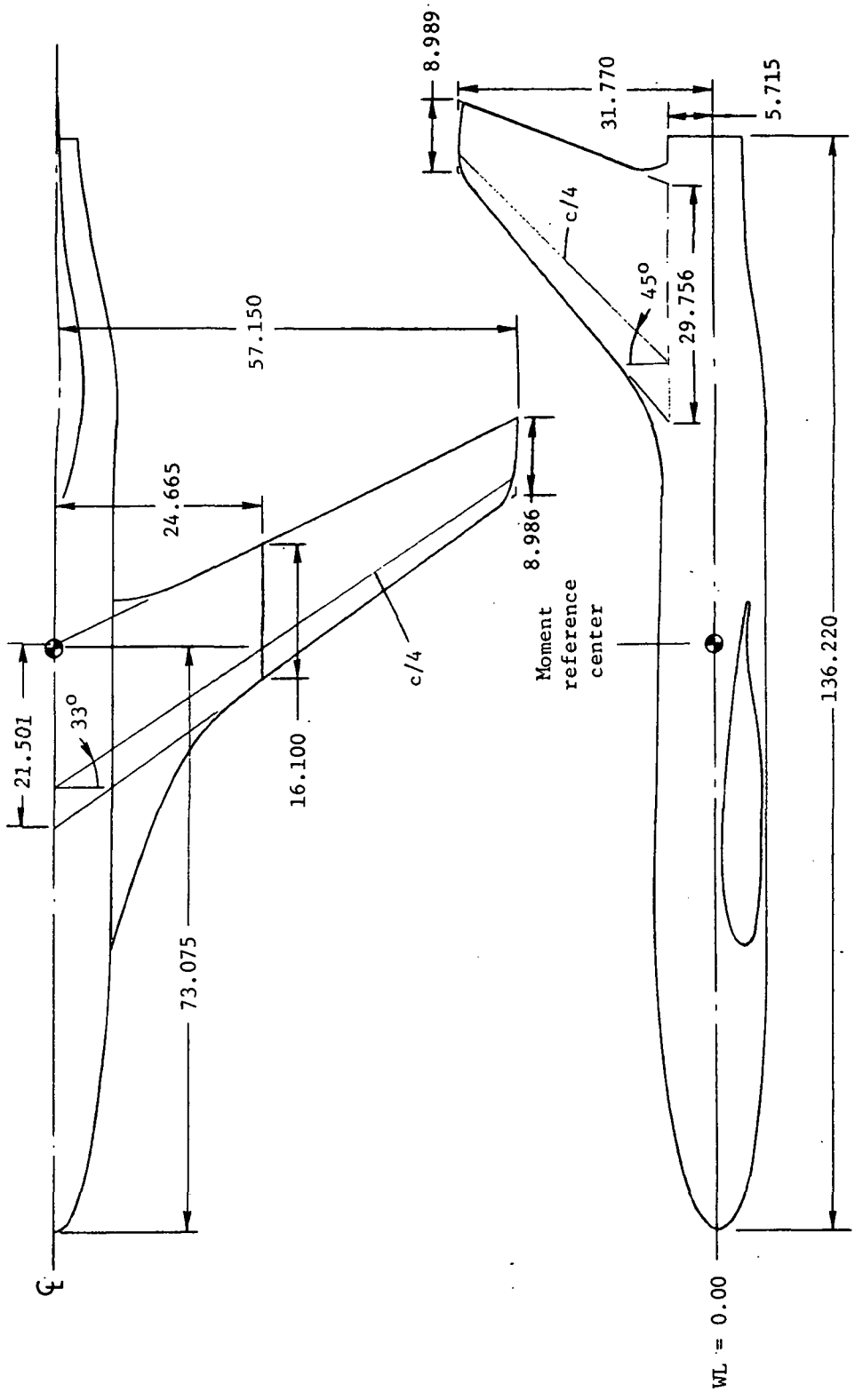
TABLE III.- WING PLANFORM COORDINATES

x', cm	y, cm
14.241	0
48.206	11.041
58.662	14.733
63.248	17.779
65.614	20.094
67.198	22.085
68.953	24.557
92.099	57.150
101.085	57.150
81.740	17.728
78.296	2.915
78.296	0



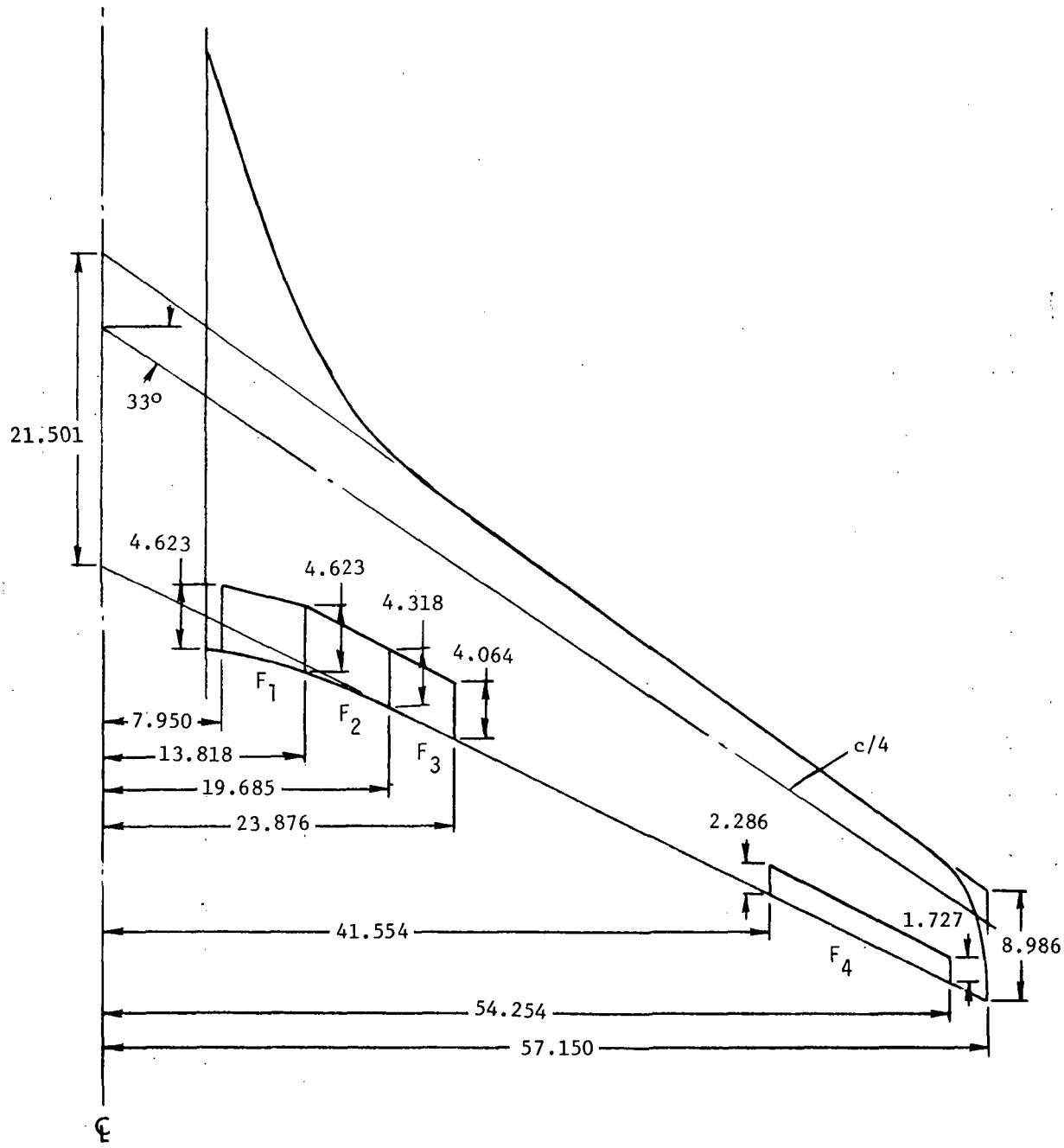
(a) Axis system. Positive directions of forces, moments, and angles are indicated by arrows.

Figure 1.- Details of model and tunnel geometry. Dimensions are in centimeters unless otherwise specified.



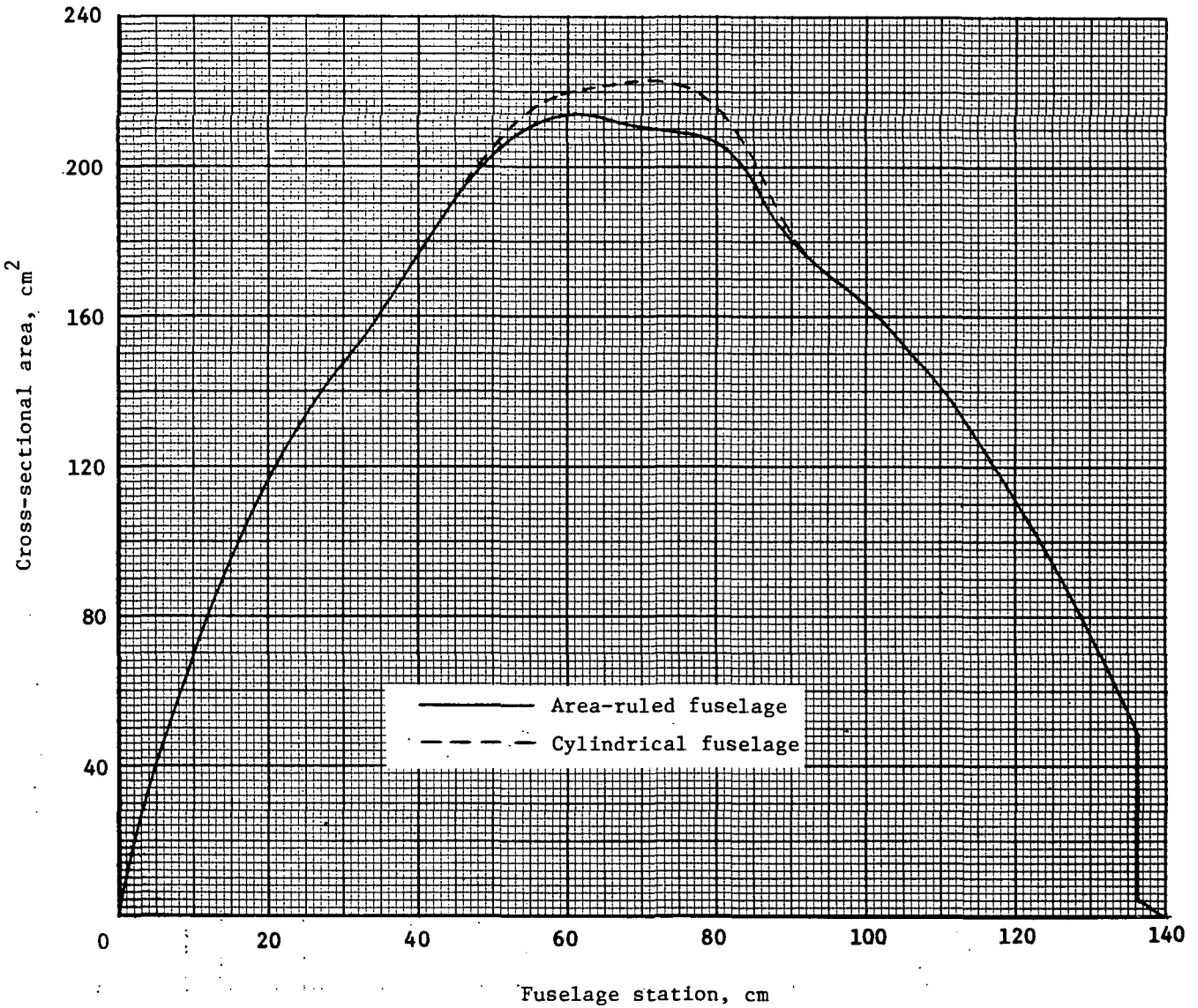
(b) General arrangement of model.

Figure 1.- Continued.



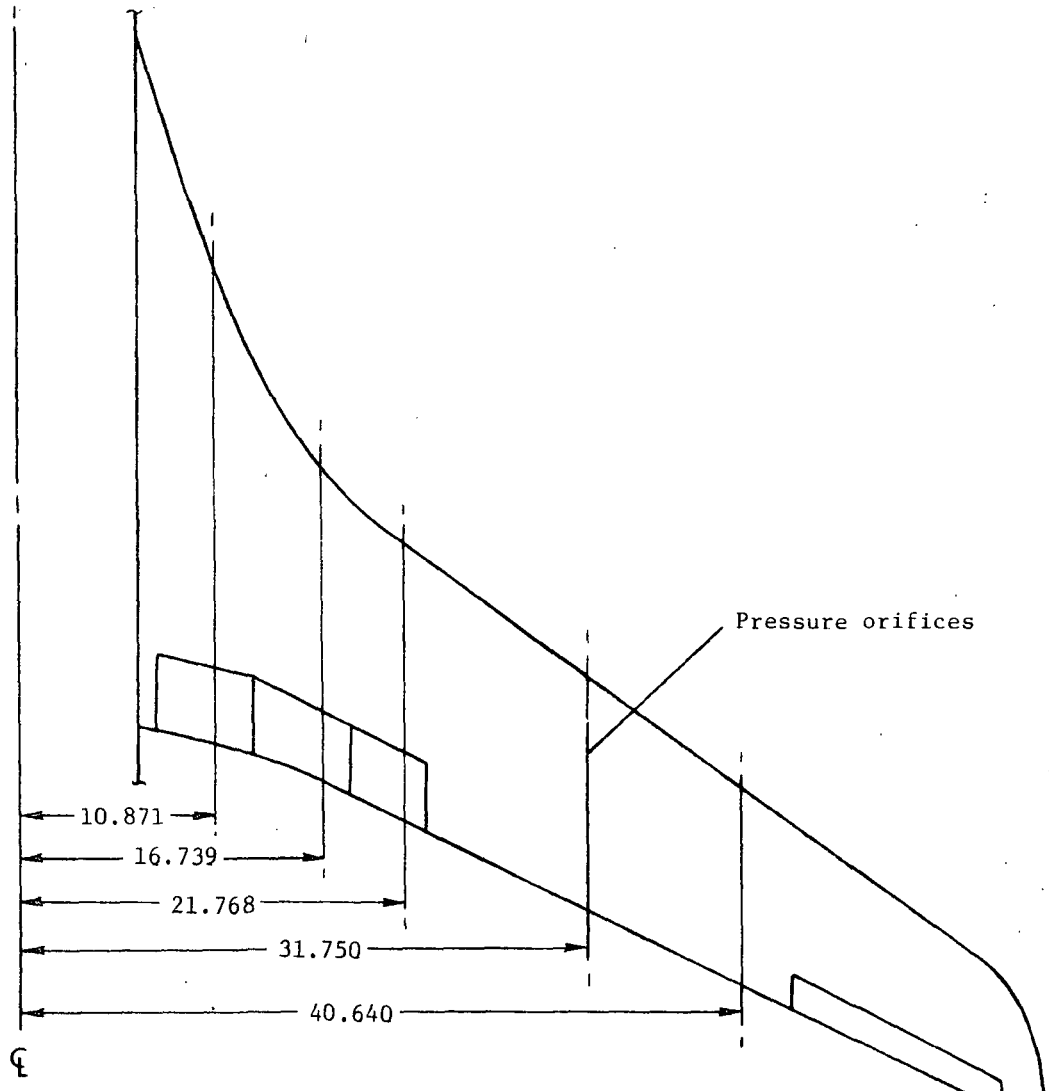
(c) Details of wing trailing-edge control surfaces.

Figure 1.- Continued.



(d) Cross-sectional area distribution of model.

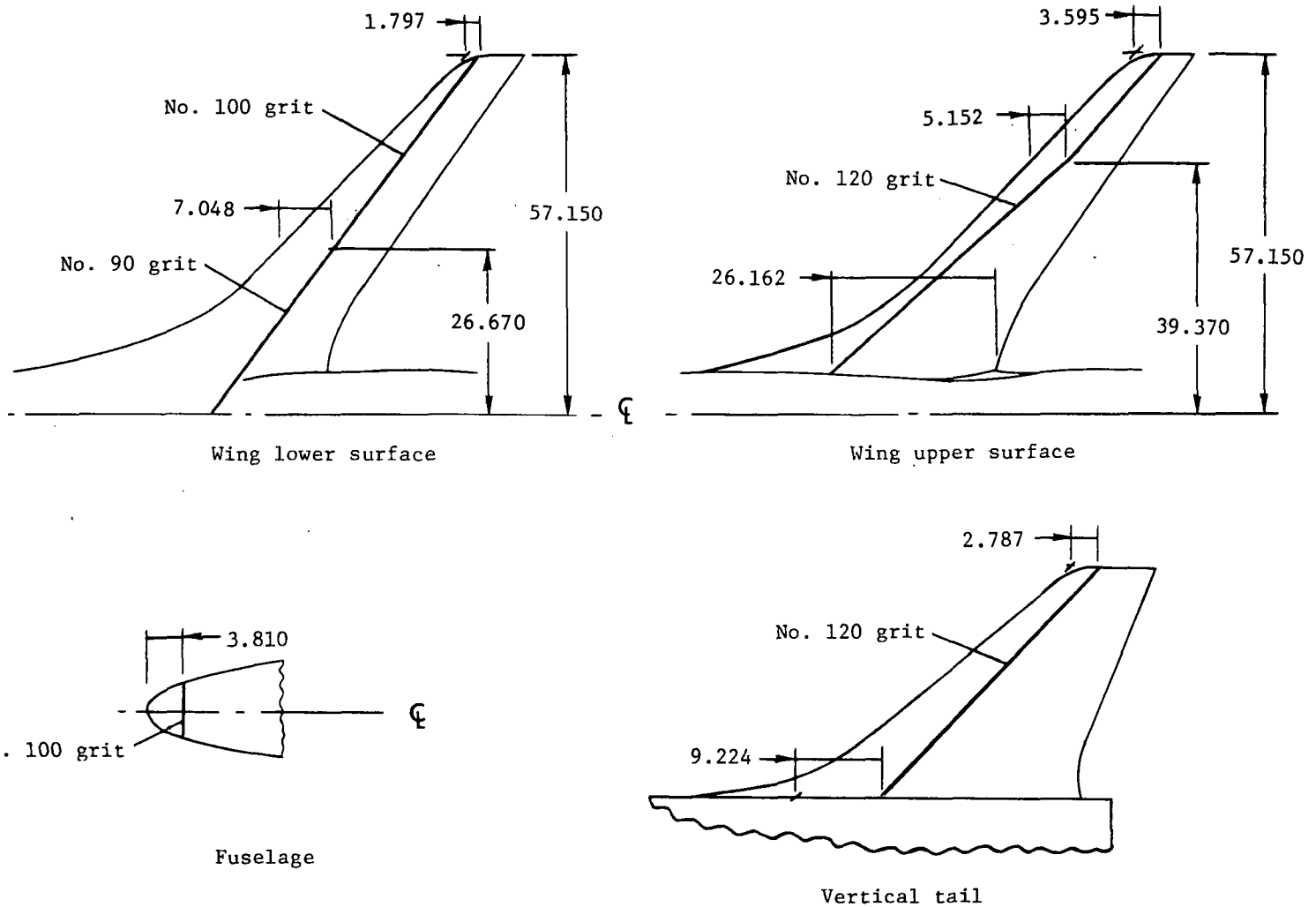
Figure 1.- Continued.



Span station	40.640	31.750	21.768	16.739	10.871
η	0.7111	0.5556	0.3809	0.2929	0.1902
Chord	12.461	14.318	16.563	20.437	31.590

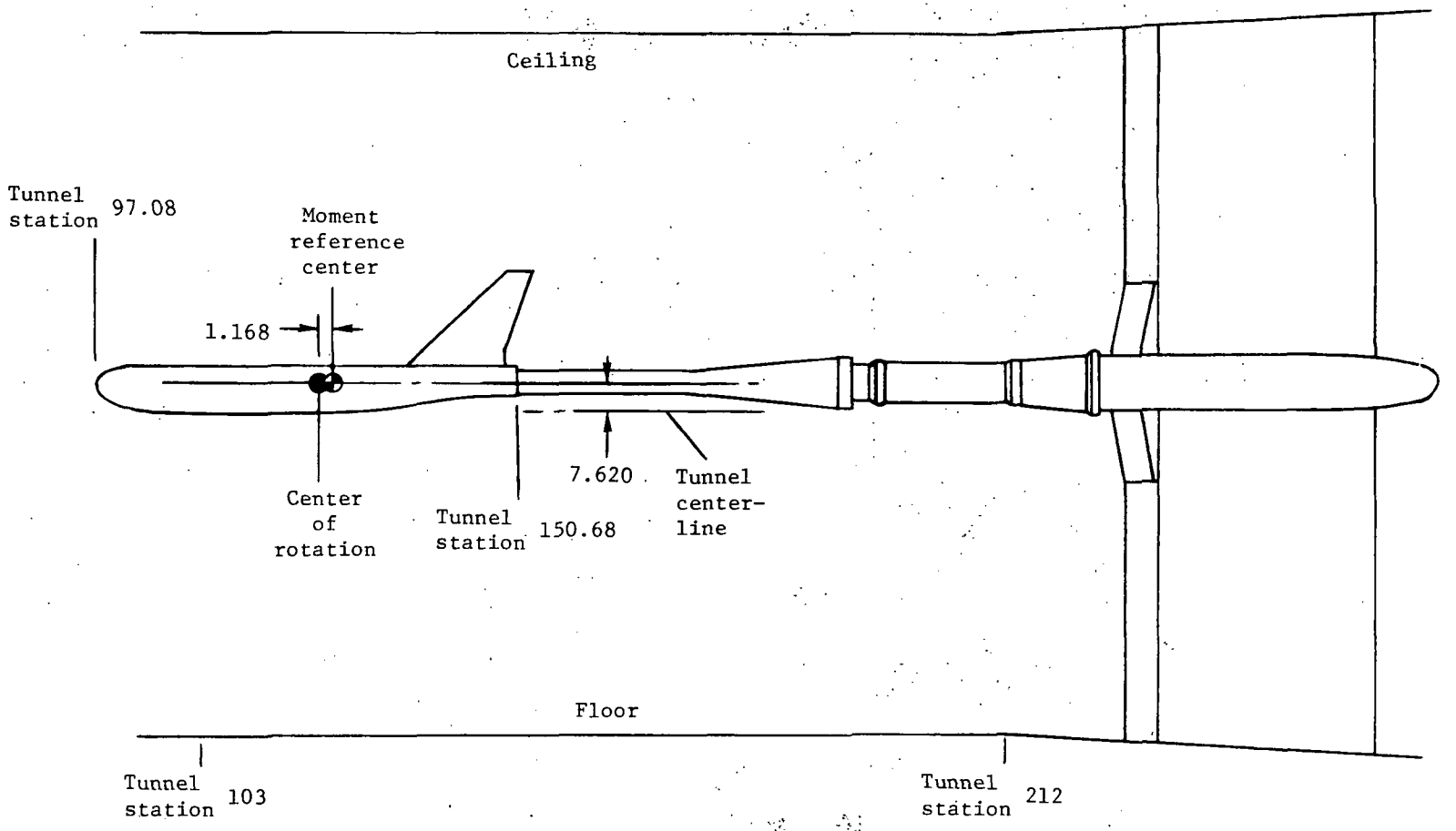
(e) Wing pressure orifice locations. See table IV for longitudinal location of pressure orifices.

Figure 1.- Continued.



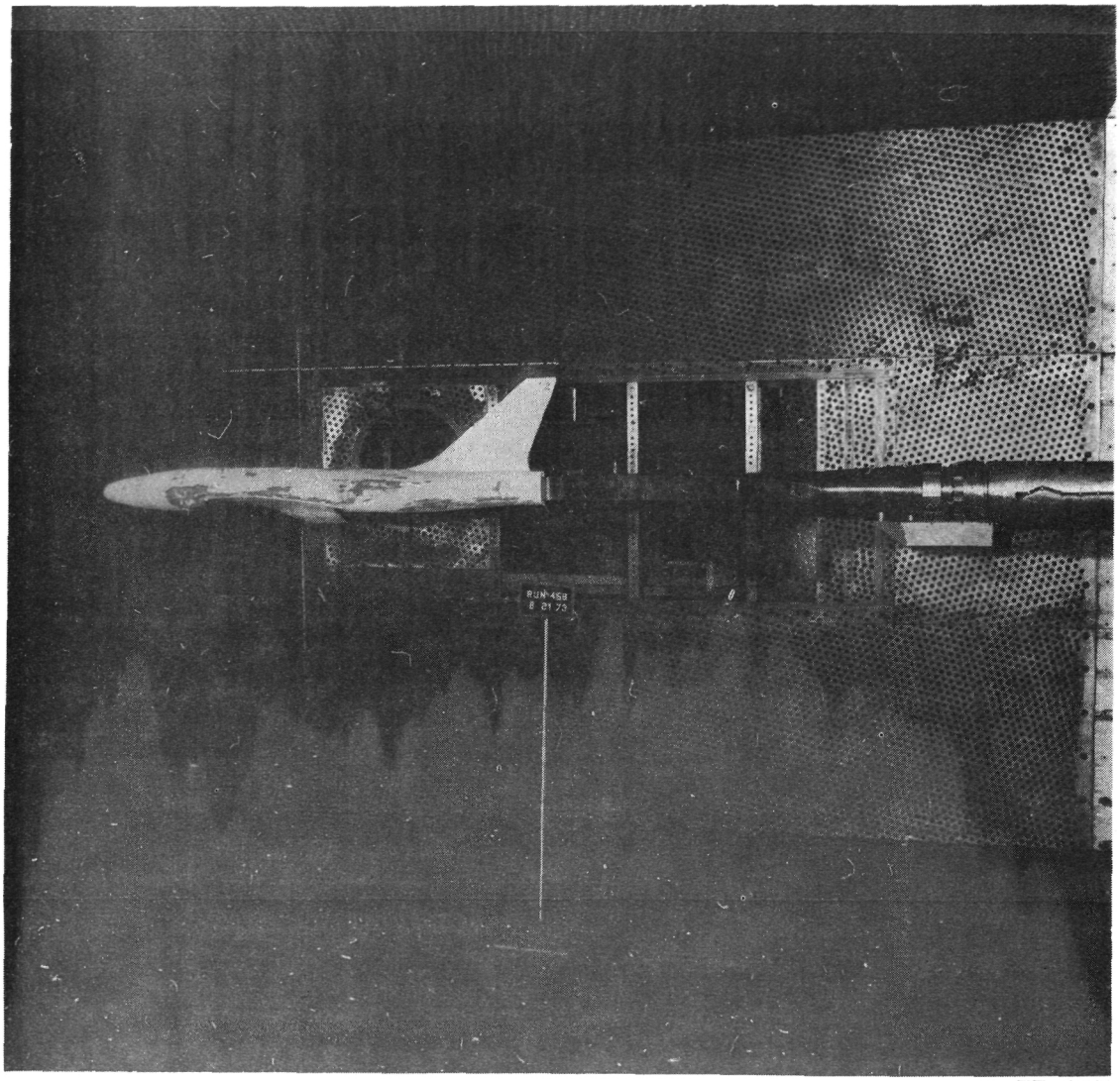
(f) Model transition-strip locations.

Figure 1.- Continued.



(g) Installation of model in tunnel.

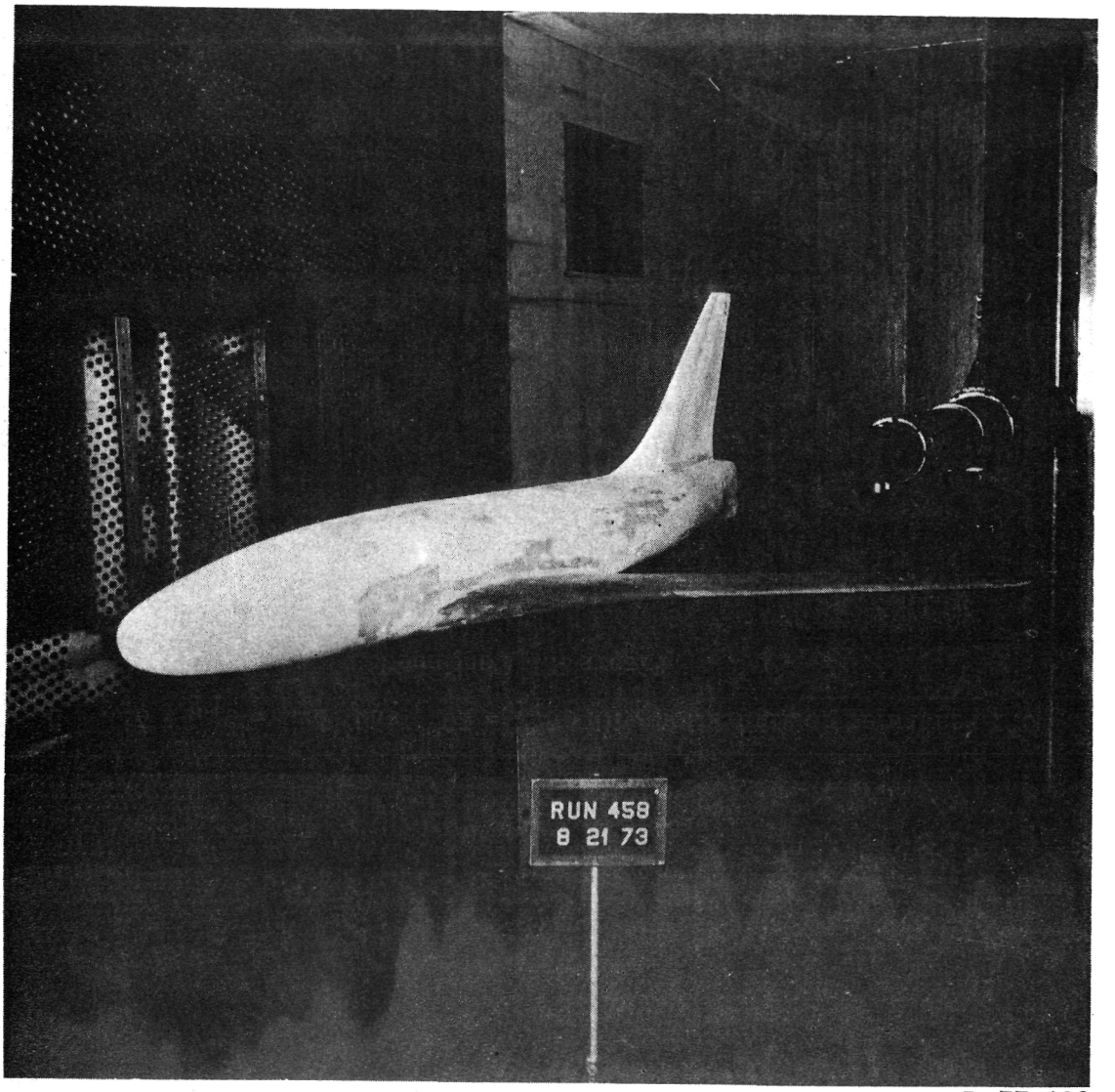
Figure 1.- Concluded.



L-77-197

(a) Model installation; area-ruled configuration.

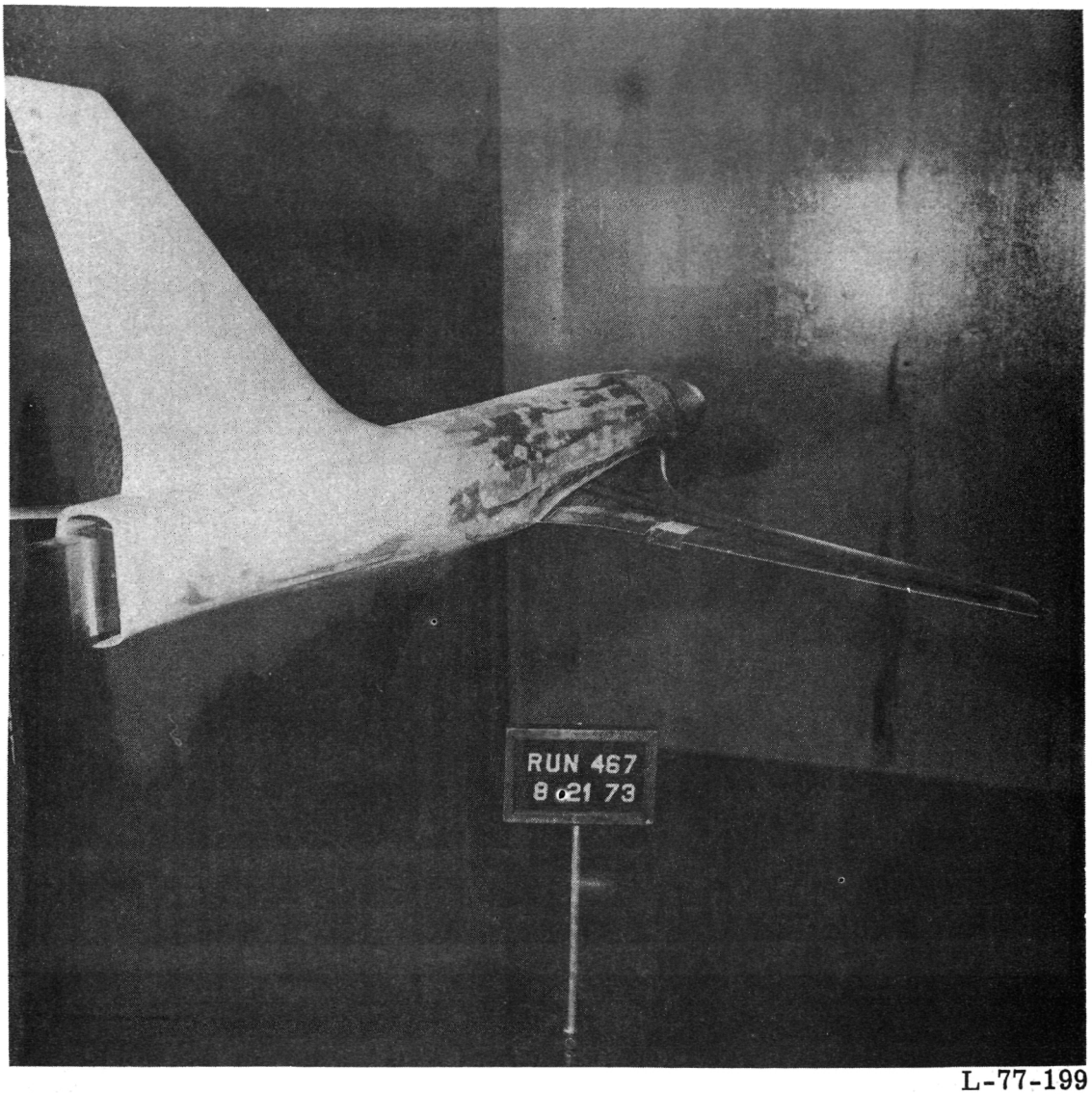
Figure 2.- Model mounted in Calspan 8-Foot Transonic Wind Tunnel.



L-77-198

(b) Area-ruled configuration.

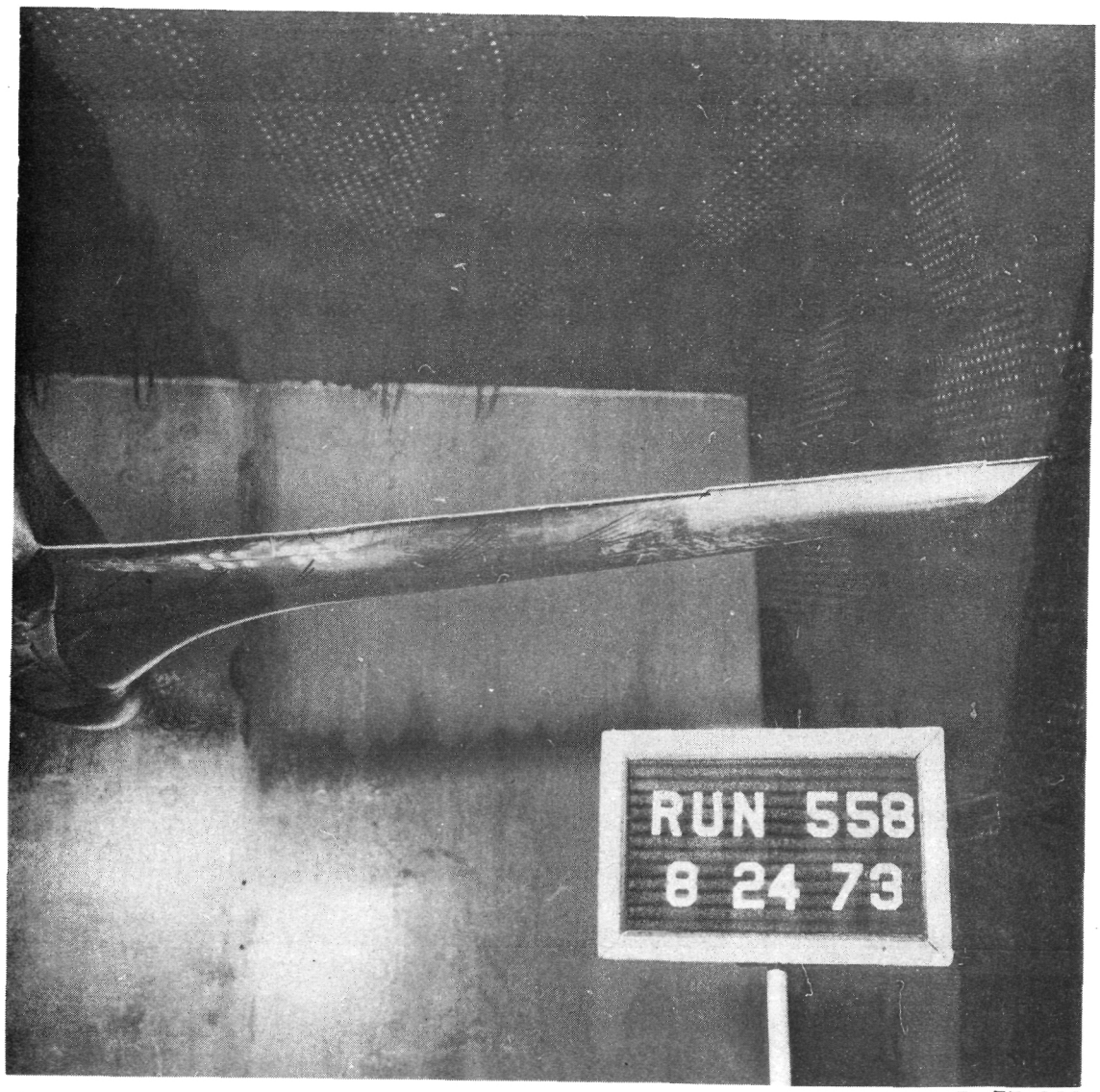
Figure 2.- Continued.



L-77-199

(c) Area-ruled configuration with $\delta_{F3} = 10^{o}$ and $\delta_{F1} = \delta_{F2} = \delta_{F4} = 0$.

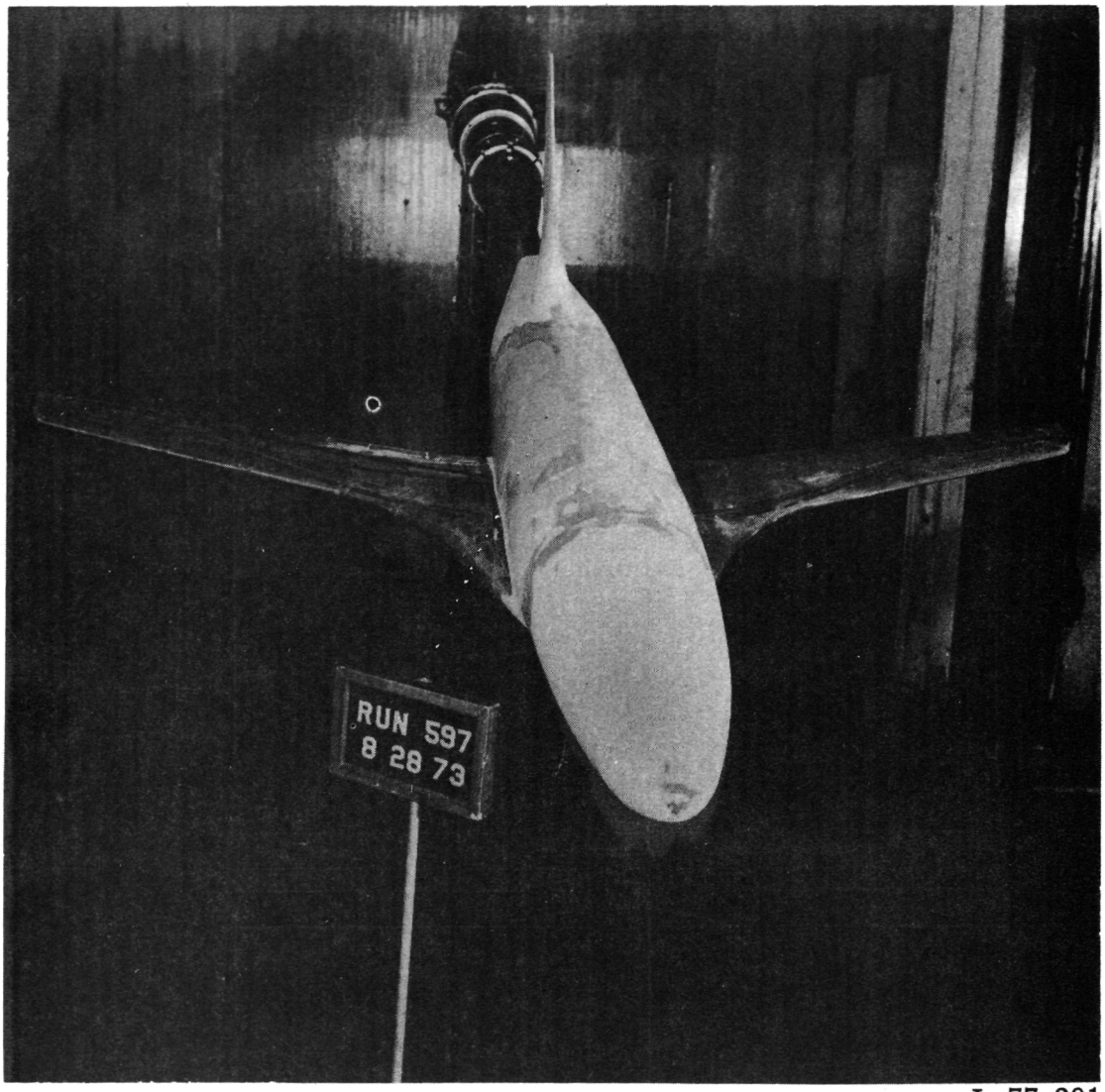
Figure 2.- Continued.



L-77-200

(d) Area-ruled configuration with $\delta_{F4} = -4^{o}$ and $\delta_{F1} = \delta_{F2} = \delta_{F3} = 0$.

Figure 2.- Continued.



L-77-201

(e) Cylindrical configuration.

Figure 2.- Concluded.

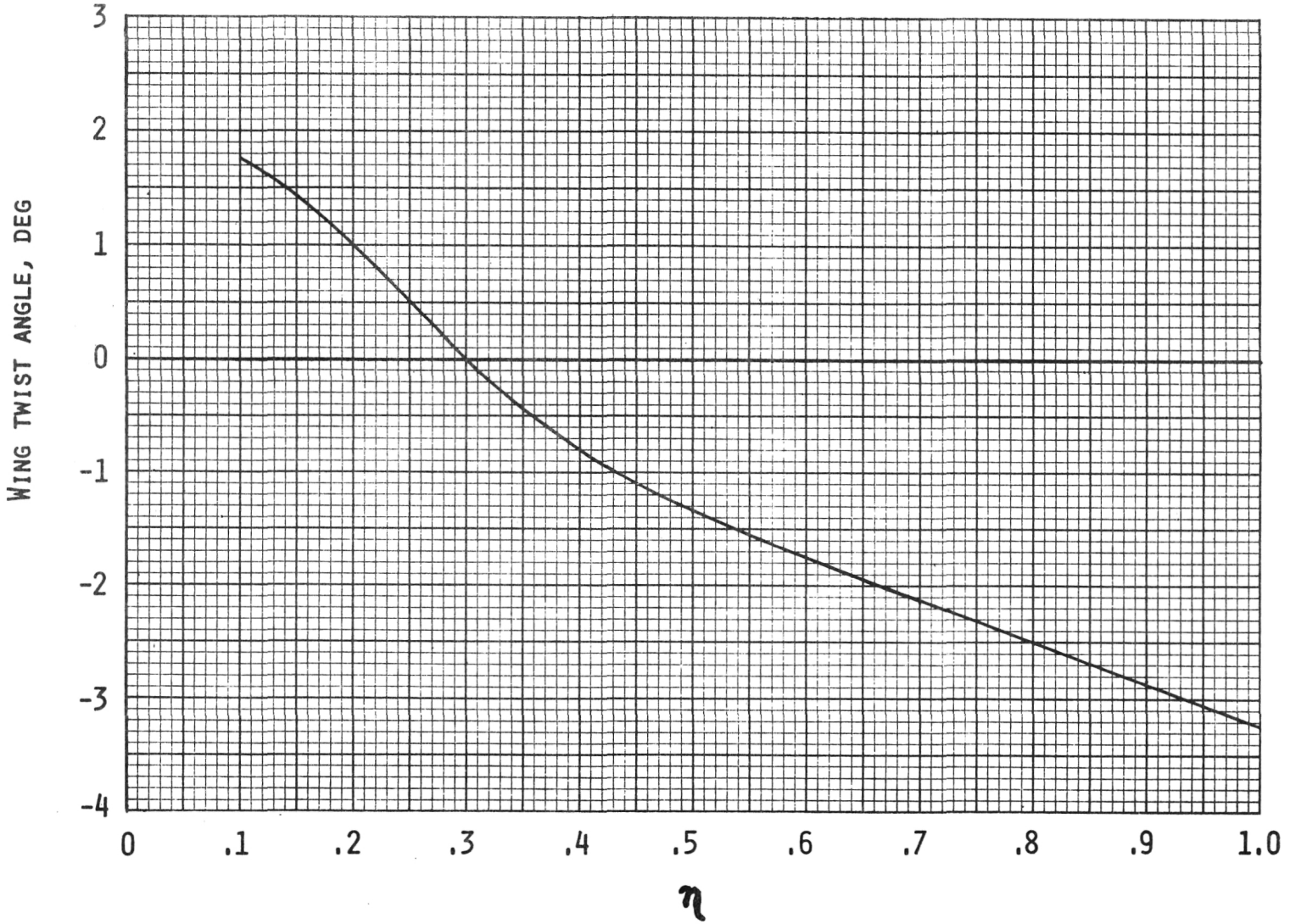
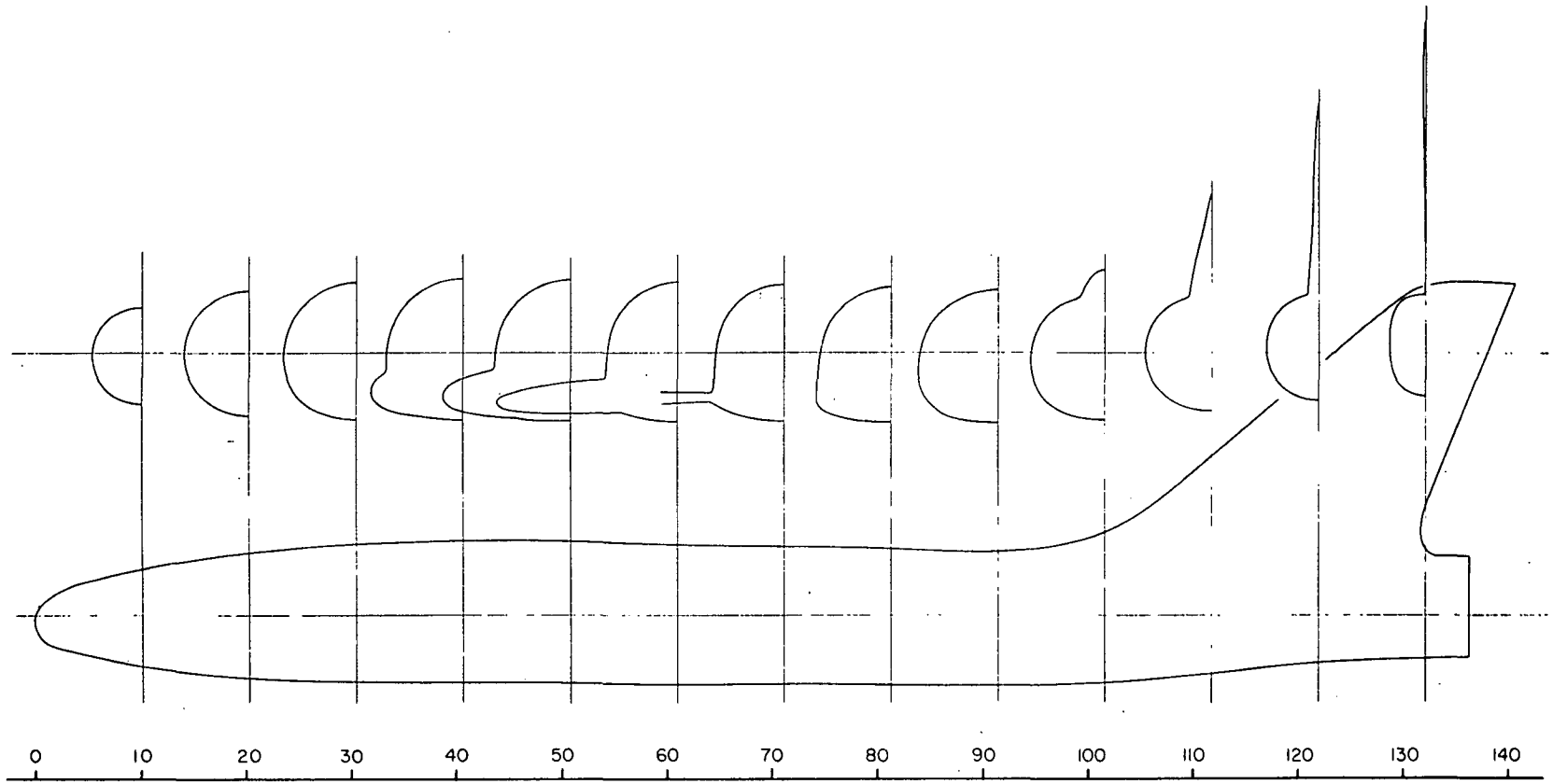
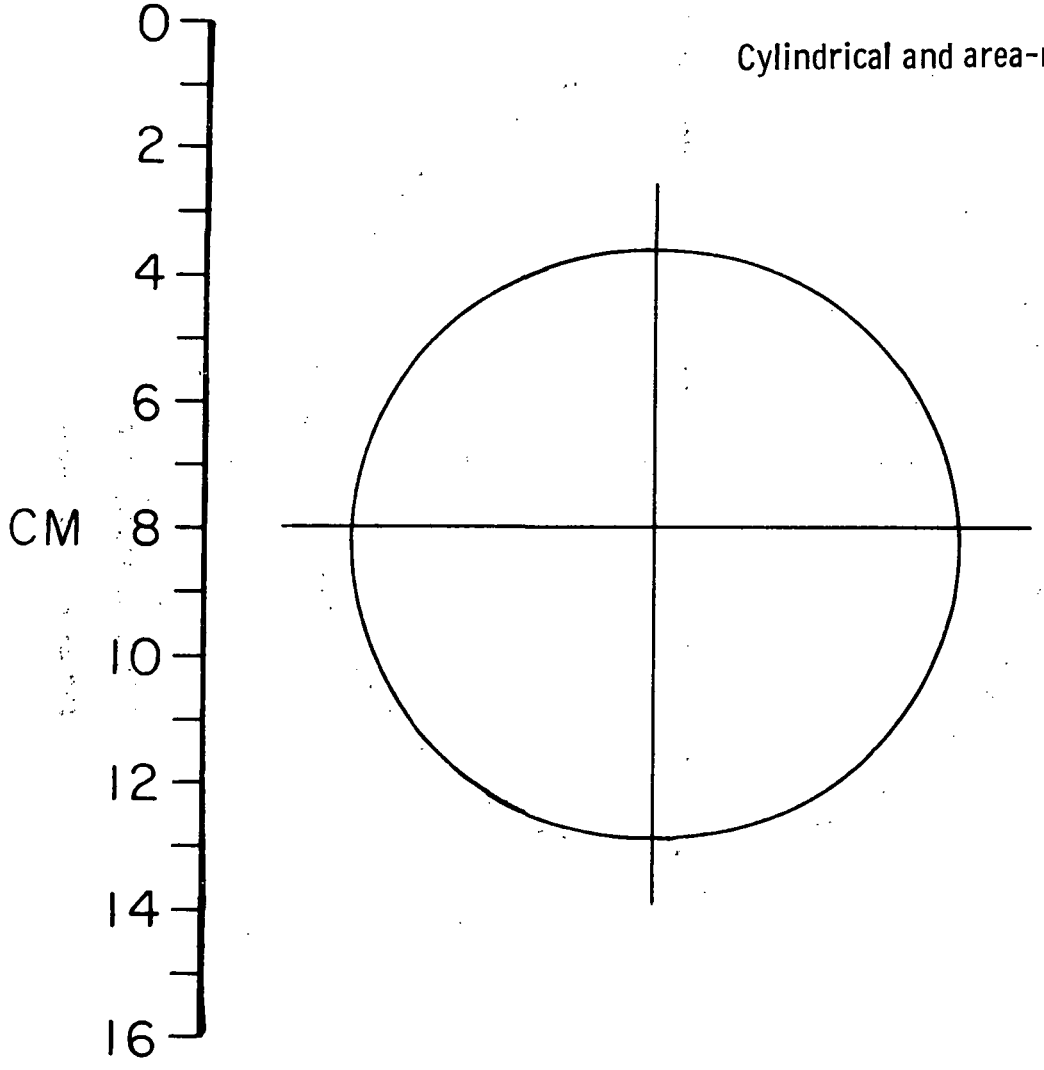


Figure 3.- Wing twist distribution.



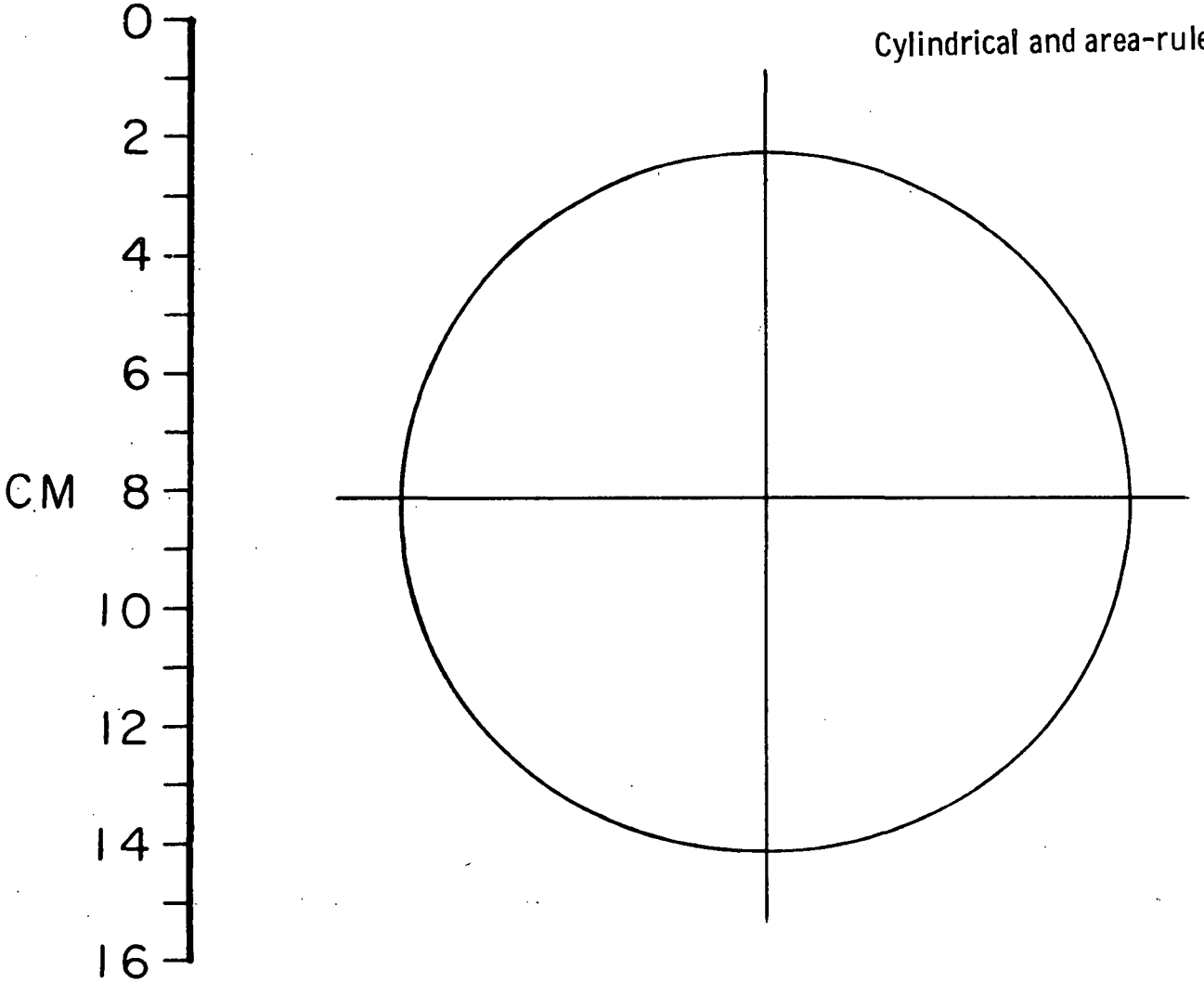
(a) Longitudinal development of fuselage cross sections for area-ruled configuration.

Figure 4.- Fuselage cross sections for area-ruled and cylindrical configurations.



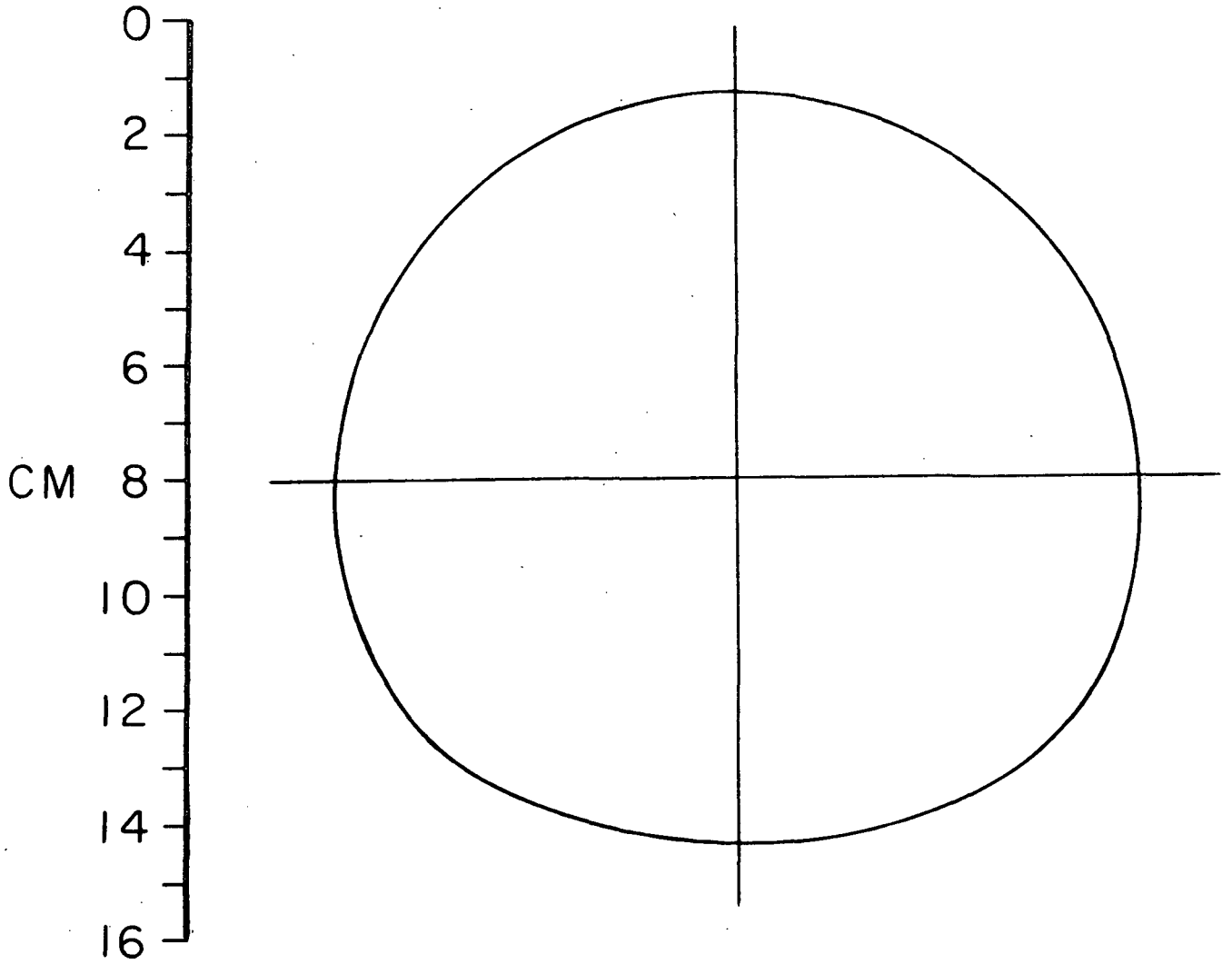
(b) 10.16 cm from nose.

Figure 4.- Continued.



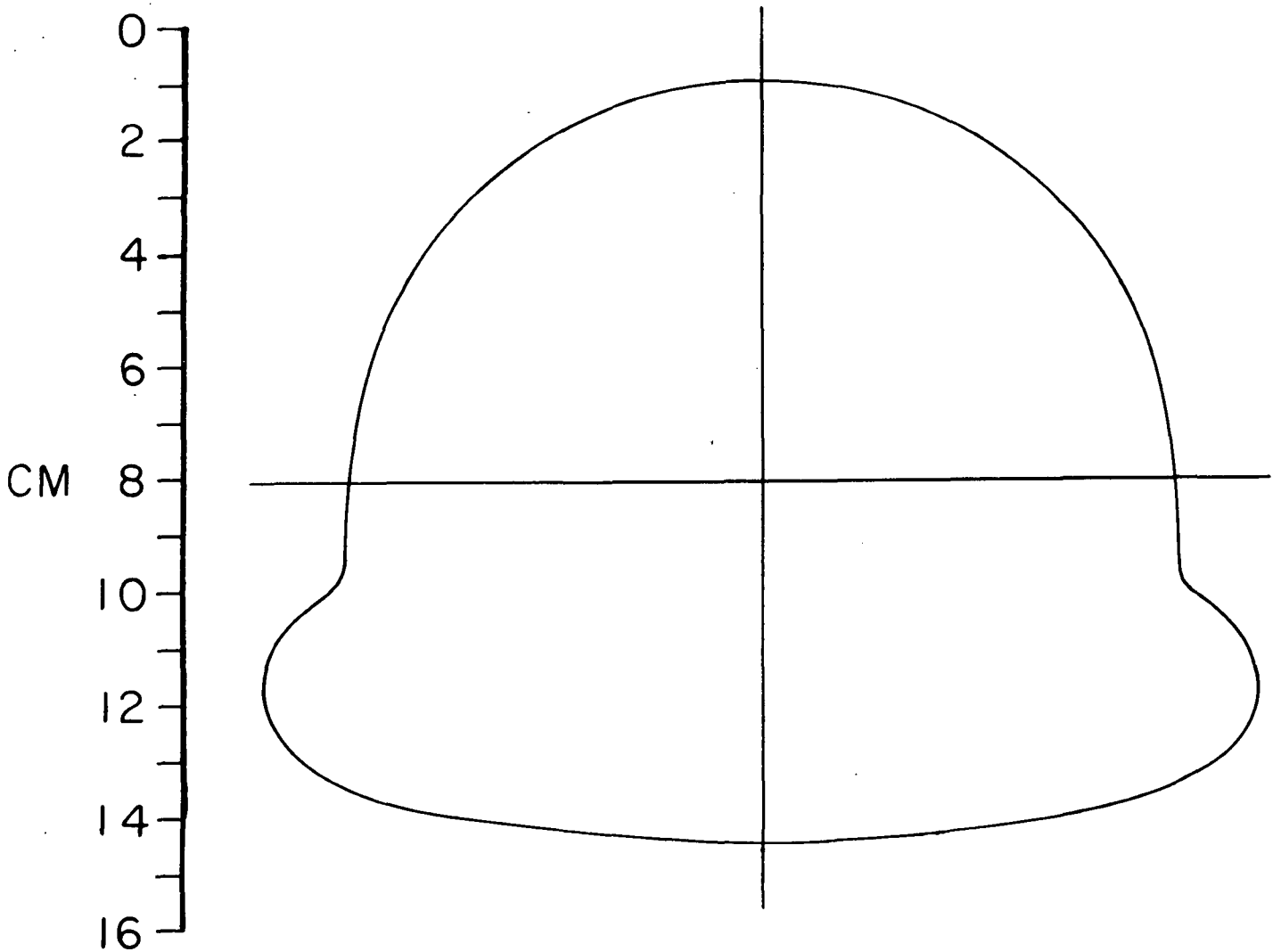
(c) 20.32 cm from nose.

Figure 4.- Continued.



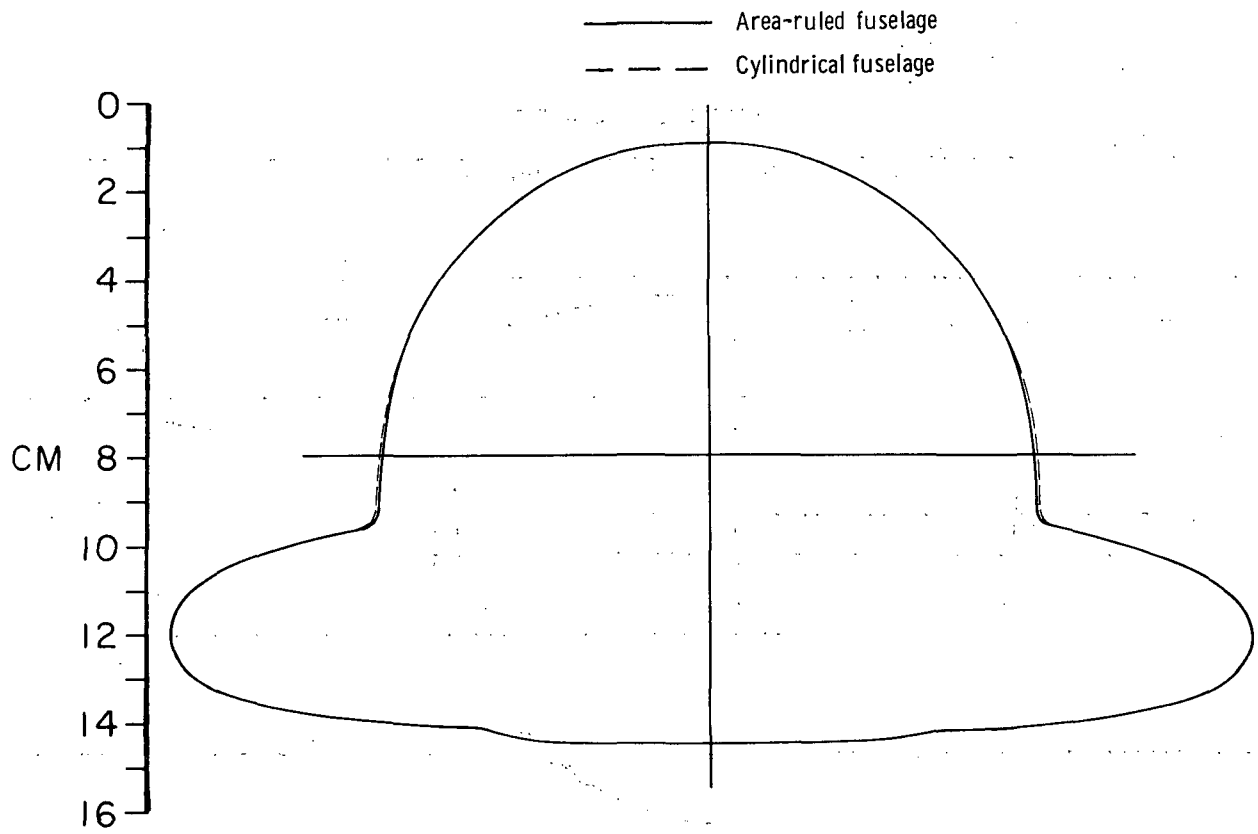
(d) 30.48 cm from nose.

Figure 4.- Continued.



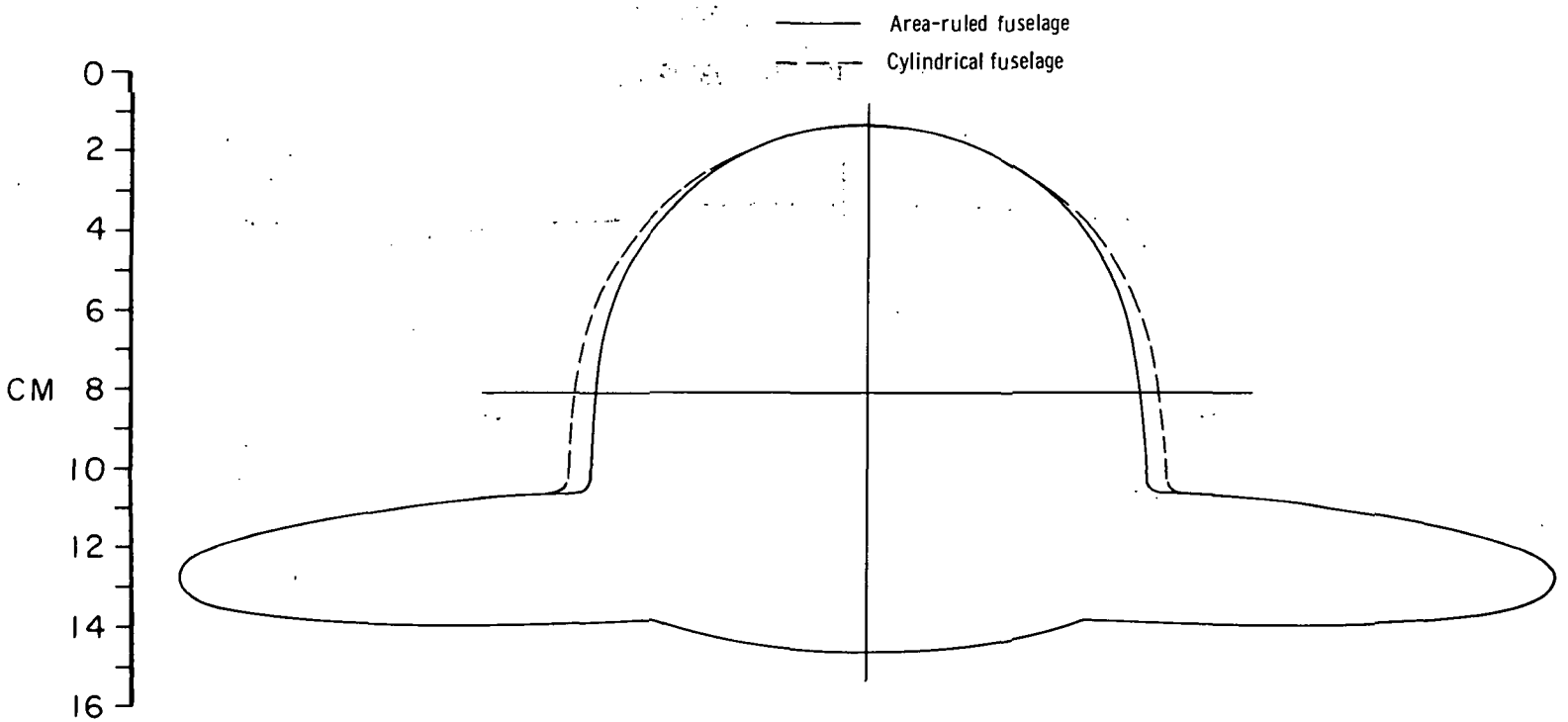
(e) 40.64 cm from nose.

Figure 4.- Continued.



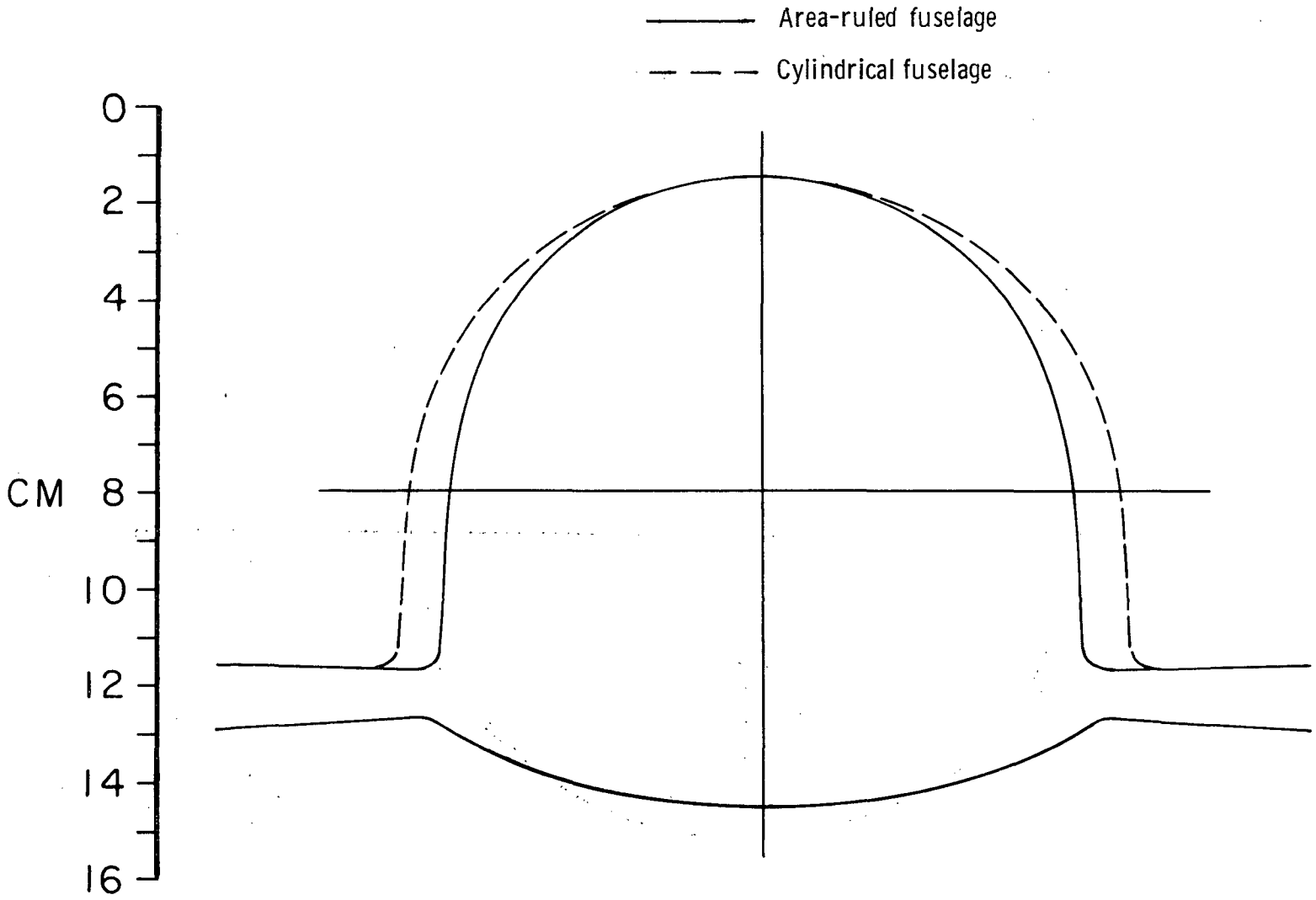
(f) 50.80 cm from nose.

Figure 4.- Continued.



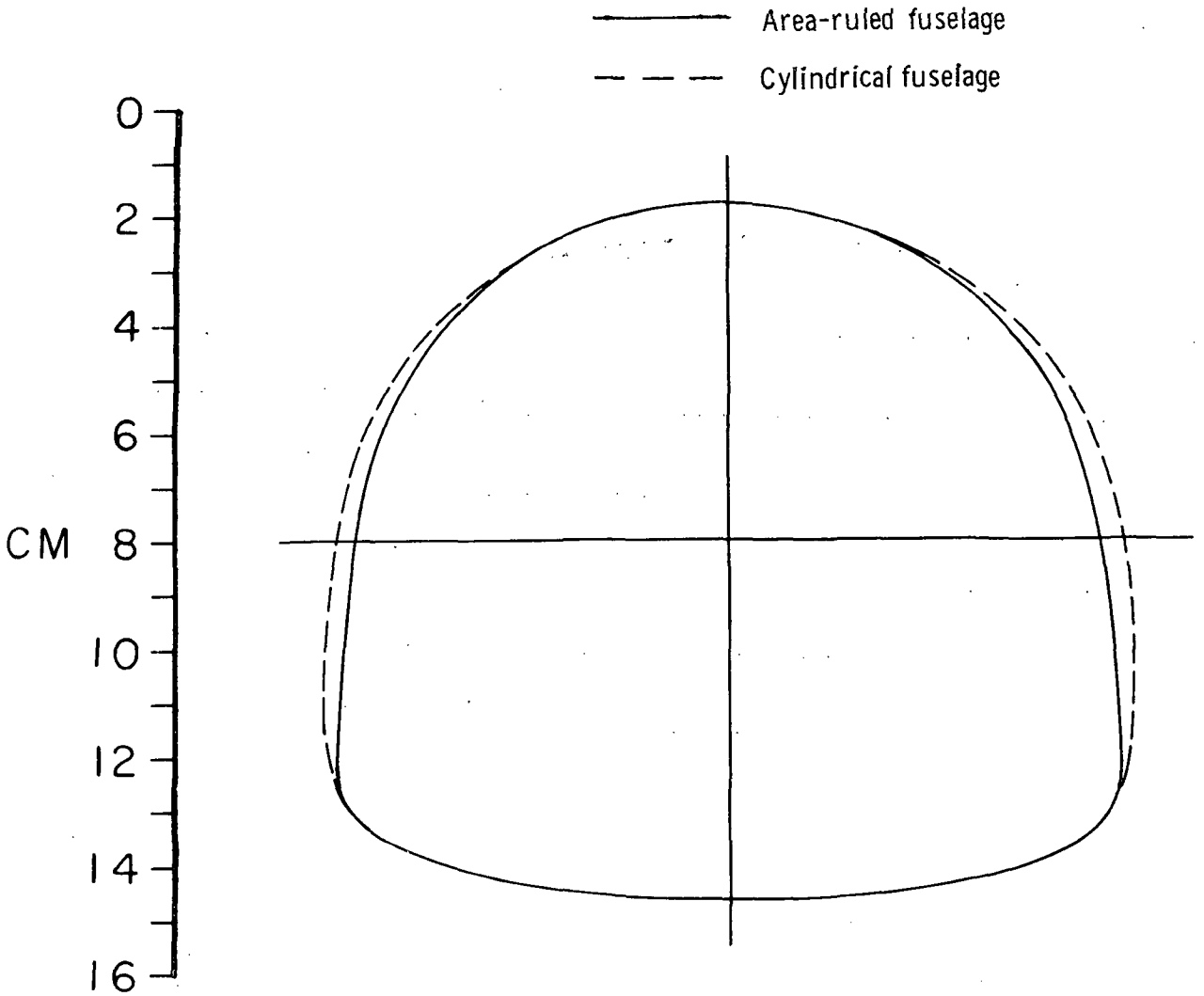
(g) 60.96 cm from nose.

Figure 4.- Continued.



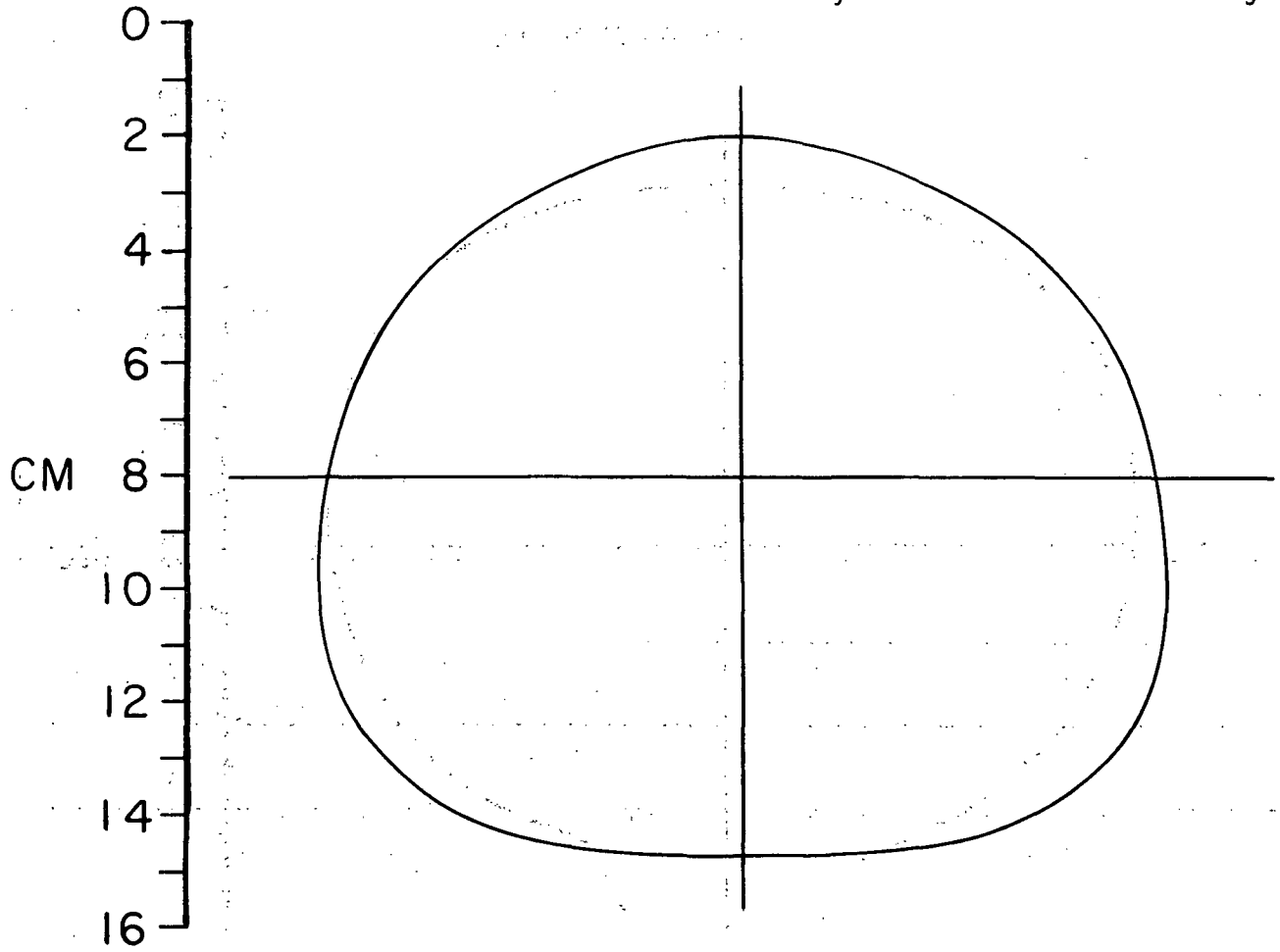
(h) 71.12 cm from nose.

Figure 4.- Continued.



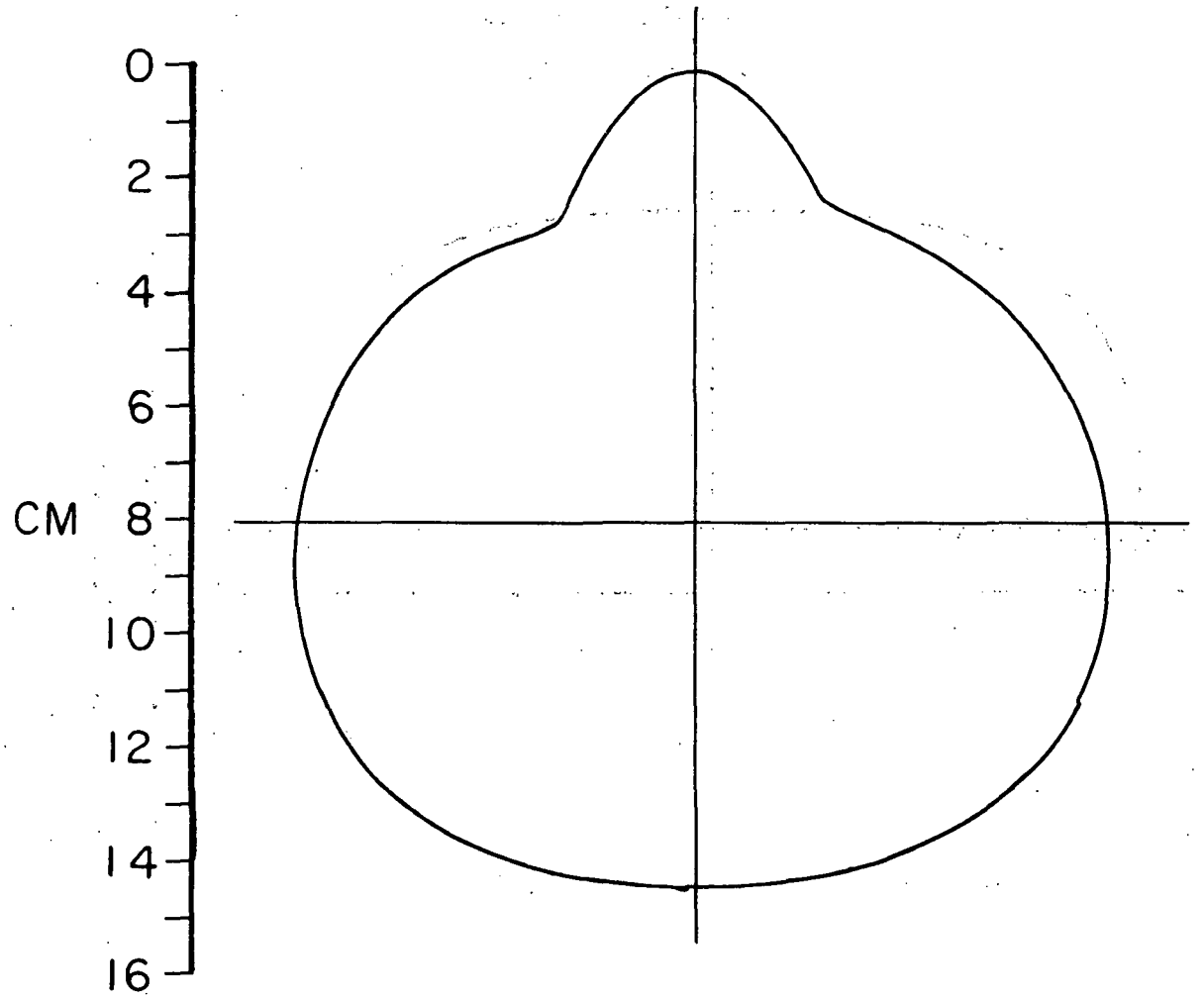
(i) 81.28 cm from nose.

Figure 4.- Continued.



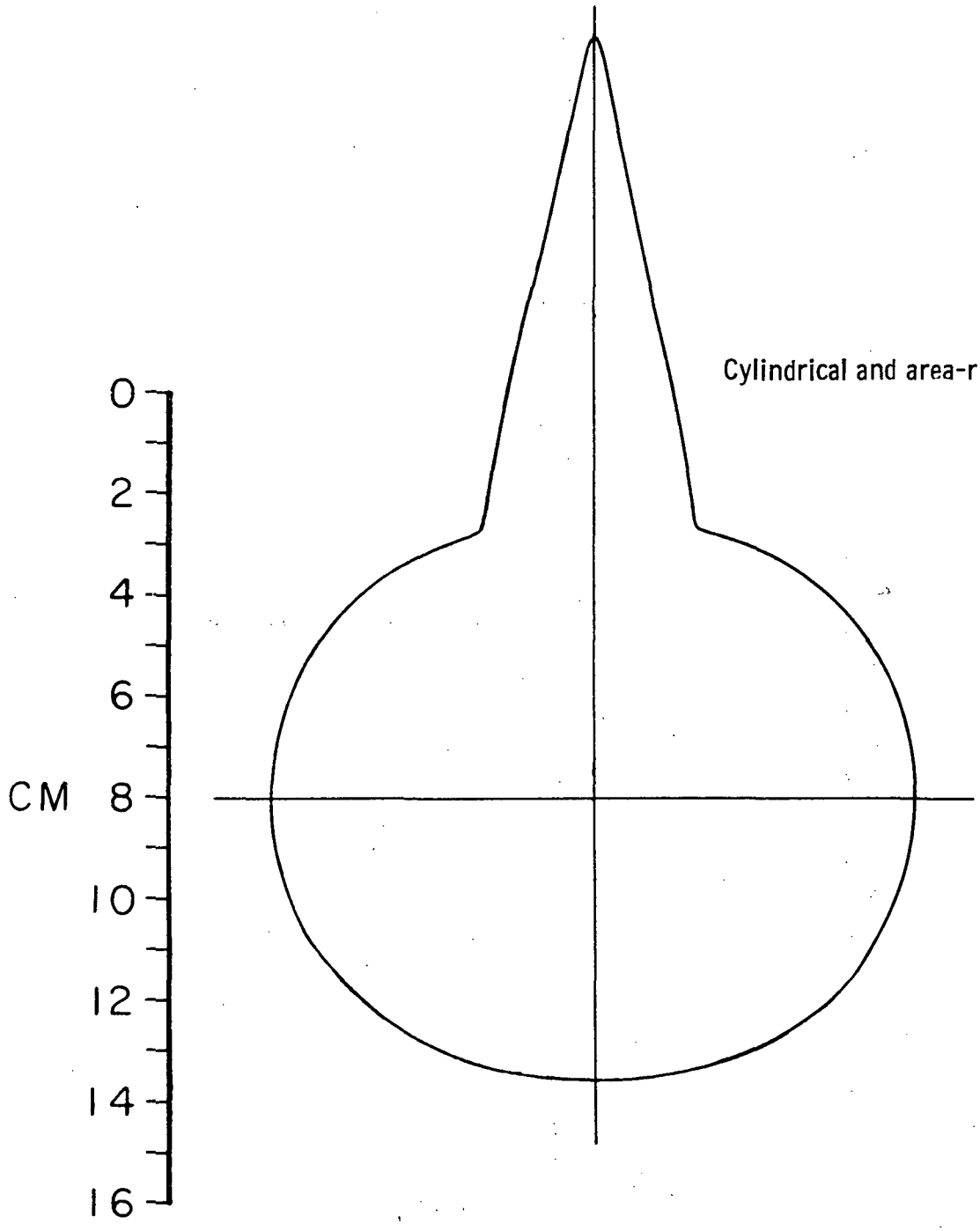
(j) 91.44 cm from nose.

Figure 4.- Continued.



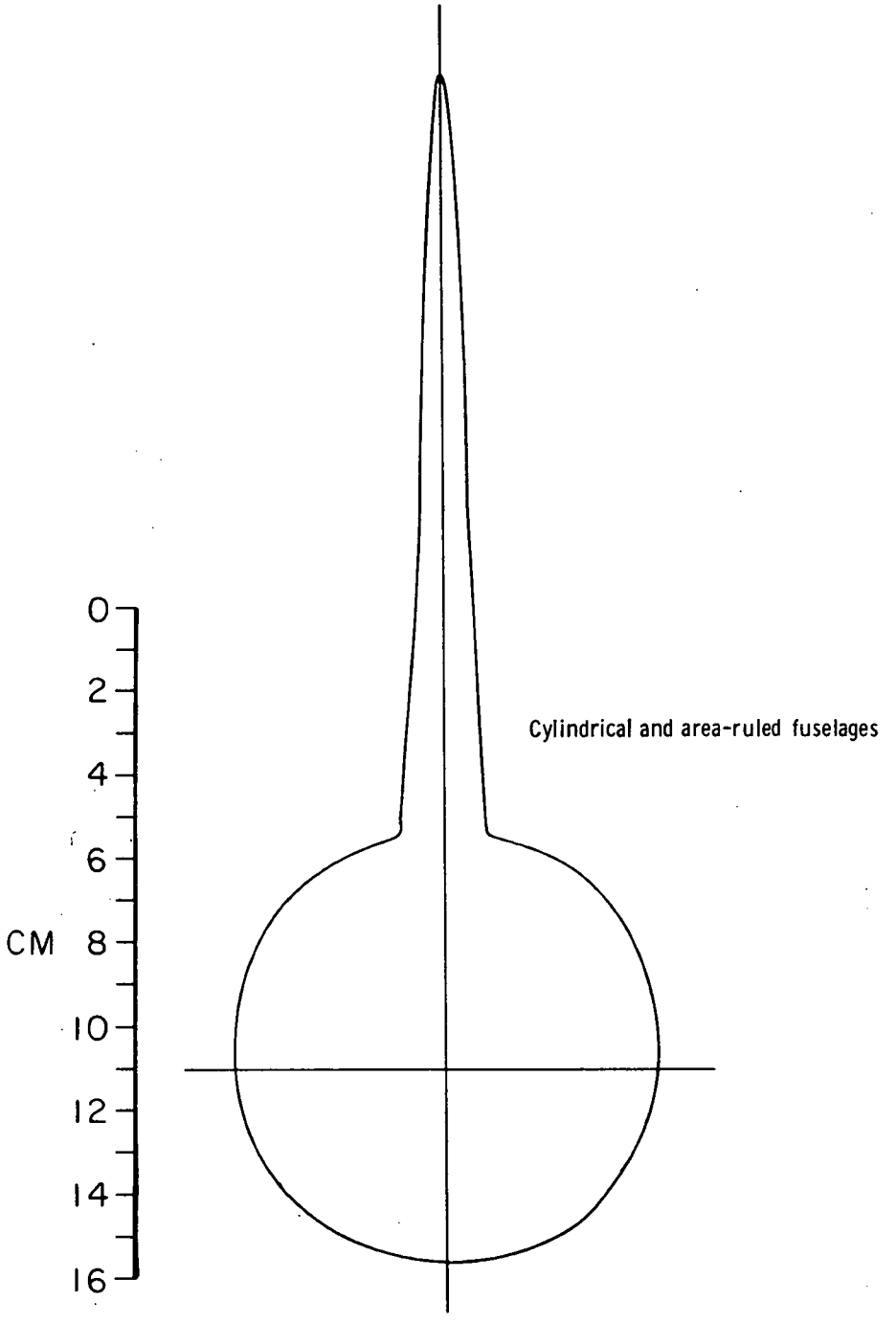
(k) 101.60 cm from nose.

Figure 4.- Continued.



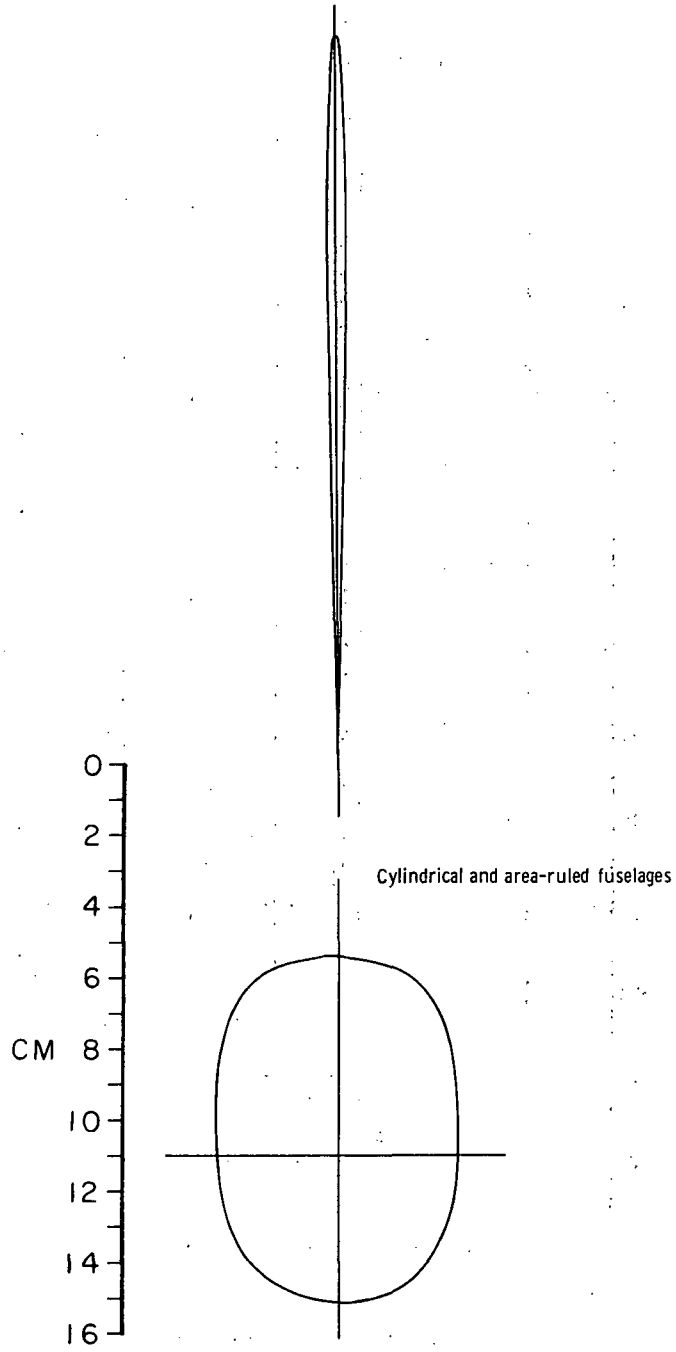
(l) 111.76 cm from nose.

Figure 4.- Continued.



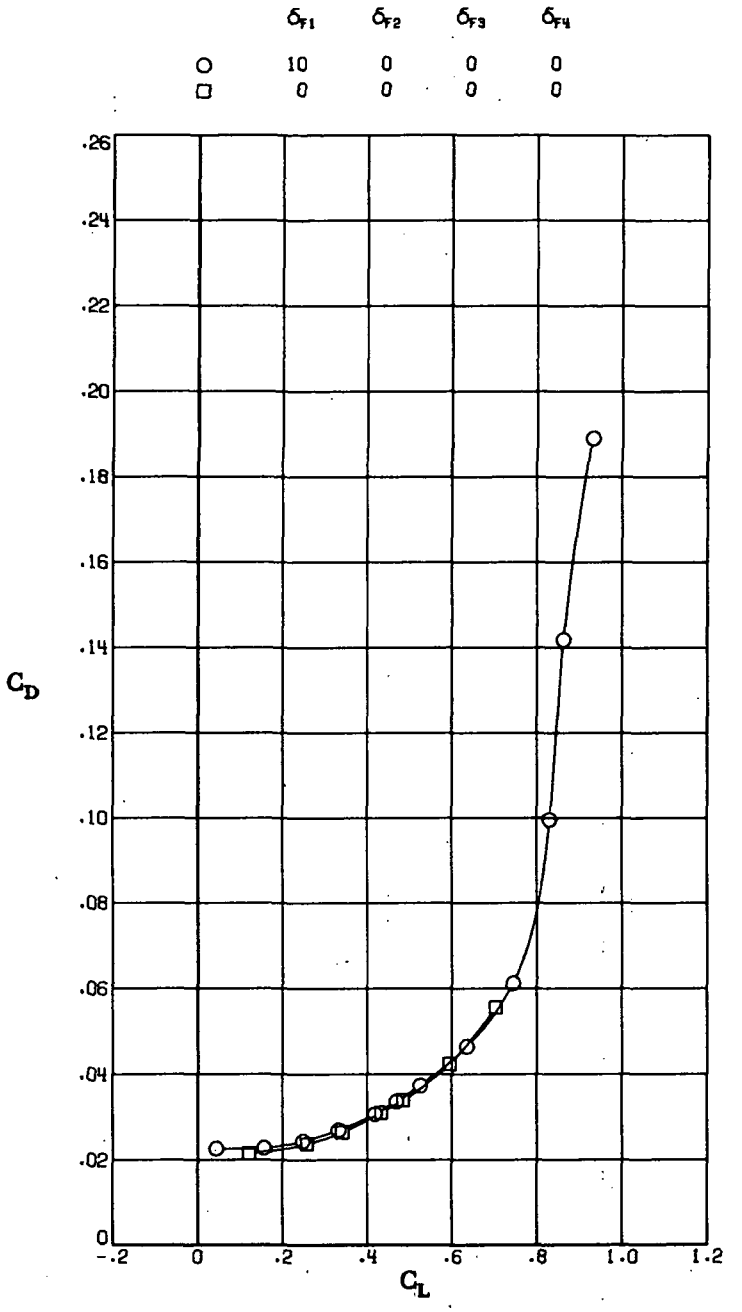
(m) 121.92 cm from nose.

Figure 4.- Continued.



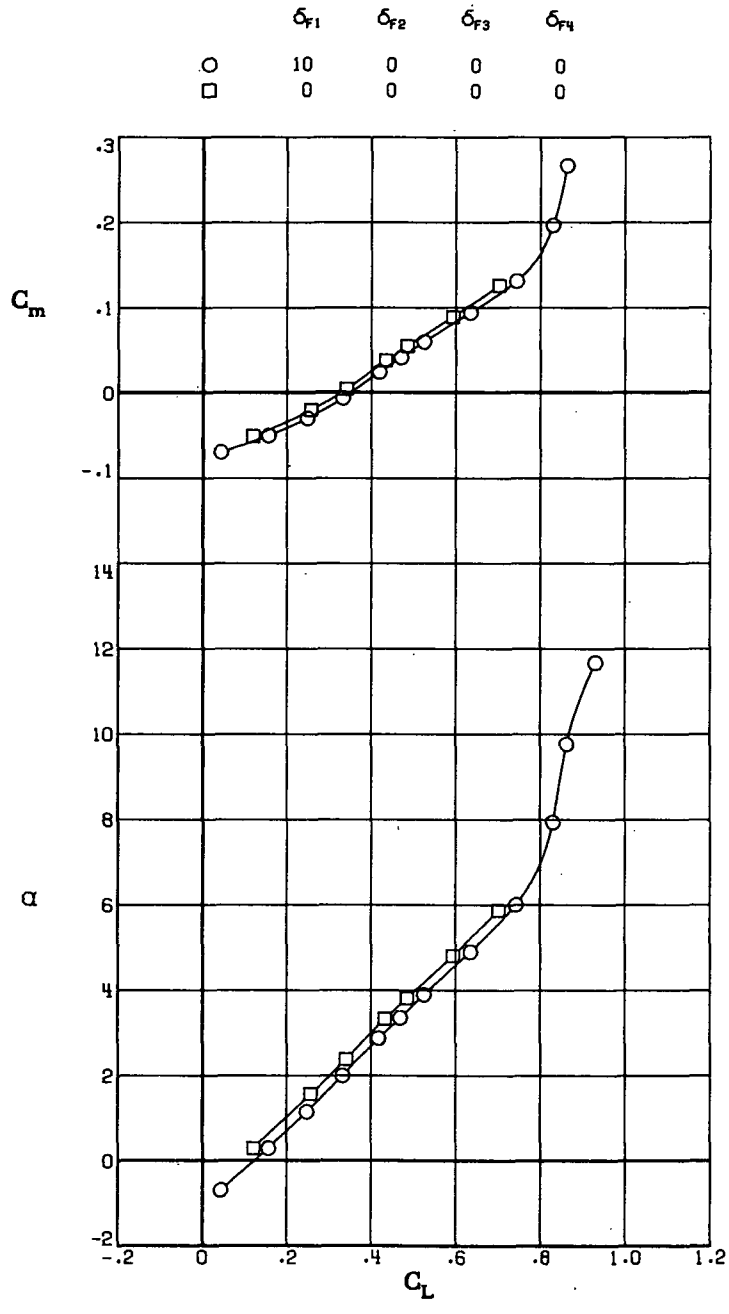
(n) 132.08 cm from nose.

Figure 4.- Concluded.



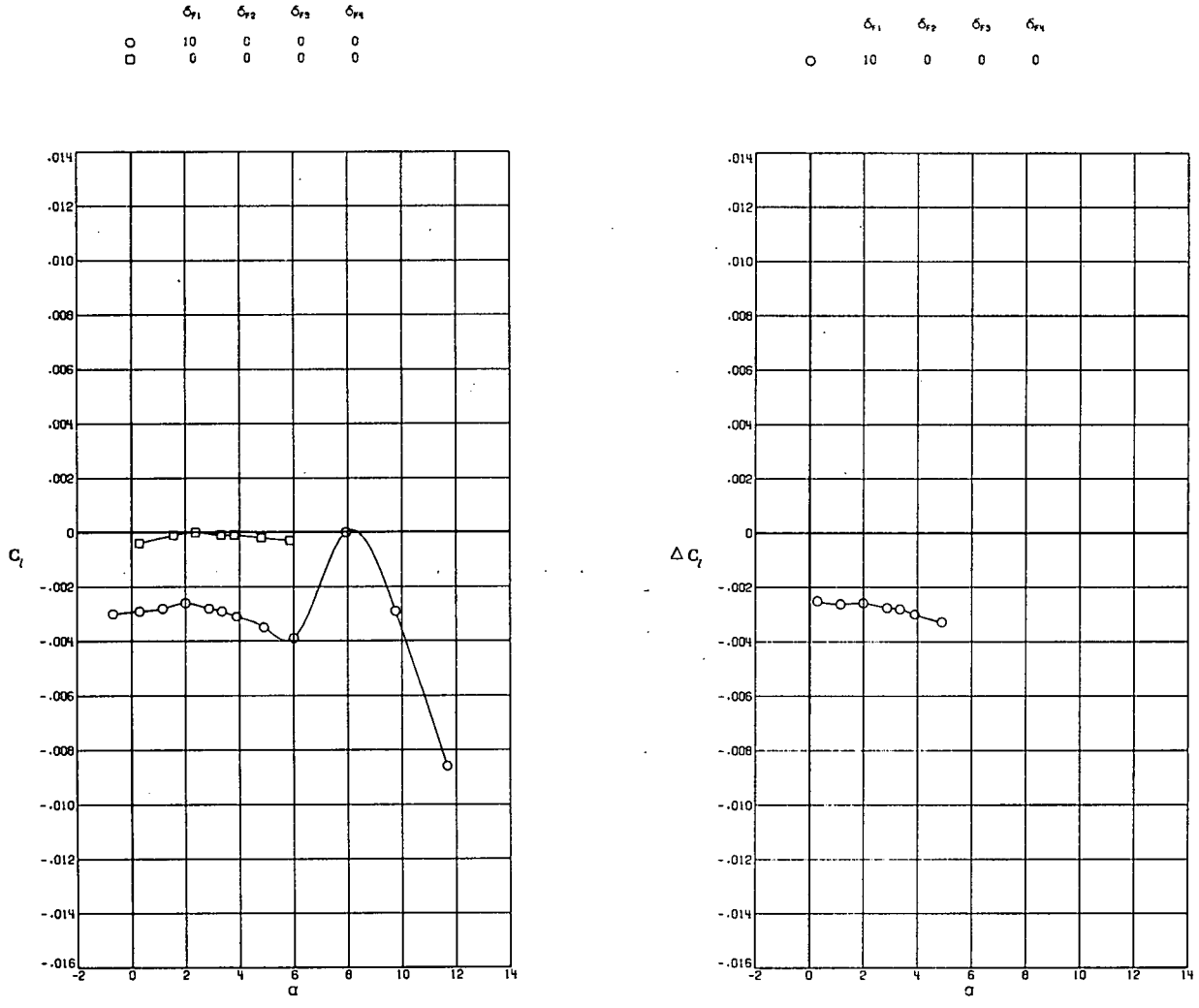
(a) Drag characteristics.

Figure 5.- Effect of F_1 trailing-edge control deflection on aerodynamic characteristics of model with area-ruled fuselage at $M_\infty = 0.80$.



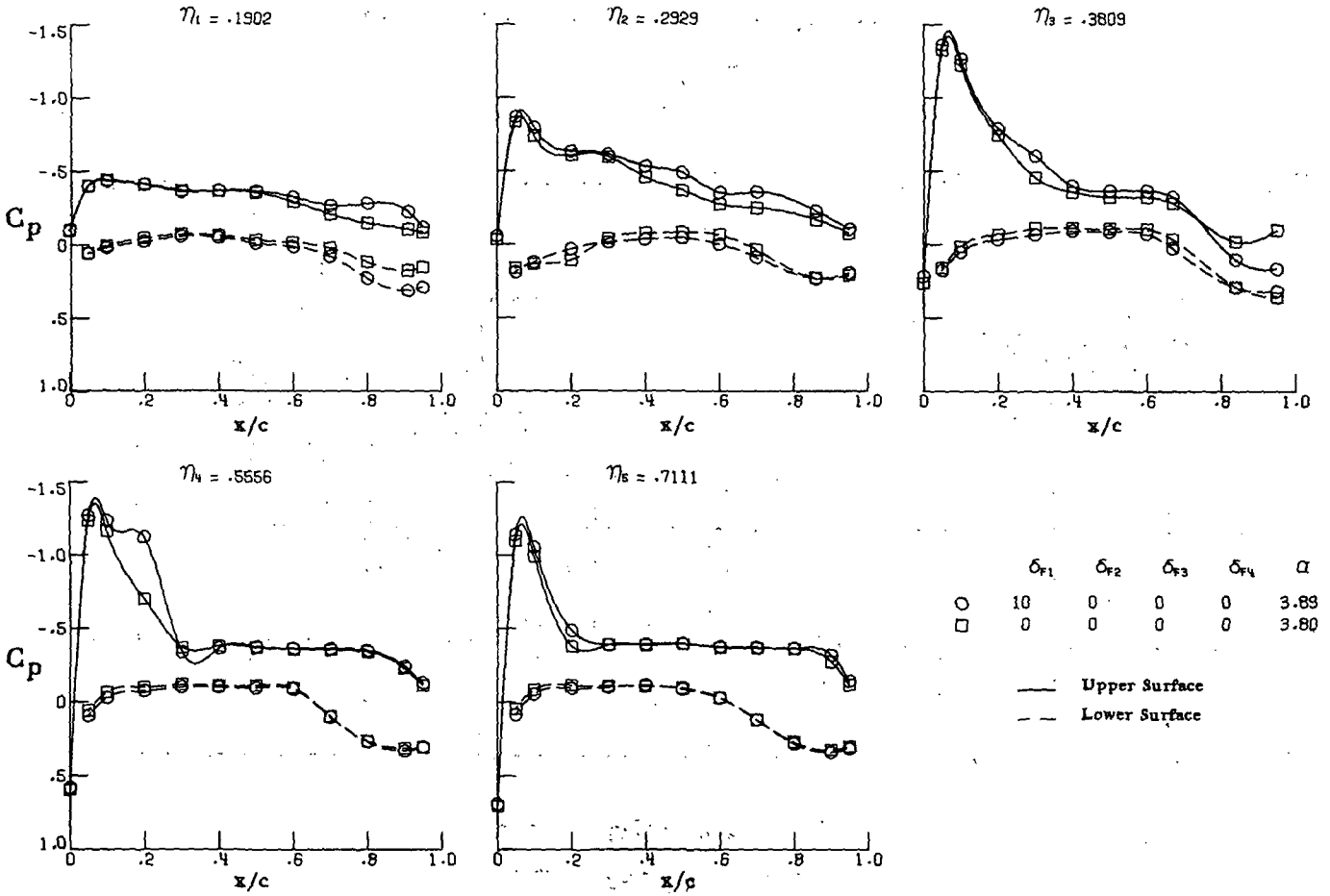
(b) Lift and pitch characteristics.

Figure 5.- Continued.



(c) Rolling-moment characteristics.

Figure 5.- Continued.



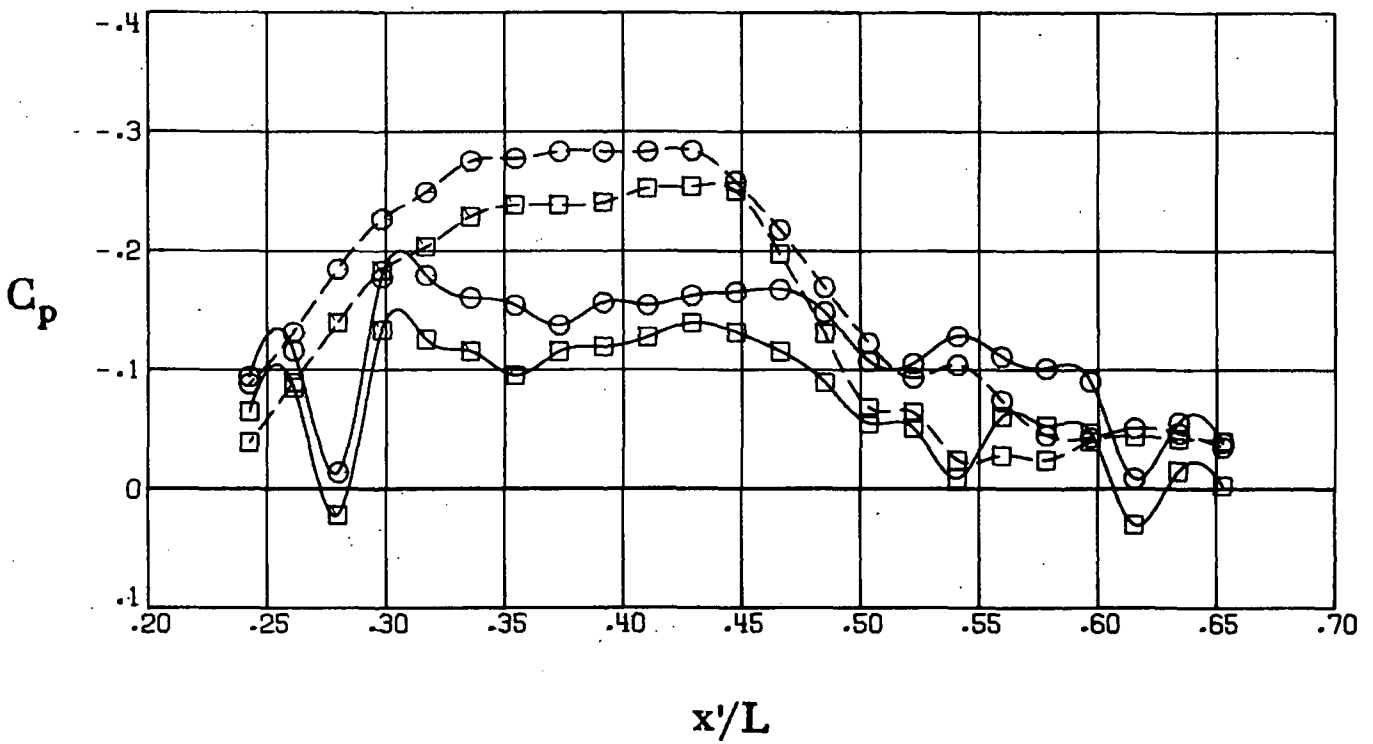
(d) Selected wing pressure distributions.

Figure 5.- Continued.

	δ_{F1}	δ_{F2}	δ_{F3}	δ_{F4}	α
○	10	0	0	0	3.89
□	0	0	0	0	3.80

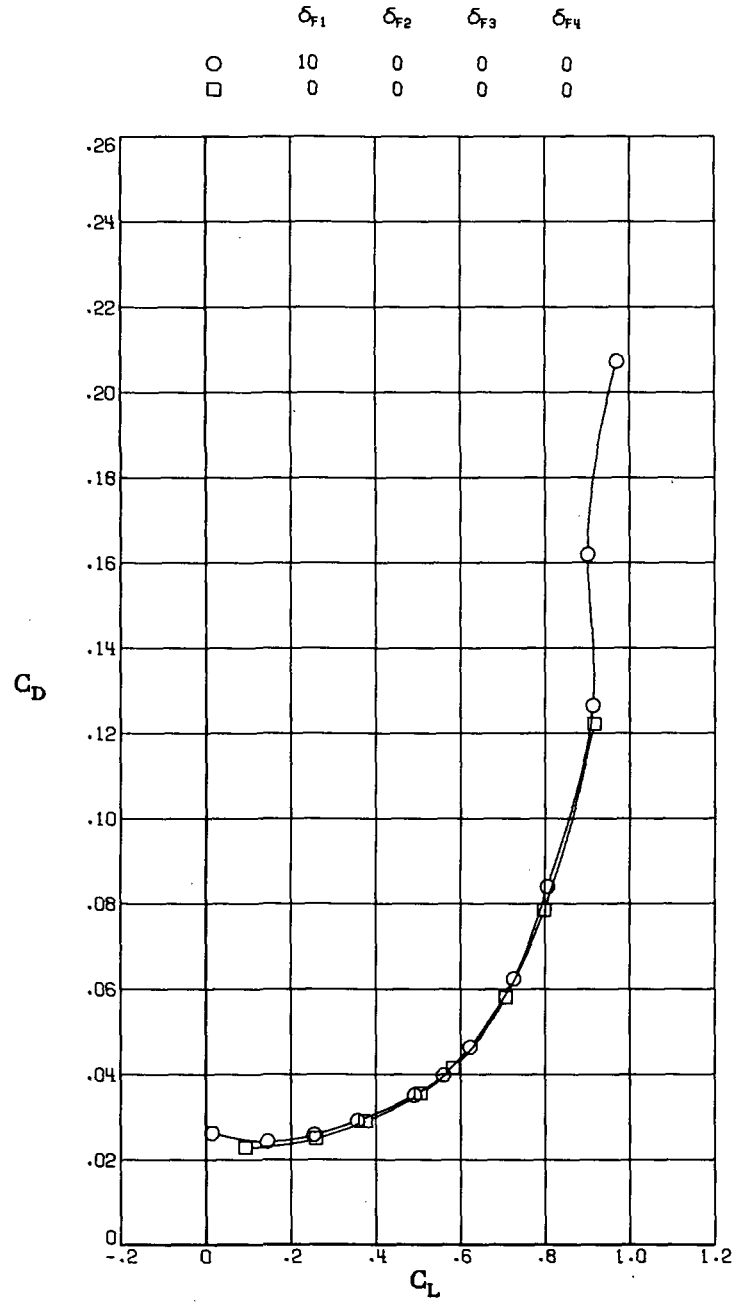
—— Top Centerline

– – Right Side



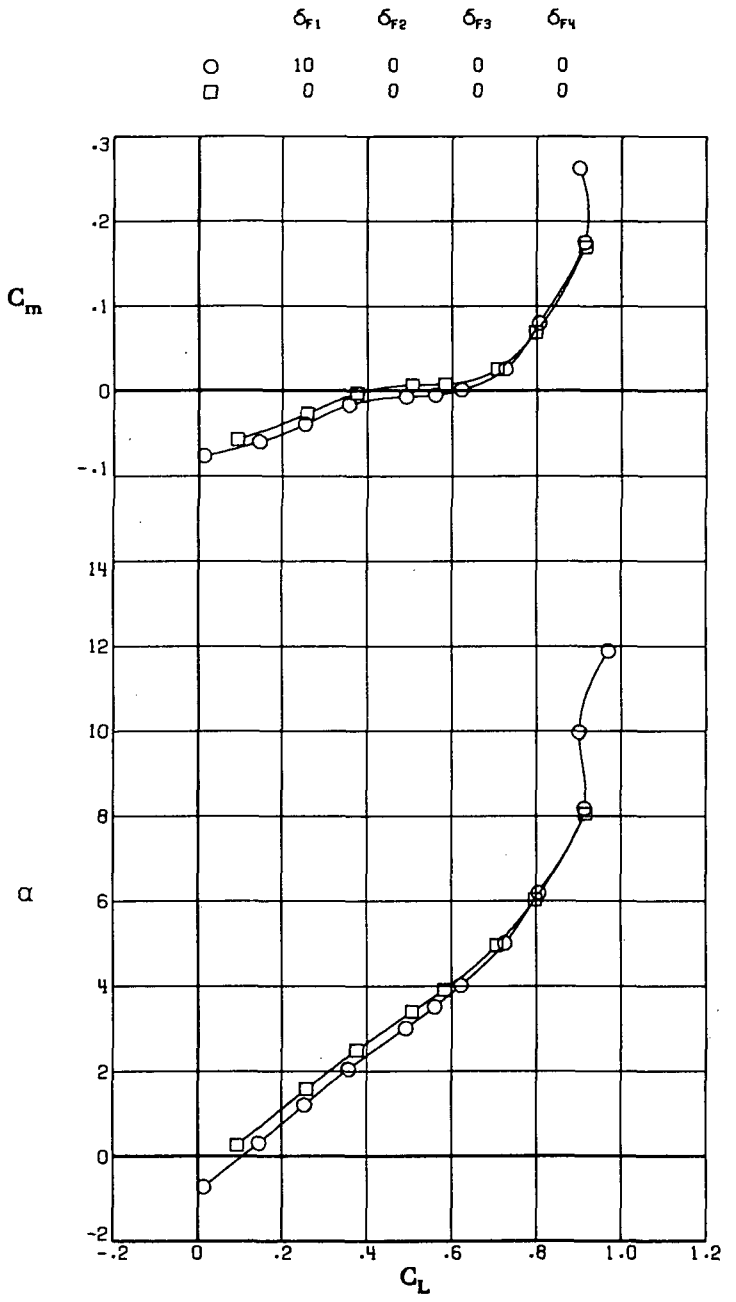
(e) Selected fuselage pressure distributions.

Figure 5.- Concluded.



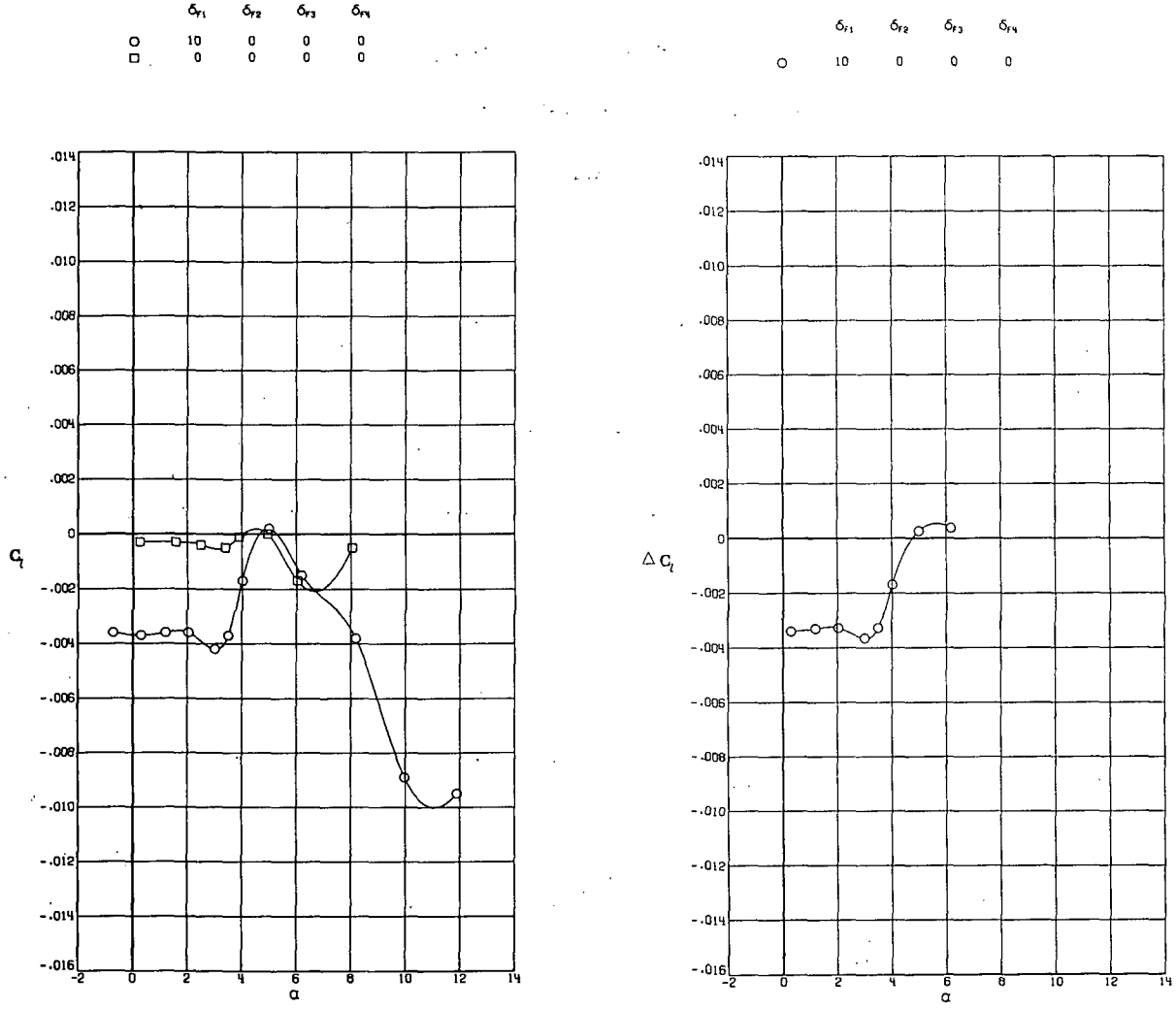
(a) Drag characteristics.

Figure 6.- Effect of F_1 trailing-edge control deflection on aerodynamic characteristics of model with area-ruled fuselage at $M_\infty = 0.90$.



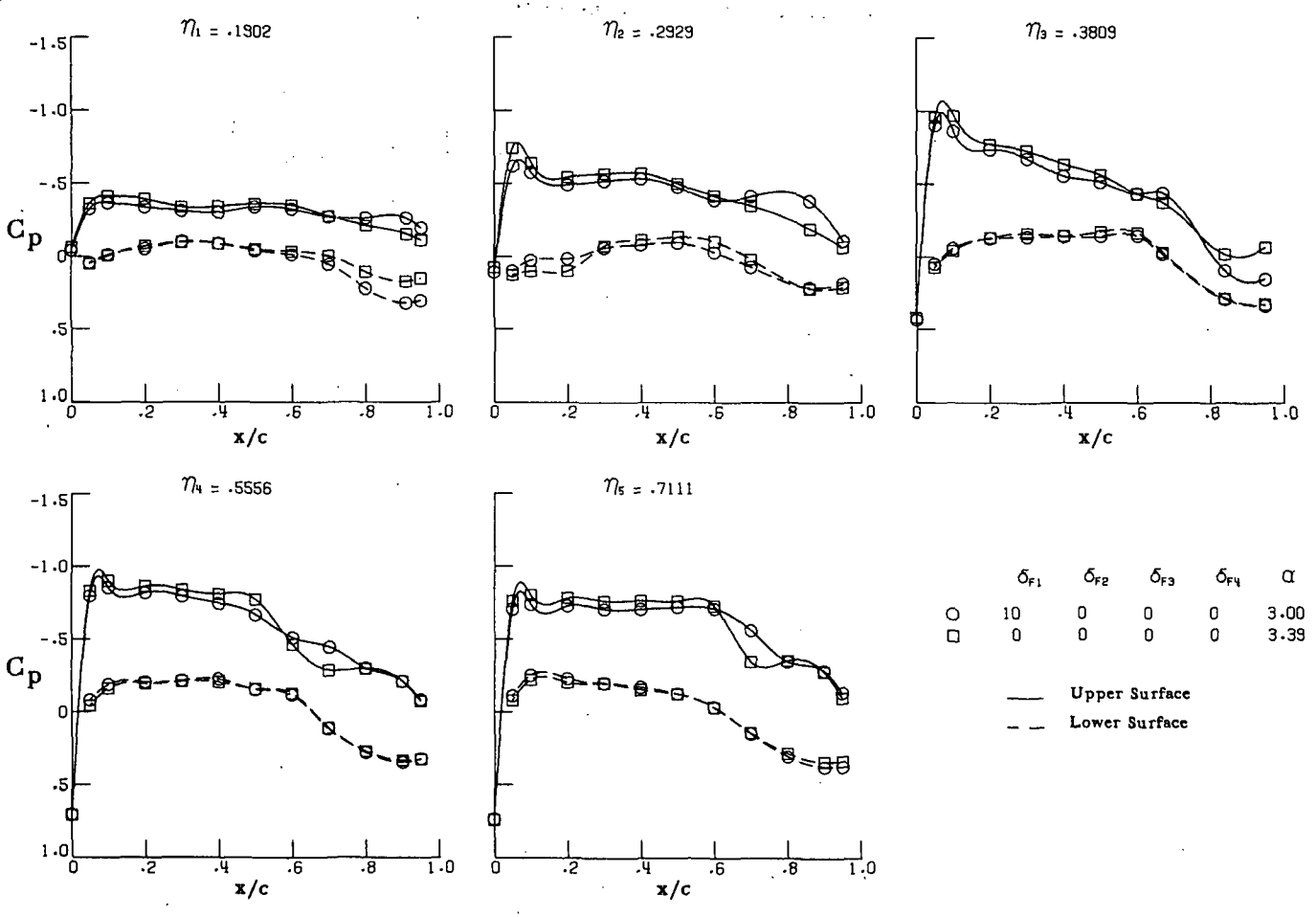
(b) Lift and pitch characteristics.

Figure 6.- Continued.



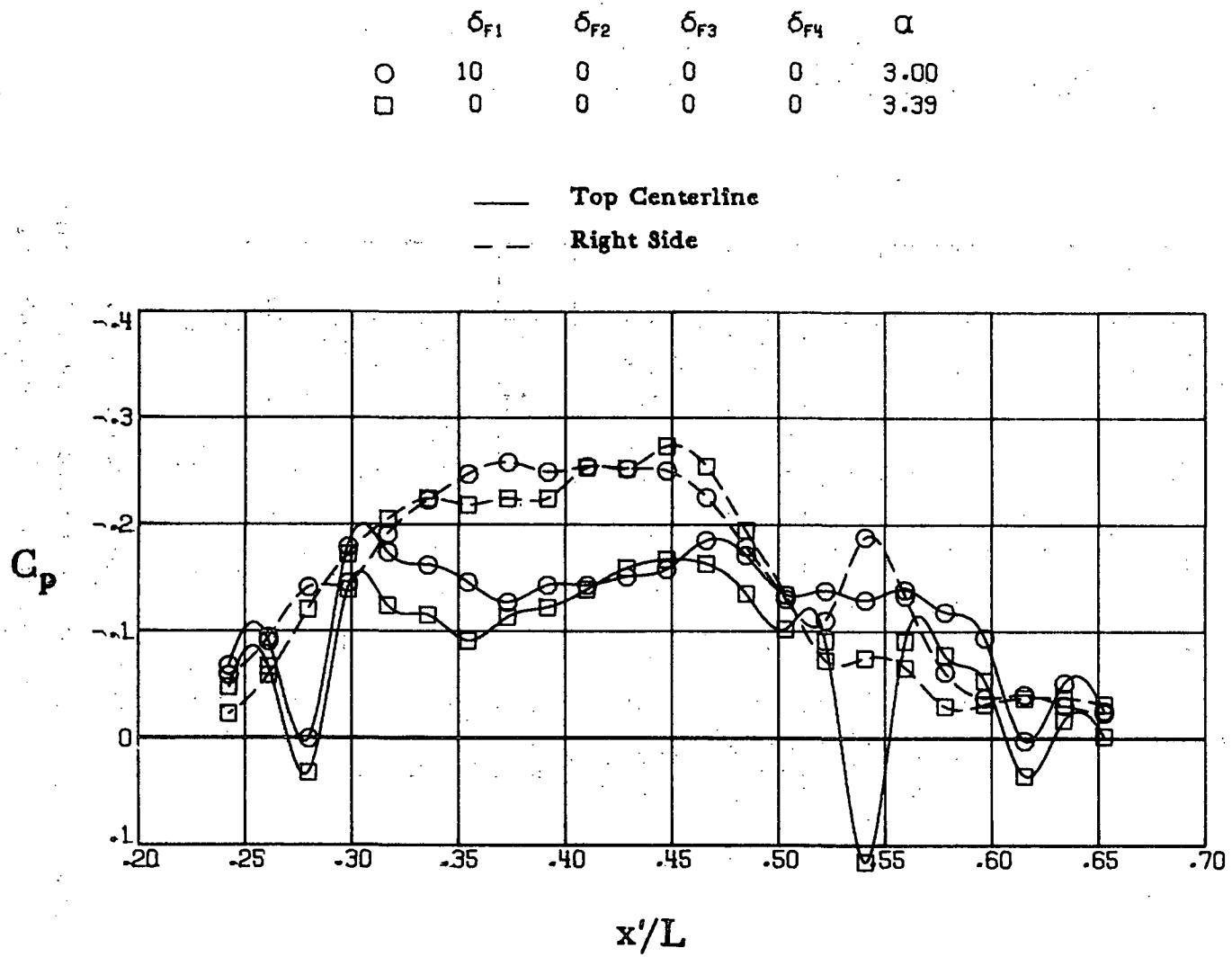
(c) Rolling-moment characteristics.

Figure 6.- Continued.



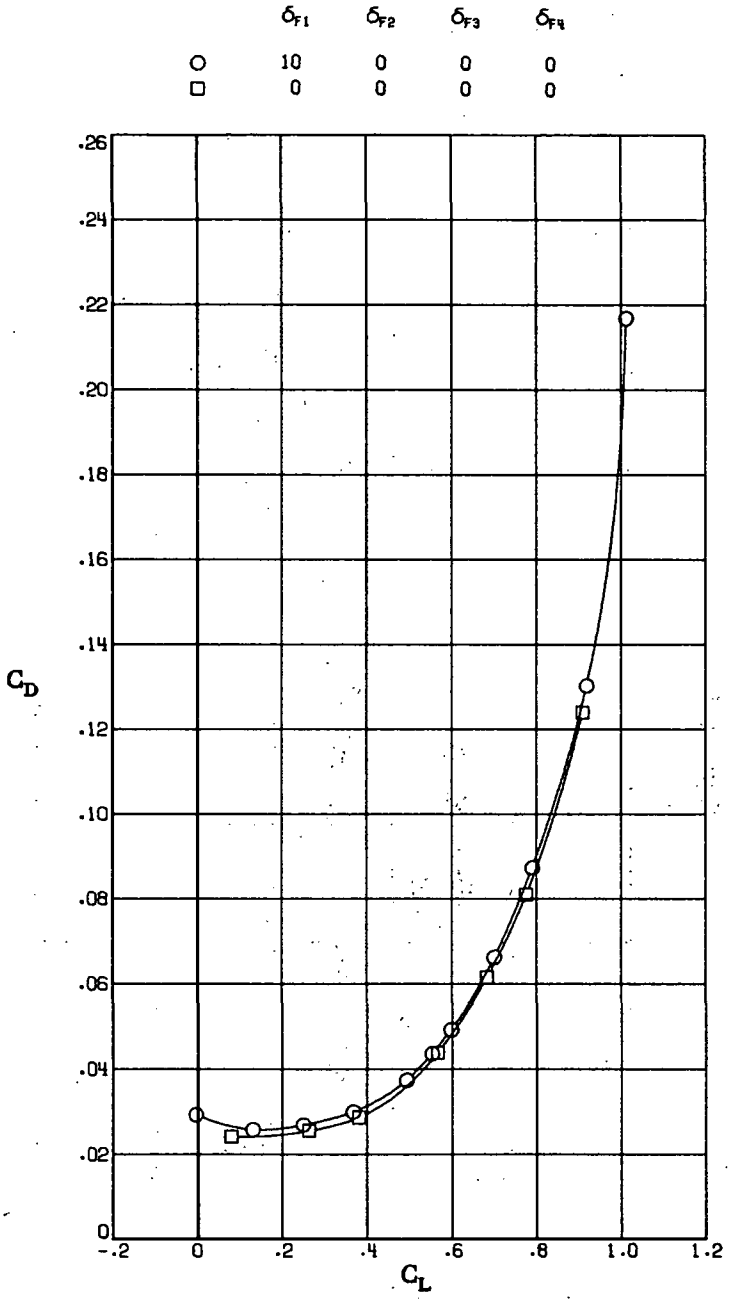
(d) Selected wing pressure distributions.

Figure 6.- Continued.



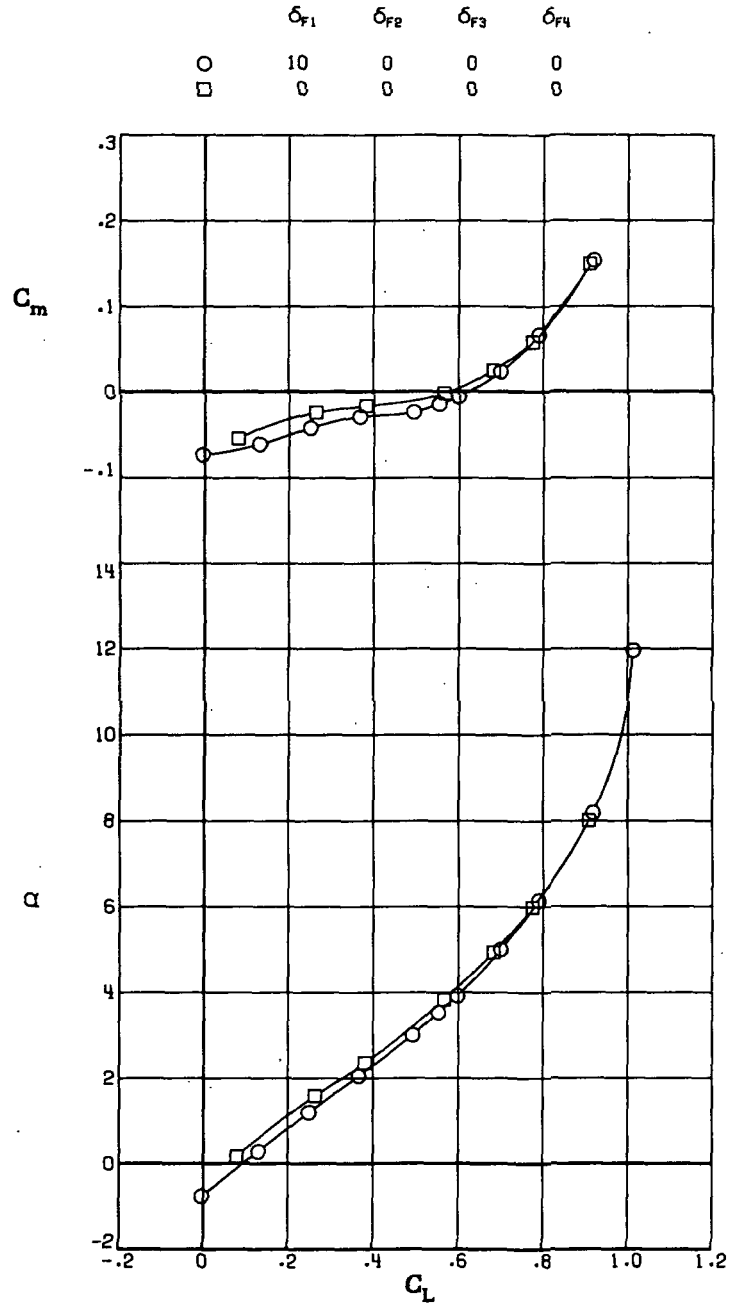
(e) Selected fuselage pressure distributions.

Figure 6.- Concluded.



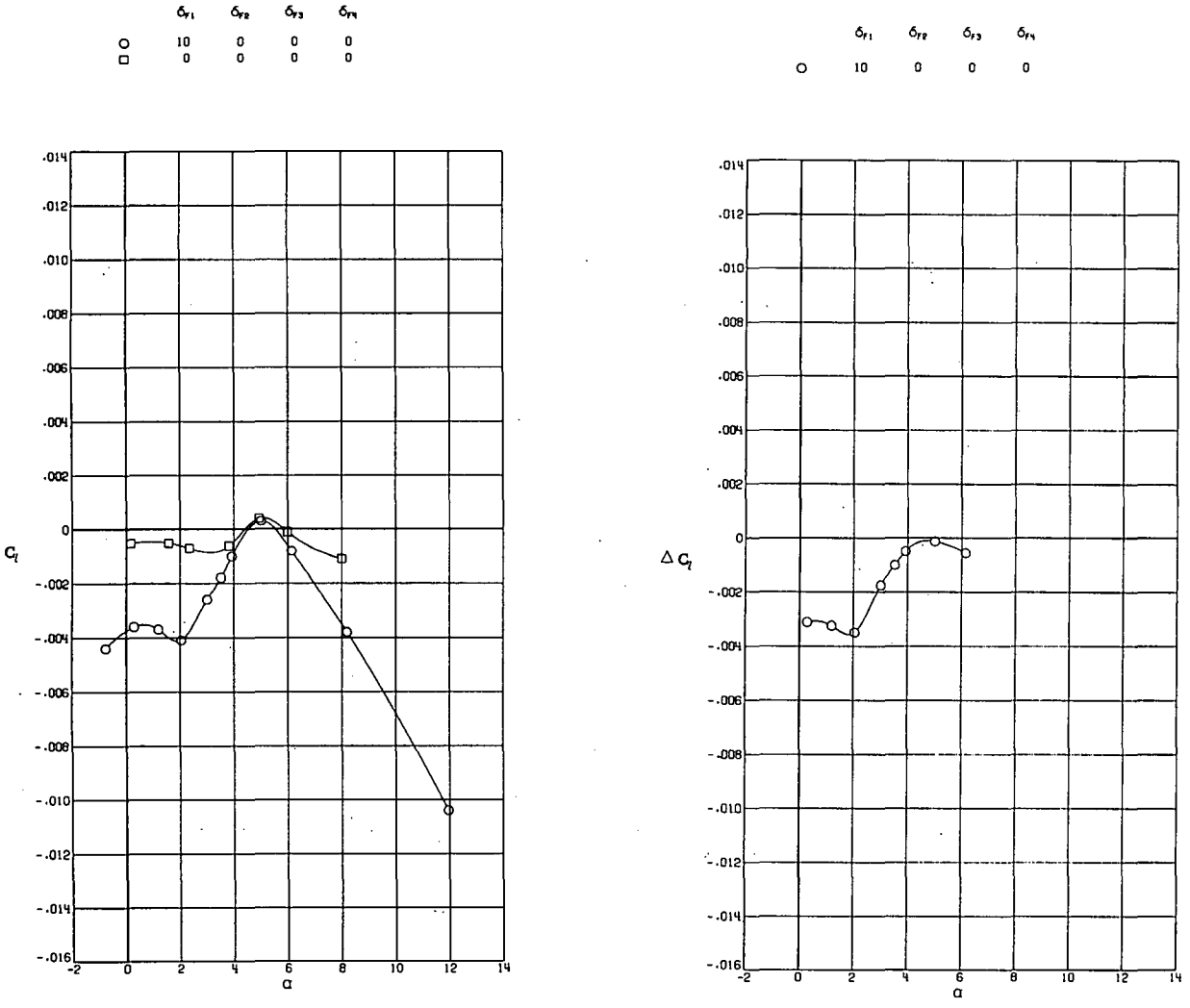
(a) Drag characteristics.

Figure 7.- Effect of F_1 trailing-edge control deflection on aerodynamic characteristics of model with area-ruled fuselage at $M_\infty = 0.92$.



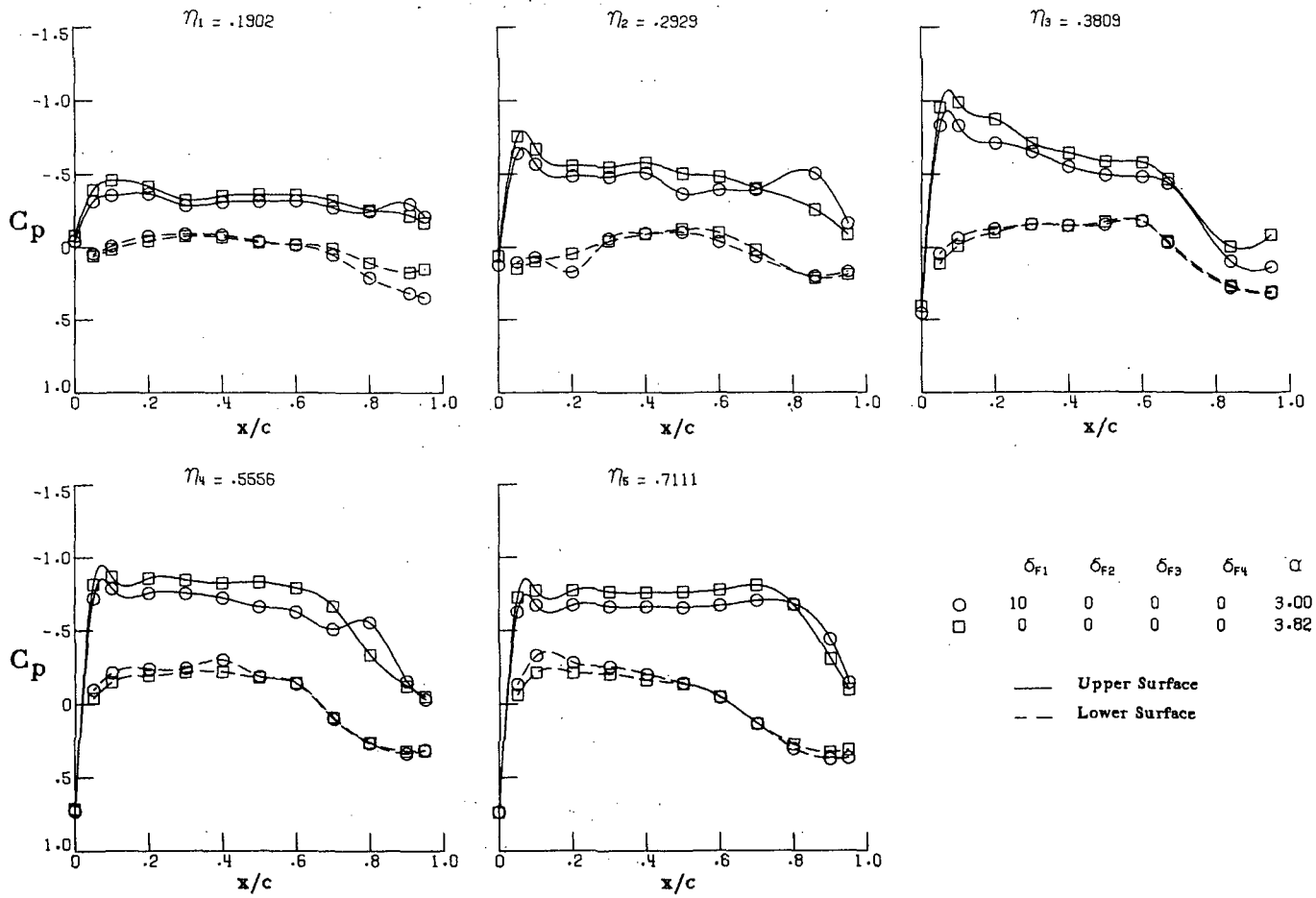
(b) Lift and pitch characteristics.

Figure 7.- Continued.



(c) Rolling-moment characteristics.

Figure 7.- Continued.



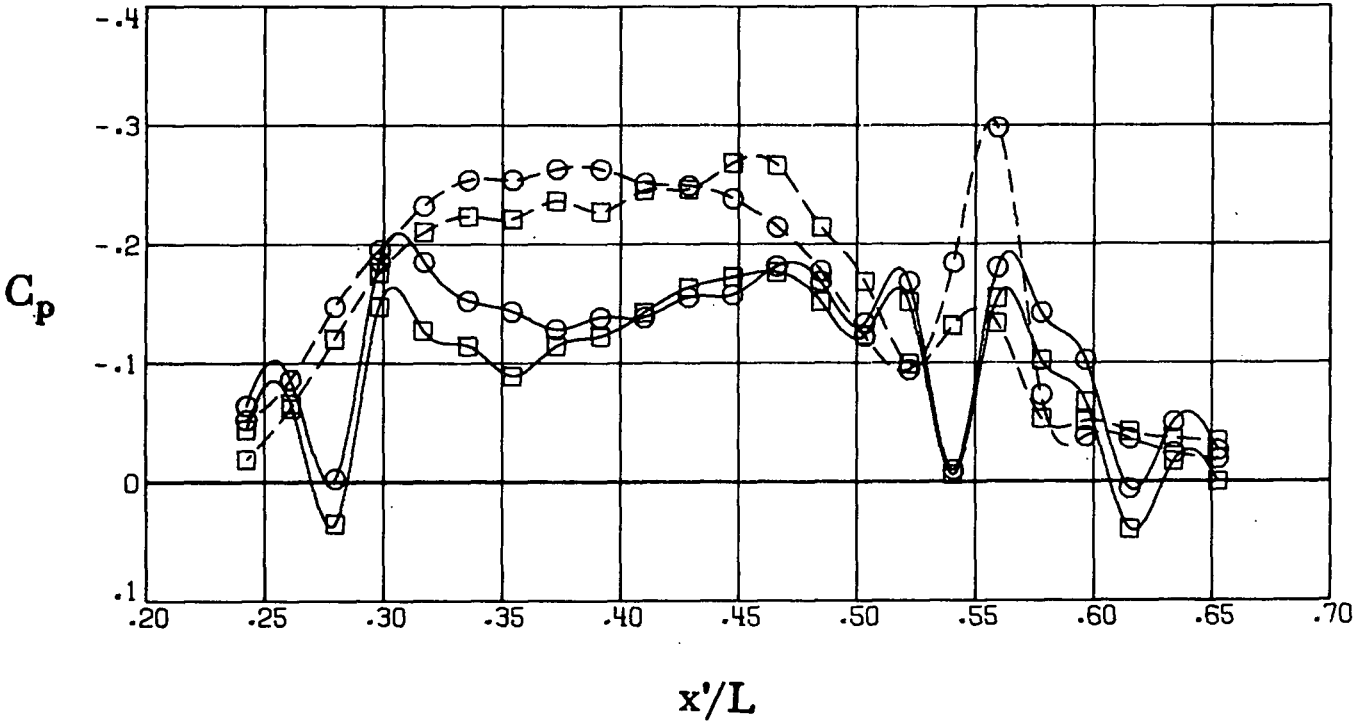
(d) Selected wing pressure distributions.

Figure 7.- Continued.

	δ_{F1}	δ_{F2}	δ_{F3}	δ_{F4}	α
○	10	0	0	0	3.00
□	0	0	0	0	3.82

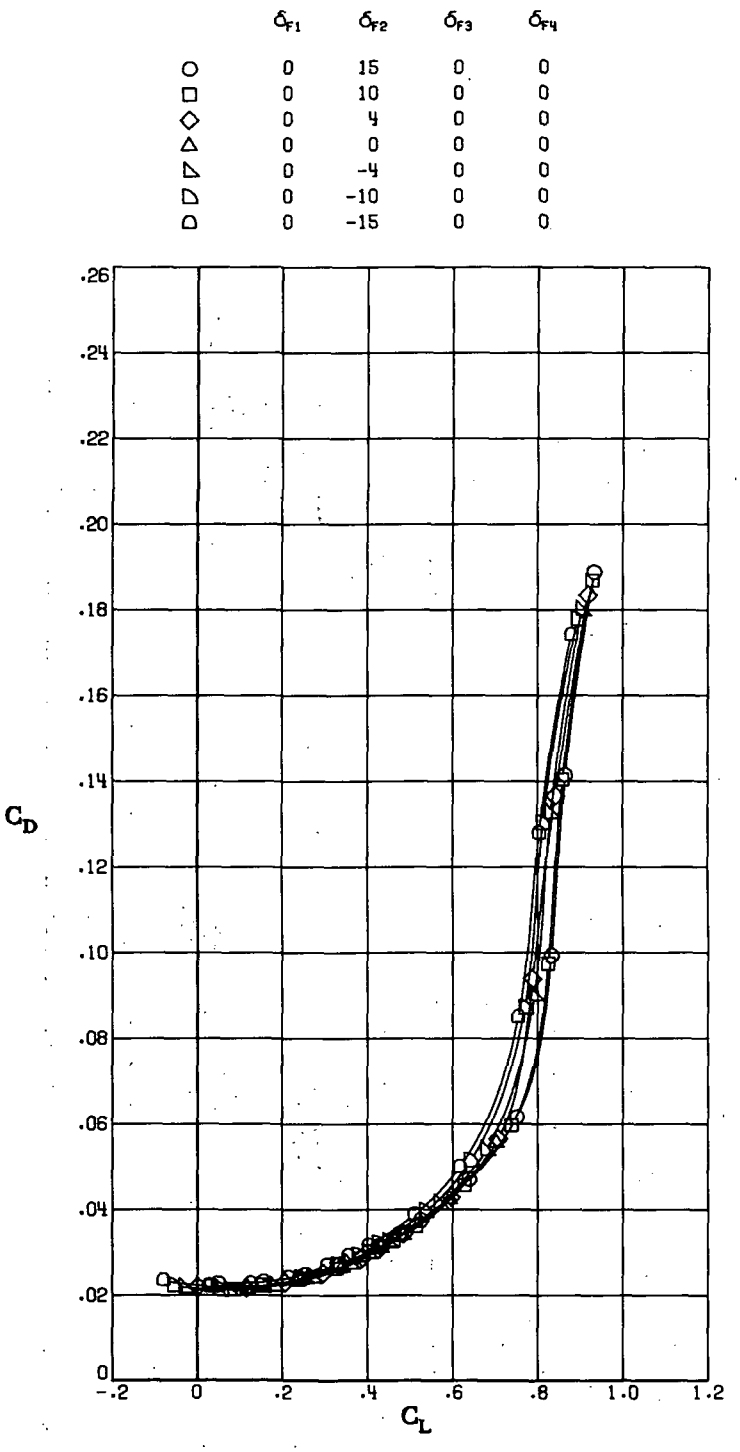
—— Top Centerline

– – Right Side



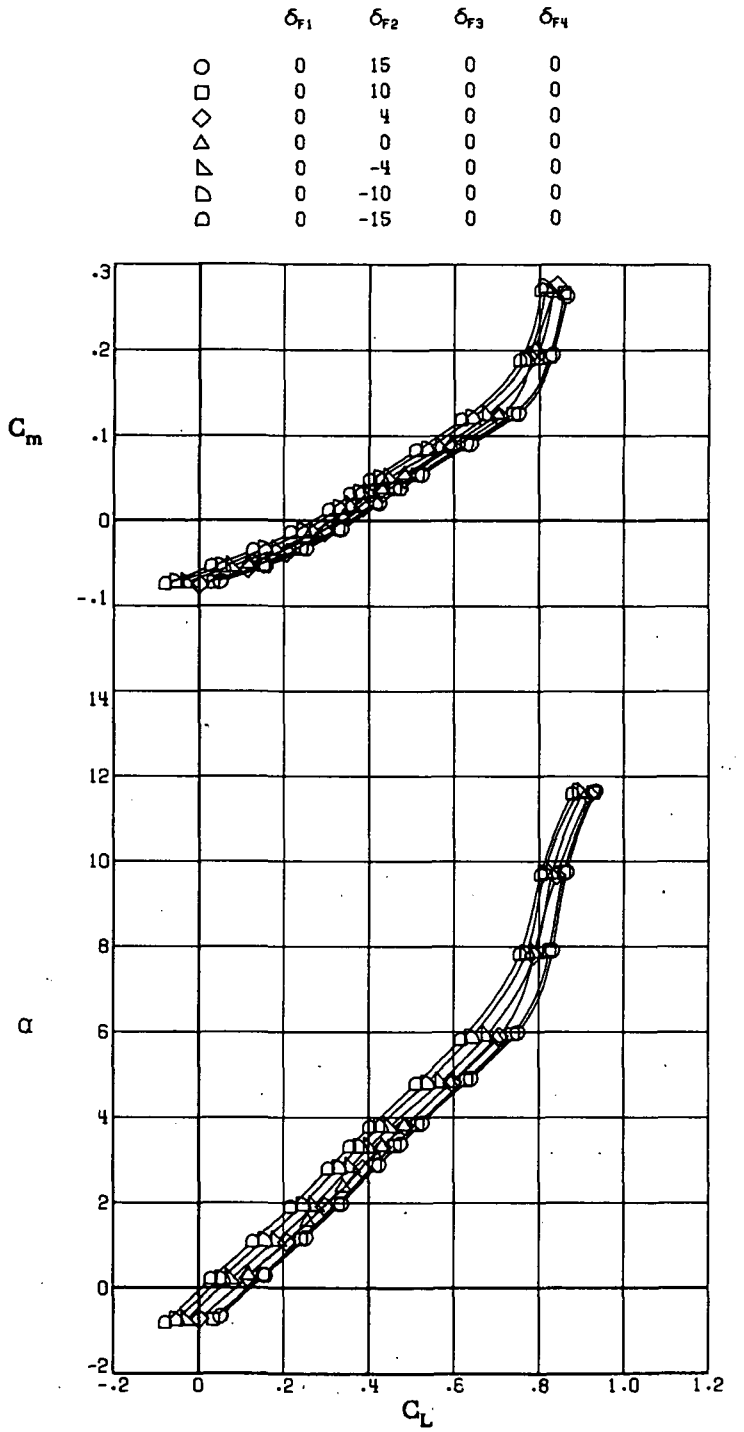
(e) Selected fuselage pressure distributions.

Figure 7.- Concluded.



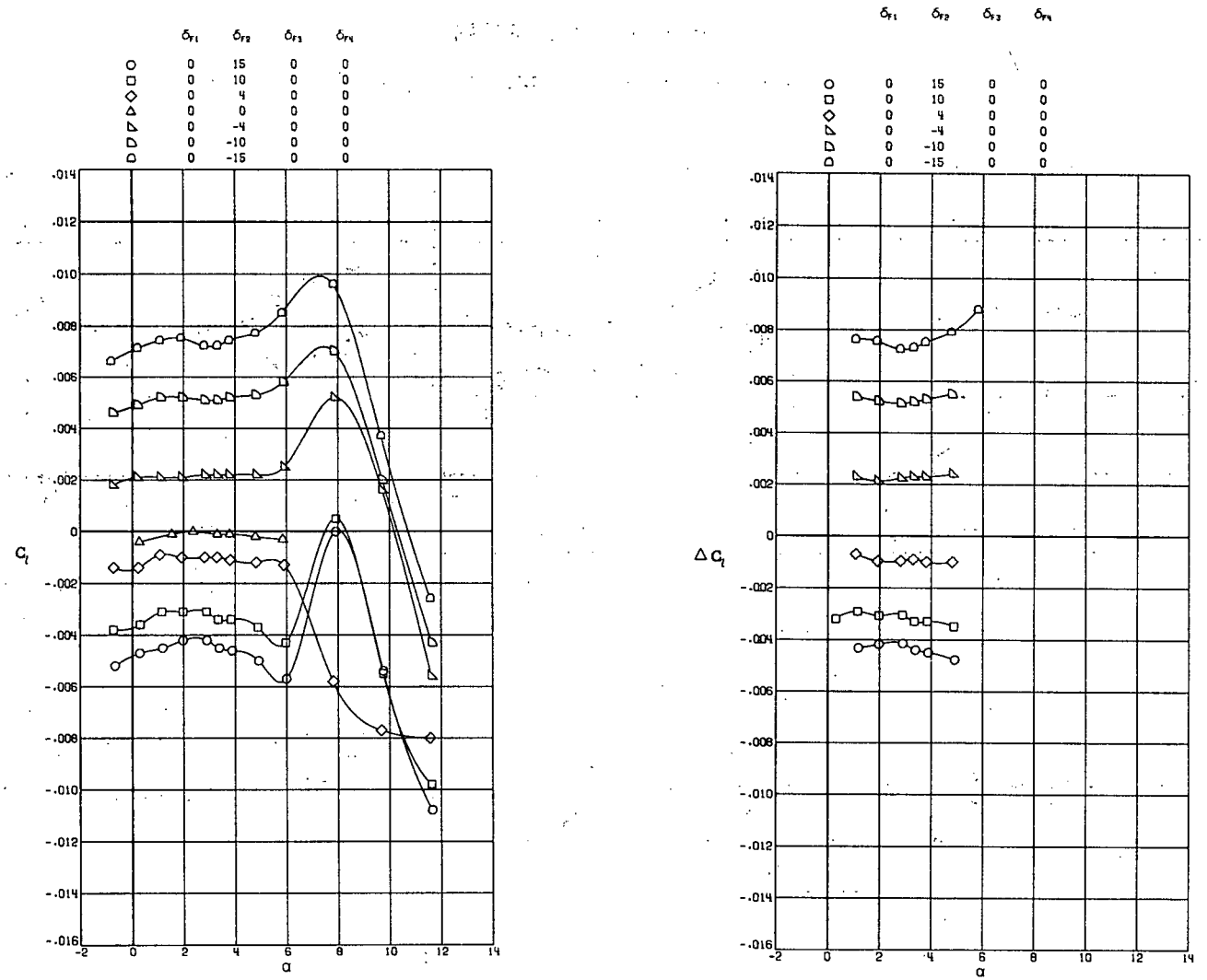
(a) Drag characteristics.

Figure 8.- Effect of F_2 trailing-edge control deflection on aerodynamic characteristics of model with area-ruled fuselage at $M_\infty = 0.80$.



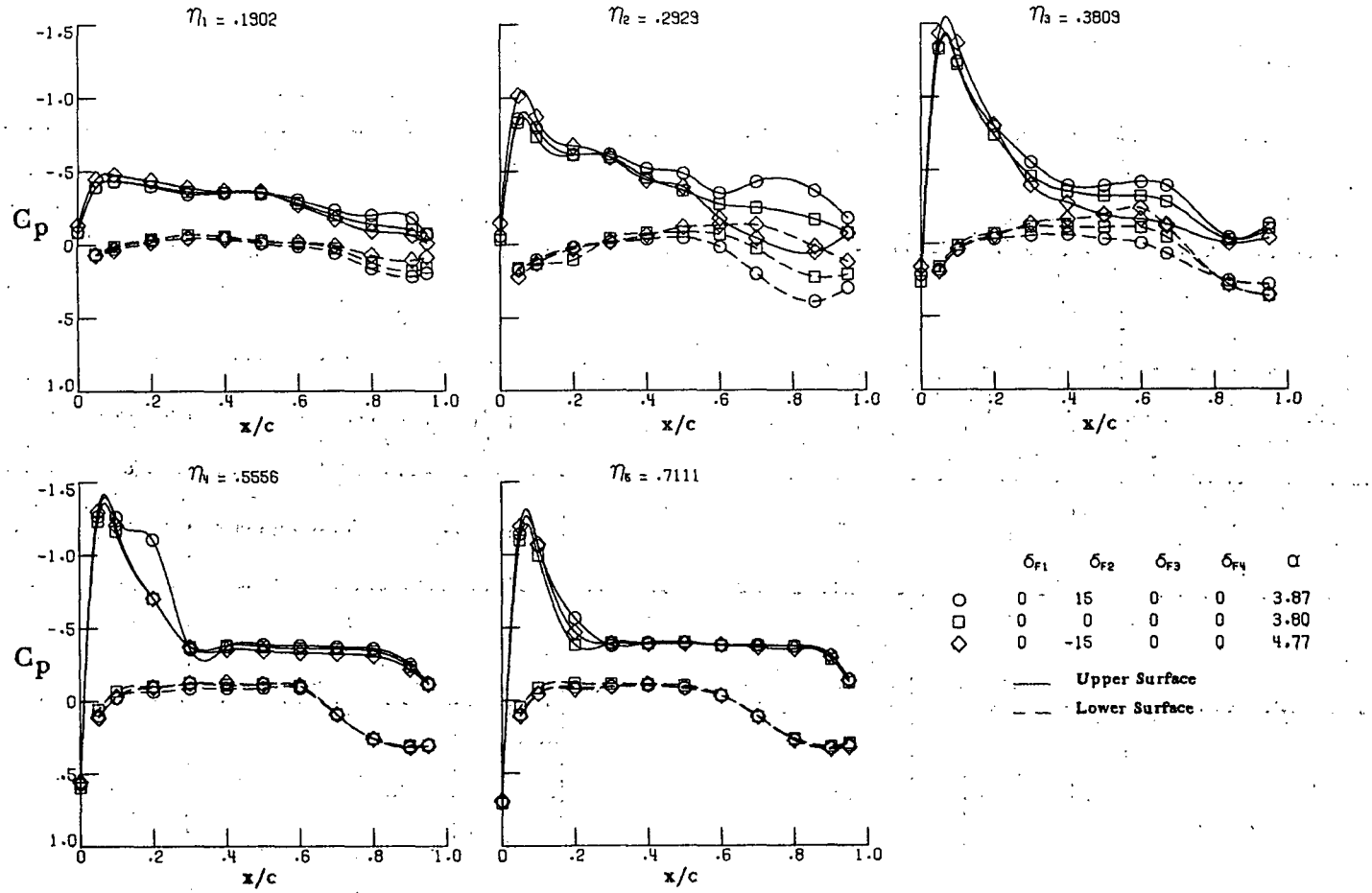
(b) Lift and pitch characteristics.

Figure 8.- Continued.



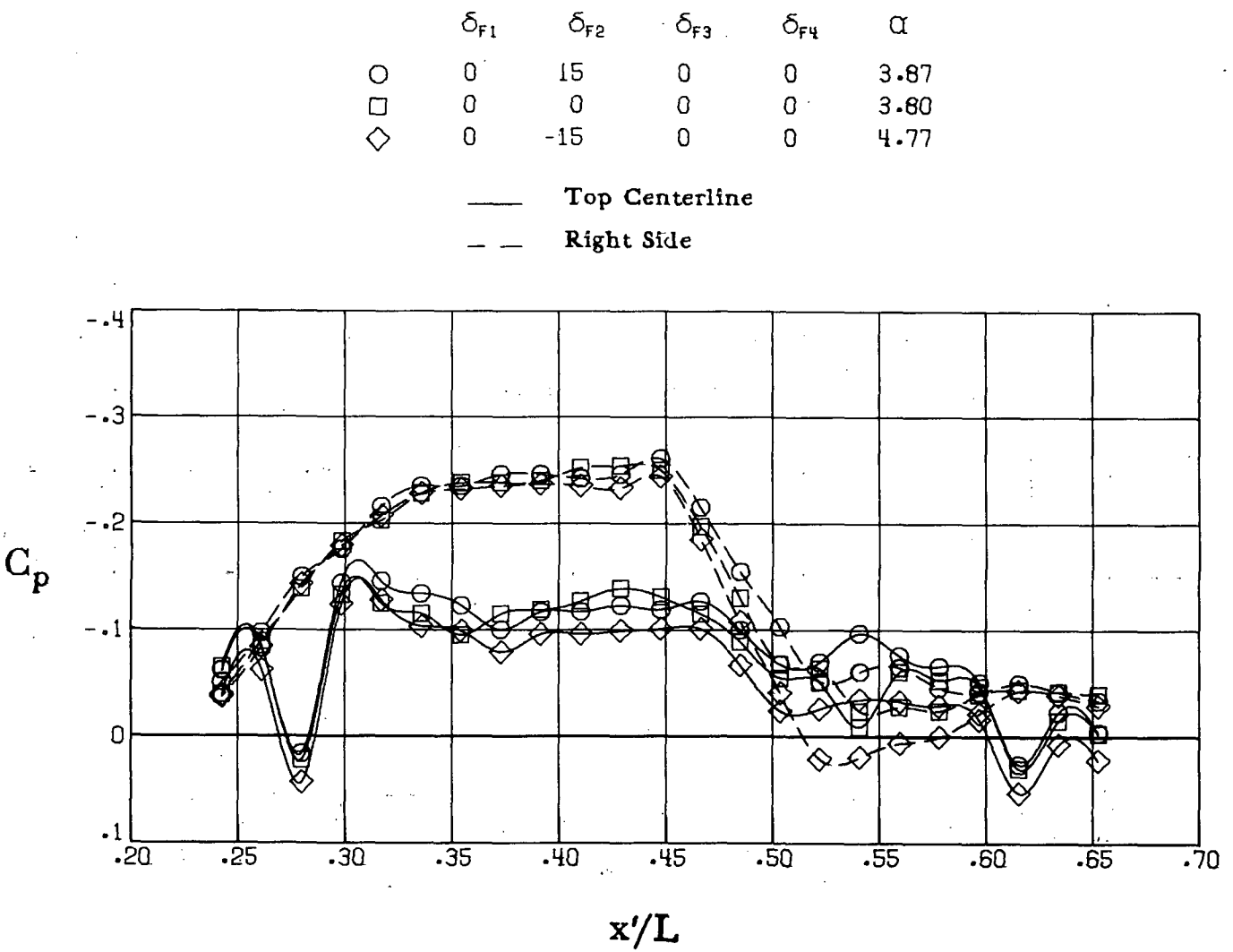
(c) Rolling-moment characteristics.

Figure 8.- Continued.



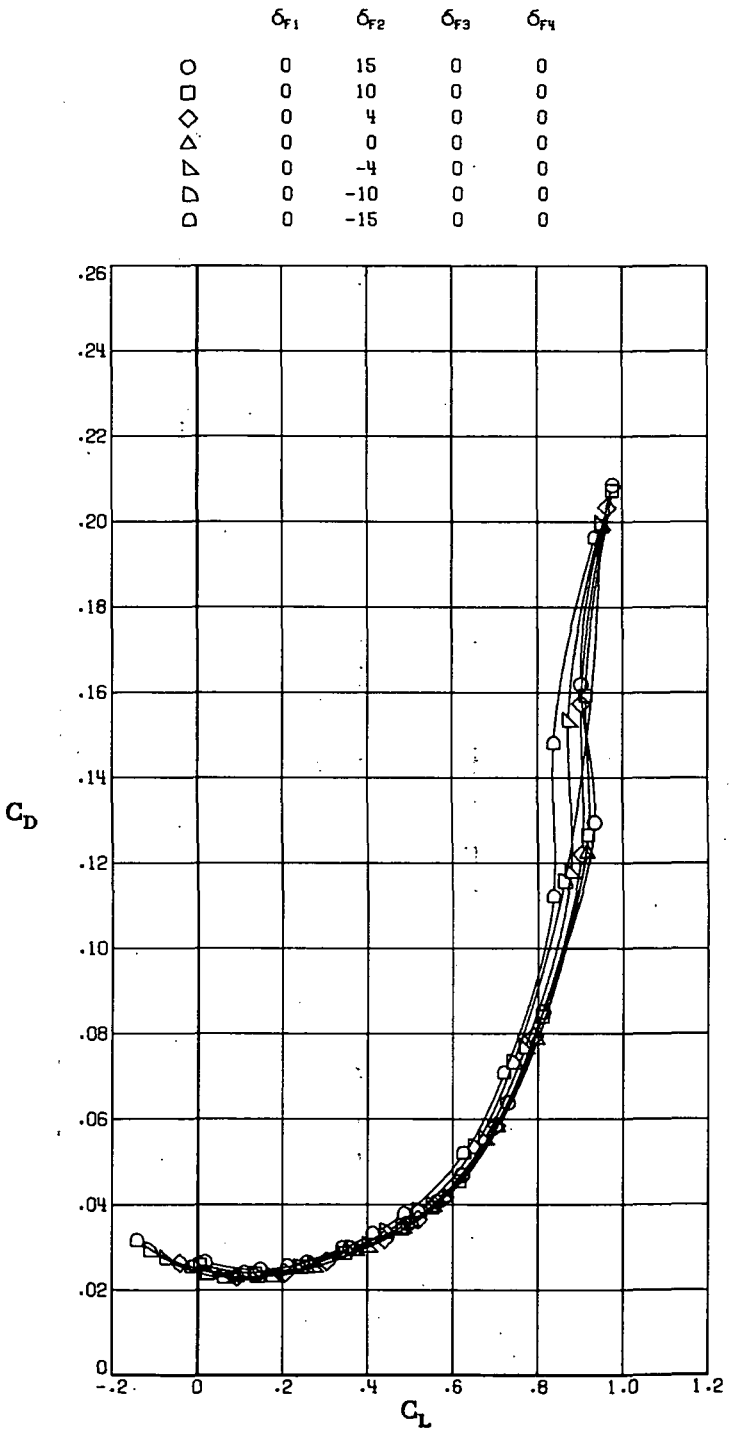
(d) Selected wing pressure distributions.

Figure 8.- Continued.



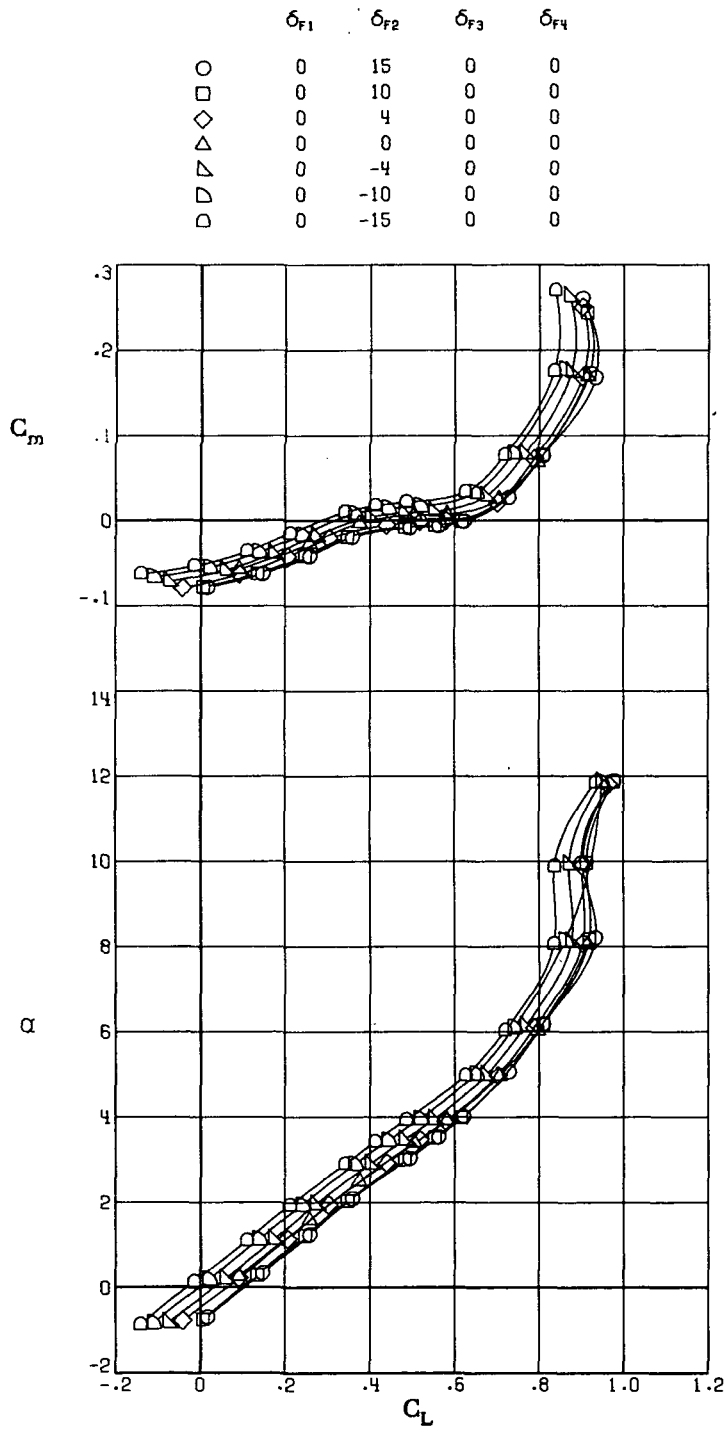
(e) Selected fuselage pressure distributions.

Figure 8.- Concluded.



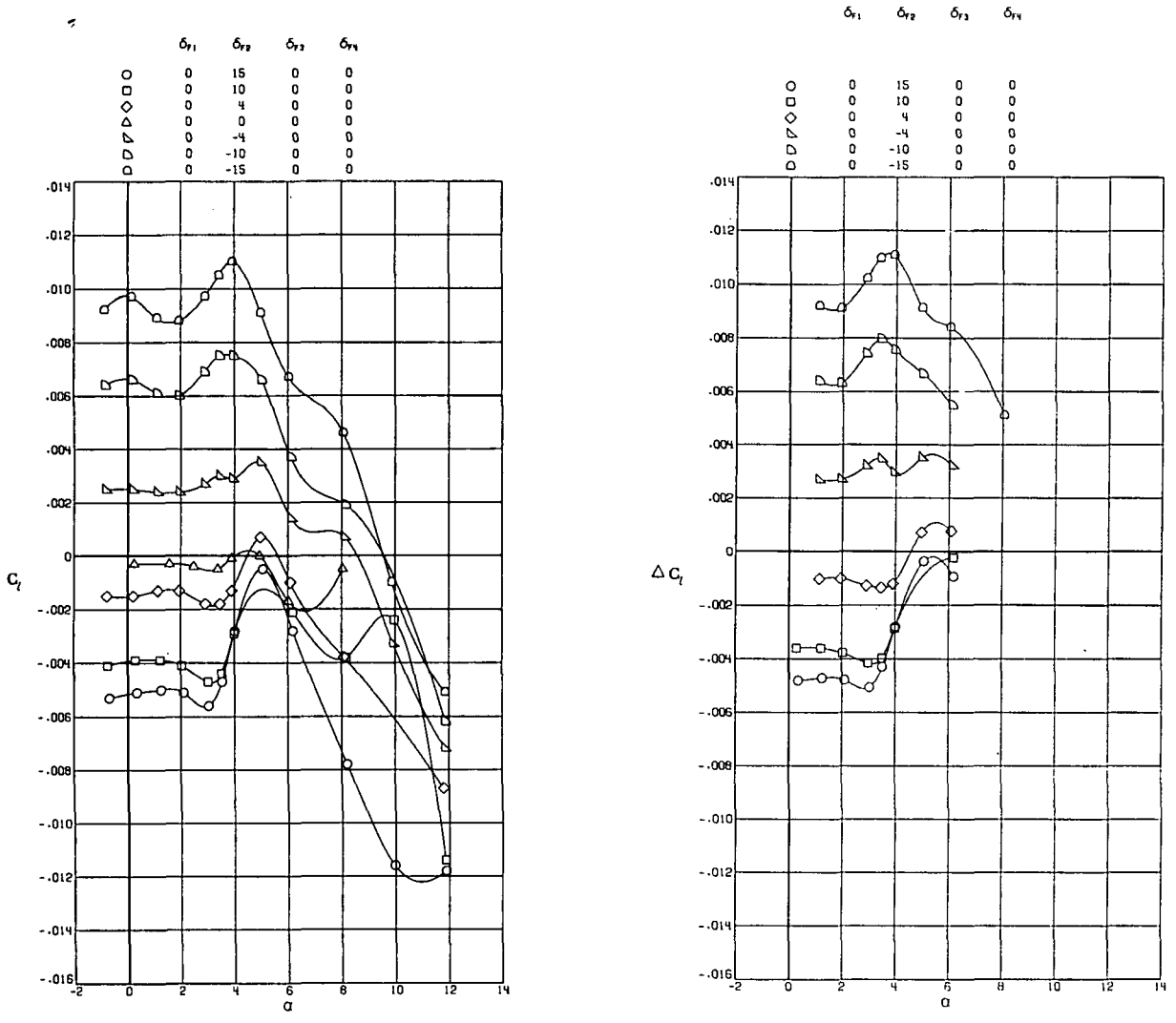
(a) Drag characteristics.

Figure 9.- Effect of F_2 trailing-edge control deflection on aerodynamic characteristics of model with area-ruled fuselage at $M_\infty = 0.90$.



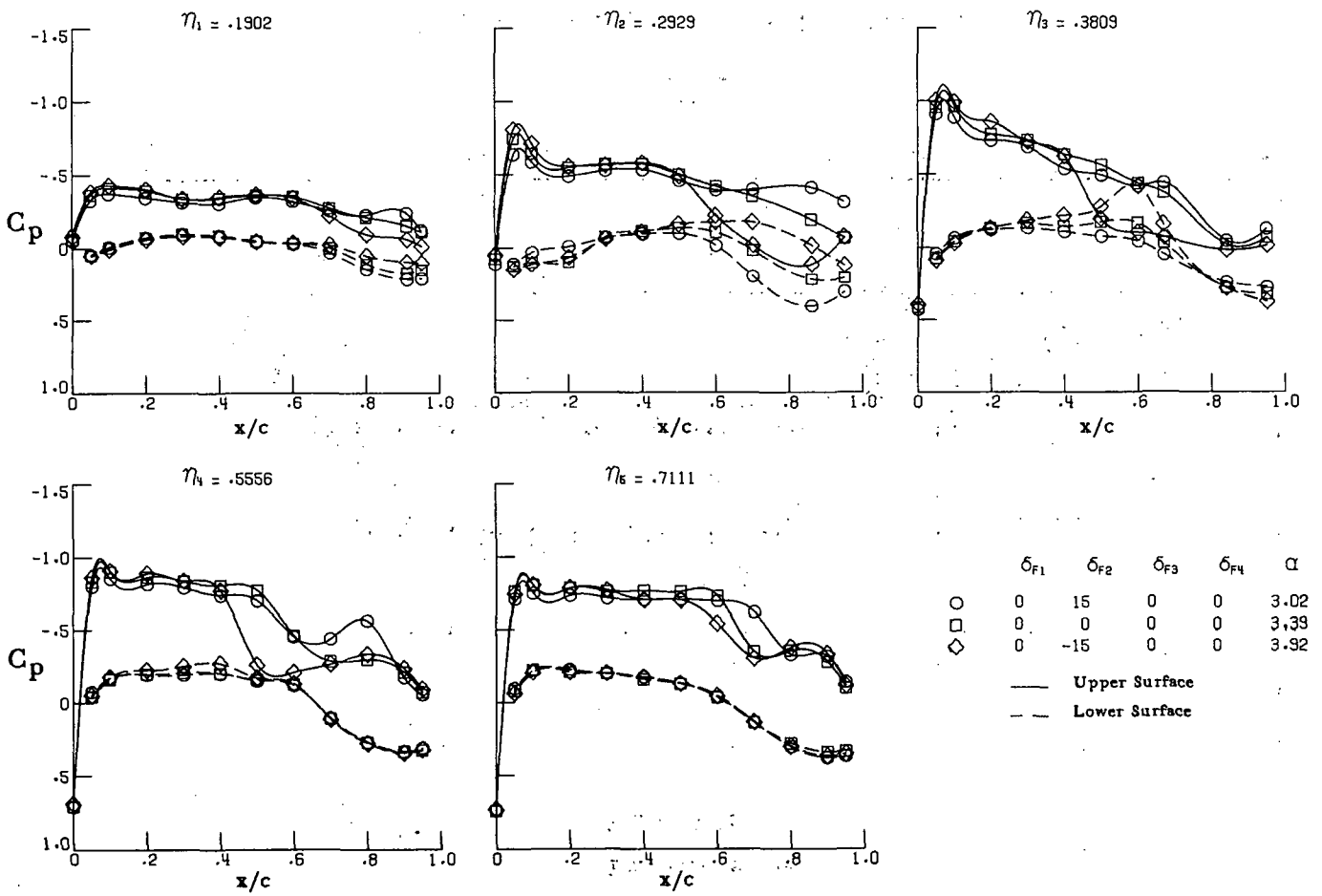
(b) Lift and pitch characteristics.

Figure 9.- Continued.



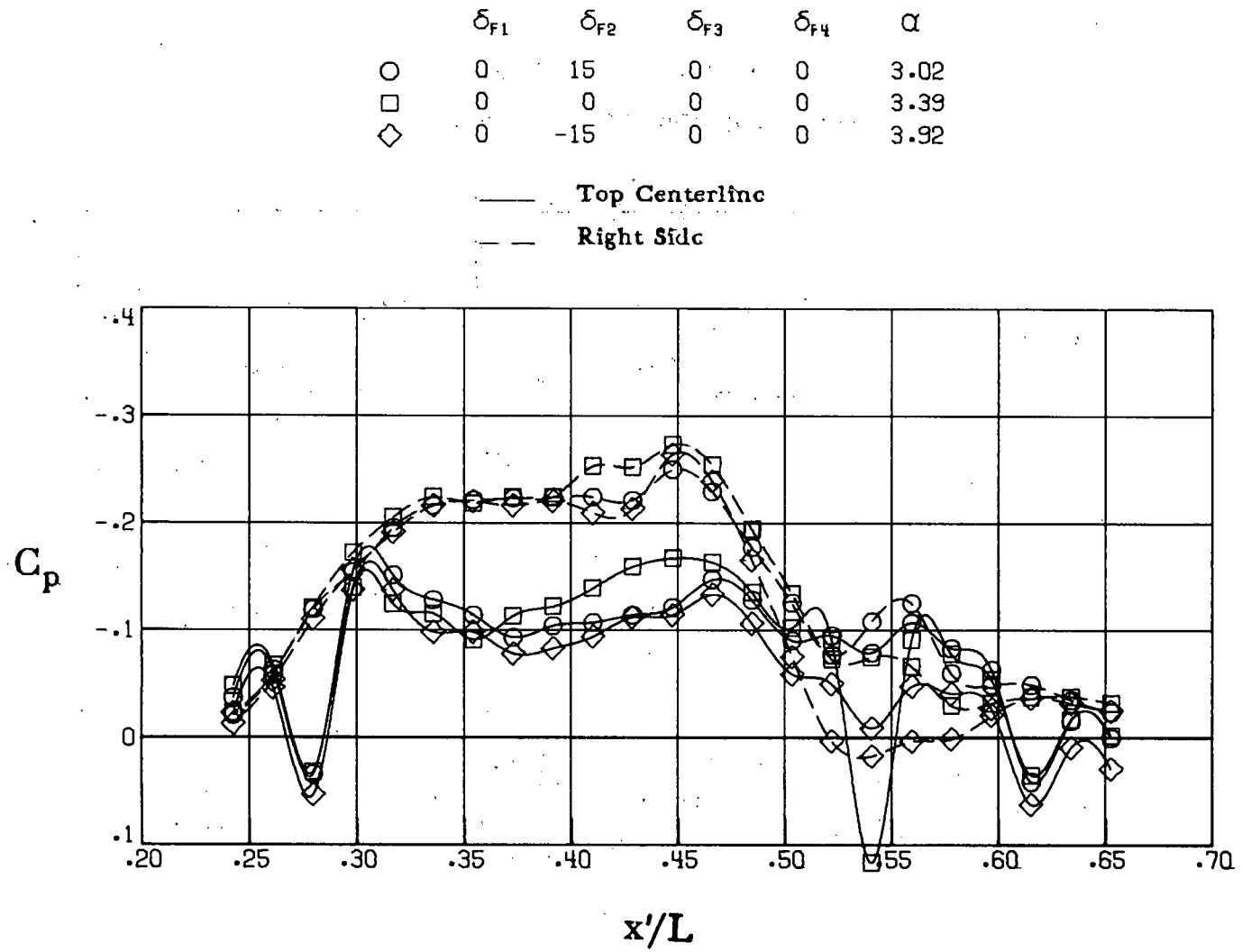
(c) Rolling-moment characteristics.

Figure 9.- Continued.



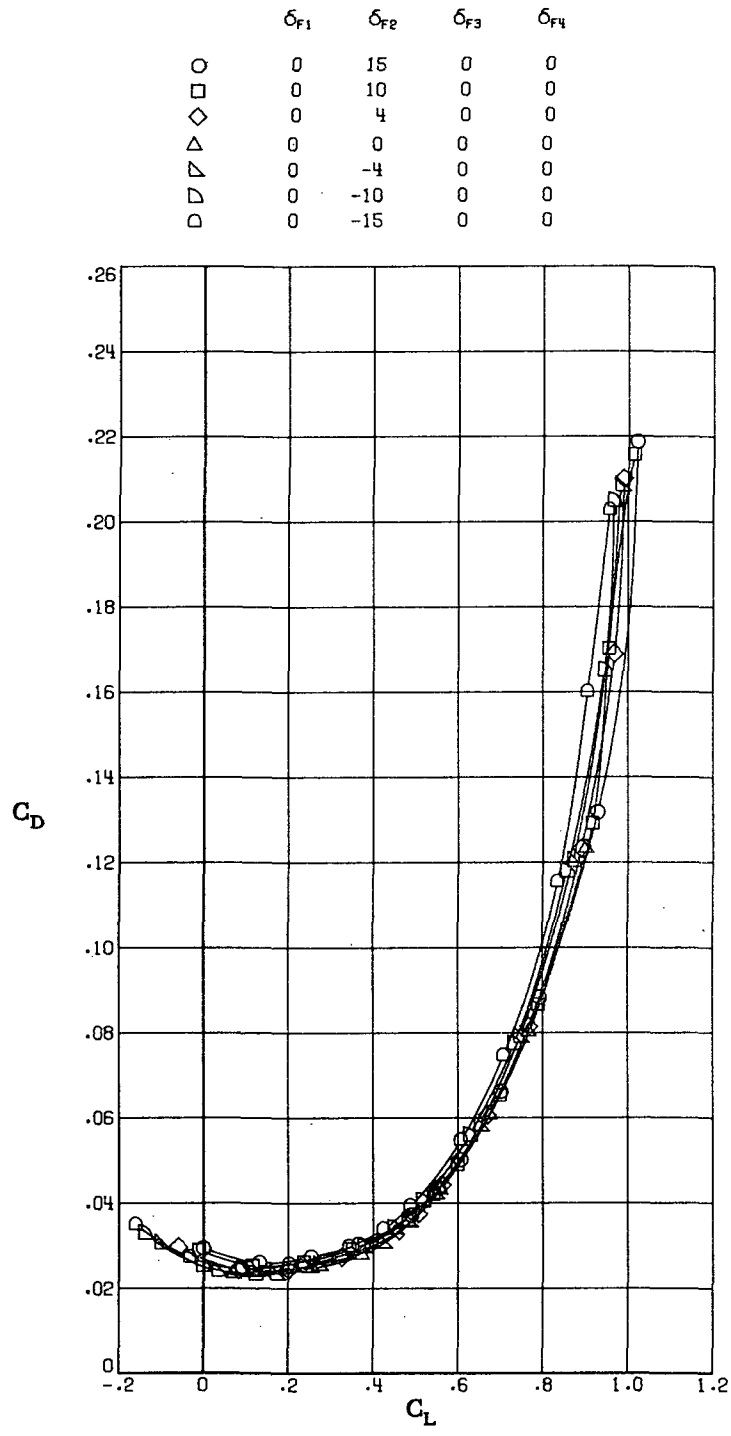
(d) Selected wing pressure distributions.

Figure 9.- Continued.



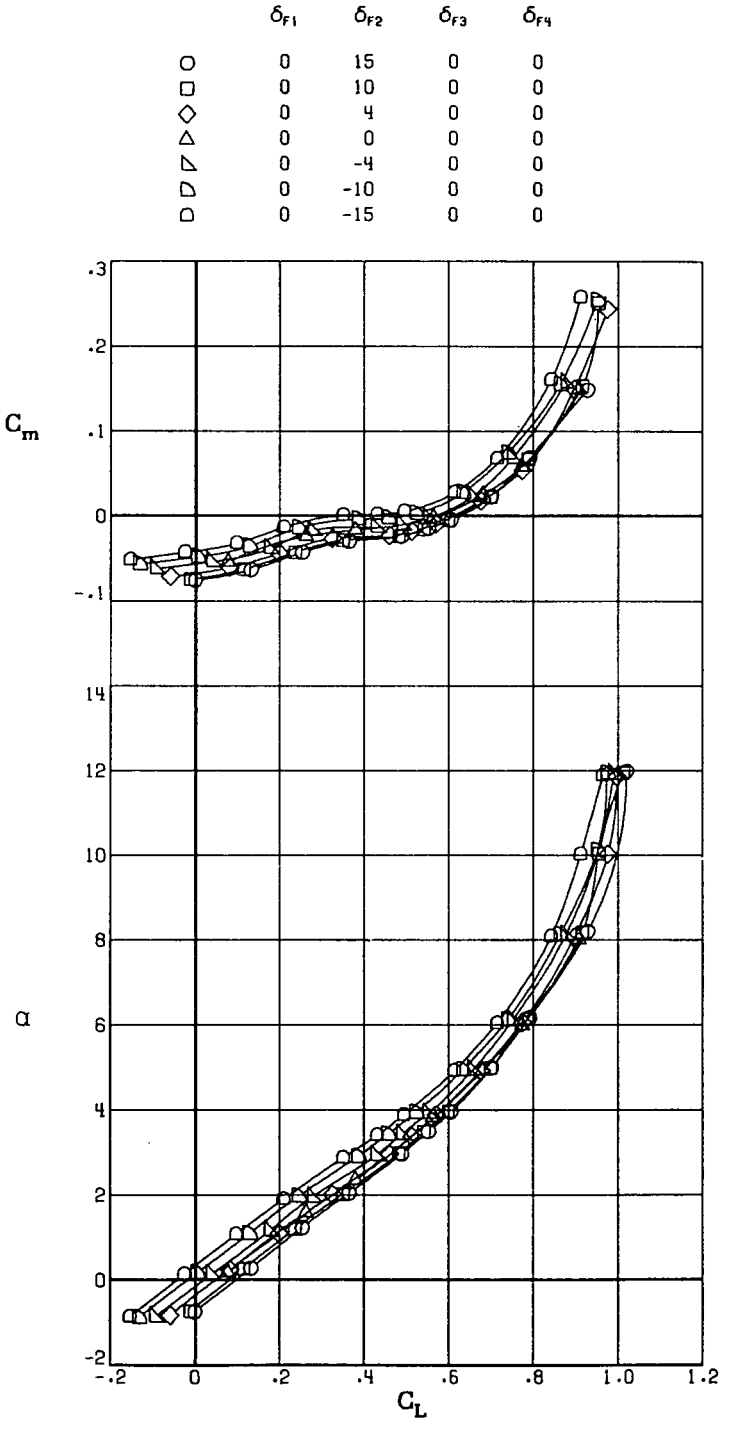
(e) Selected fuselage pressure distributions.

Figure 9.- Concluded.



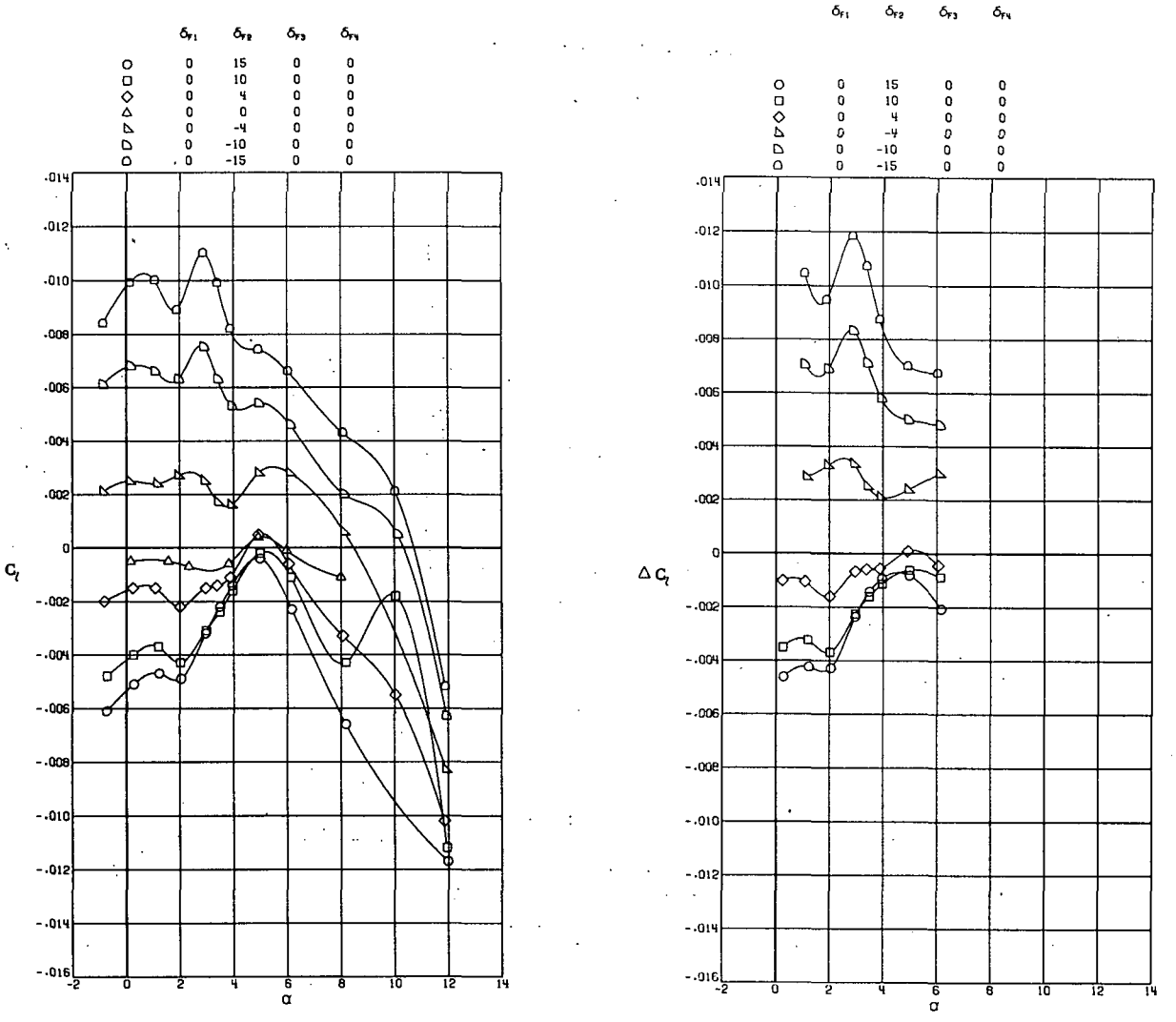
(a) Drag characteristics.

Figure 10.- Effect of F_2 trailing-edge control deflection on aerodynamic characteristics of model with area-ruled fuselage at $M_\infty = 0.92$.



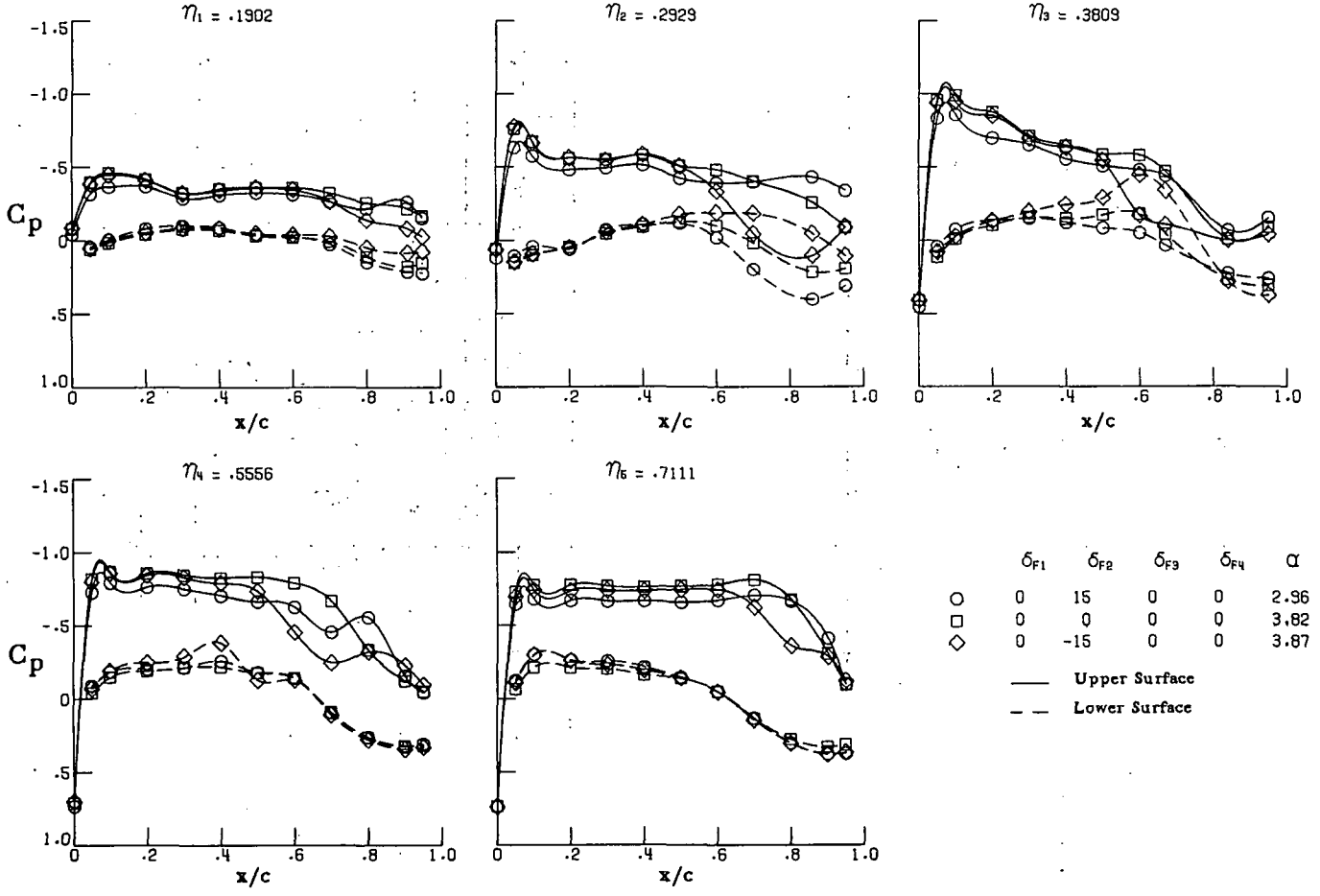
(b) Lift and pitch characteristics.

Figure 10.- Continued.



(c) Rolling-moment characteristics.

Figure 10.- Continued.



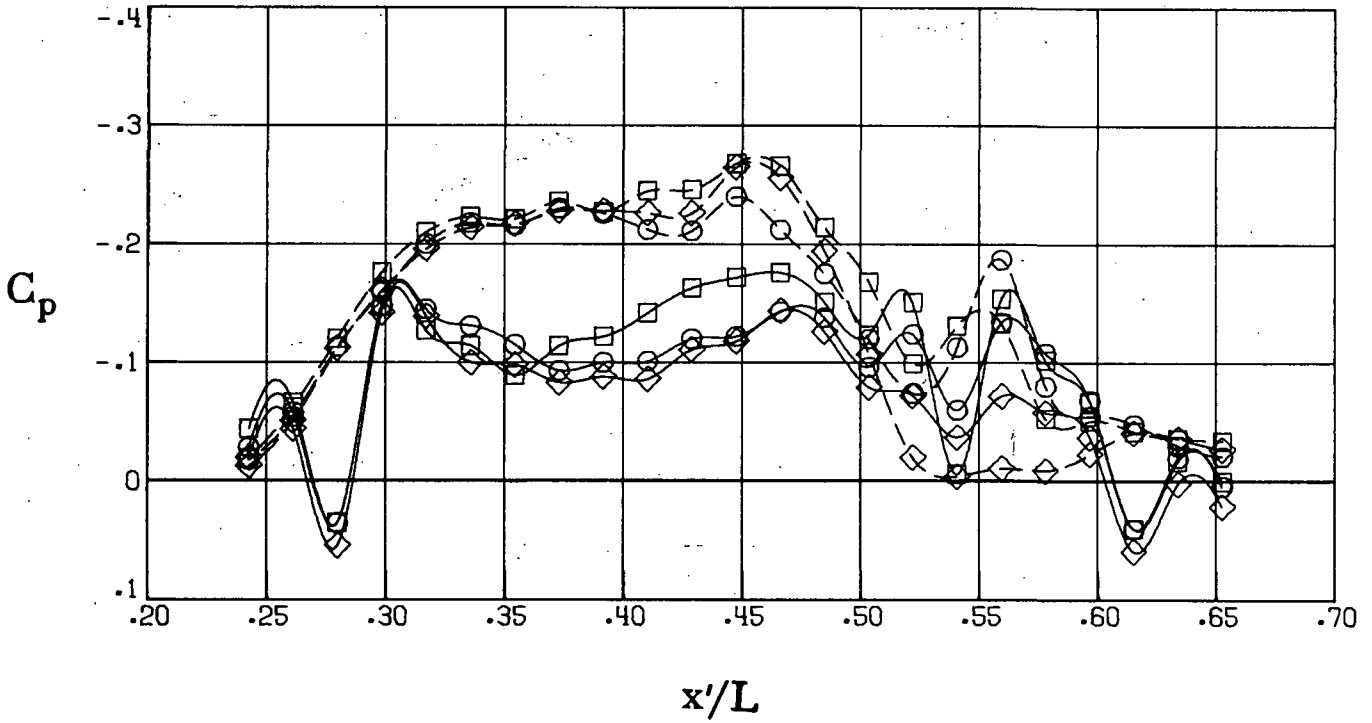
(d) Selected wing pressure distributions.

Figure 10.- Continued.

	δ_{F1}	δ_{F2}	δ_{F3}	δ_{F4}	α'
○	0	15	0	0	2.96
□	0	0	0	0	3.82
◇	0	-15	0	0	3.87

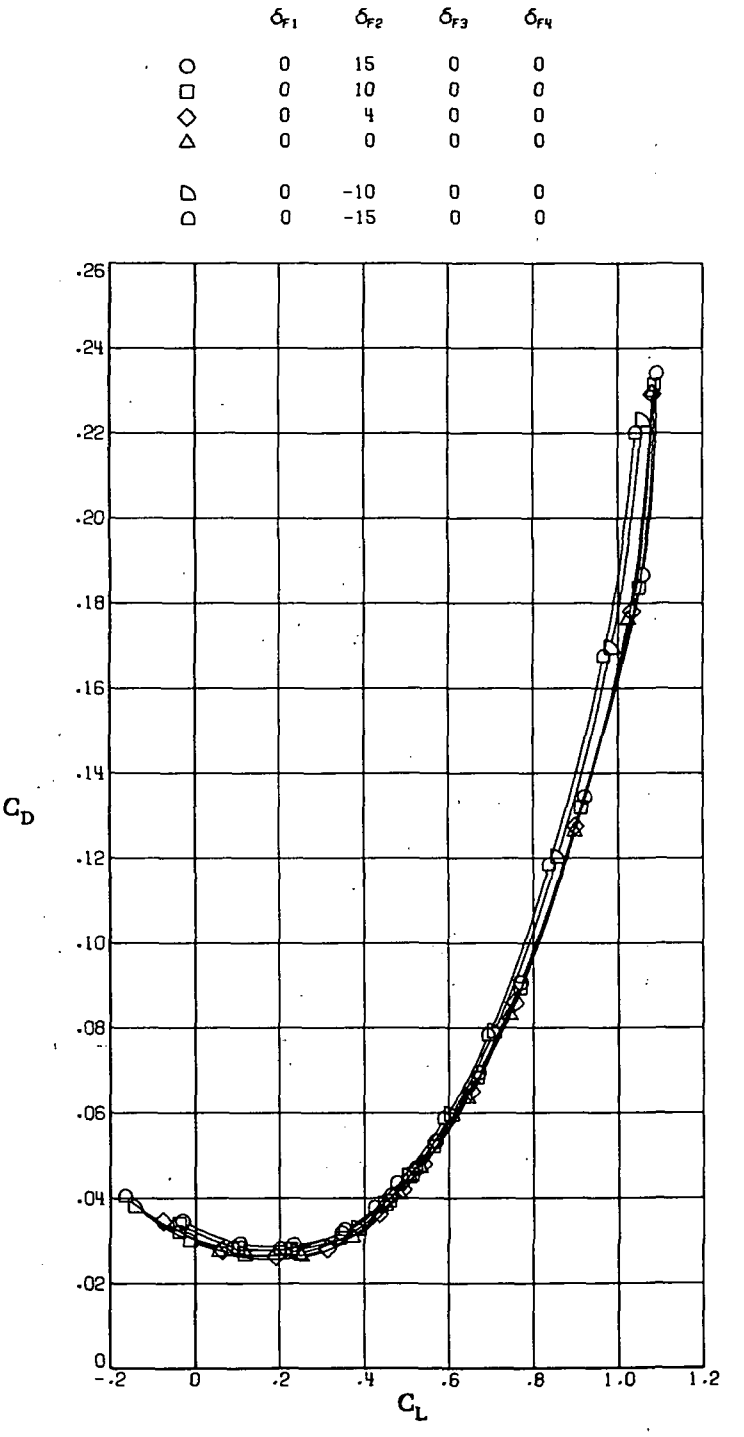
—— Top Centerline

– – Right Side



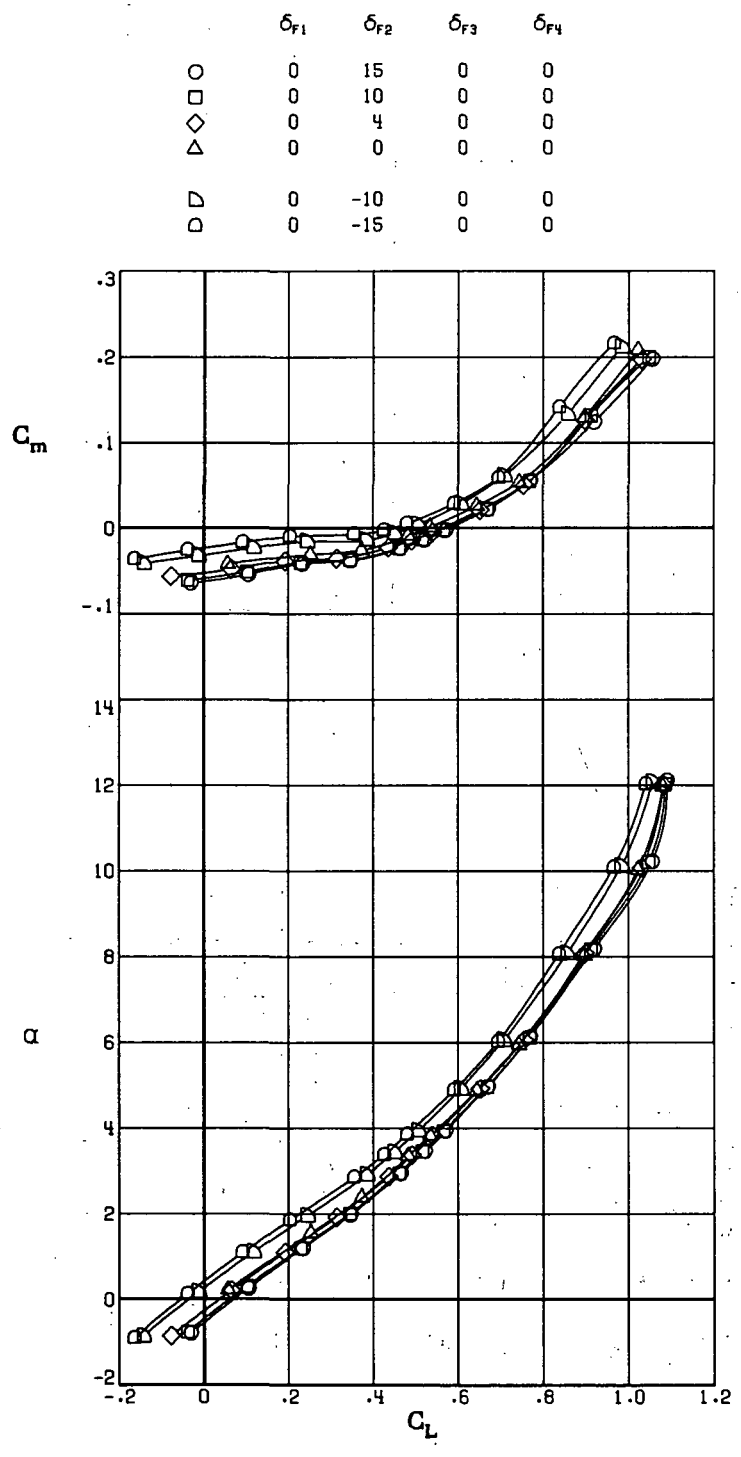
(e) Selected fuselage pressure distributions.

Figure 10.- Concluded.



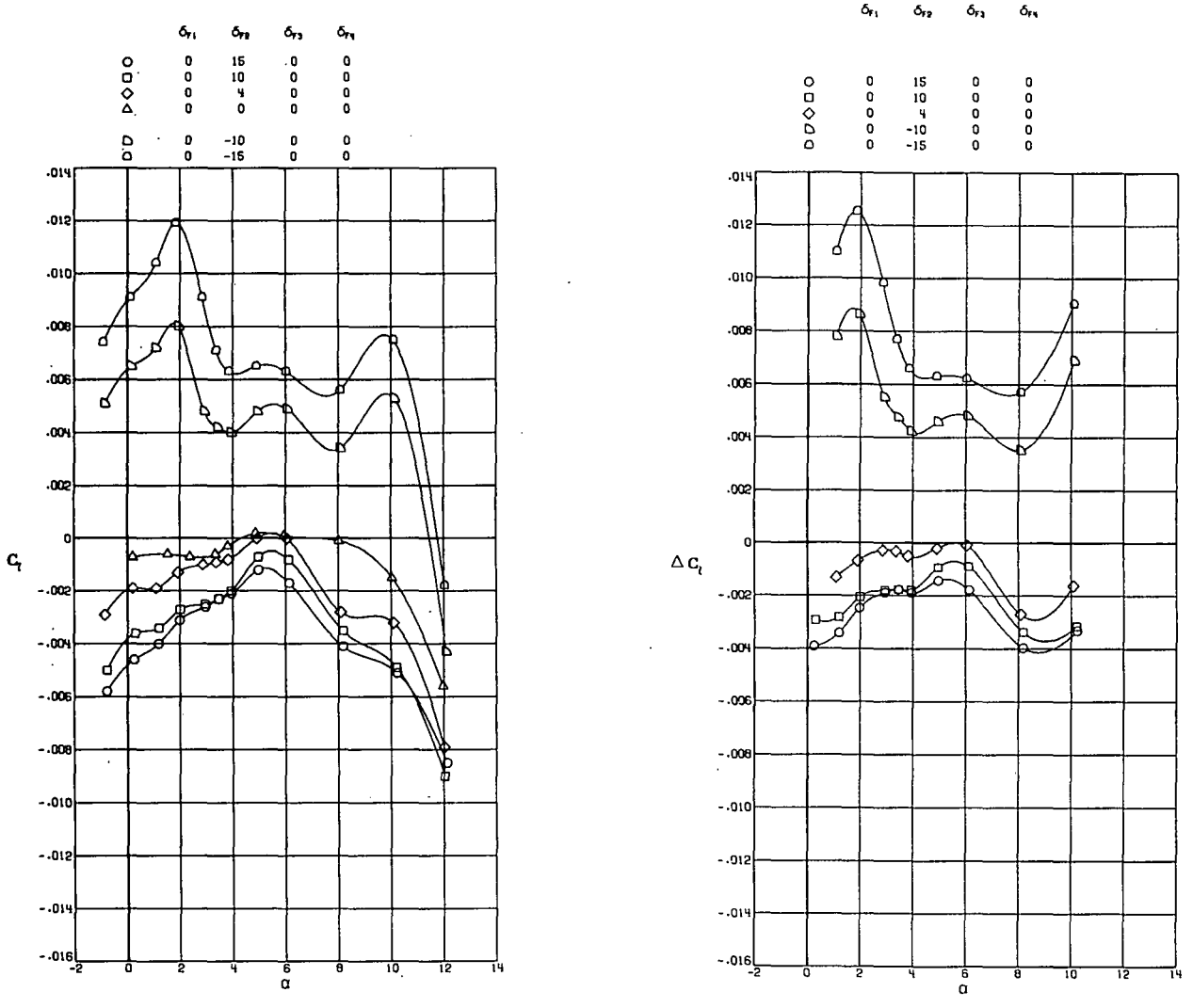
(a) Drag characteristics.

Figure 11.- Effect of F_2 trailing-edge control deflection on aerodynamic characteristics of model with area-ruled fuselage at $M_\infty = 0.94$.



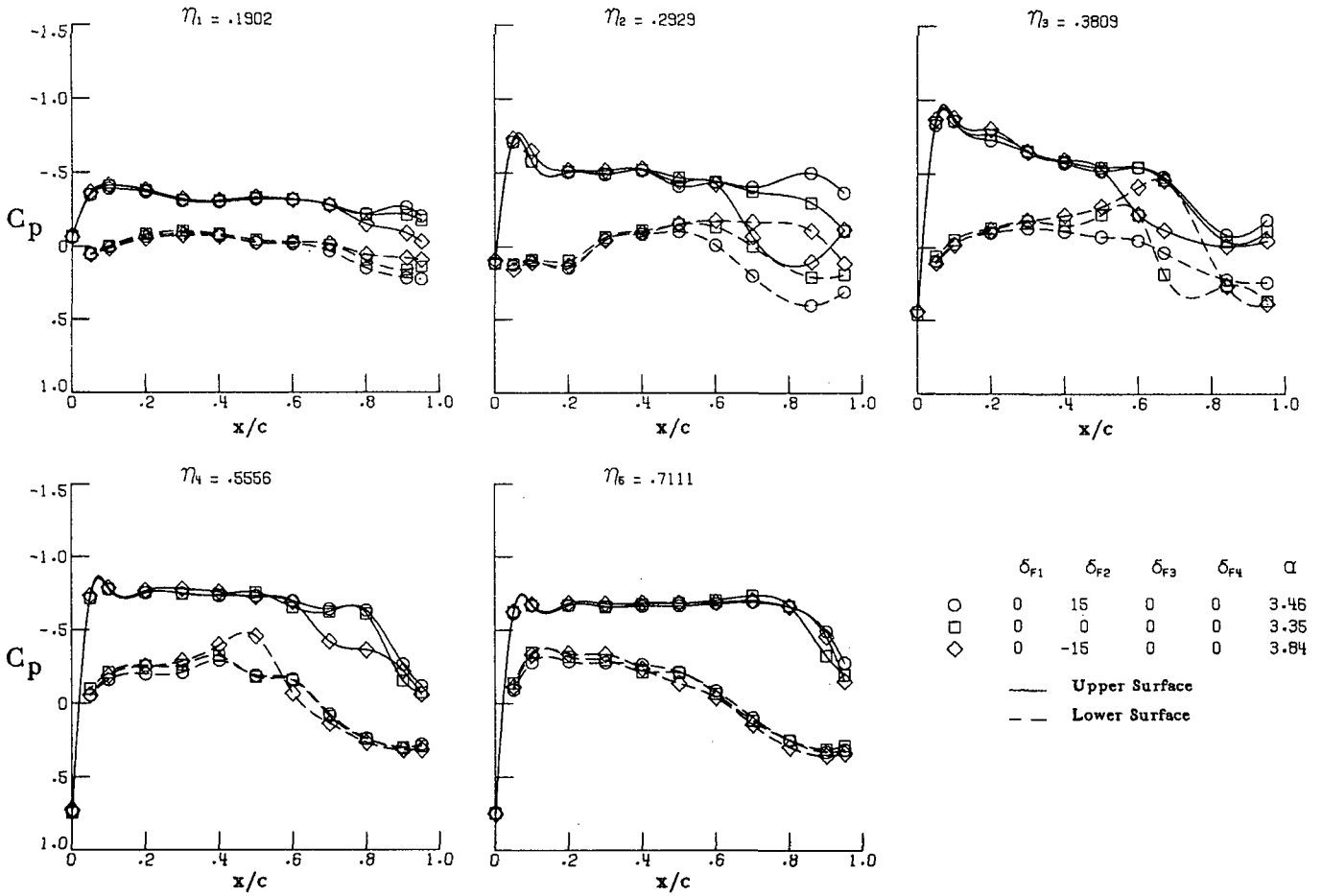
(b) Lift and pitch characteristics.

Figure 11.- Continued.



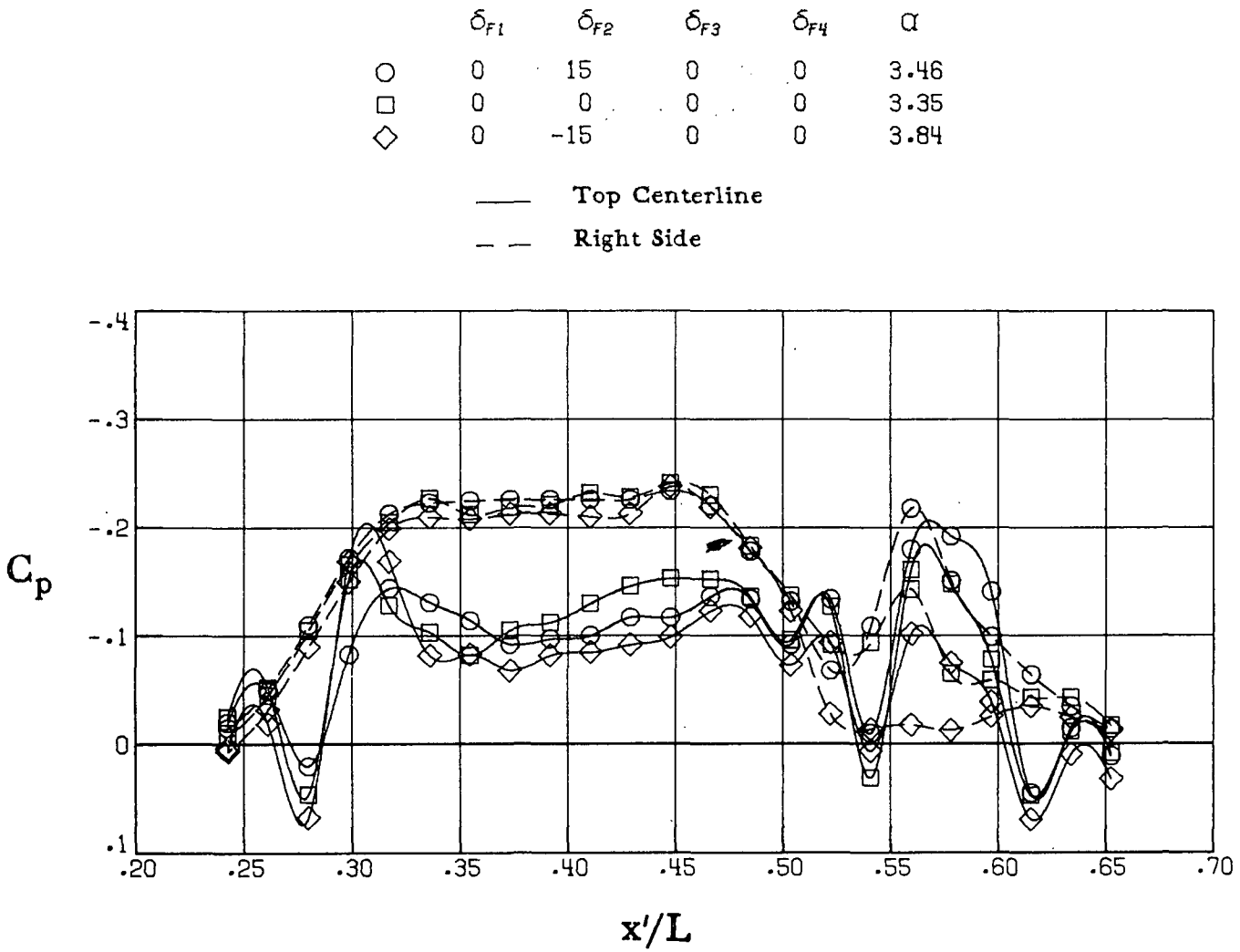
(c) Rolling-moment characteristics.

Figure 11.- Continued.



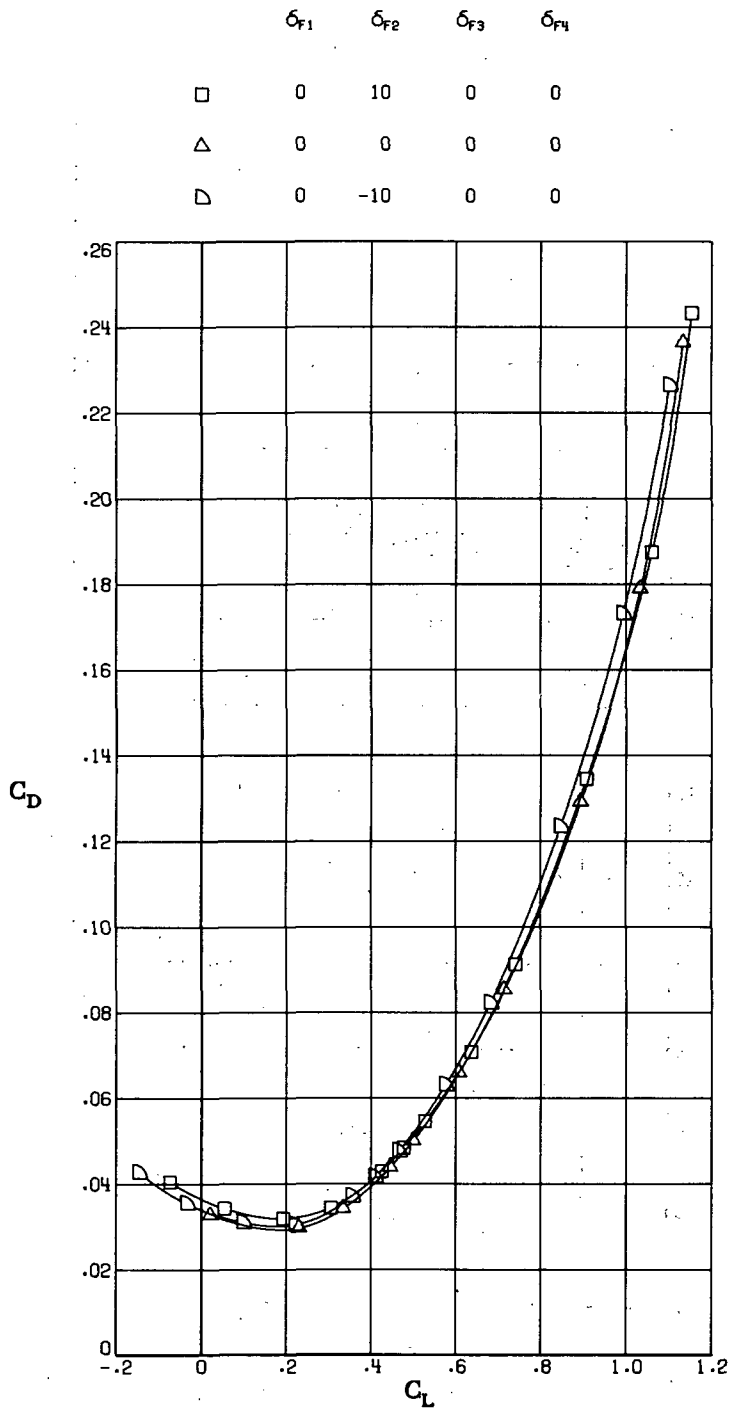
(d) Selected wing pressure distributions.

Figure 11.- Continued.



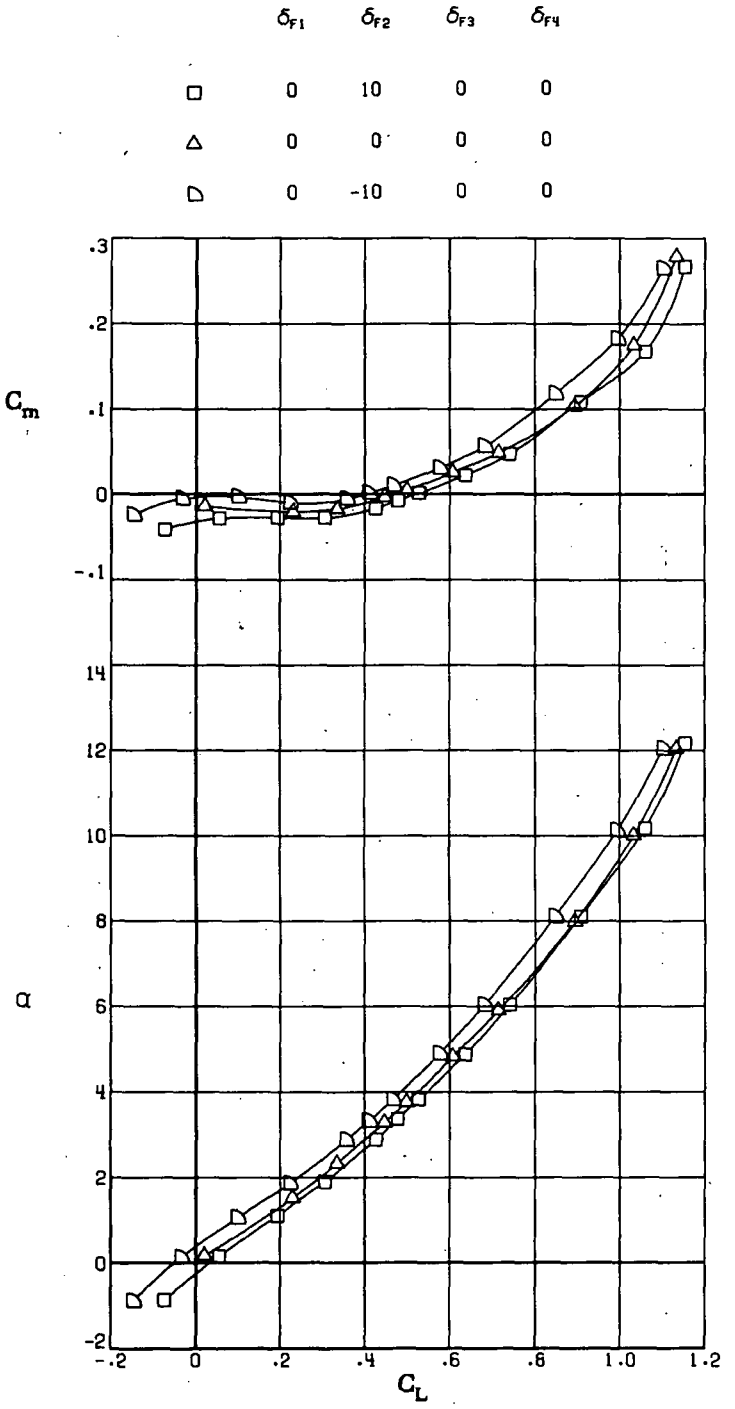
(e) Selected fuselage pressure distributions.

Figure 11.- Concluded.



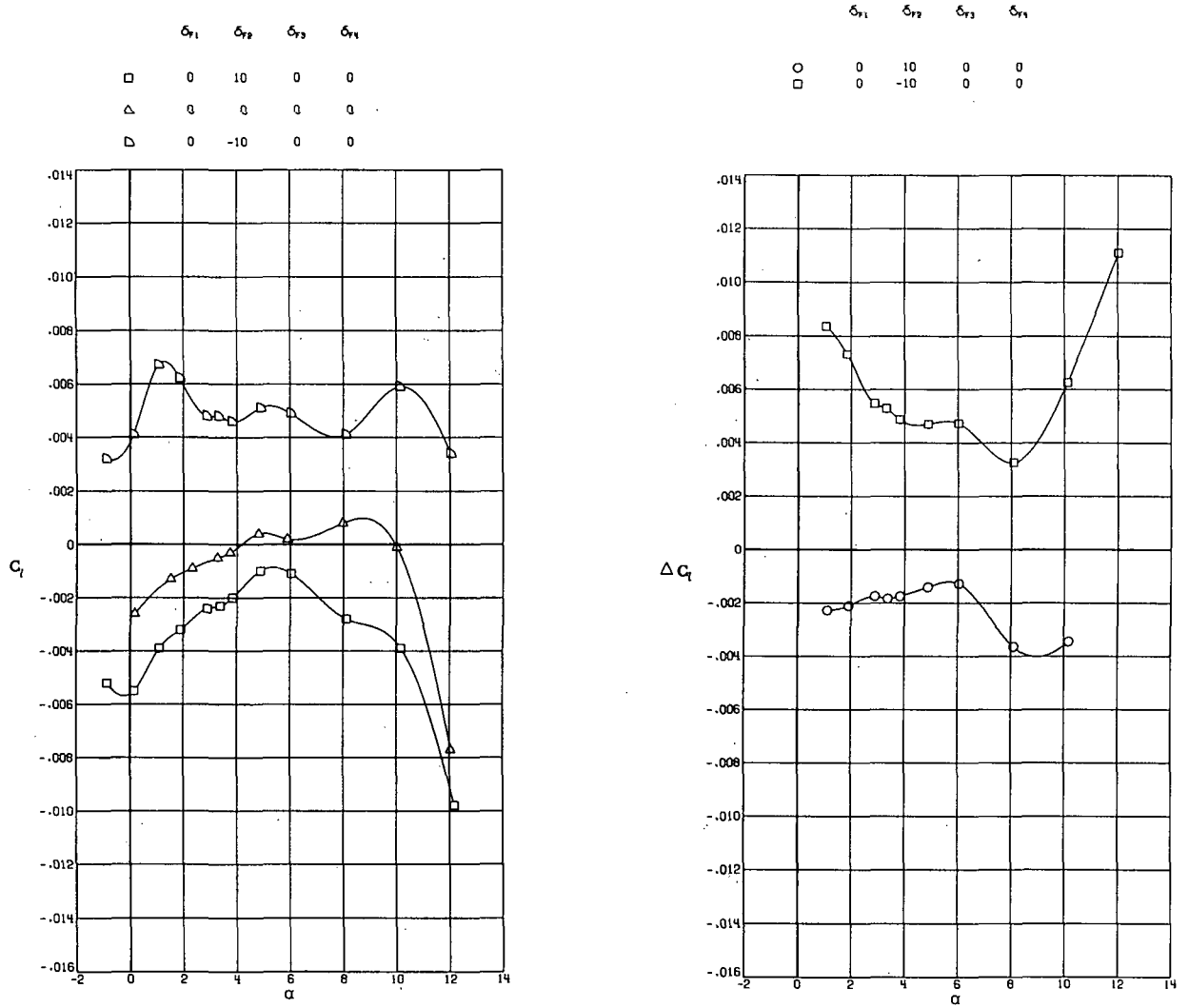
(a) Drag characteristics.

Figure 12.- Effect of F_2 trailing-edge control deflection on aerodynamic characteristics of model with area-ruled fuselage at $M_\infty = 0.96$.



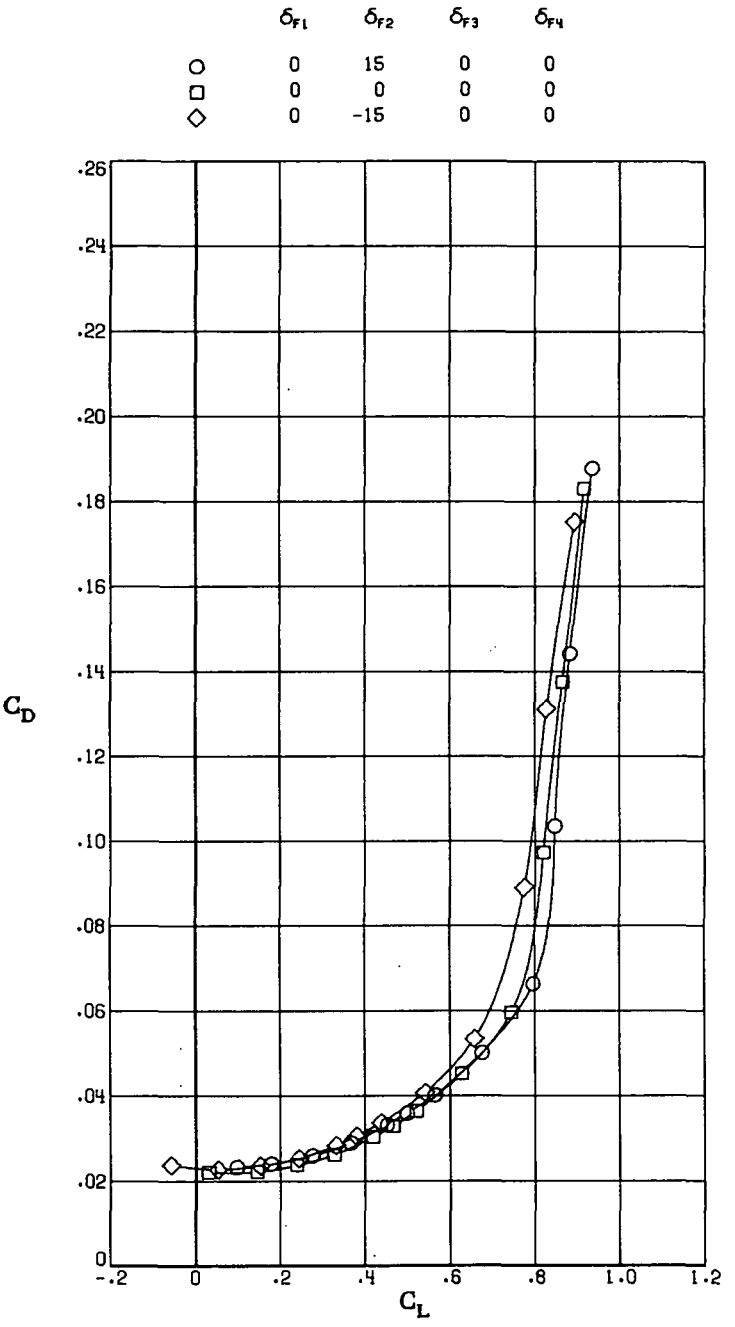
(b) Lift and pitch characteristics.

Figure 12.- Continued.



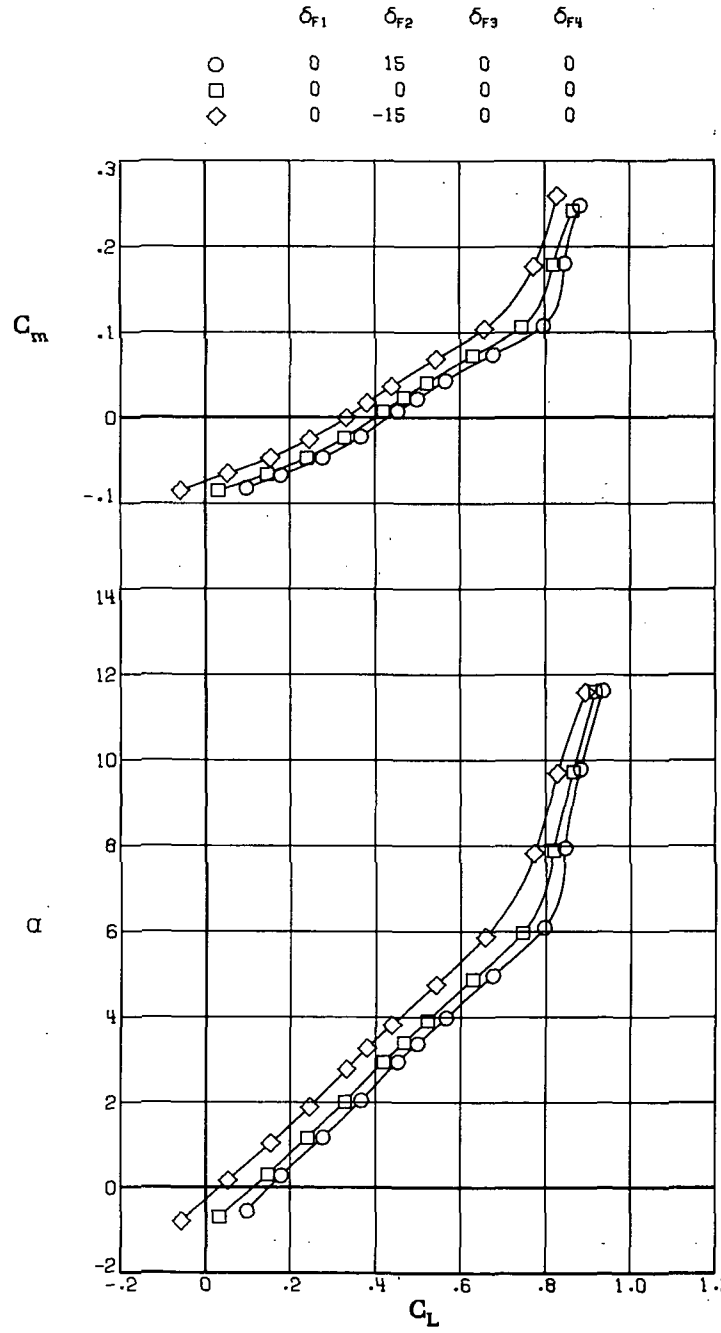
(c) Rolling-moment characteristics.

Figure 12.- Concluded.



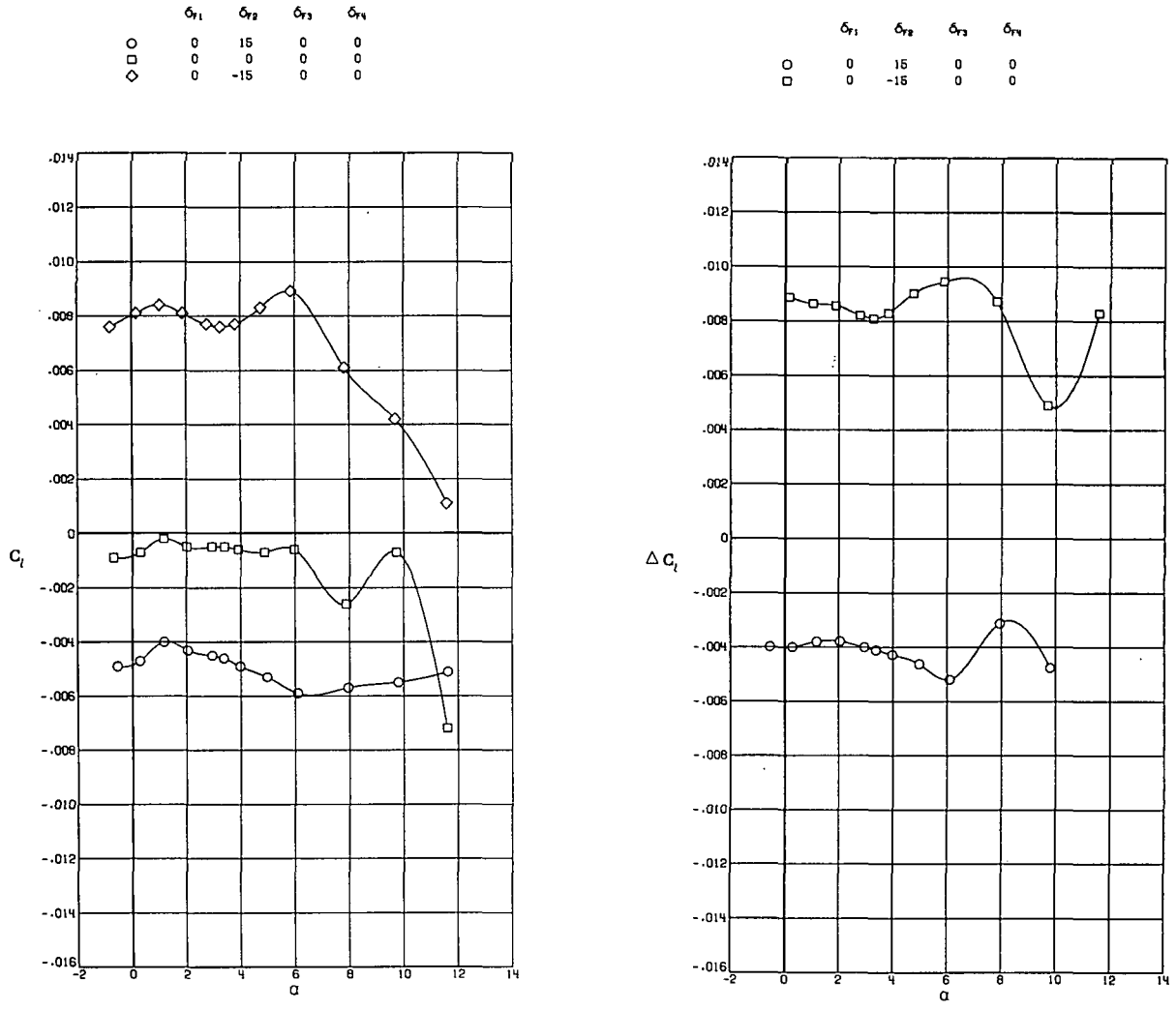
(a) Drag characteristics.

Figure 13.- Effect of F_2 trailing-edge control deflection on aerodynamic characteristics of model with cylindrical fuselage at $M_\infty = 0.80$.



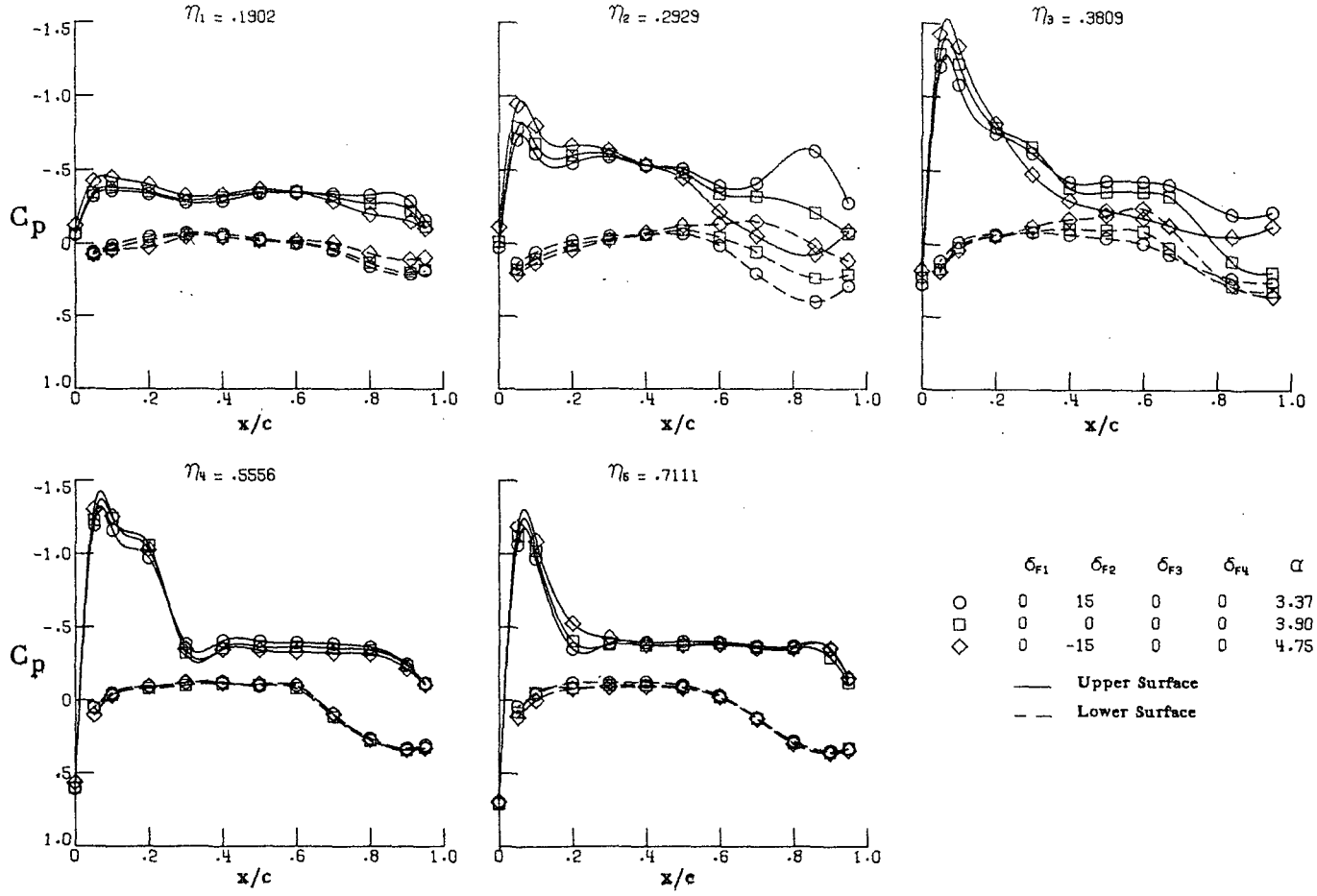
(b) Lift and pitch characteristics.

Figure 13.- Continued.



(c) Rolling-moment characteristics.

Figure 13.- Continued.

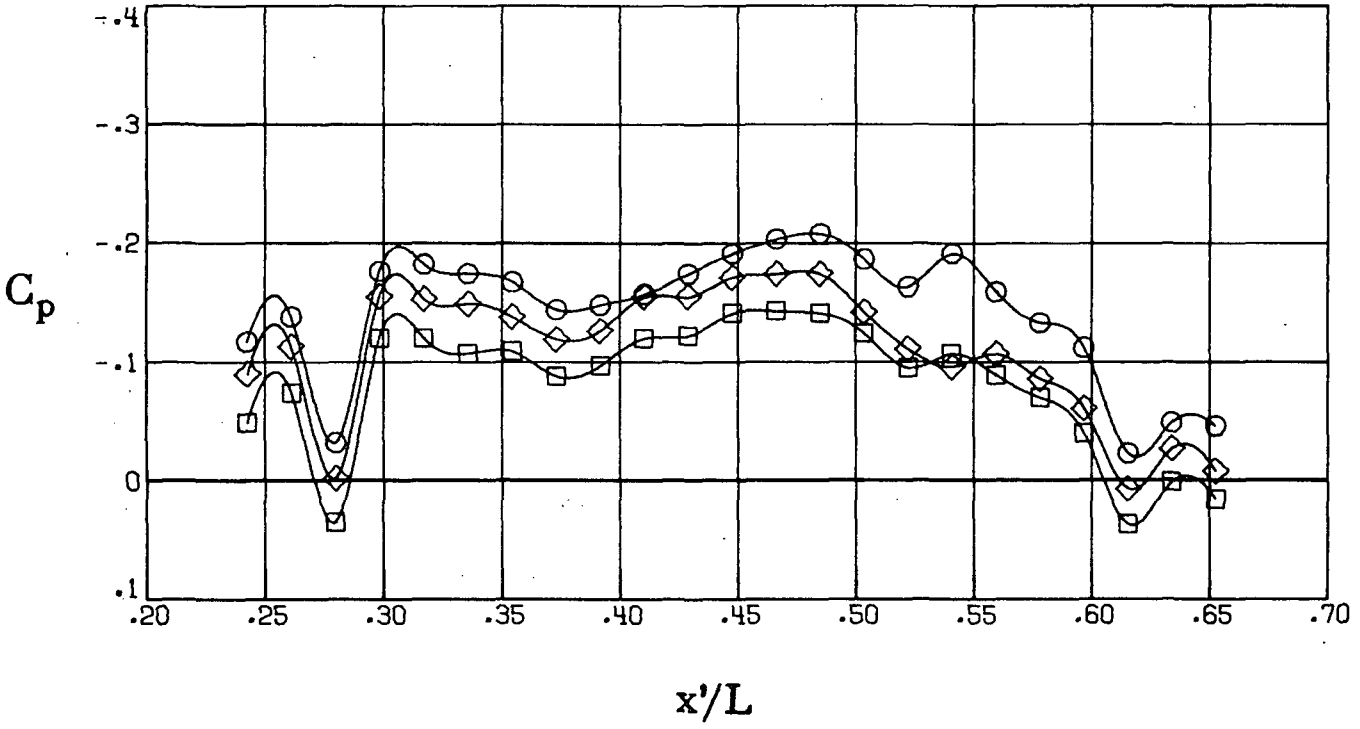


(d) Selected wing pressure distributions.

Figure 13.- Continued.

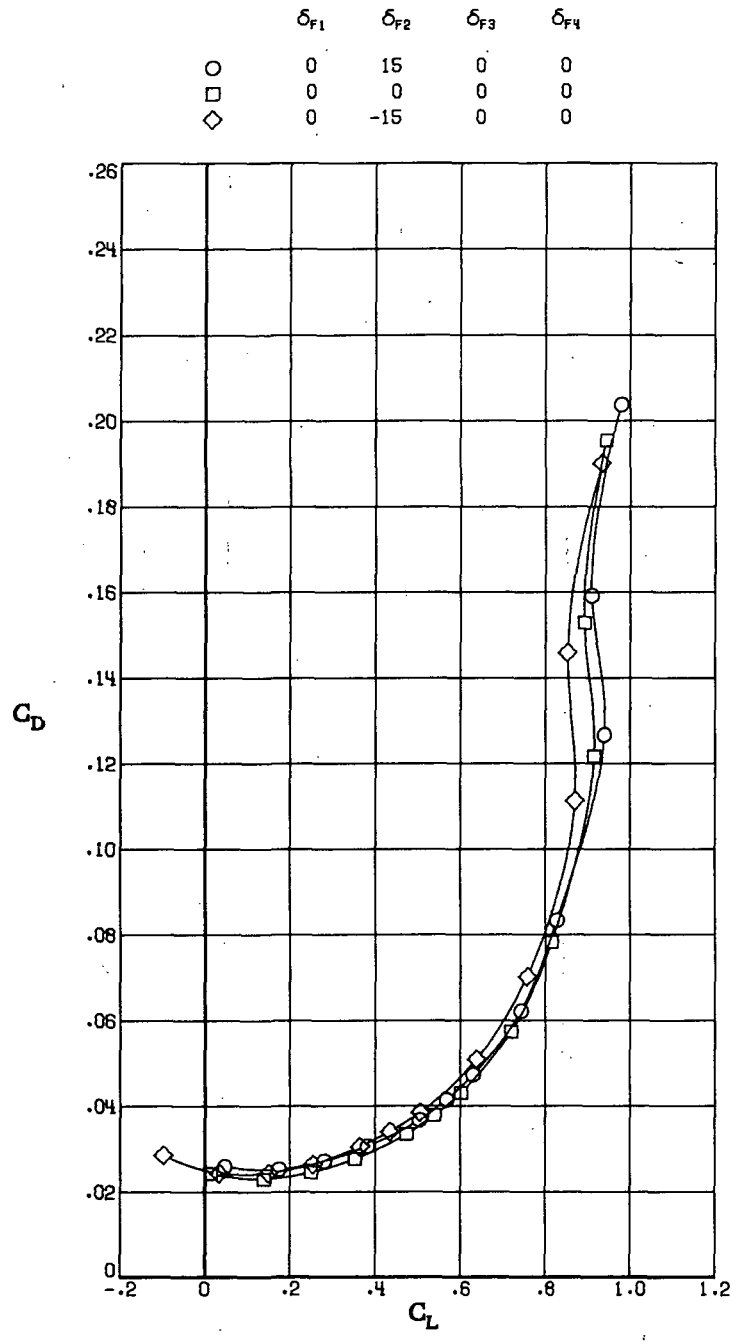
	δ_{F1}	δ_{F2}	δ_{F3}	δ_{F4}	α
○	0	15	0	0	3.37
□	0	0	0	0	3.90
◇	0	-15	0	0	4.75

—— Top Centerline



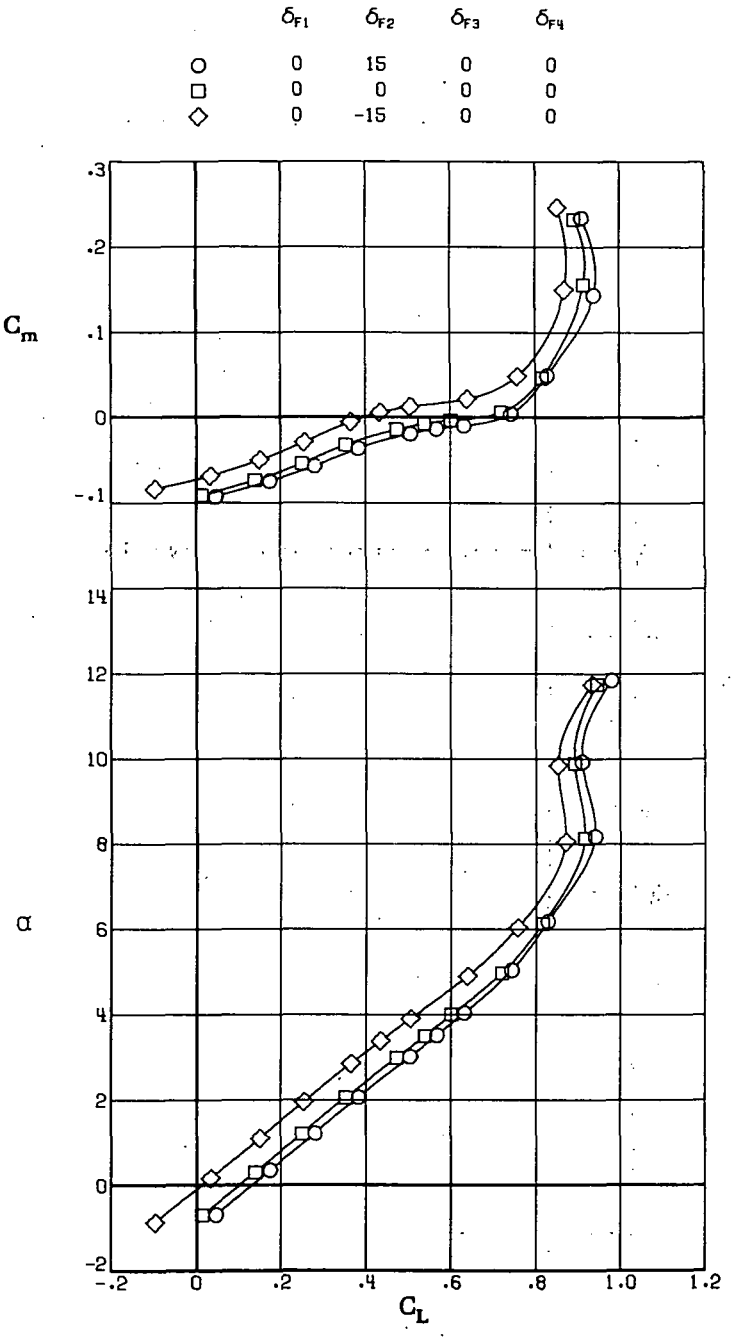
(e) Selected fuselage pressure distributions.

Figure 13.- Concluded.



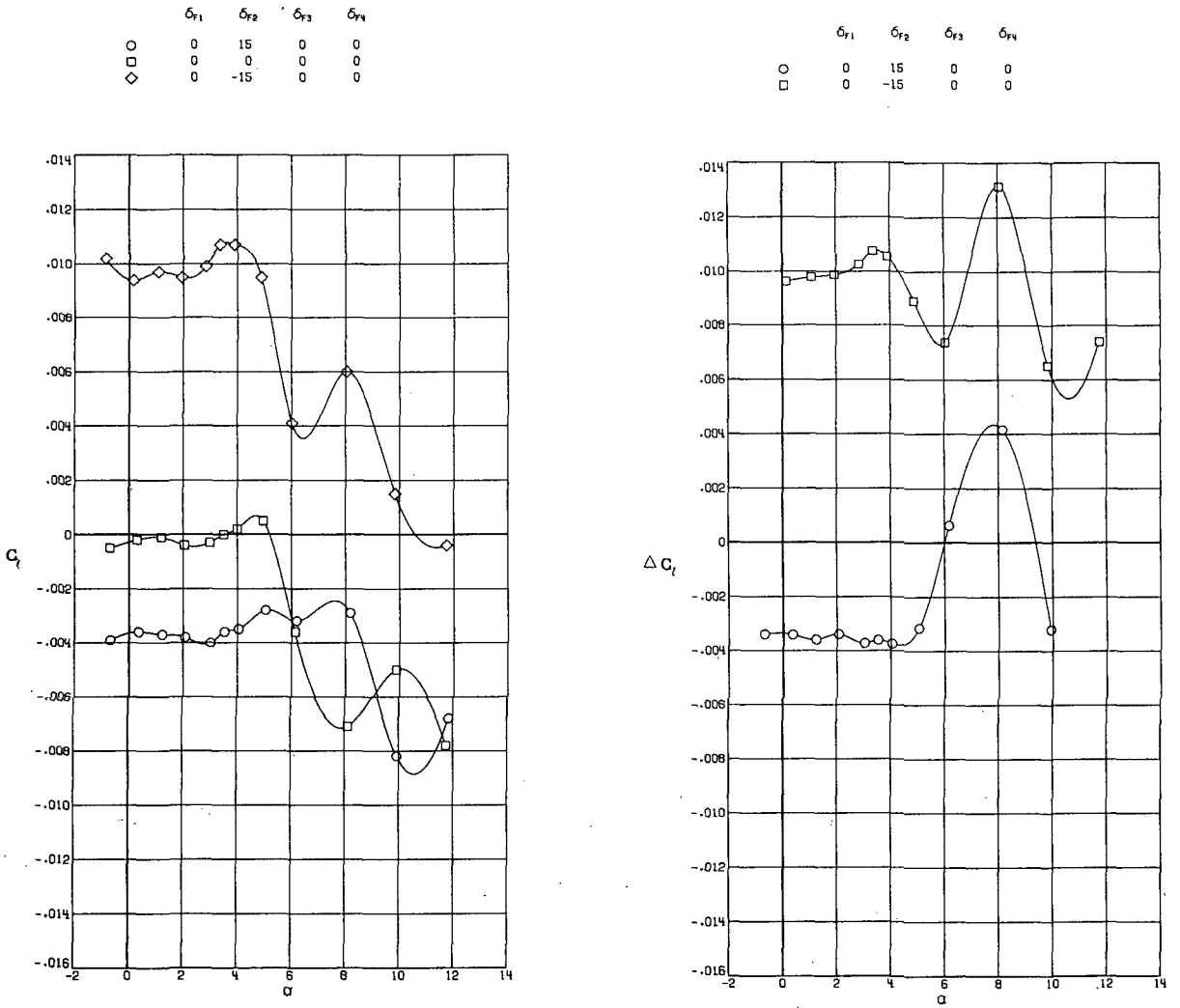
(a) Drag characteristics.

Figure 14.- Effect of F_2 trailing-edge control deflection on aerodynamic characteristics of model with cylindrical fuselage at $M_\infty = 0.88$.



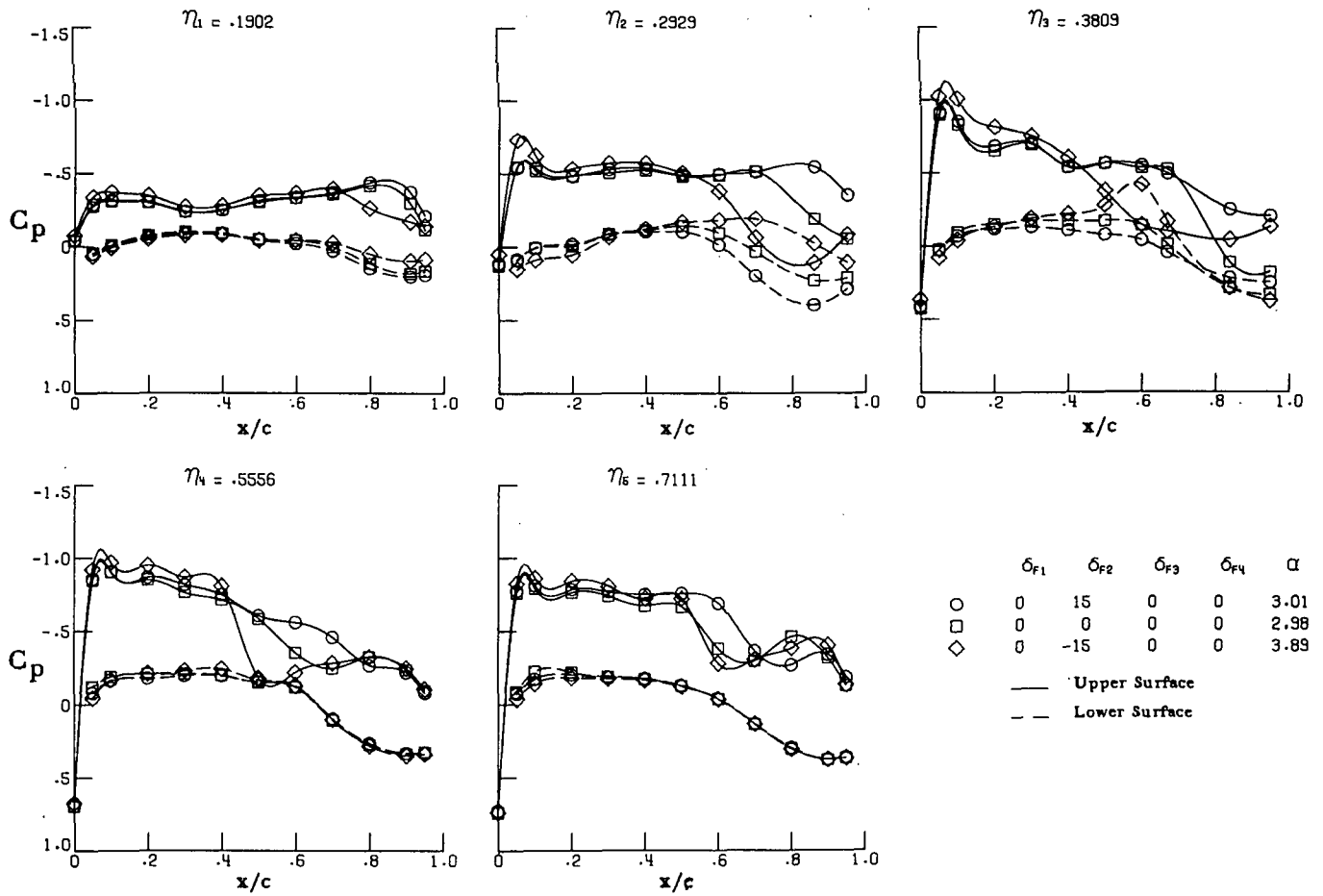
(b) Lift and pitch characteristics.

Figure 14.- Continued.



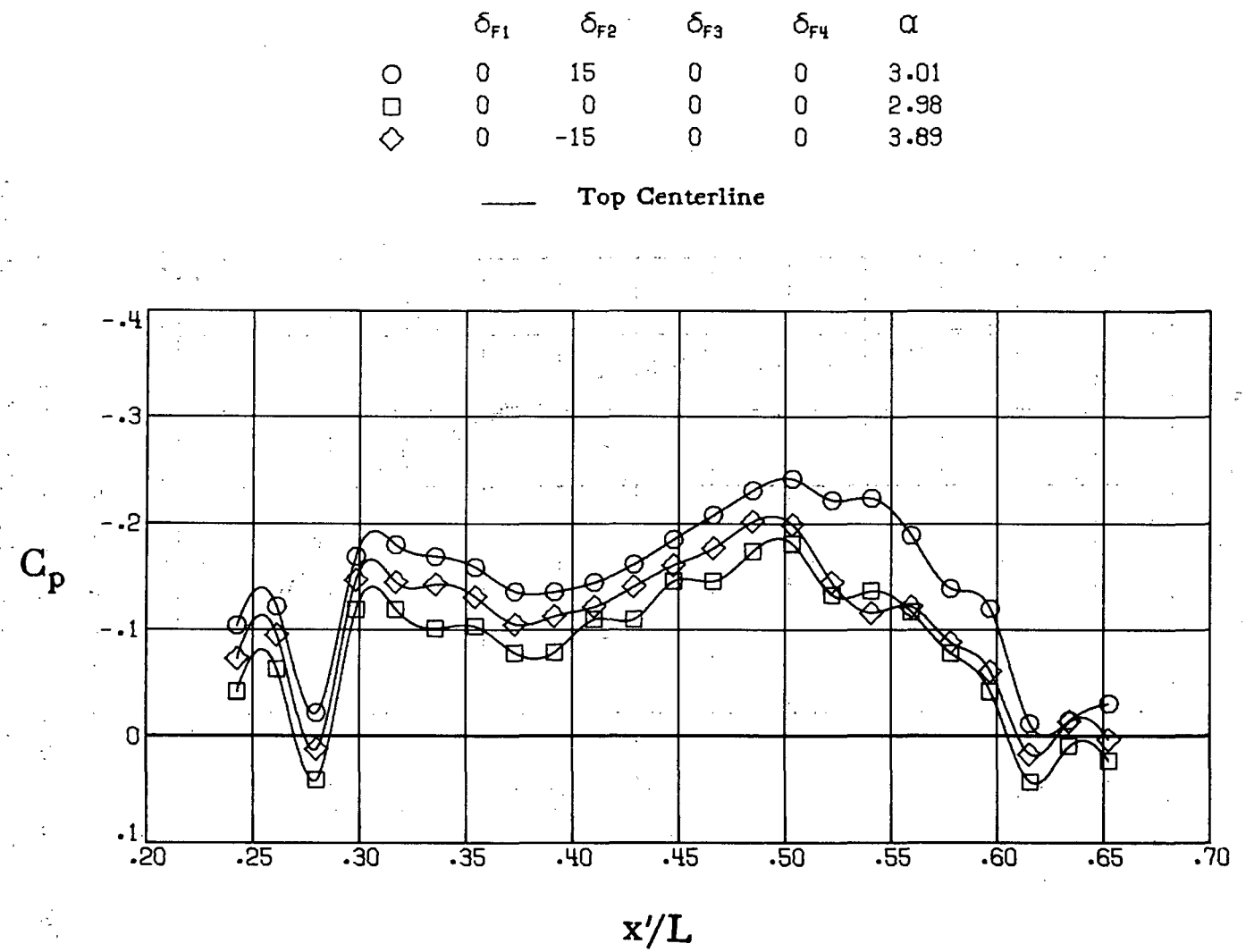
(c) Rolling-moment characteristics.

Figure 14.- Continued.



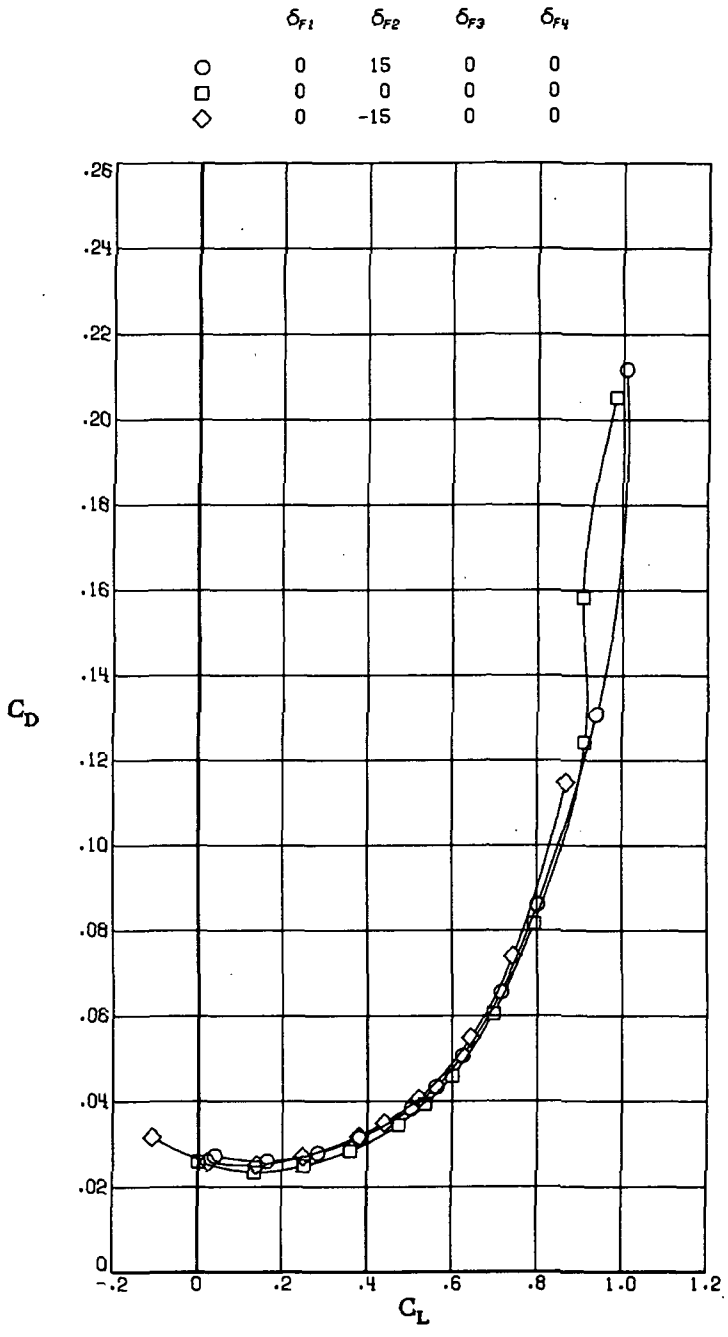
(d) Selected wing pressure distributions.

Figure 14.- Continued.



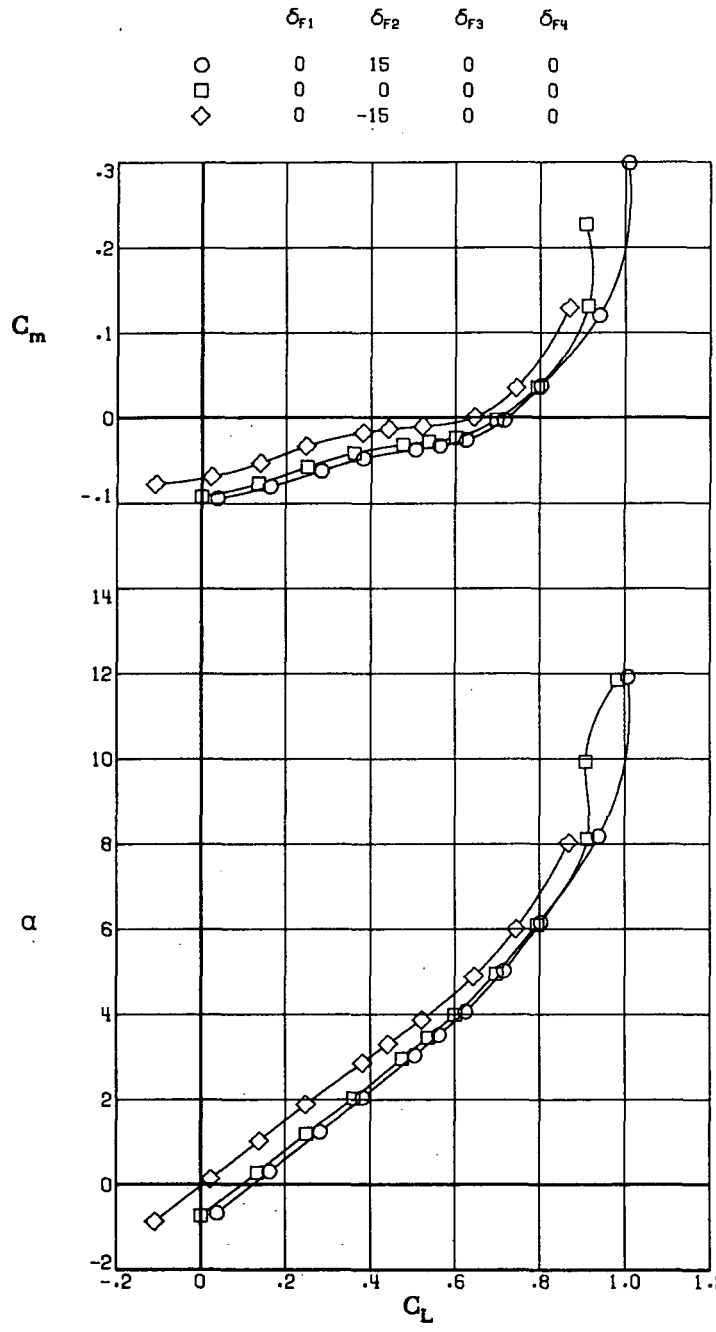
(e) Selected fuselage pressure distributions.

Figure 14.- Concluded.



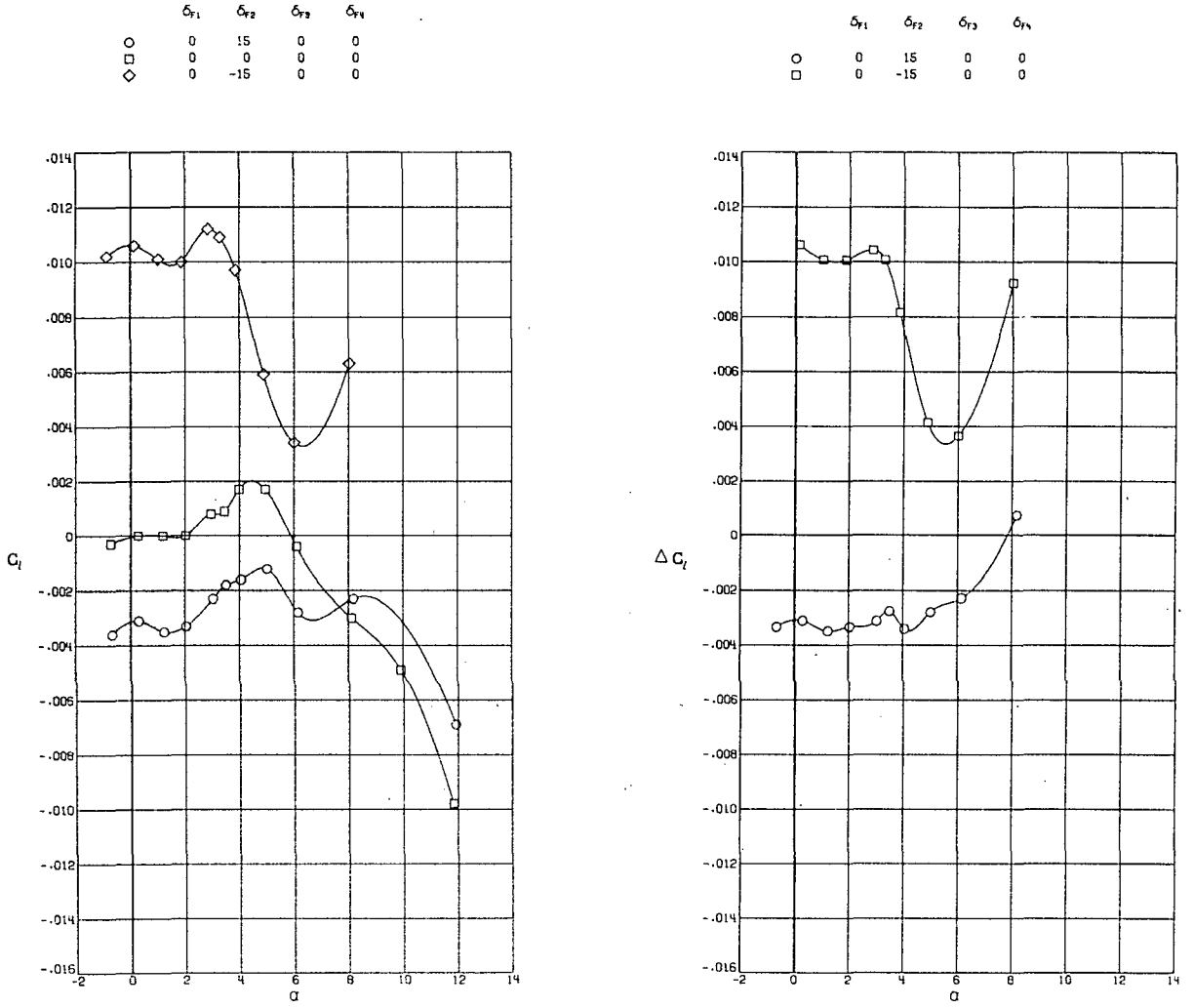
(a) Drag characteristics.

Figure 15.- Effect of F_2 trailing-edge control deflection on aerodynamic characteristics of model with cylindrical fuselage at $M_\infty = 0.90$.



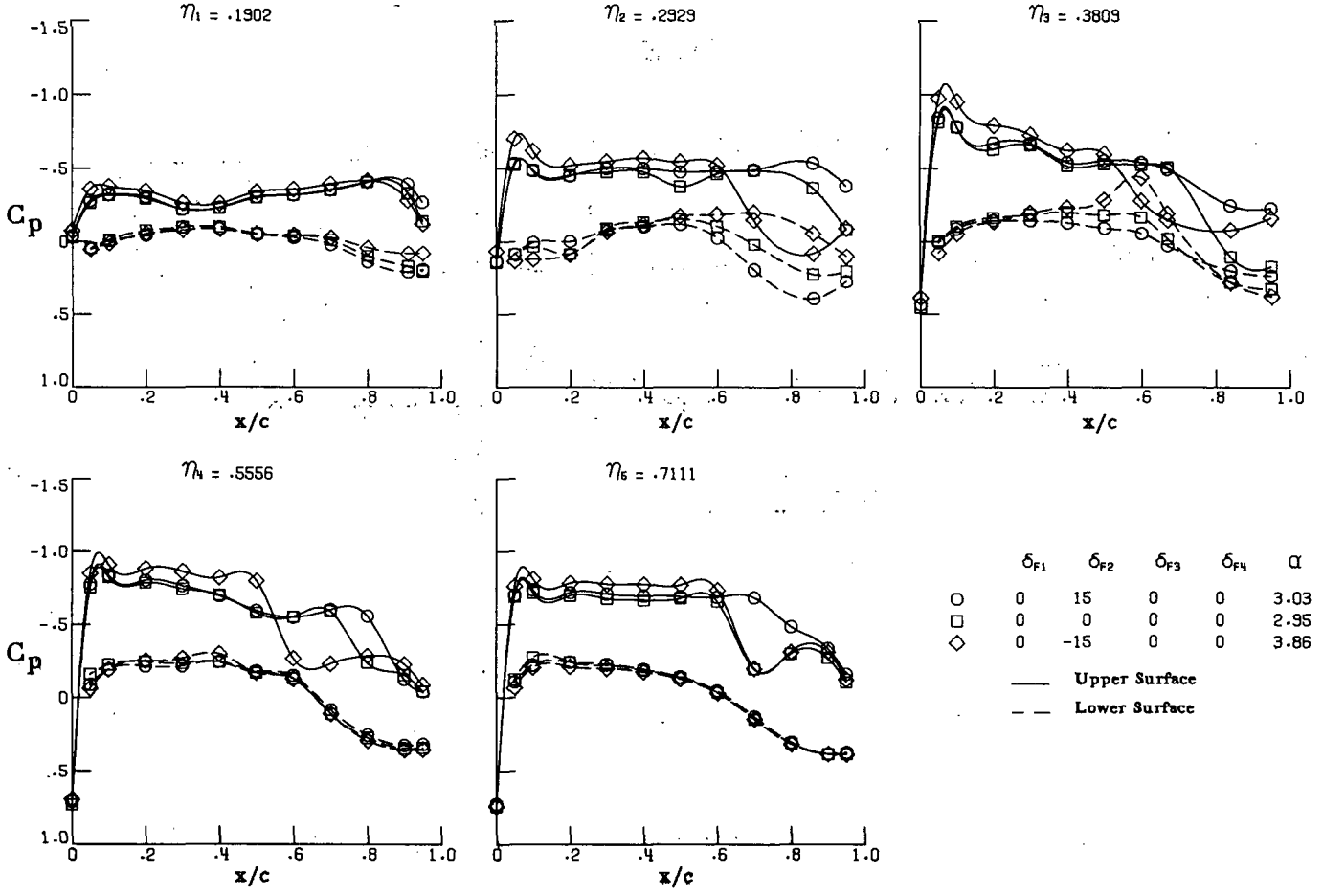
(b) Lift and pitch characteristics.

Figure 15.- Continued.



(c) Rolling-moment characteristics.

Figure 15.- Continued.

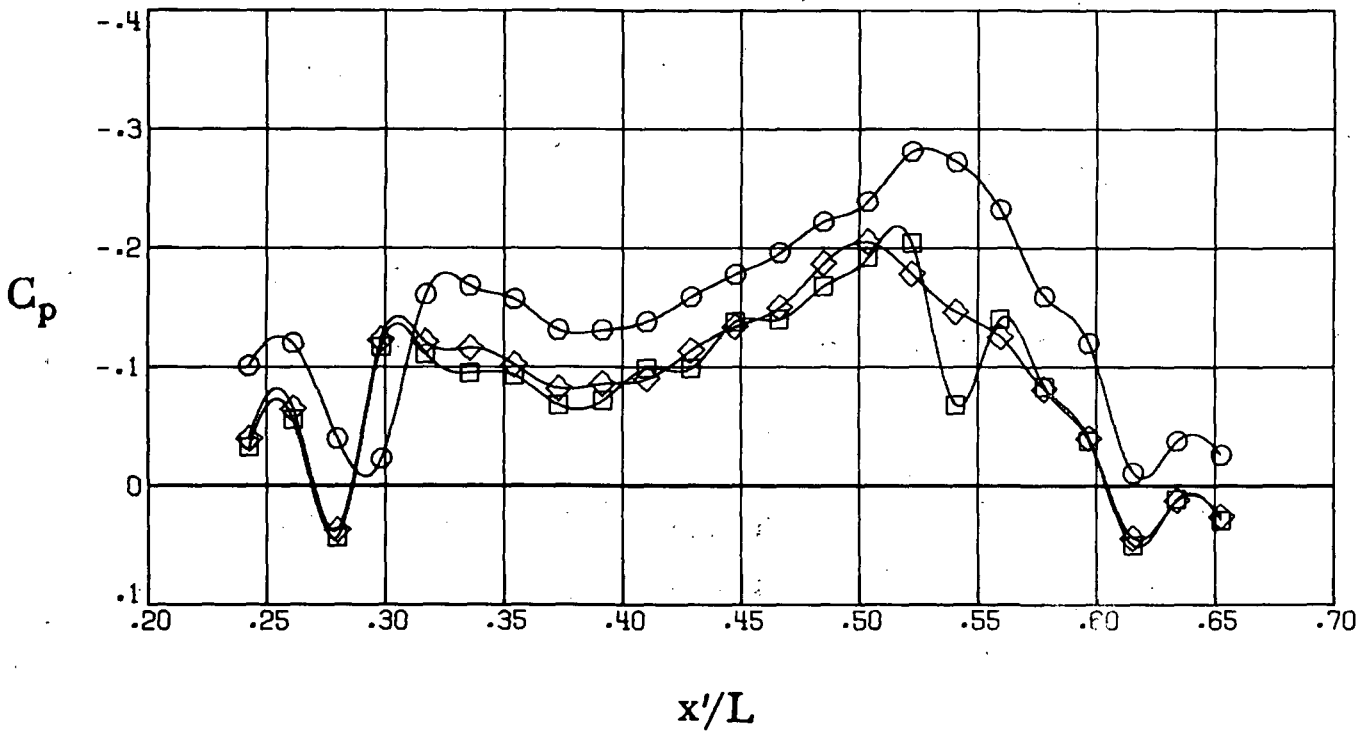


(d) Selected wing pressure distributions.

Figure 15.- Continued.

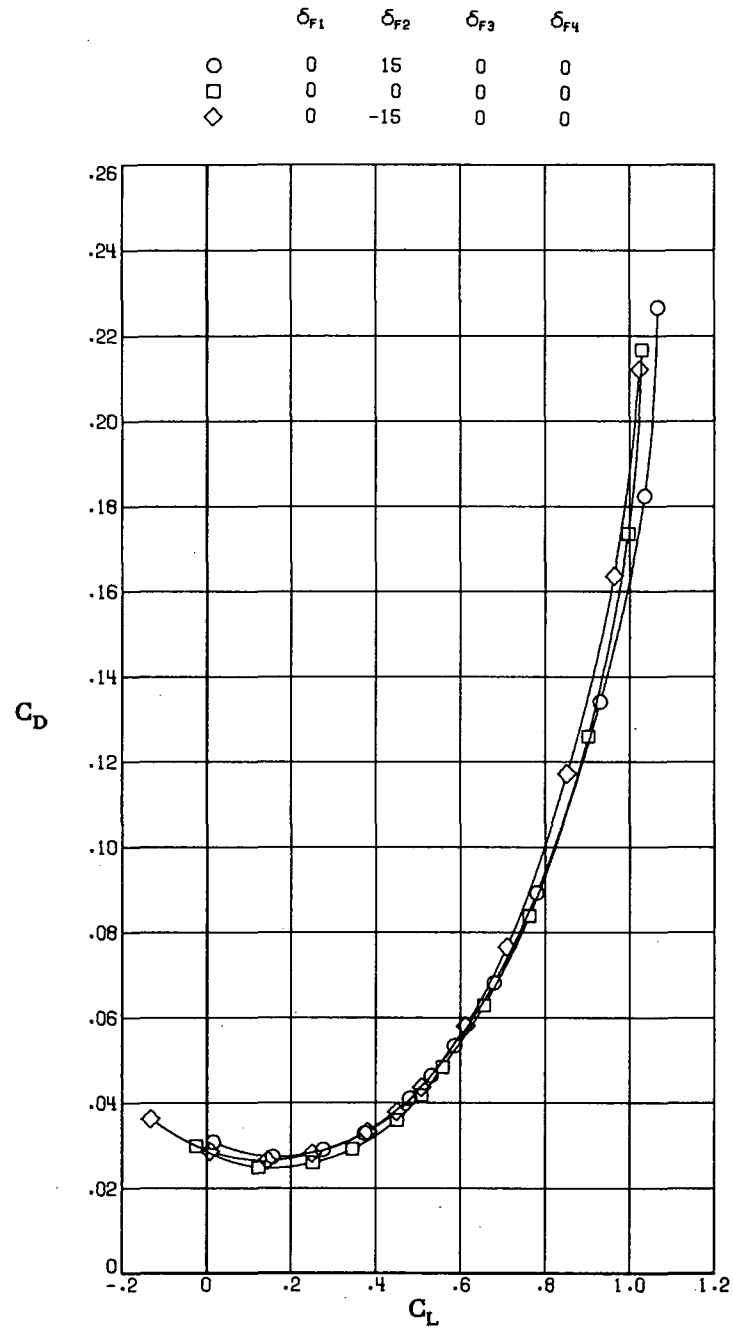
	δ_{F1}	δ_{F2}	δ_{F3}	δ_{F4}	α
○	0	15	0	0	3.03
□	0	0	0	0	2.95
◇	0	-15	0	0	3.86

—— Top Centerline



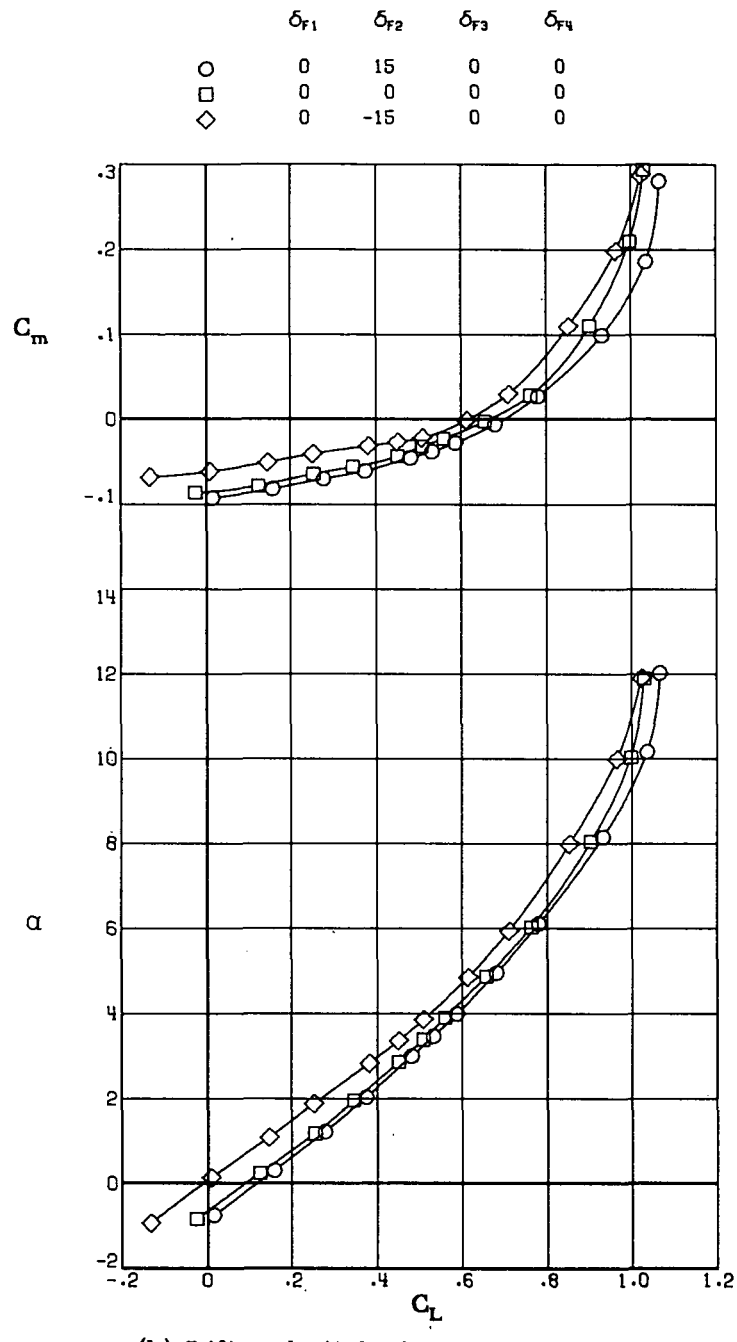
(e) Selected fuselage pressure distributions.

Figure 15.- Concluded.



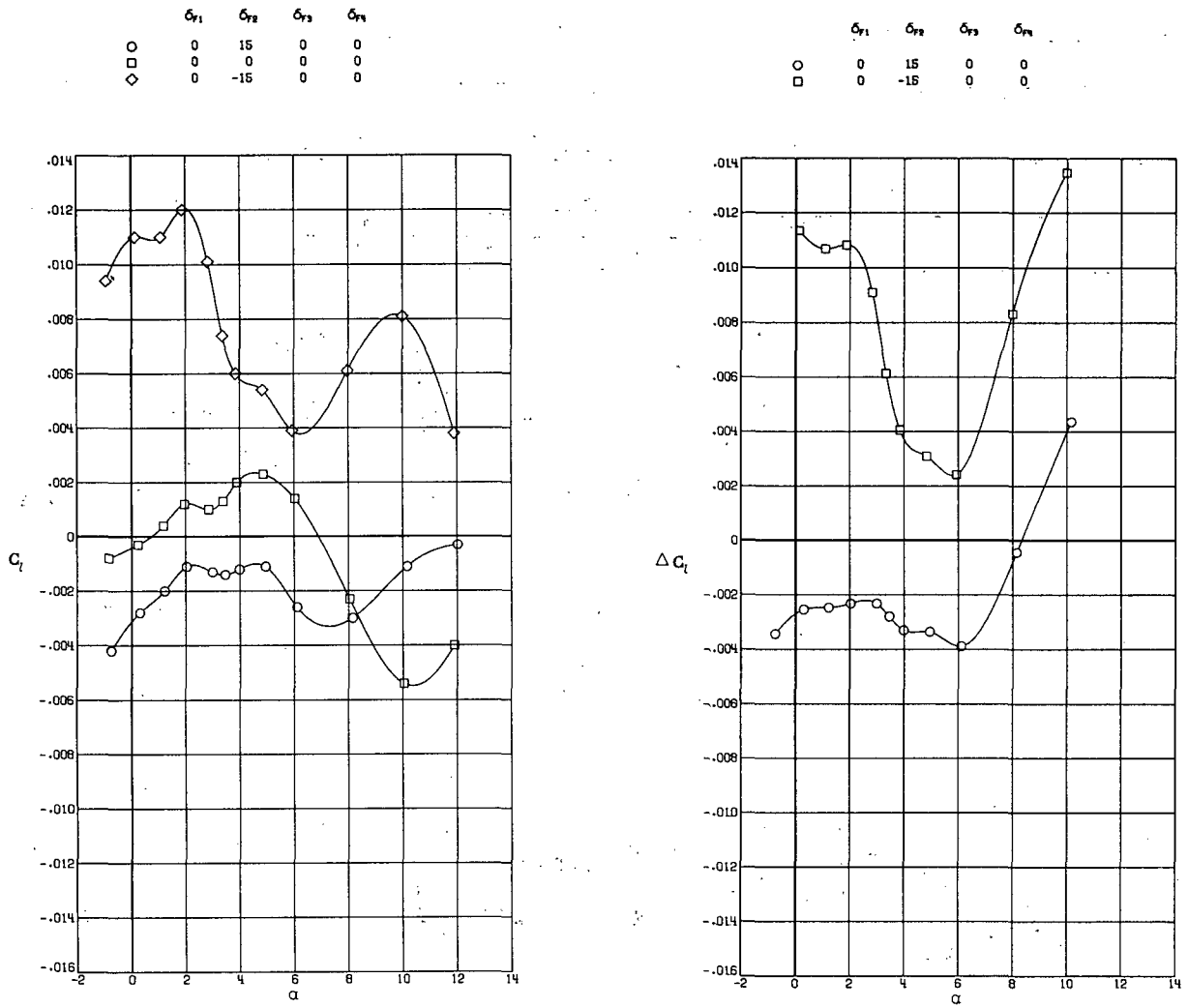
(a) Drag characteristics.

Figure 16.- Effect of F_2 trailing-edge control deflection on aerodynamic characteristics of model with cylindrical fuselage at $M_\infty = 0.92$.



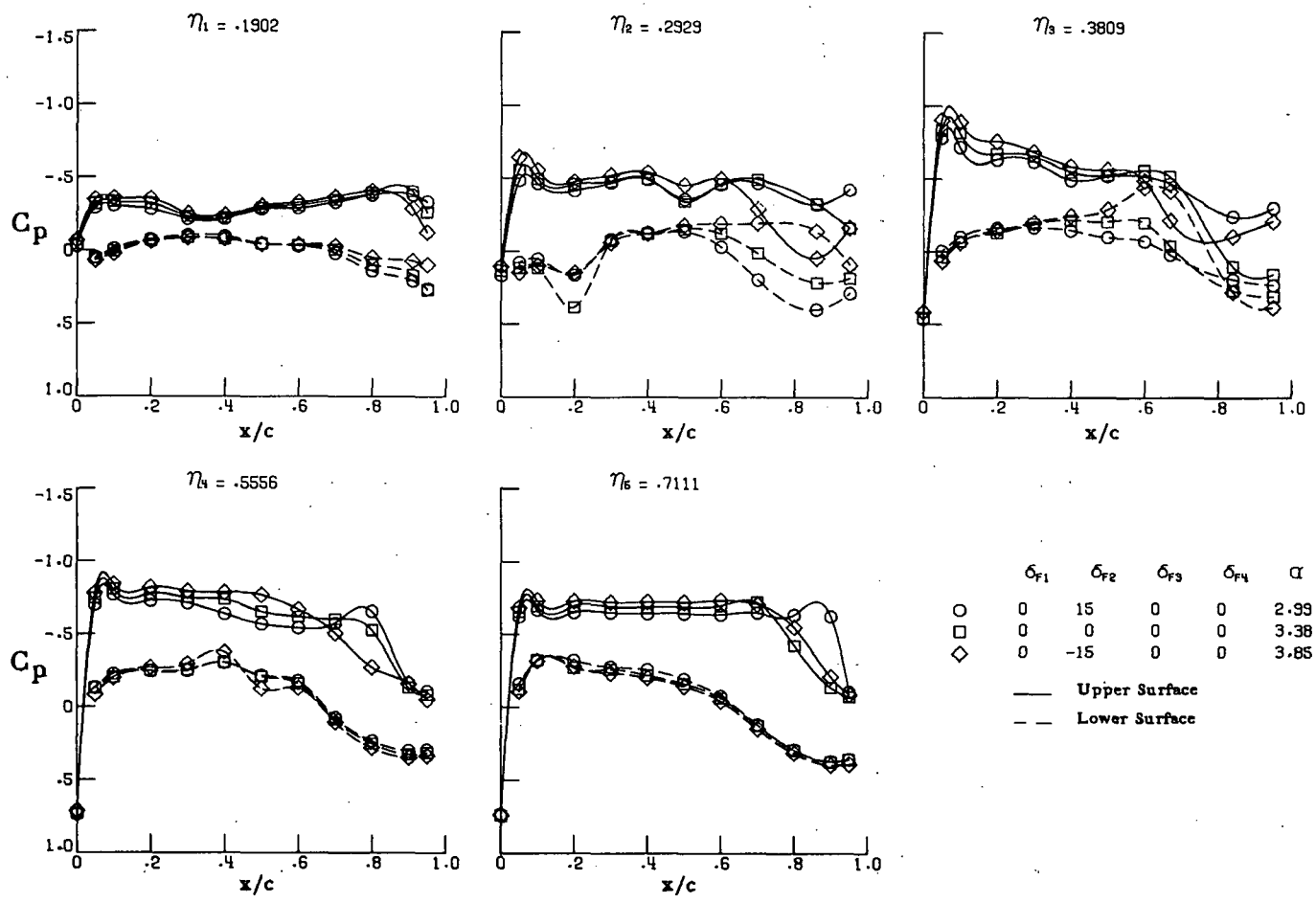
(b) Lift and pitch characteristics.

Figure 16.- Continued.



(c) Rolling-moment characteristics.

Figure 16.- Continued.

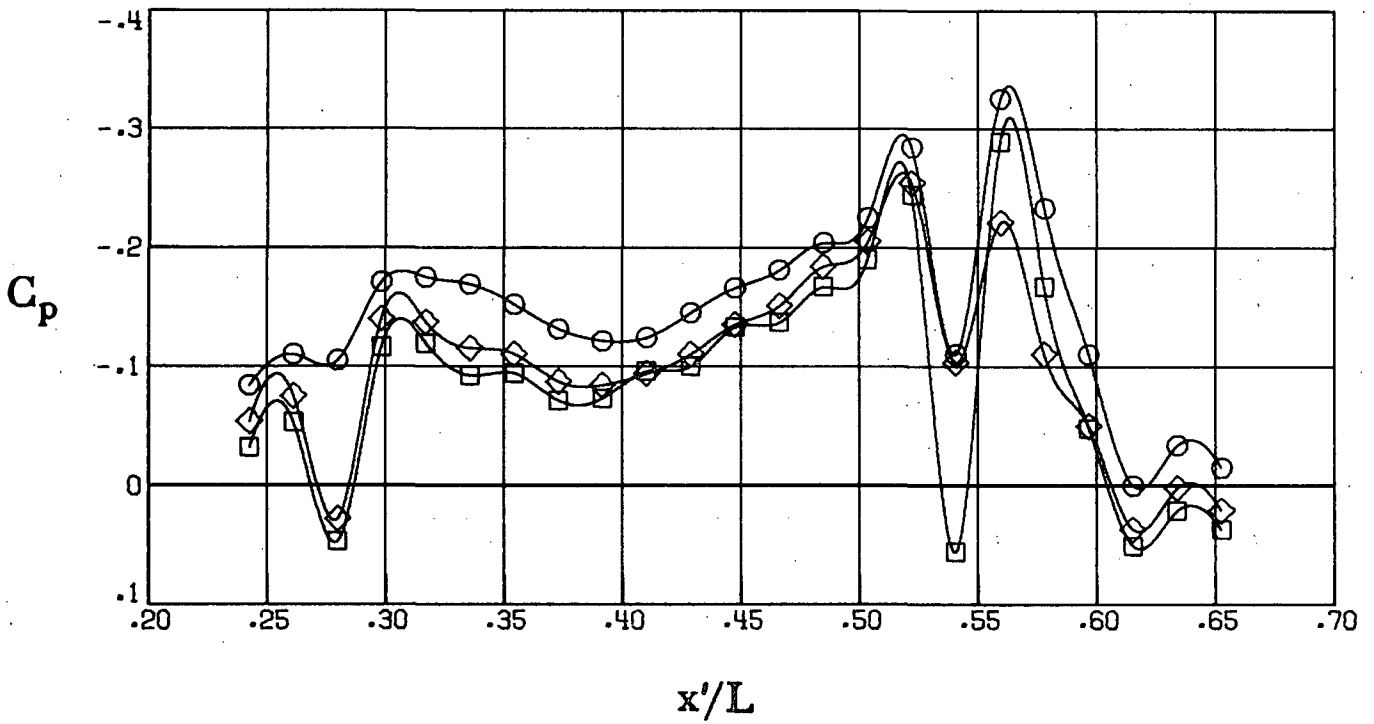


(d) Selected wing pressure distributions.

Figure 16.- Continued.

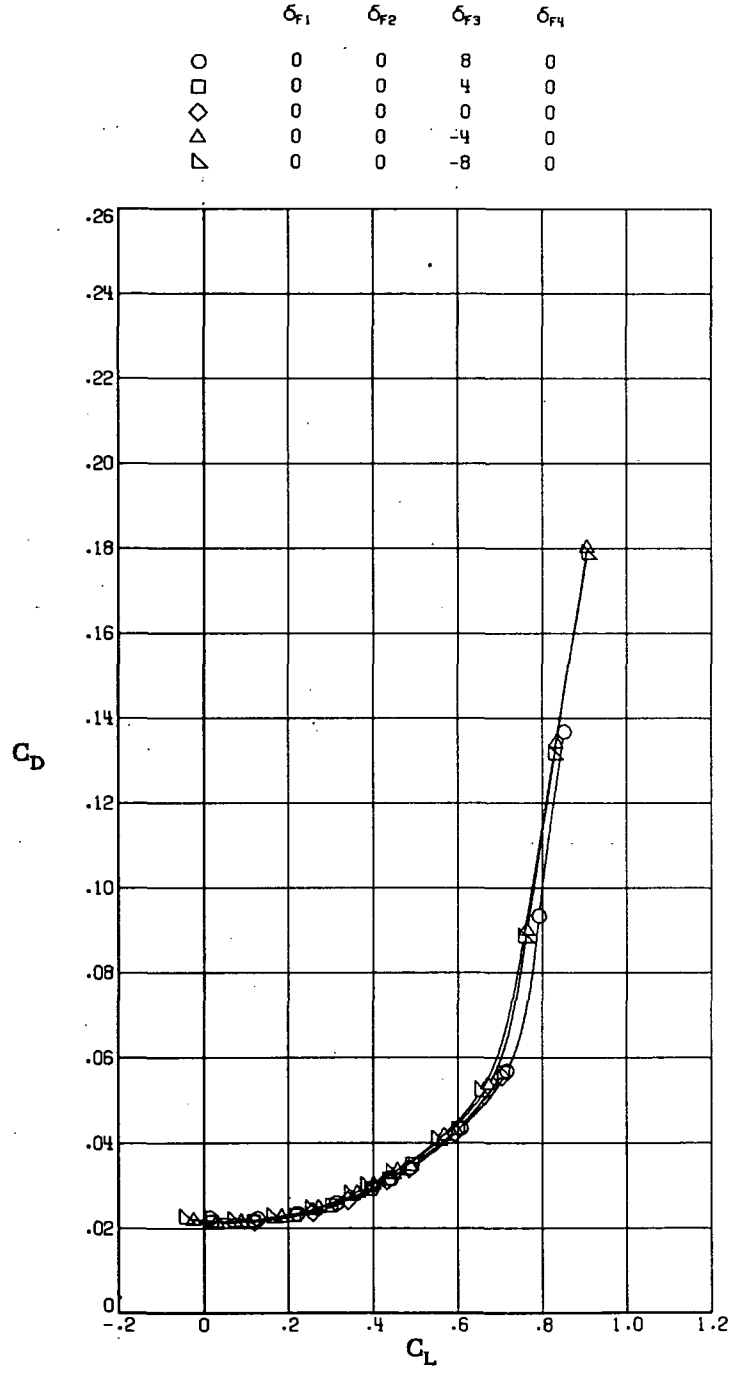
	δ_{F1}	δ_{F2}	δ_{F3}	δ_{F4}	α
○	0	15	0	0	2.99
□	0	0	0	0	3.38
◇	0	-15	0	0	3.85

—— Top Centerline



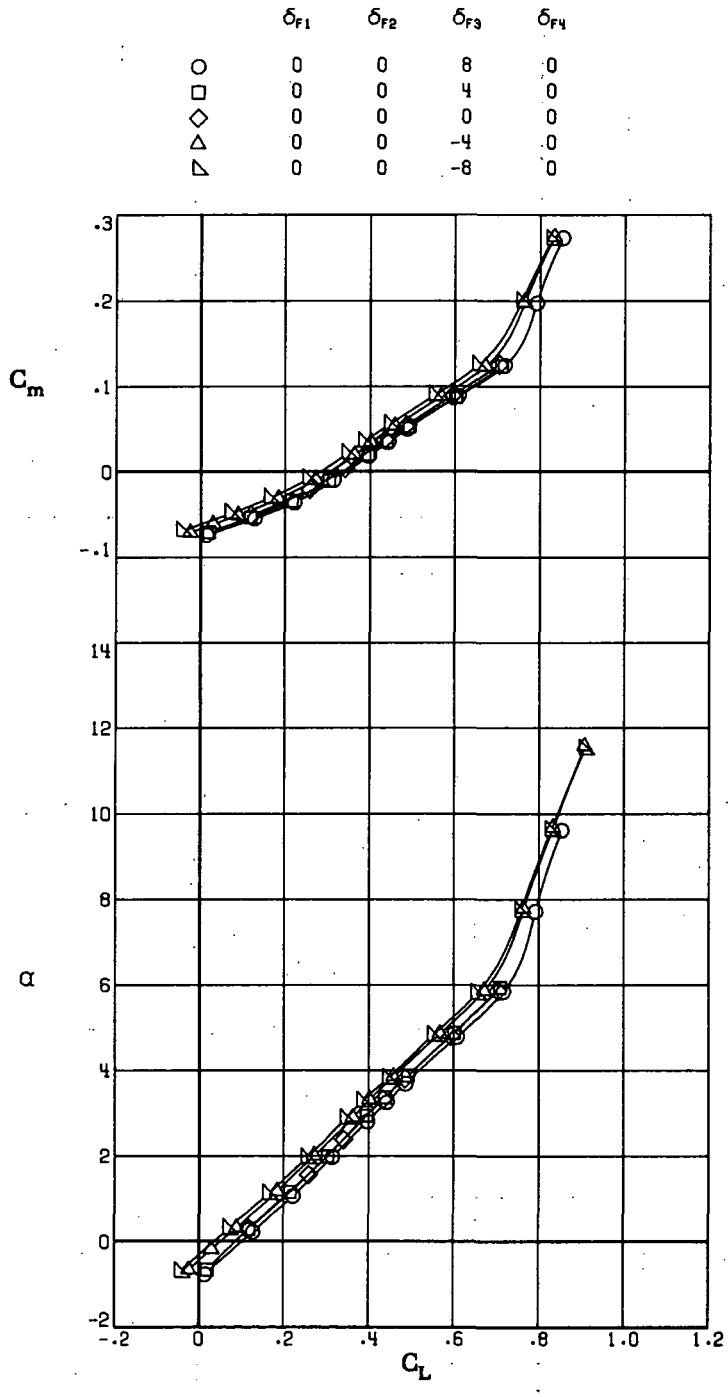
(e) Selected fuselage pressure distributions.

Figure 16.- Concluded.



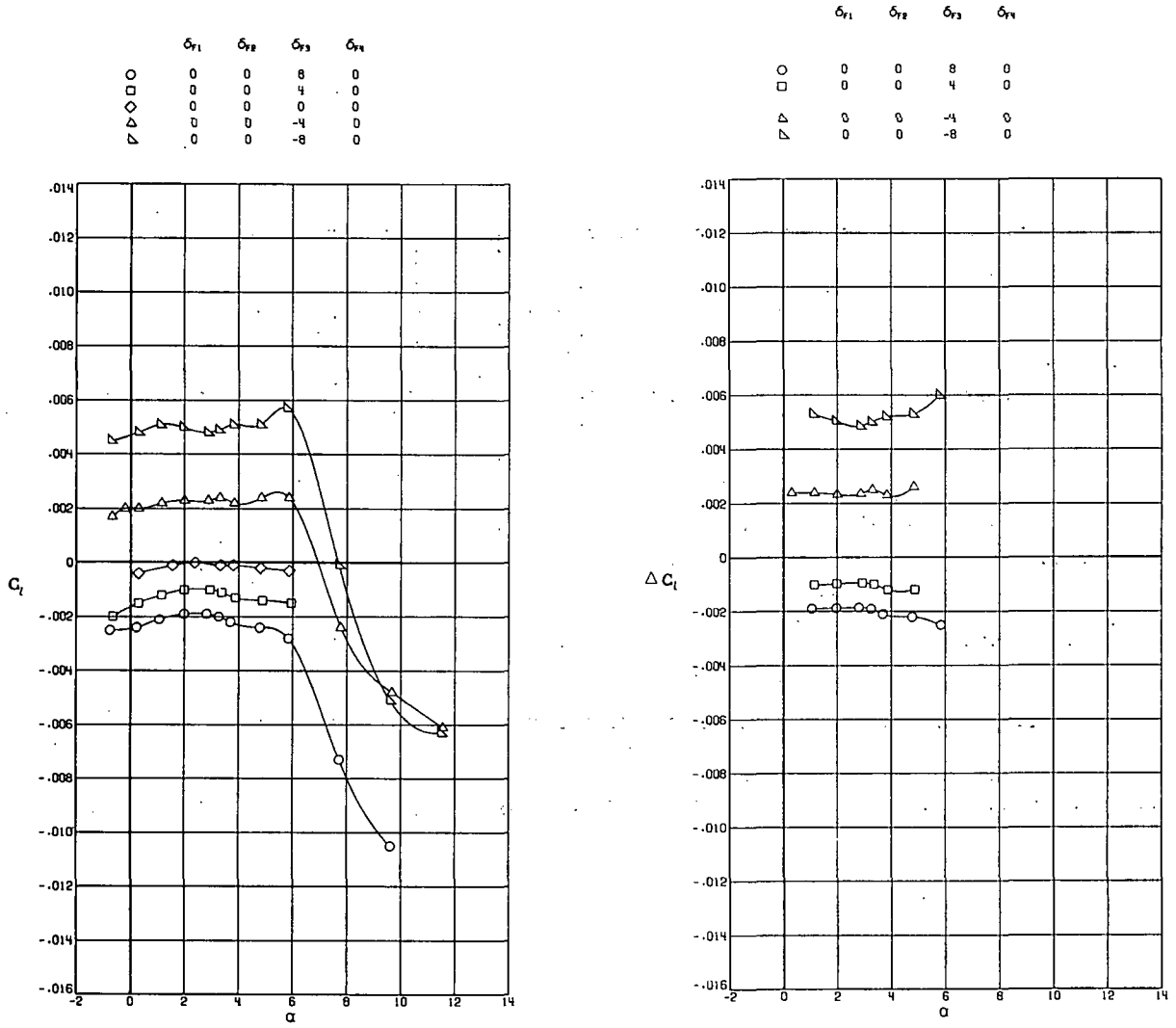
(a) Drag characteristics.

Figure 17.- Effect of F_3 trailing-edge control deflection on aerodynamic characteristics of model with area-ruled fuselage at $M_\infty = 0.80$.



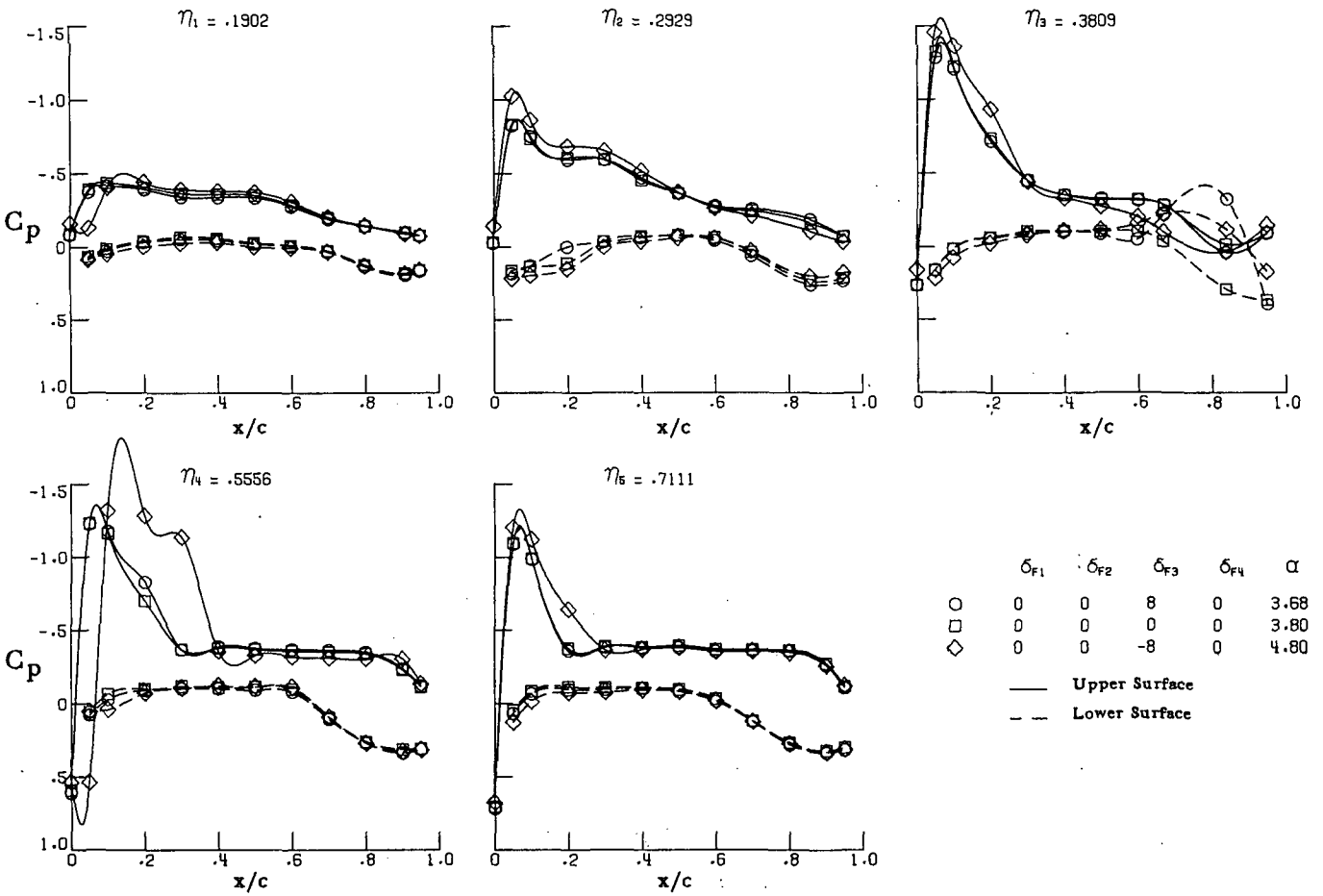
(b) Lift and pitch characteristics.

Figure 17.- Continued.



(c) Rolling-moment characteristics.

Figure 17.- Continued.



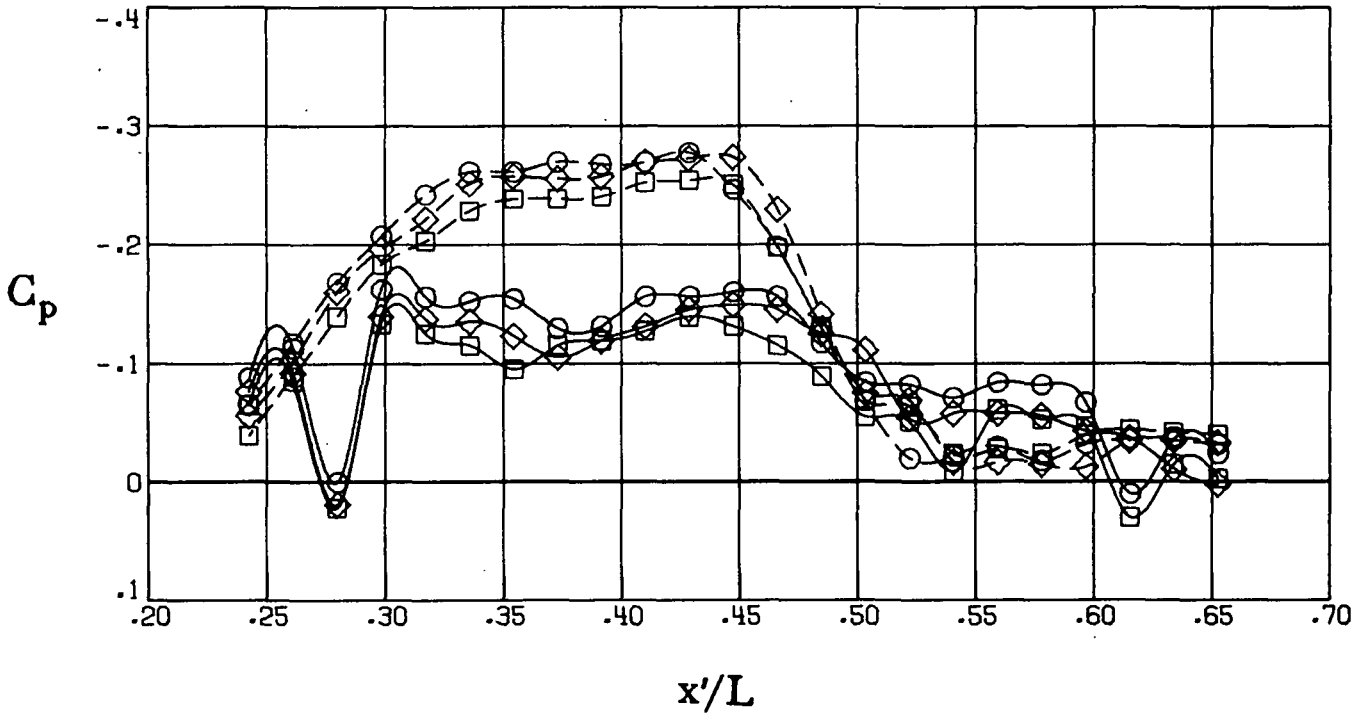
(d) Selected wing pressure distributions.

Figure 17.- Continued.

	δ_{F1}	δ_{F2}	δ_{F3}	δ_{F4}	α
○	0	0	8	0	3.68
□	0	0	0	0	3.80
◇	0	0	-8	0	4.80

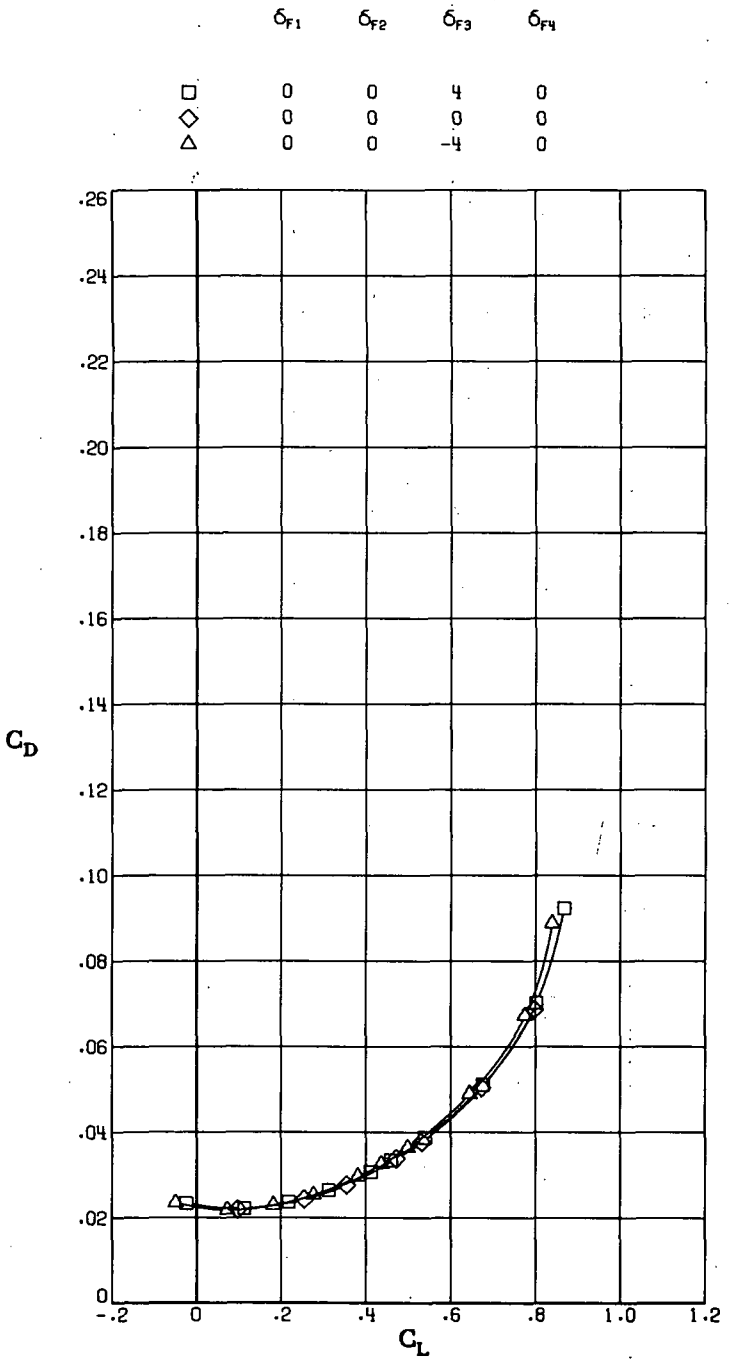
—— Top Centerline

– – Right Side



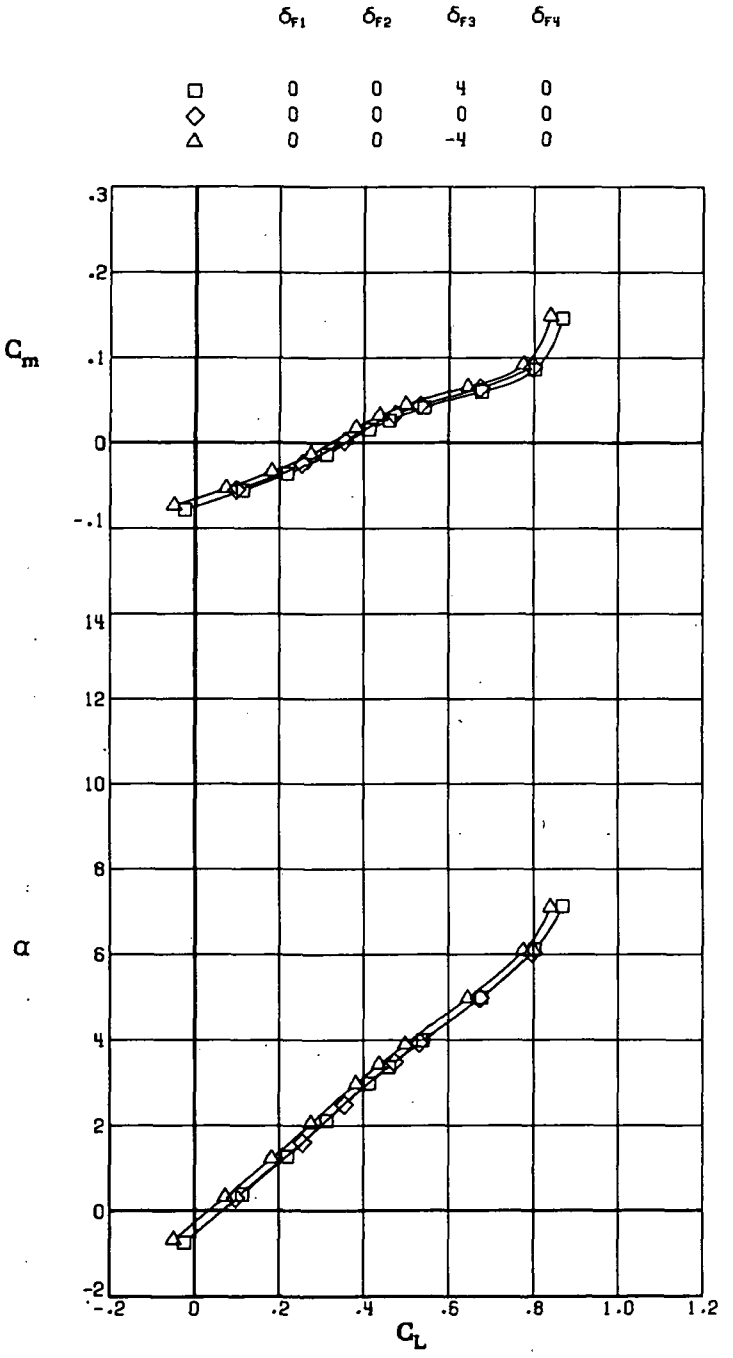
(e) Selected fuselage pressure distributions.

Figure 17.- Concluded.



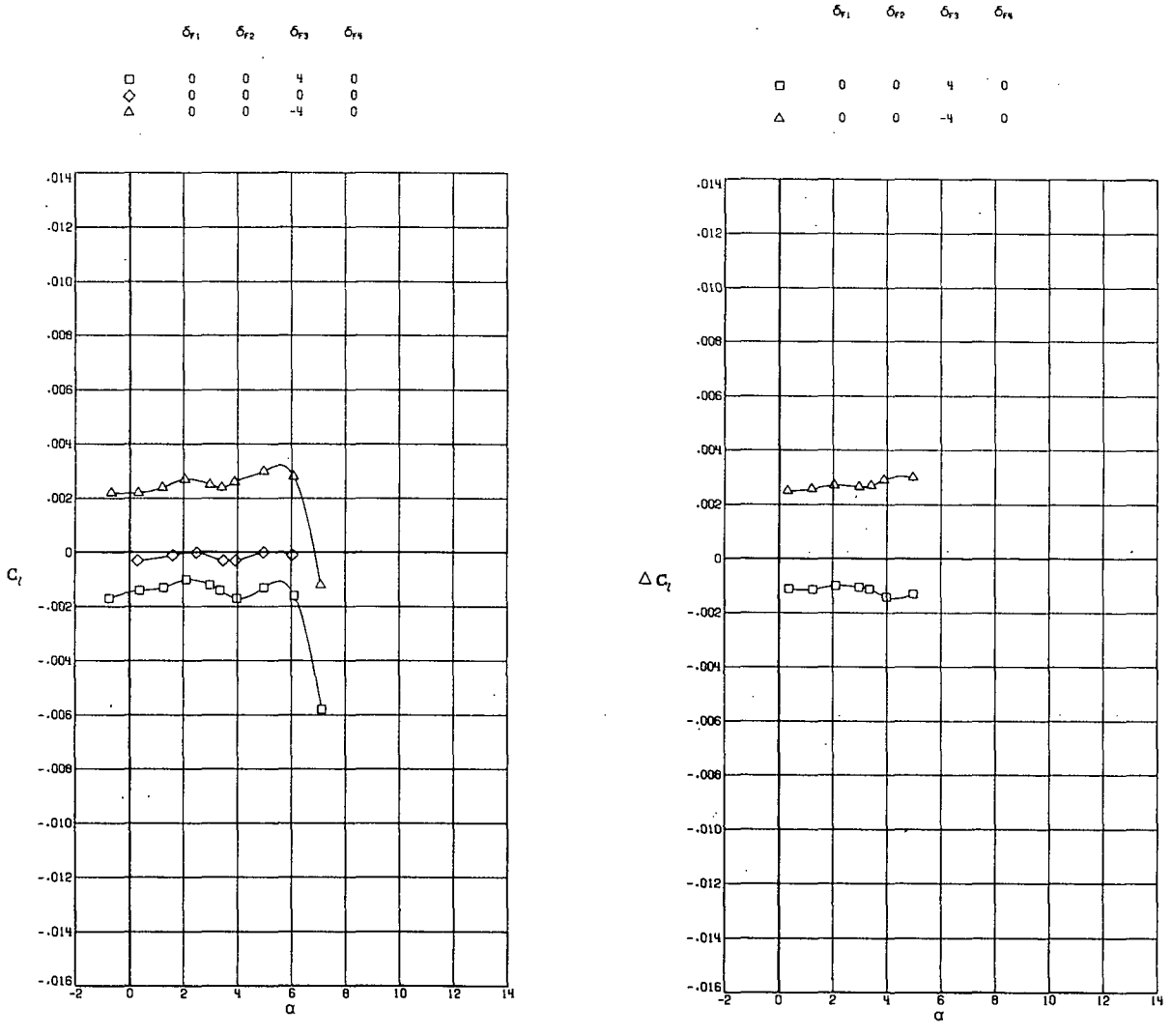
(a) Drag characteristics.

Figure 18.- Effect of F_3 trailing-edge control deflection on aerodynamic characteristics of model with area-ruled fuselage at $M_\infty = 0.86$.



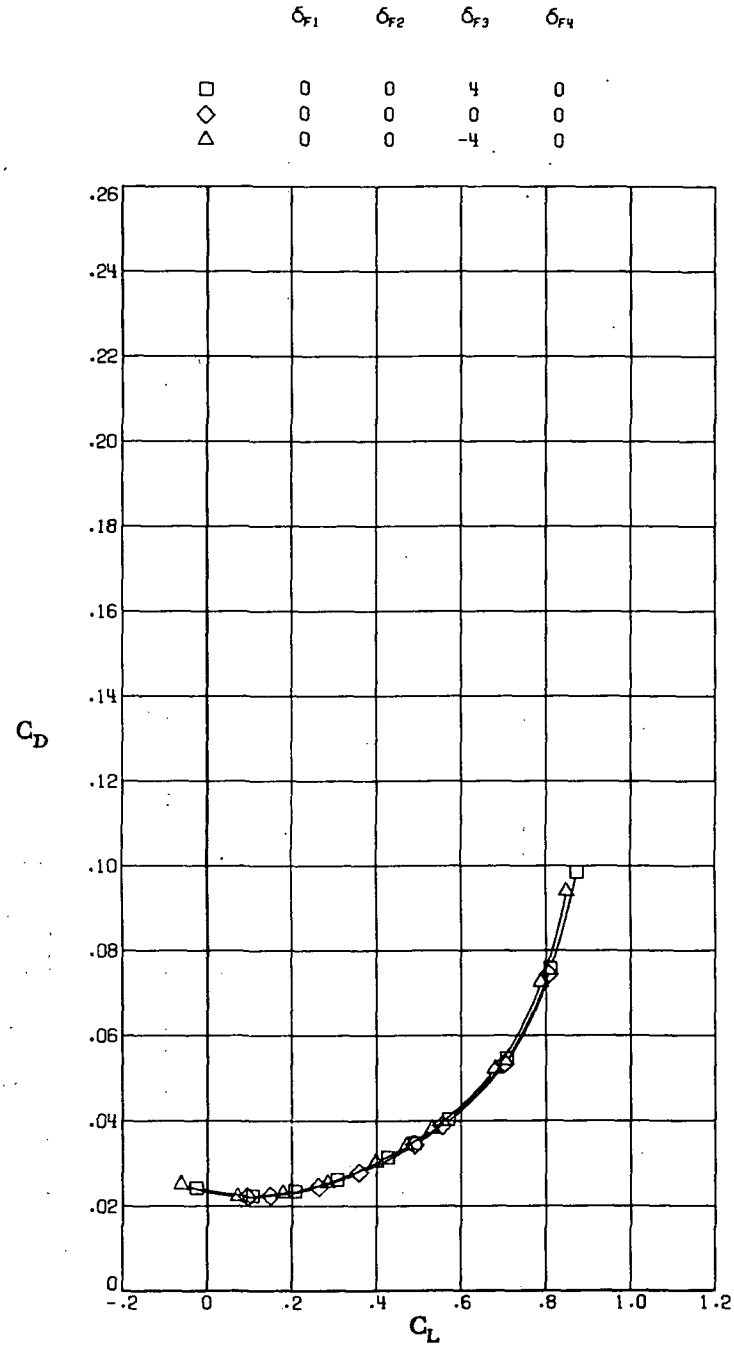
(b) Lift and pitch characteristics.

Figure 18.- Continued.



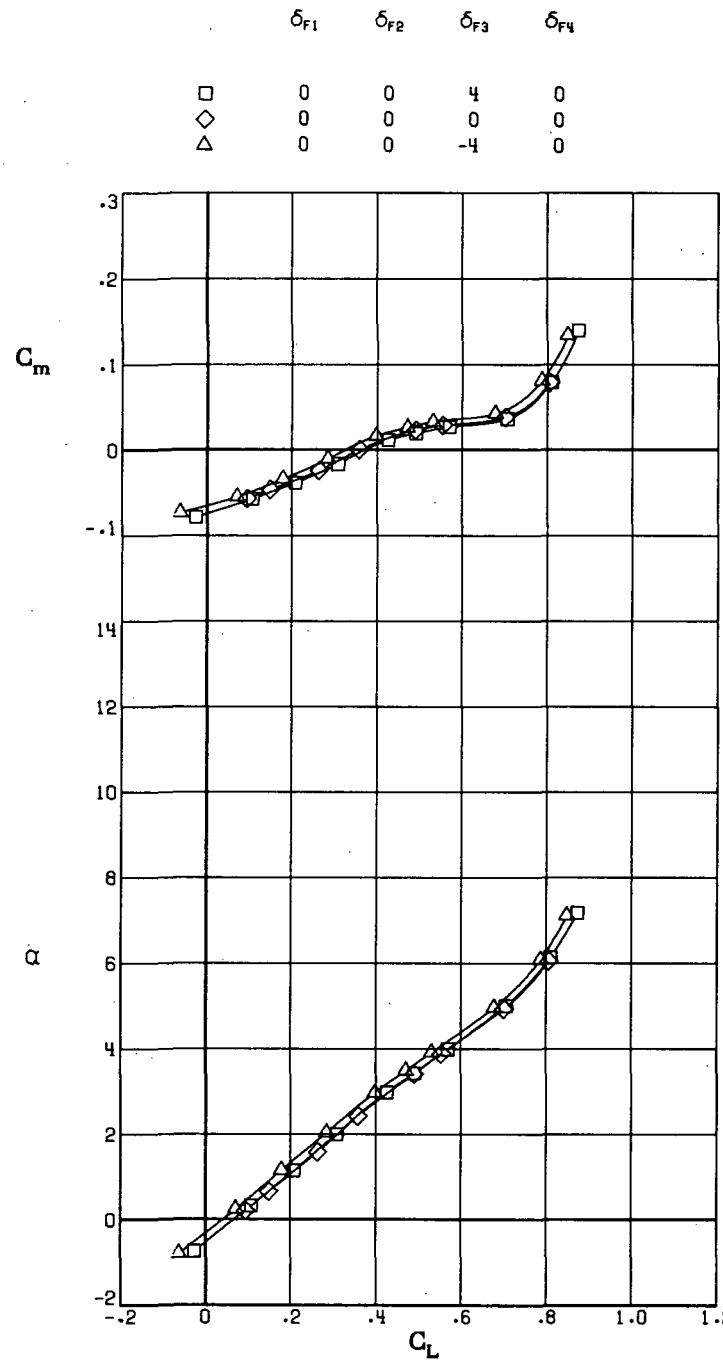
(c) Rolling-moment characteristics.

Figure 18.- Concluded.



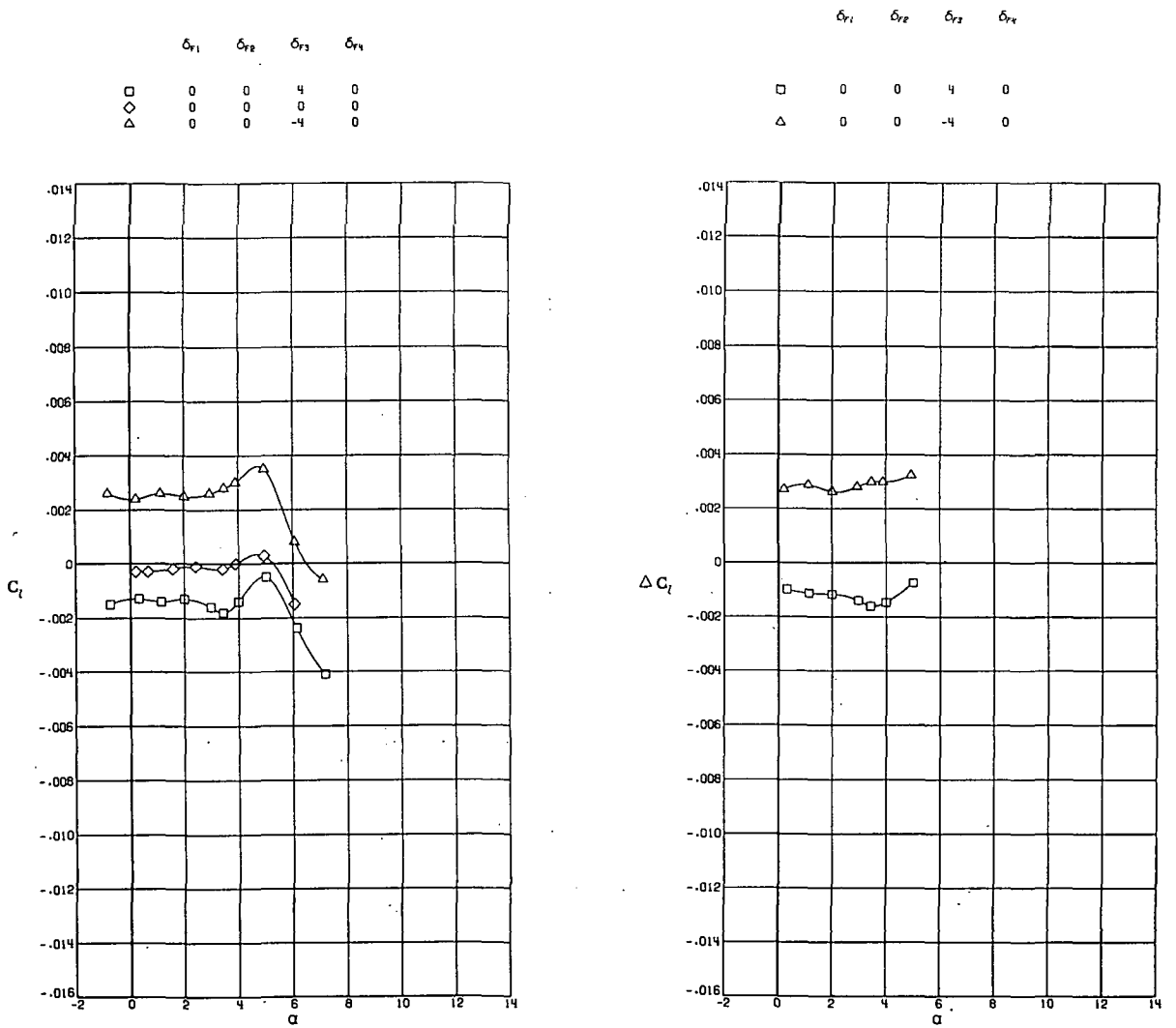
(a) Drag characteristics.

Figure 19.- Effect of F_3 trailing-edge control deflection on aerodynamic characteristics of model with area-ruled fuselage at $M_\infty = 0.88$.



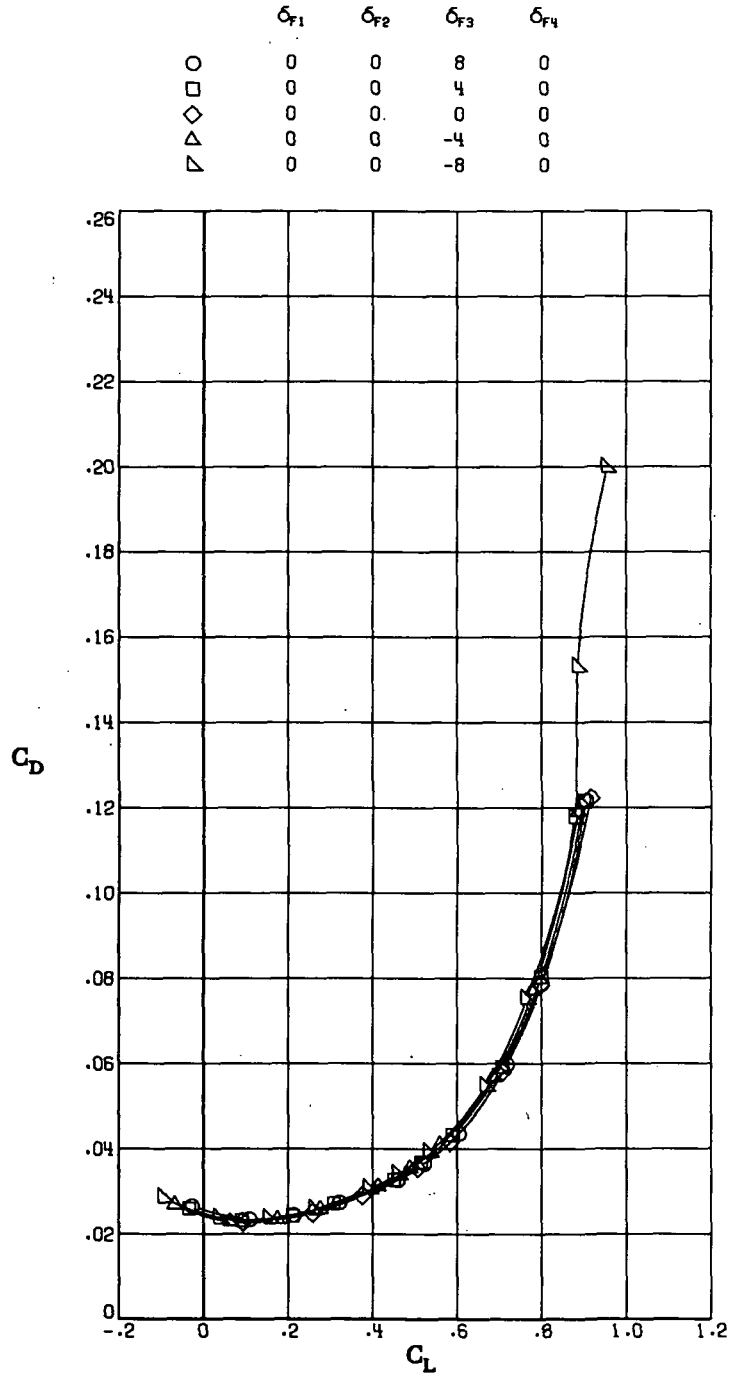
(b) Lift and pitch characteristics.

Figure 19.- Continued.



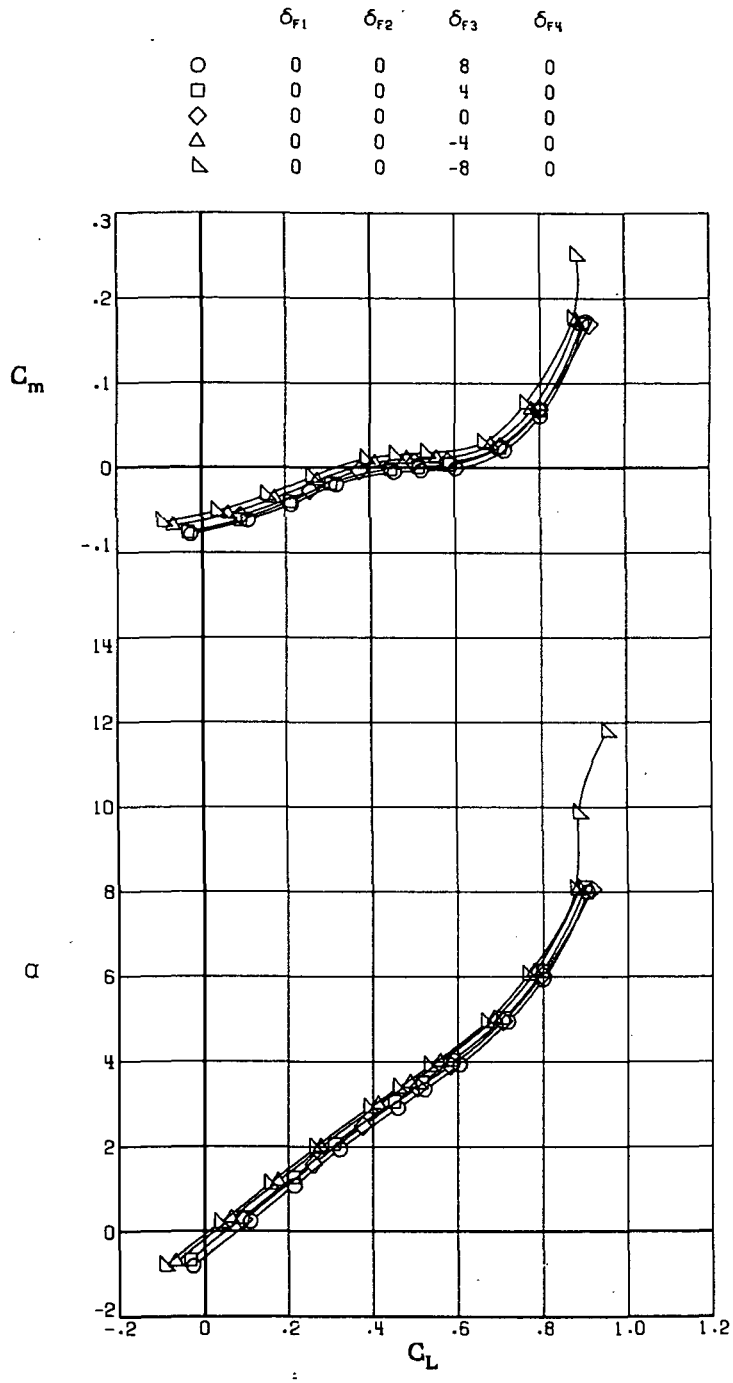
(c) Rolling-moment characteristics.

Figure 19.- Concluded.



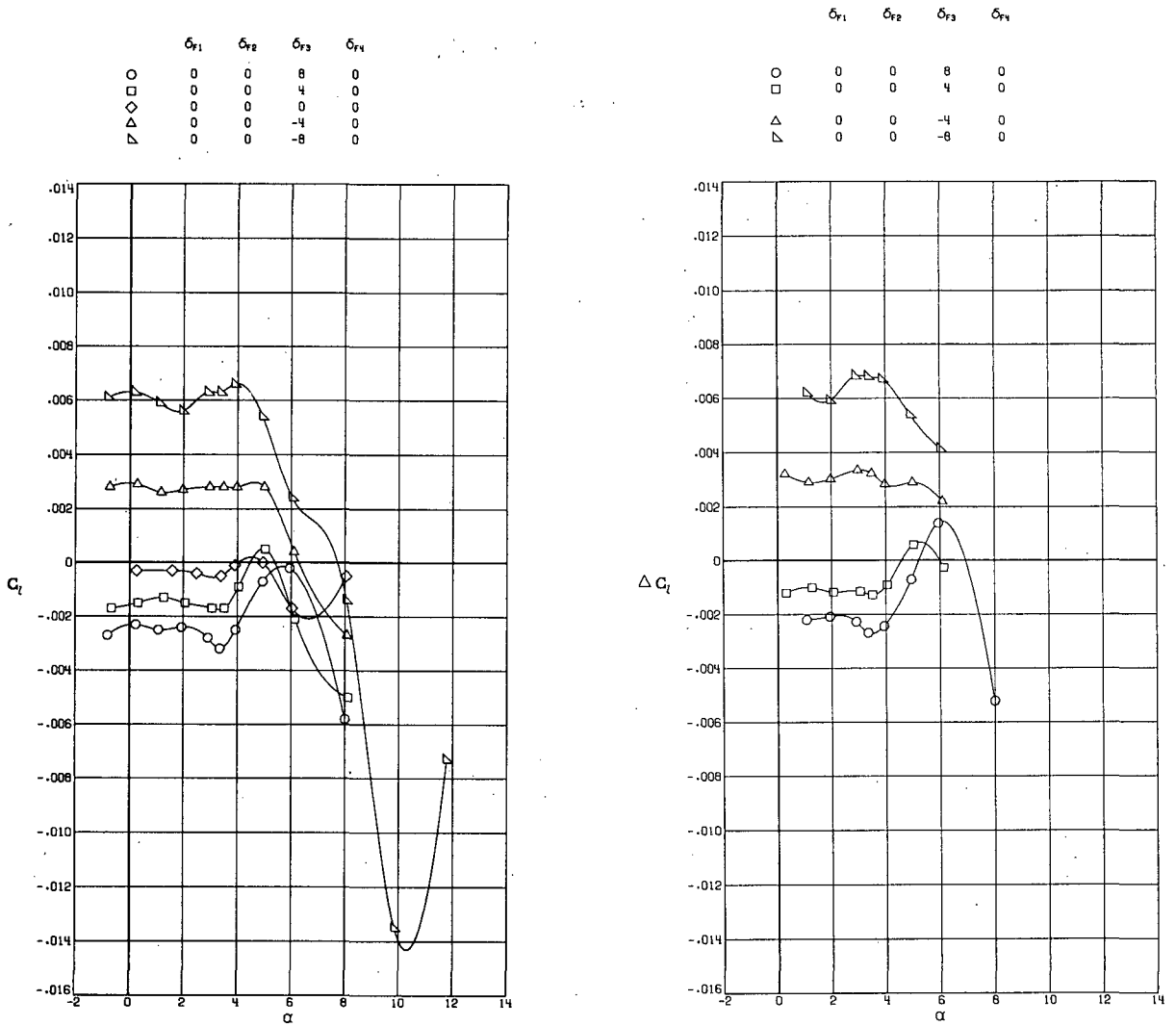
(a) Drag characteristics.

Figure 20.- Effect of F_3 trailing-edge control deflection on aerodynamic characteristics of model with area-ruled fuselage at $M_\infty = 0.90$.



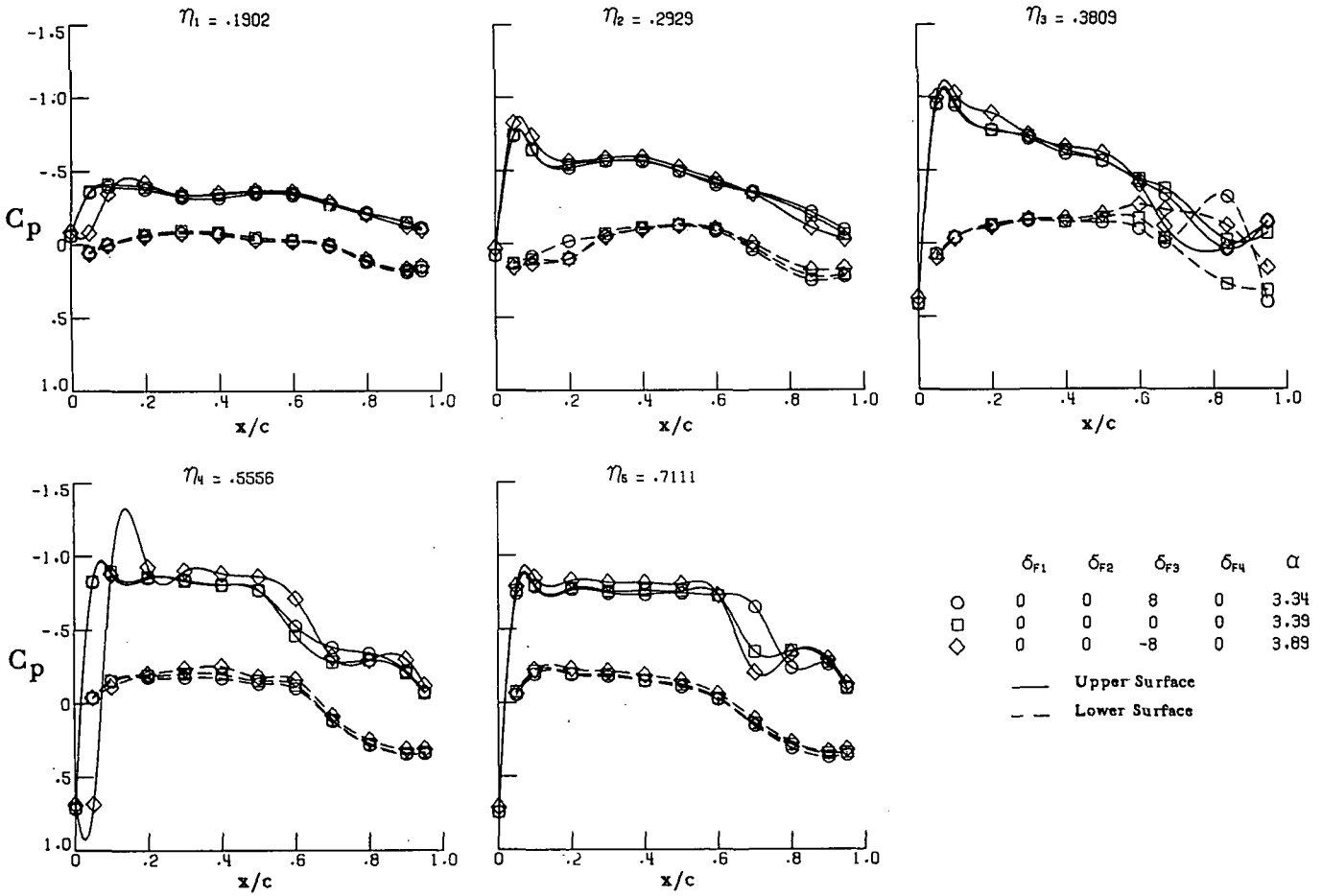
(b) Lift and pitch characteristics.

Figure 20.- Continued.



(c) Rolling-moment characteristics.

Figure 20.- Continued.



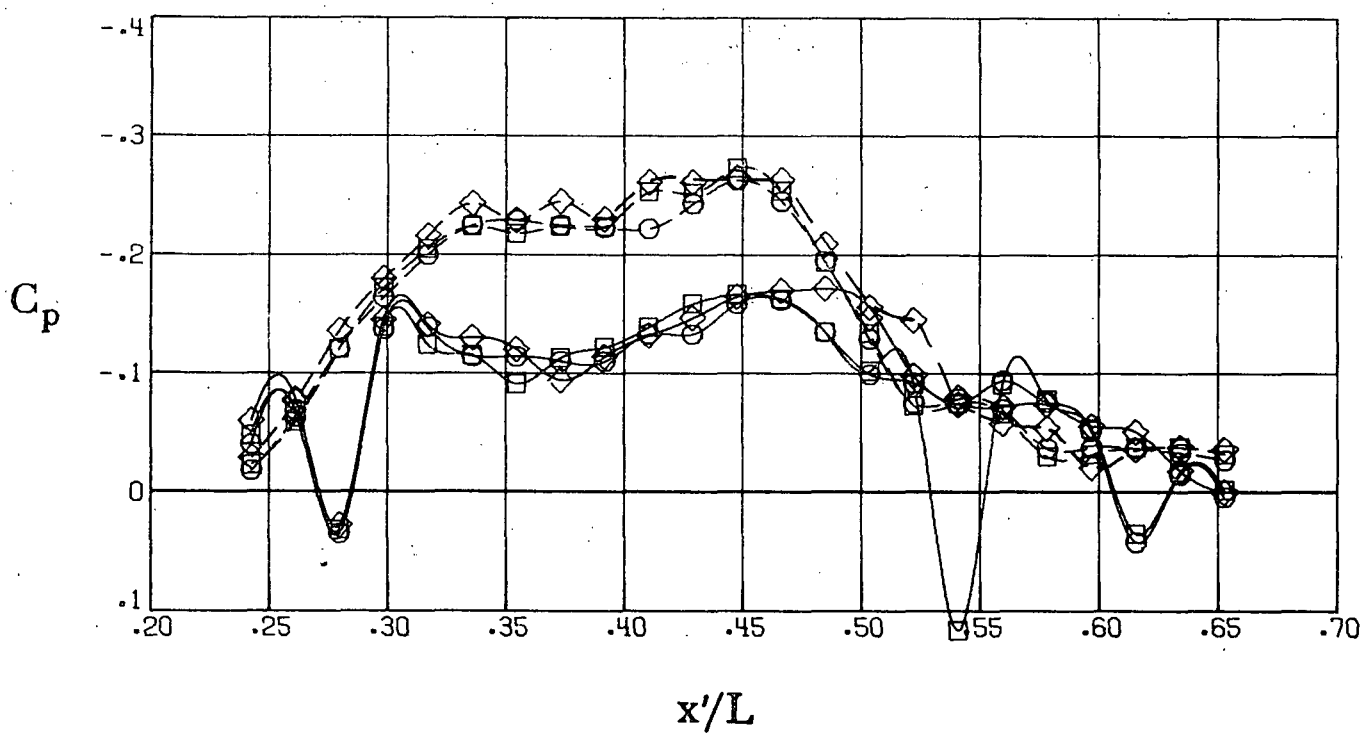
(d) Selected wing pressure distributions.

Figure 20.- Continued.

	δ_{F1}	δ_{F2}	δ_{F3}	δ_{F4}	α
○	0	0	8	0	3.34
□	0	0	0	0	3.39
◇	0	0	-8	0	3.89

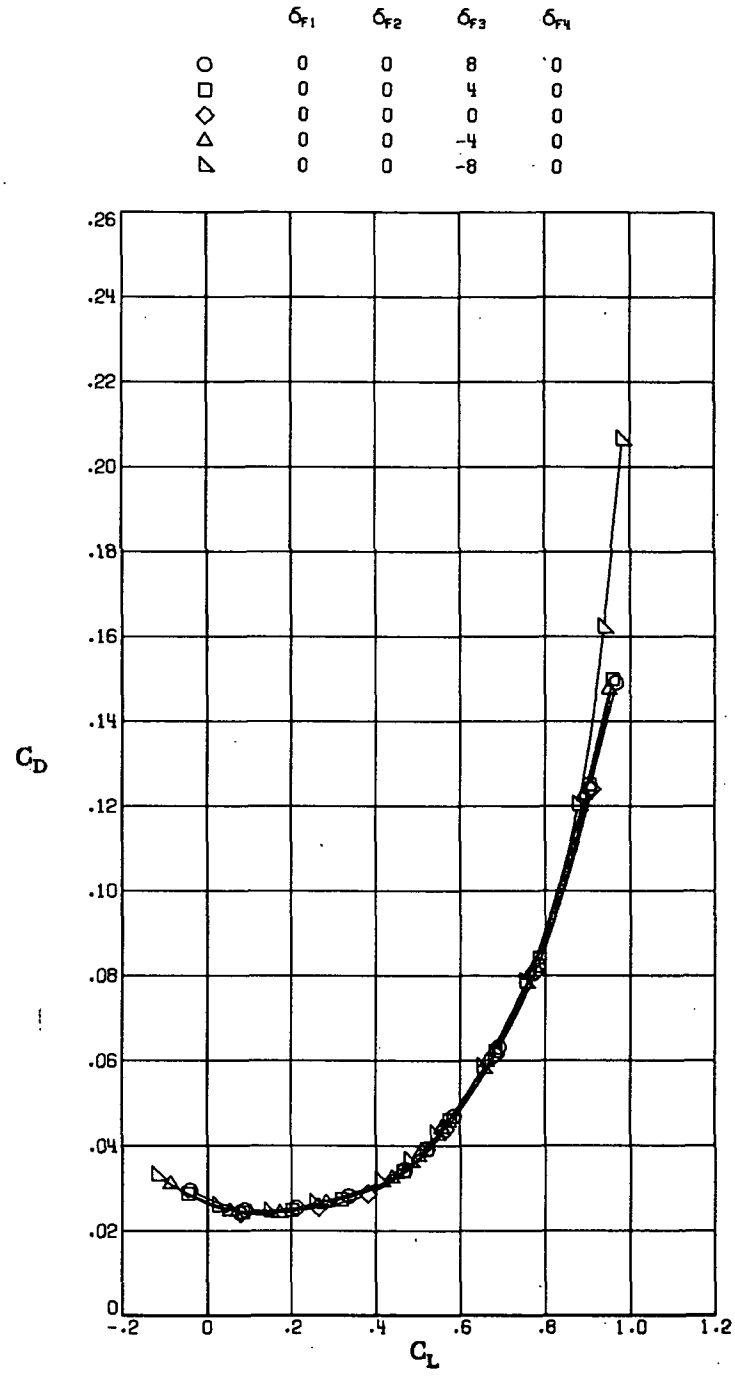
—— Top Centerline

– – Right Side



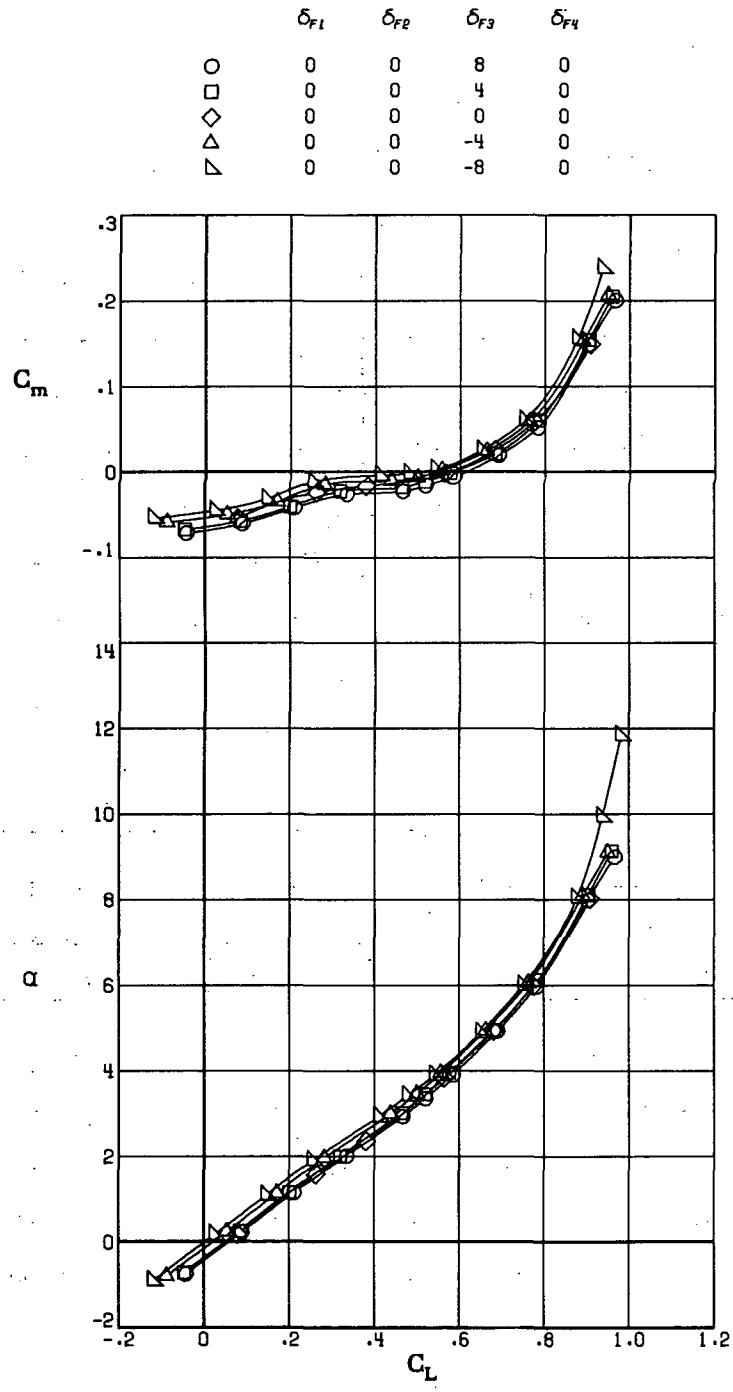
(e) Selected fuselage pressure distributions.

Figure 20.- Concluded.



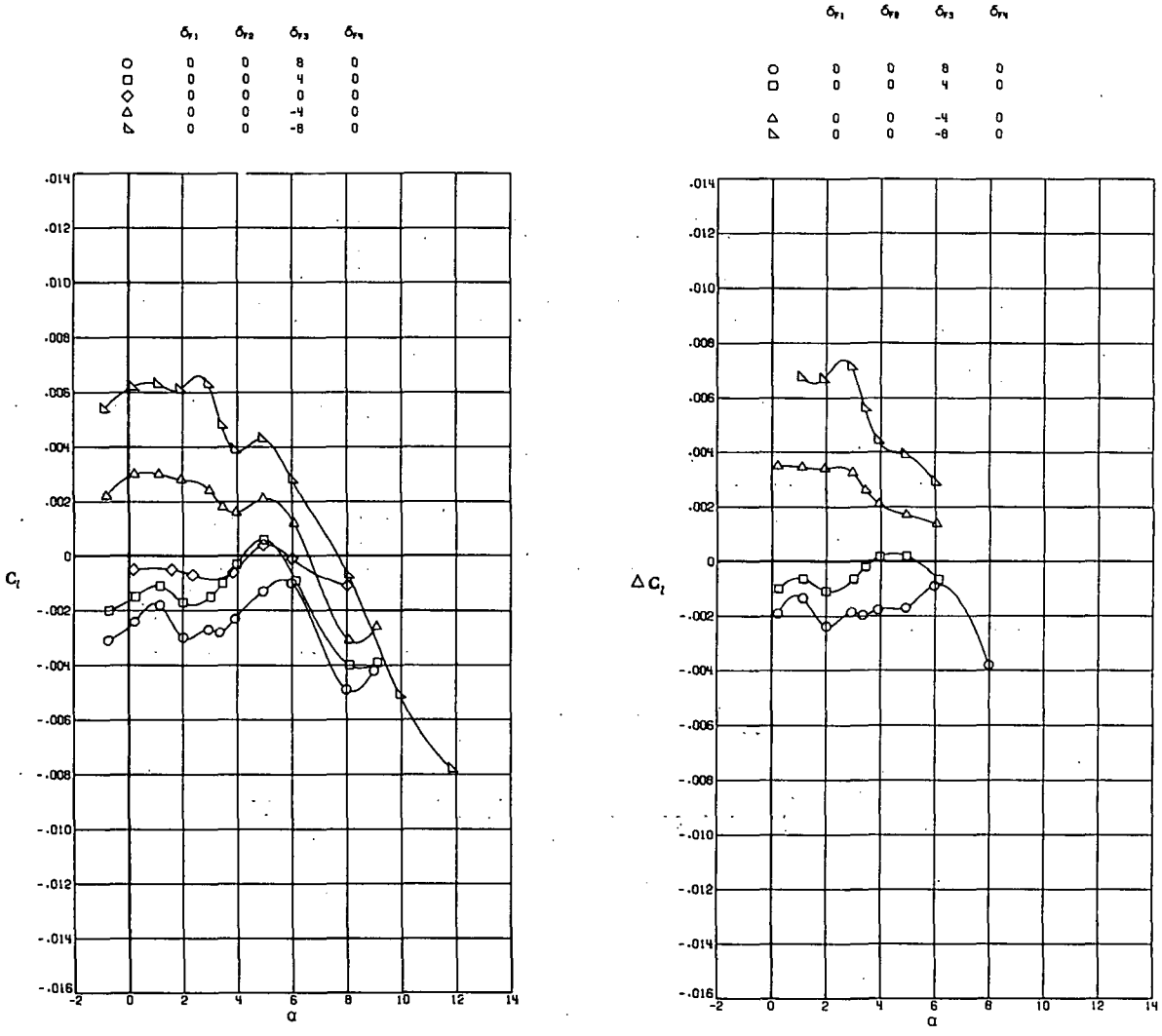
(a) Drag characteristics.

Figure 21.- Effect of F_3 trailing-edge control deflection on aerodynamic characteristics of model with area-ruled fuselage at $M_\infty = 0.92$.



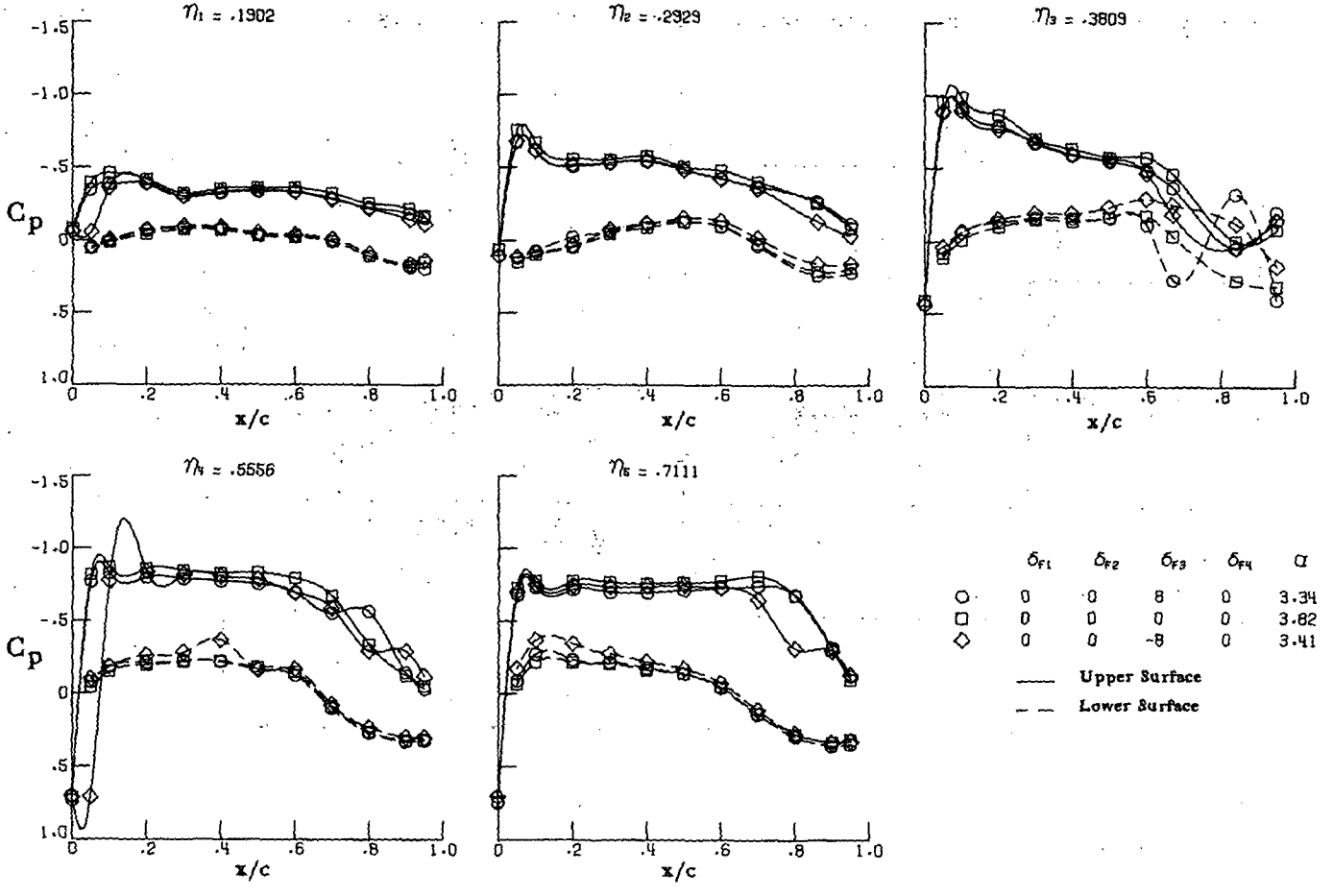
(b) Lift and pitch characteristics.

Figure 21.- Continued.



(c) Rolling-moment characteristics.

Figure 21.- Continued.



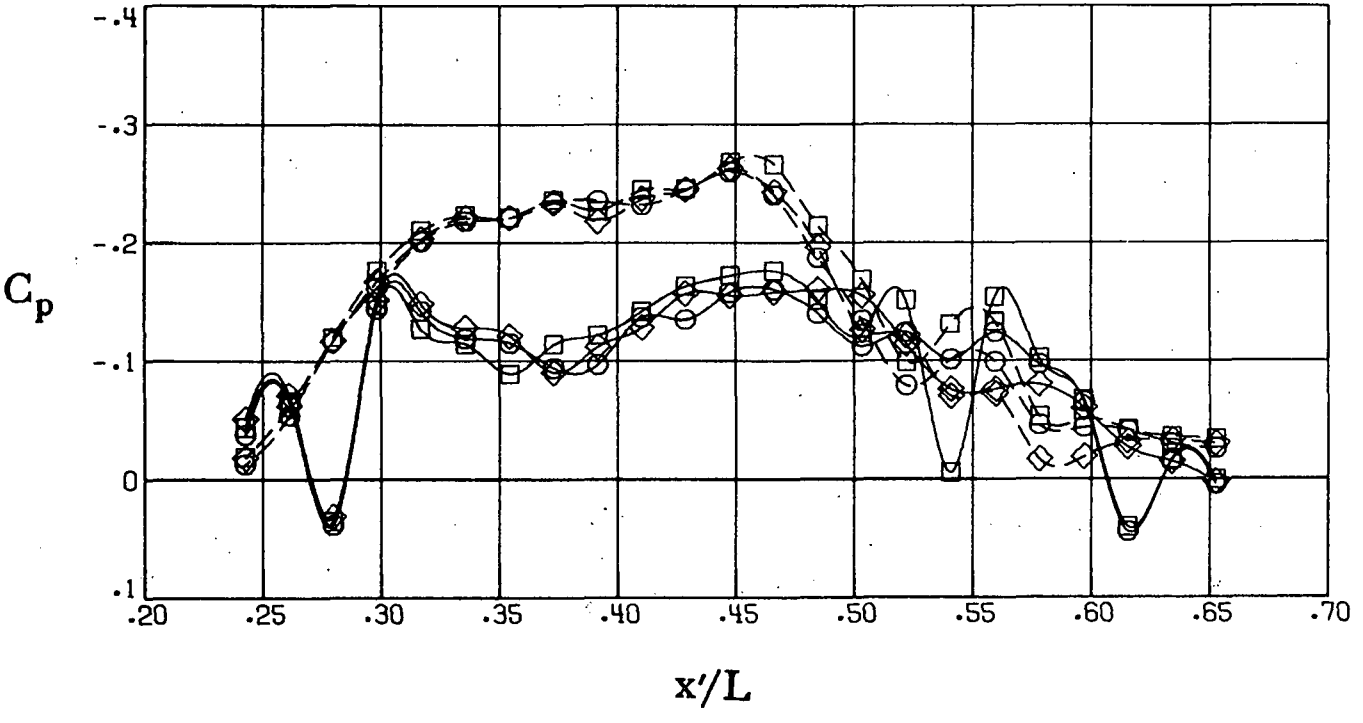
(d) Selected wing pressure distributions.

Figure 21.- Continued.

	δ_{F1}	δ_{F2}	δ_{F3}	δ_{F4}	α
○	0	0	8	0	3.34
□	0	0	0	0	3.82
◇	0	0	-8	0	3.41

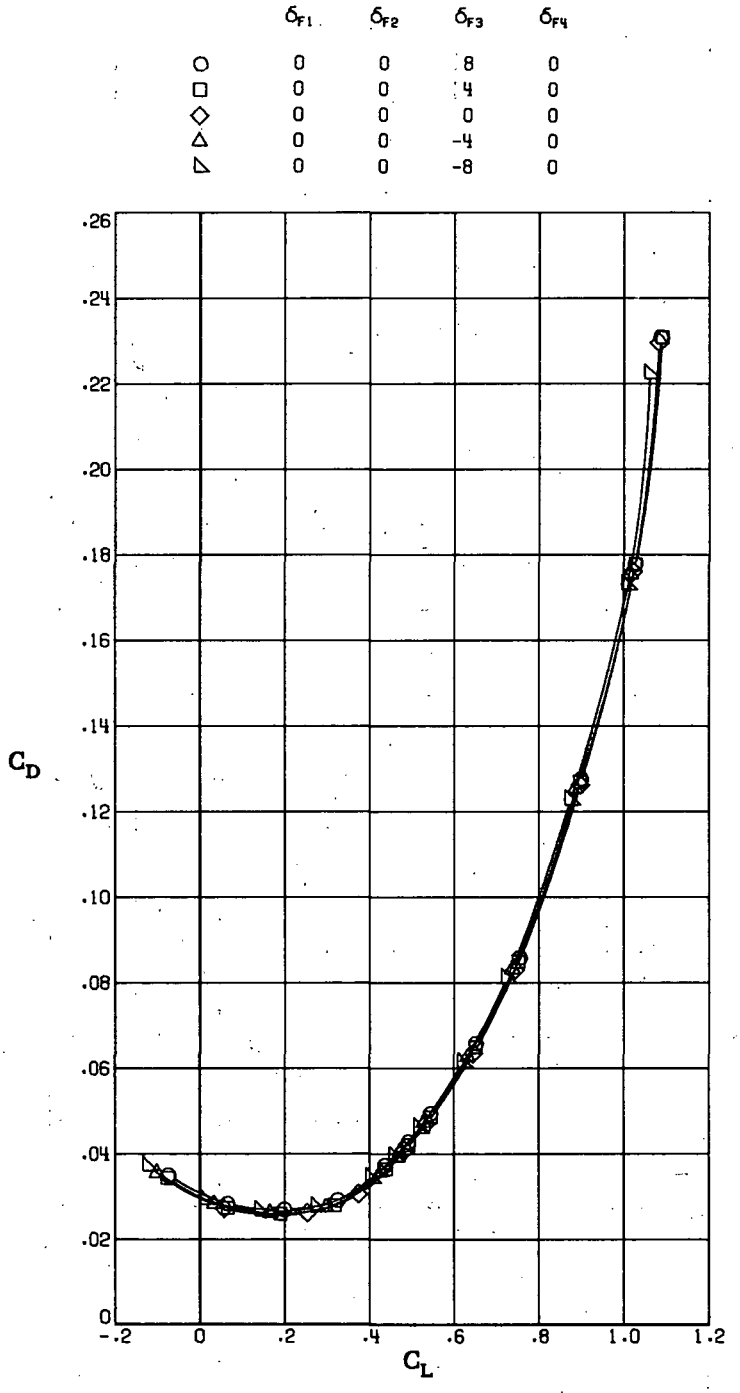
—— Top Centerline

– – Right Side



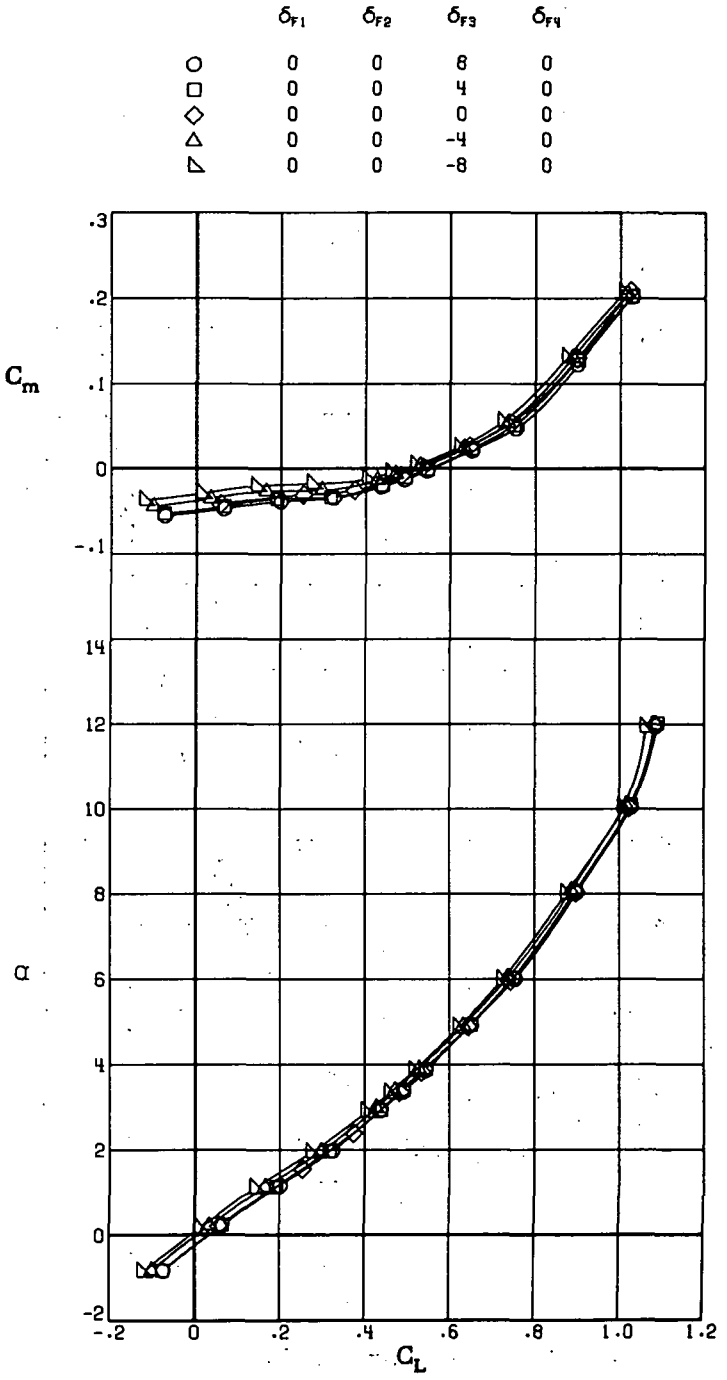
(e) Selected fuselage pressure distributions.

Figure 21.- Concluded.



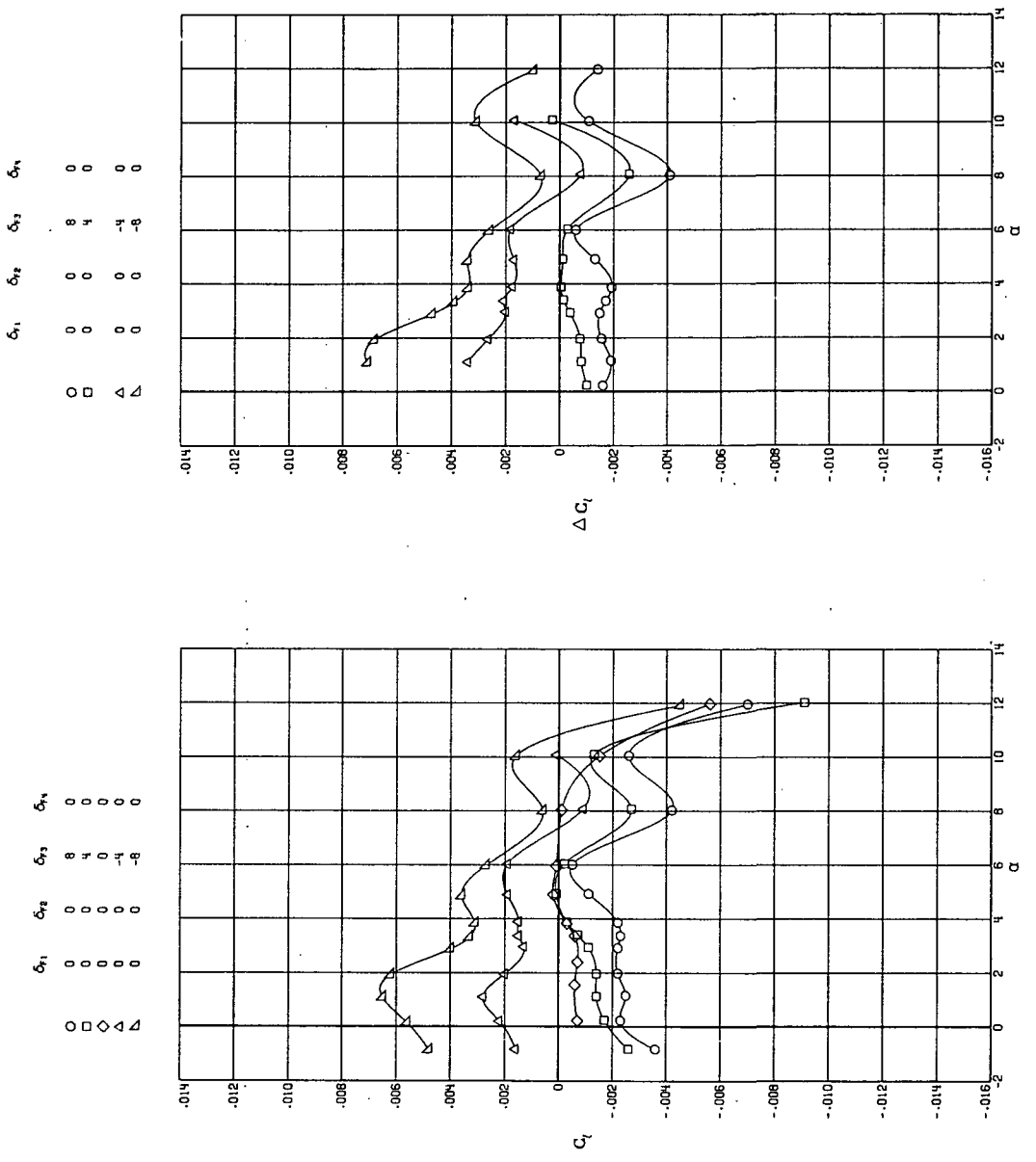
(a) Drag characteristics.

Figure 22.- Effect of F_3 trailing-edge control deflection on aerodynamic characteristics of model with area-ruled fuselage at $M_\infty = 0.94$.



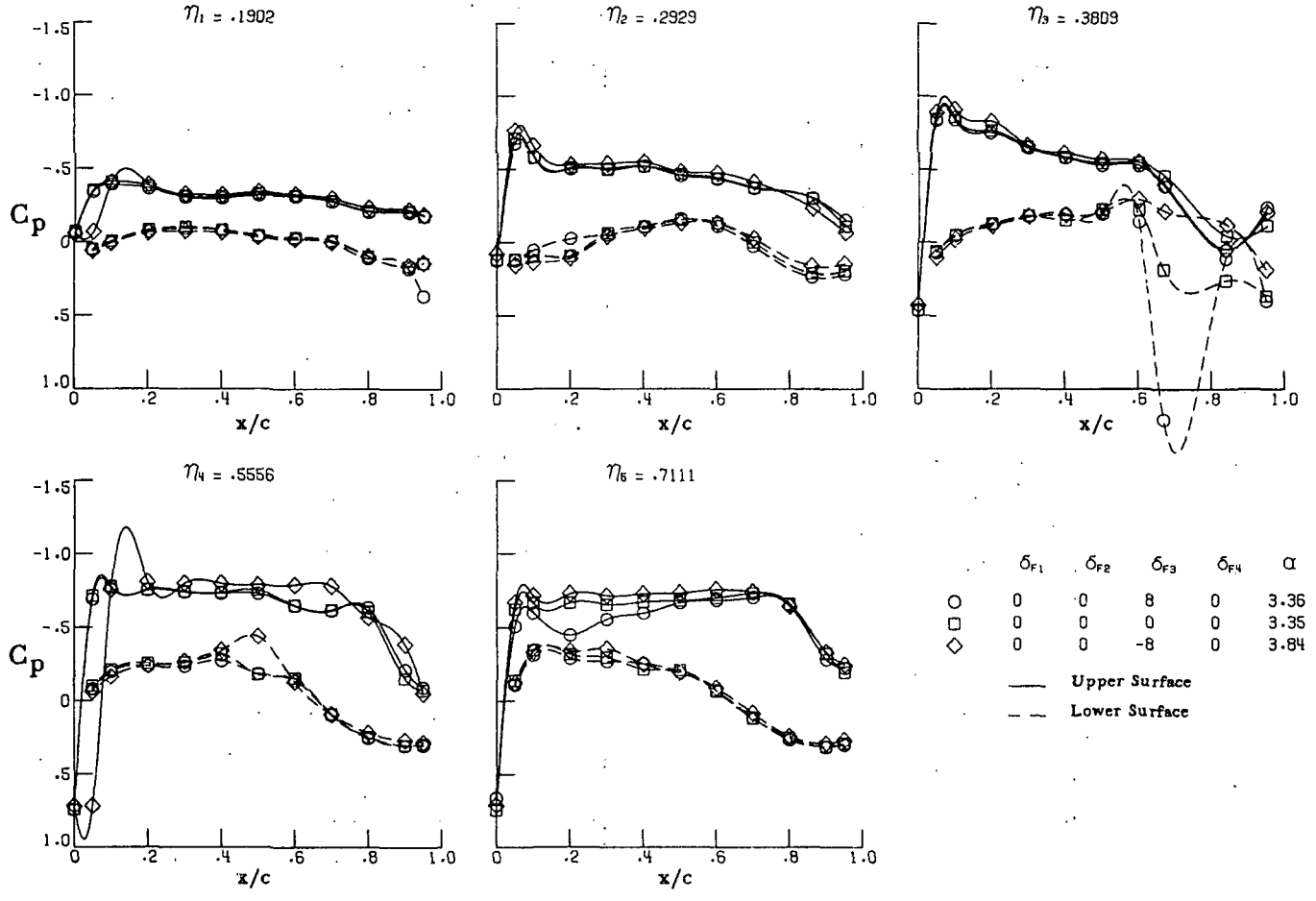
(b) Lift and pitch characteristics.

Figure 22.- Continued.



(c) Rolling-moment characteristics.

Figure 22.- Continued.



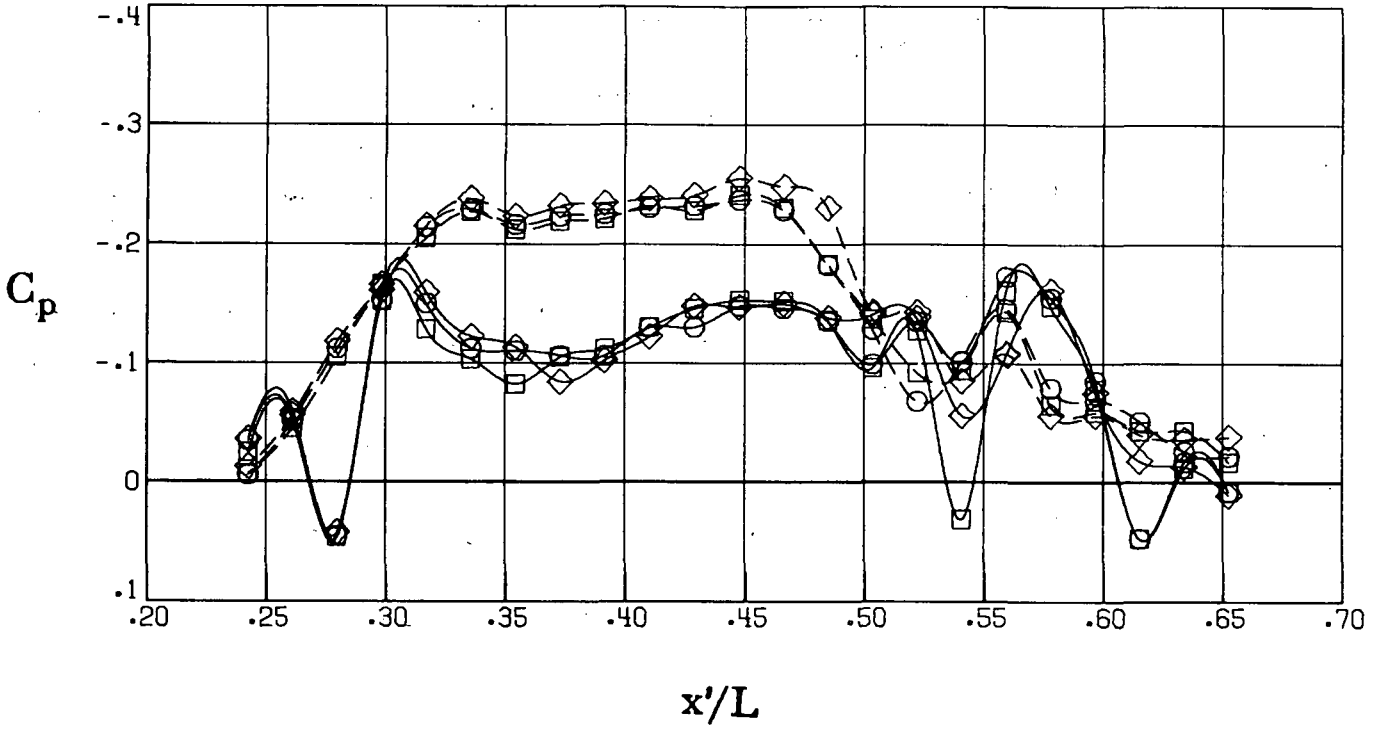
(d) Selected wing pressure distributions.

Figure 22.- Continued.

	δ_{F1}	δ_{F2}	δ_{F3}	δ_{F4}	α
○	0	0	8	0	3.36
□	0	0	0	0	3.35
◇	0	0	-8	0	3.84

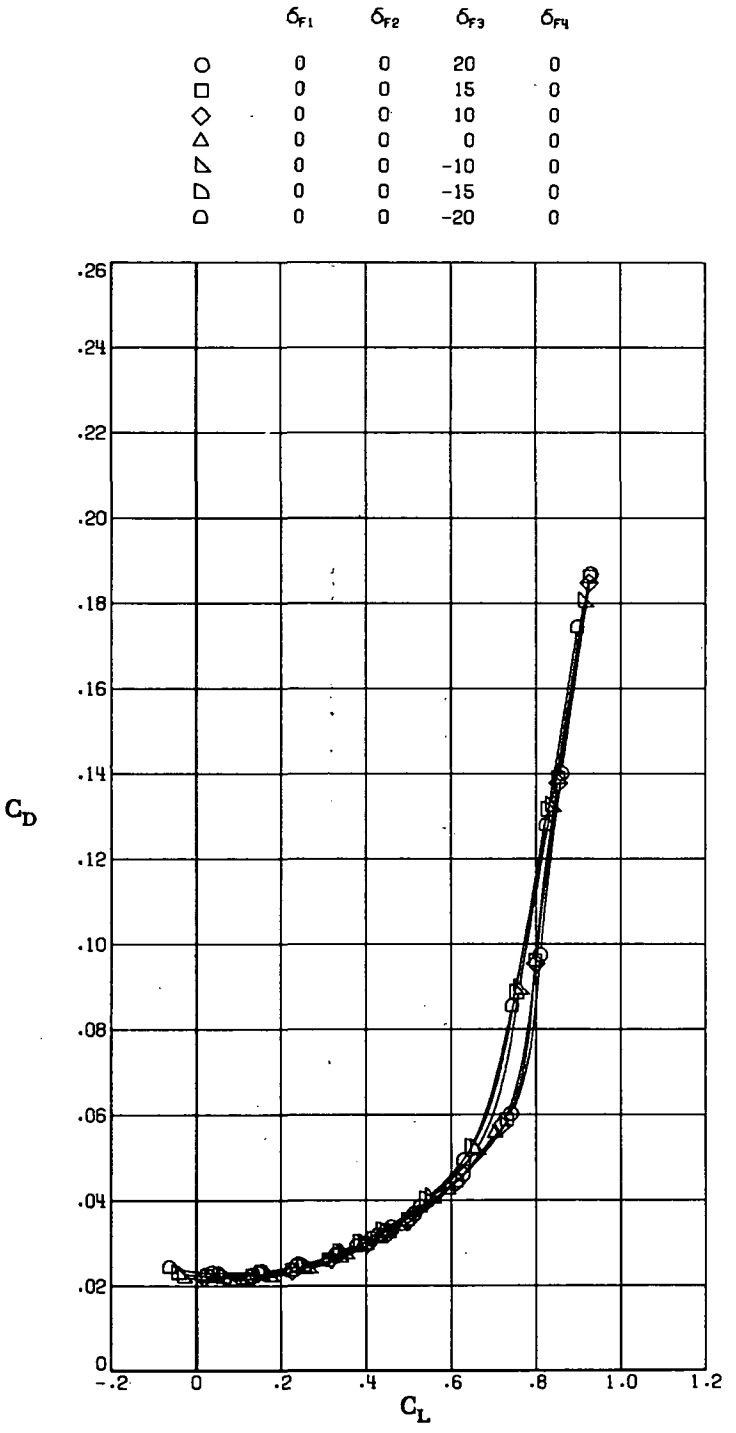
—— Top Centerline

— — Right Side



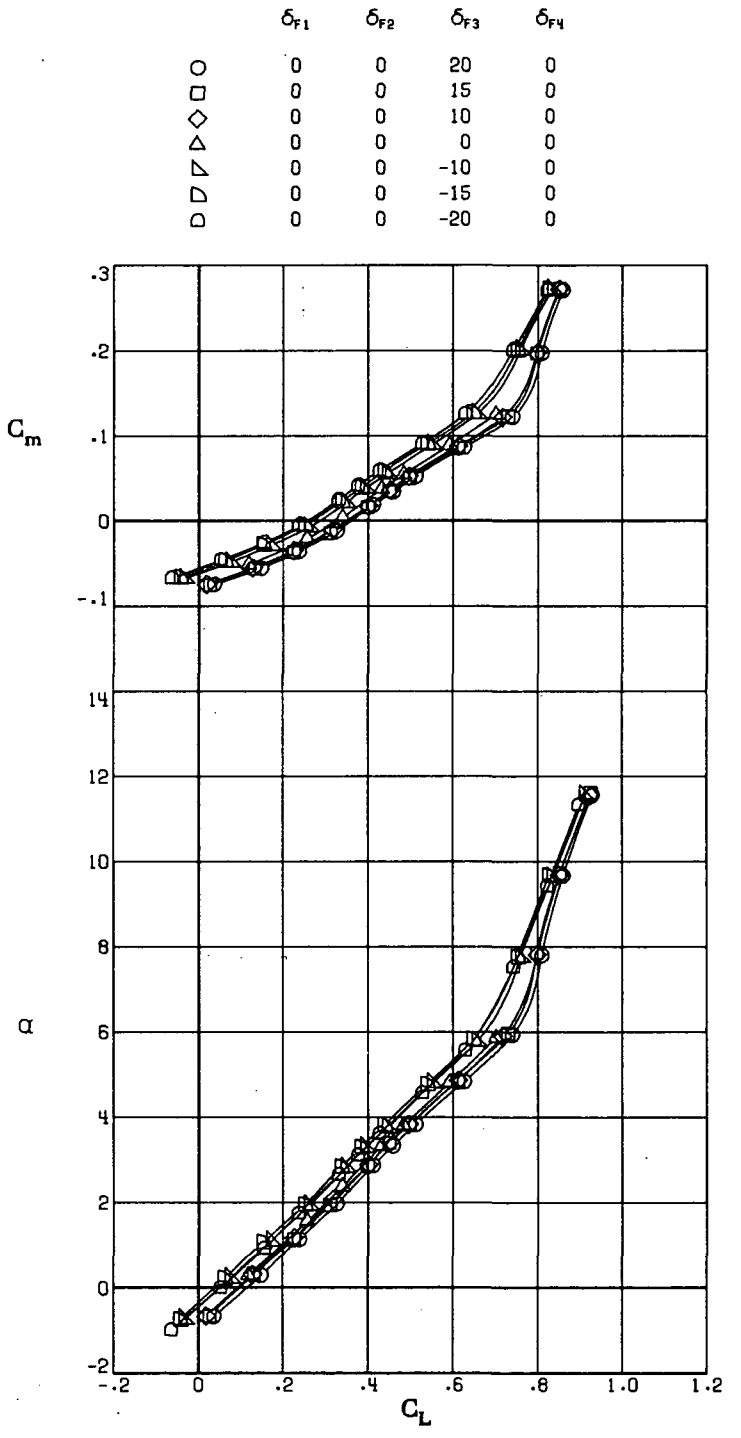
(e) Selected fuselage pressure distributions.

Figure 22.- Concluded.



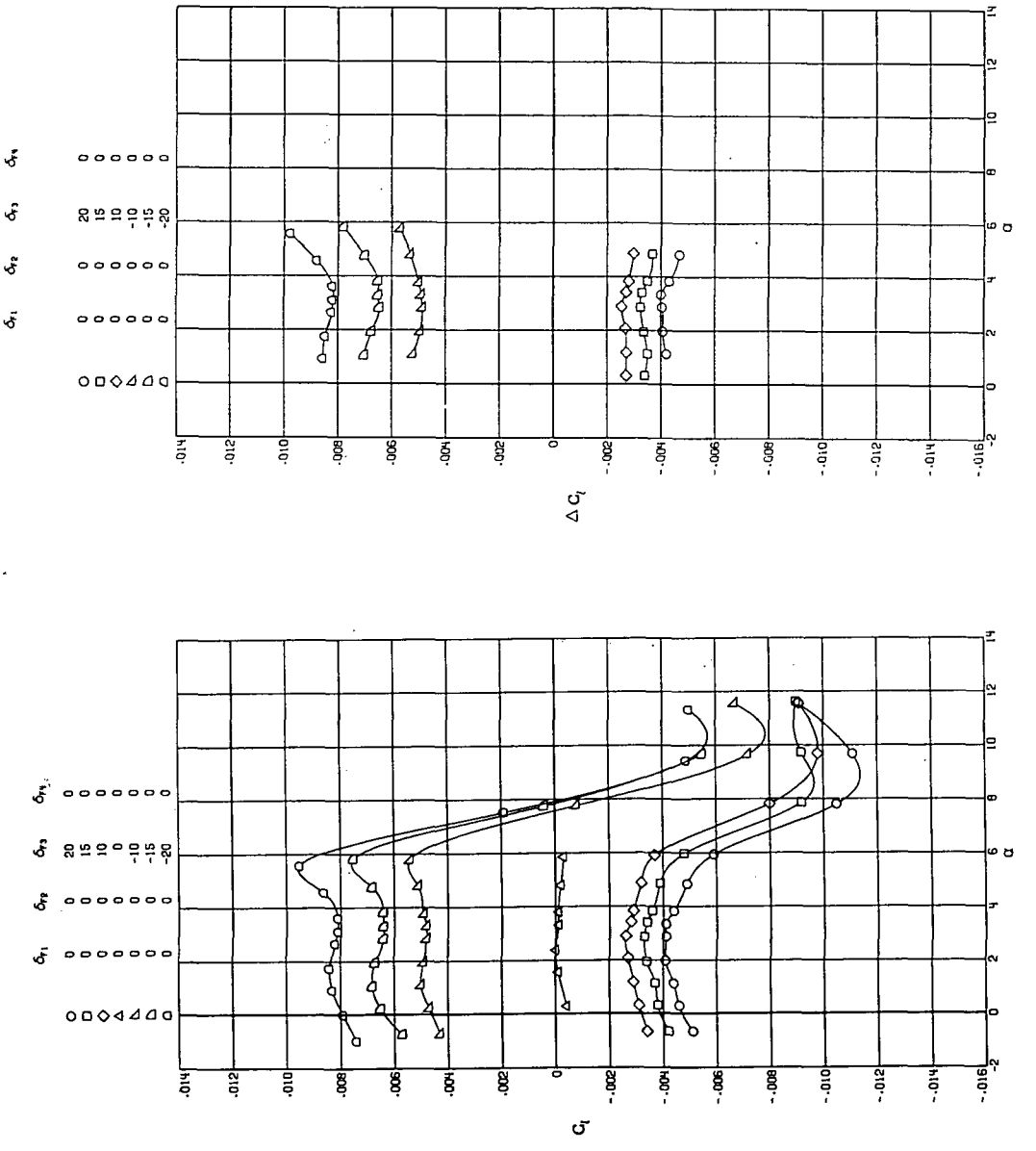
(a) Drag characteristics.

Figure 23.- Effect of F_3 trailing-edge control deflection on aerodynamic characteristics of model with area-ruled fuselage at $M_\infty = 0.80$.



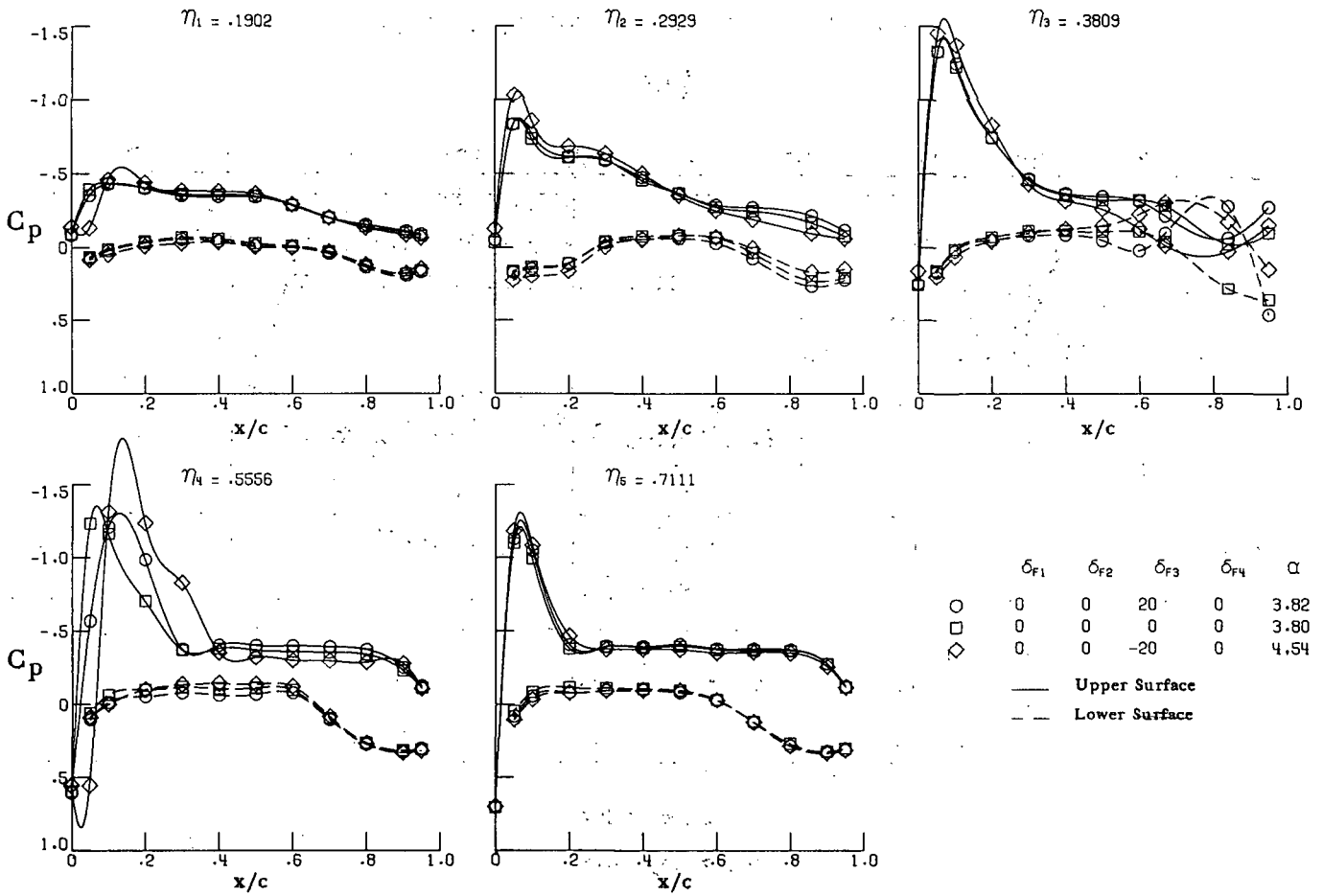
(b) Lift and pitch characteristics.

Figure 23.- Continued.



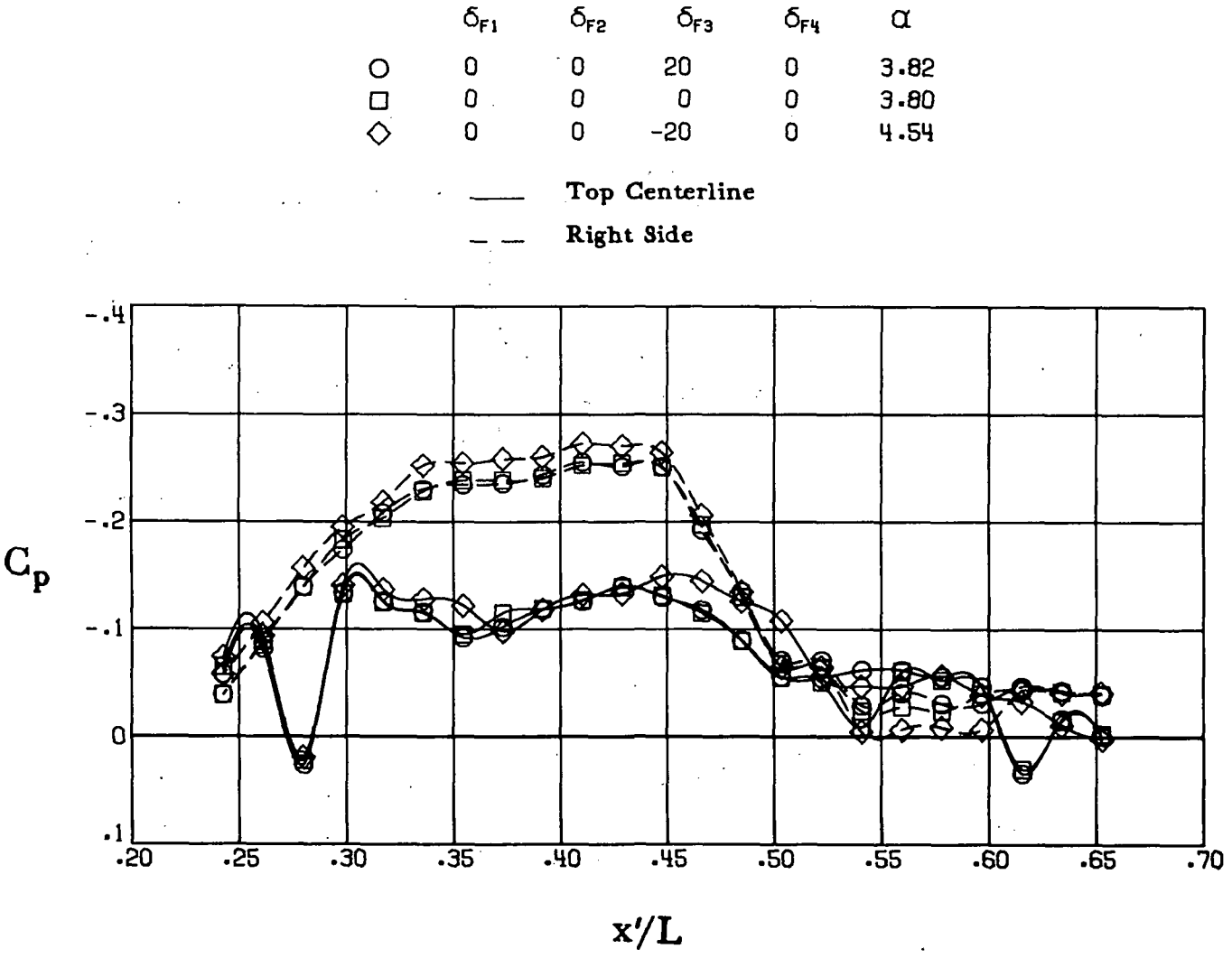
(c) Rolling-moment characteristics.

Figure 23.- Continued.



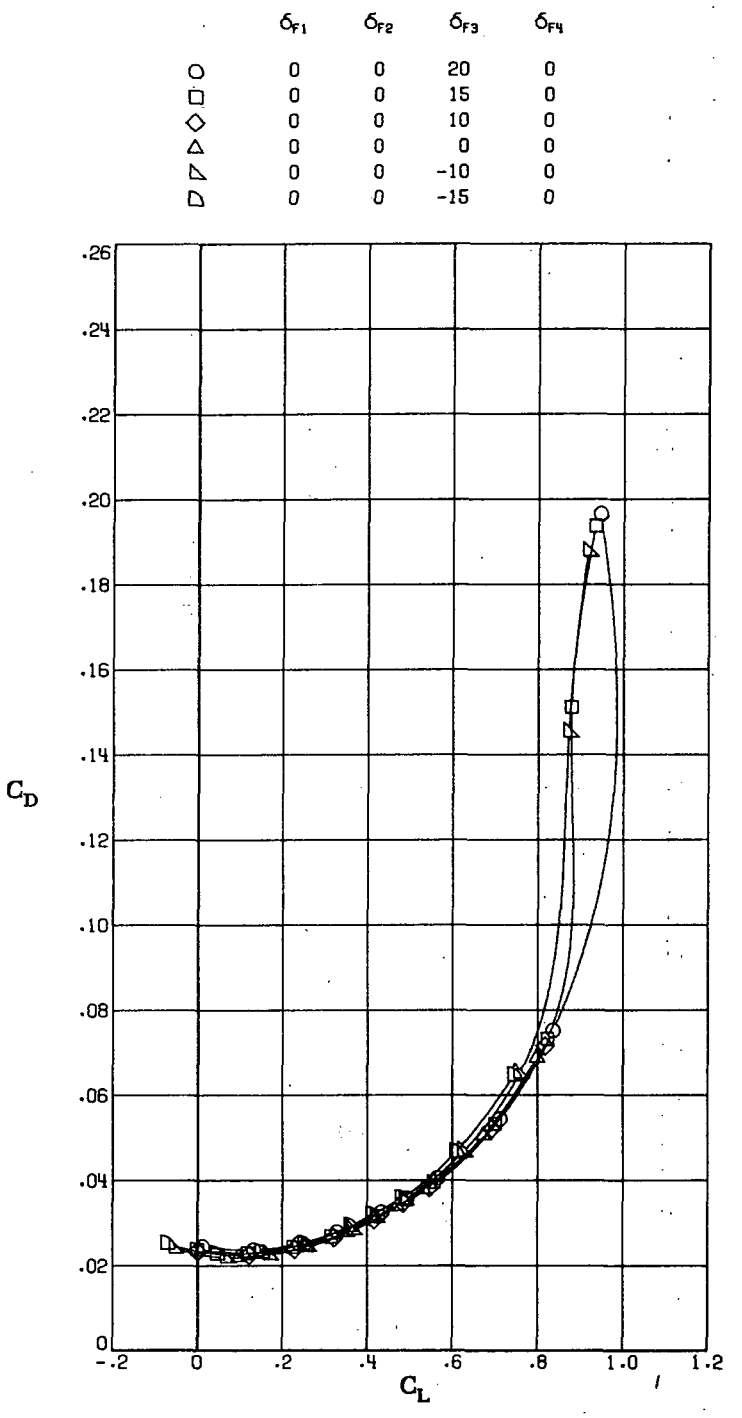
(d) Selected wing pressure distributions.

Figure 23.- Continued.



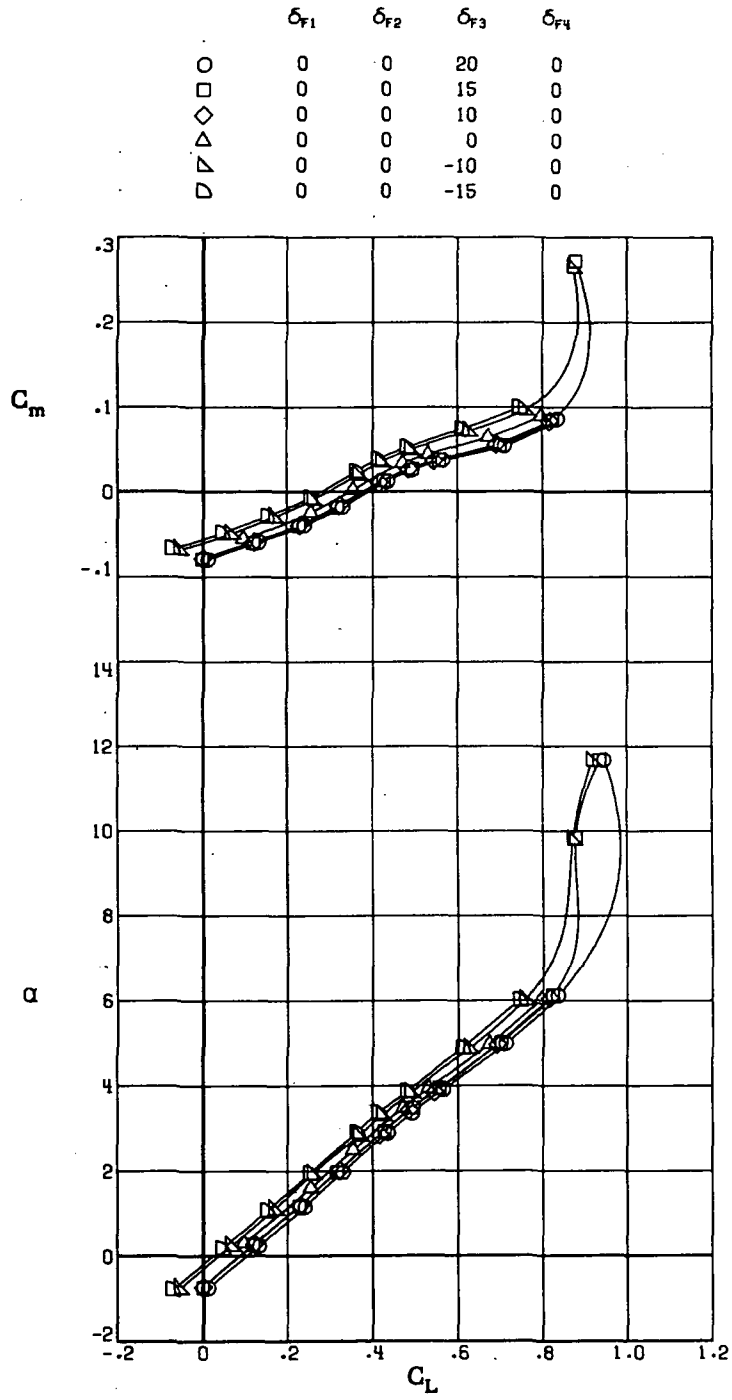
(e) Selected fuselage pressure distributions.

Figure 23.- Concluded.



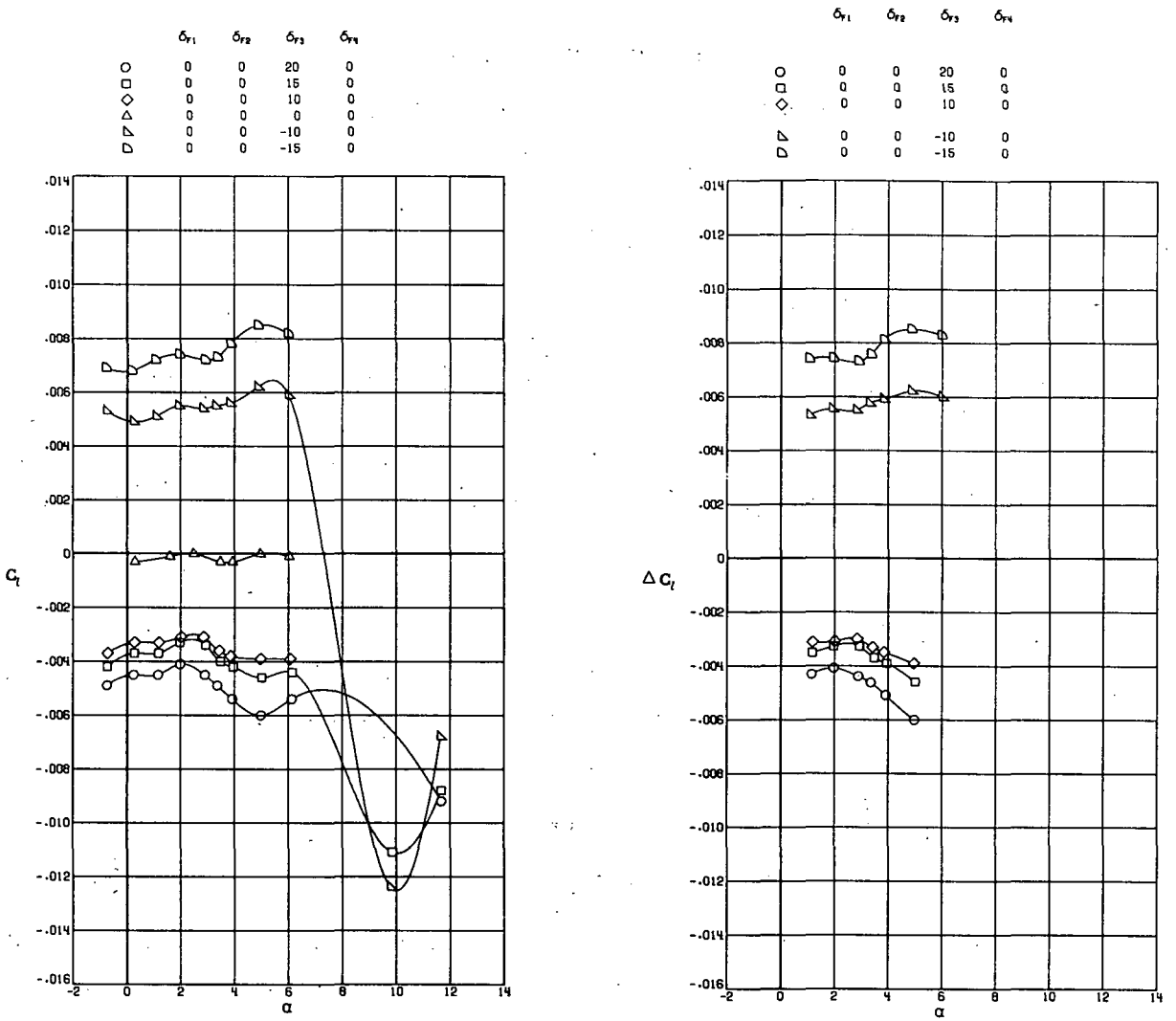
(a) Drag characteristics.

Figure 24.- Effect of F_3 trailing-edge control deflection on aerodynamic characteristics of model with area-ruled fuselage at $M_\infty = 0.86$.



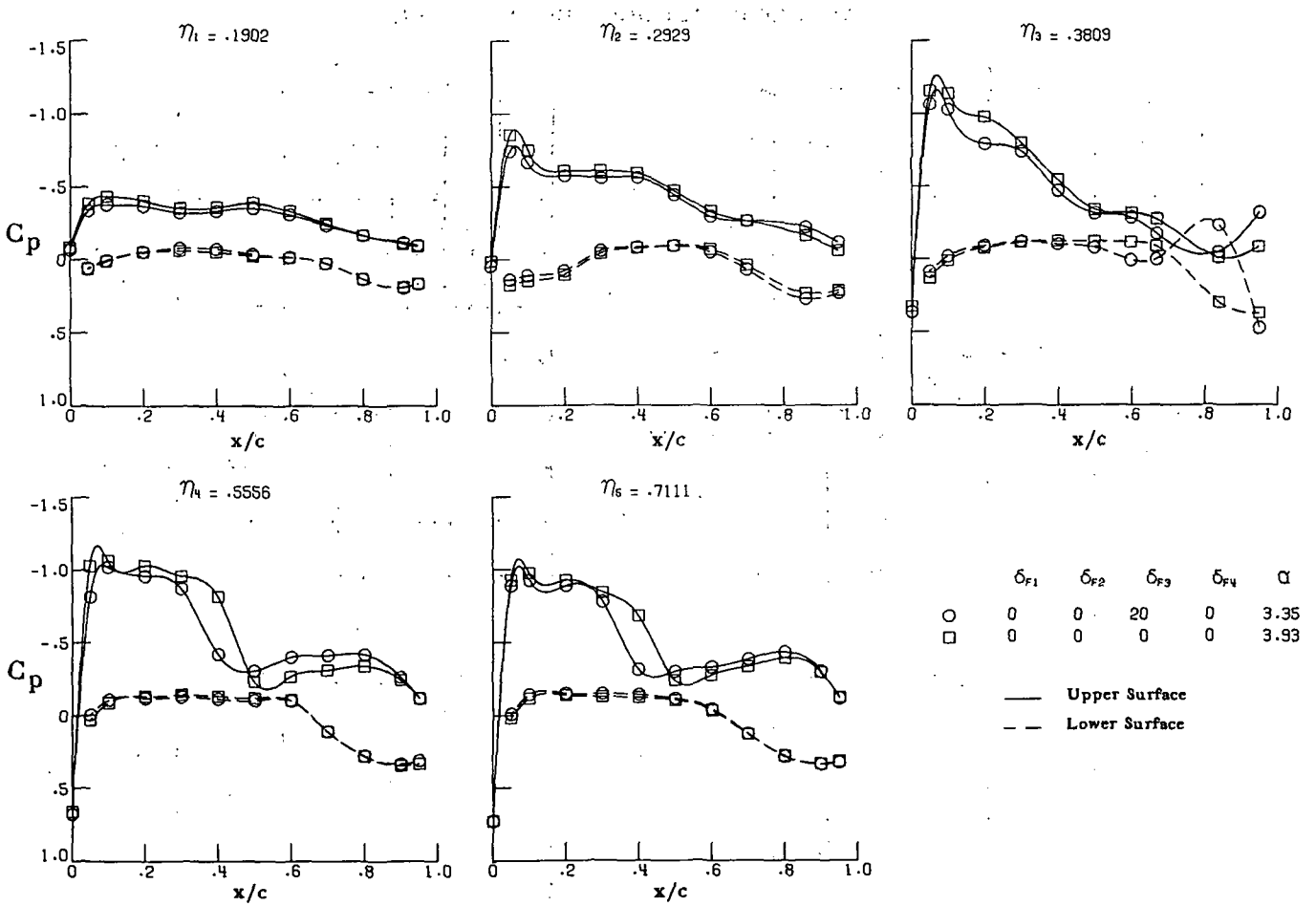
(b) Lift and pitch characteristics.

Figure 24.- Continued.



(c) Rolling-moment characteristics.

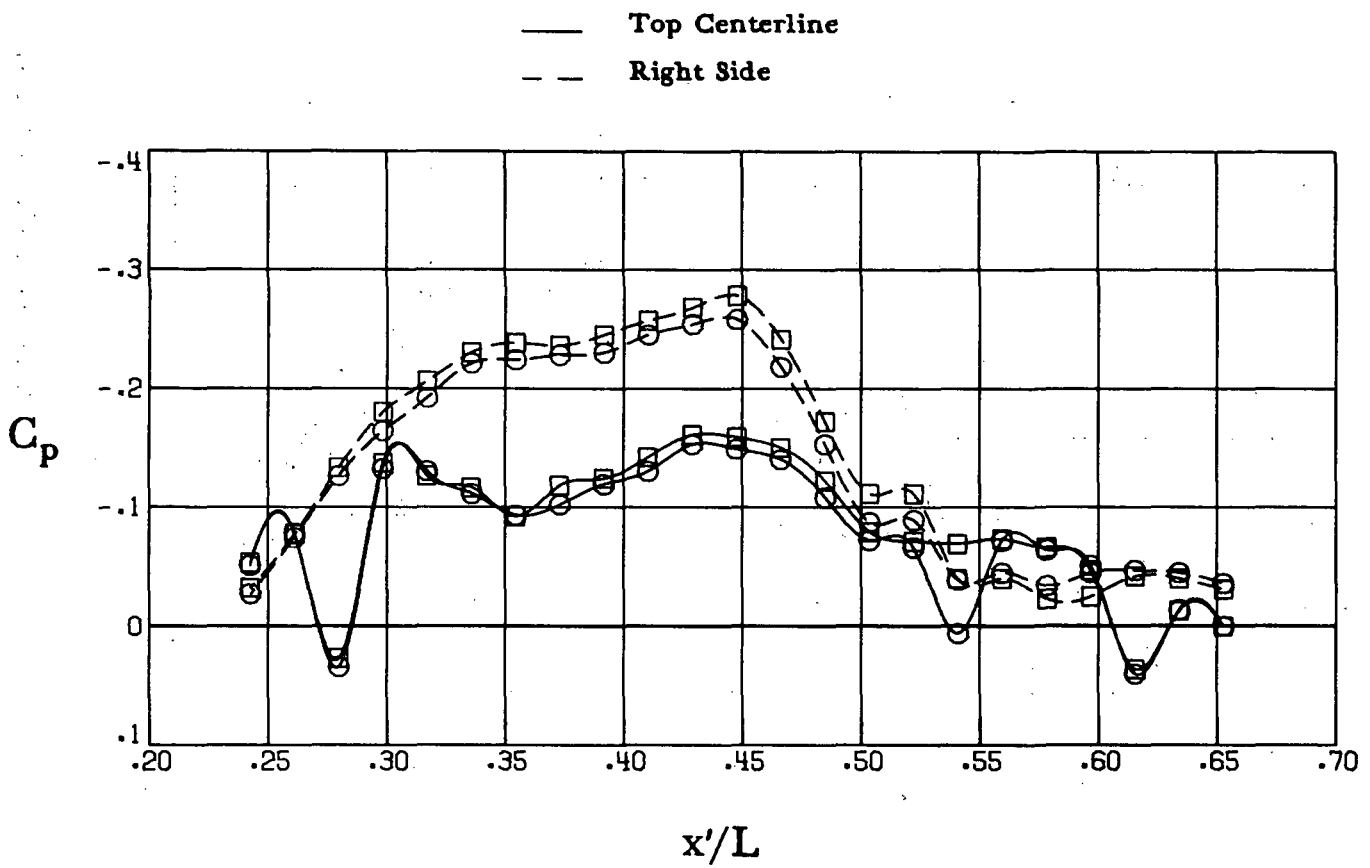
Figure 24.- Continued.



(d) Selected wing pressure distributions.

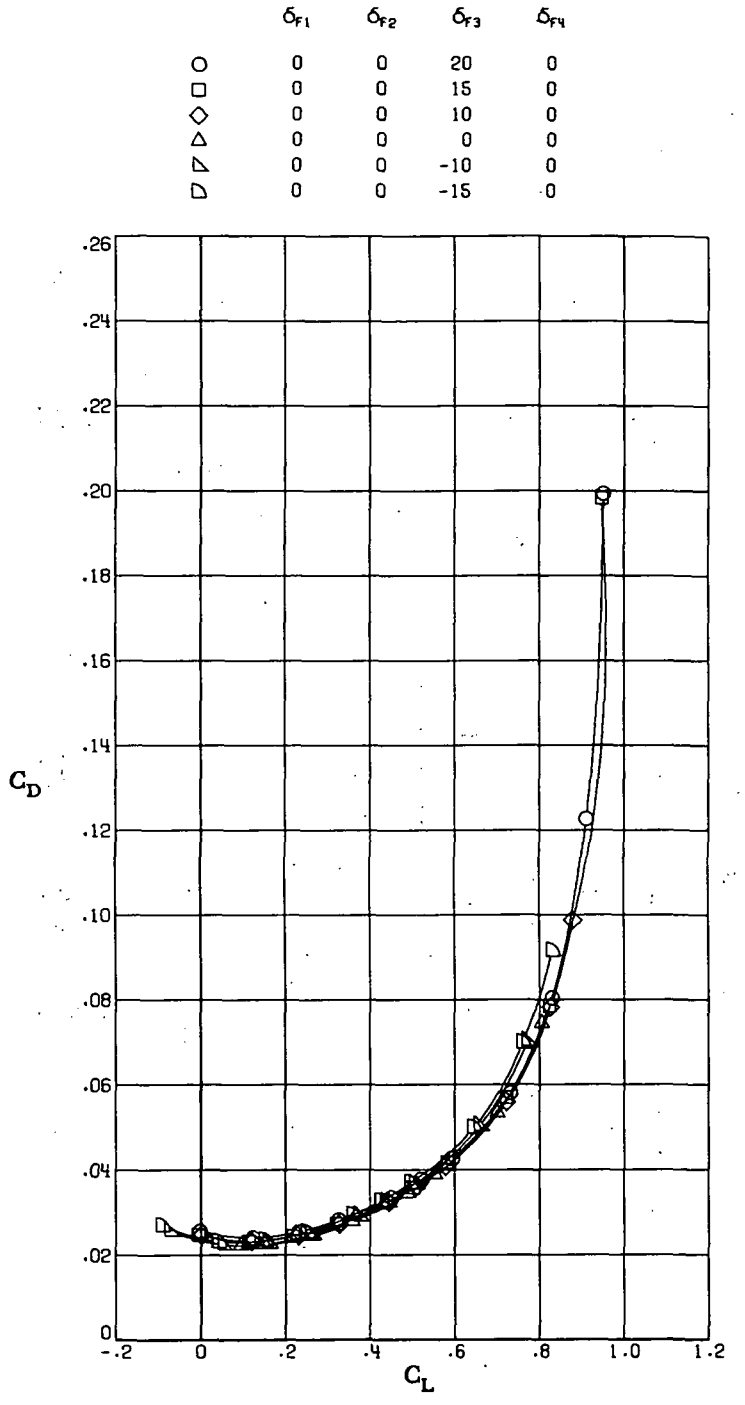
Figure 24.- Continued.

	δ_{F1}	δ_{F2}	δ_{F3}	δ_{F4}	α
○	0	0	20	0	3.35
□	0	0	0	0	3.93



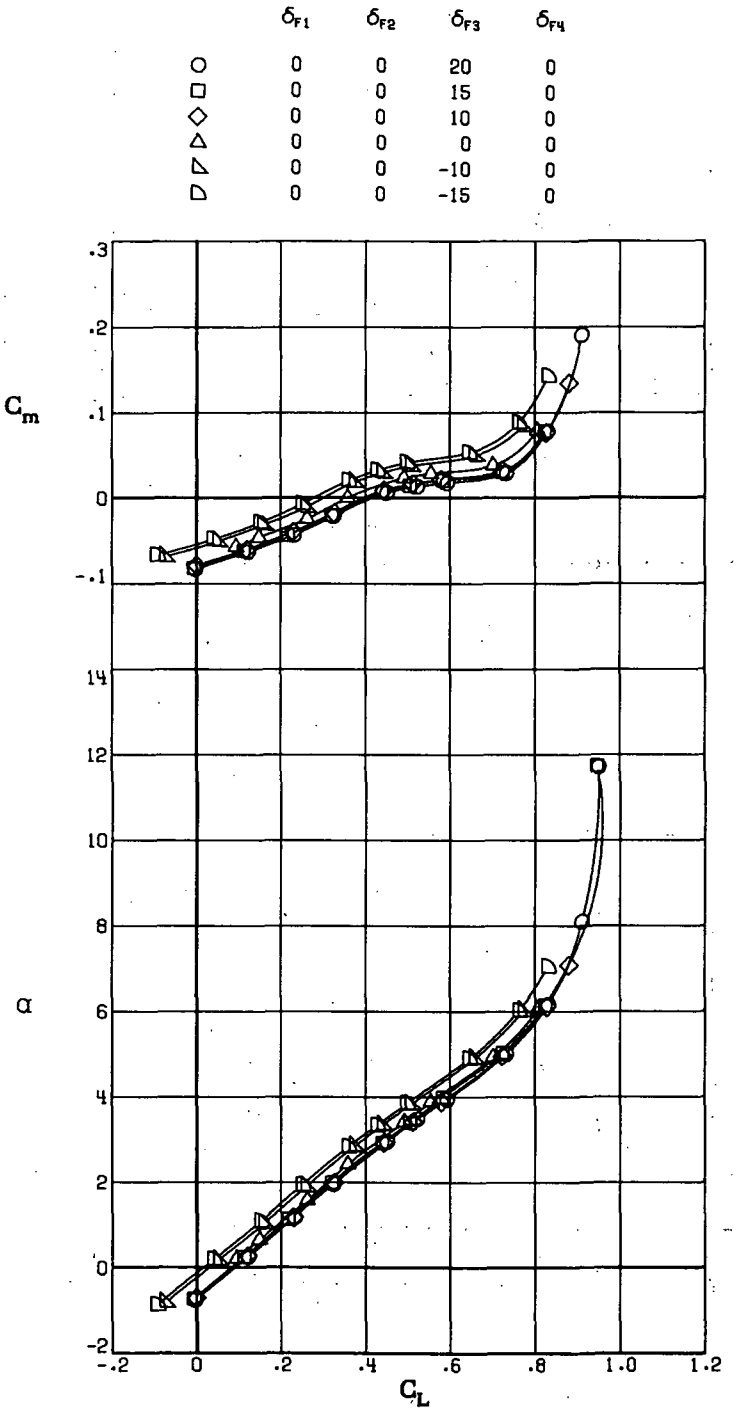
(e) Selected fuselage pressure distributions.

Figure 24.- Concluded.



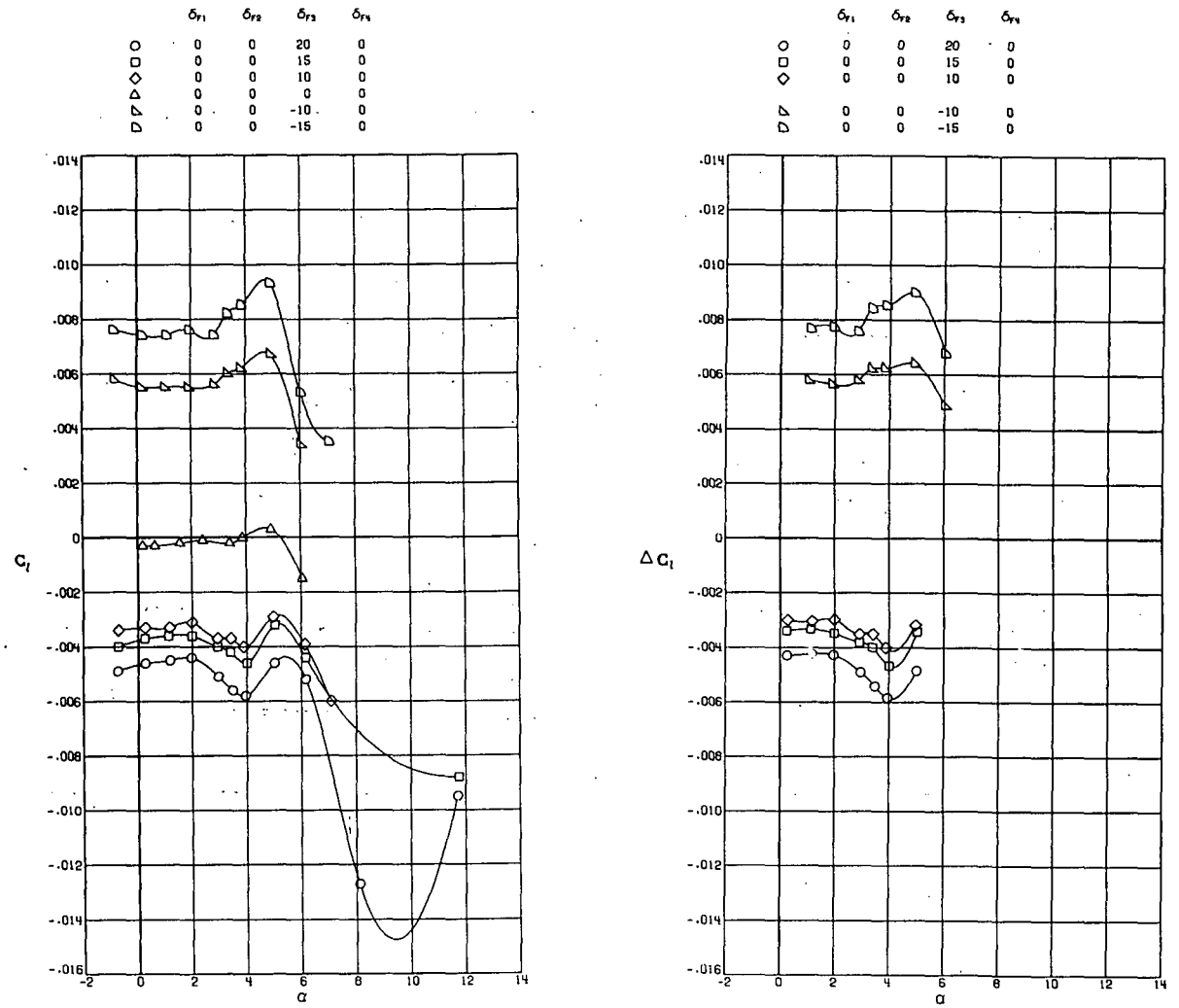
(a) Drag characteristics.

Figure 25.- Effect of F_3 trailing-edge control deflection on aerodynamic characteristics of model with area-ruled fuselage at $M_\infty = 0.88$.



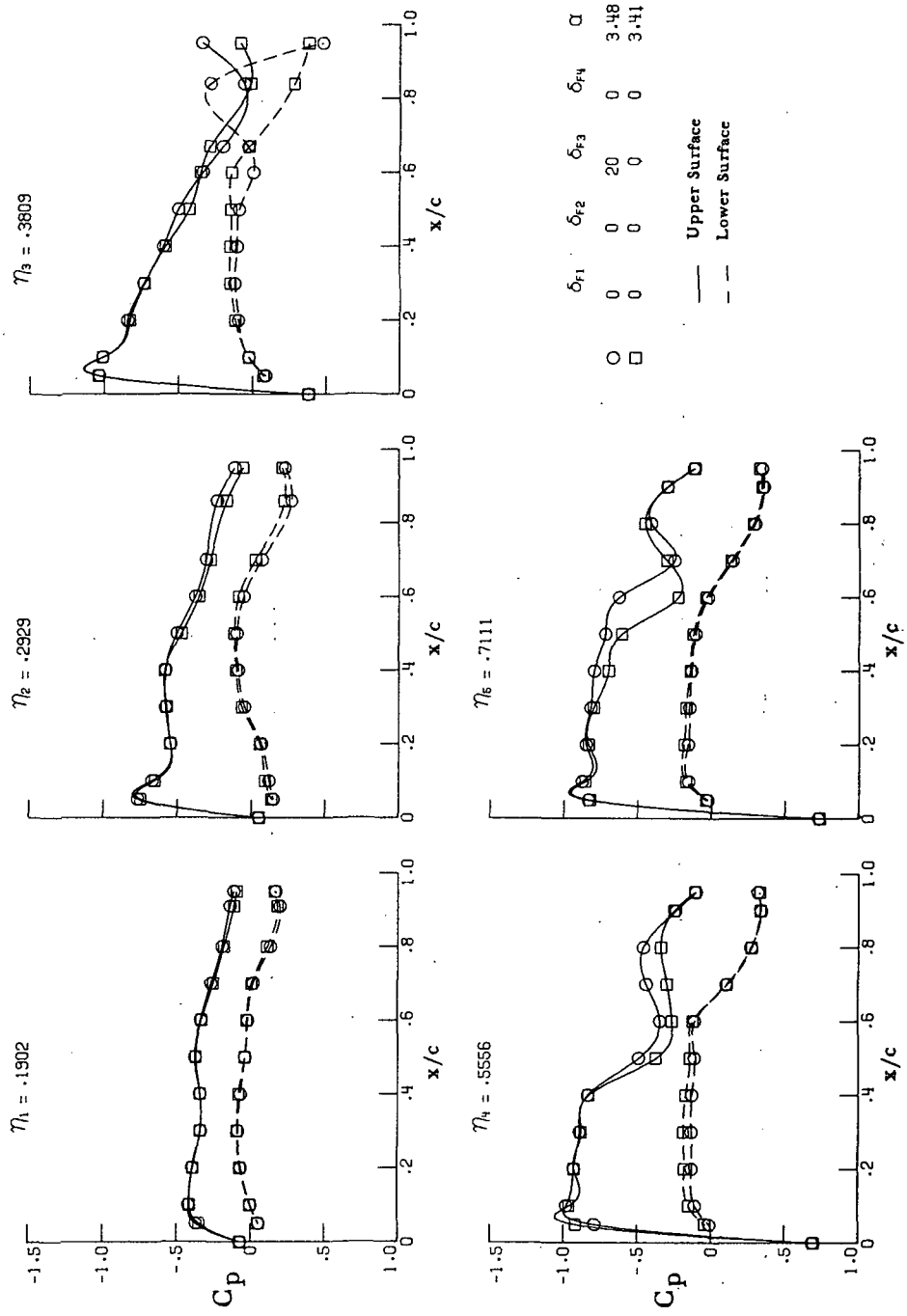
(b) Lift and pitch characteristics.

Figure 25.- Continued.



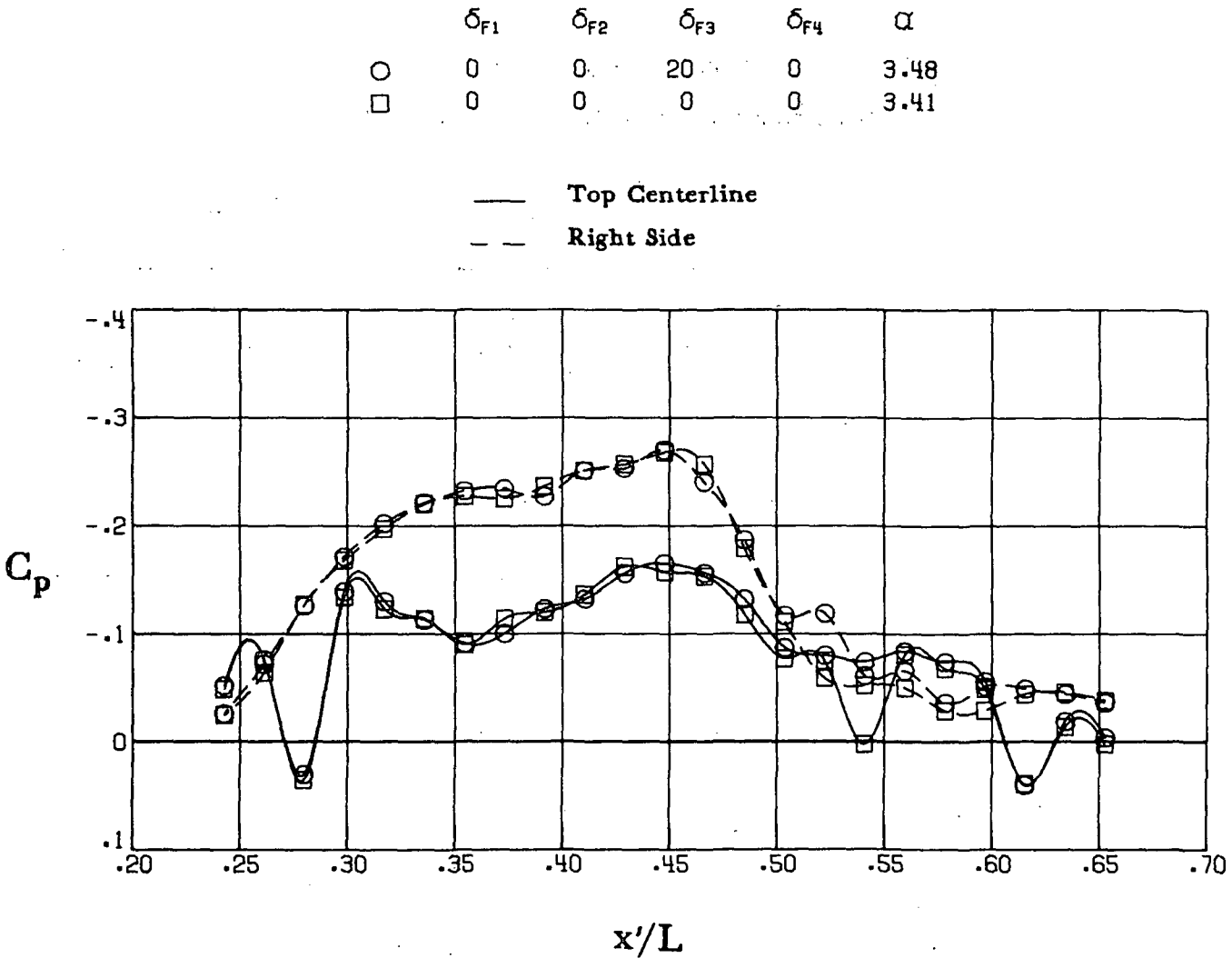
(c) Rolling-moment characteristics.

Figure 25.- Continued.



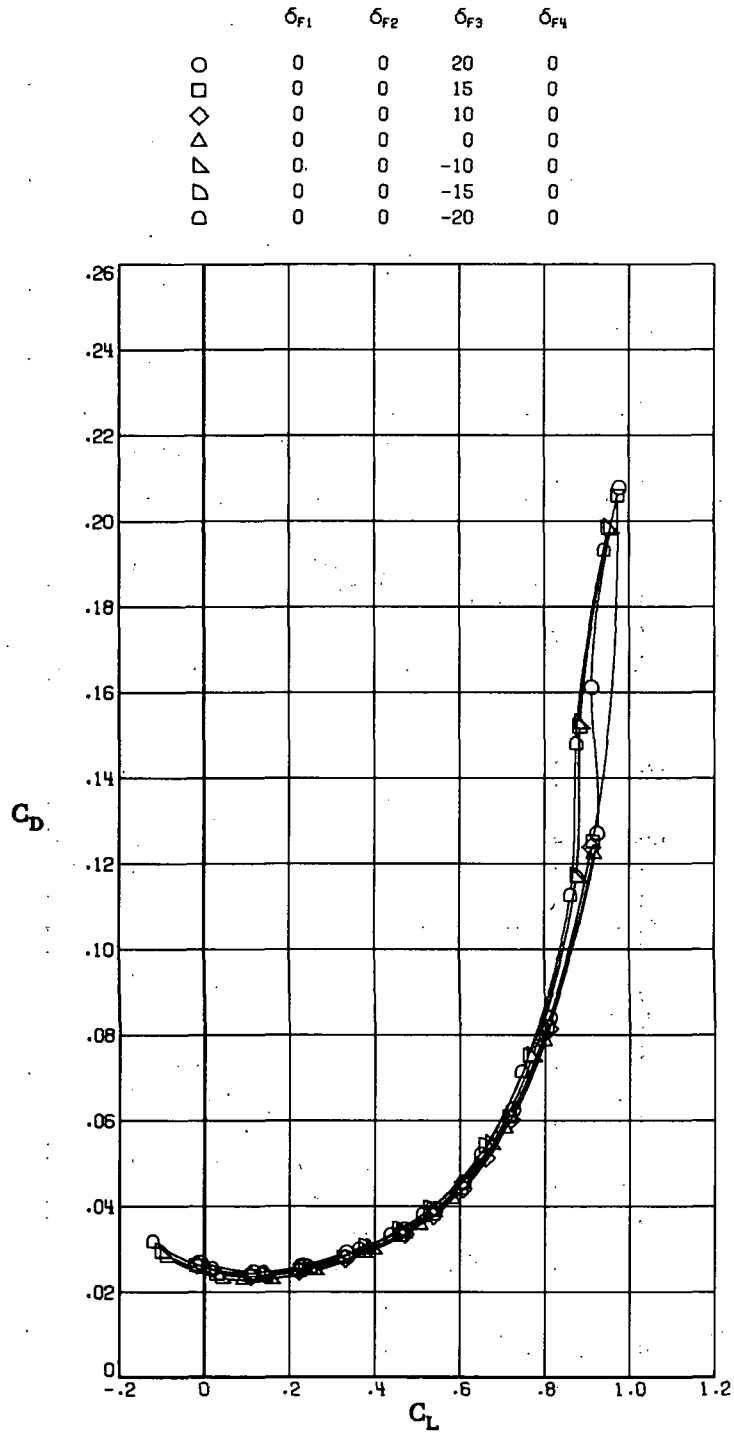
(d) Selected wing pressure distributions.

Figure 25.- Continued.



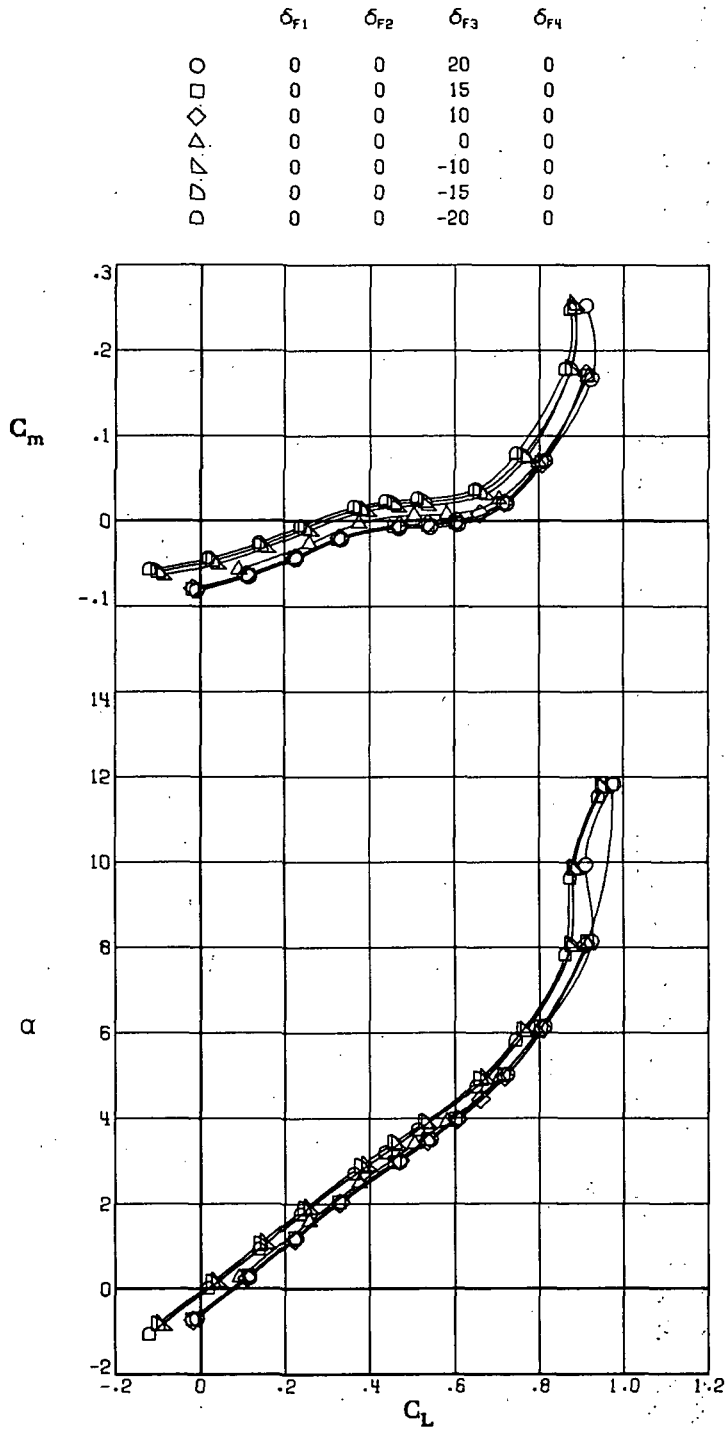
(e) Selected fuselage pressure distributions.

Figure 25.- Concluded.



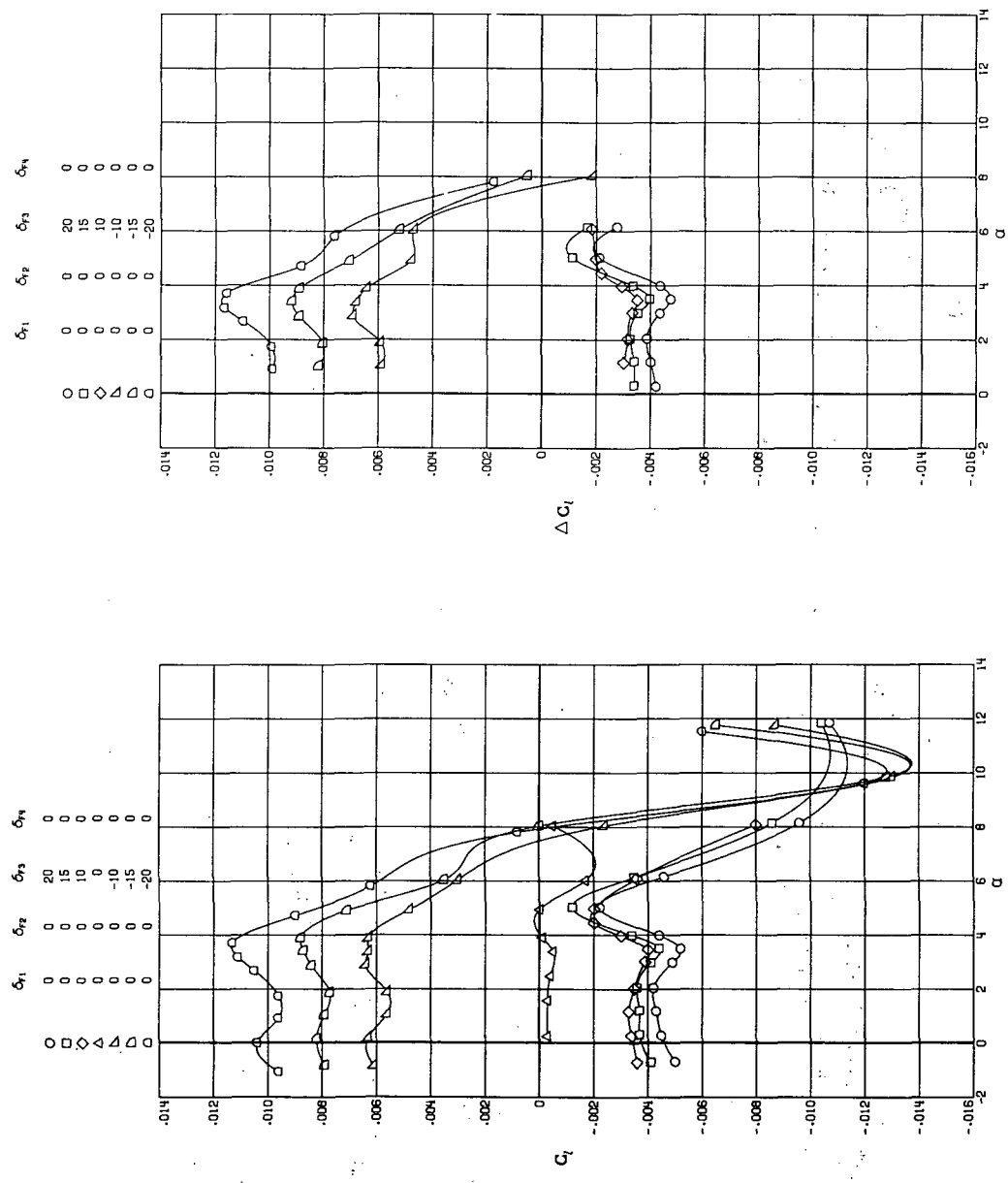
(a) Drag characteristics.

Figure 26.- Effect of F_3 trailing-edge control deflection on aerodynamic characteristics of model with area-ruled fuselage at $M_\infty = 0.90$.



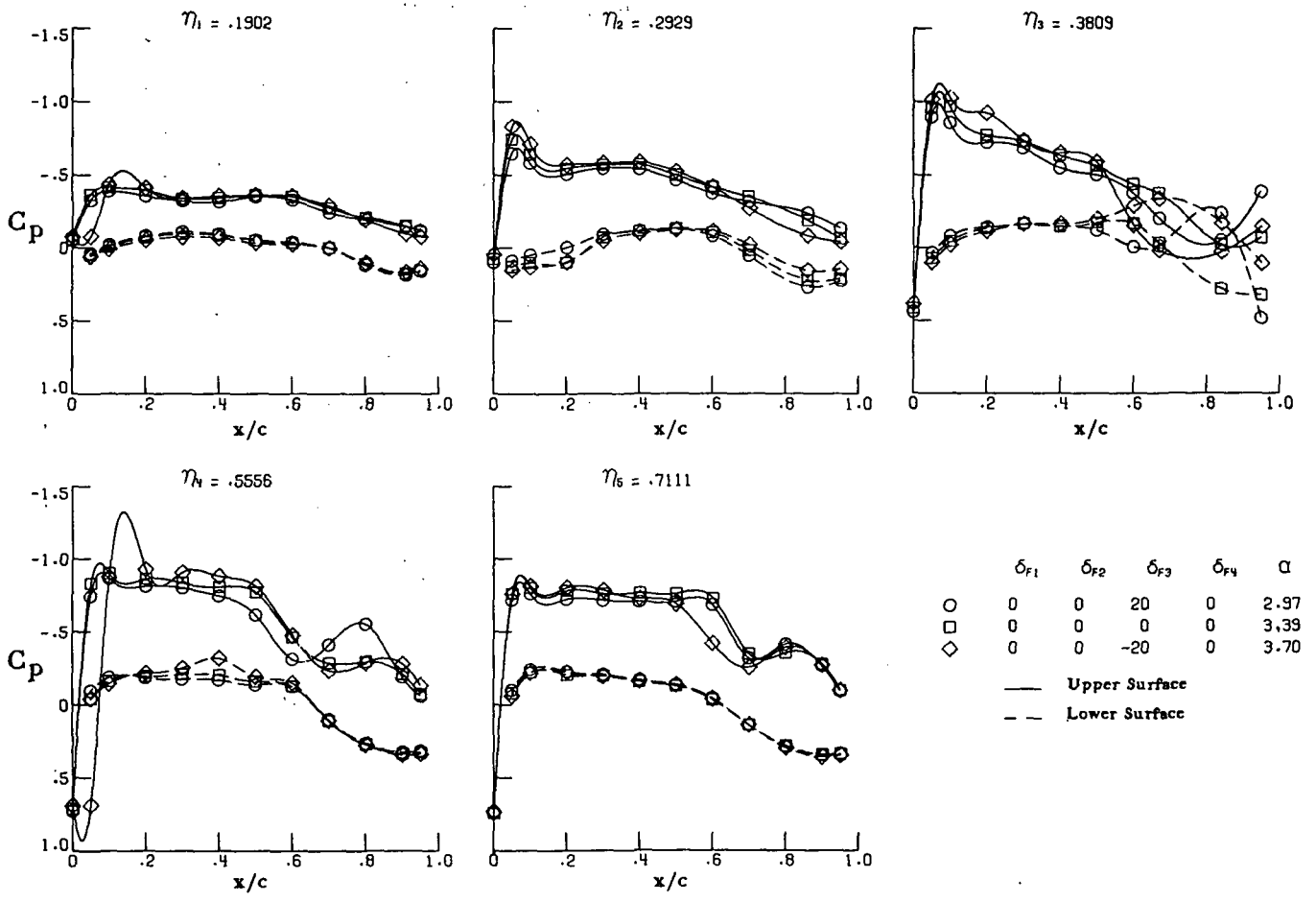
(b) Lift and pitch characteristics.

Figure 26.- Continued.



(c) Rolling-moment characteristics.

Figure 26.- Continued.



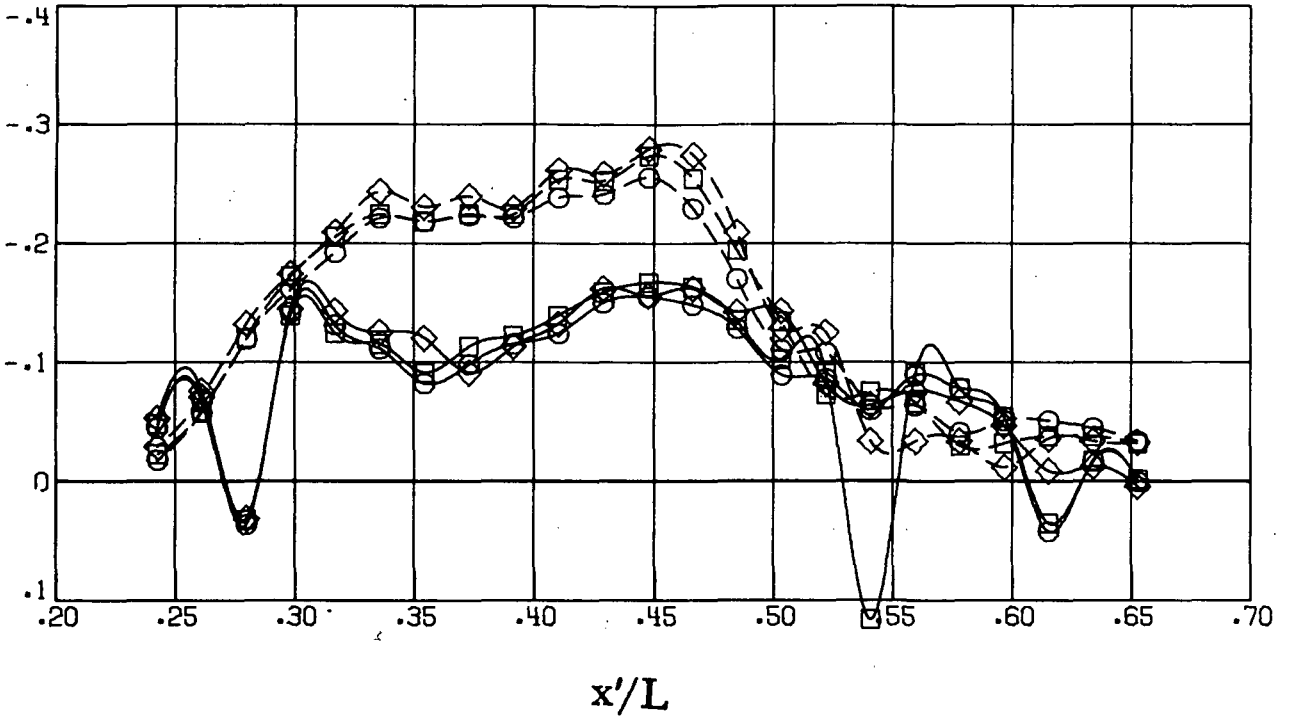
(d) Selected wing pressure distributions.

Figure 26.- Continued.

	δ_{F1}	δ_{F2}	δ_{F3}	δ_{F4}	α
○	0	0	20	0	2.97
□	0	0	0	0	3.39
◇	0	0	-20	0	3.70

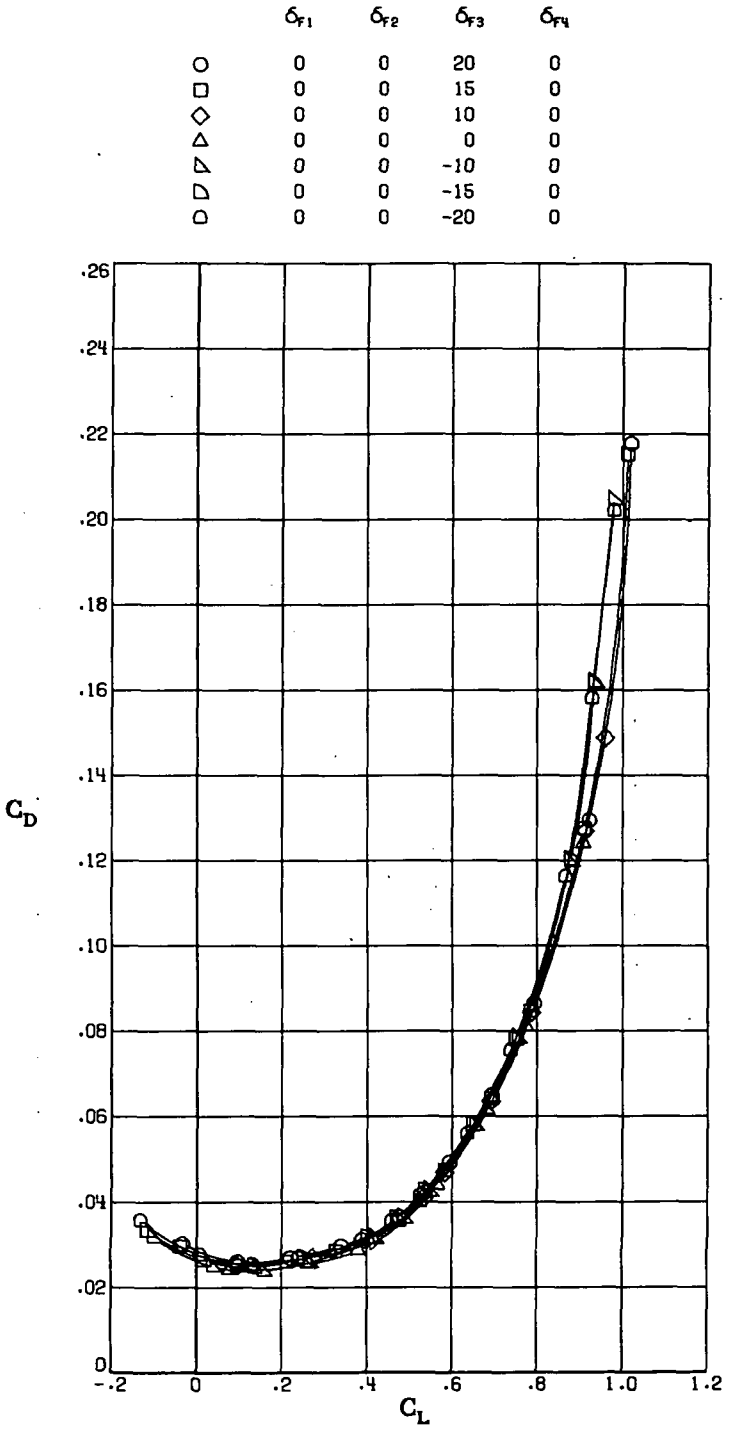
—— Top Centerline

– – Right Side



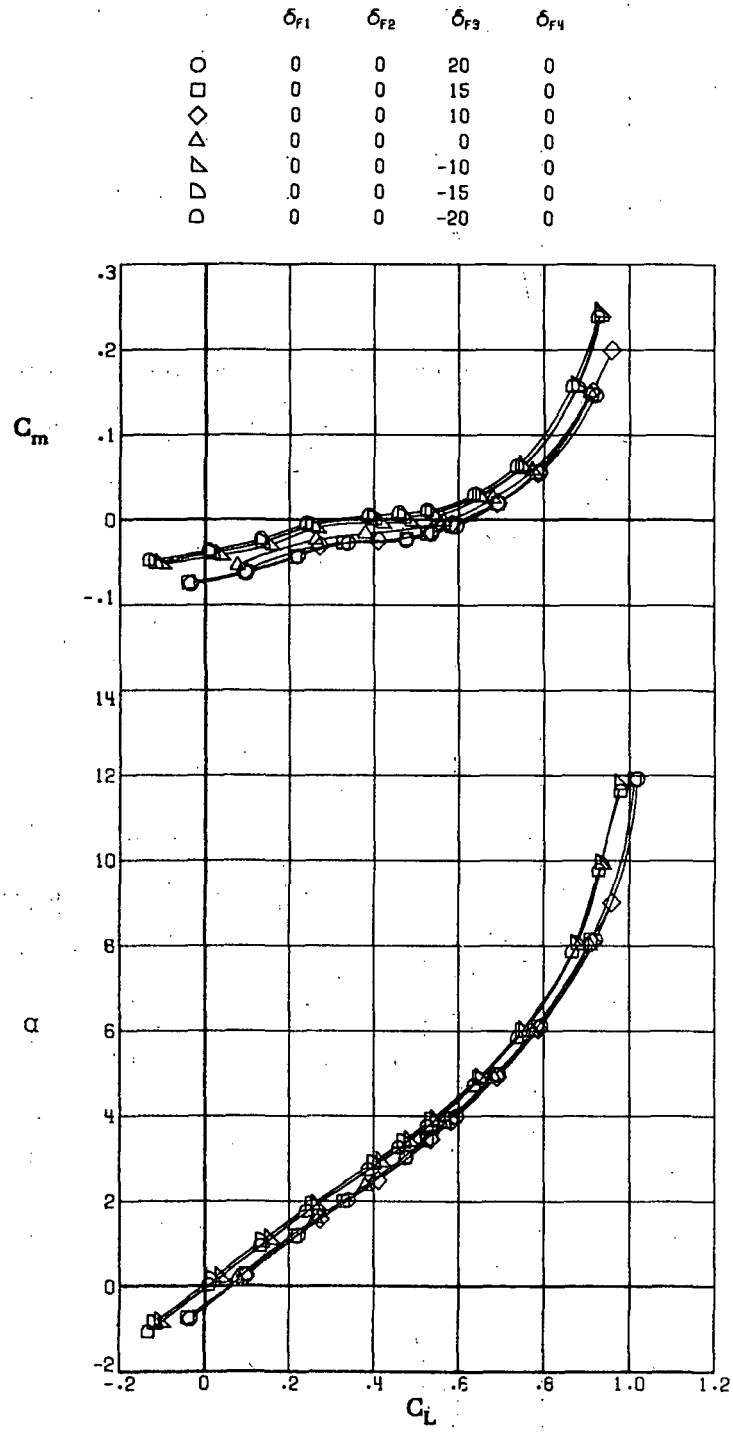
(e) Selected fuselage pressure distributions.

Figure 26.- Concluded.



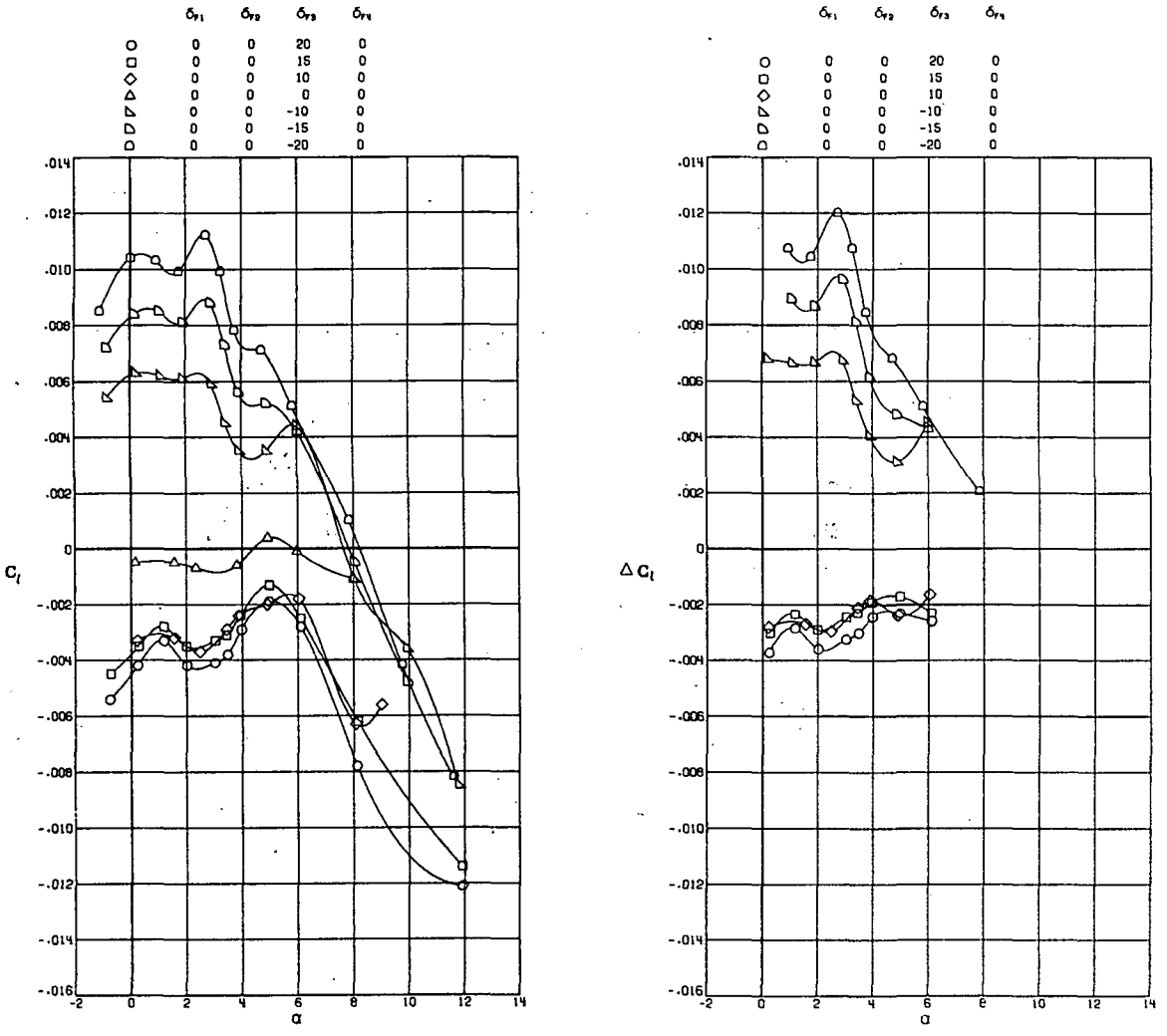
(a) Drag characteristics.

Figure 27.- Effect of F_3 trailing-edge control deflection on aerodynamic characteristics of model with area-ruled fuselage at $M_\infty = 0.92$.



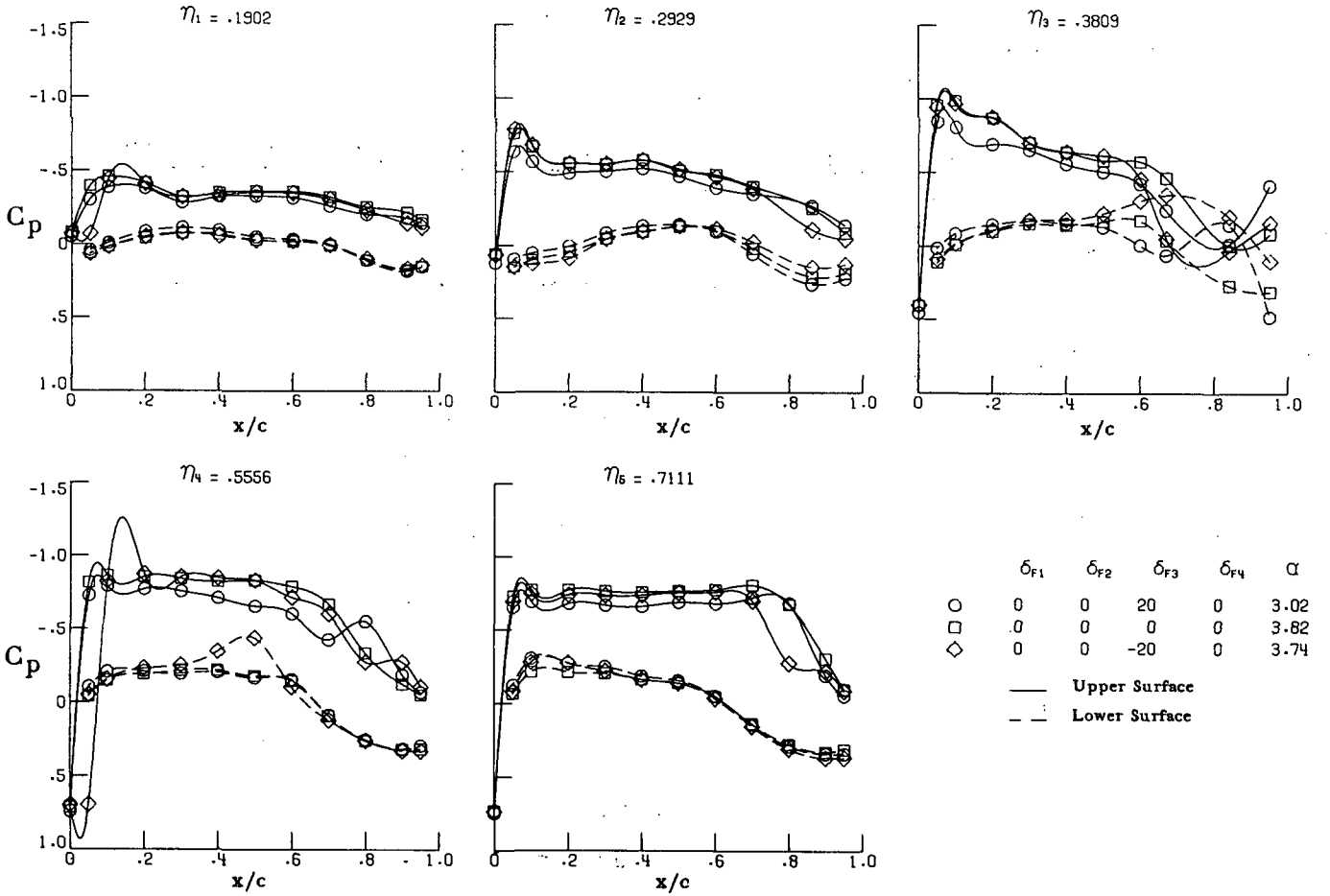
(b) Lift and pitch characteristics.

Figure 27.- Continued.



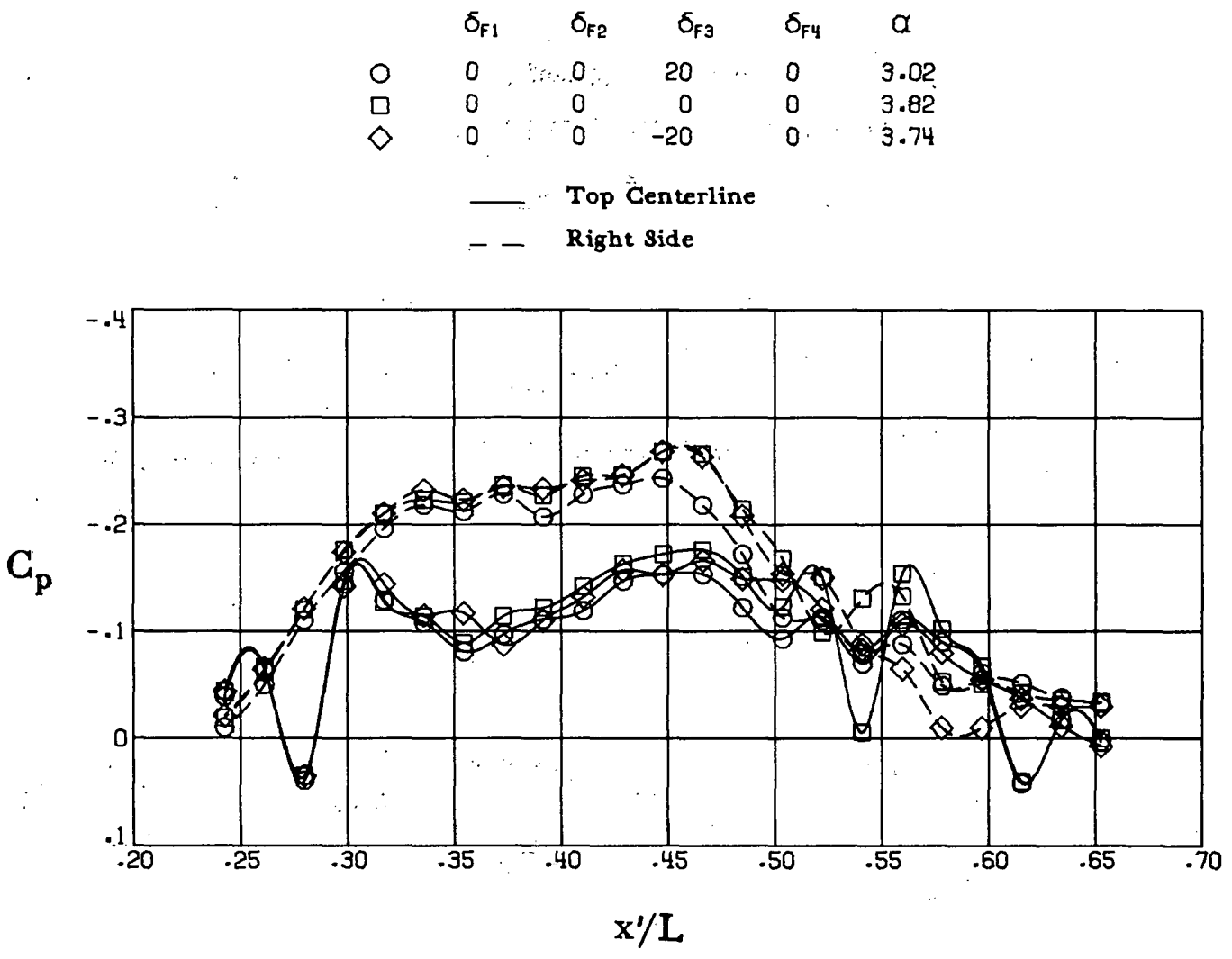
(c) Rolling-moment characteristics.

Figure 27.- Continued.



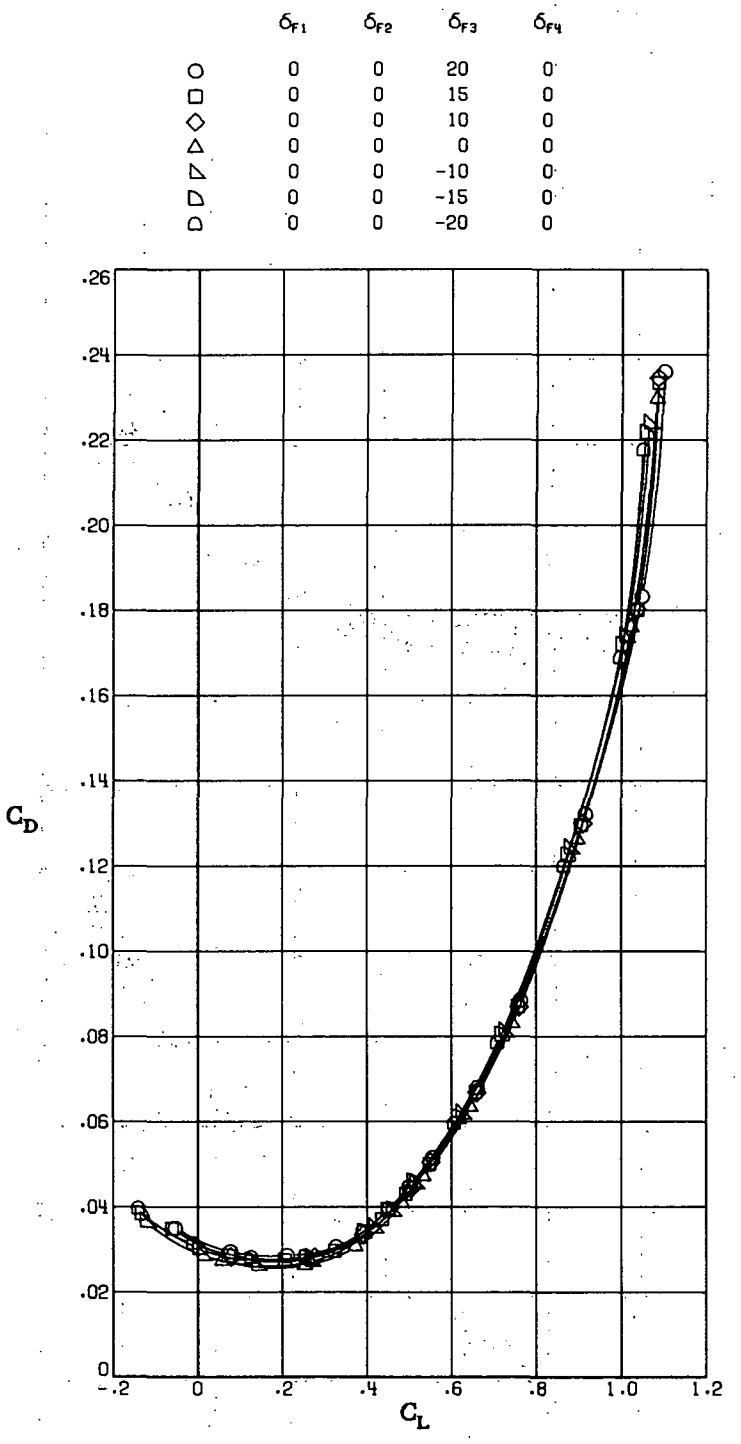
(d) Selected wing pressure distributions.

Figure 27.- Continued.



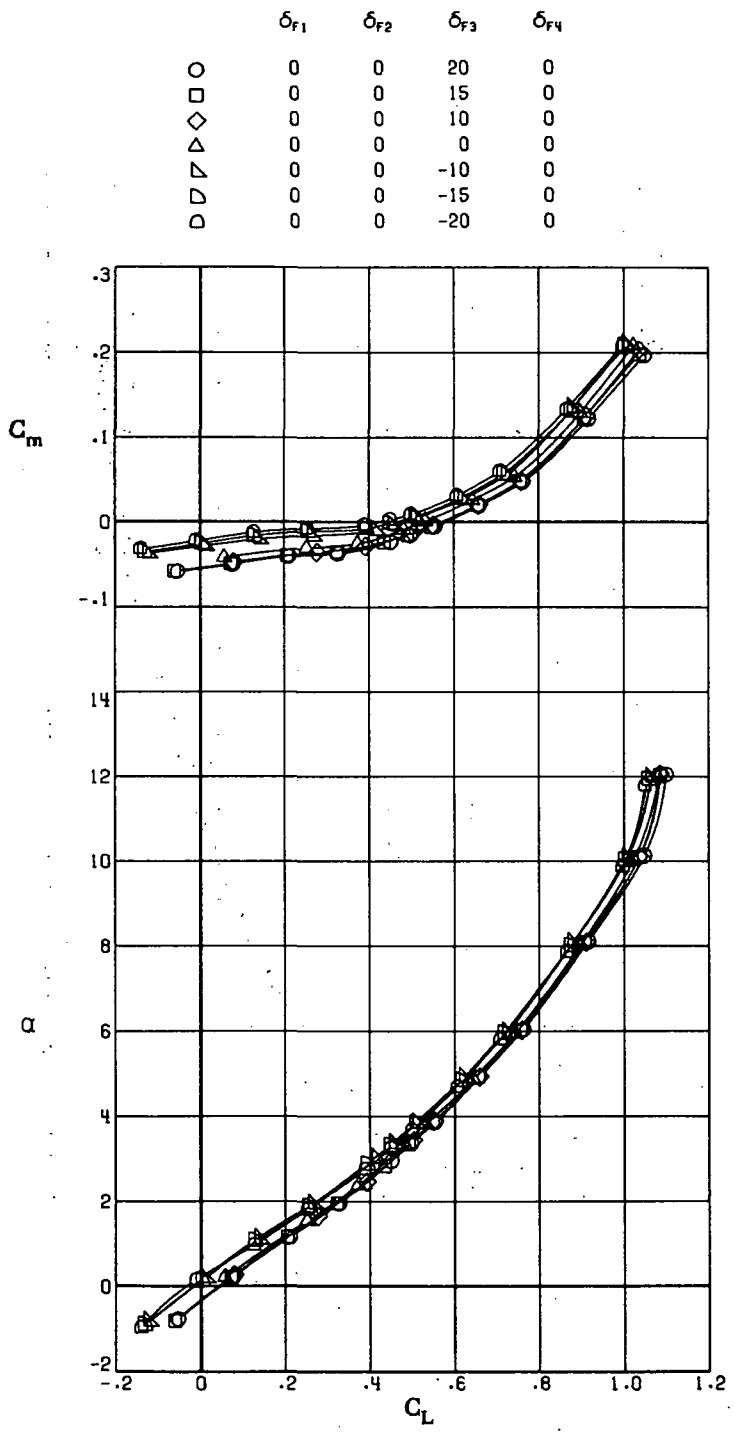
(e) Selected fuselage pressure distributions.

Figure 27.- Concluded.



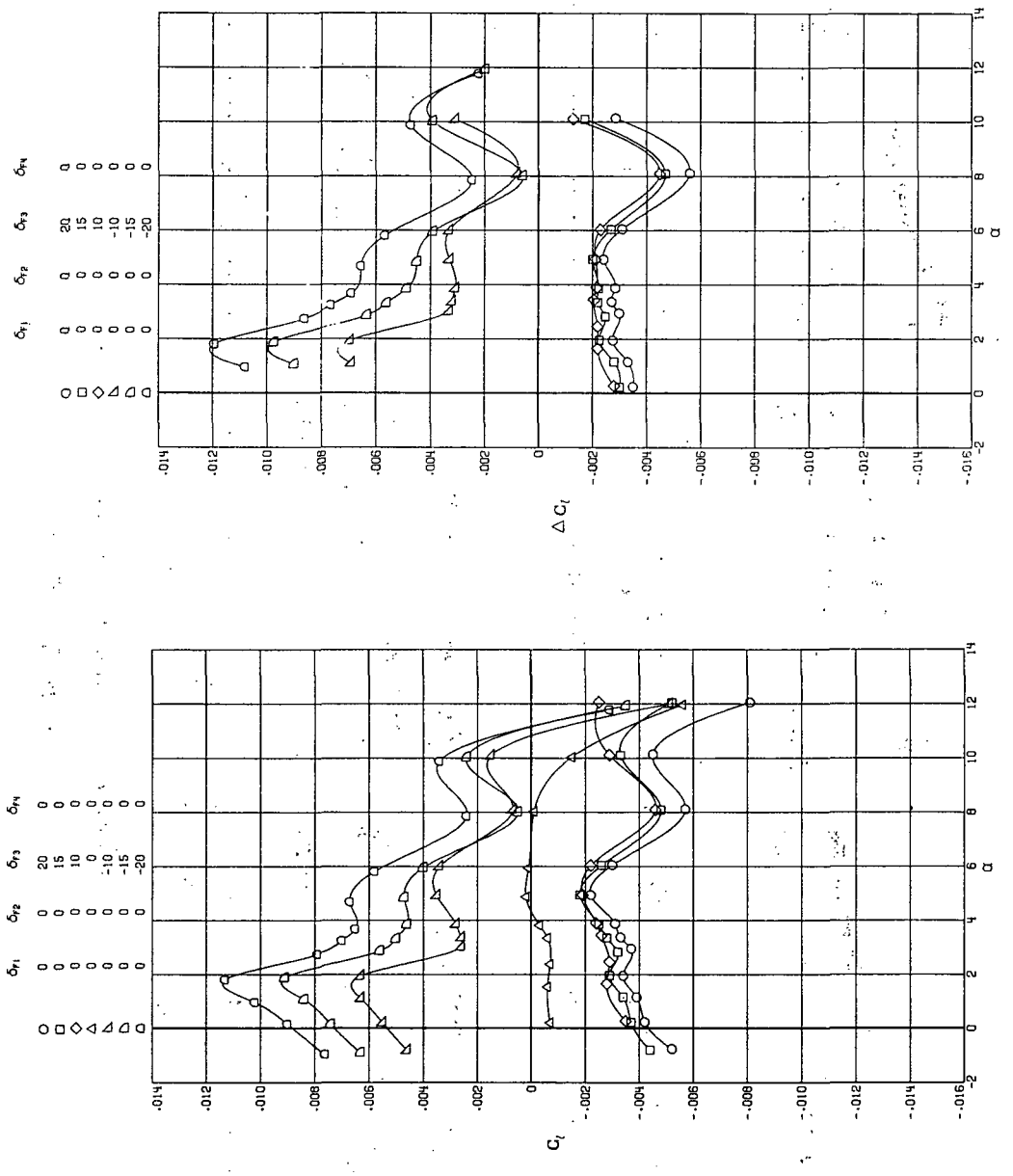
(a) Drag characteristics.

Figure 28.- Effect of F_3 trailing-edge control deflection on aerodynamic characteristics of model with area-ruled fuselage at $M_\infty = 0.94$.



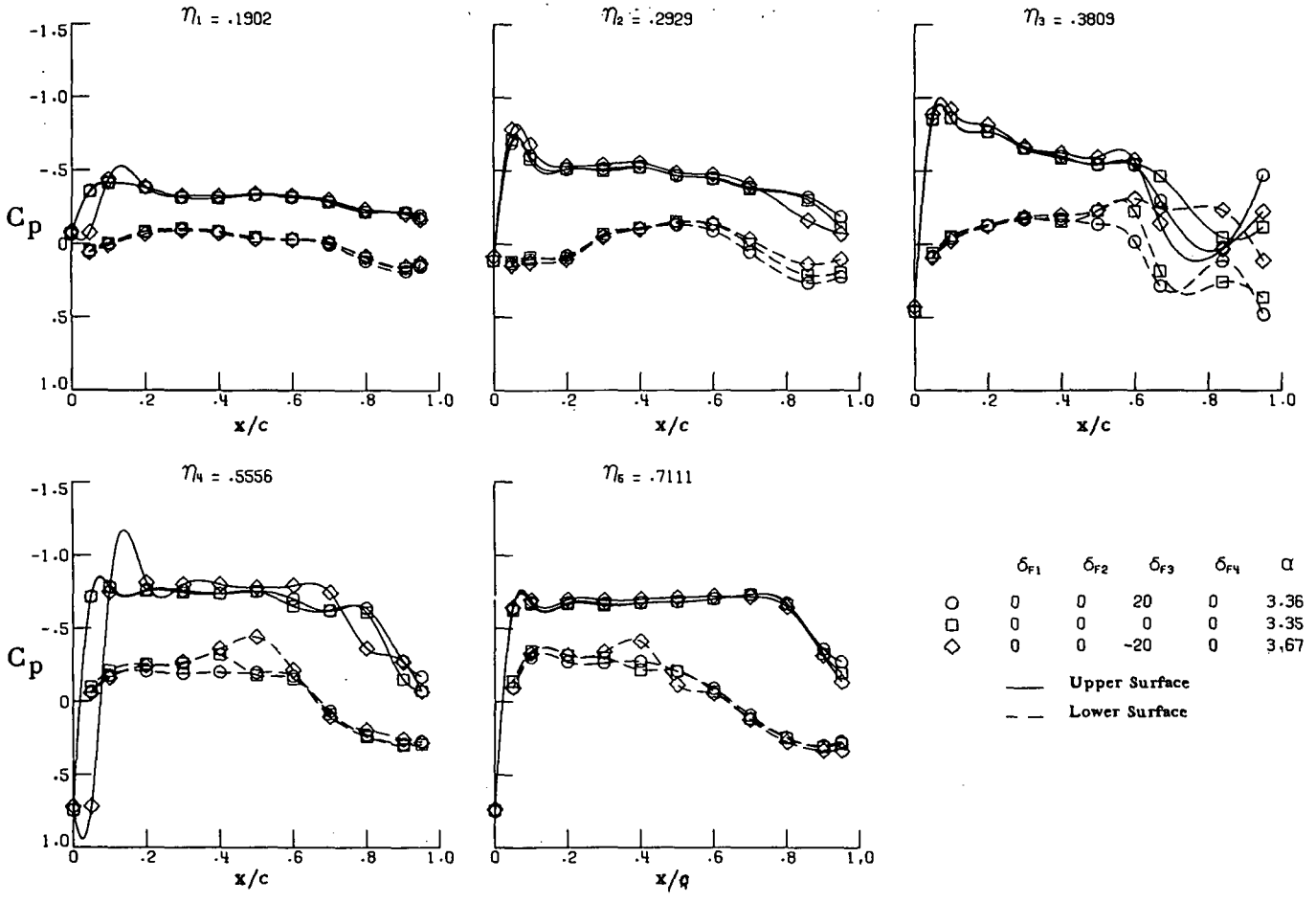
(b) Lift and pitch characteristics.

Figure 28.- Continued.



(c) Rolling-moment characteristics.

Figure 28.- Continued.



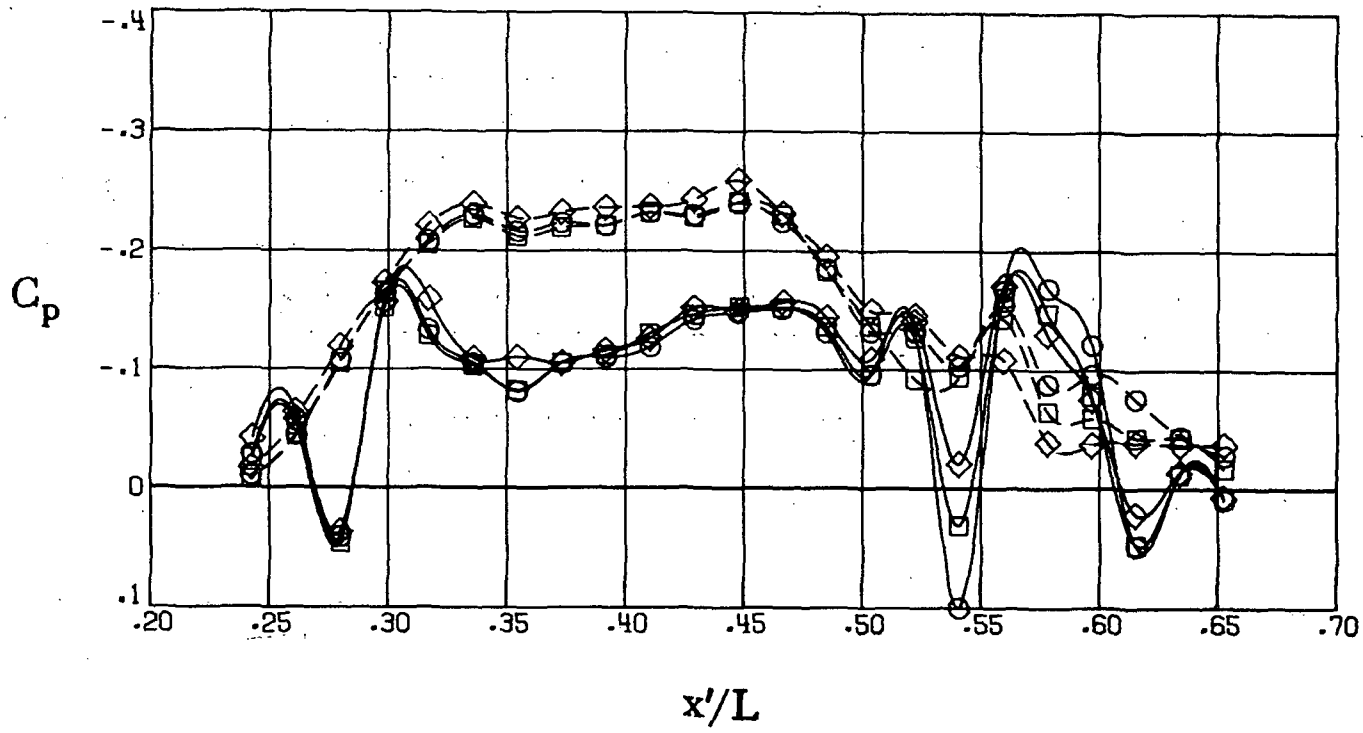
(d) Selected wing pressure distributions.

Figure 28.- Continued.

	δ_{F1}	δ_{F2}	δ_{F3}	δ_{F4}	α
○	0	0	20	0	3.36
□	0	0	0	0	3.35
◇	0	0	-20	0	3.67

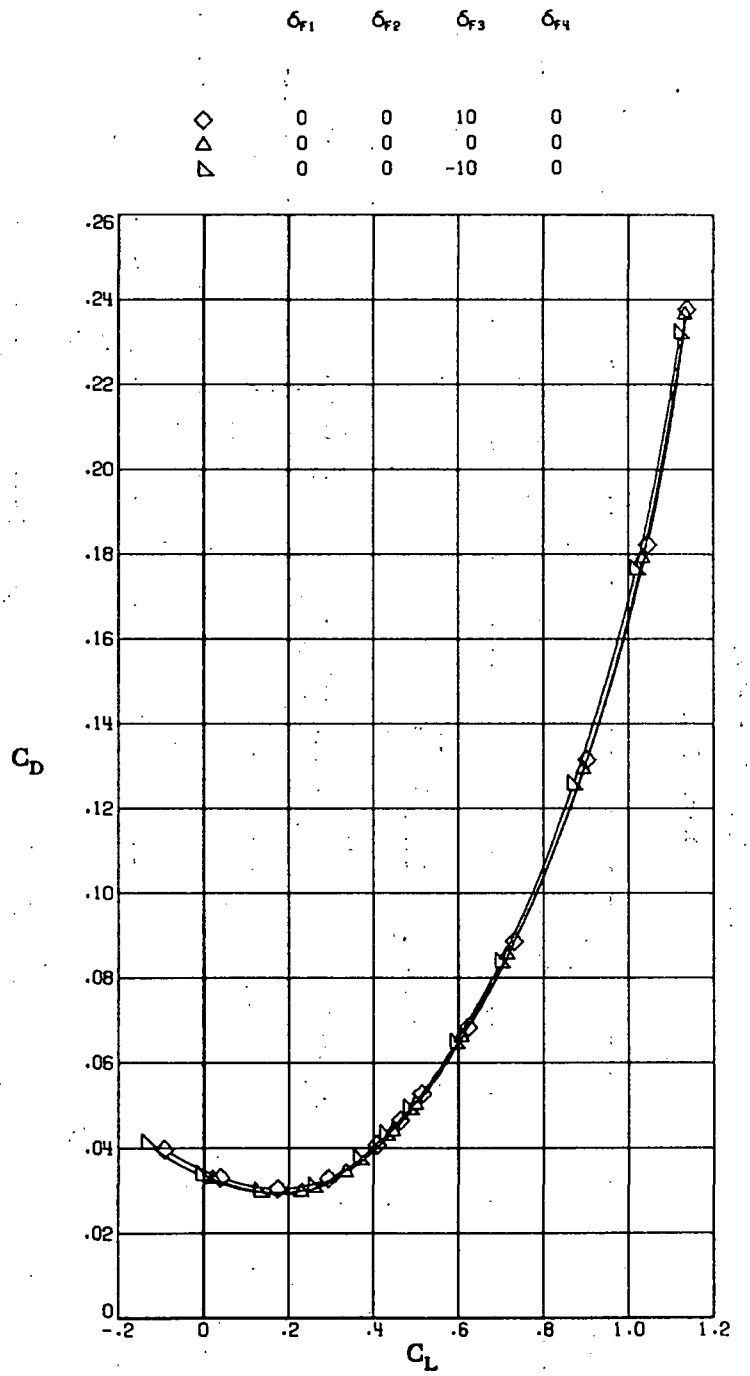
—— Top Centerline

– – Right Side



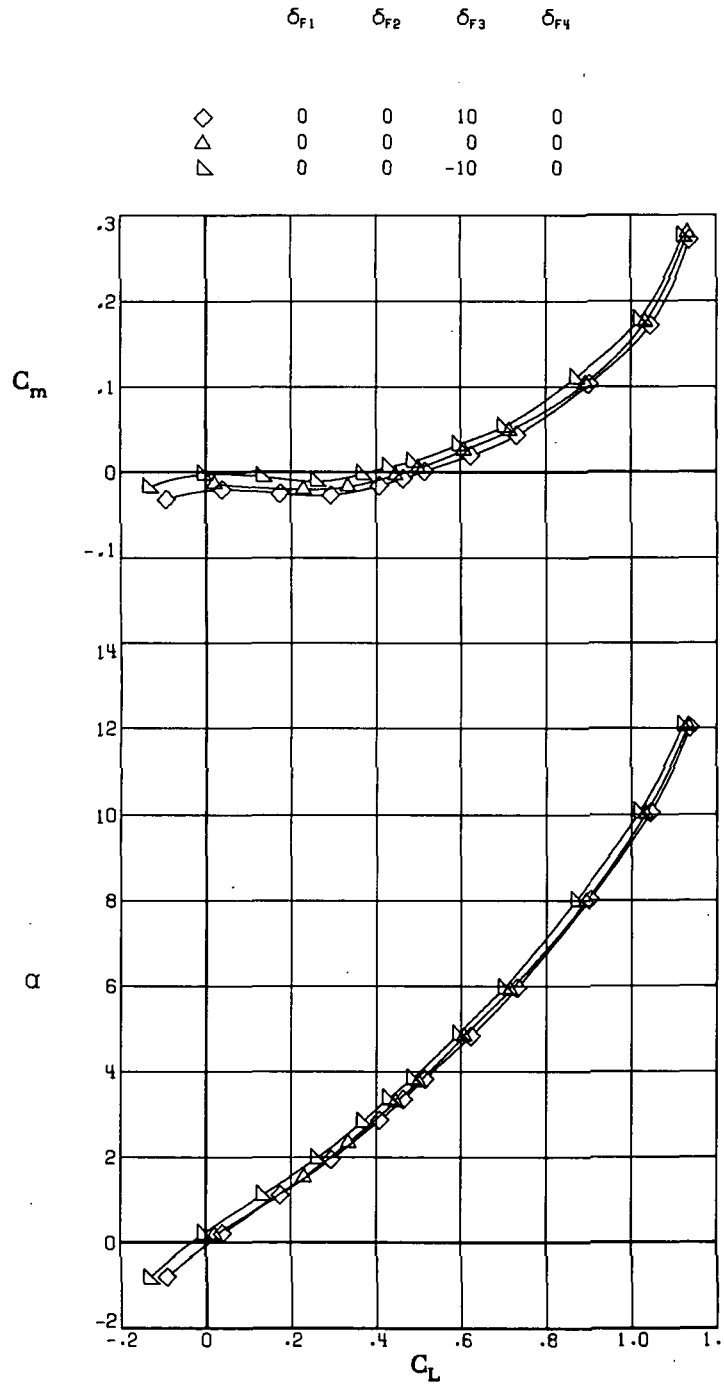
(e) Selected fuselage pressure distributions.

Figure 28.- Concluded.



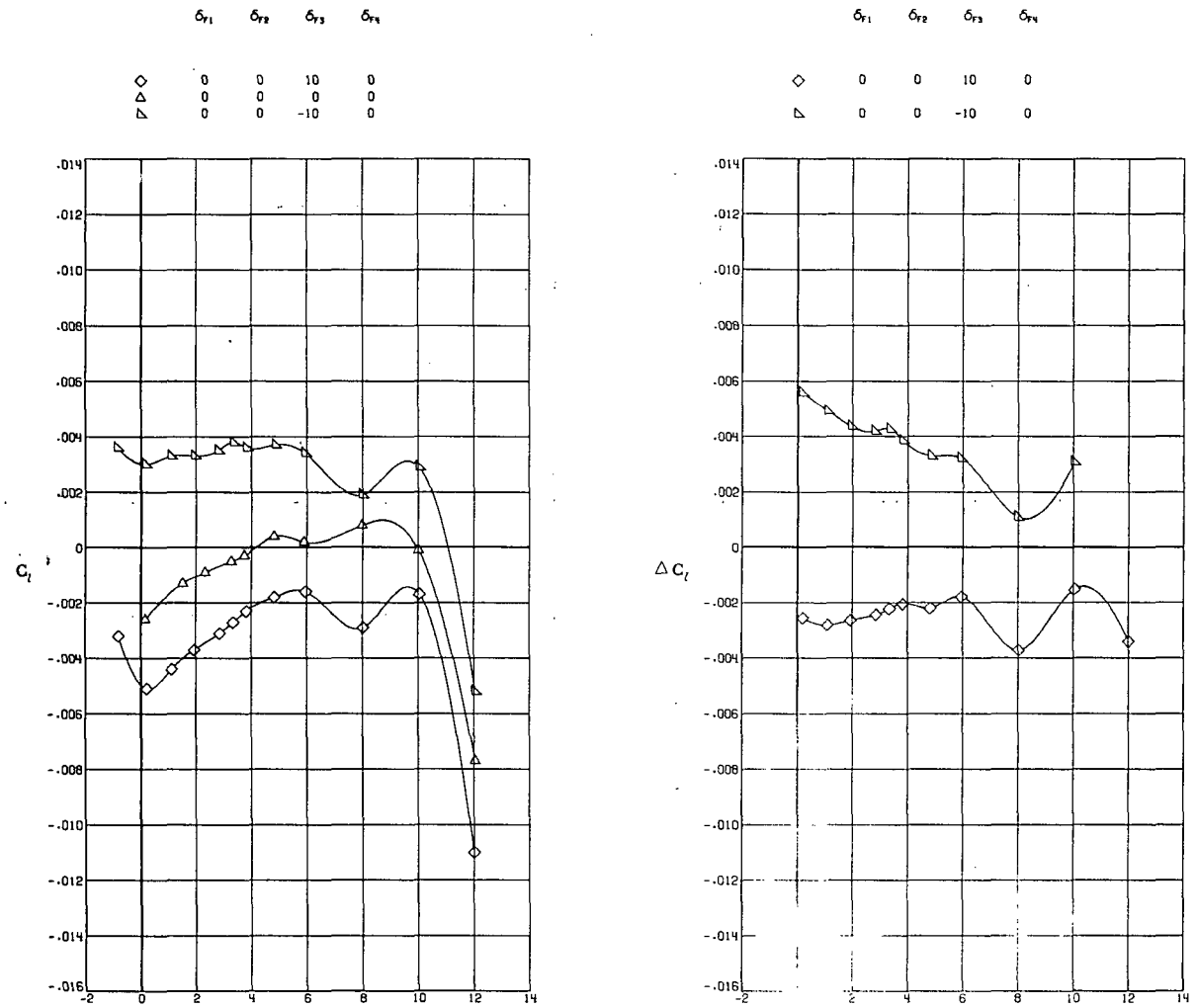
(a) Drag characteristics.

Figure 29.- Effect of F_3 trailing-edge control deflection on aerodynamic characteristics of model with area-ruled fuselage at $M_\infty = 0.96$.



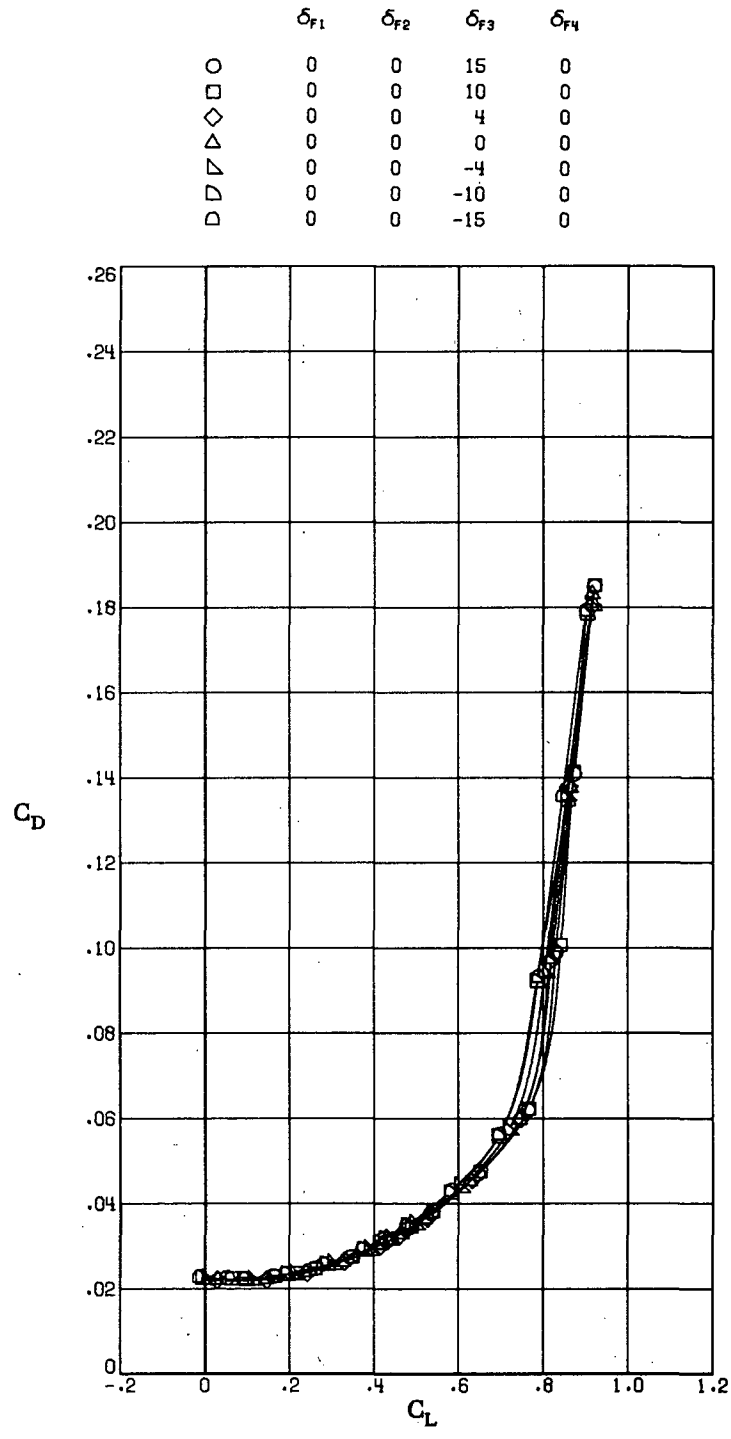
(b) Lift and pitch characteristics.

Figure 29.- Continued.



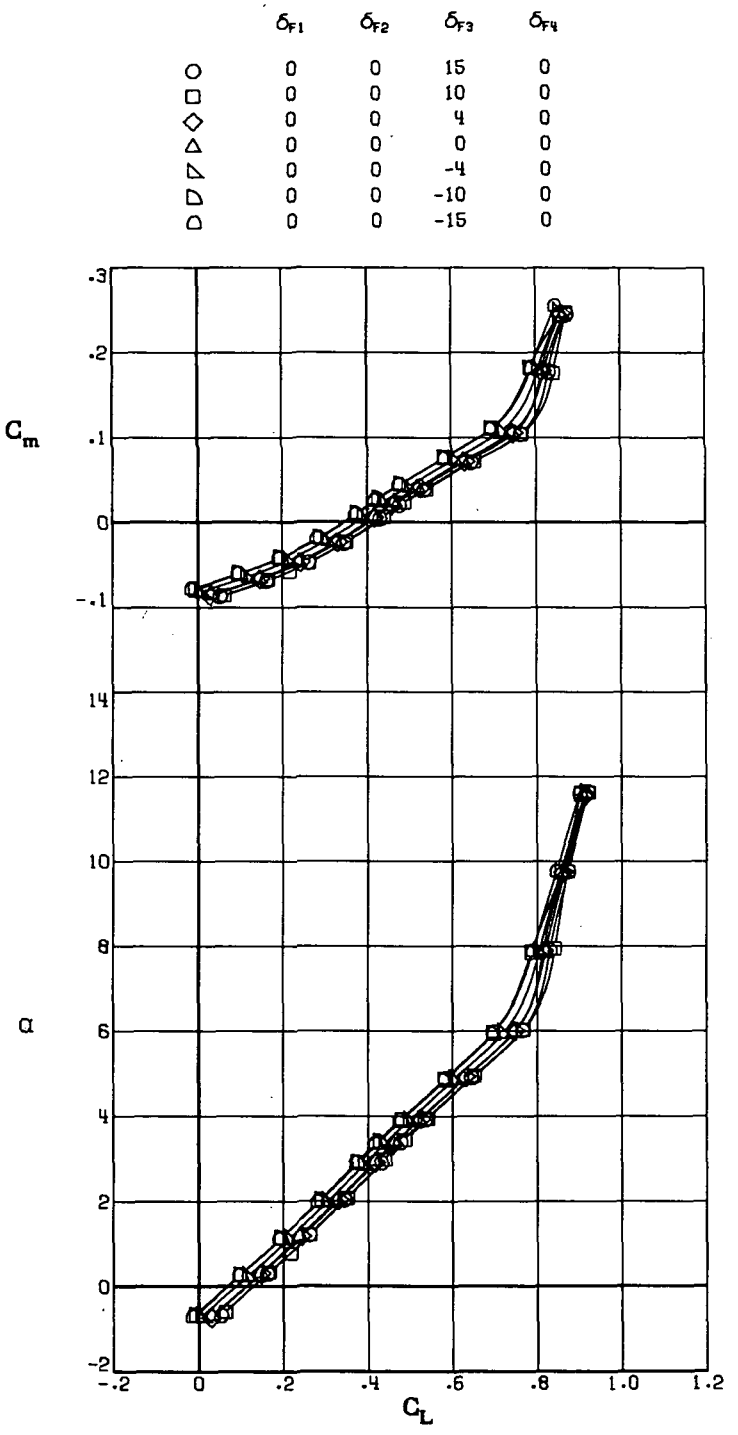
(c) Rolling-moment characteristics.

Figure 29.- Concluded.



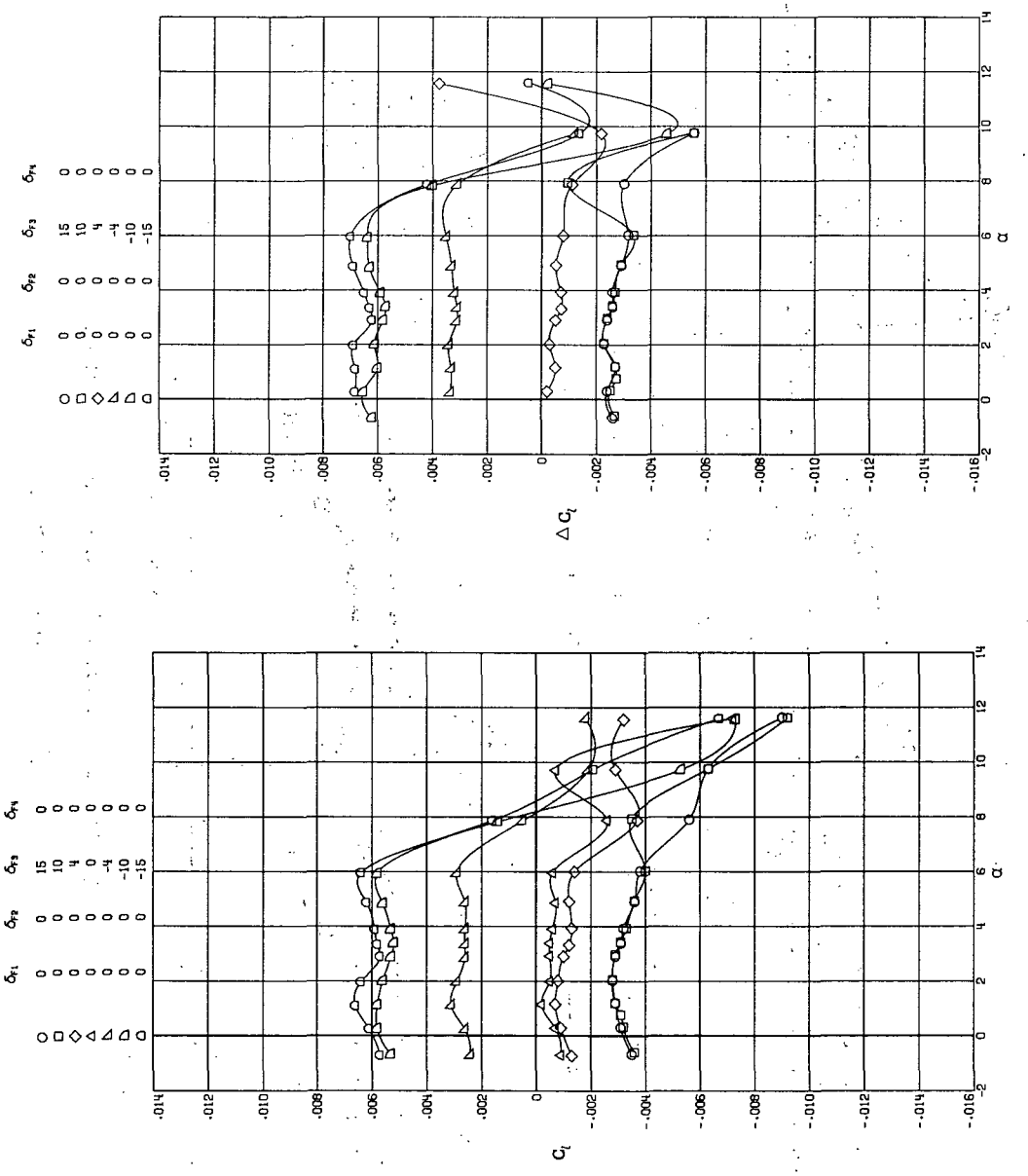
(a) Drag characteristics.

Figure 30.- Effect of F_3 trailing-edge control deflection on aerodynamic characteristics of model with cylindrical fuselage at $M_\infty = 0.80$.



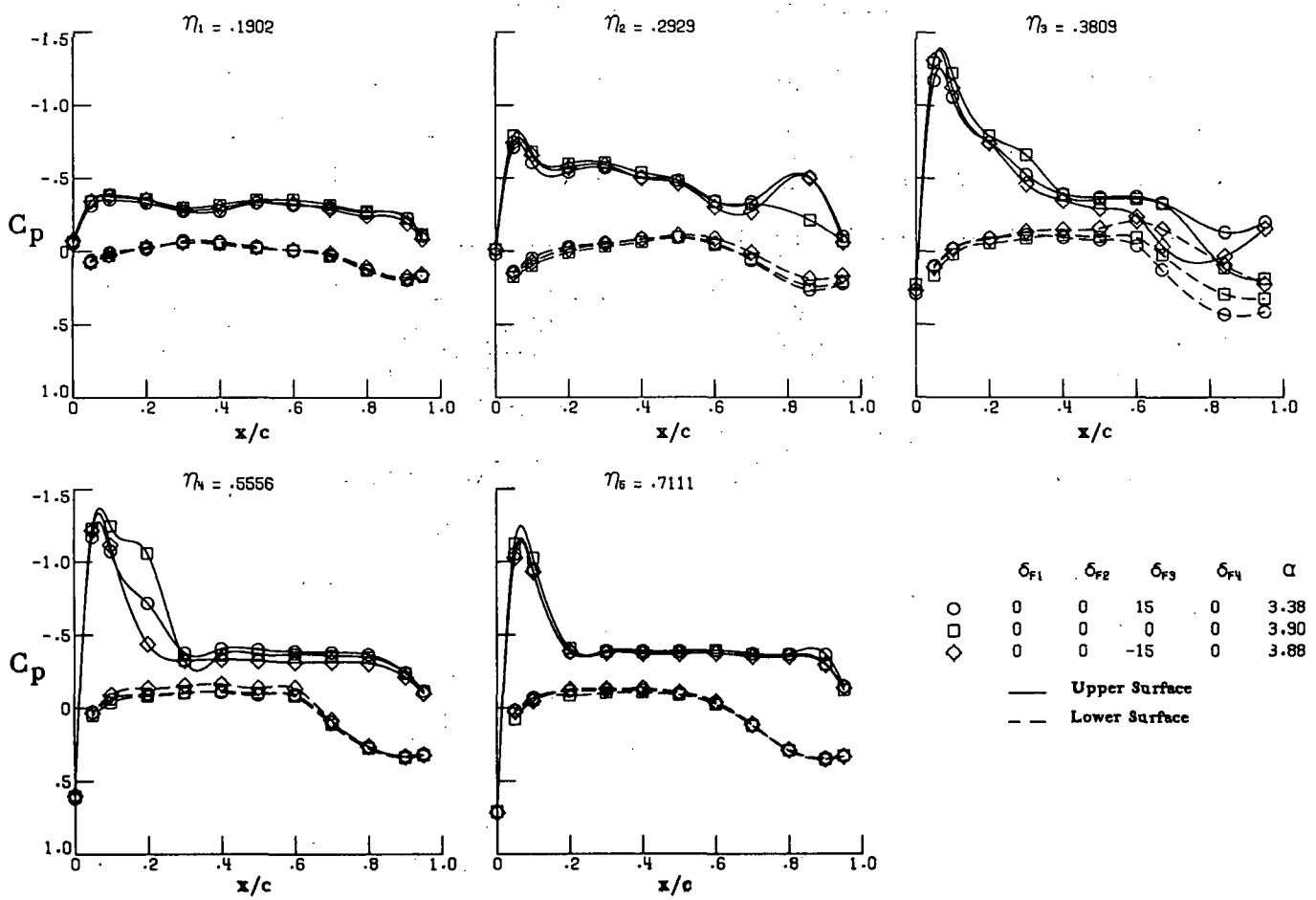
(b) Lift and pitch characteristics.

Figure 30.- Continued.



(c) Rolling-moment characteristics.

Figure 30.- Continued.

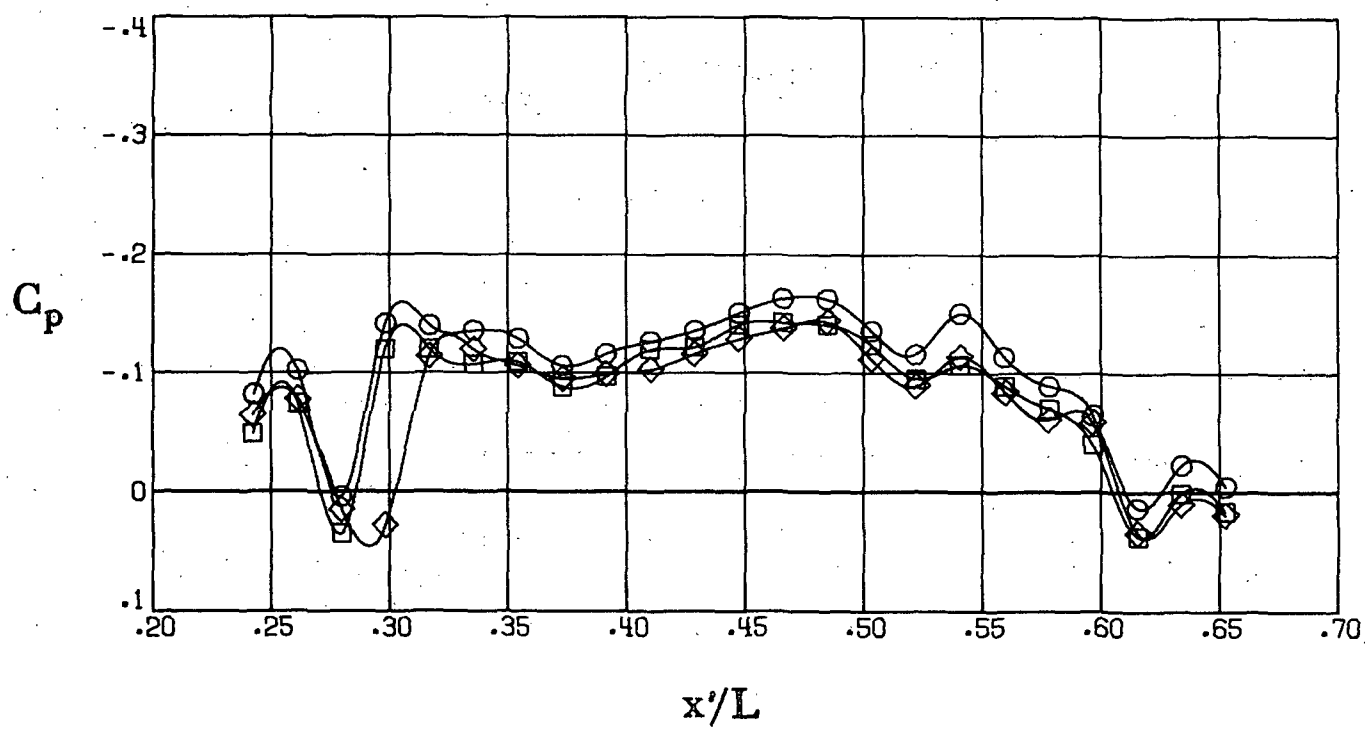


(d) Selected wing pressure distributions.

Figure 30.- Continued.

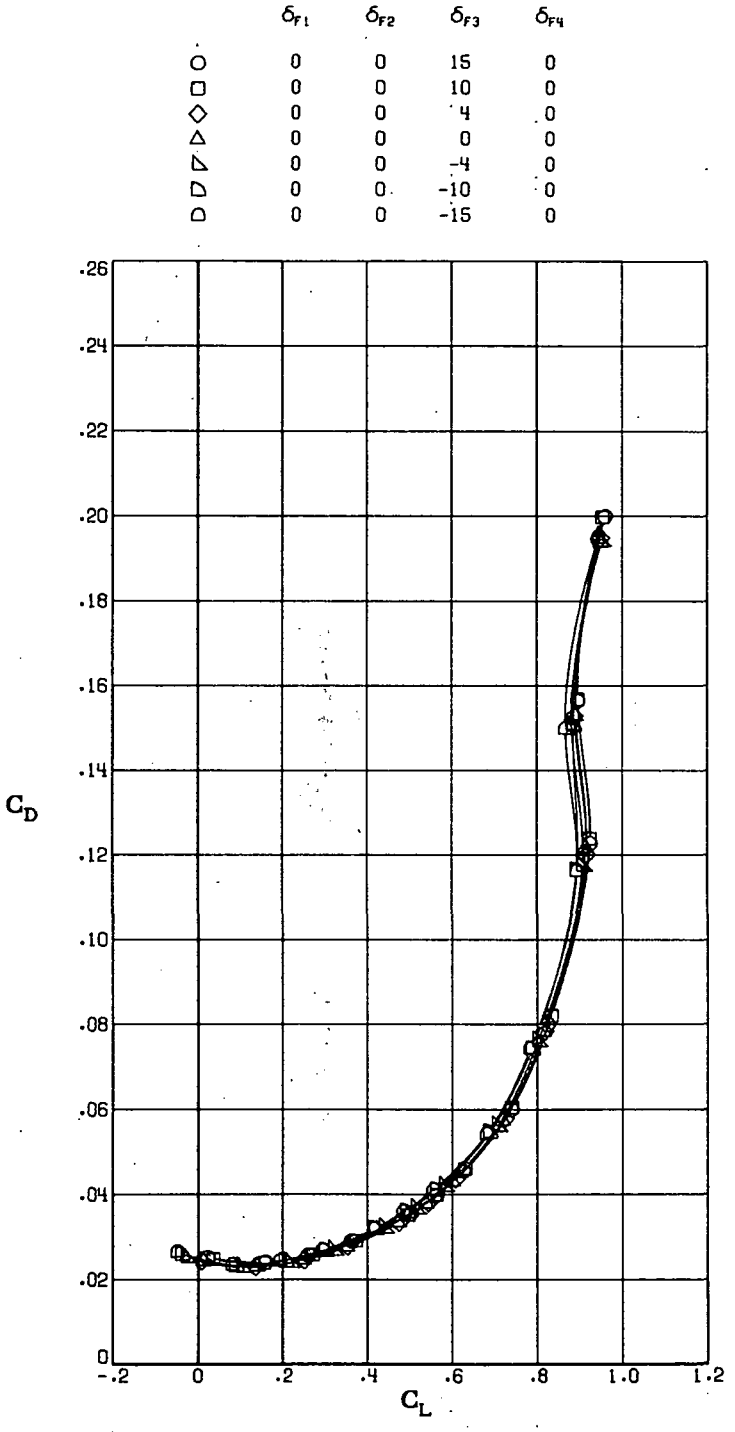
	δ_{F1}	δ_{F2}	δ_{F3}	δ_{F4}	α
○	0	0	15	0	3.38
□	0	0	0	0	3.90
◇	0	0	-15	0	3.88

—— Top Centerline



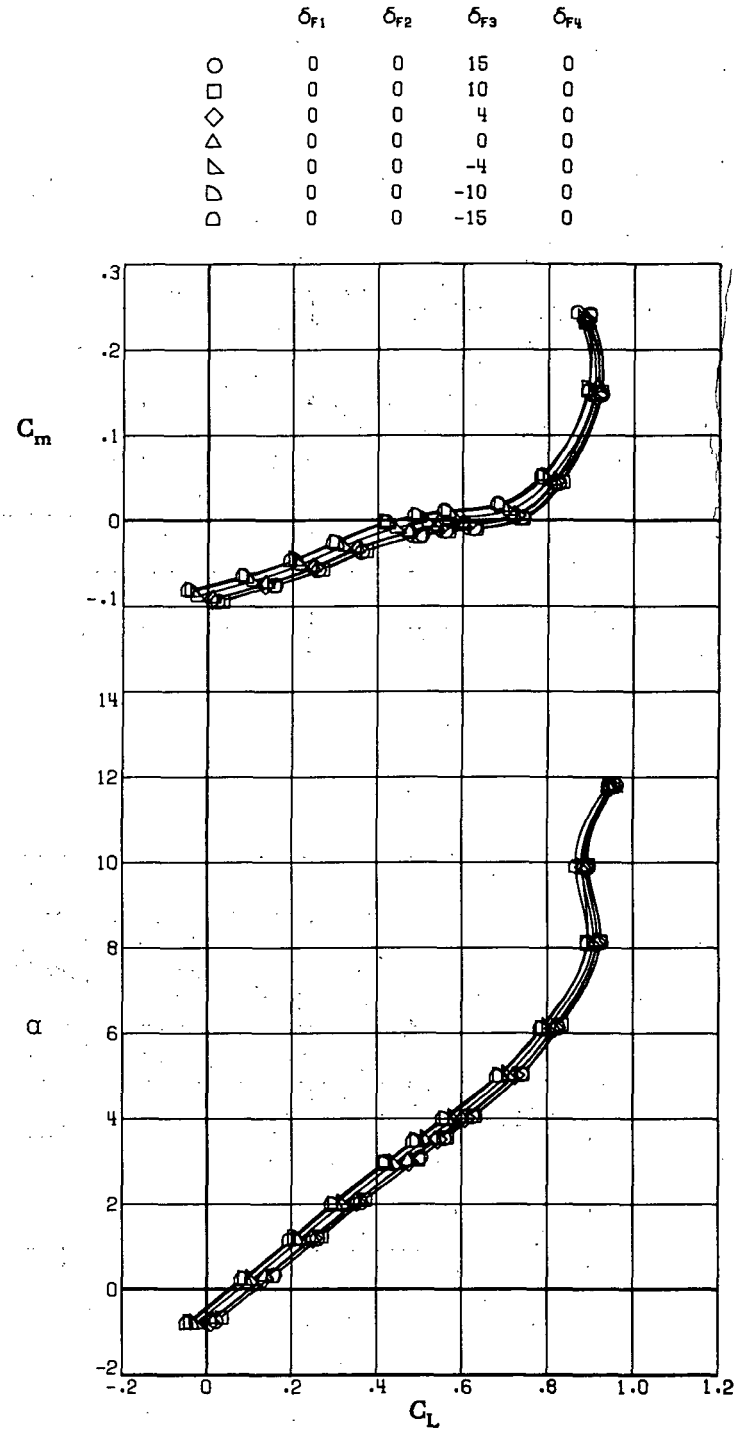
(e) Selected fuselage pressure distributions.

Figure 30.- Concluded.



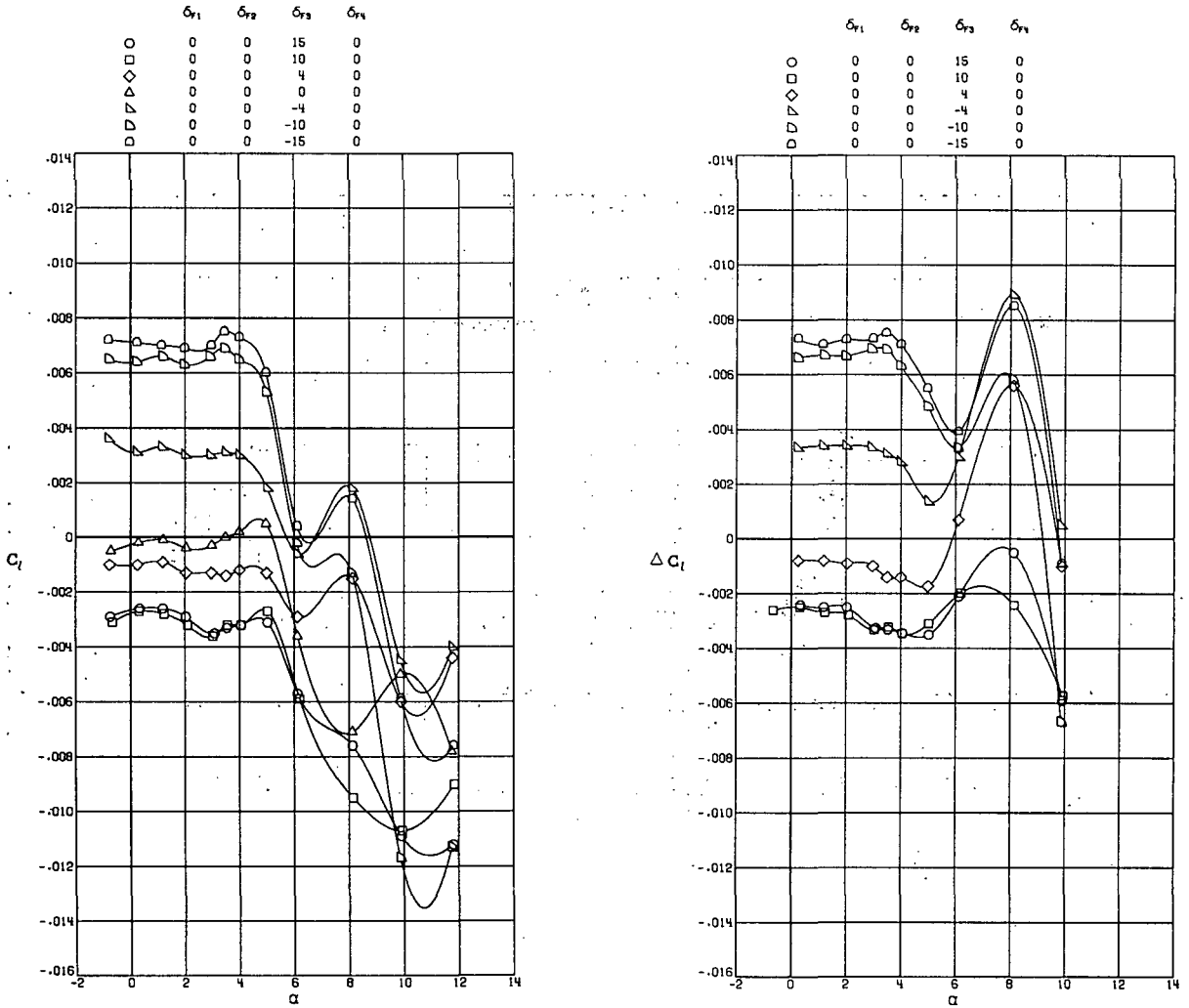
(a) Drag characteristics.

Figure 31.- Effect of F_3 trailing-edge control deflection on aerodynamic characteristics of model with cylindrical fuselage at $M_\infty = 0.88$.



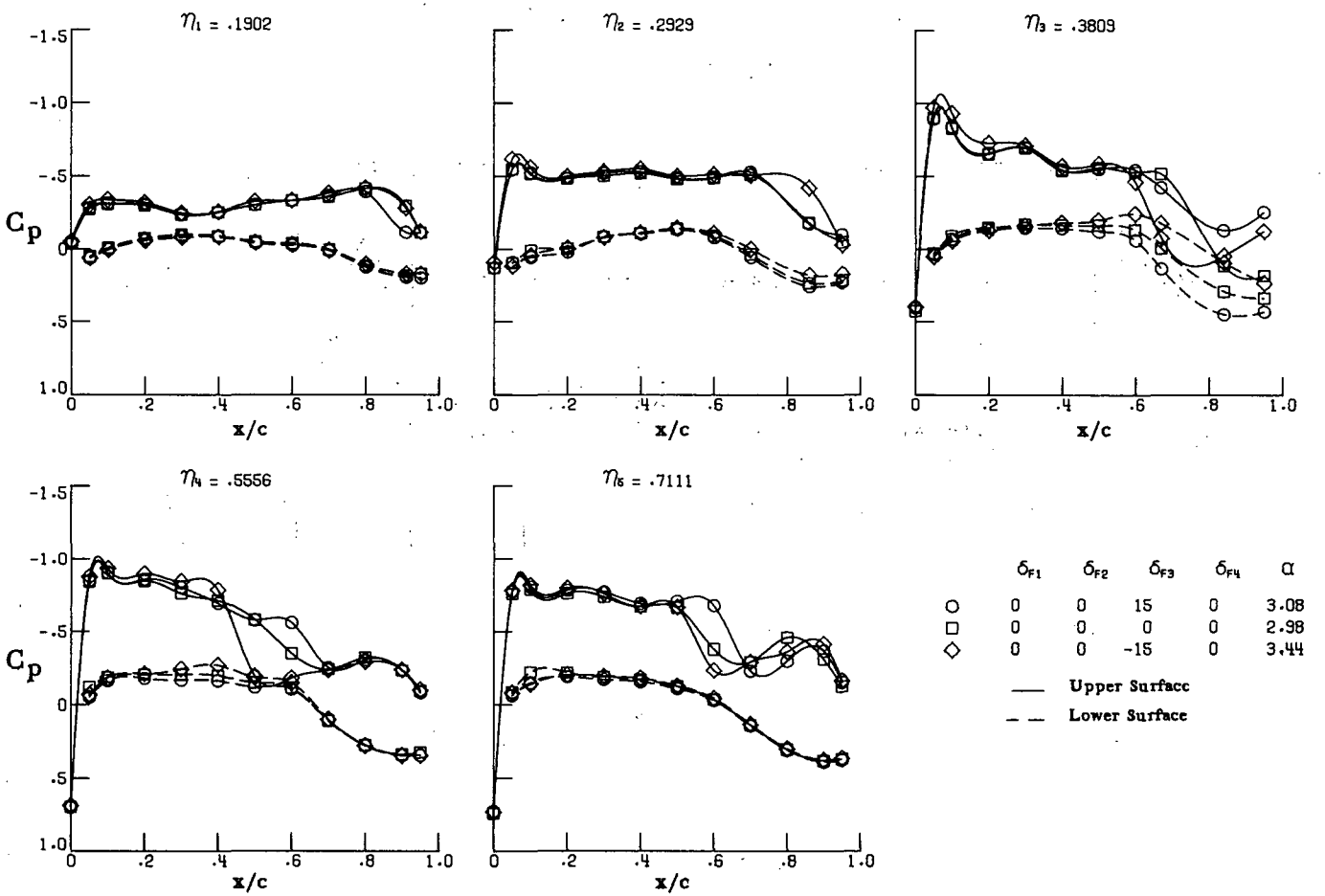
(b) Lift and pitch characteristics.

Figure 31.- Continued.



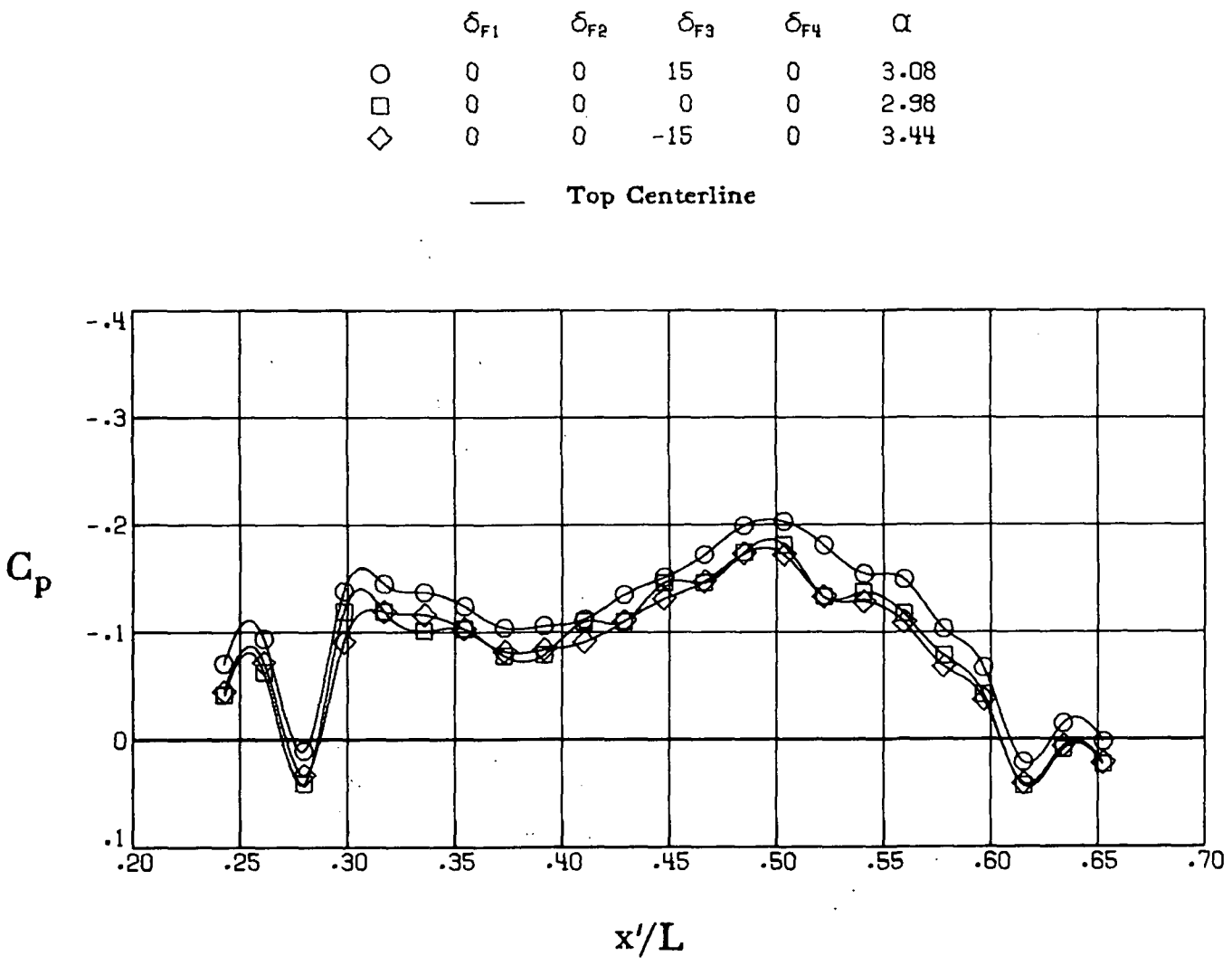
(c) Rolling-moment characteristics.

Figure 31.- Continued.



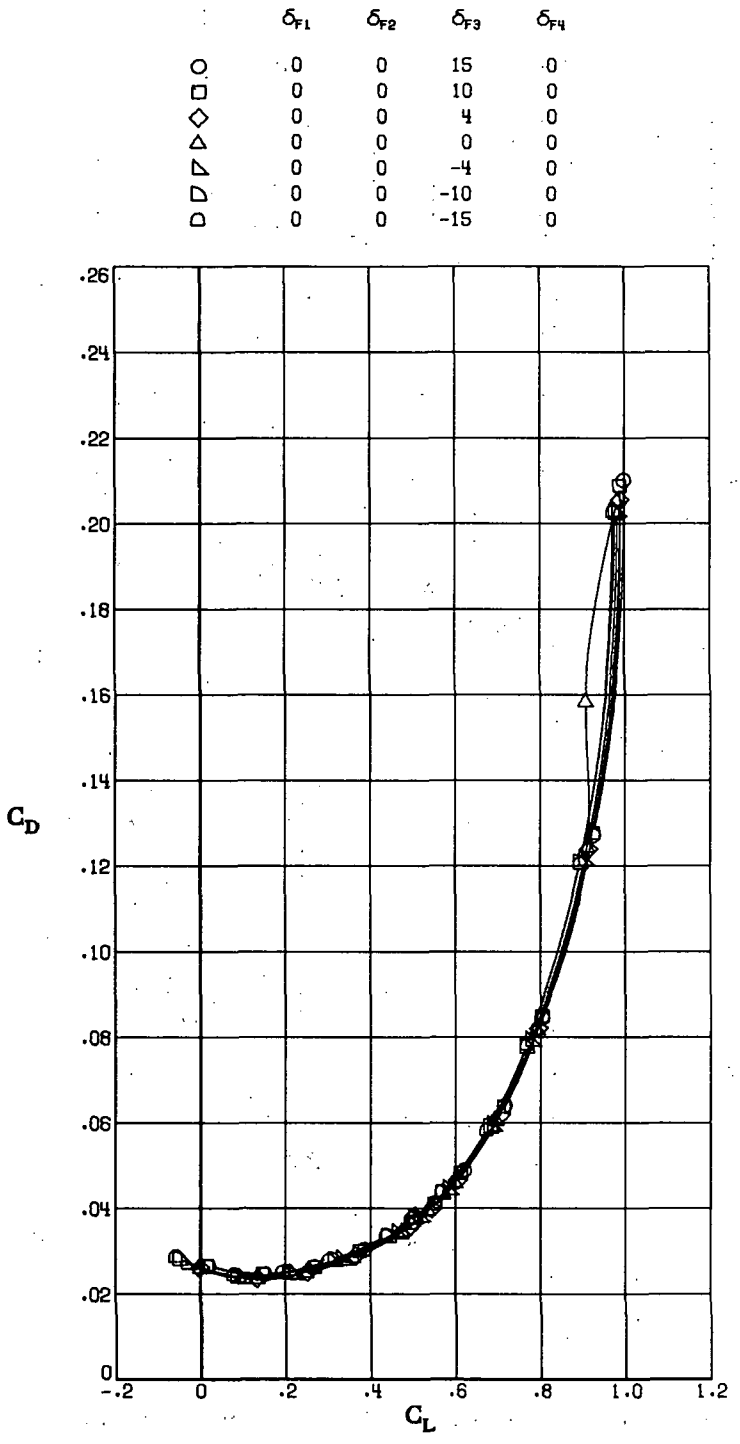
(d) Selected wing pressure distributions.

Figure 31.- Continued.



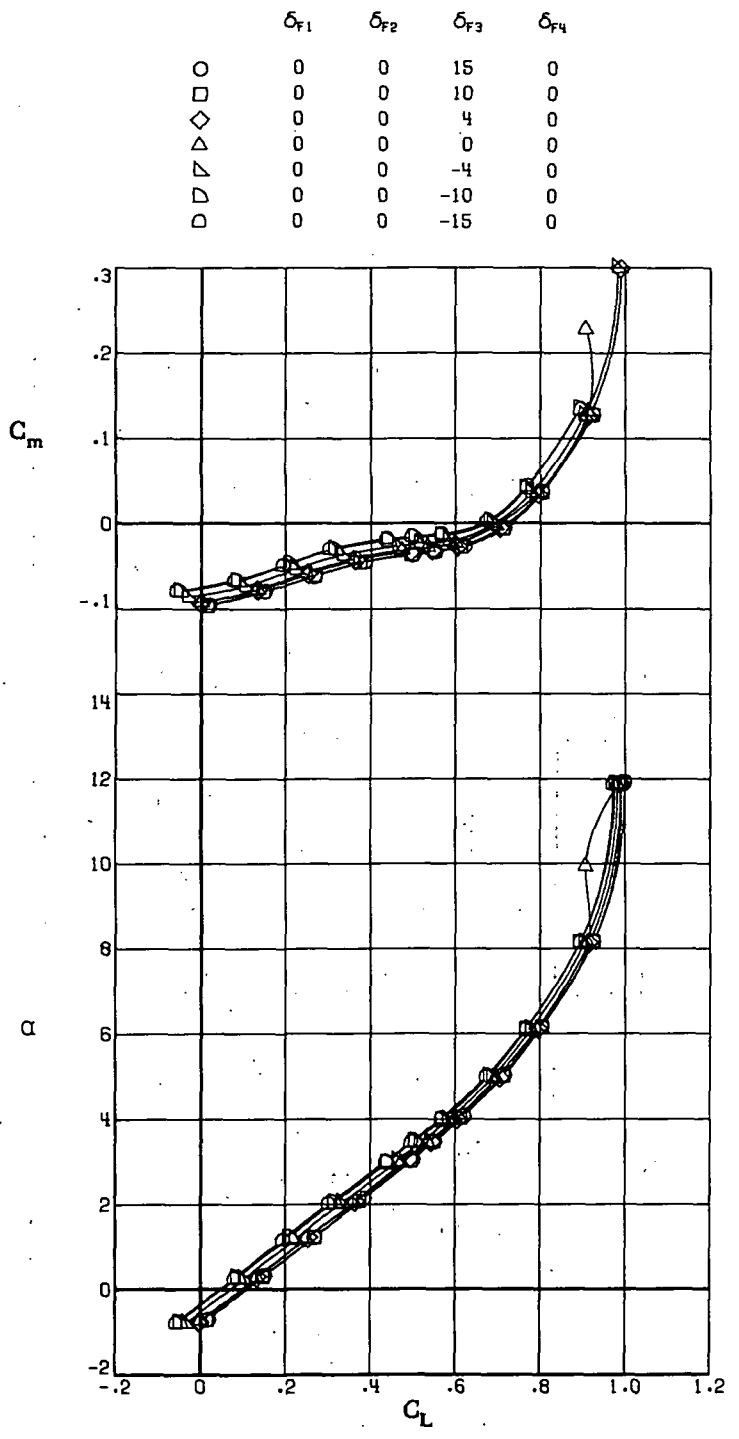
(e) Selected fuselage pressure distributions.

Figure 31.- Concluded.



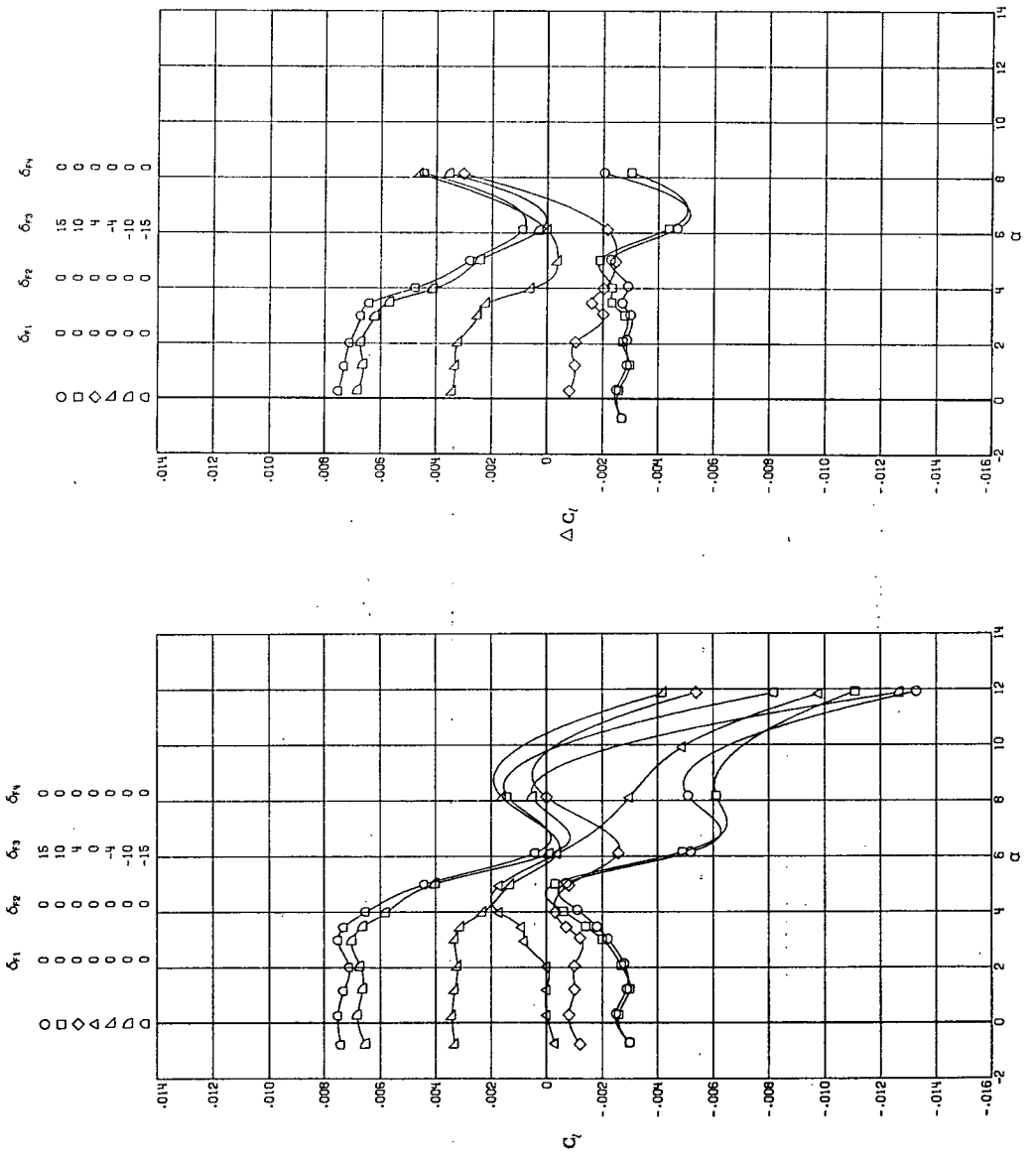
(a) Drag characteristics.

Figure 32.- Effect of F_3 trailing-edge control deflection on aerodynamic characteristics of model with cylindrical fuselage at $M_\infty = 0.90$.



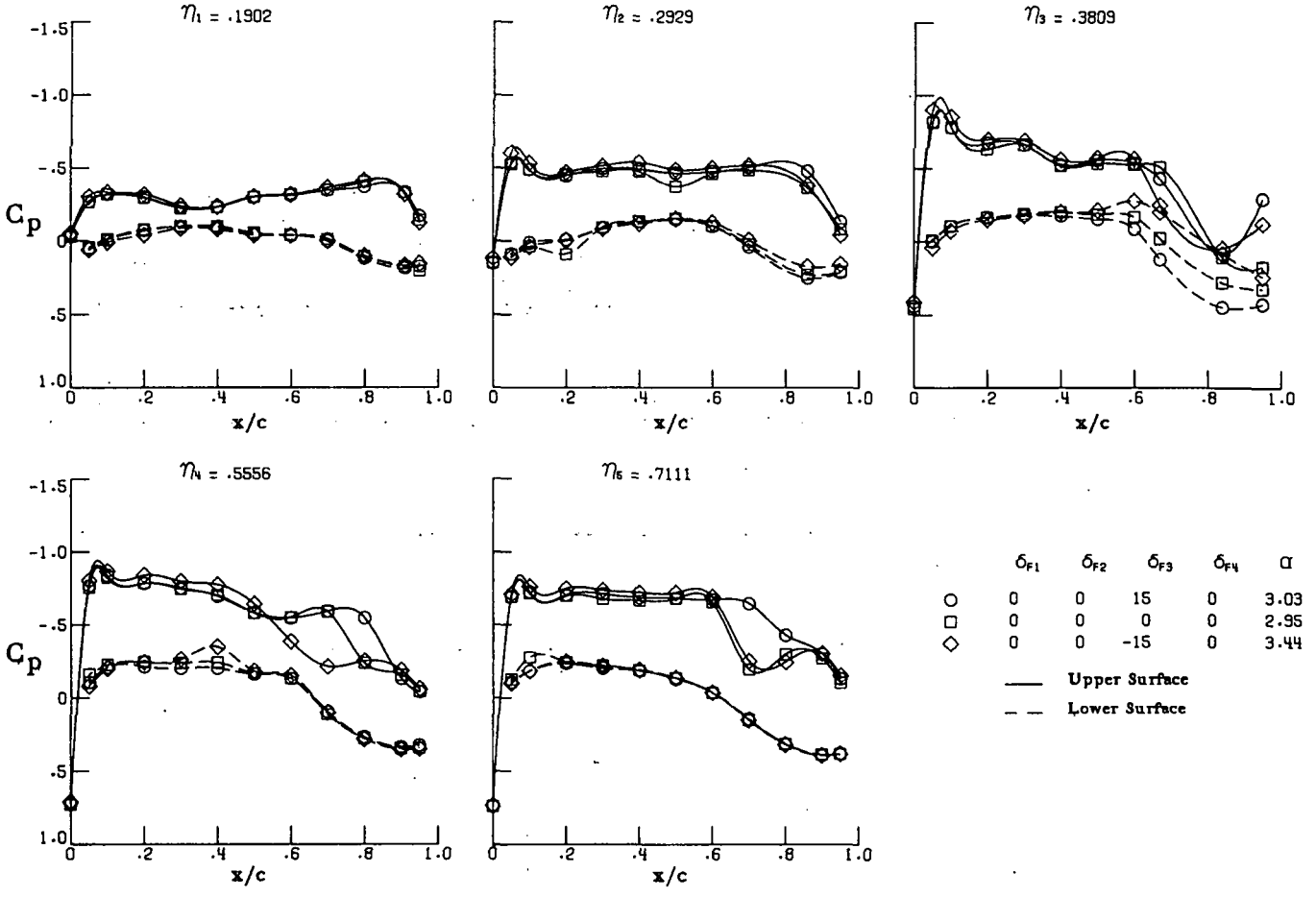
(b) Lift and pitch characteristics.

Figure 32.- Continued.



(c) Rolling-moment characteristics.

Figure 32.- Continued.

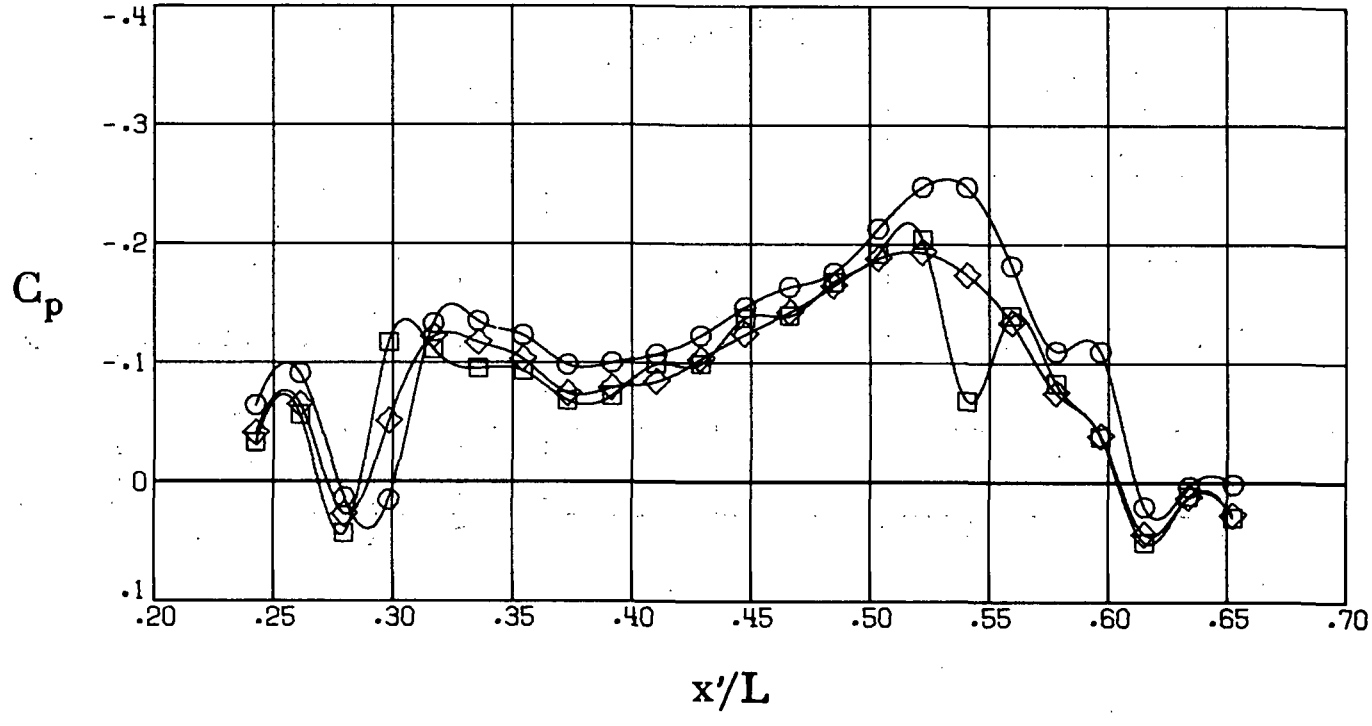


(d) Selected wing pressure distributions.

Figure 32.- Continued.

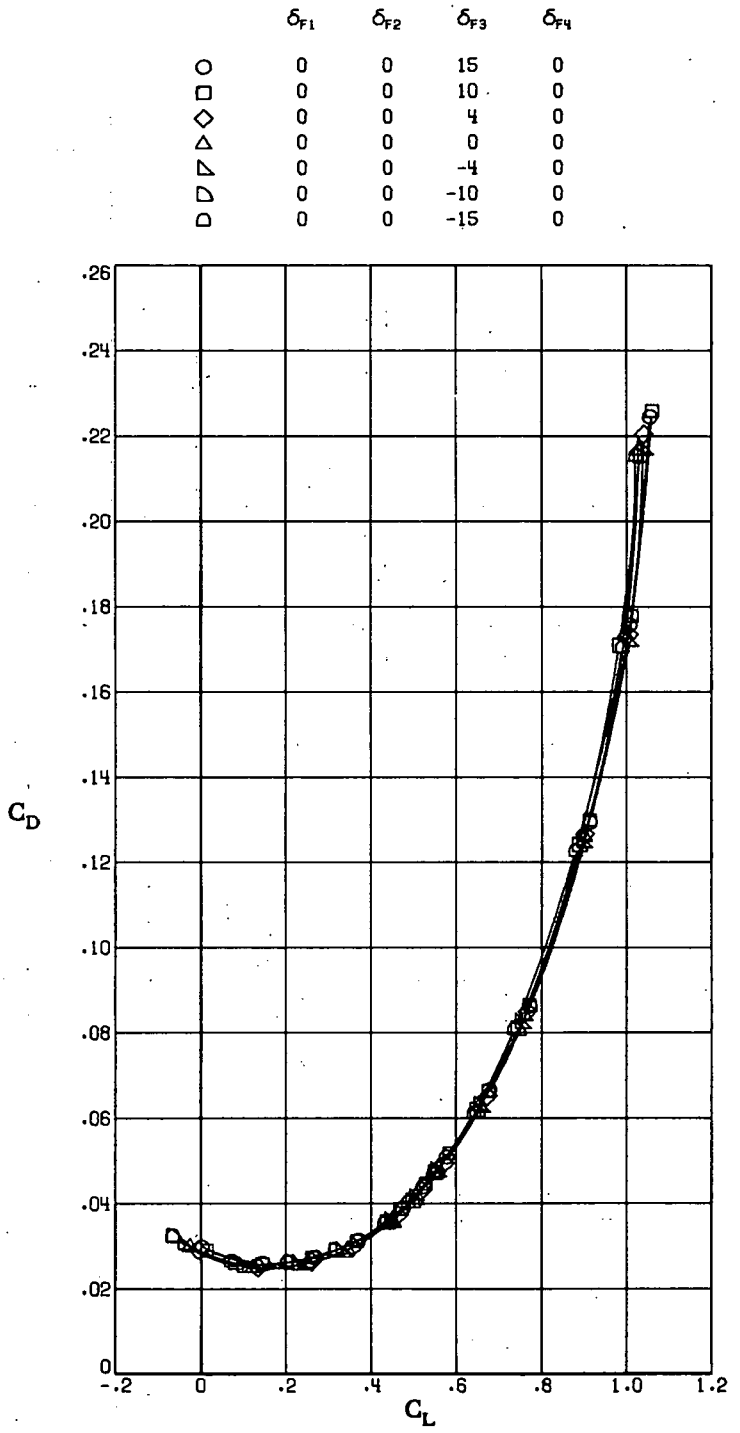
	δ_{F1}	δ_{F2}	δ_{F3}	δ_{F4}	α
○	0	0	15	0	3.03
□	0	0	0	0	2.95
◇	0	0	-15	0	3.44

—— Top Centerline



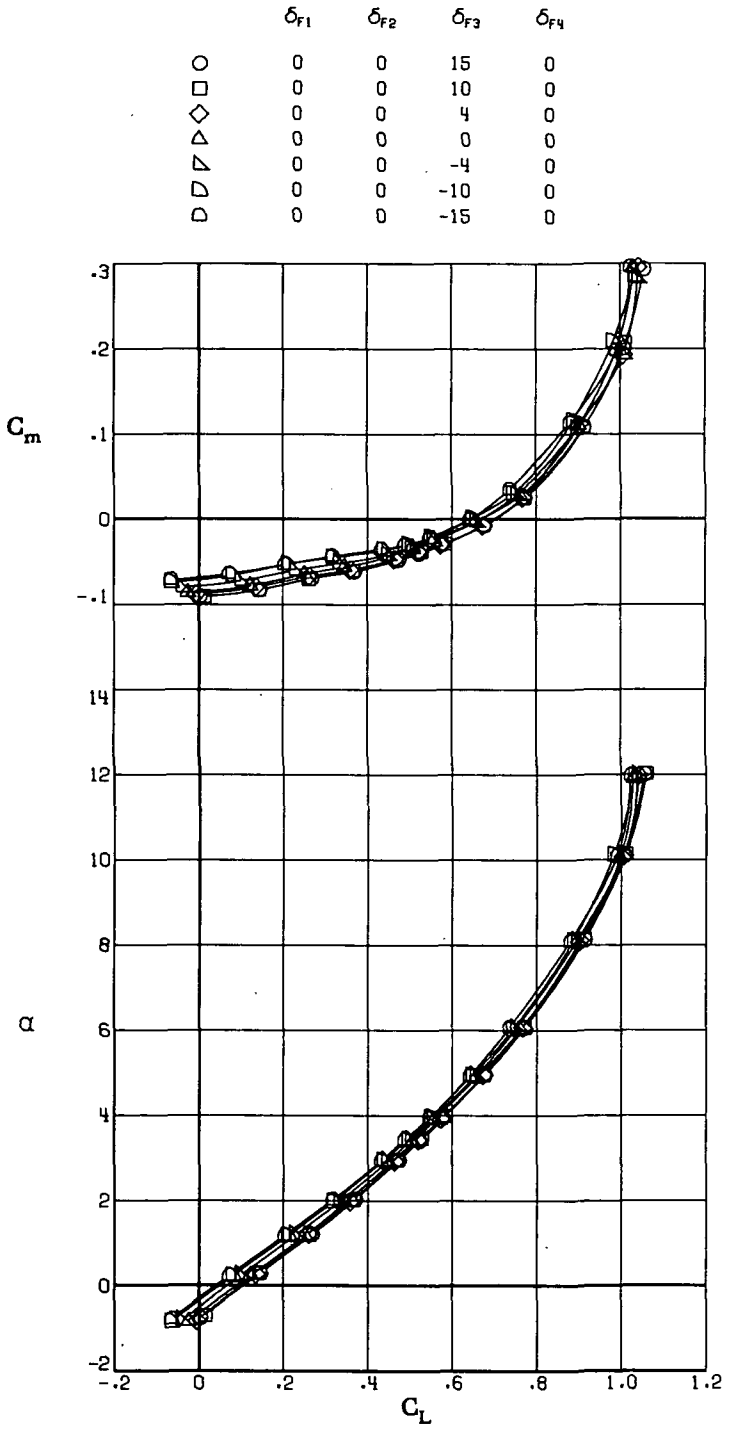
(e) Selected fuselage pressure distributions.

Figure 32.- Concluded.



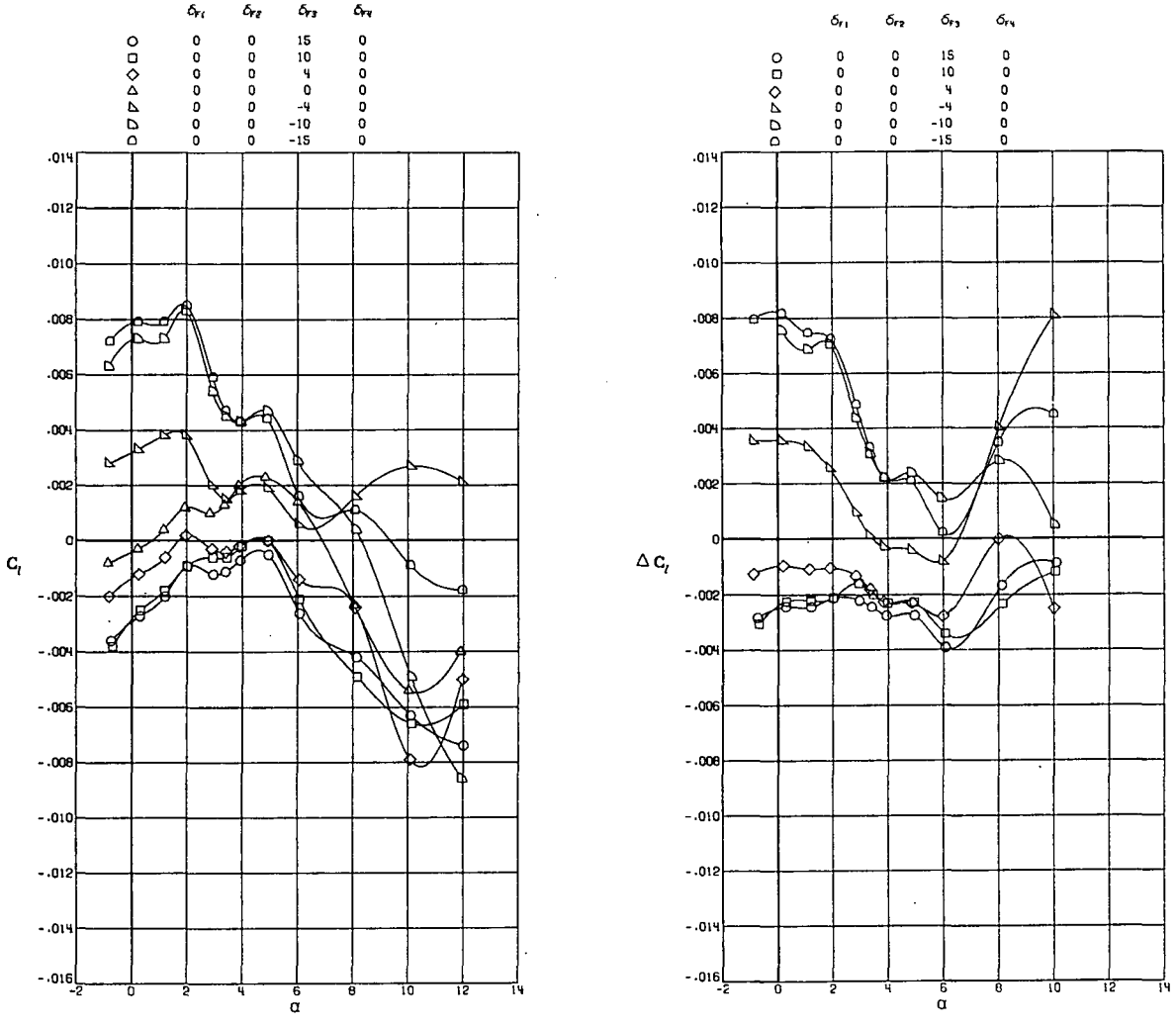
(a) Drag characteristics.

Figure 33.- Effect of F_3 trailing-edge control deflection on aerodynamic characteristics of model with cylindrical fuselage at $M_\infty = 0.92$.



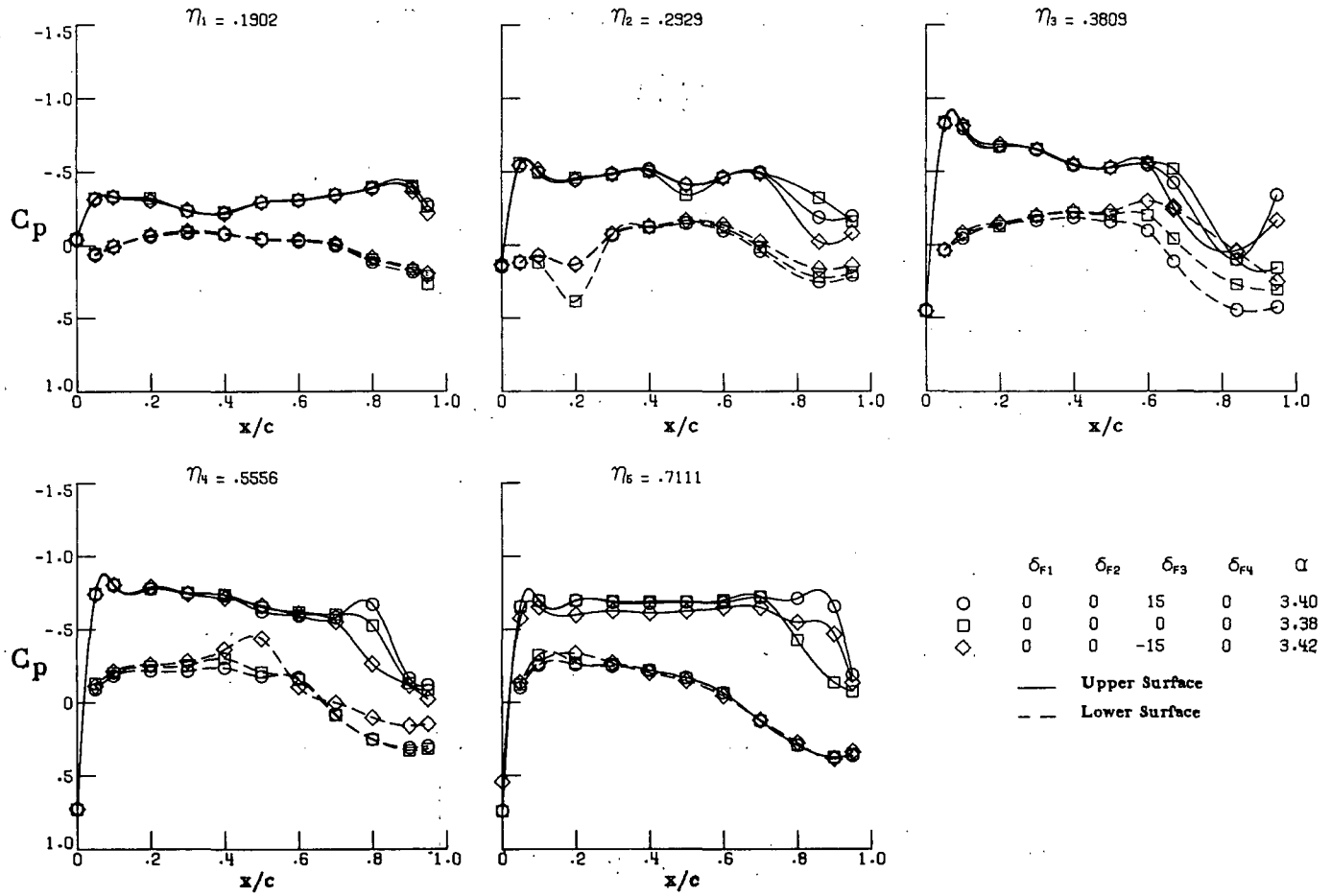
(b) Lift and pitch characteristics.

Figure 33.- Continued.



(c) Rolling-moment characteristics.

Figure 33.- Continued.

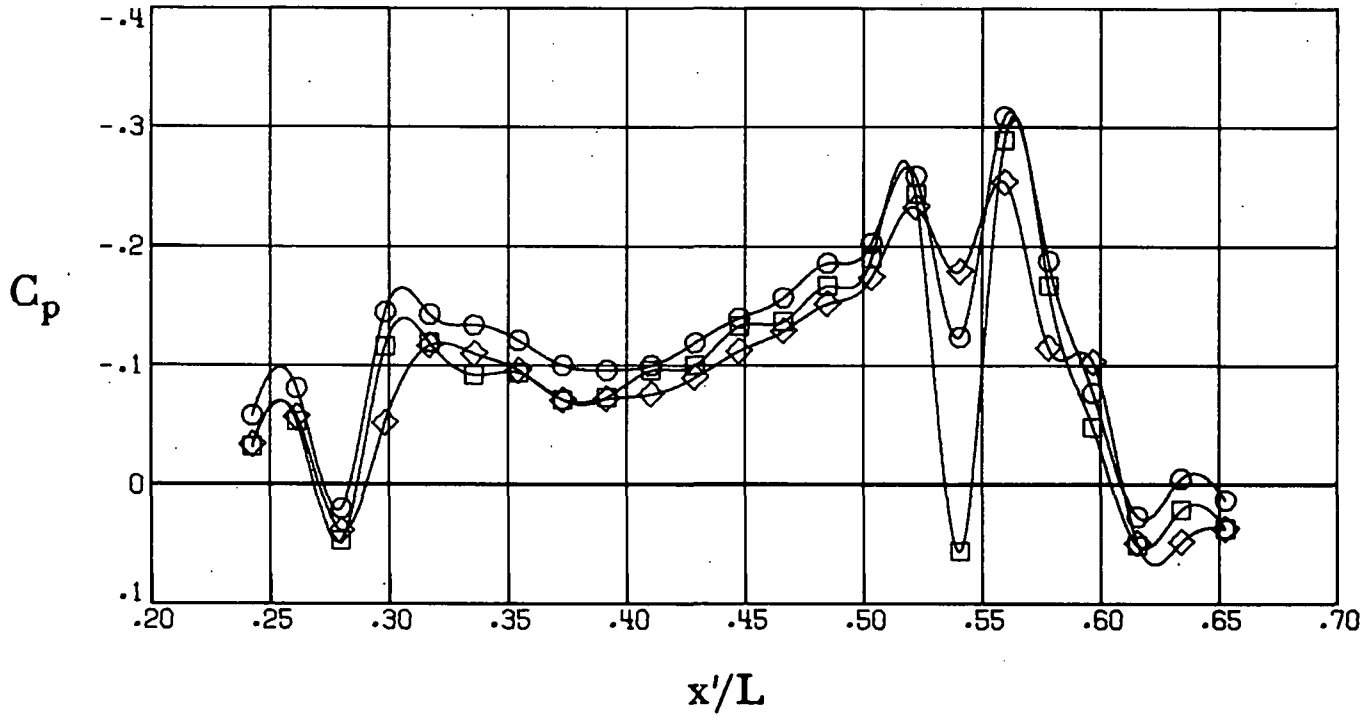


(d) Selected wing pressure distributions.

Figure 33.- Continued.

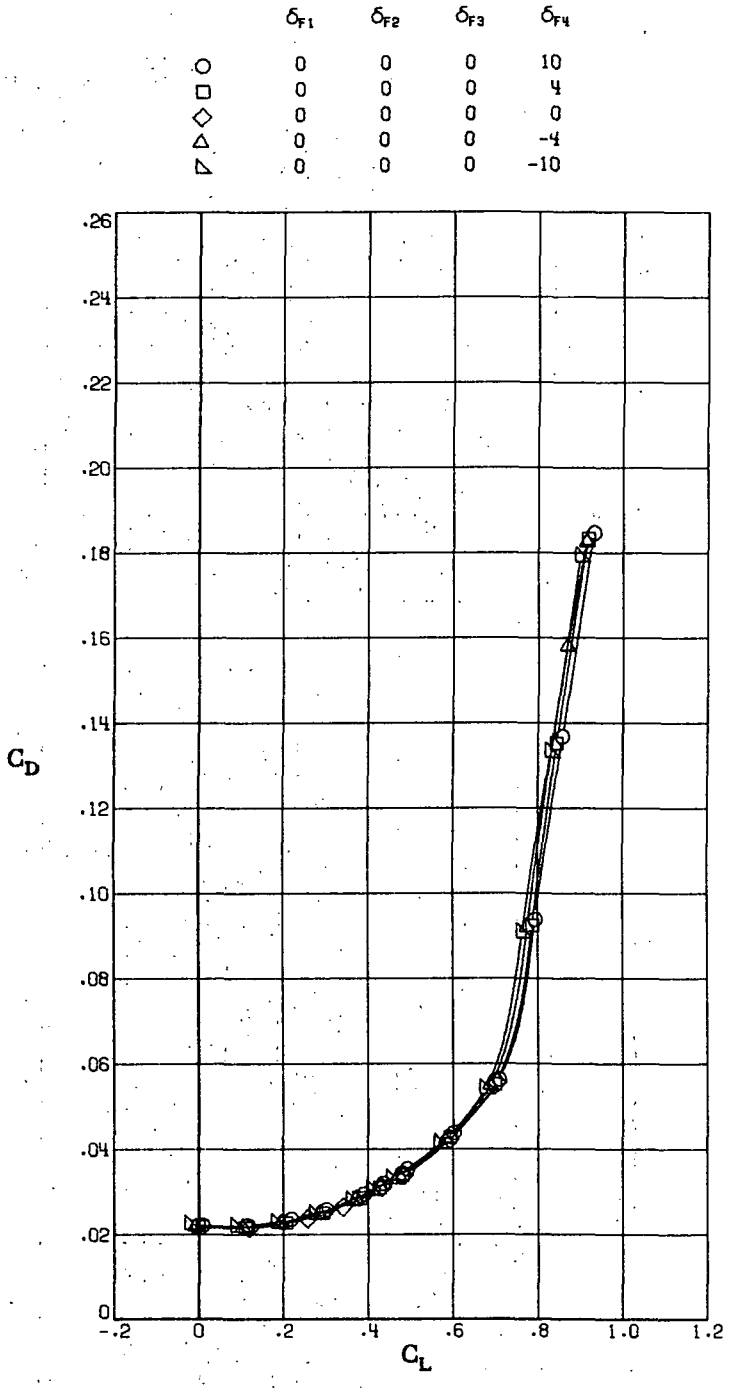
	δ_{F1}	δ_{F2}	δ_{F3}	δ_{F4}	α
○	0	0	15	0	3.40
□	0	0	0	0	3.38
◇	0	0	-15	0	3.42

—— Top Centerline



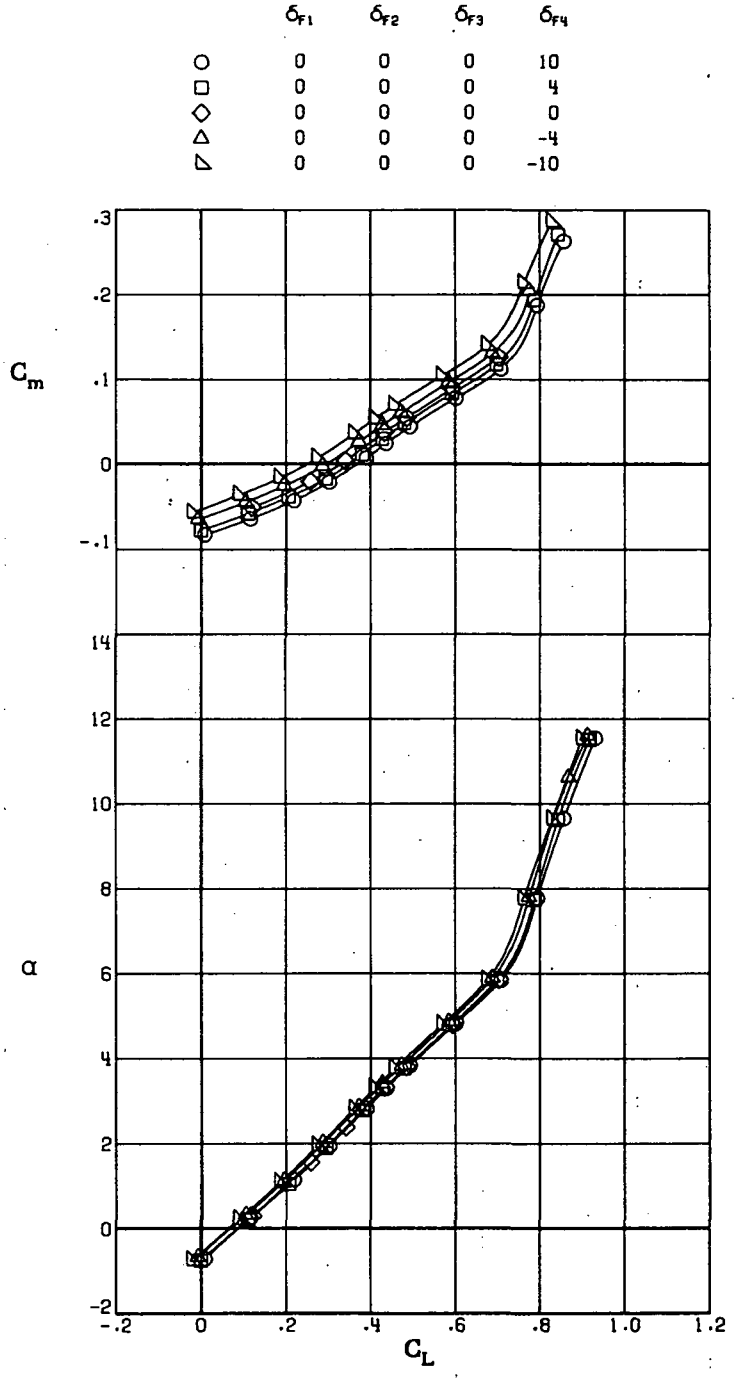
(e) Selected fuselage pressure distributions.

Figure 33.- Concluded.



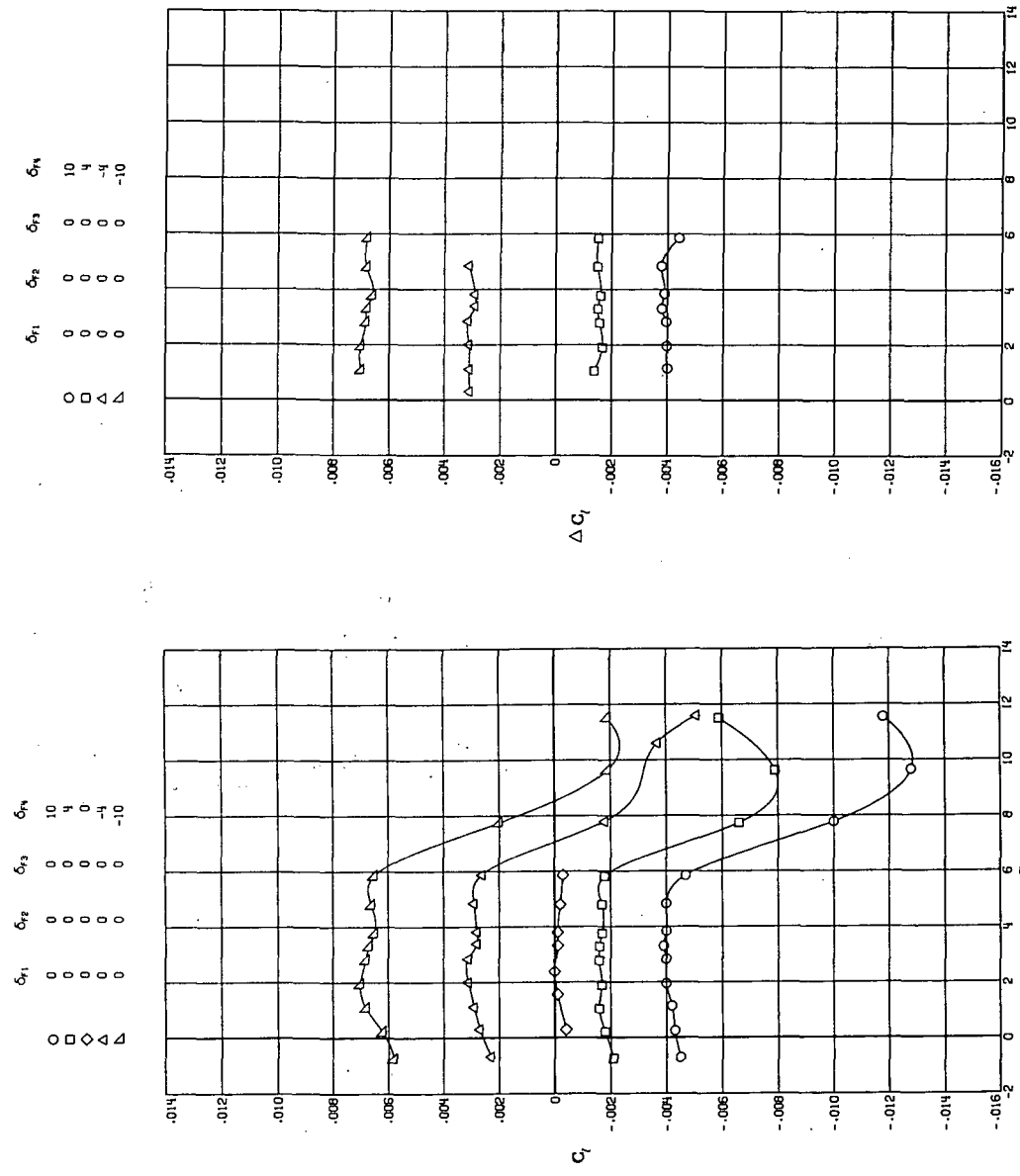
(a) Drag characteristics.

Figure 34.- Effect of F_4 trailing-edge control deflection on aerodynamic characteristics of model with area-ruled fuselage at $M_\infty = 0.80$.



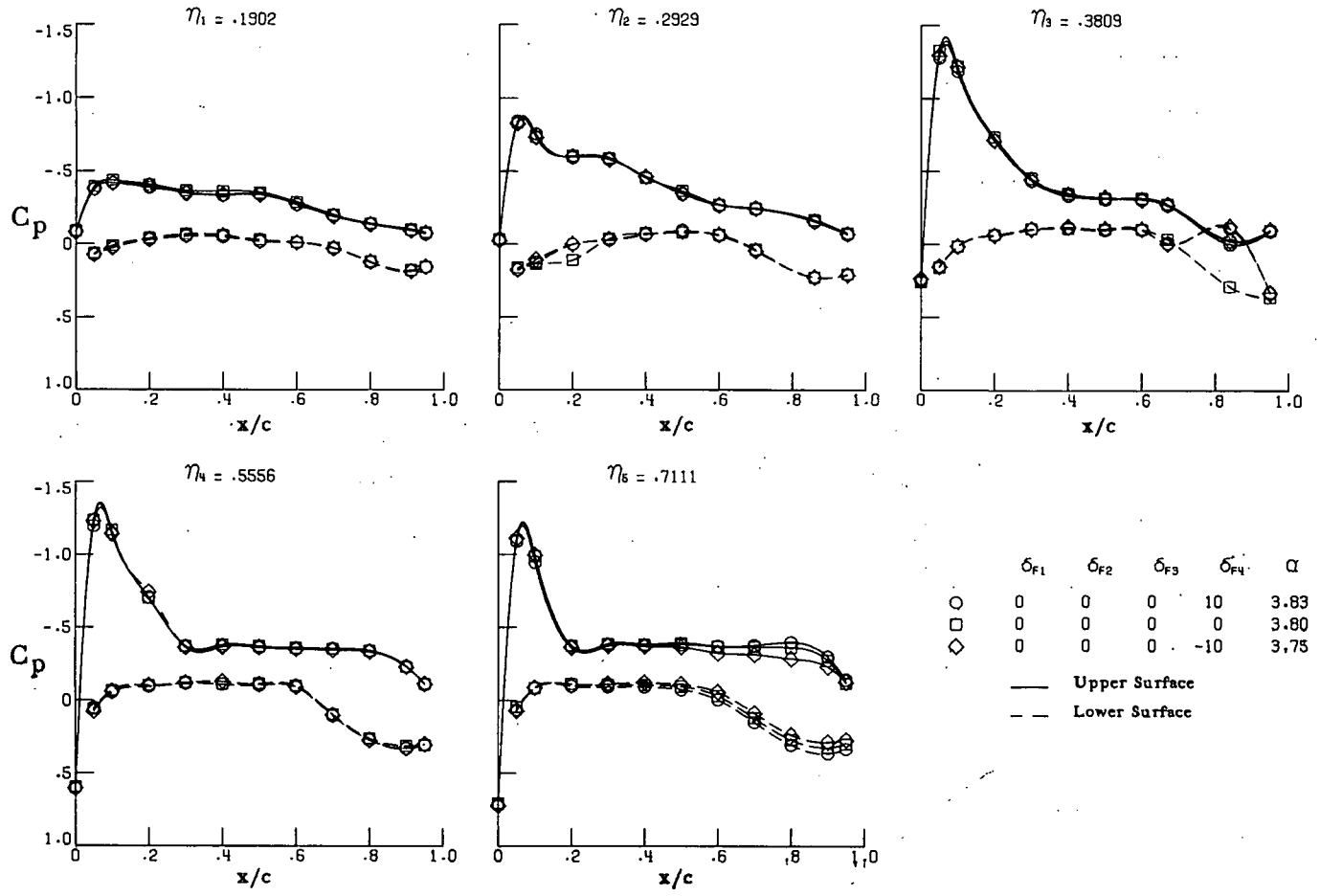
(b) Lift and pitch characteristics.

Figure 34.- Continued.



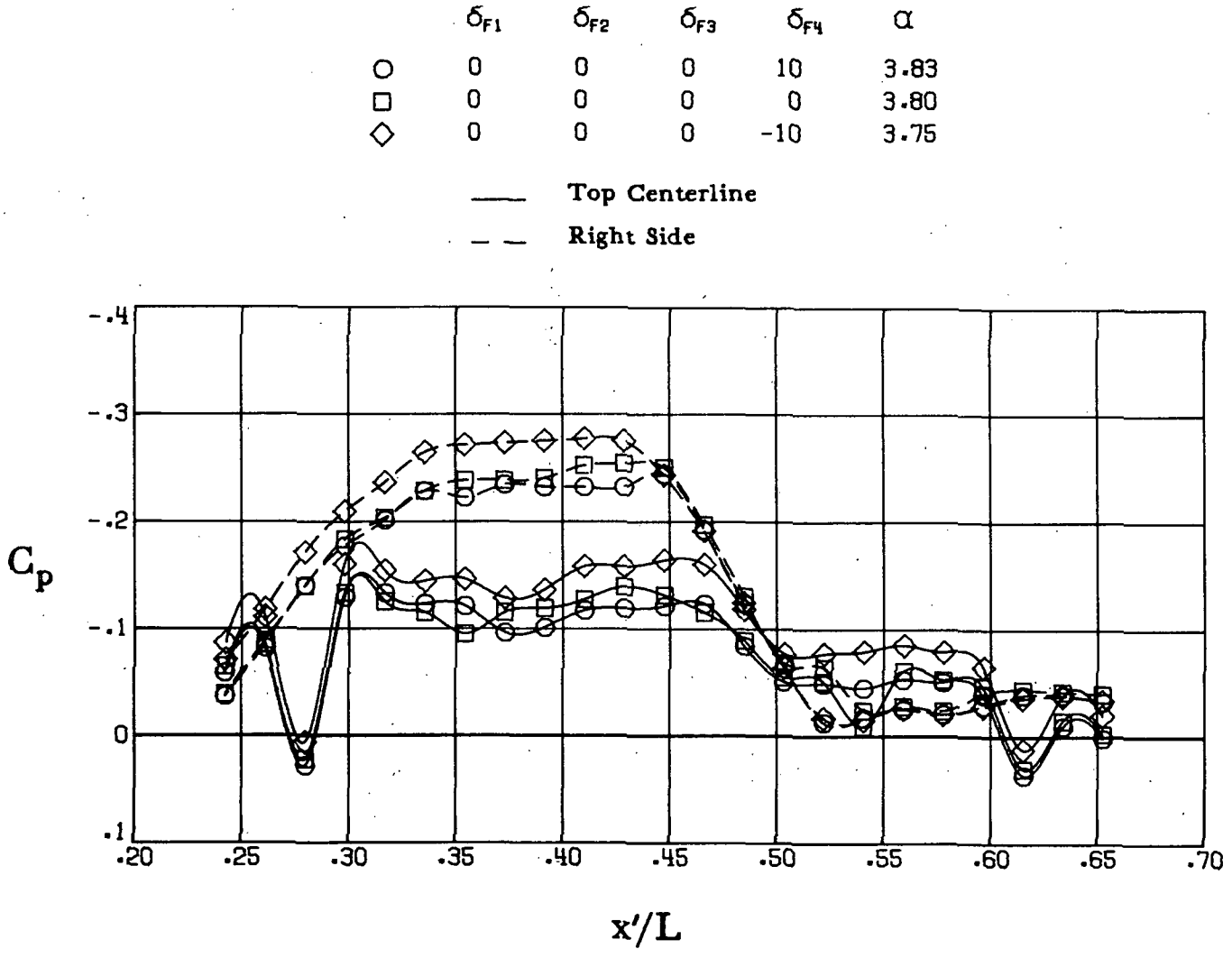
(c) Rolling-moment characteristics.

Figure 34.- Continued.



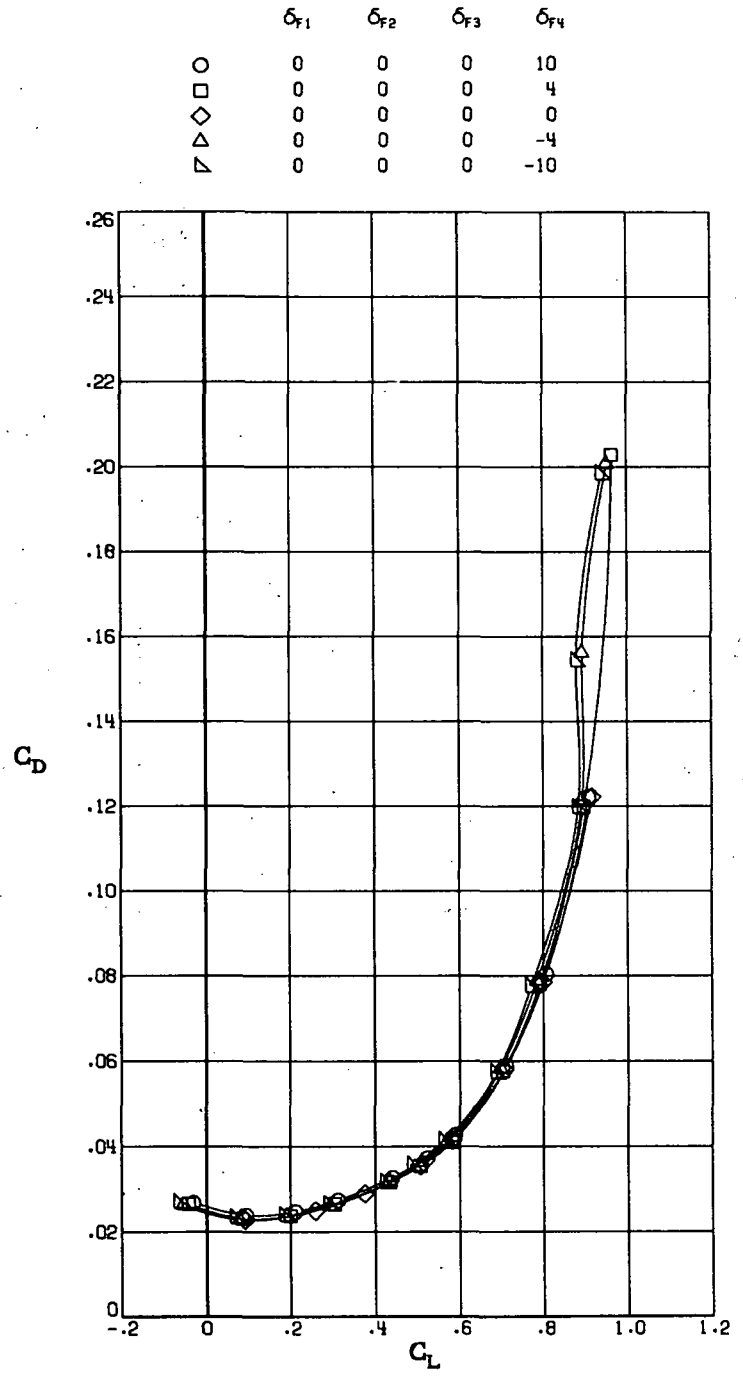
(d) Selected wing pressure distributions.

Figure 34.- Continued.



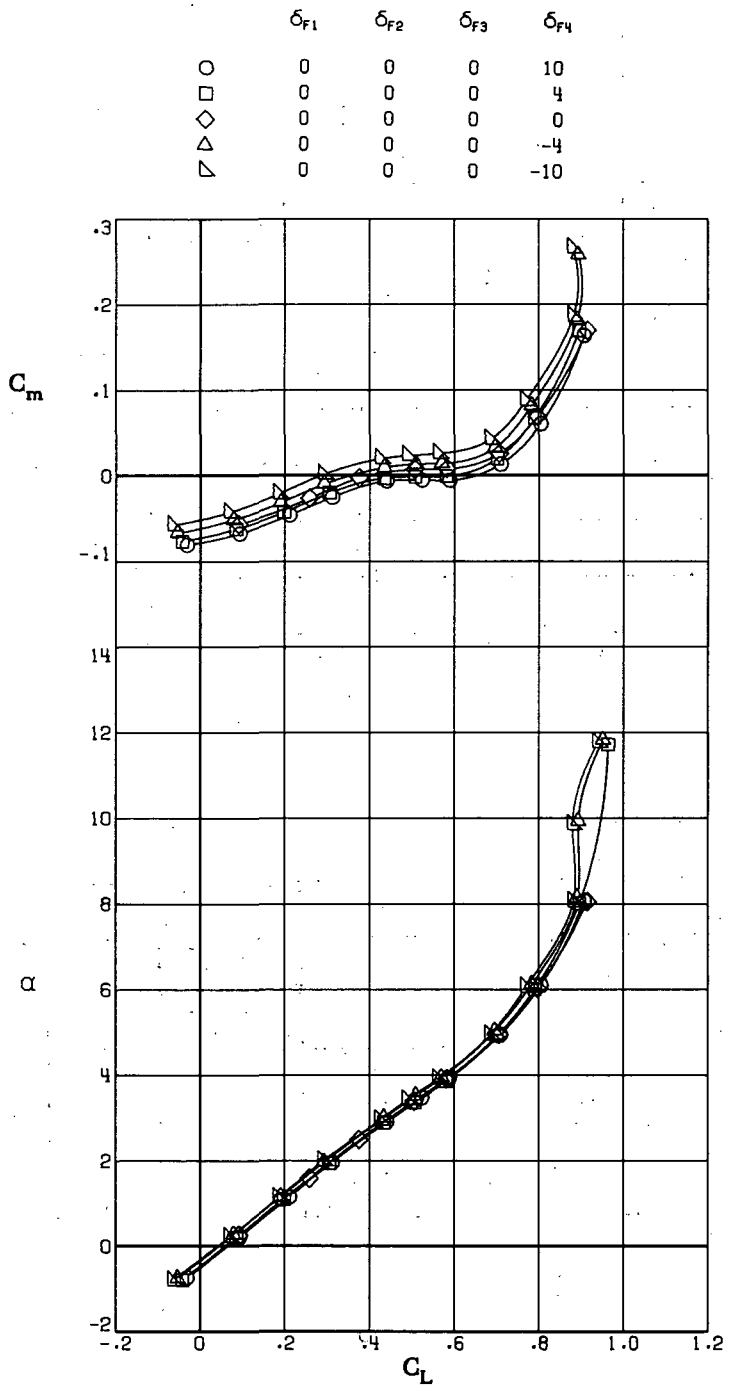
(e) Selected fuselage pressure distributions.

Figure 34.- Concluded.



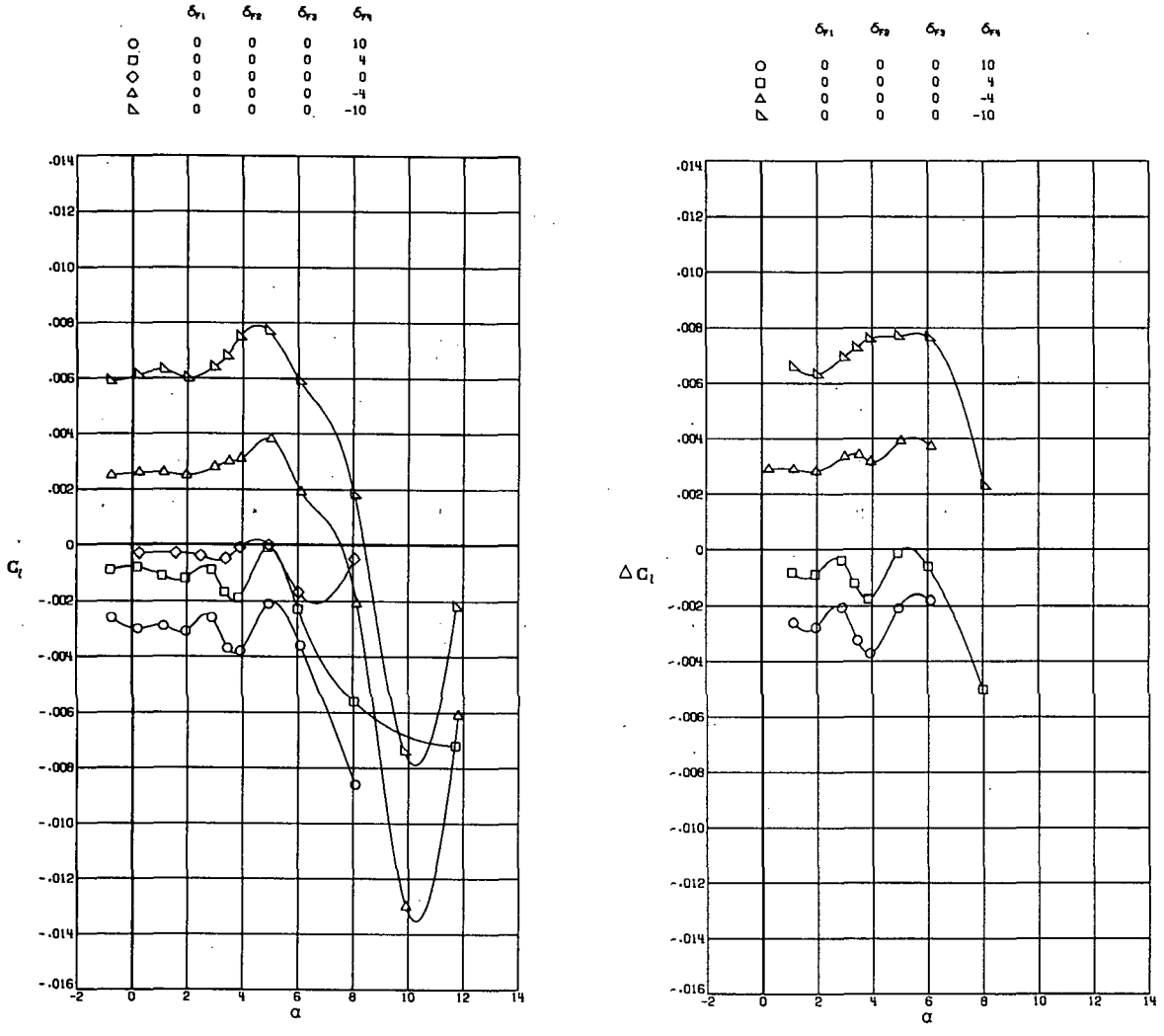
(a) Drag characteristics.

Figure 35.- Effect of F_4 trailing-edge control deflection on aerodynamic characteristics of model with area-ruled fuselage at $M_\infty = 0.90$.



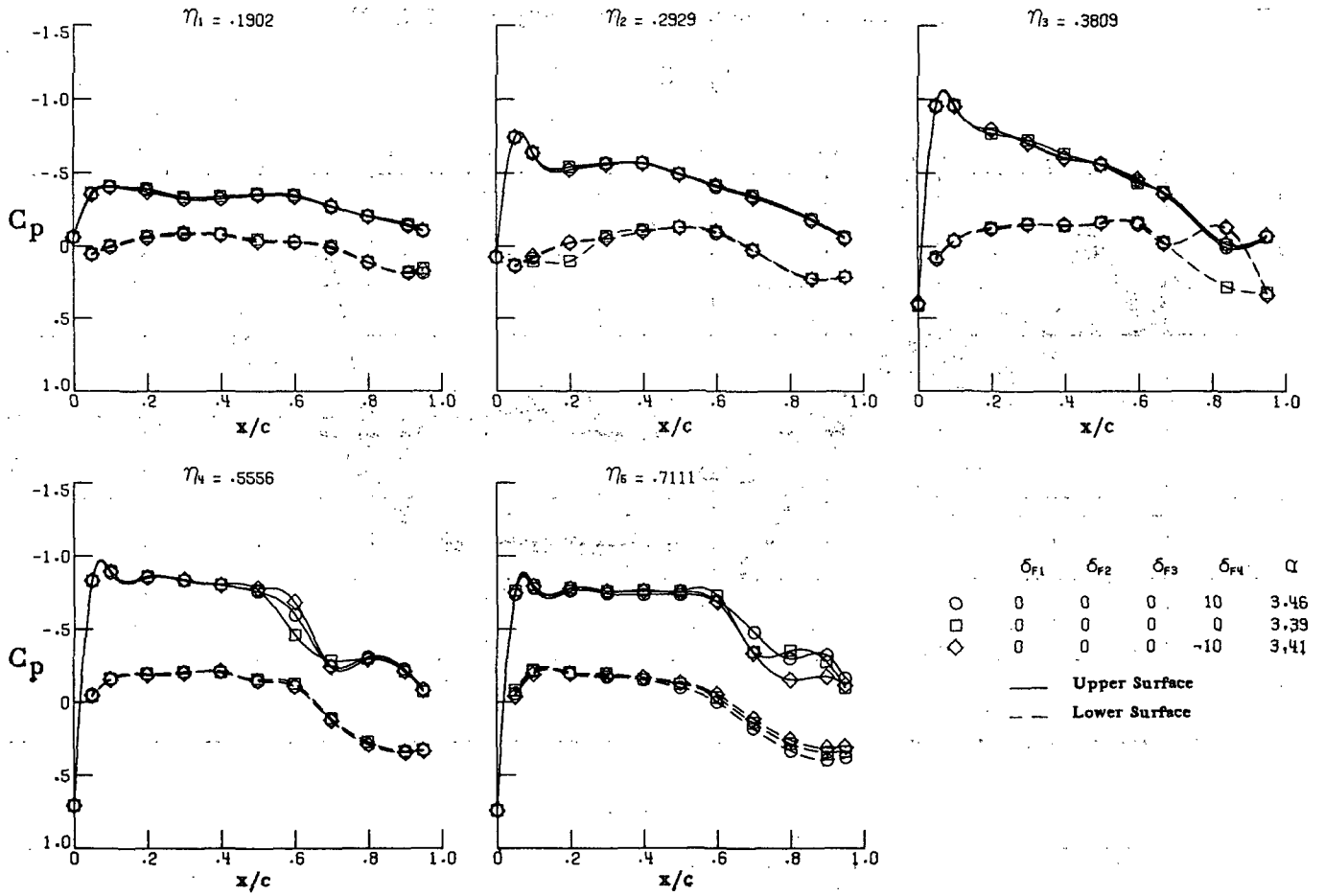
(b) Lift and pitch characteristics.

Figure 35.- Continued.



(c) Rolling-moment characteristics.

Figure 35.- Continued.



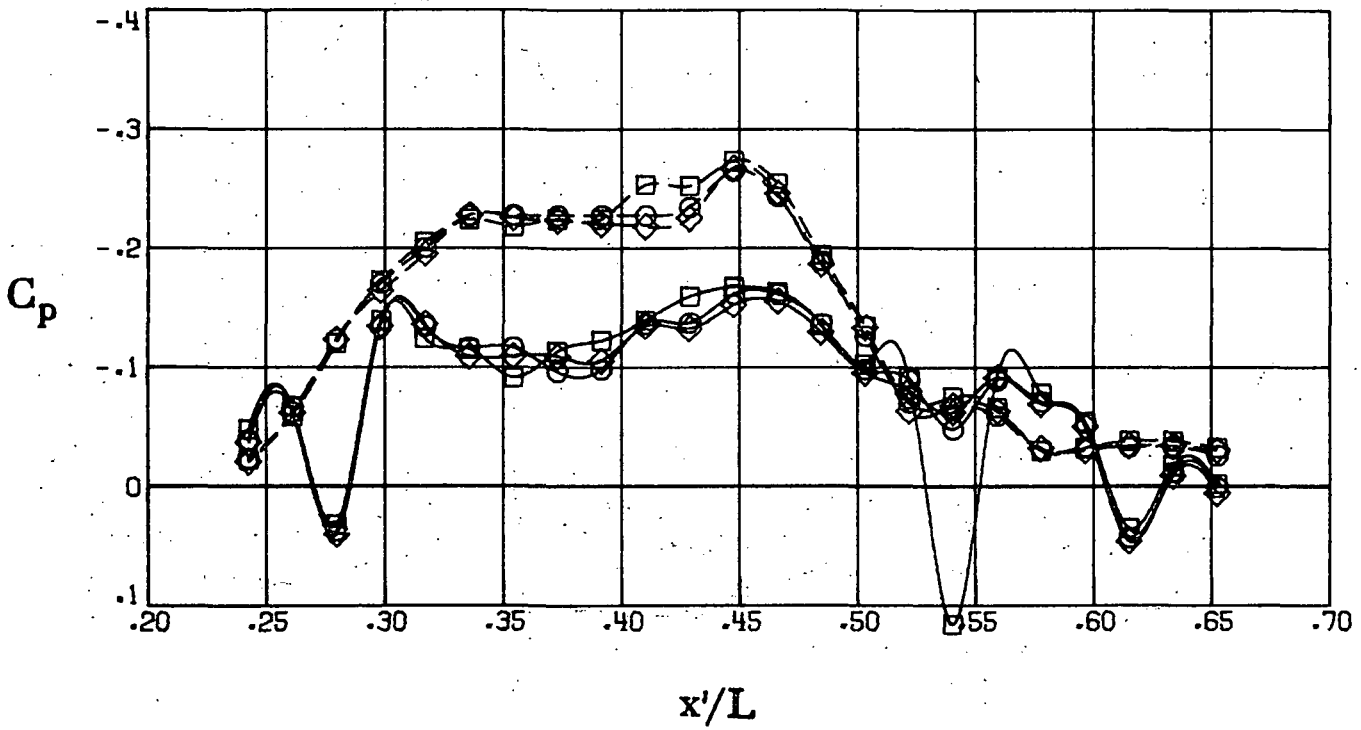
(d) Selected wing pressure distributions.

Figure 35.- Continued.

	δ_{F1}	δ_{F2}	δ_{F3}	δ_{F4}	α
○	0	0	0	10	3.46
□	0	0	0	0	3.39
◇	0	0	0	-10	3.41

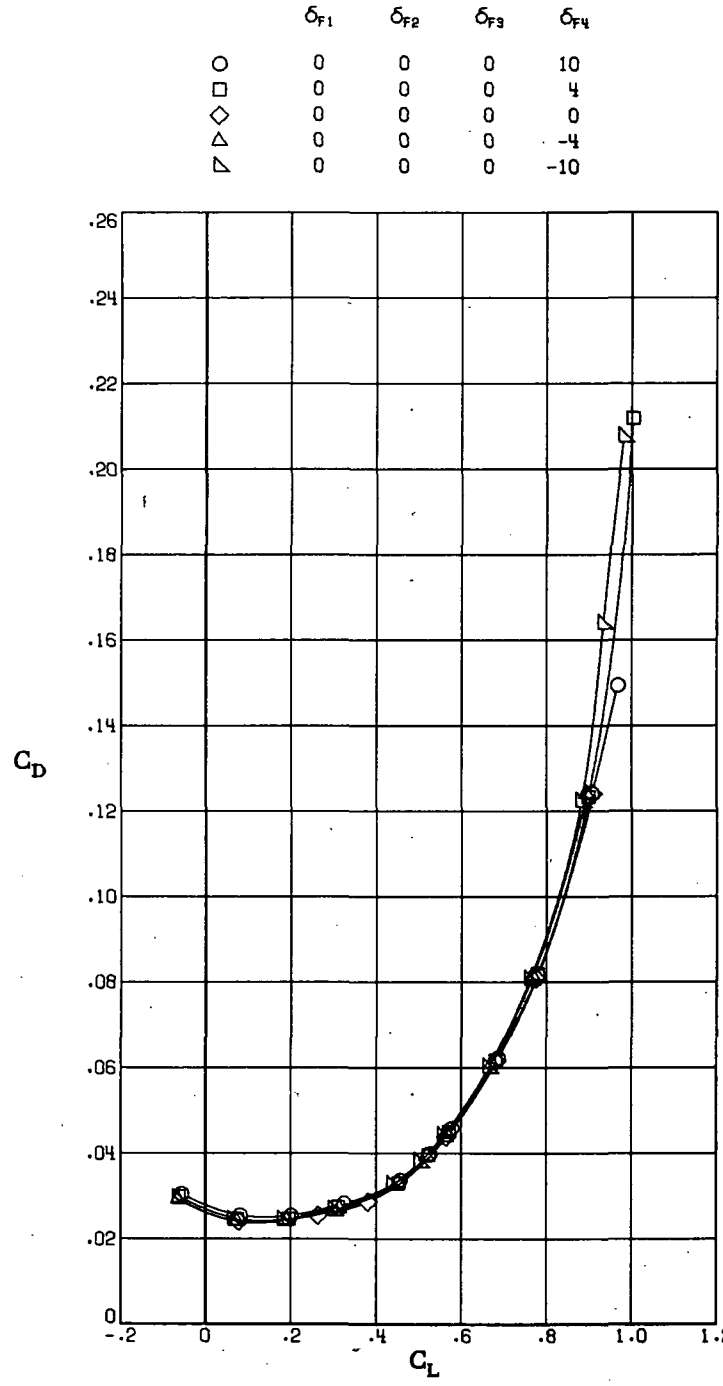
—— Top Centerline

– – Right Side



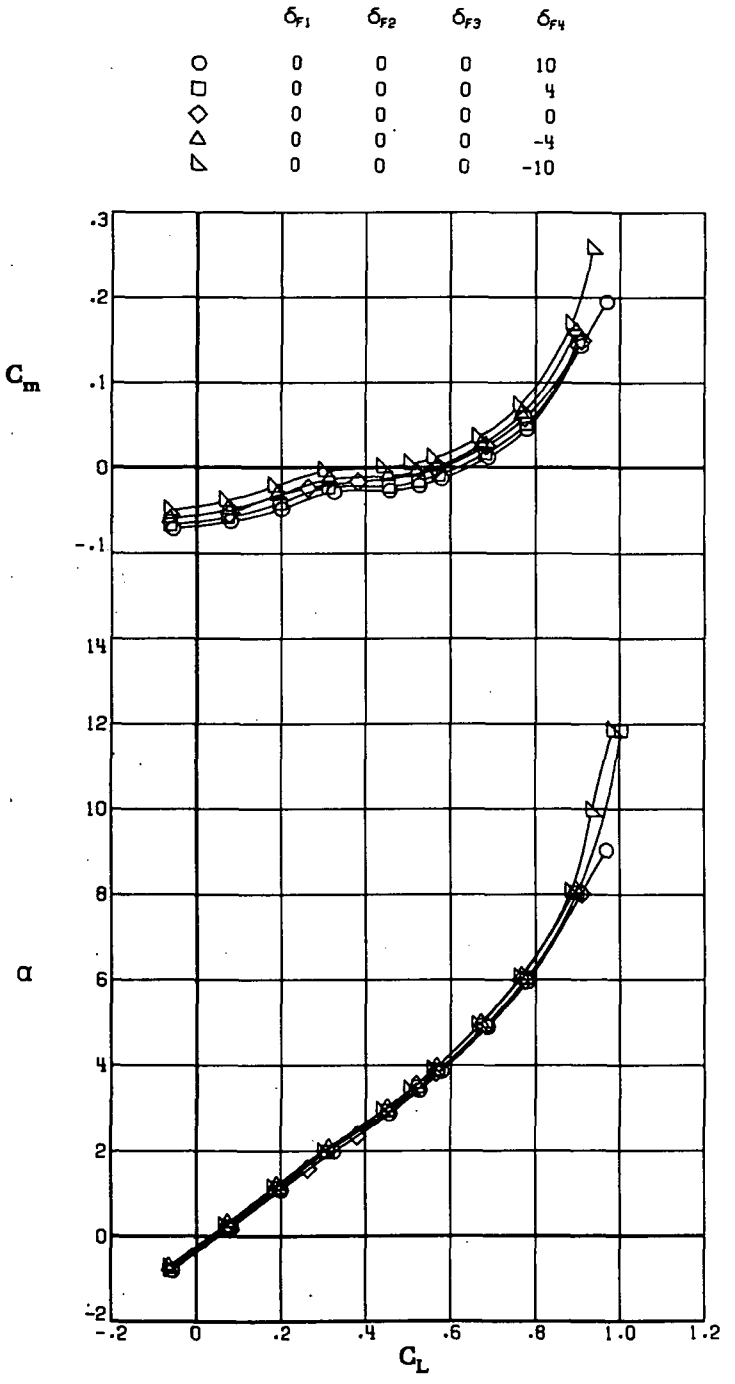
(e) Selected fuselage pressure distributions.

Figure 35.- Concluded.



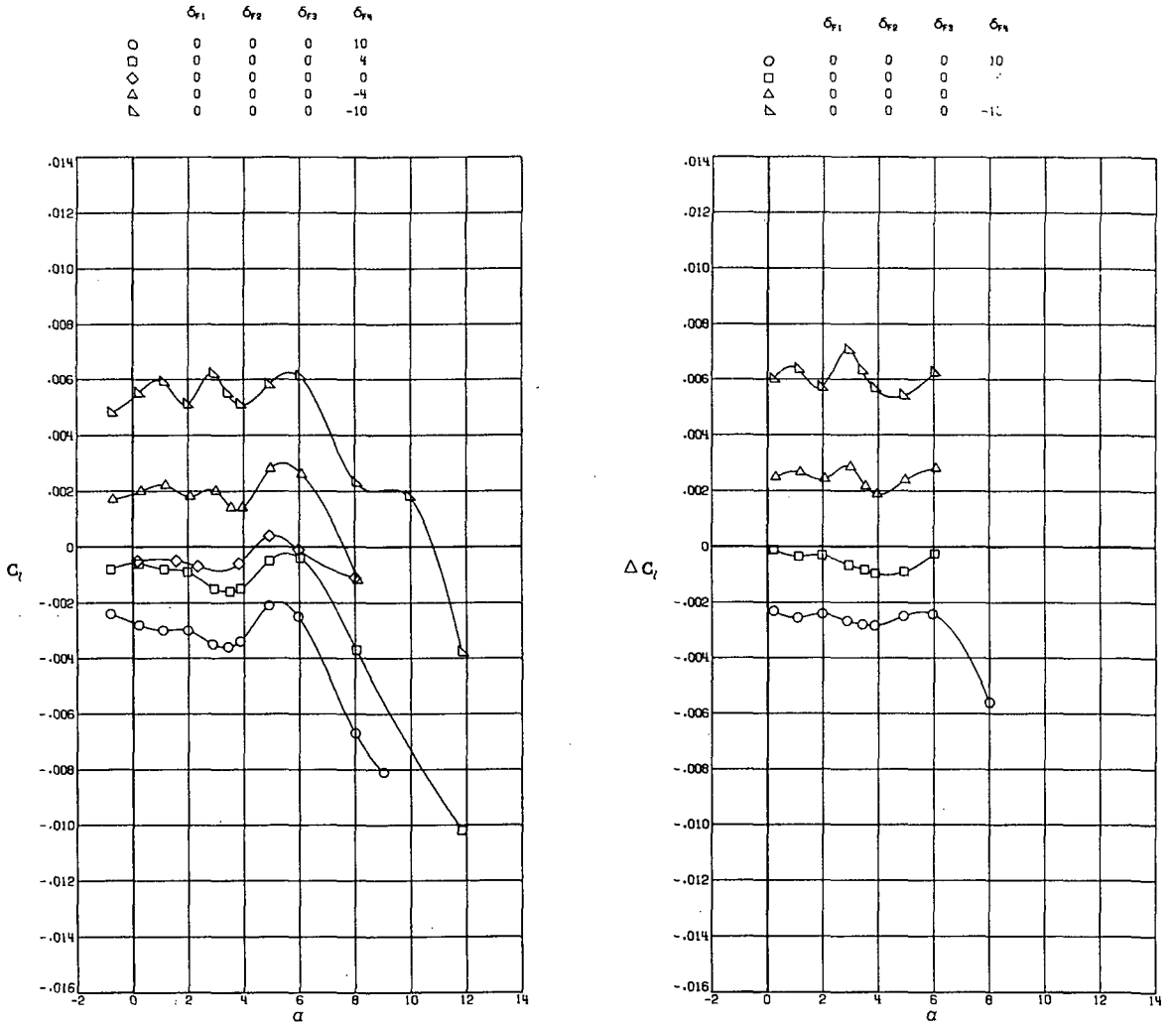
(a) Drag characteristics.

Figure 36.- Effect of F_4 trailing-edge control deflection on aerodynamic characteristics of model with area-ruled fuselage at $M_\infty = 0.92$.



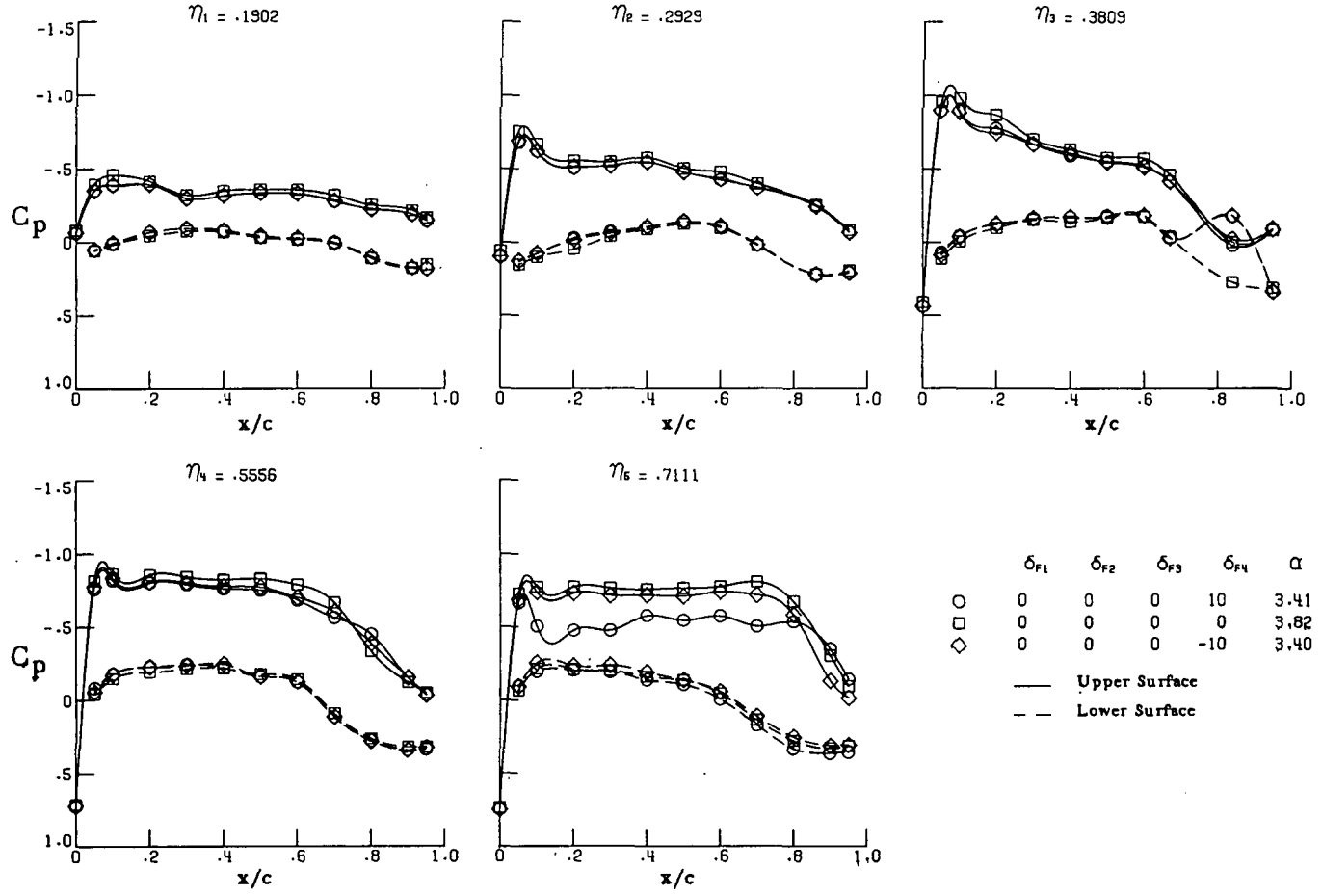
(b) Lift and pitch characteristics.

Figure 36.- Continued.



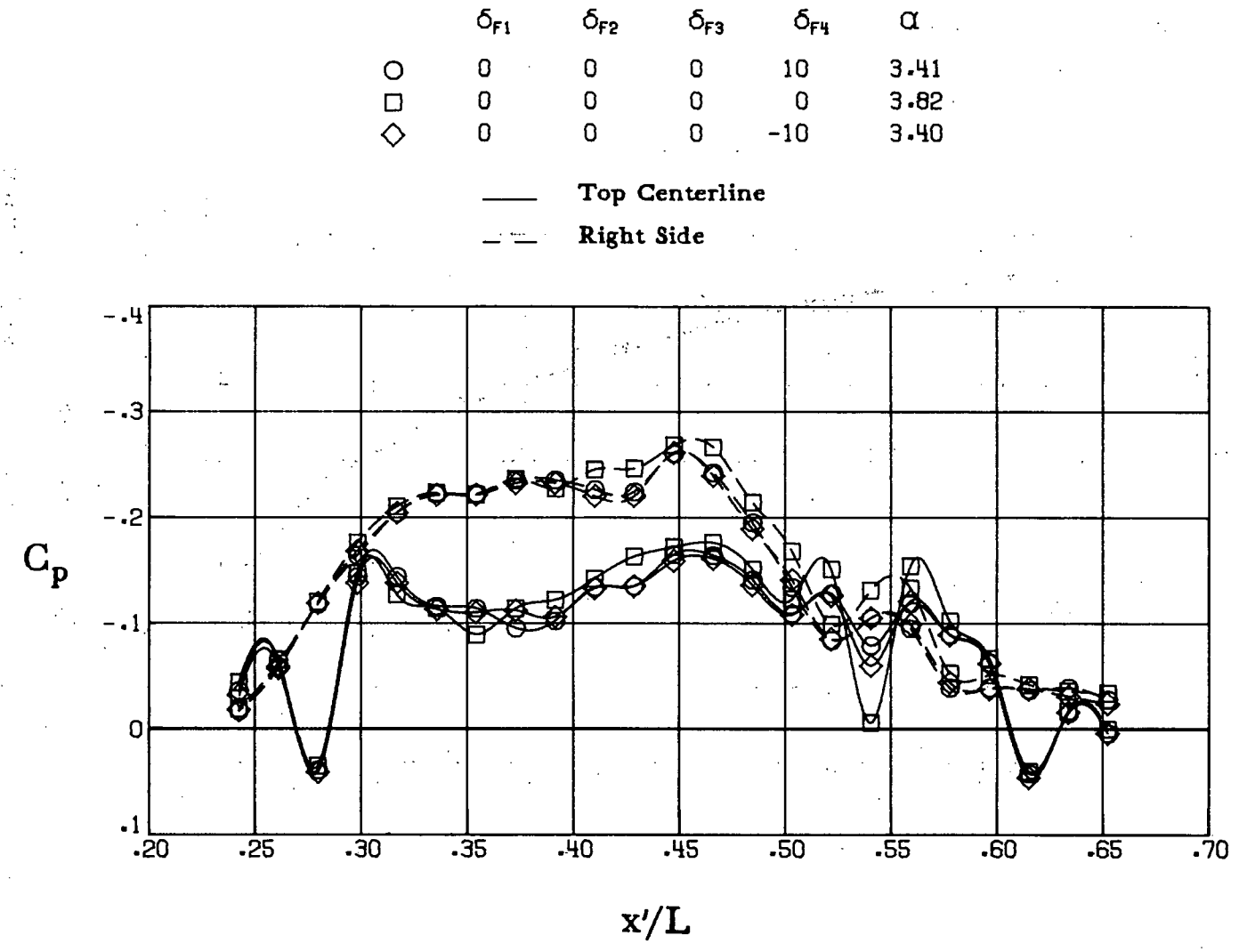
(c) Rolling-moment characteristics.

Figure 36.- Continued.



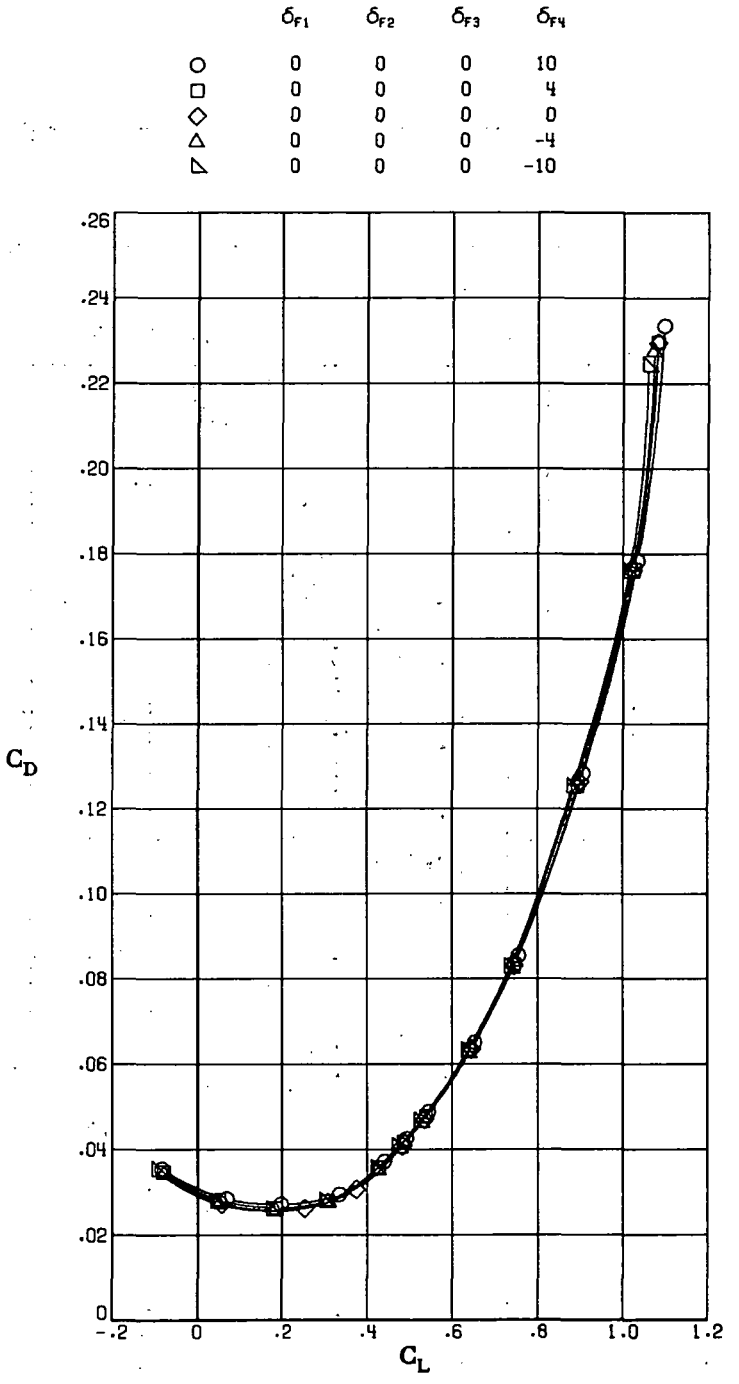
(d) Selected wing pressure distributions.

Figure 36.- Continued.



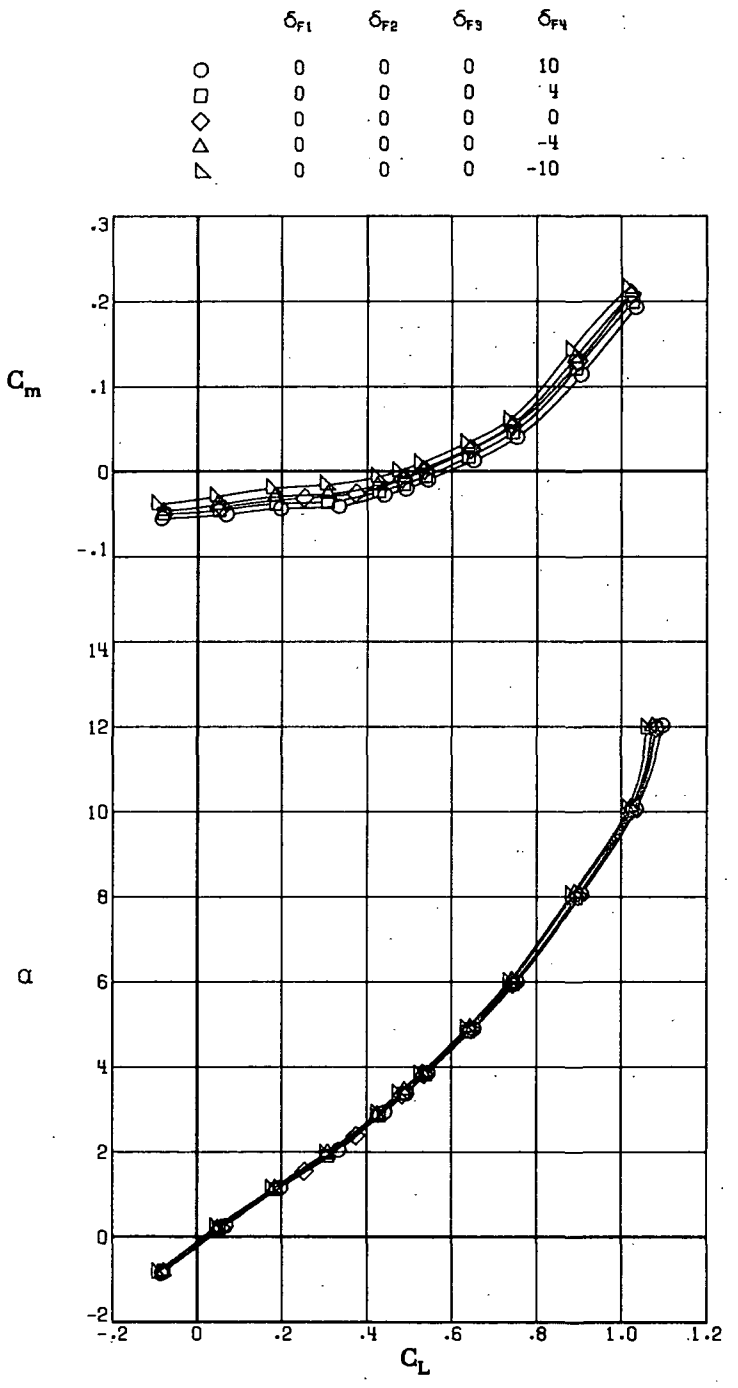
(e) Selected fuselage pressure distributions.

Figure 36.- Concluded.



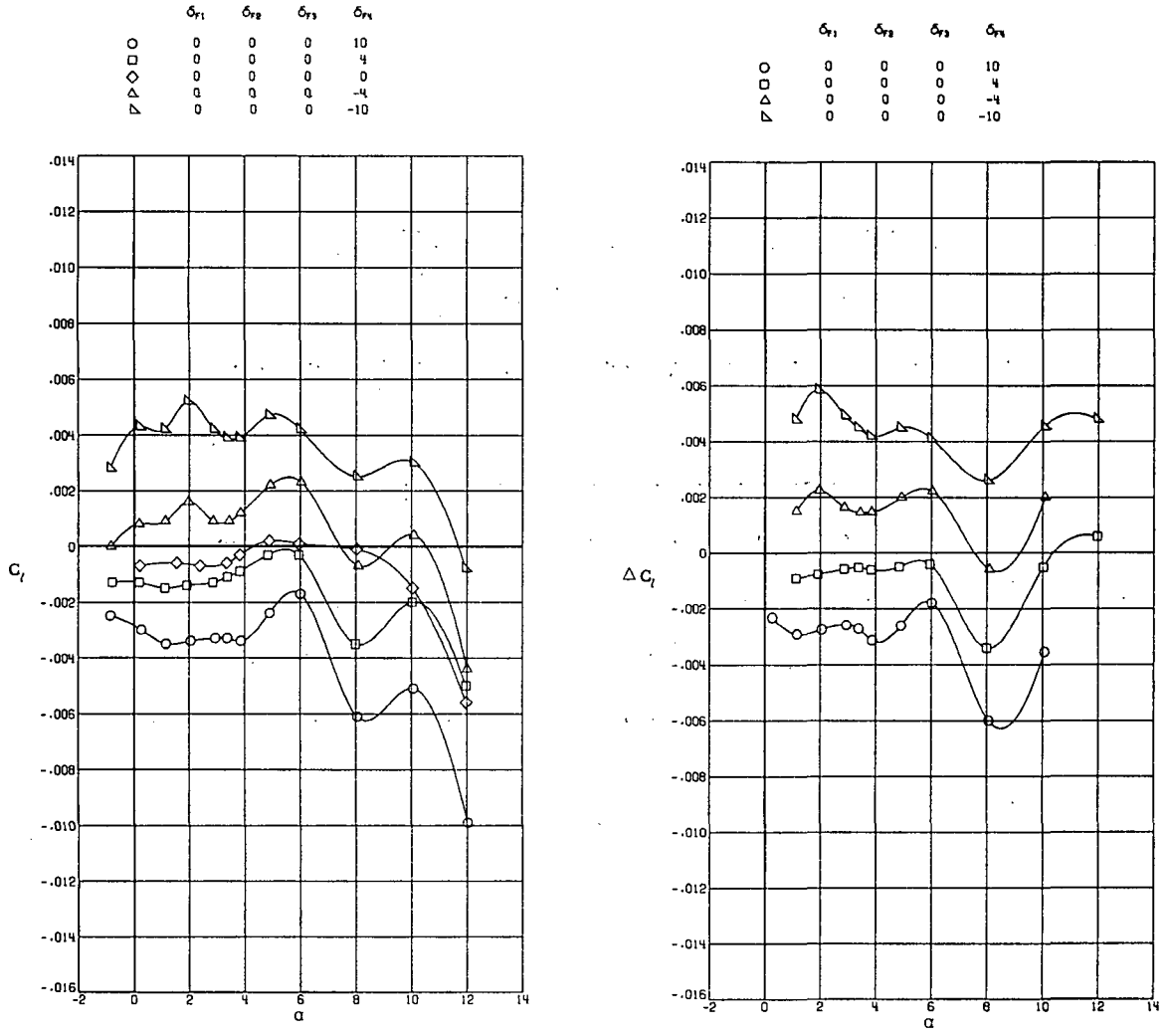
(a) Drag characteristics.

Figure 37.- Effect of F_4 trailing-edge control deflection on aerodynamic characteristics of model with area-ruled fuselage at $M_\infty = 0.94$.



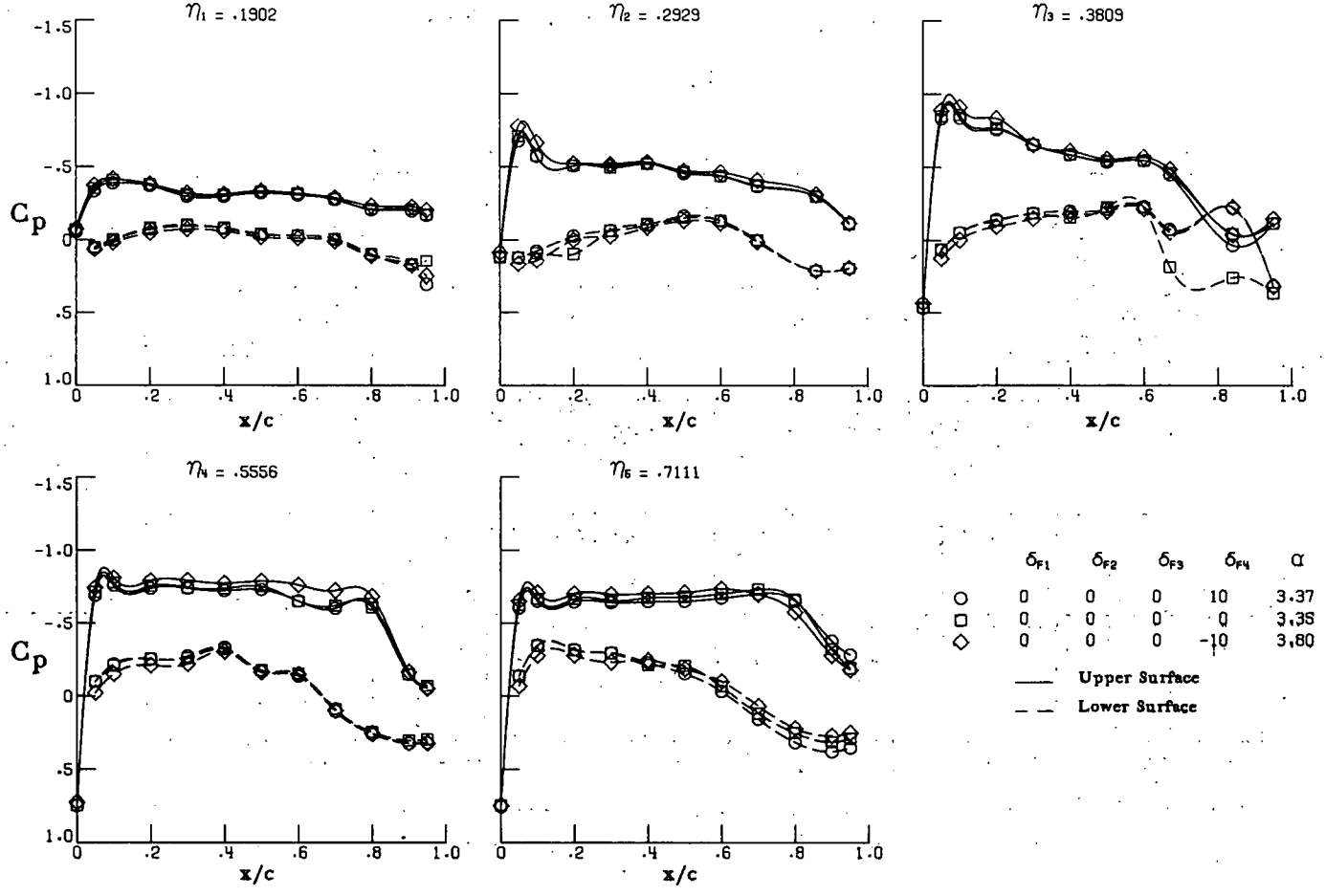
(b) Lift and pitch characteristics.

Figure 37.- Continued.



(c) Rolling-moment characteristics.

Figure 37.- Continued.



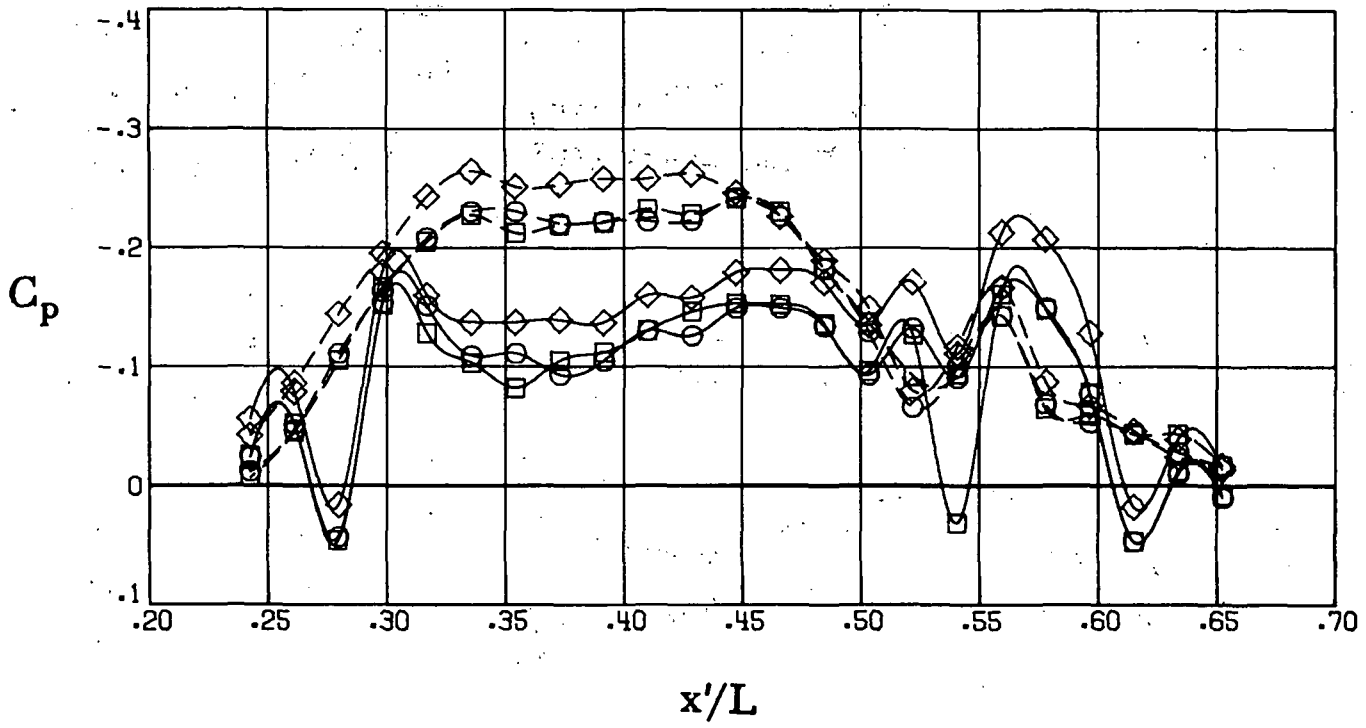
(d) Selected wing pressure distributions.

Figure 37.- Continued.

	δ_{F1}	δ_{F2}	δ_{F3}	δ_{F4}	α
○	0	0	0	10	3.37
□	0	0	0	0	3.35
◇	0	0	0	-10	3.80

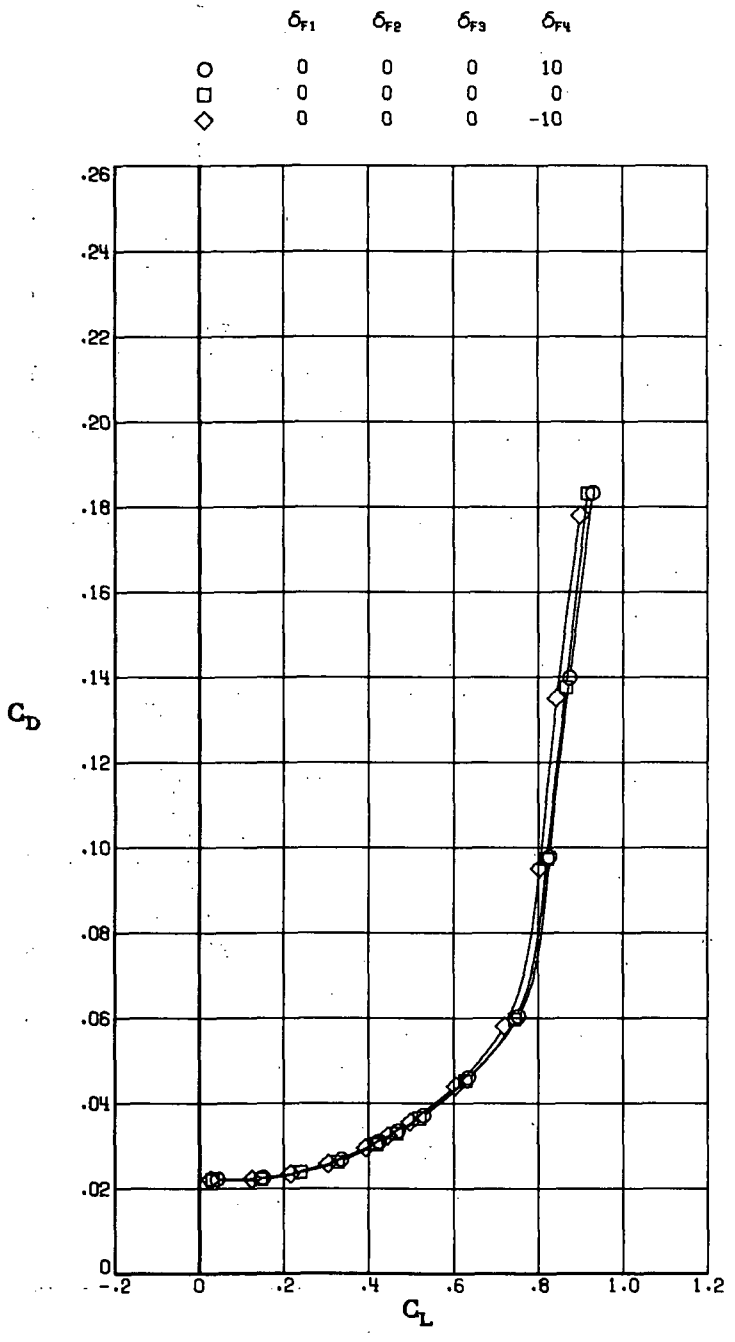
—— Top Centerline

– – Right Side



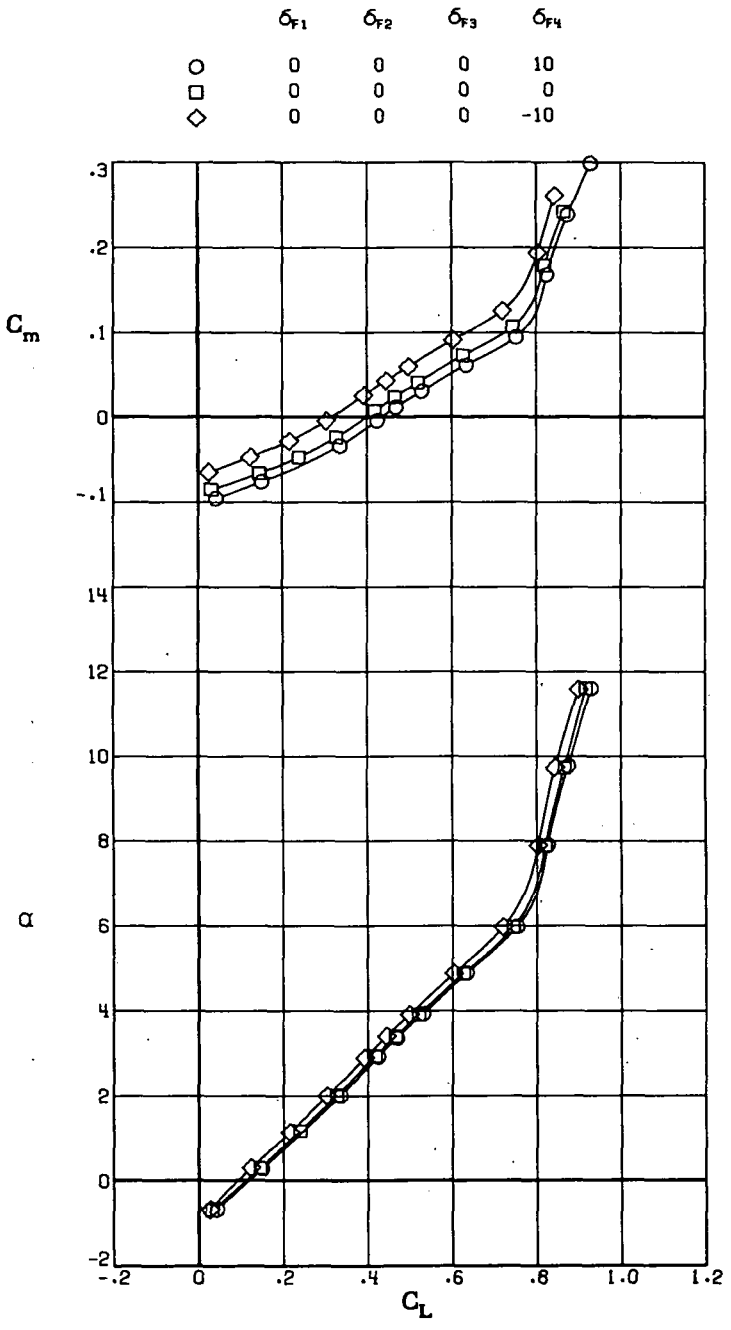
(e) Selected fuselage pressure distributions.

Figure 37.- Concluded.



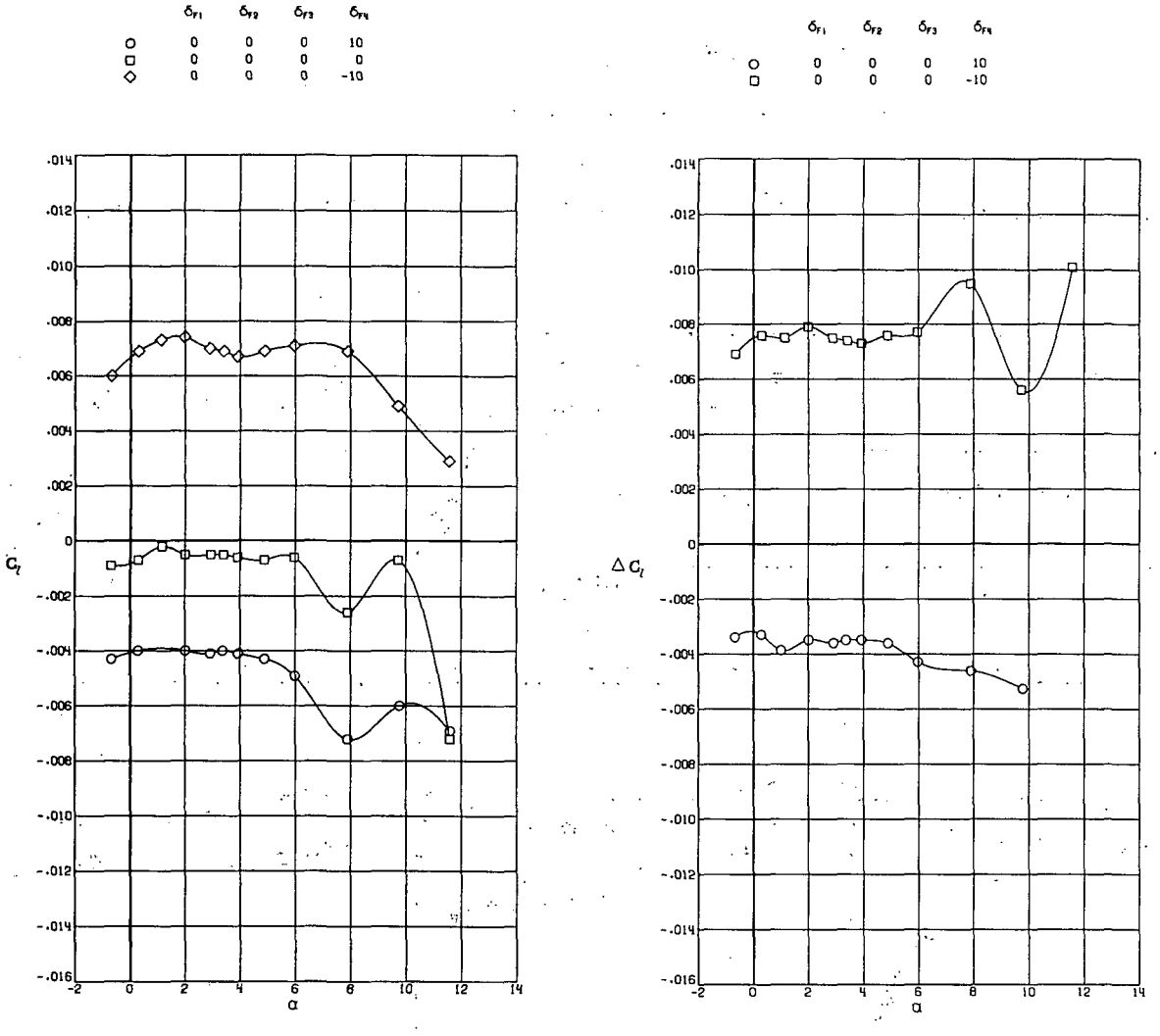
(a) Drag characteristics.

Figure 38.- Effect of F_4 trailing-edge control deflection on aerodynamic characteristics of model with cylindrical fuselage at $M_\infty = 0.80$.



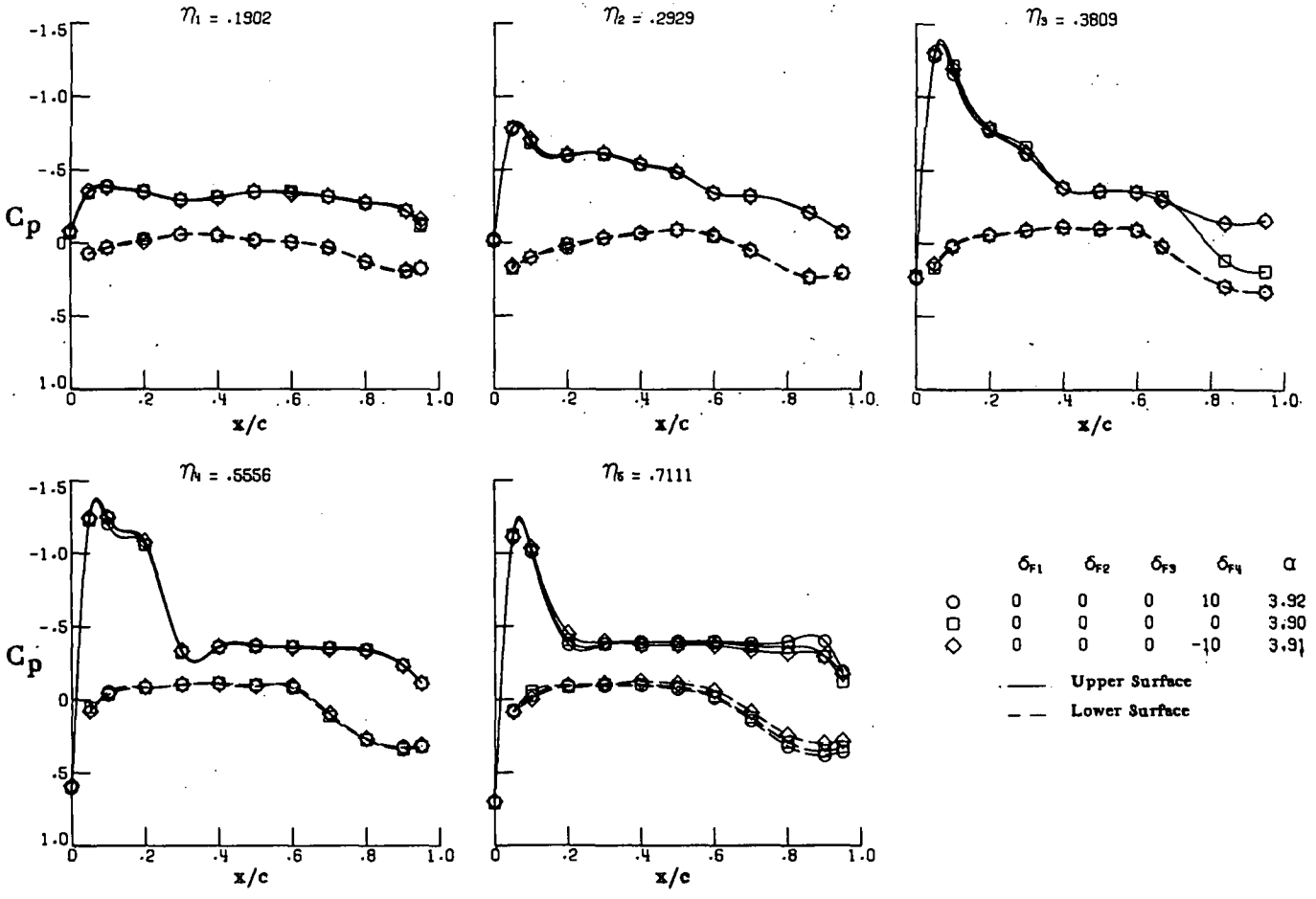
(b) Lift and pitch characteristics.

Figure 38.- Continued.



(c) Rolling-moment characteristics.

Figure 38.- Continued.

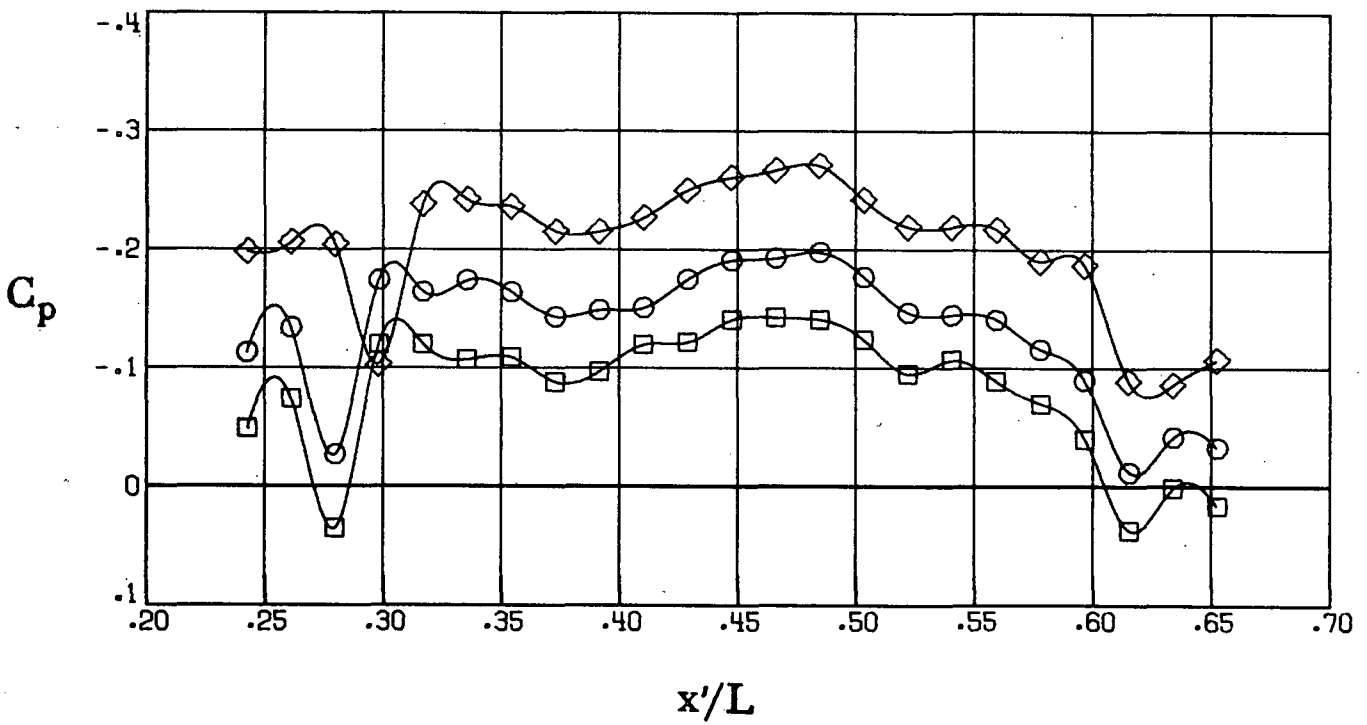


(d) Selected wing pressure distributions.

Figure 38.- Continued.

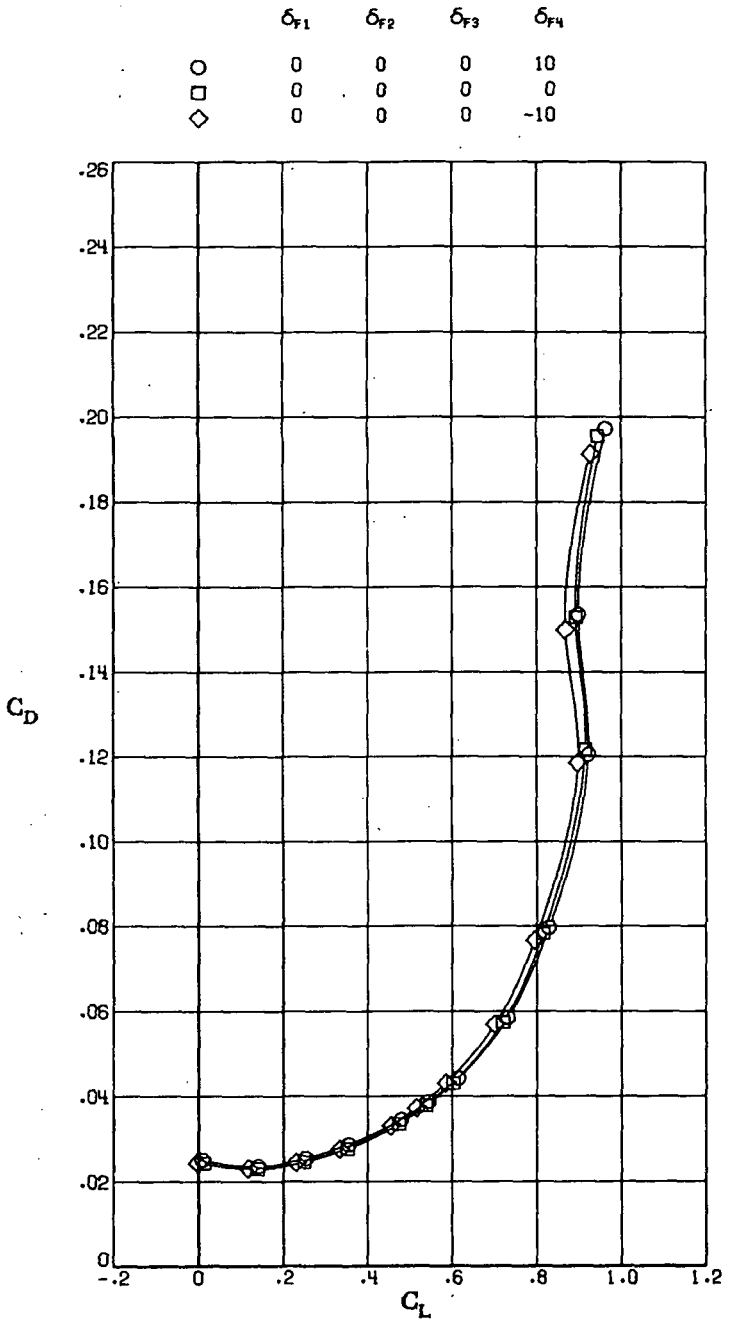
	δ_{F1}	δ_{F2}	δ_{F3}	δ_{F4}	α
○	0	0	0	10	3.92
□	0	0	0	0	3.90
◇	0	0	0	-10	3.91

—— Top Centerline



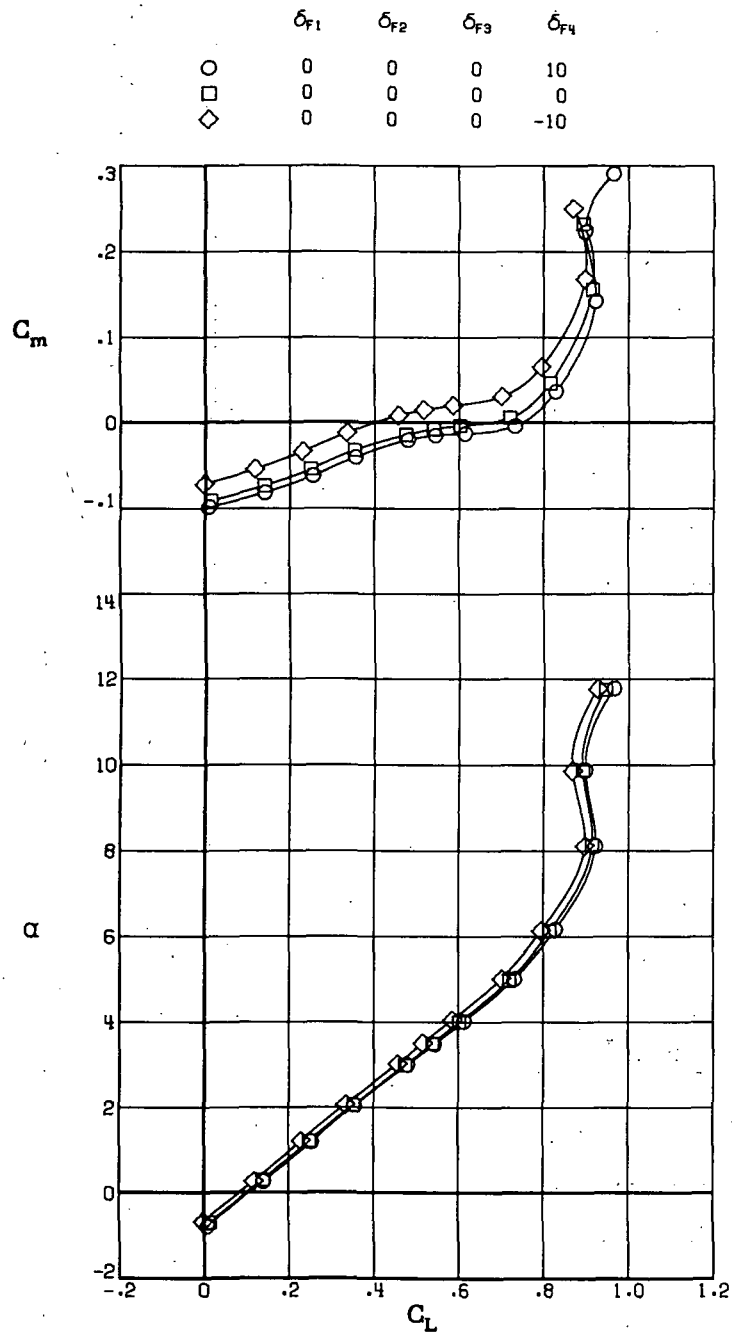
(e) Selected fuselage pressure distributions.

Figure 38.- Concluded.



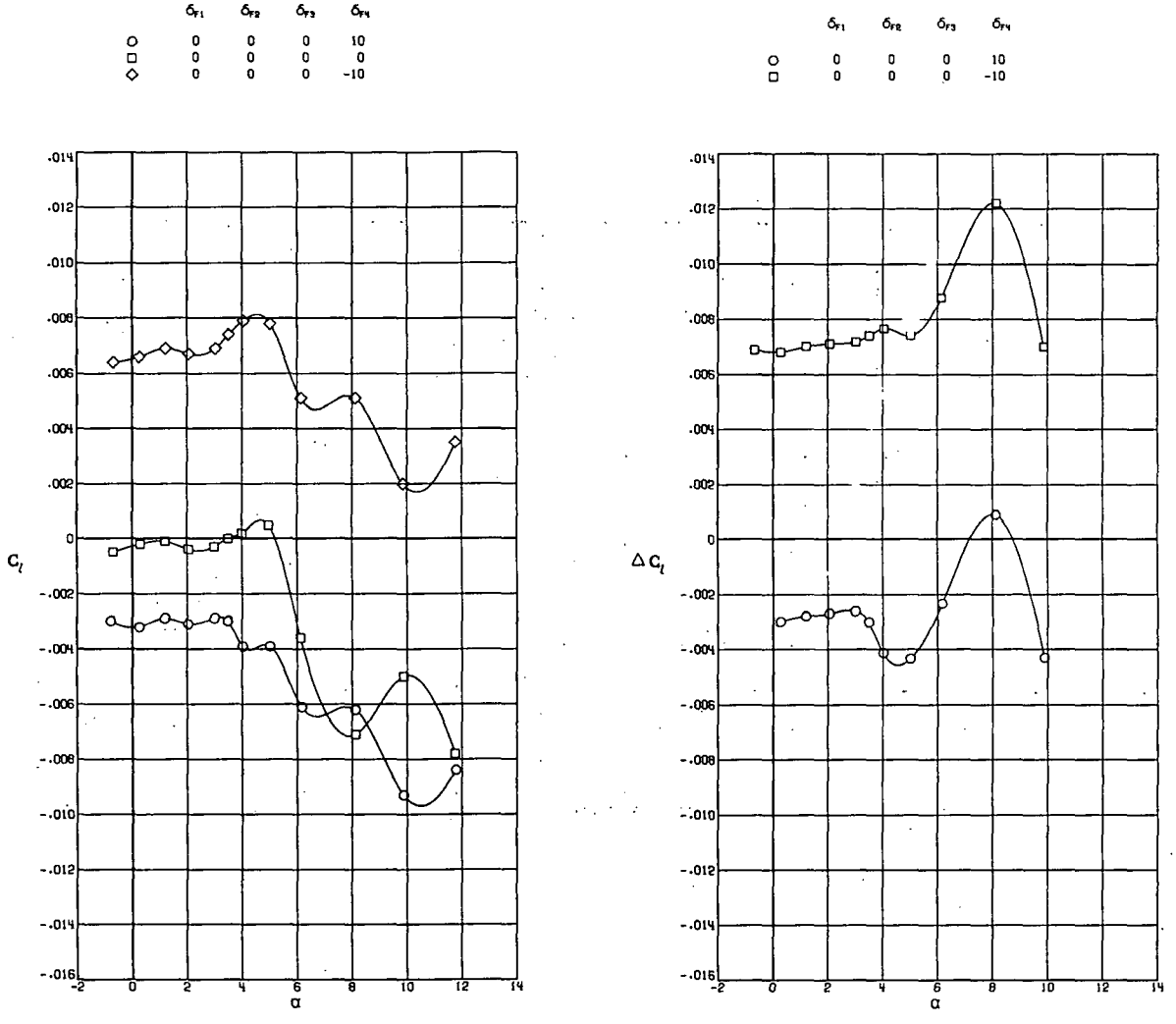
(a) Drag characteristics.

Figure 39.- Effect of F_4 trailing-edge control deflection on aerodynamic characteristics of model with cylindrical fuselage at $M_\infty = 0.88$.



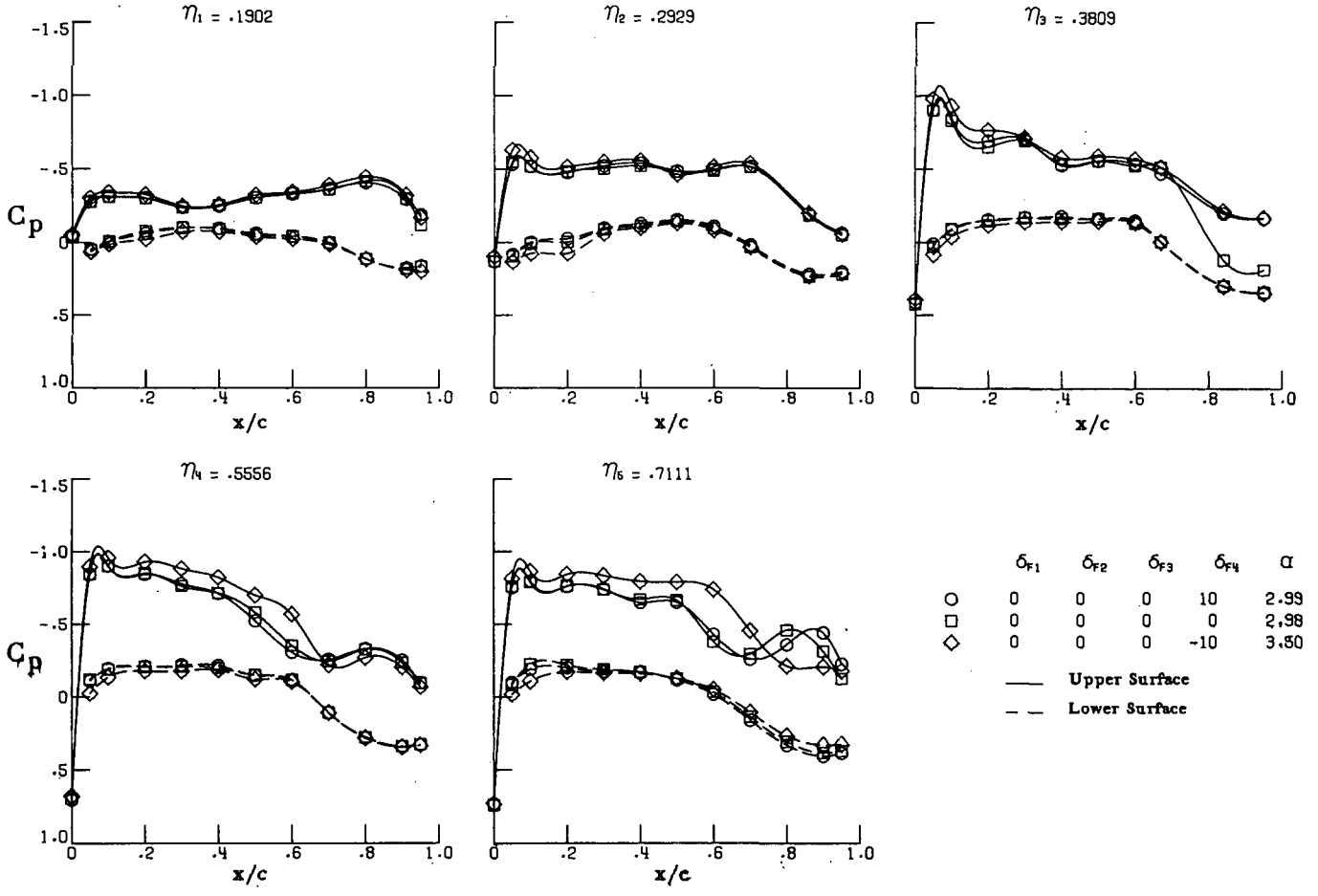
(b) Lift and pitch characteristics.

Figure 39.- Continued.



(c) Rolling-moment characteristics.

Figure 39.- Continued.

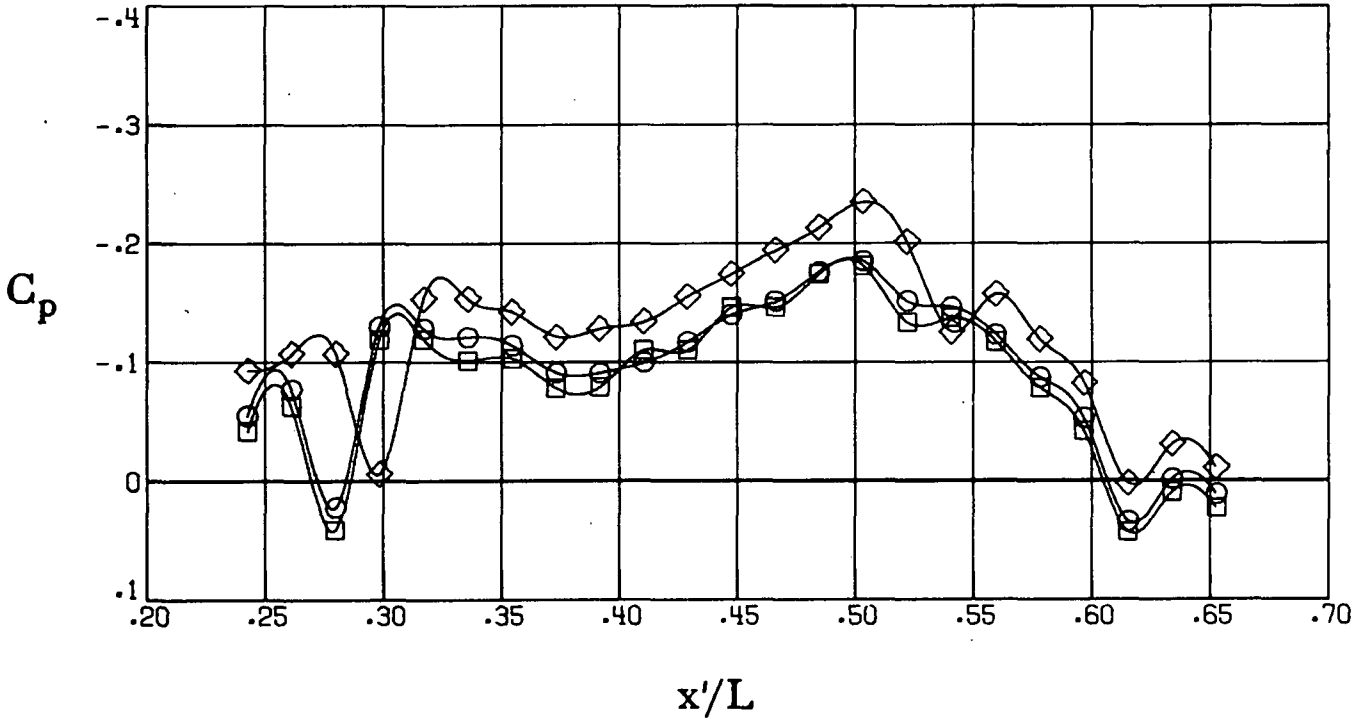


(d) Selected wing pressure distributions.

Figure 39.- Continued.

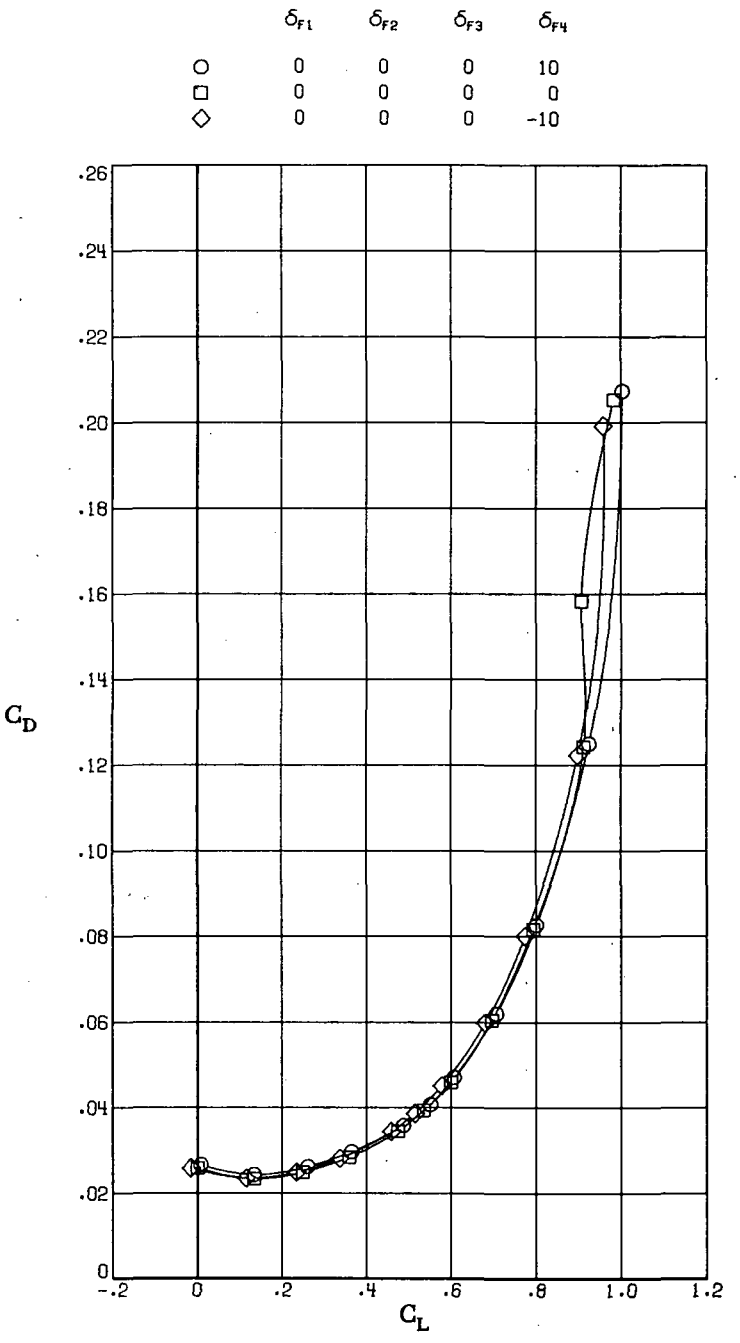
	δ_{F1}	δ_{F2}	δ_{F3}	δ_{F4}	α
○	0	0	0	10	2.99
□	0	0	0	0	2.98
◇	0	0	0	-10	3.50

—— Top Centerline



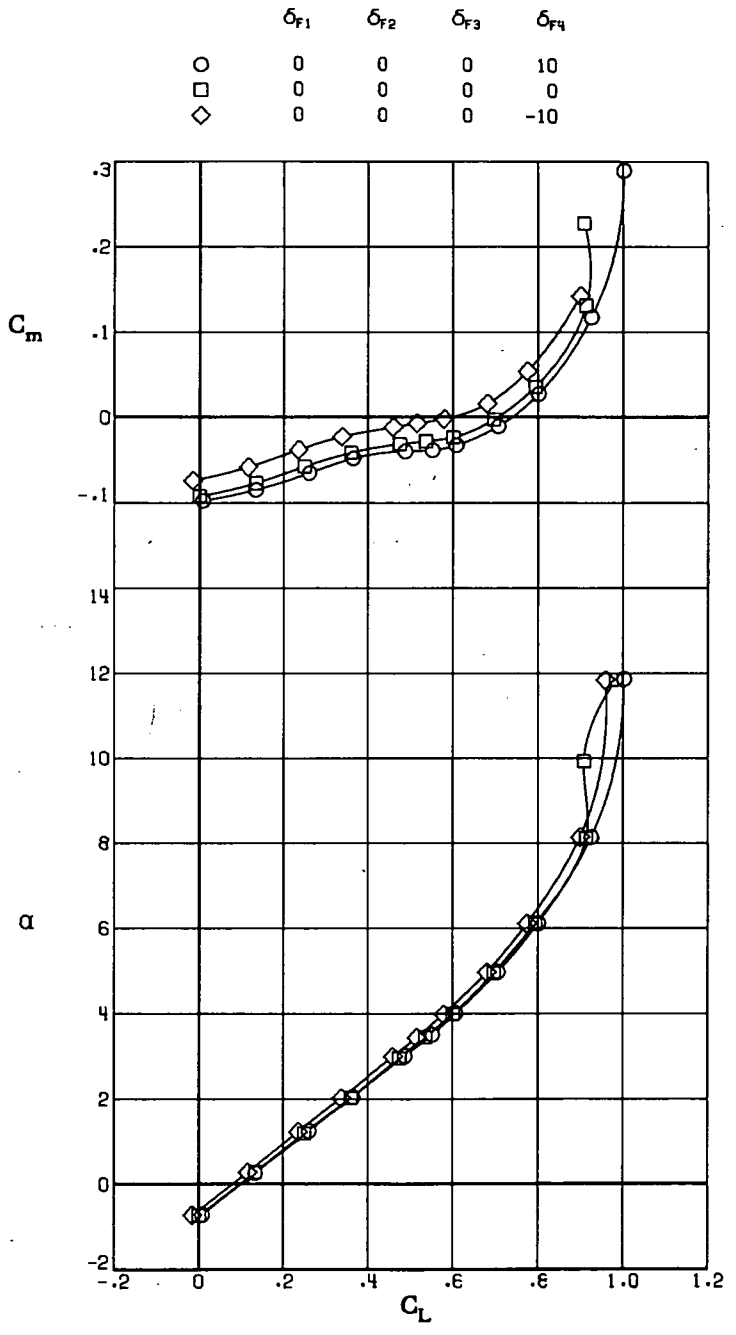
(e) Selected fuselage pressure distributions.

Figure 39.- Concluded.



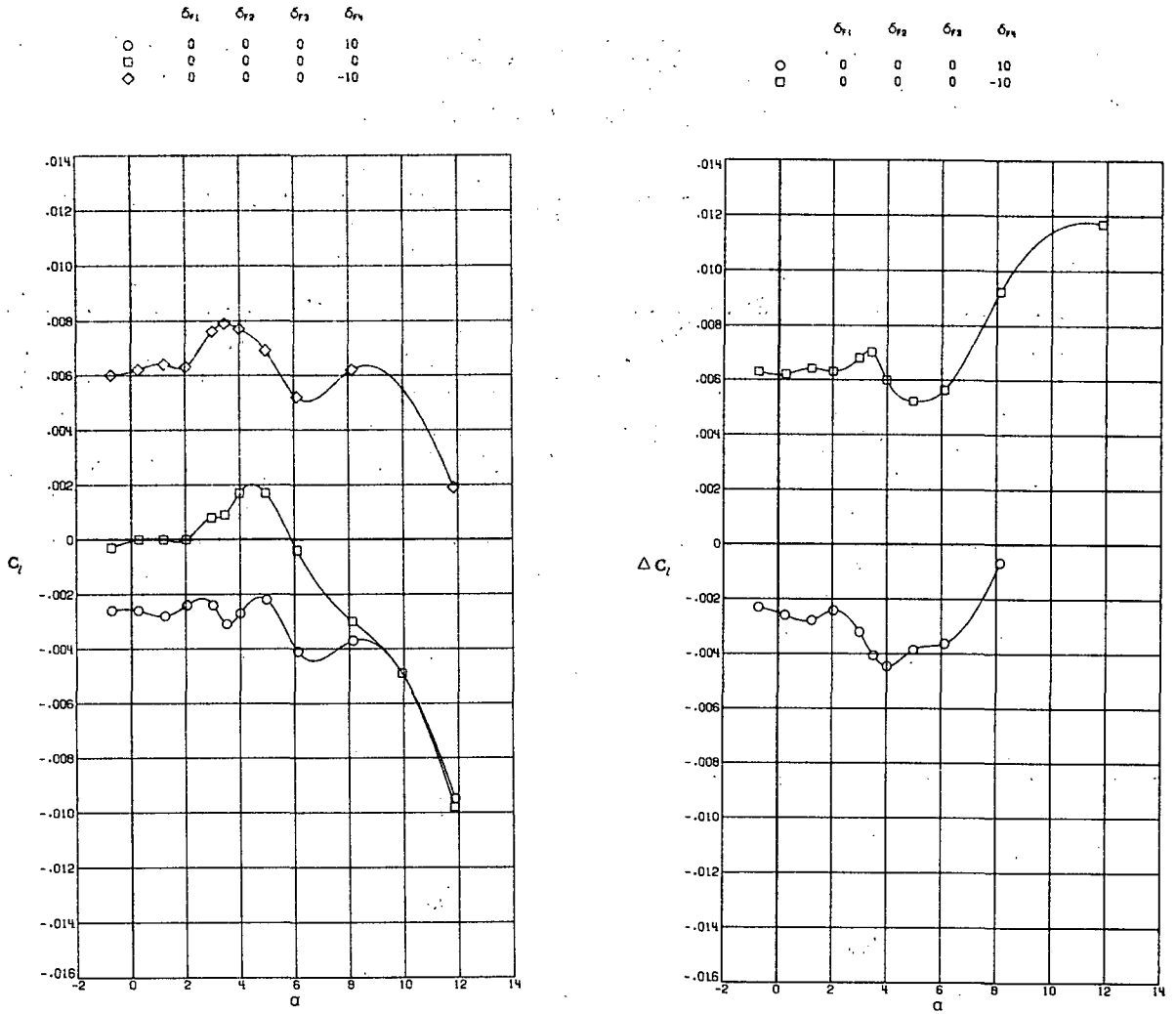
(a) Drag characteristics.

Figure 40.- Effect of F_4 trailing-edge control deflection on aerodynamic characteristics of model with cylindrical fuselage at $M_\infty = 0.90$.



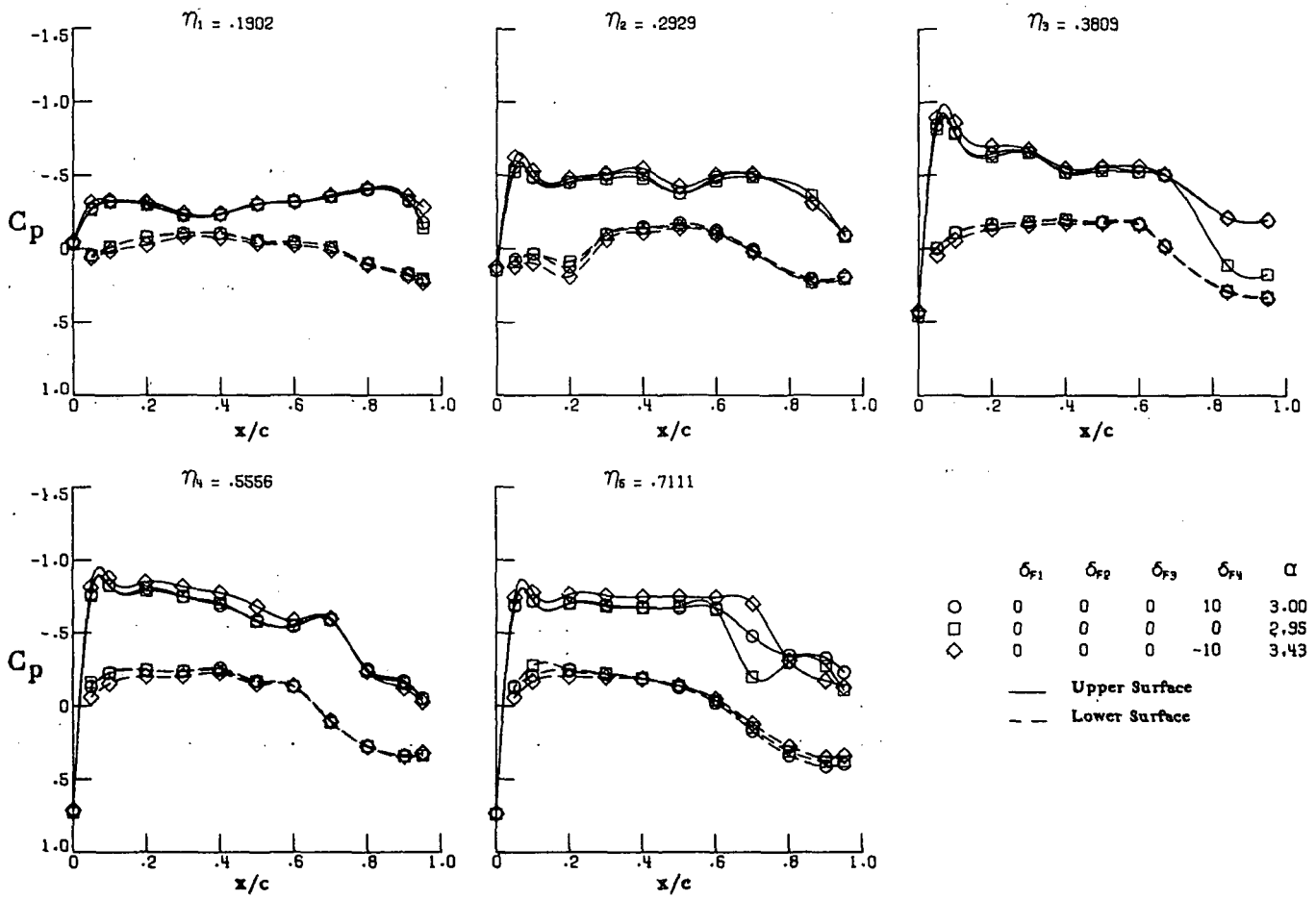
(b) Lift and pitch characteristics.

Figure 40.- Continued.



(c) Rolling-moment characteristics.

Figure 40.- Continued.

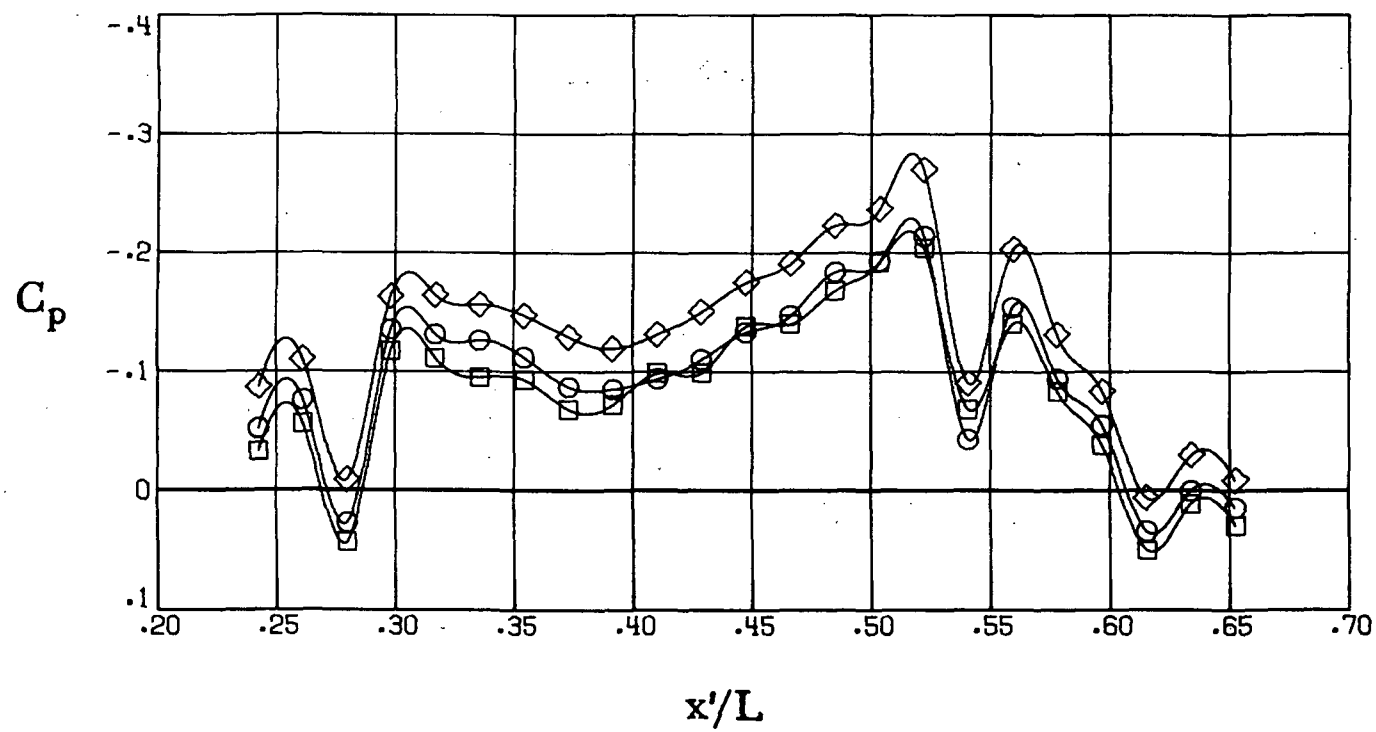


(d) Selected wing pressure distributions.

Figure 40.- Continued.

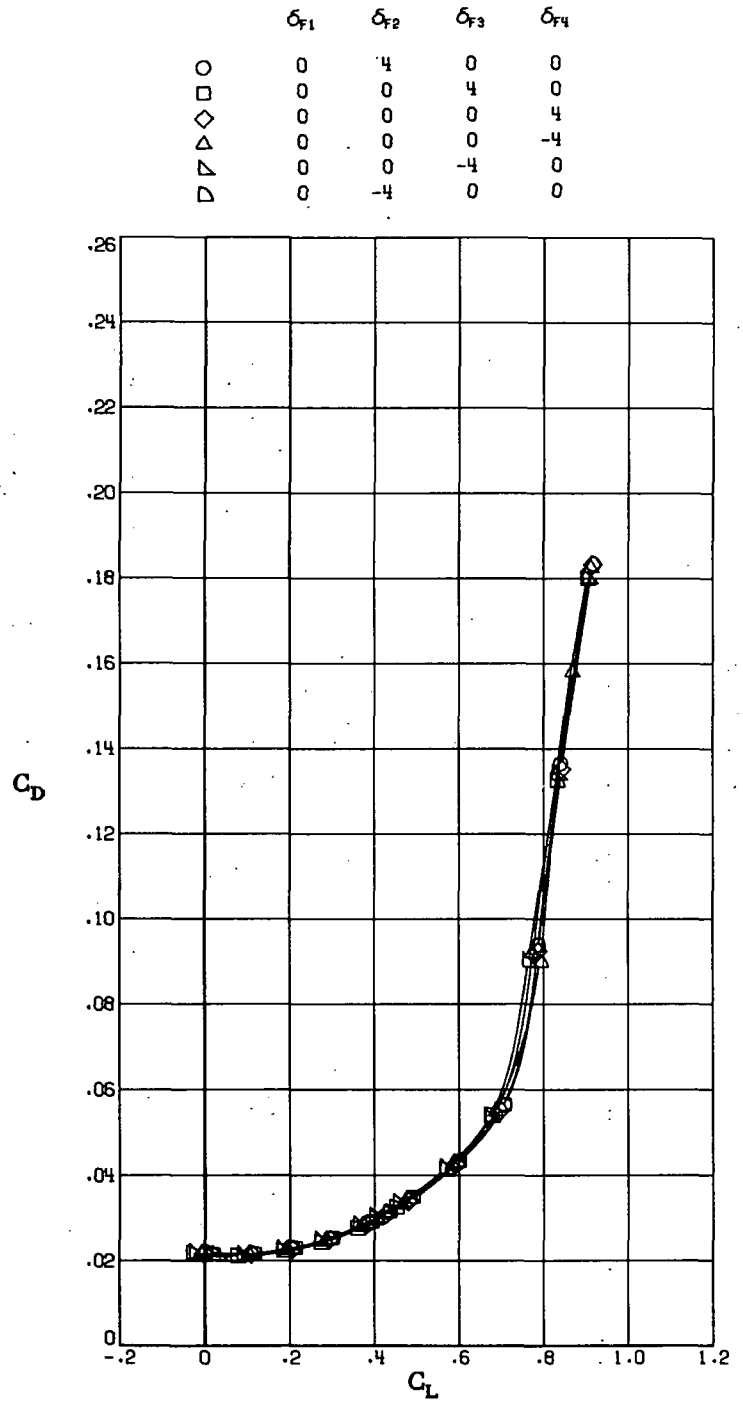
	δ_{F1}	δ_{F2}	δ_{F3}	δ_{F4}	α
○	0	0	0	10	3.00
□	0	0	0	0	2.95
◇	0	0	0	-10	3.43

—— Top Centerline



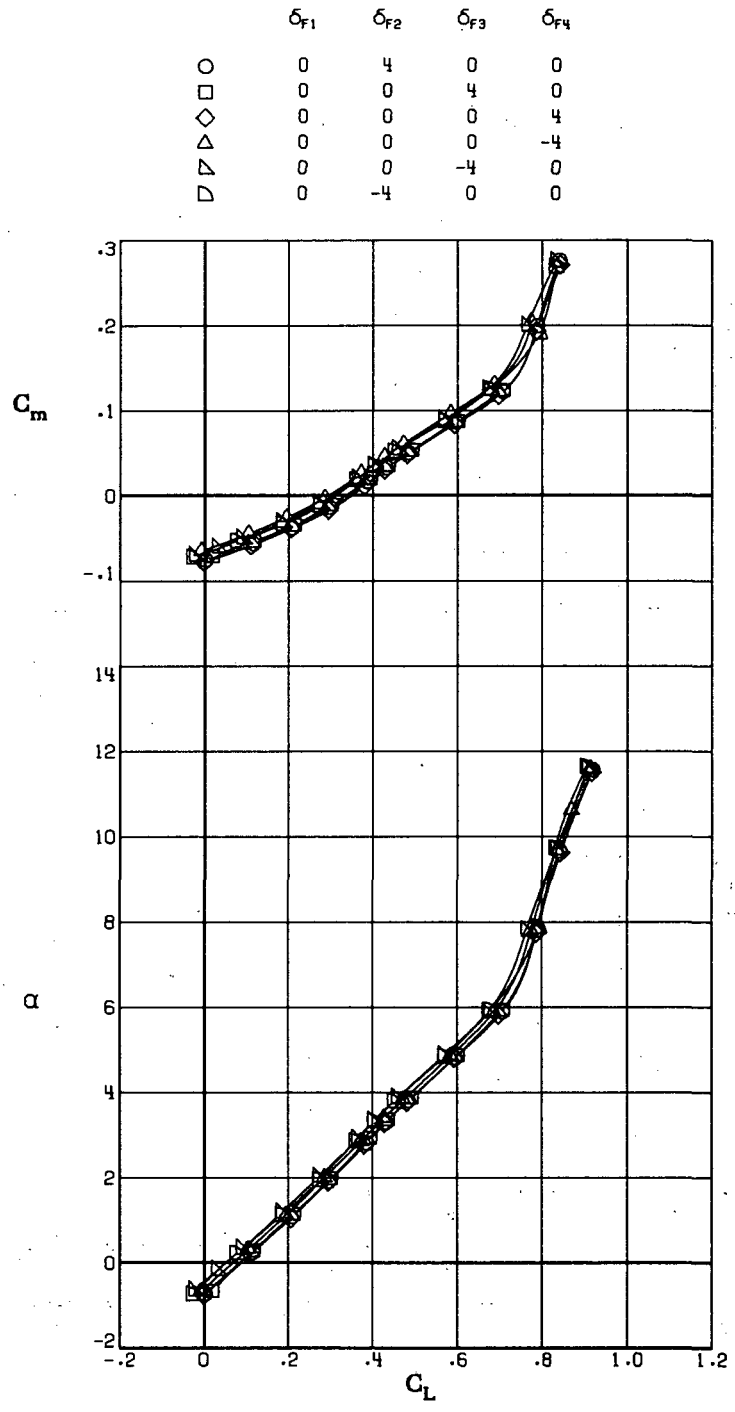
(e) Selected fuselage pressure distributions.

Figure 40.- Concluded.



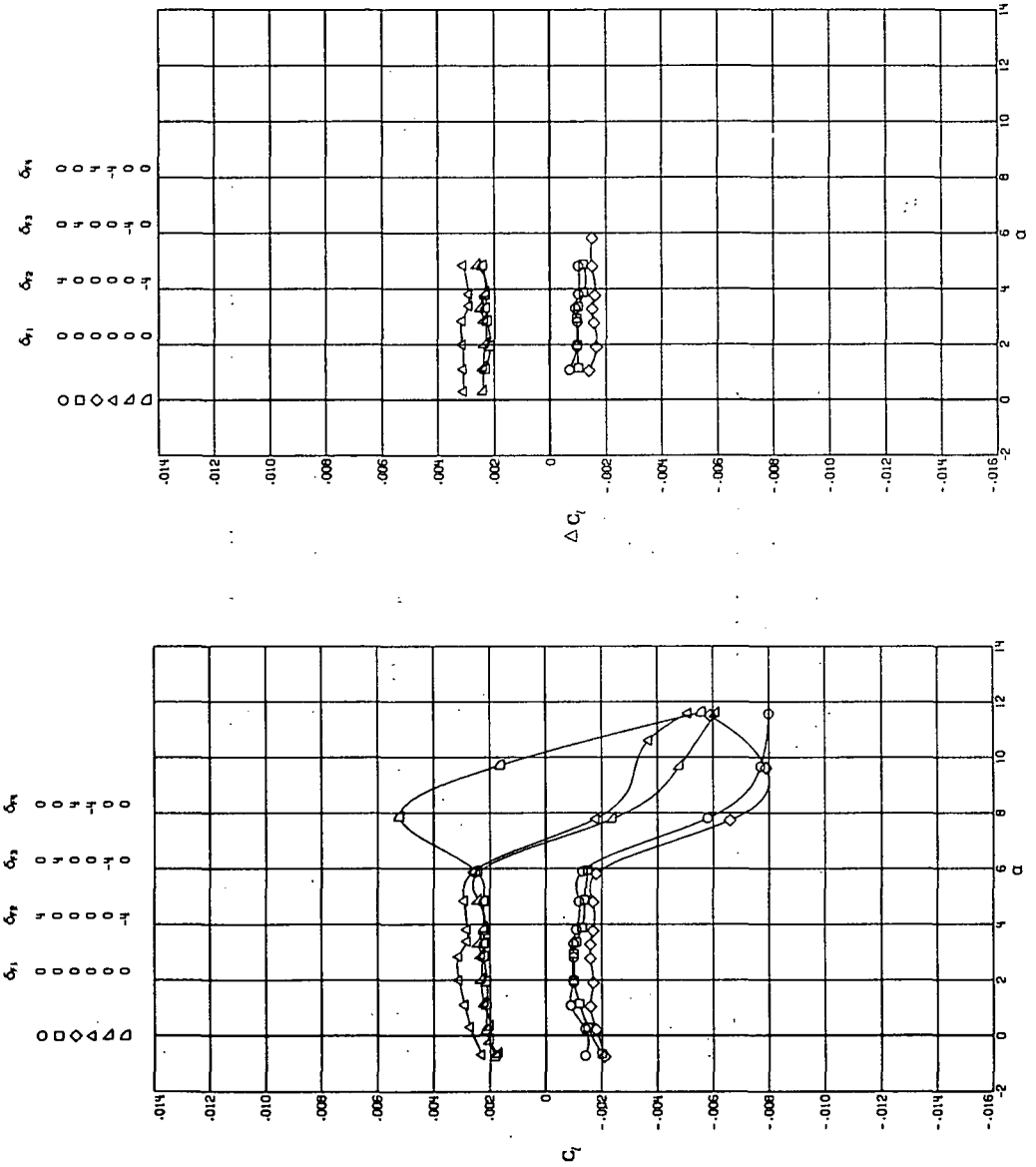
(a) Drag characteristics.

Figure 41.- Effect of spanwise location of trailing-edge control surface deflected $\pm 4^{\circ}$. Area-ruled fuselage. $M_{\infty} = 0.80$.



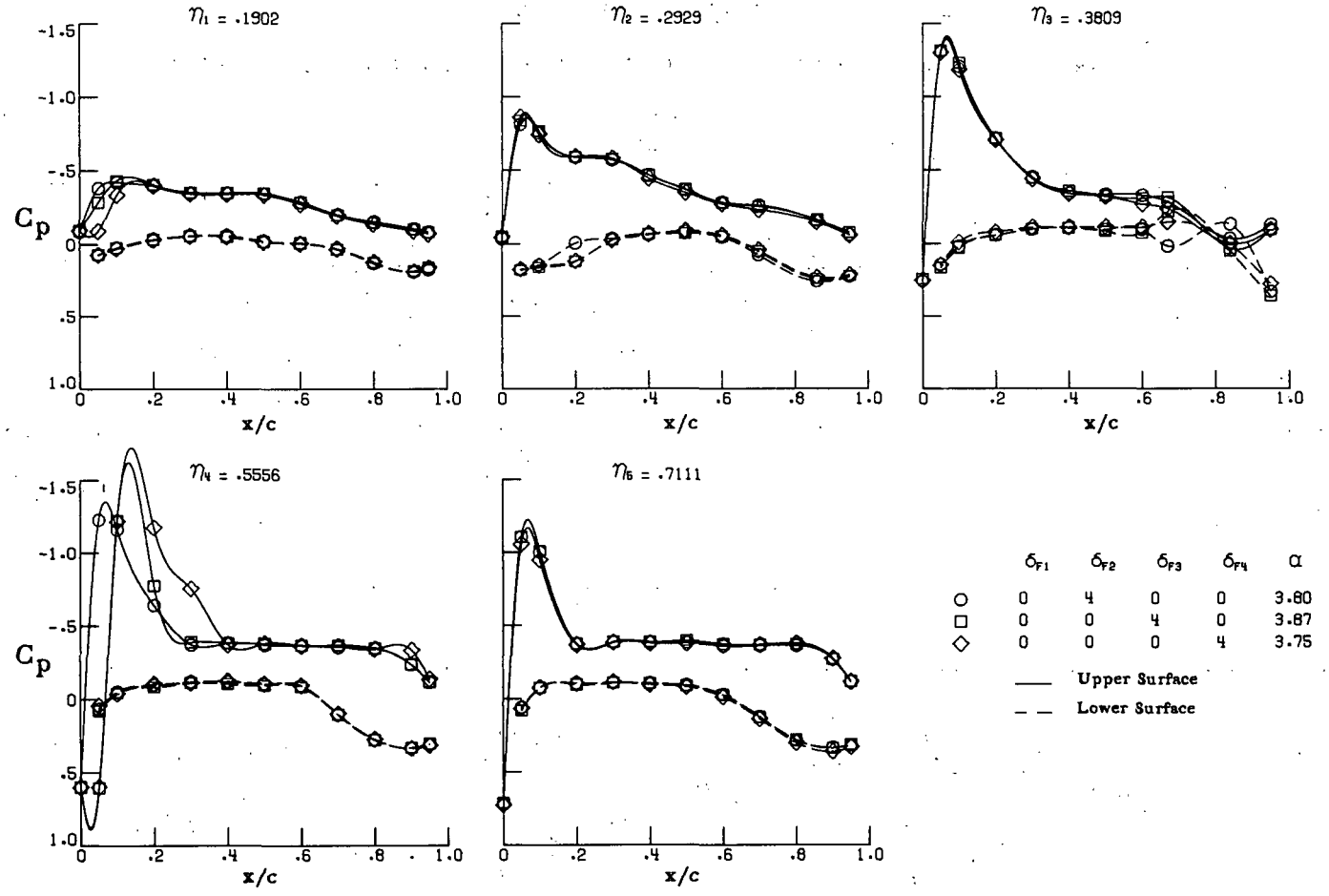
(b) Lift and pitch characteristics.

Figure 41.- Continued.



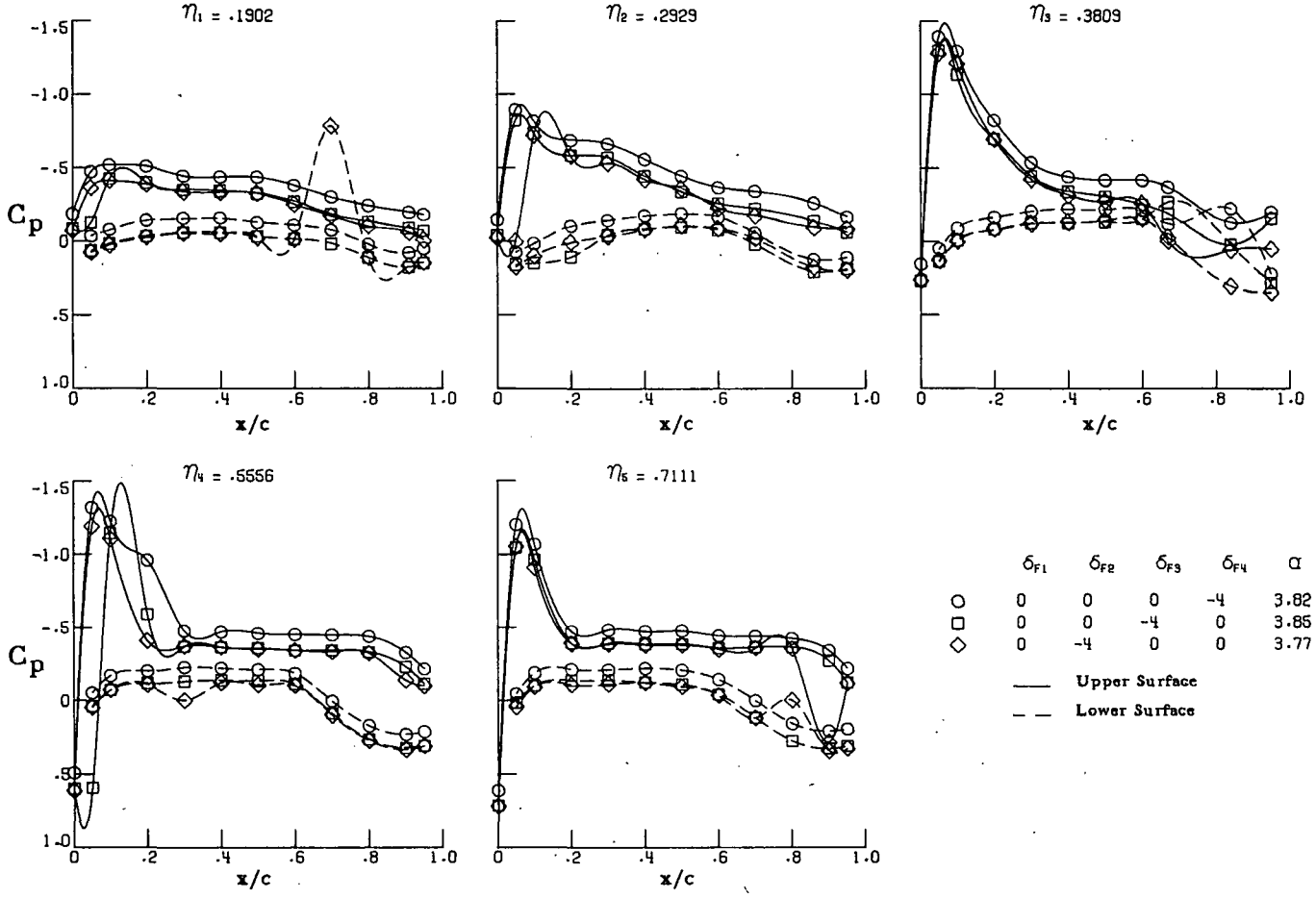
(c) Rolling-moment characteristics.

Figure 41.- Continued.



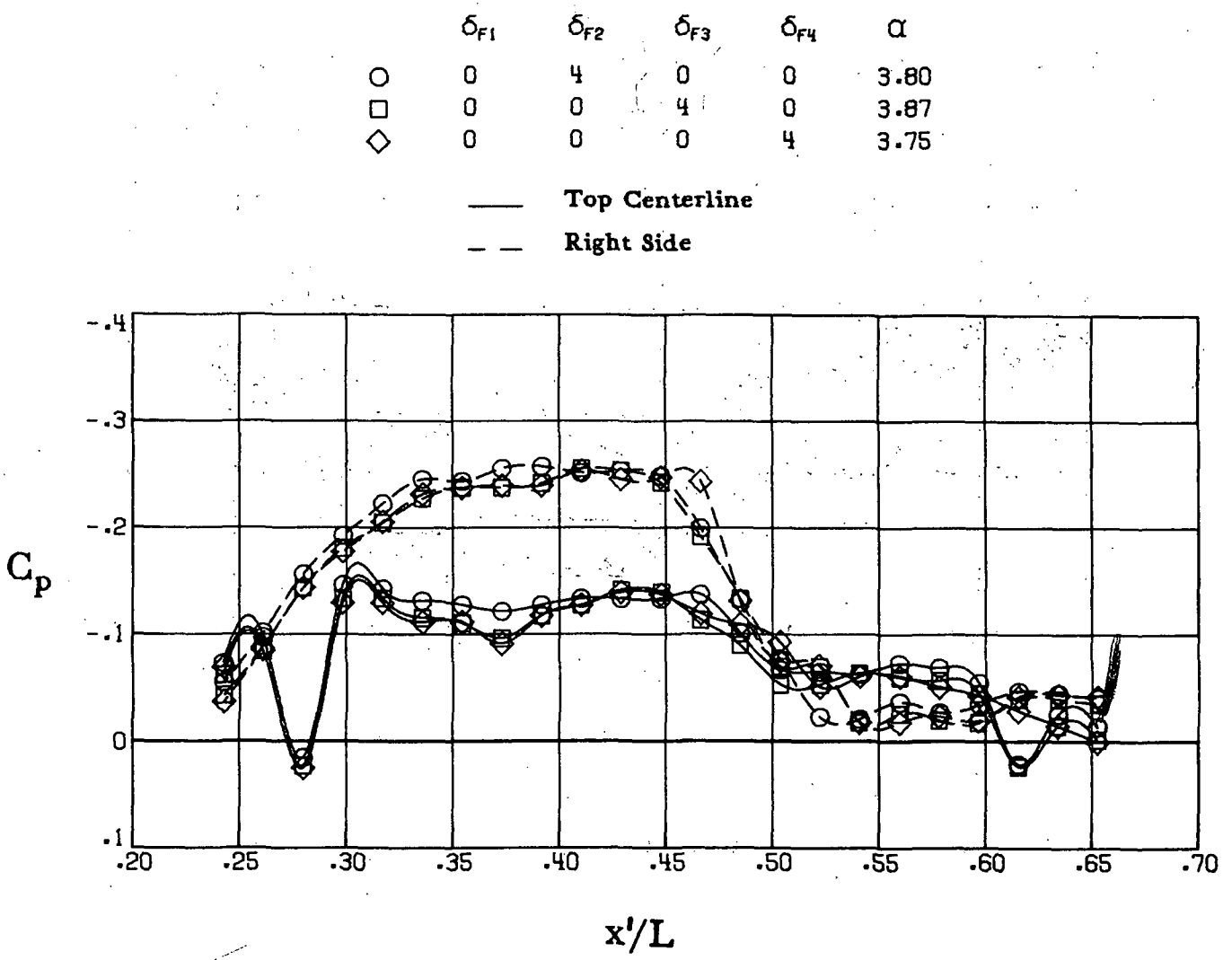
(d) Selected wing pressure distributions for control surface deflected 4^{o}.

Figure 41.- Continued.



(e) Selected wing pressure distributions for control surface deflected -4°.

Figure 41.- Continued.



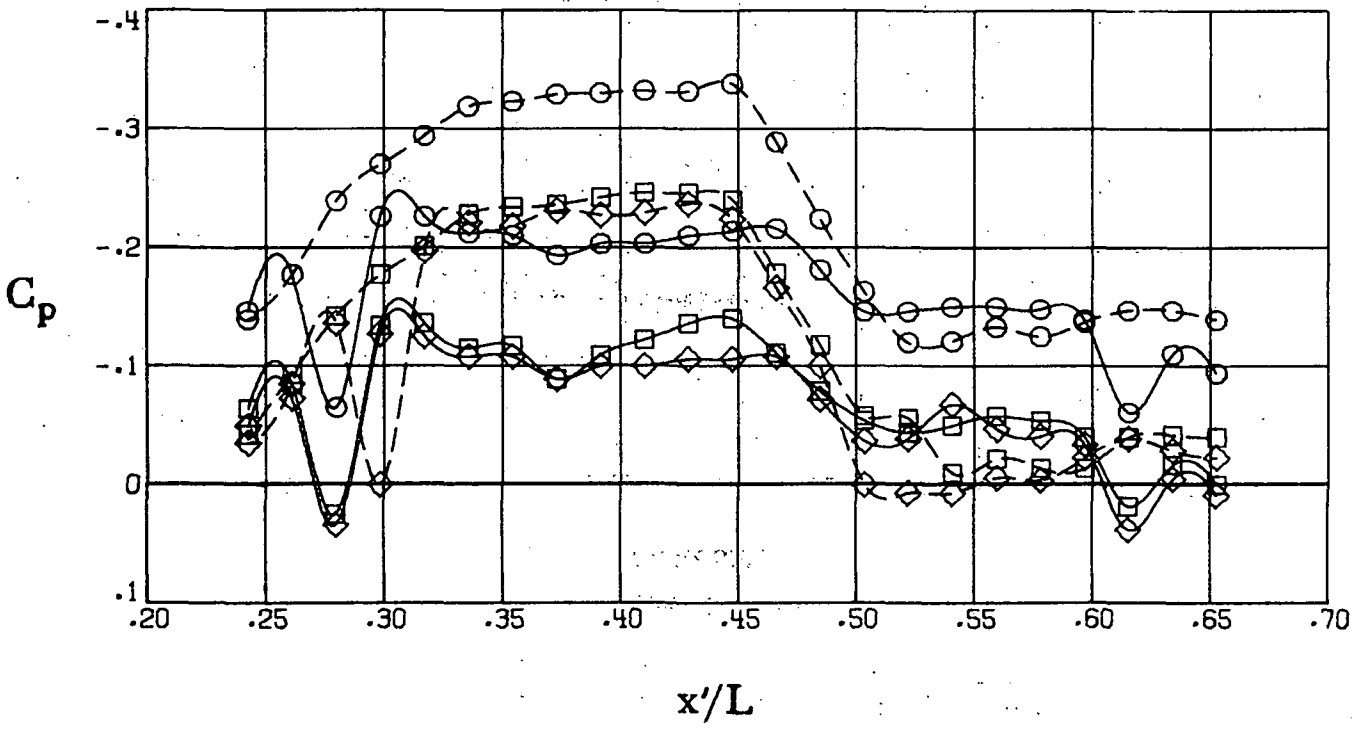
(f) Selected fuselage pressure distributions for control surface deflected 4^{o}.

Figure 41.- Continued.

	δ_{F1}	δ_{F2}	δ_{F3}	δ_{F4}	α
○	0	0	0	-4	3.82
□	0	0	-4	0	3.85
◇	0	-4	0	0	3.77

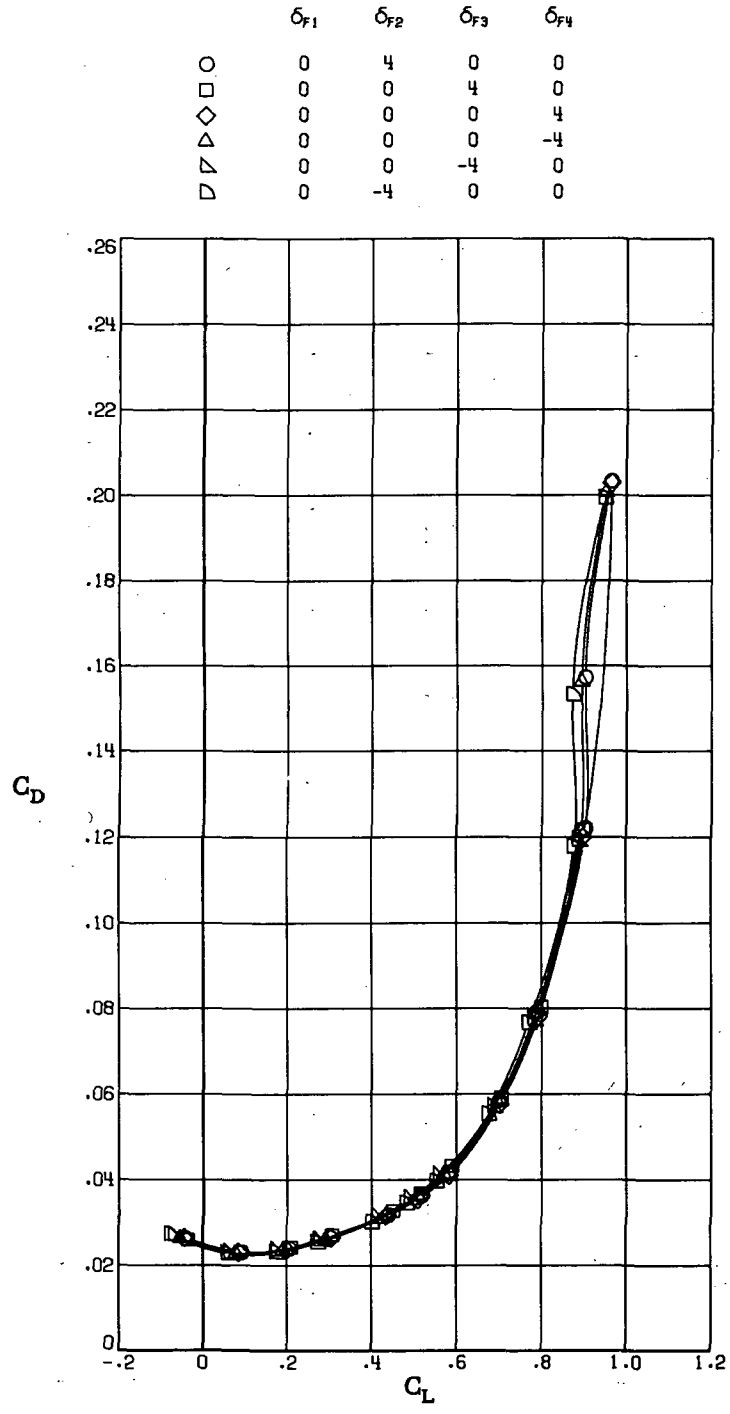
—— Top Centerline

– – Right Side



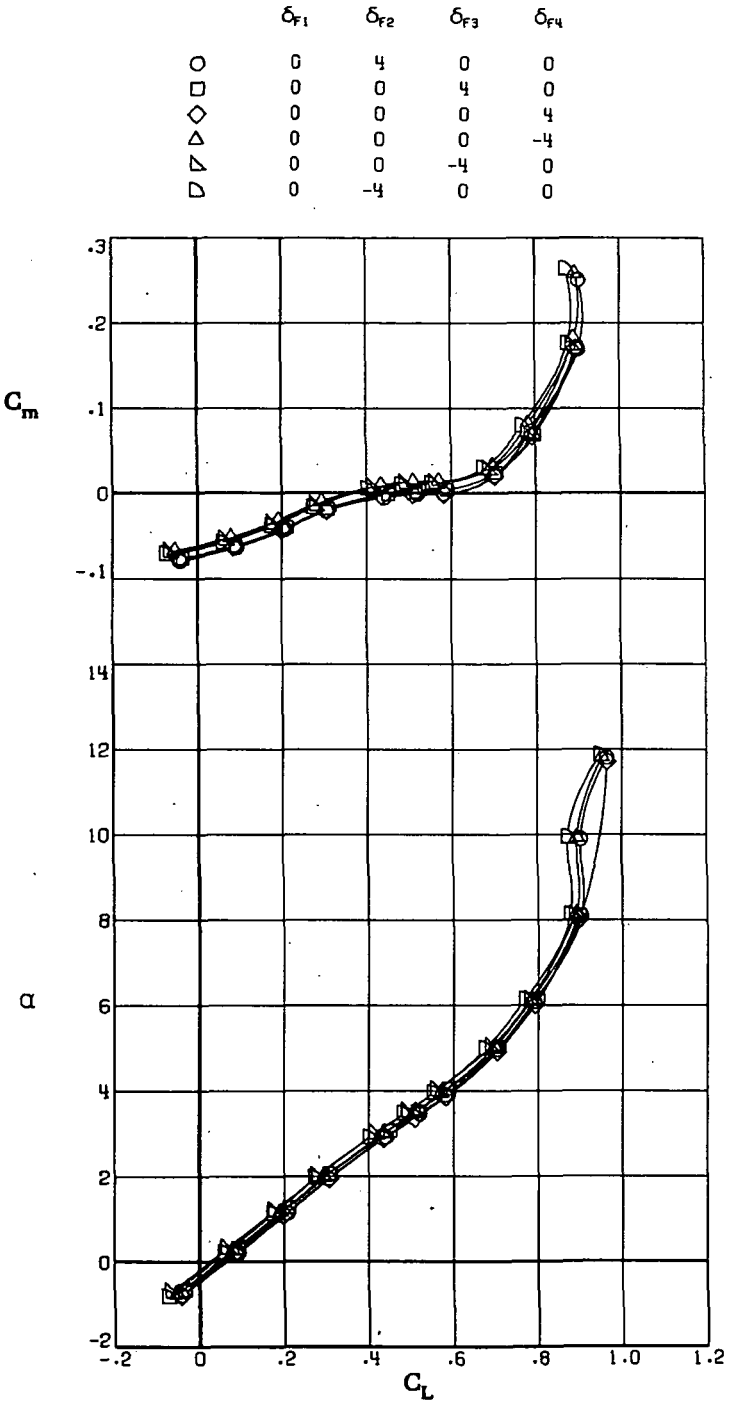
(g) Selected fuselage pressure distributions for control surface deflected -4°.

Figure 41.- Concluded.



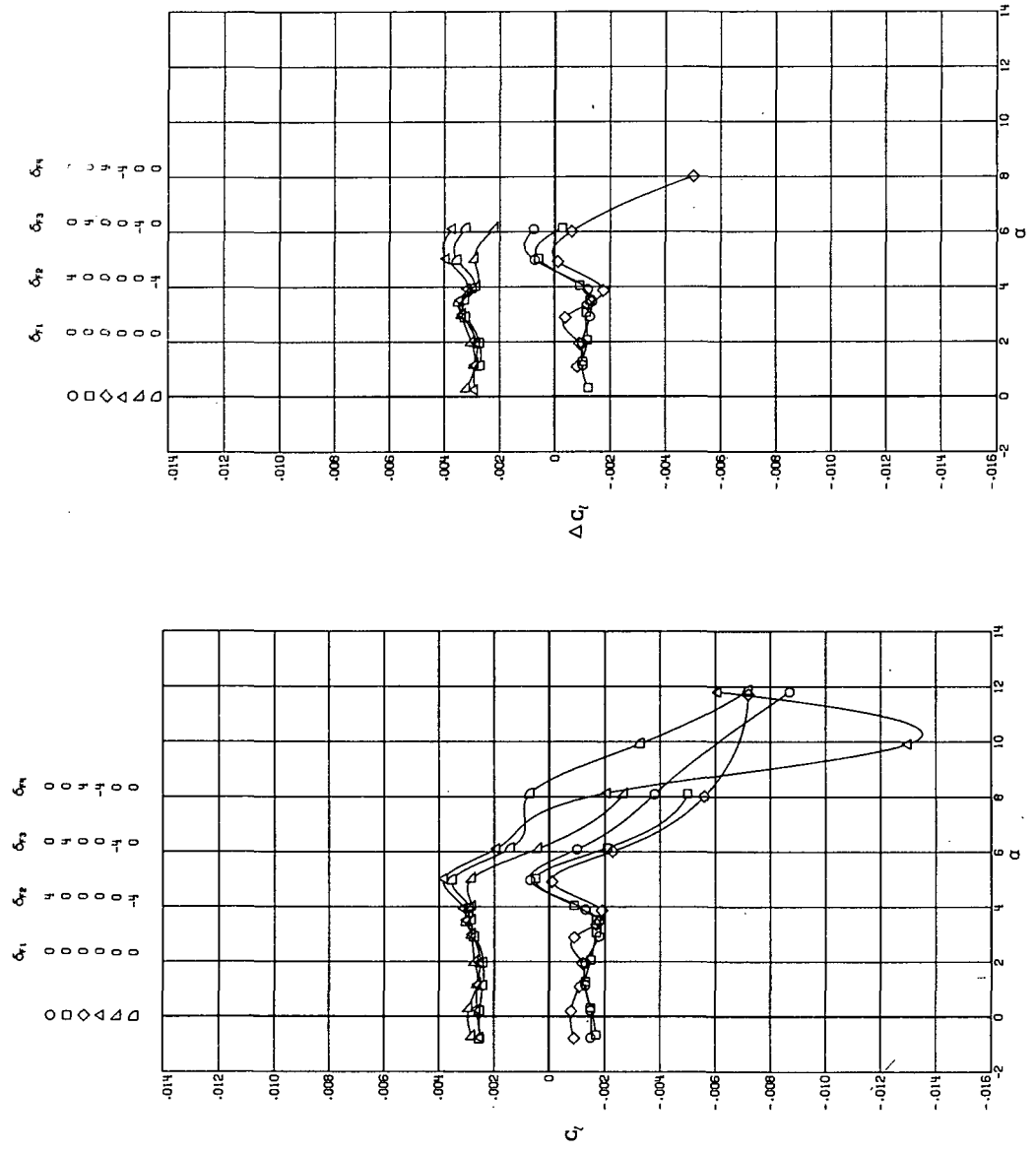
(a) Drag characteristics.

Figure 42.- Effect of spanwise location of trailing-edge control surface deflected $\pm 4^{\circ}$. Area-ruled fuselage. $M_{\infty} = 0.90$.



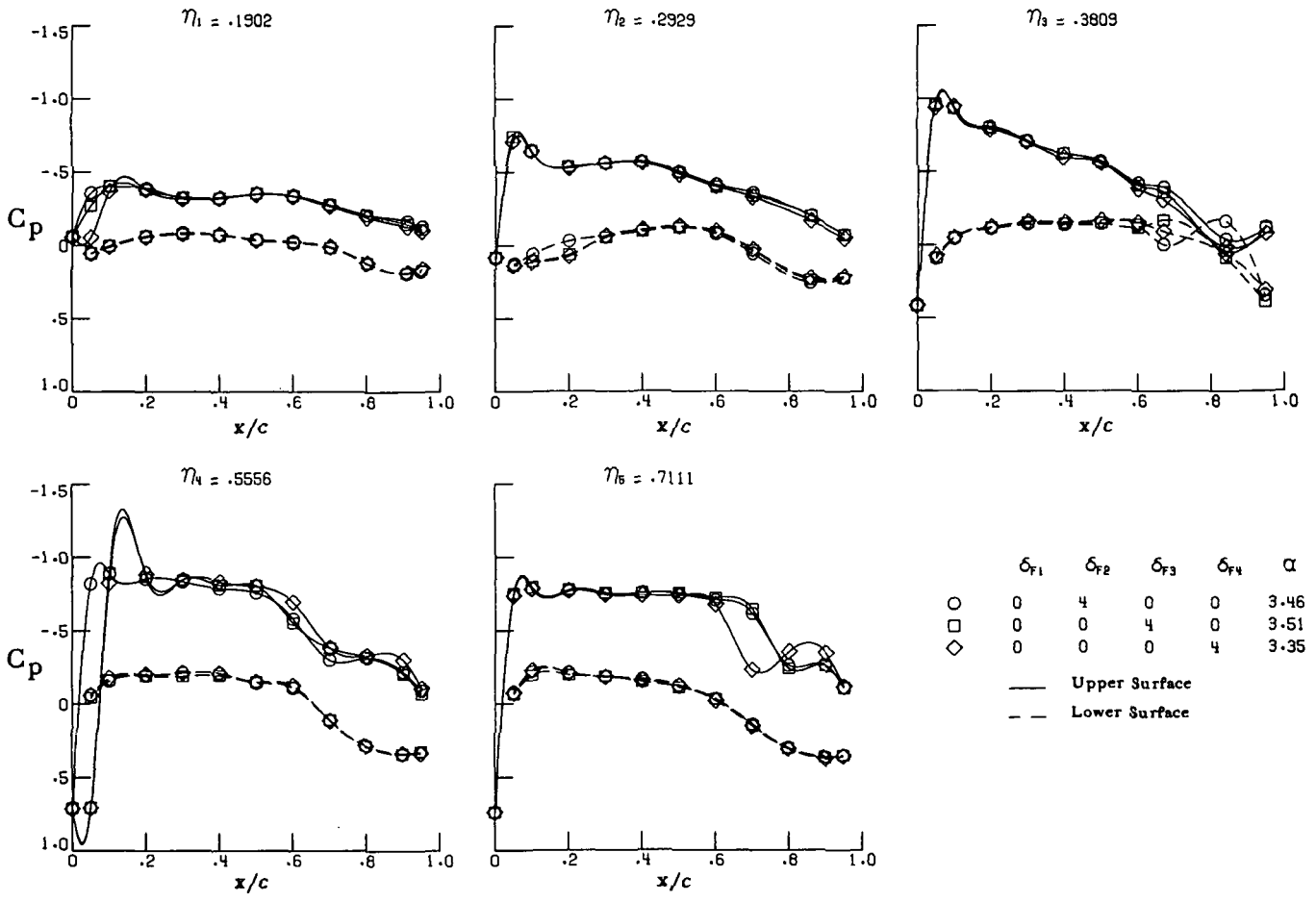
(b) Lift and pitch characteristics.

Figure 42.- Continued.



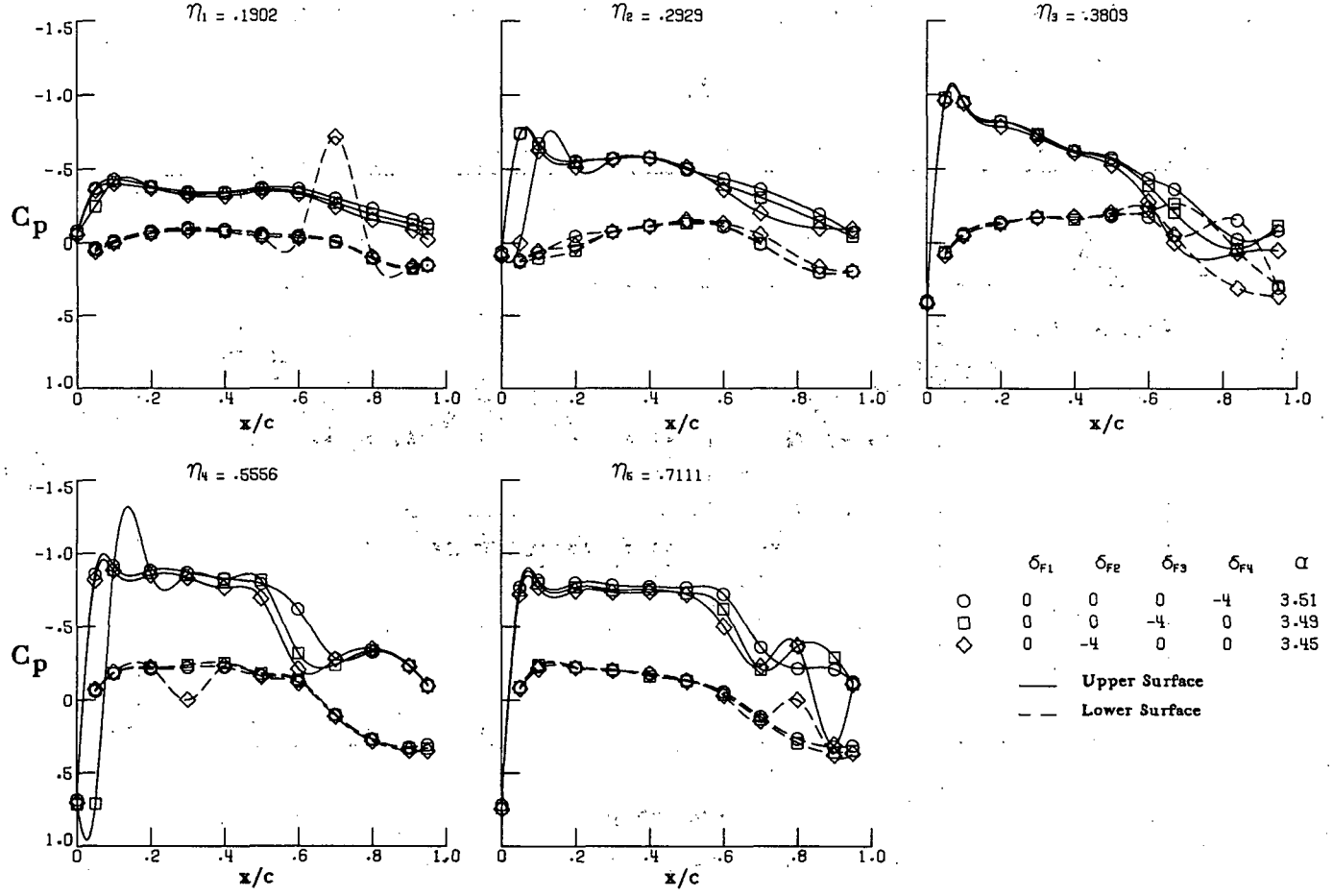
(c) Rolling-moment characteristics.

Figure 42.- Continued.



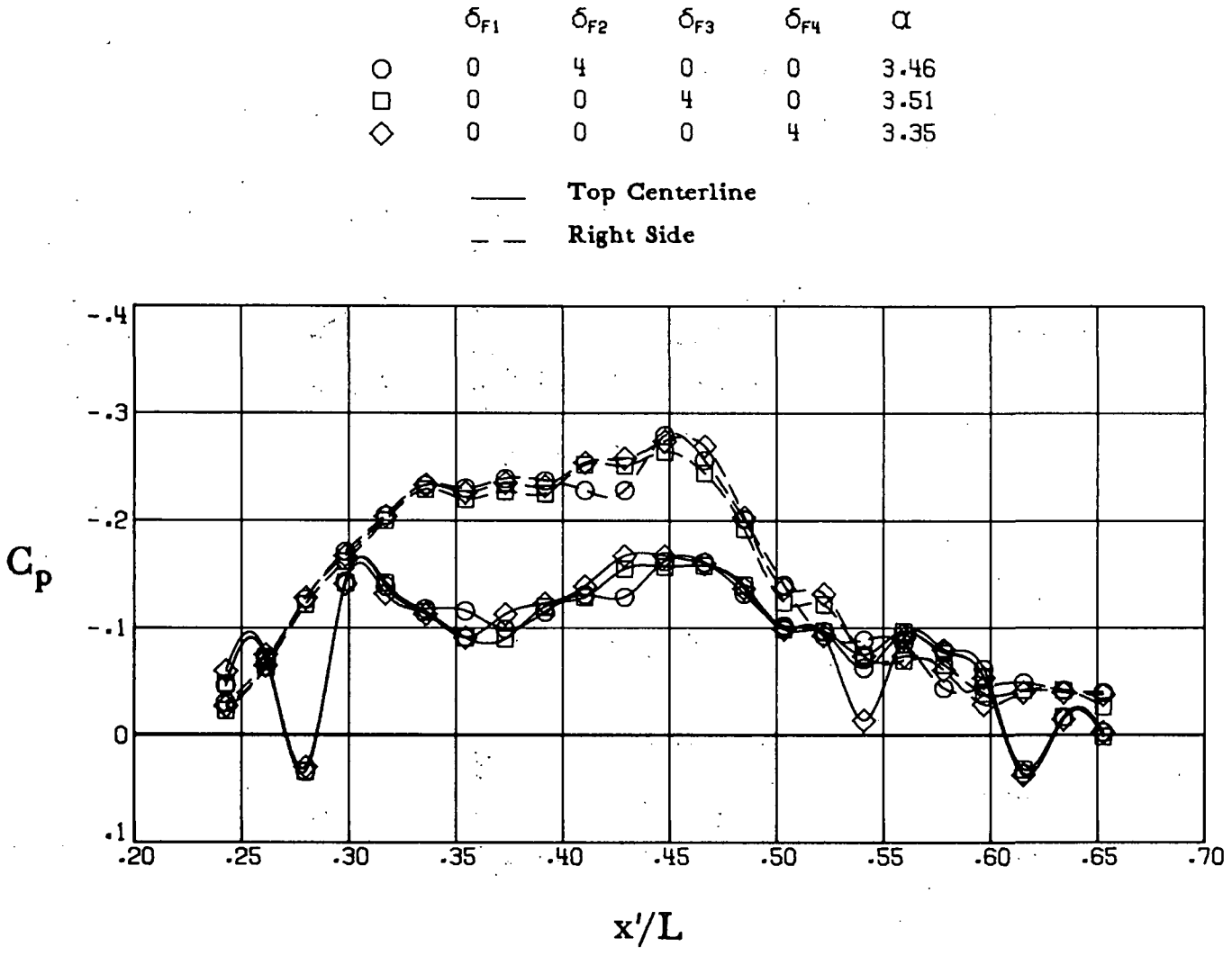
(d) Selected wing pressure distributions for control surface deflected 4^{o}.

Figure 42.- Continued.



(e) Selected wing pressure distributions for control surface deflected -4^{o}.

Figure 42.- Continued.



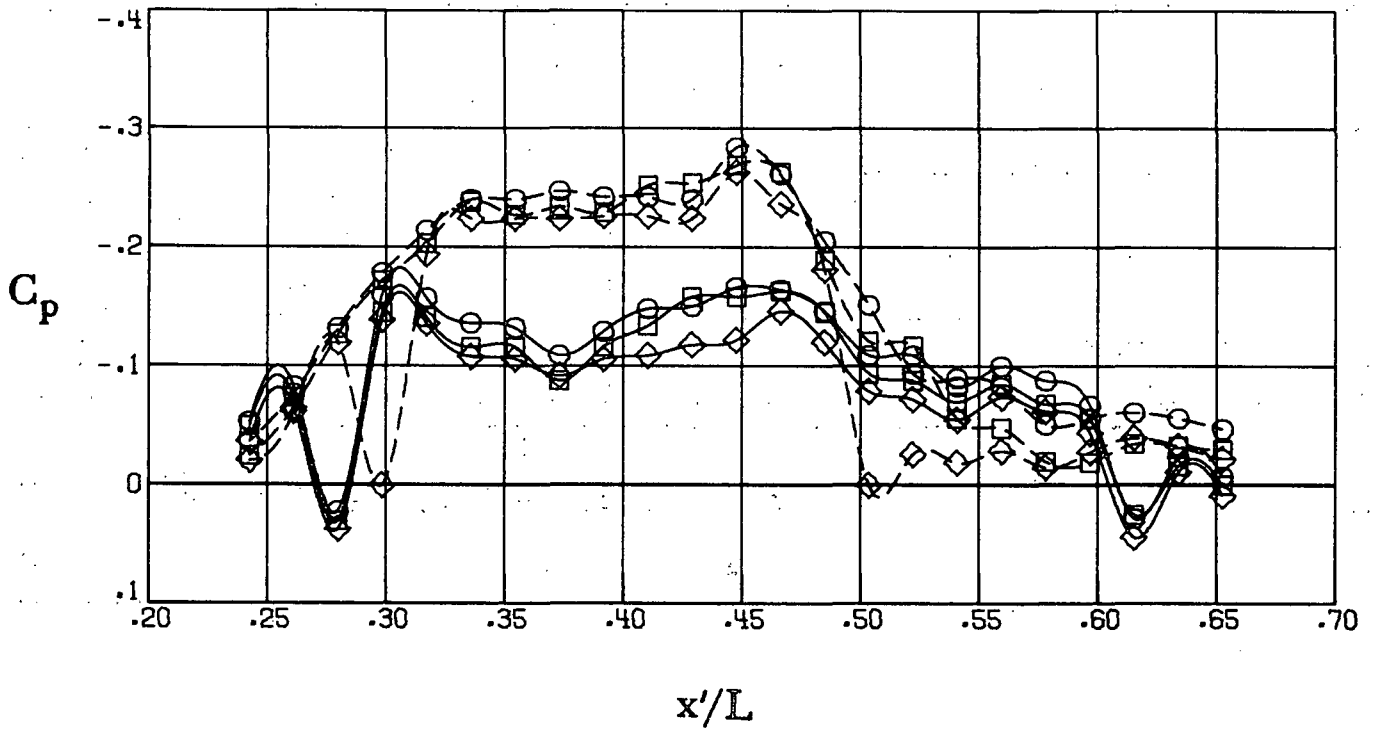
(f) Selected fuselage pressure distributions for control surface deflected 4^{o}.

Figure 42.- Continued.

	δ_{F1}	δ_{F2}	δ_{F3}	δ_{F4}	α
○	0	0	0	-4	3.51
□	0	0	-4	0	3.49
◇	0	-4	0	0	3.45

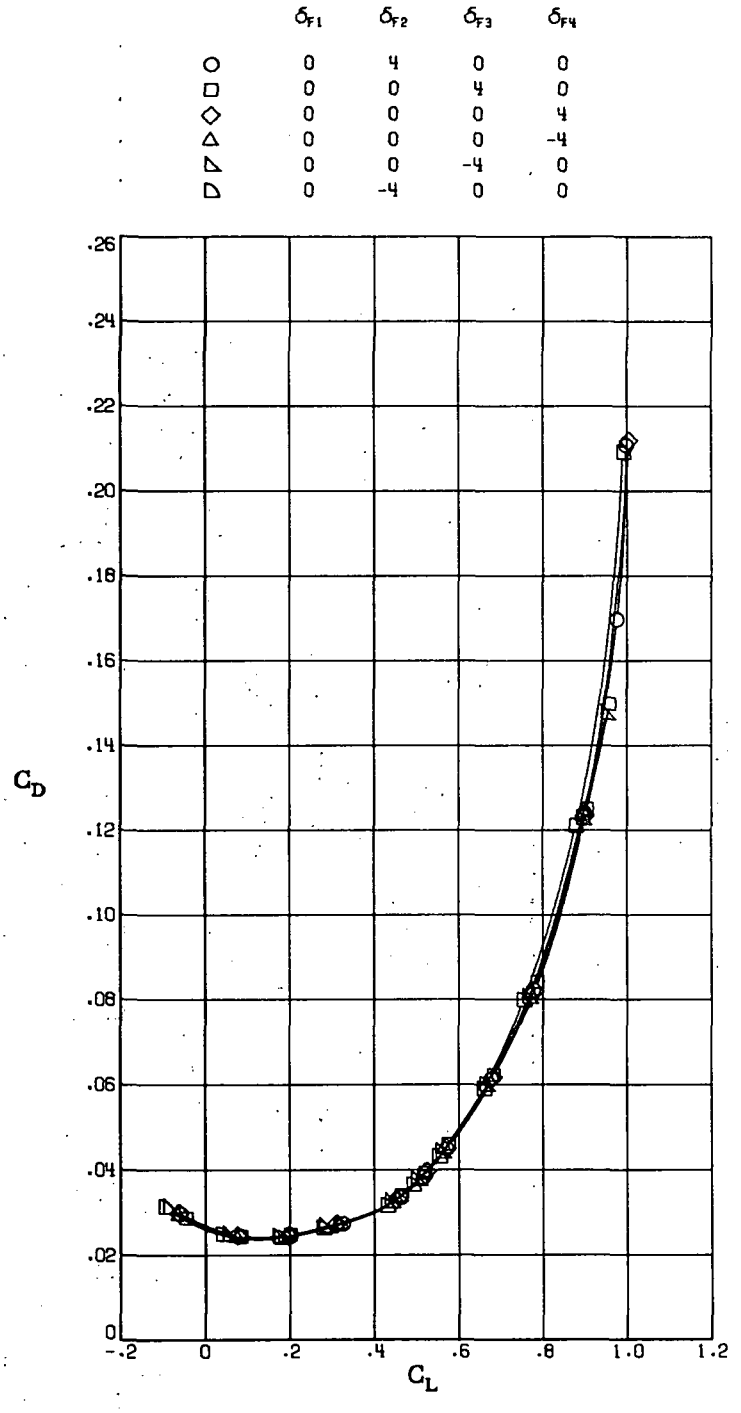
—— Top Centerline

– – Right Side



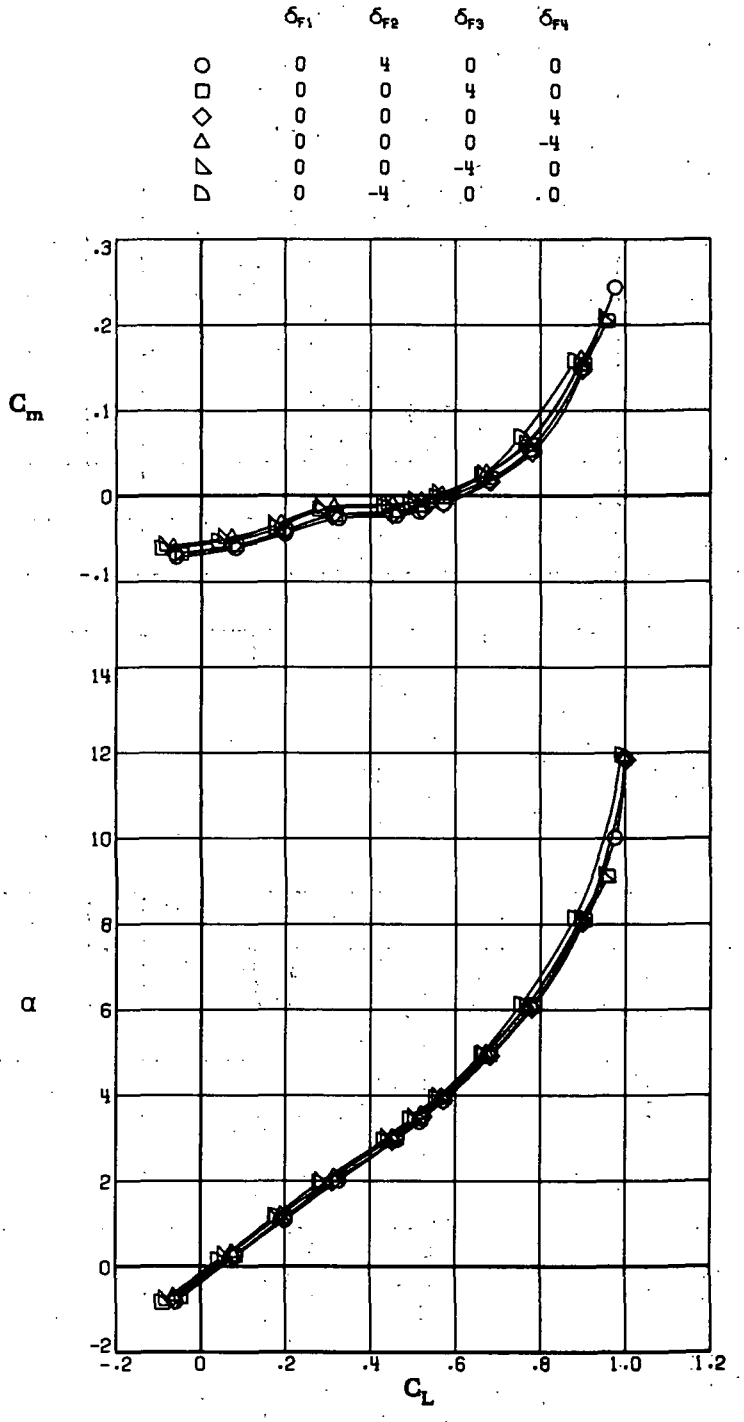
(g) Selected fuselage pressure distributions for control surface deflected -4°.

Figure 42.- Concluded.



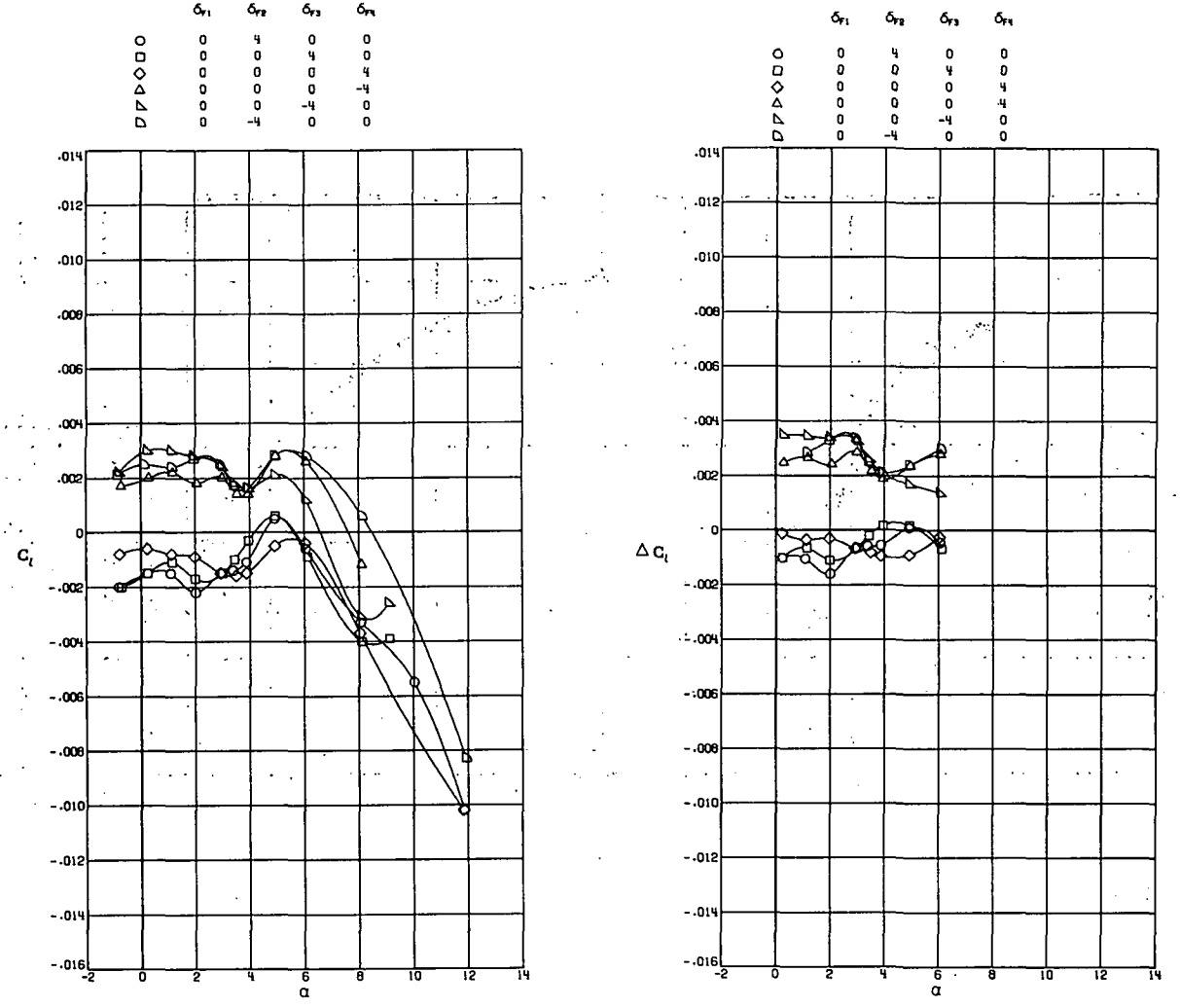
(a) Drag characteristics.

Figure 43.- Effect of spanwise location of trailing-edge control surface deflected $\pm 4^{o}$. Area-ruled fuselage. $M_{\infty} = 0.92$.



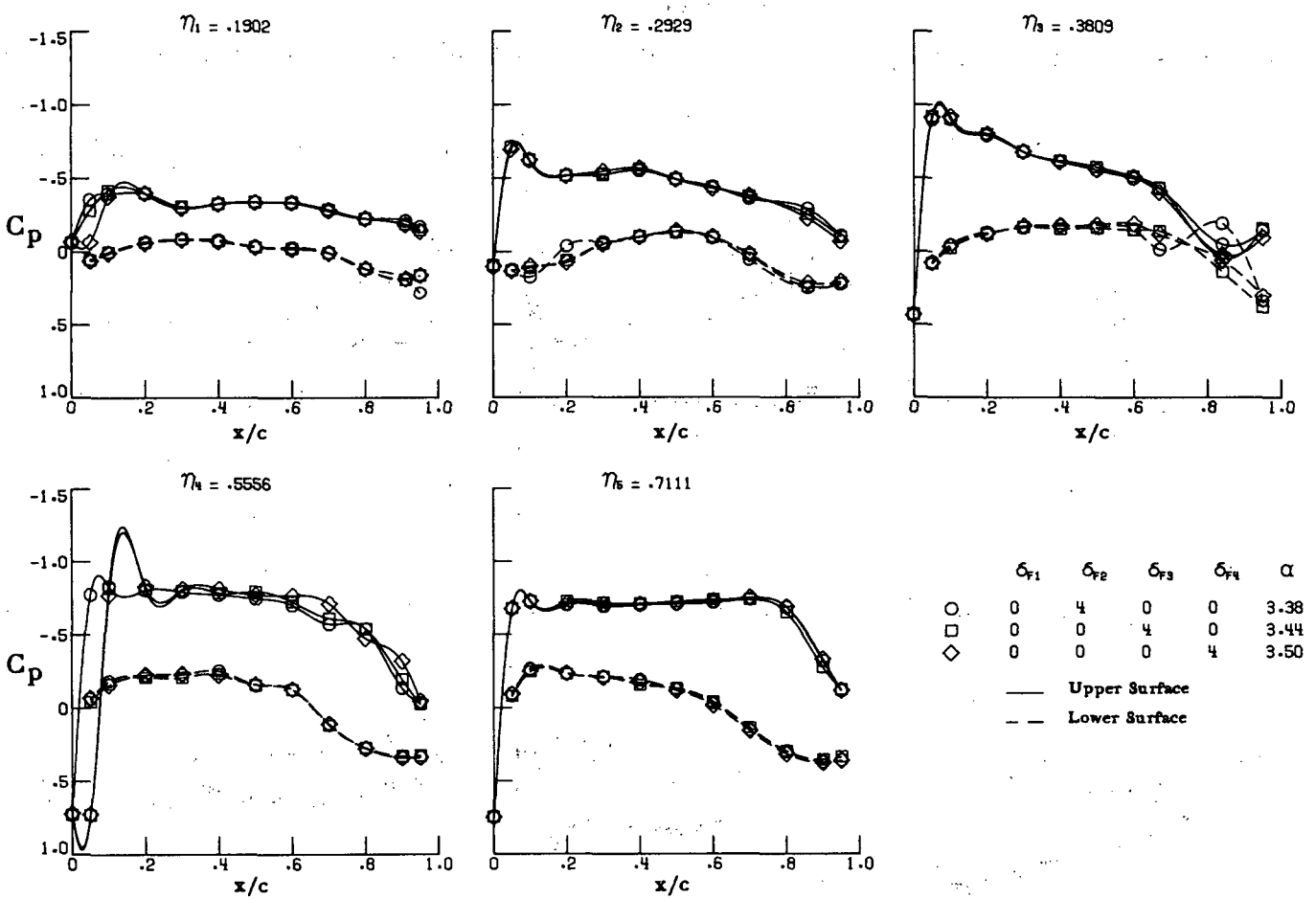
(b) Lift and pitch characteristics.

Figure 43.- Continued.



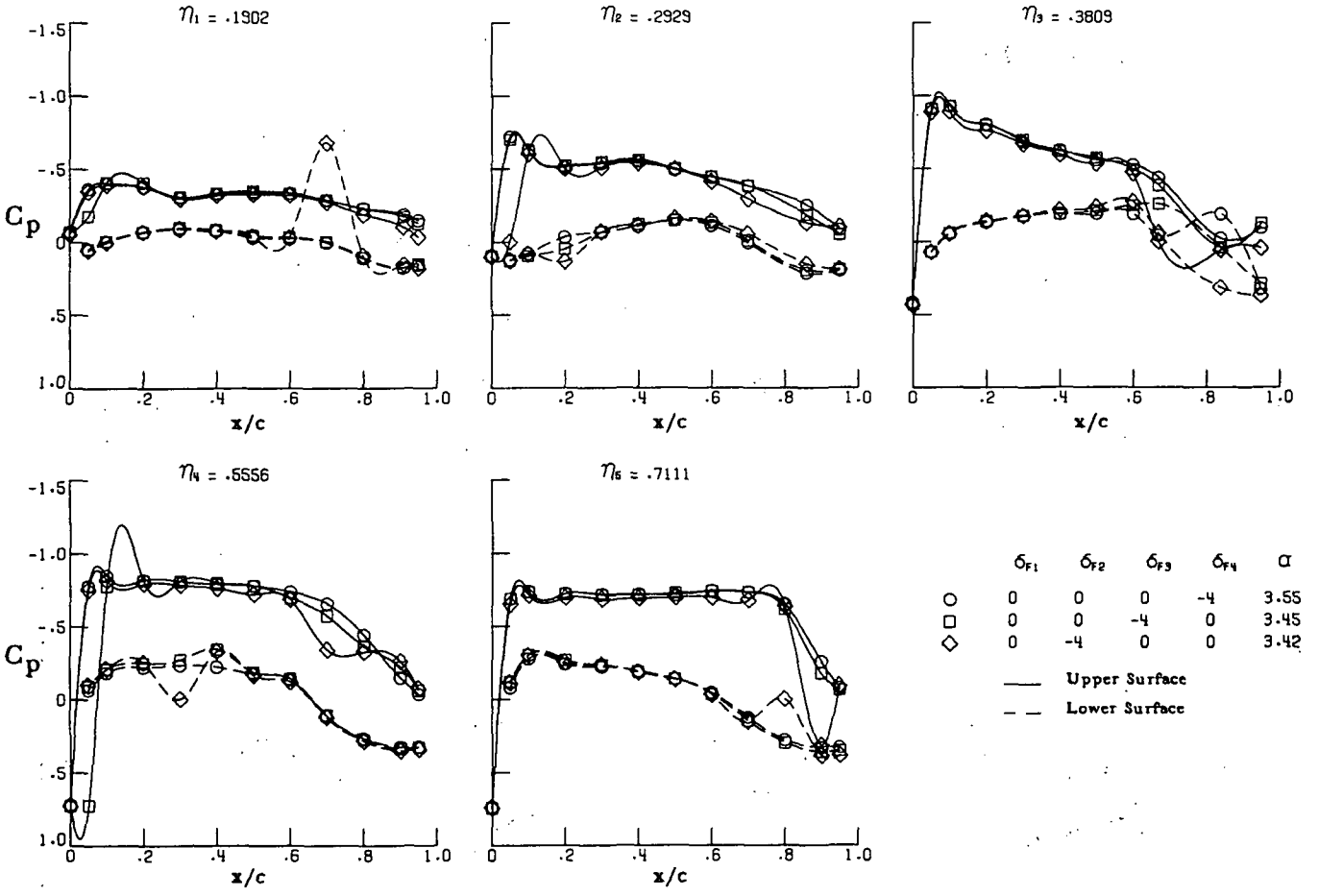
(c) Rolling-moment characteristics.

Figure 43.- Continued.



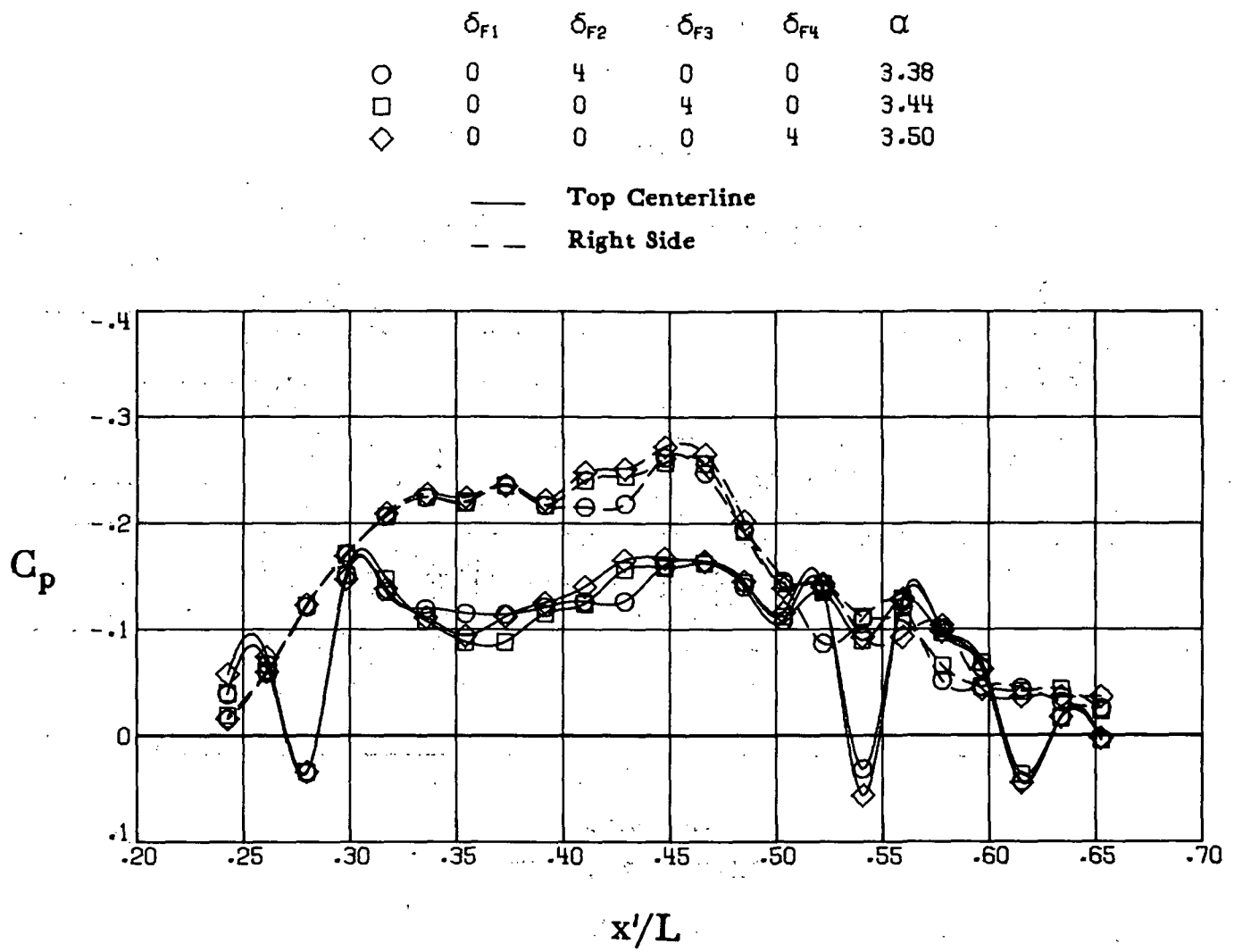
(d) Selected wing pressure distributions for control surface deflected 4^{o}.

Figure 43.- Continued.



(e) Selected wing pressure distributions for control surface deflected -4°.

Figure 43.- Continued.



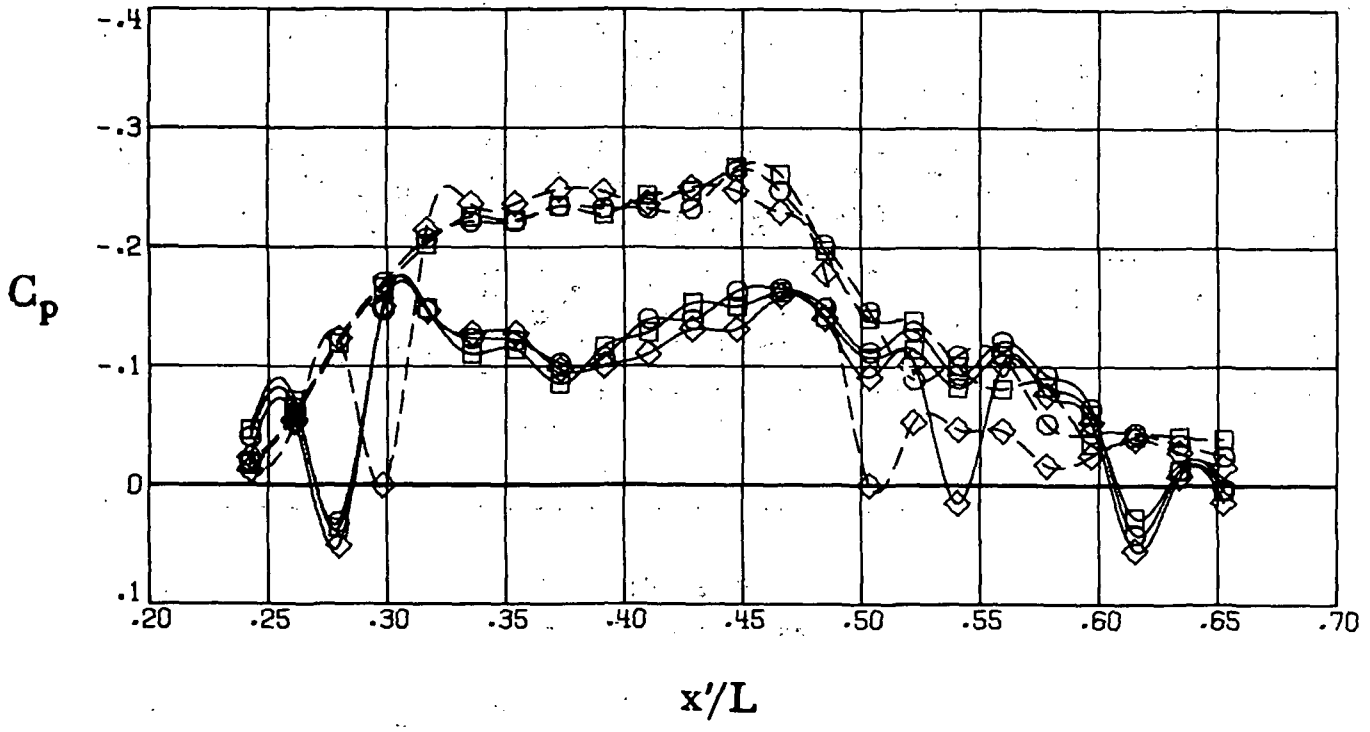
(f) Selected fuselage pressure distributions for control surface deflected 4^{o}.

Figure 43.- Continued.

	δ_{F1}	δ_{F2}	δ_{F3}	δ_{F4}	α
○	0	0	0	-4	3.55
□	0	0	-4	0	3.45
◇	0	-4	0	0	3.42

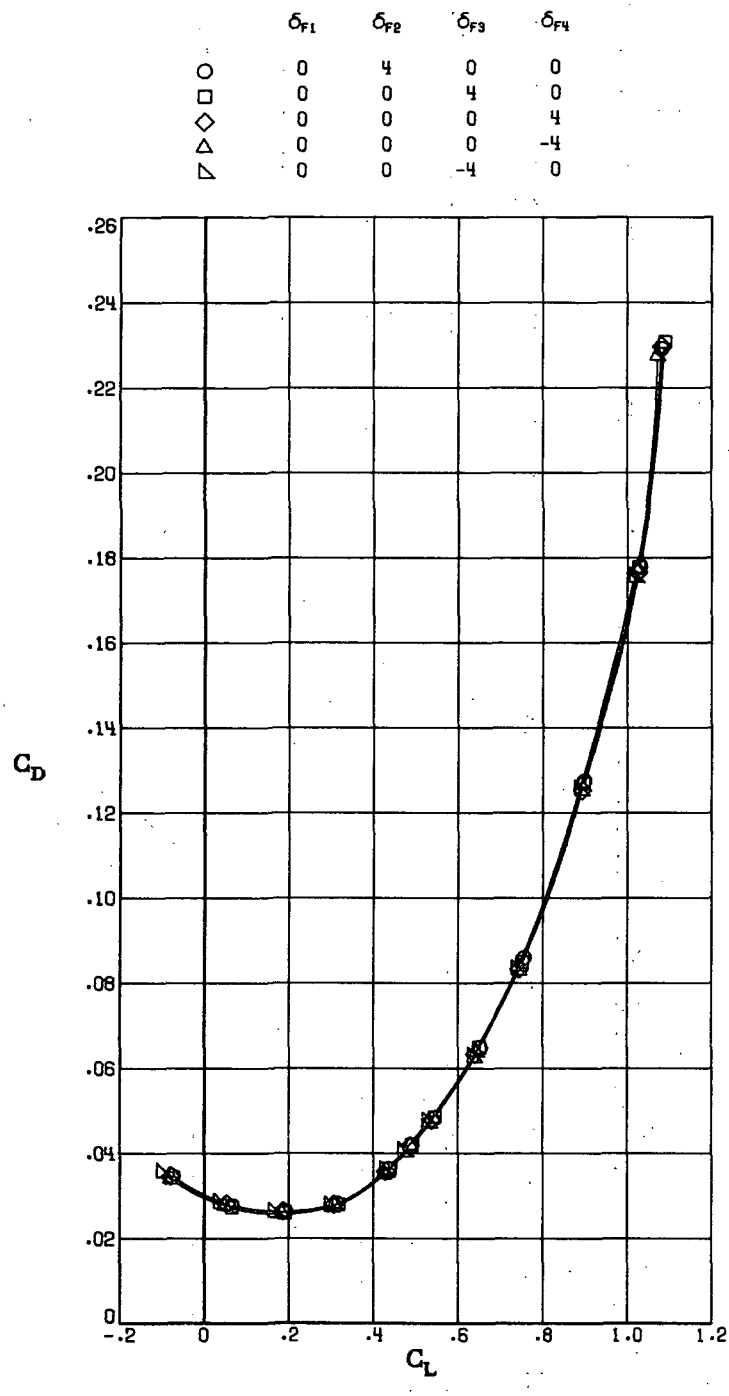
—— Top Centerline

– – Right Side



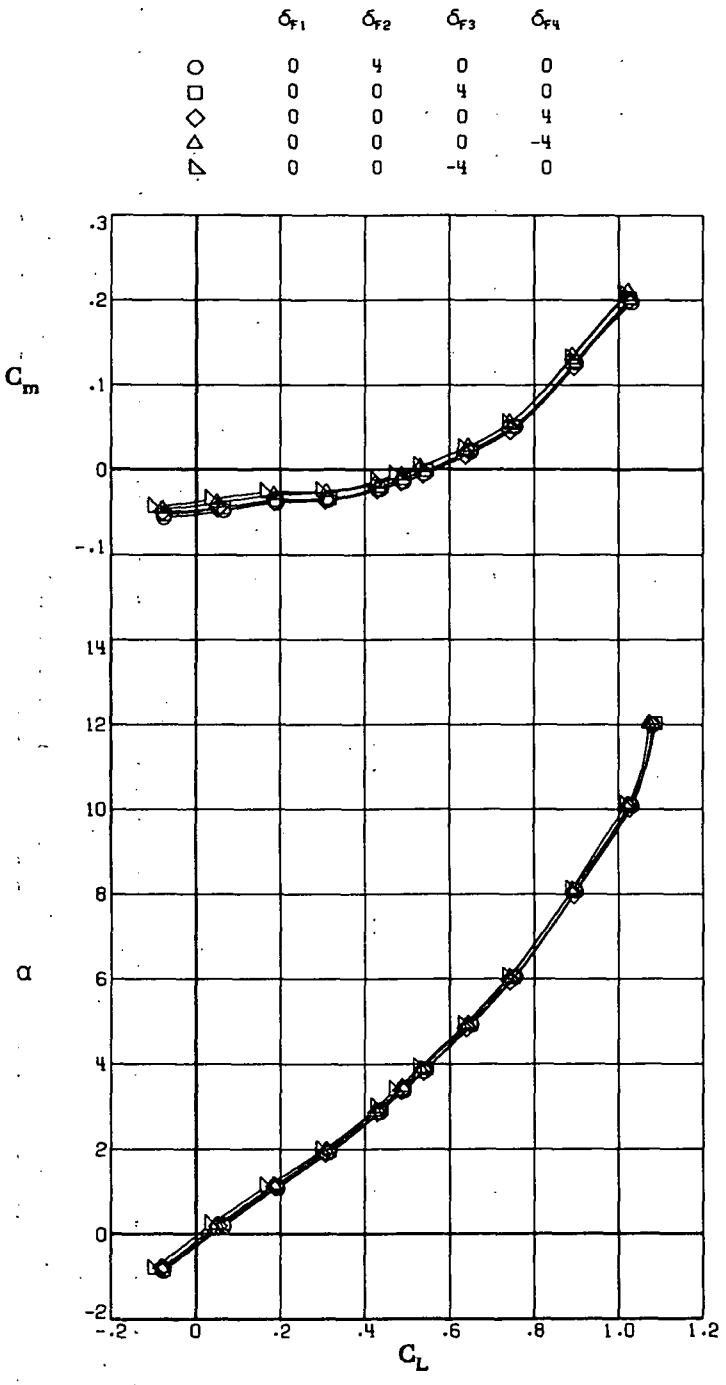
(g) Selected fuselage pressure distributions for control surface deflected -4°.

Figure 43.- Concluded.



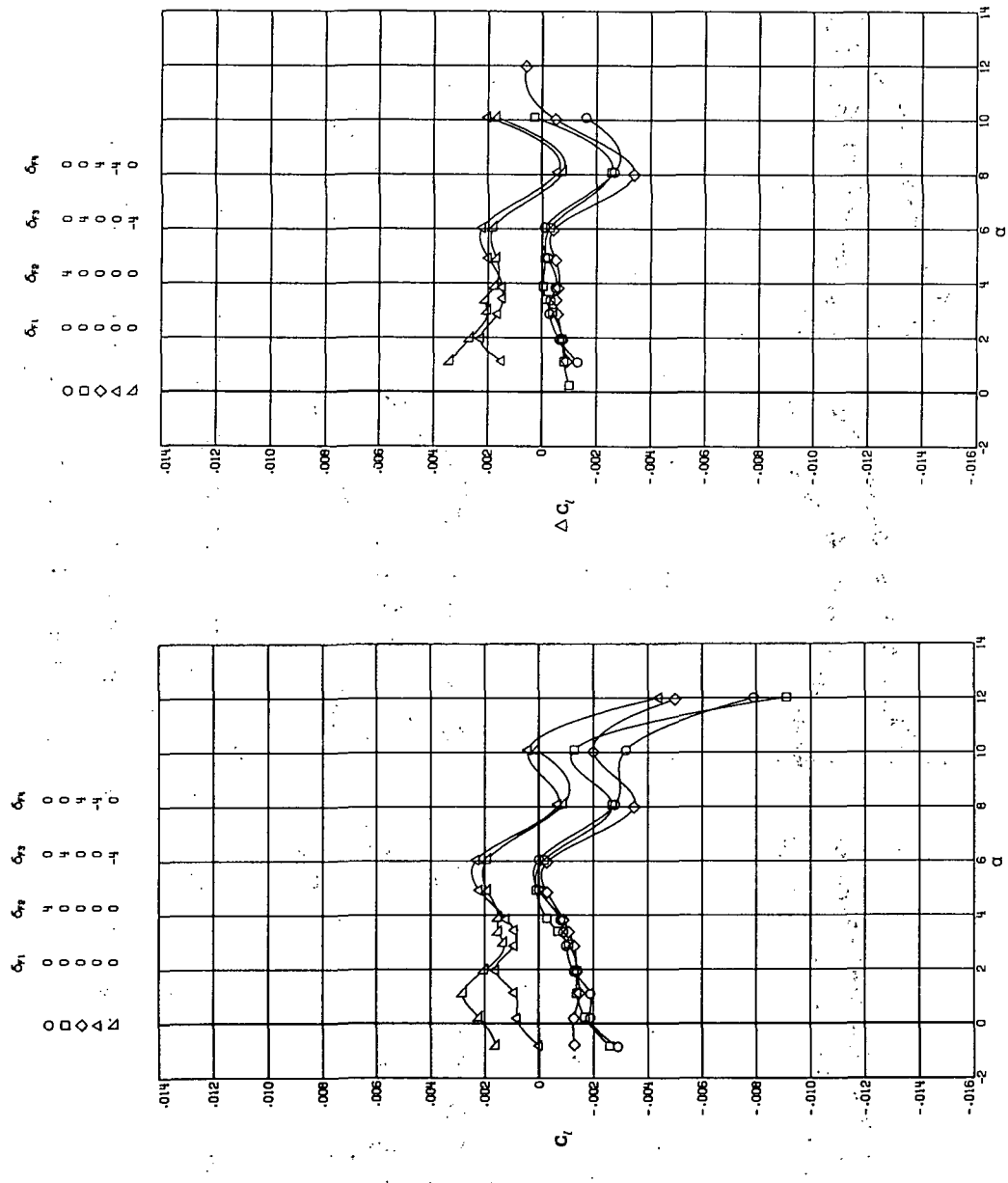
(a) Drag characteristics.

Figure 44.- Effect of spanwise location of trailing-edge control surface deflected $\pm 4^{o}$. Area-ruled fuselage. $M_{\infty} = 0.94$.



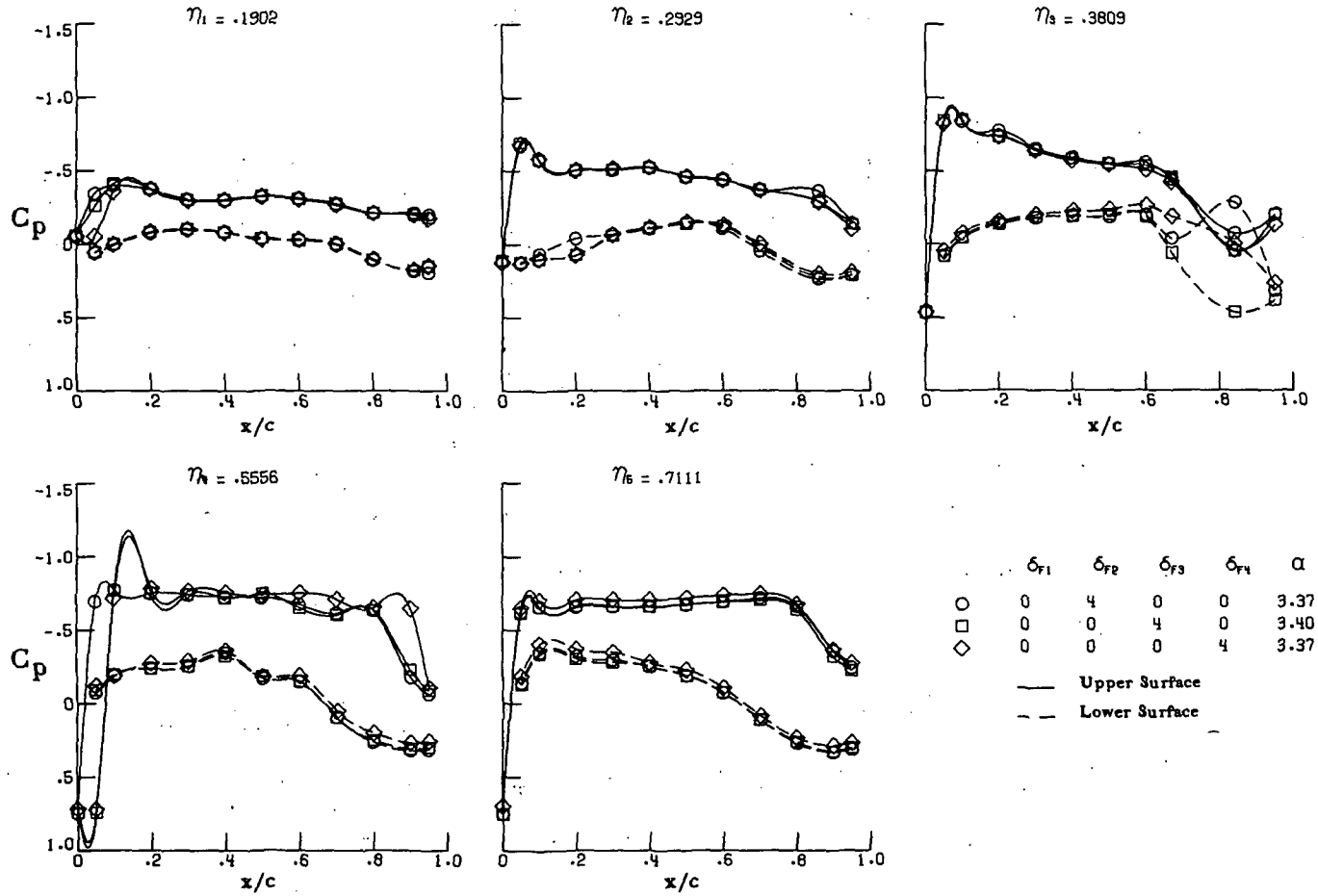
(b) Lift and pitch characteristics.

Figure 44.- Continued.



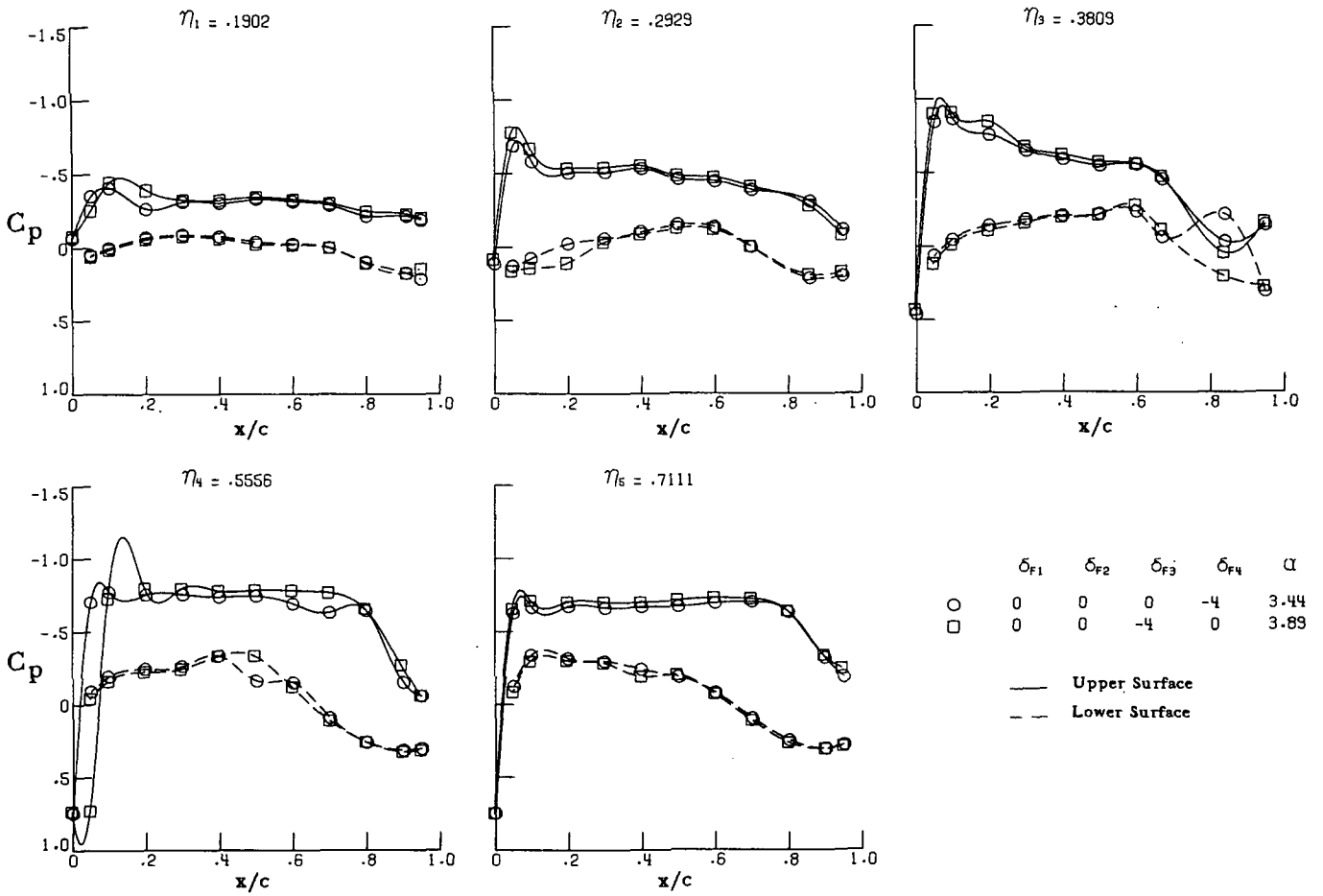
(c) Rolling-moment characteristics.

Figure 44.- Continued.



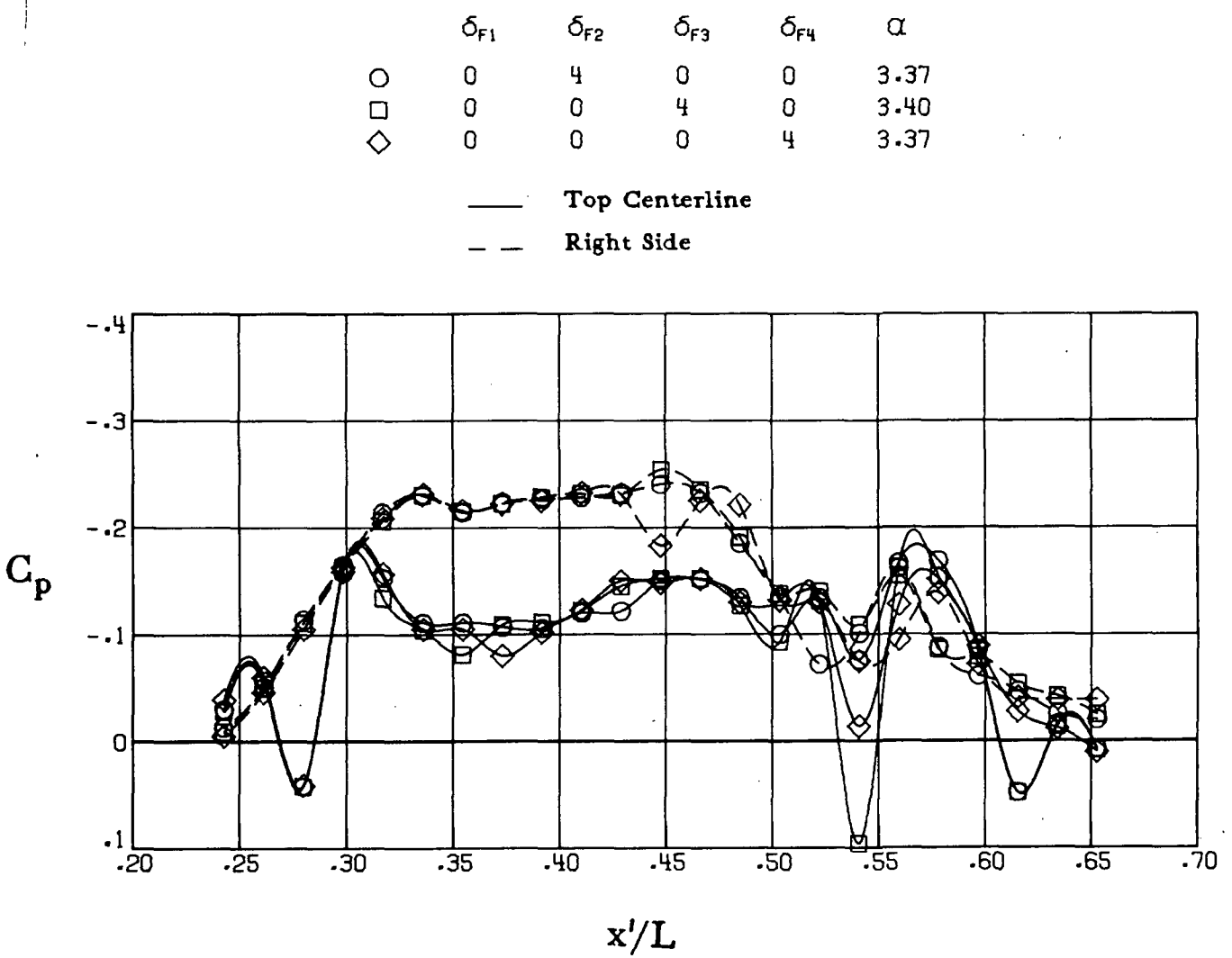
(d) Selected wing pressure distributions for control surface deflected 4^o.

Figure 44.- Continued.



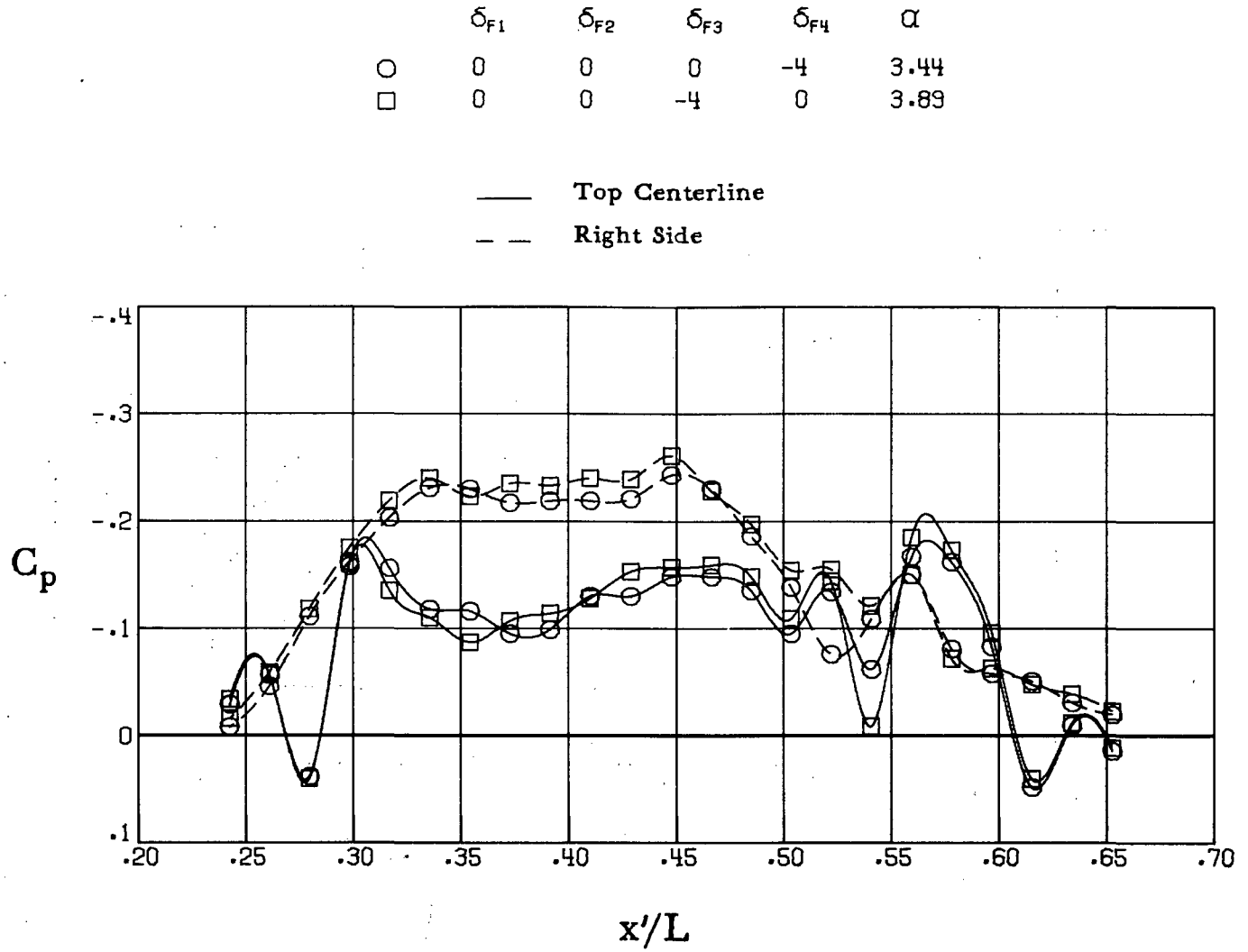
(e) Selected wing pressure distributions for control surface deflected -4^{o}.

Figure 44.- Continued.



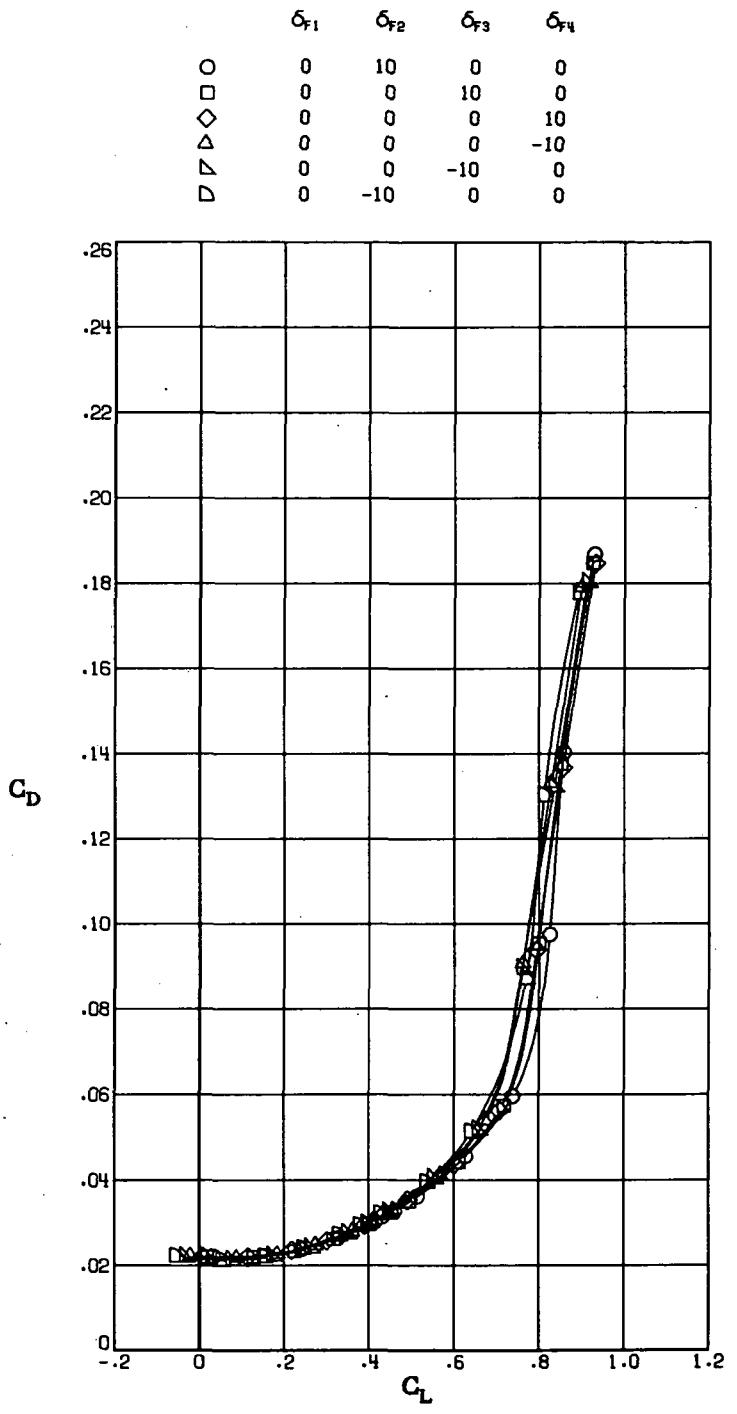
(f) Selected fuselage pressure distributions for control surface deflected 4^{o}.

Figure 44.- Continued.



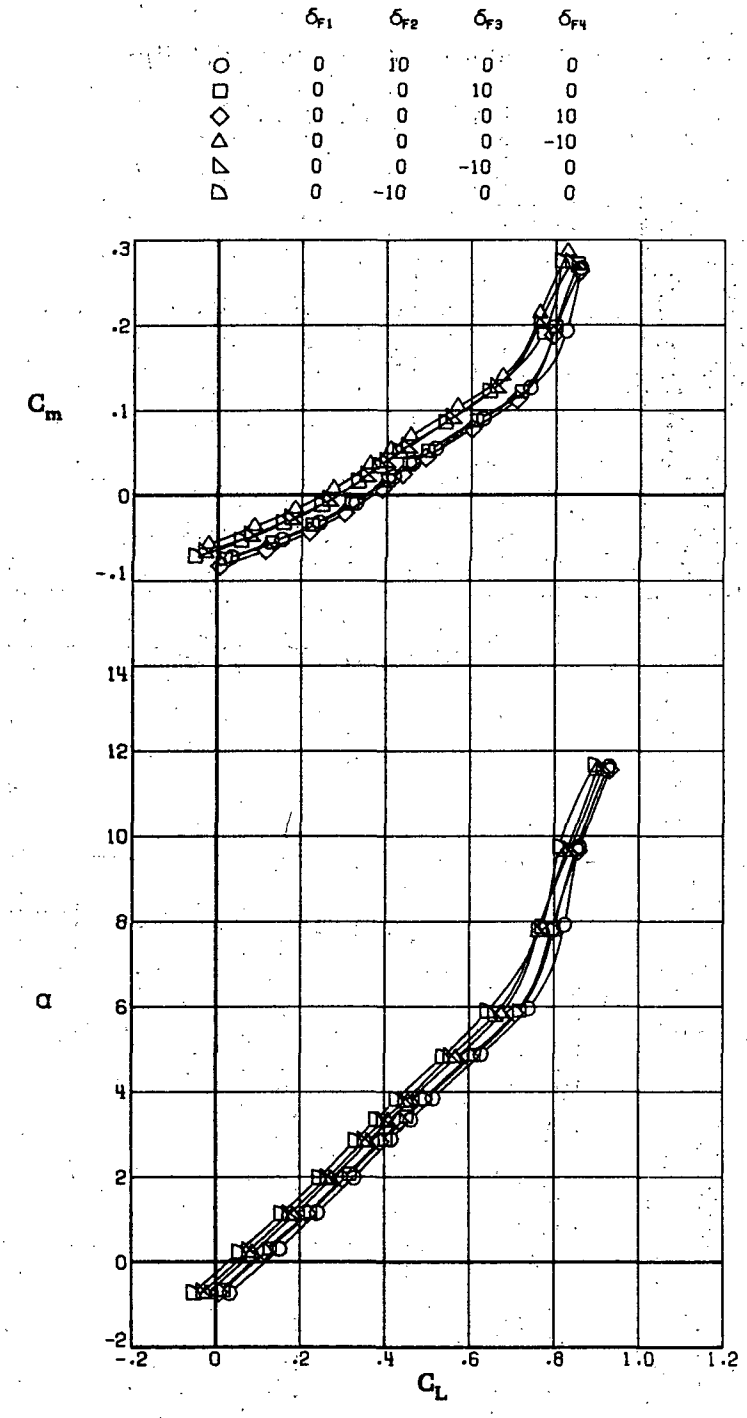
(g) Selected fuselage pressure distributions for control surface deflected -4^{o}.

Figure 44.- Concluded.



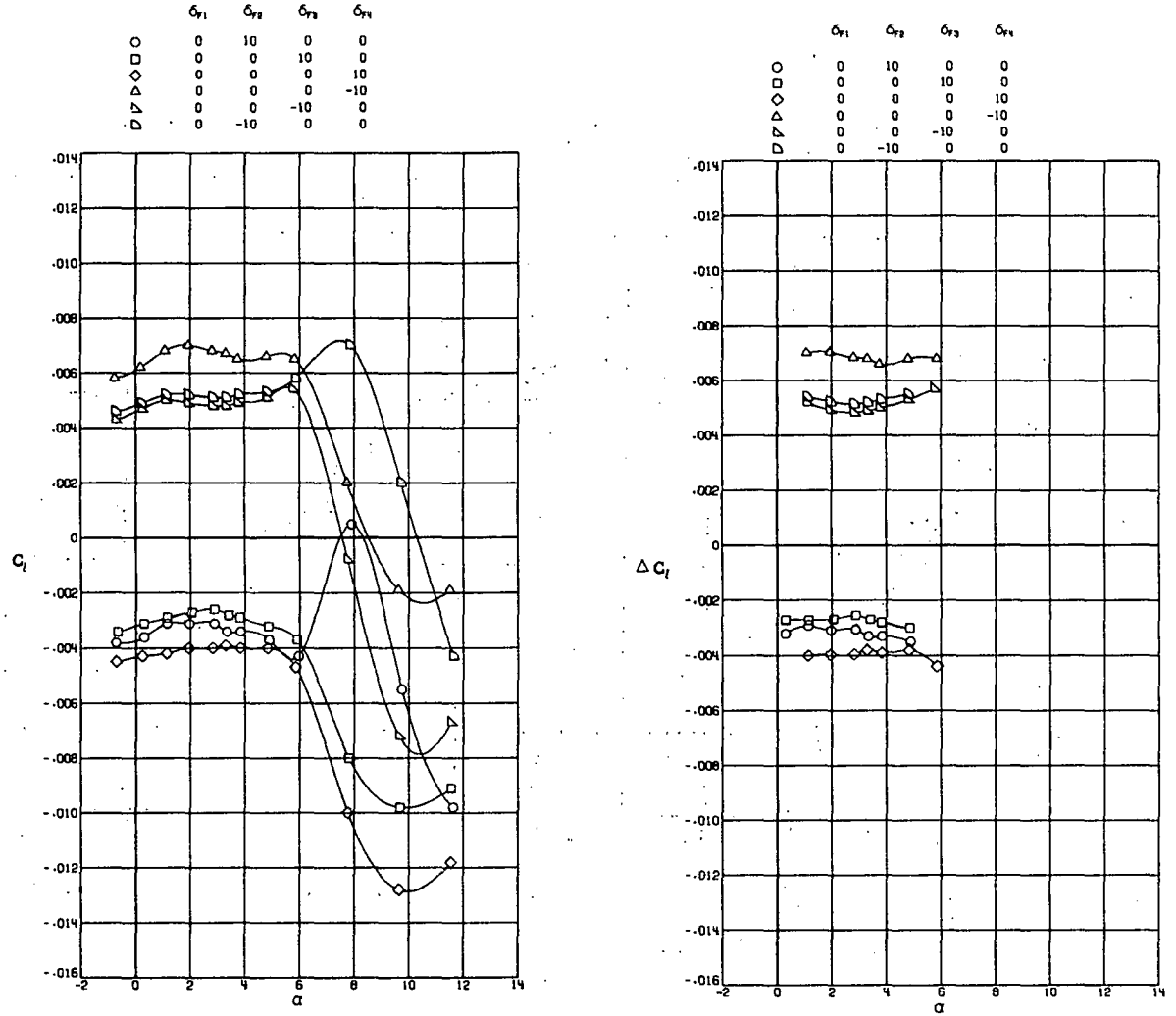
(a) Drag characteristics.

Figure 45.- Effect of spanwise location of trailing-edge control surface deflected $\pm 10^{o}$. Area-ruled fuselage. $M_{\infty} = 0.80$.



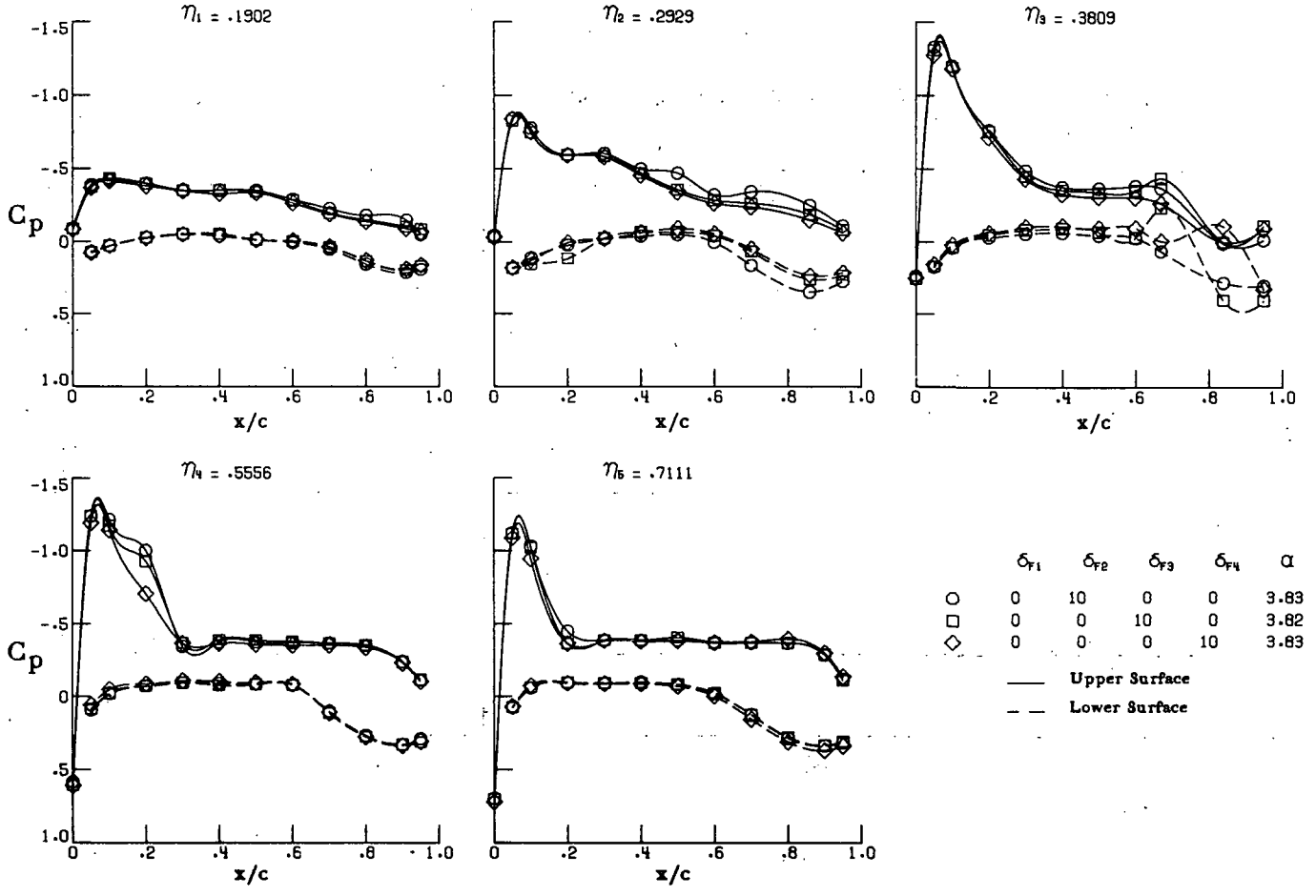
(b) Lift and pitch characteristics.

Figure 45.- Continued.



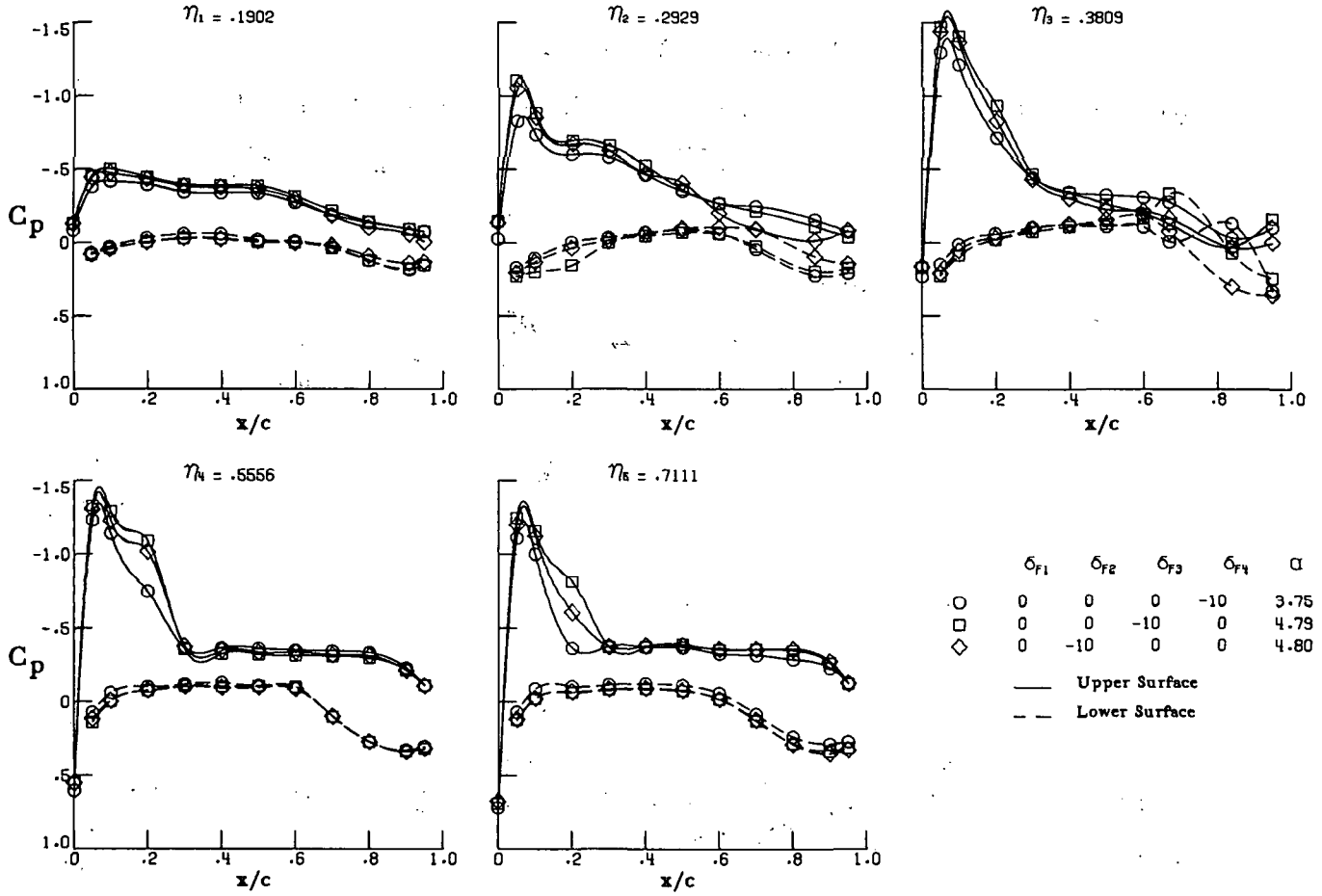
(c) Rolling-moment characteristics.

Figure 45.- Continued.



(d) Selected wing pressure distributions for control surface deflected 10^{o}.

Figure 45.- Continued.



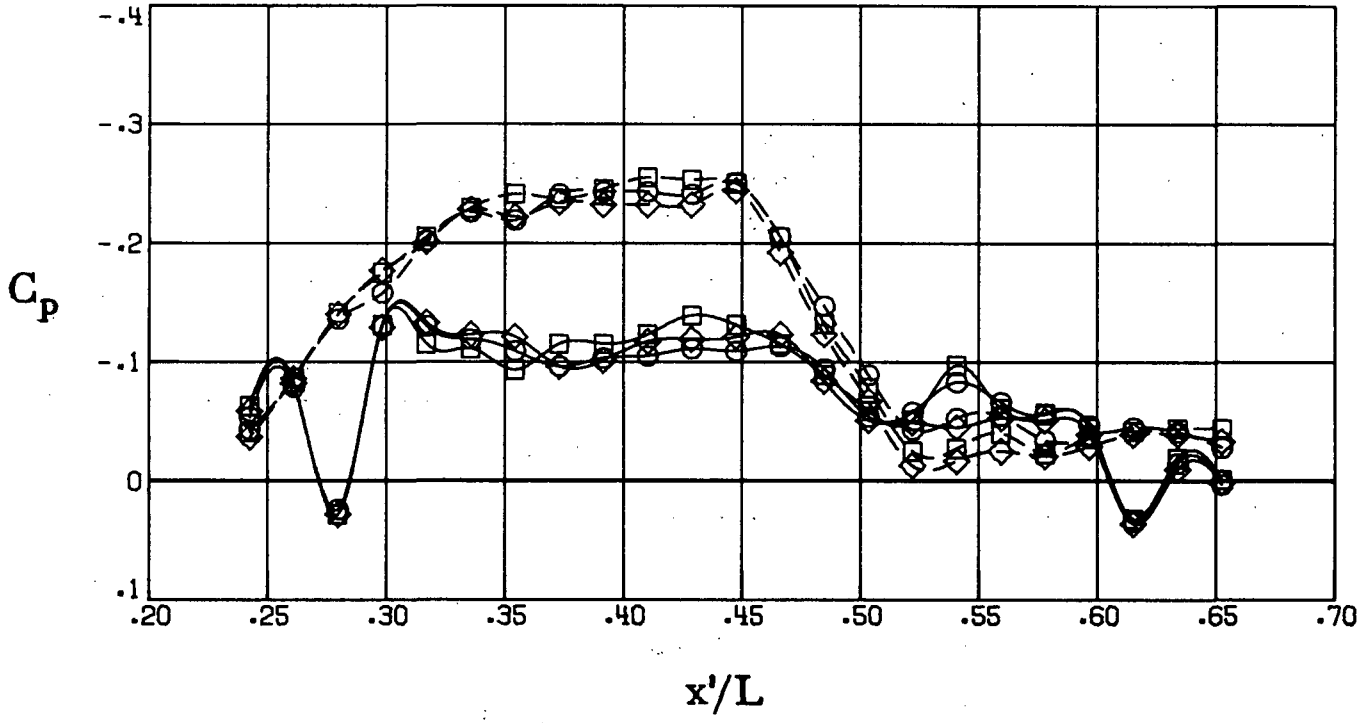
(e) Selected wing pressure distributions for control surface deflected -10°.

Figure 45.- Continued.

	δ_{F1}	δ_{F2}	δ_{F3}	δ_{F4}	α
○	0	10	0	0	3.83
□	0	0	10	0	3.82
◇	0	0	0	10	3.83

—— Top Centerline

– – Right Side



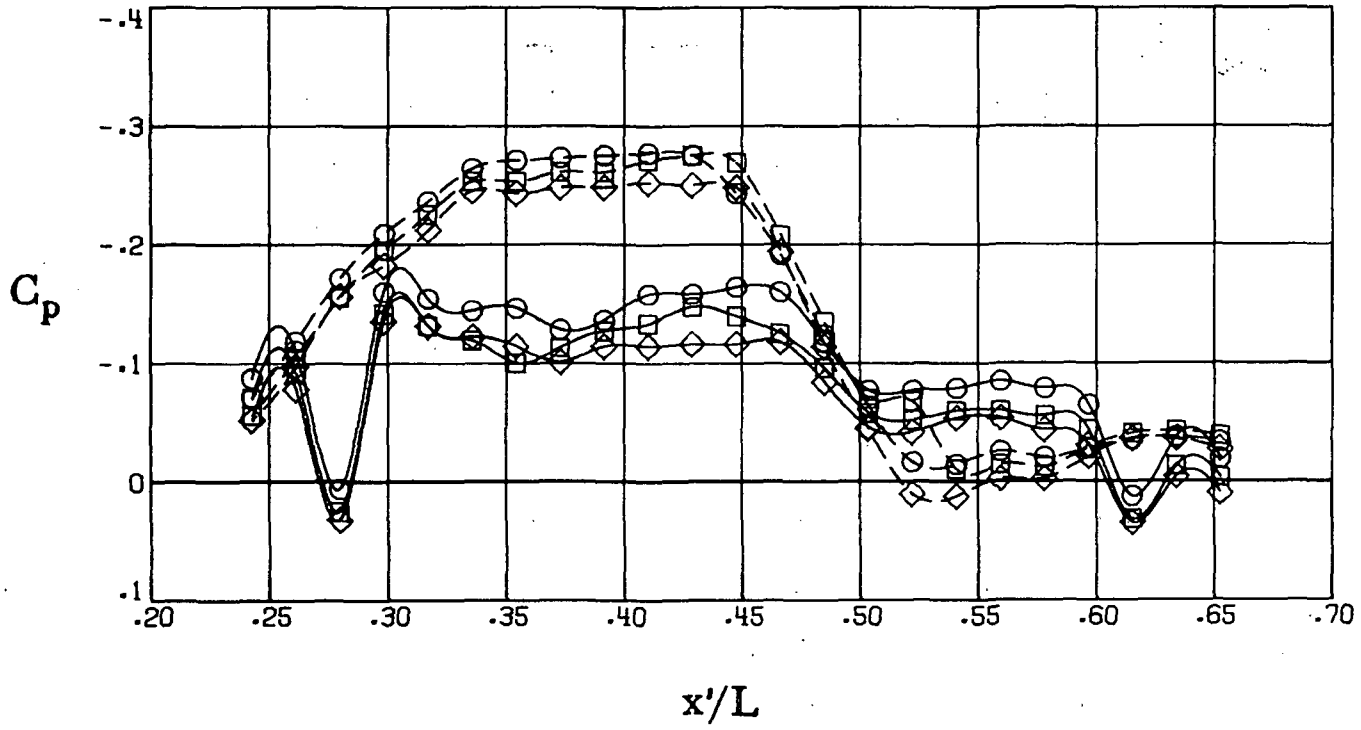
(f) Selected fuselage pressure distributions for control surface deflected 10^{o}.

Figure 45.- Continued.

	δ_{F1}	δ_{F2}	δ_{F3}	δ_{F4}	α
○	0	0	0	-10	3.75
□	0	0	-10	0	4.79
◇	0	-10	0	0	4.80

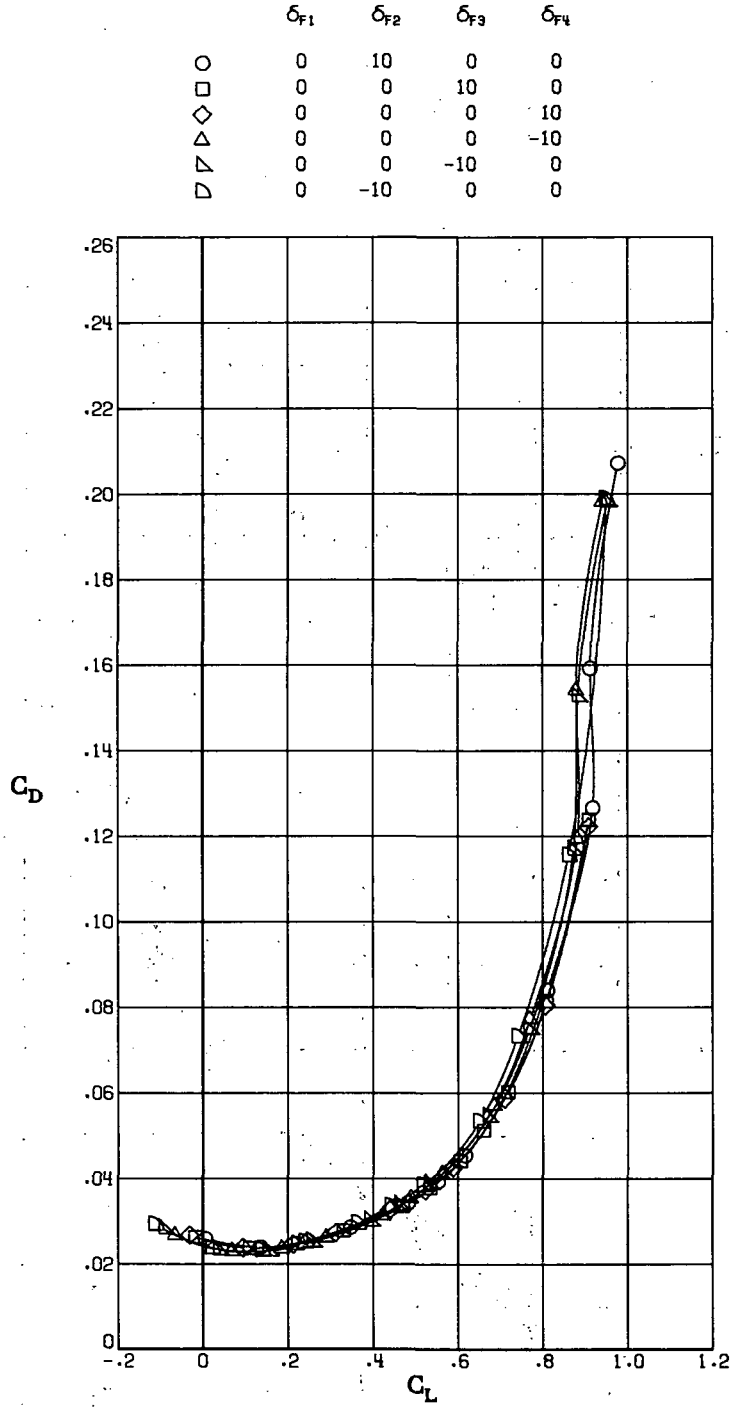
—— Top Centerline

– – Right Side



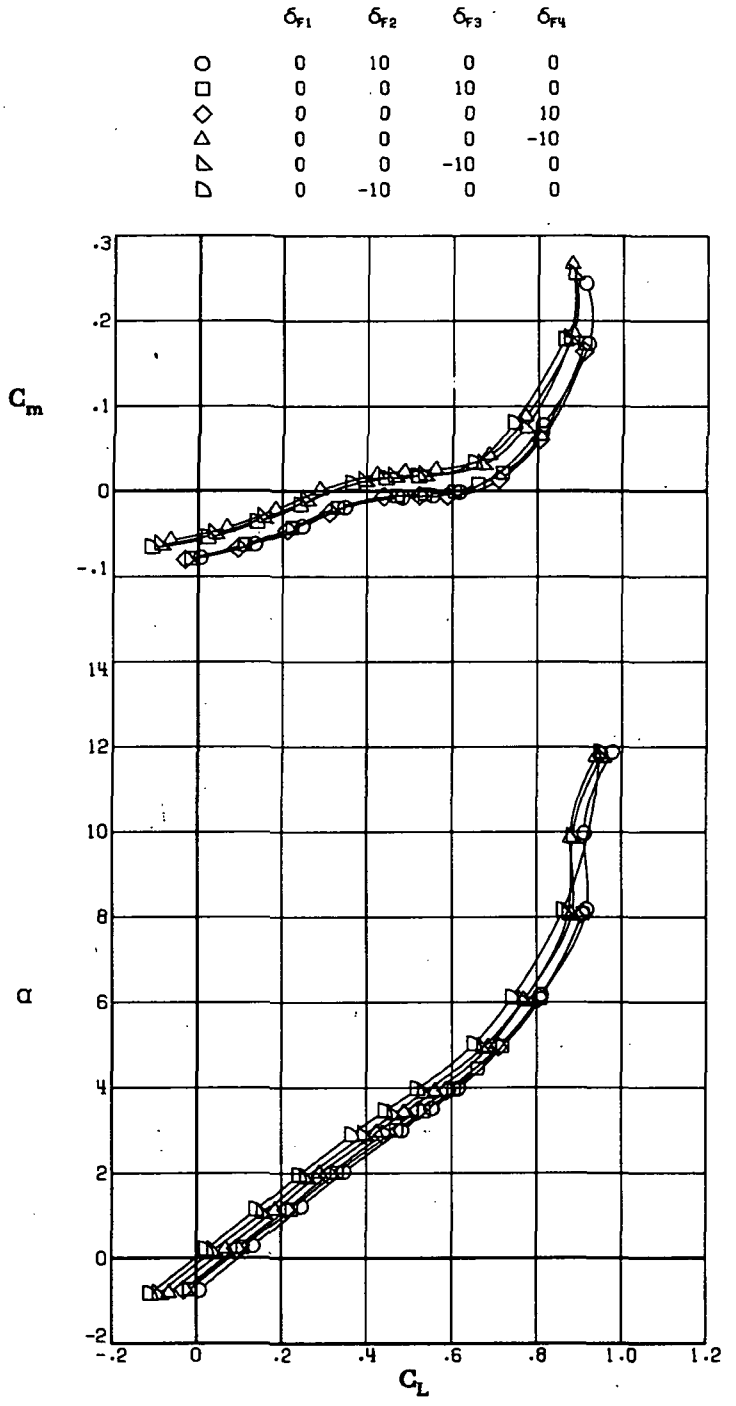
(g) Selected fuselage pressure distributions for control surface deflected -10°.

Figure 45.- Concluded.



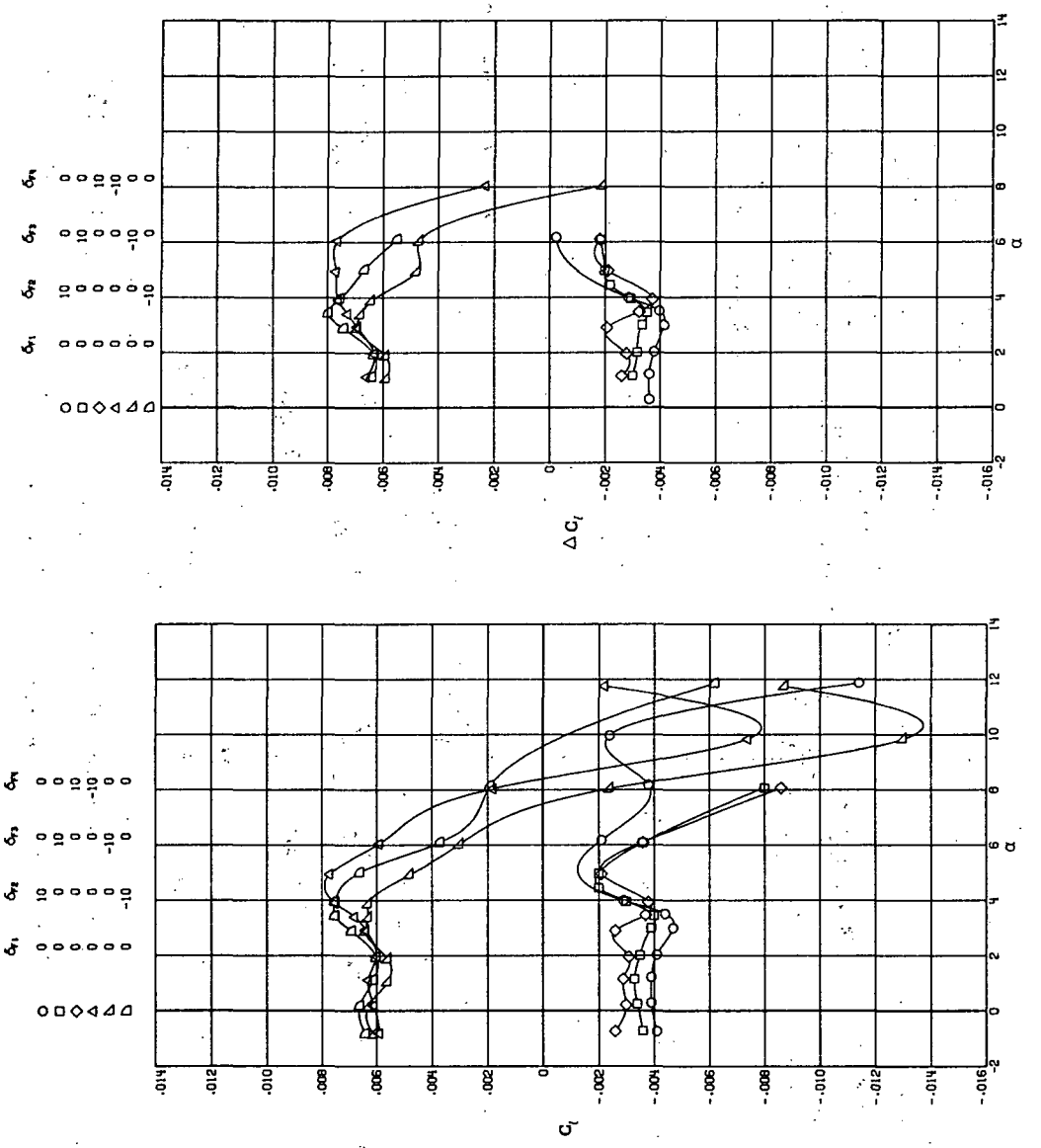
(a) Drag characteristics.

Figure 46.- Effect of spanwise location of trailing-edge control surface deflected $\pm 10^{\circ}$. Area-ruled fuselage. $M_{\infty} = 0.90$.



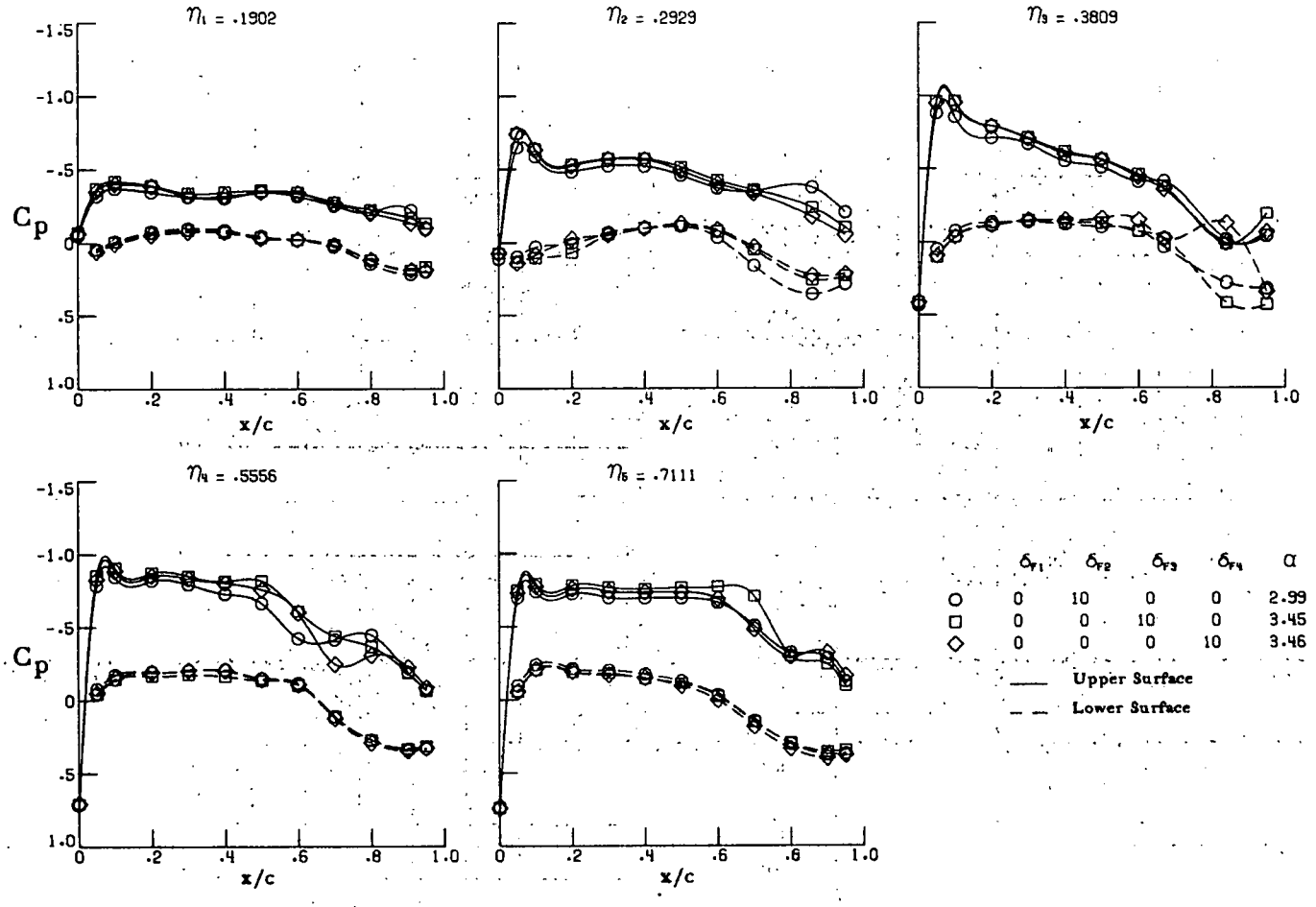
(b) Lift and pitch characteristics.

Figure 46.- Continued.



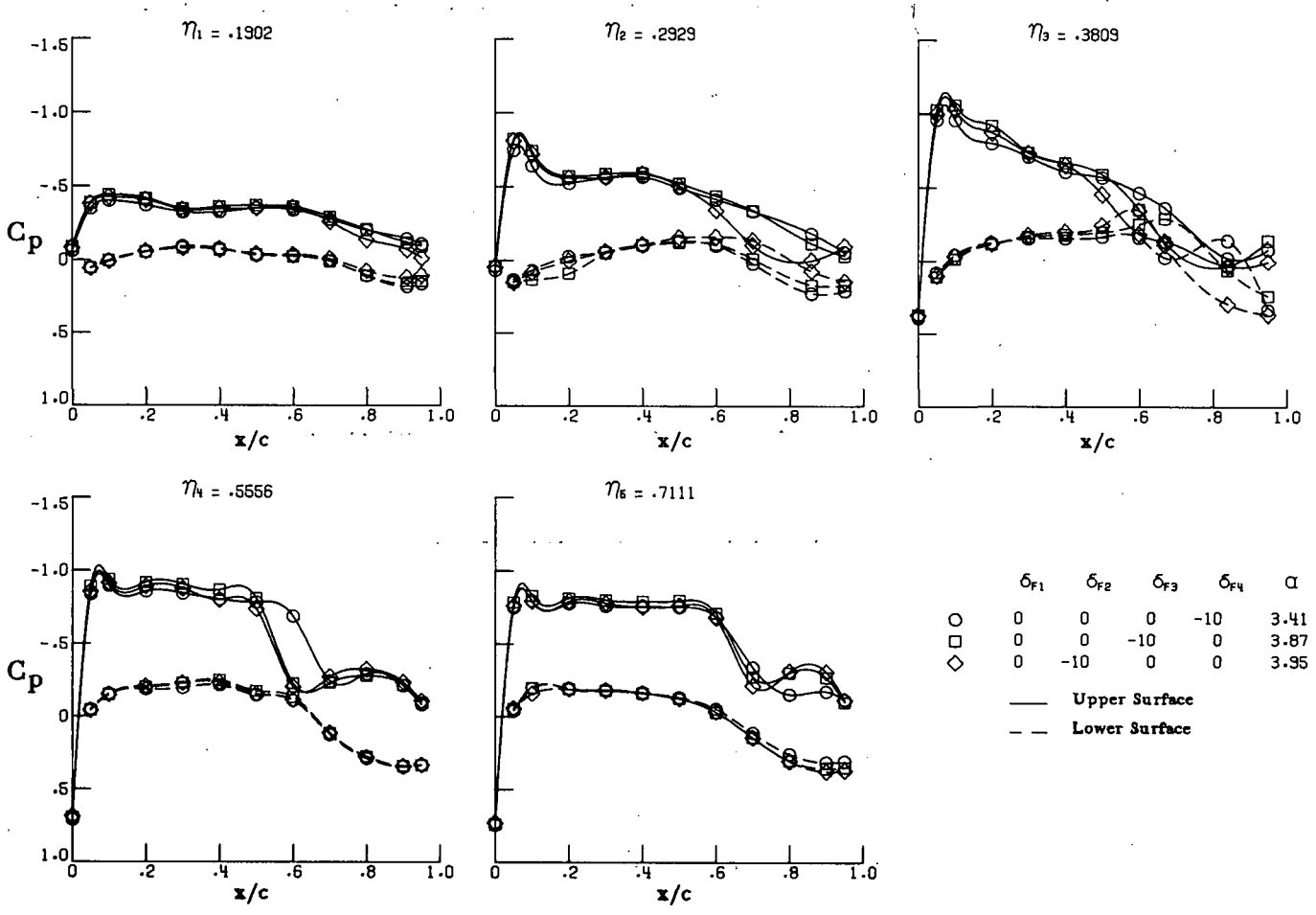
(c) Rolling-moment characteristics.

Figure 46.- Continued.



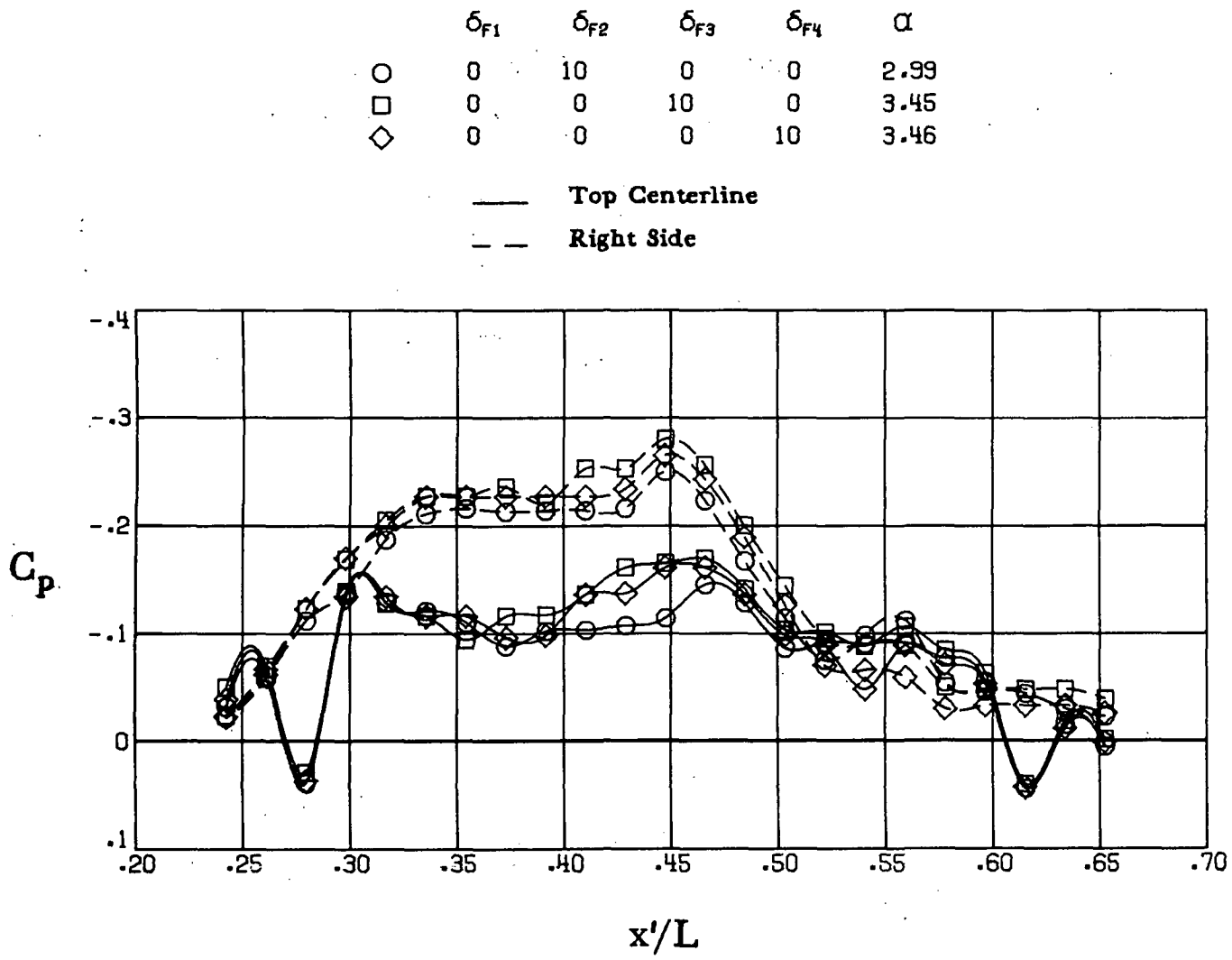
(d) Selected wing pressure distributions for control surface deflected 10^{o}.

Figure 46.- Continued.



(e) Selected wing pressure distributions for control surface deflected -10°.

Figure 46.- Continued.



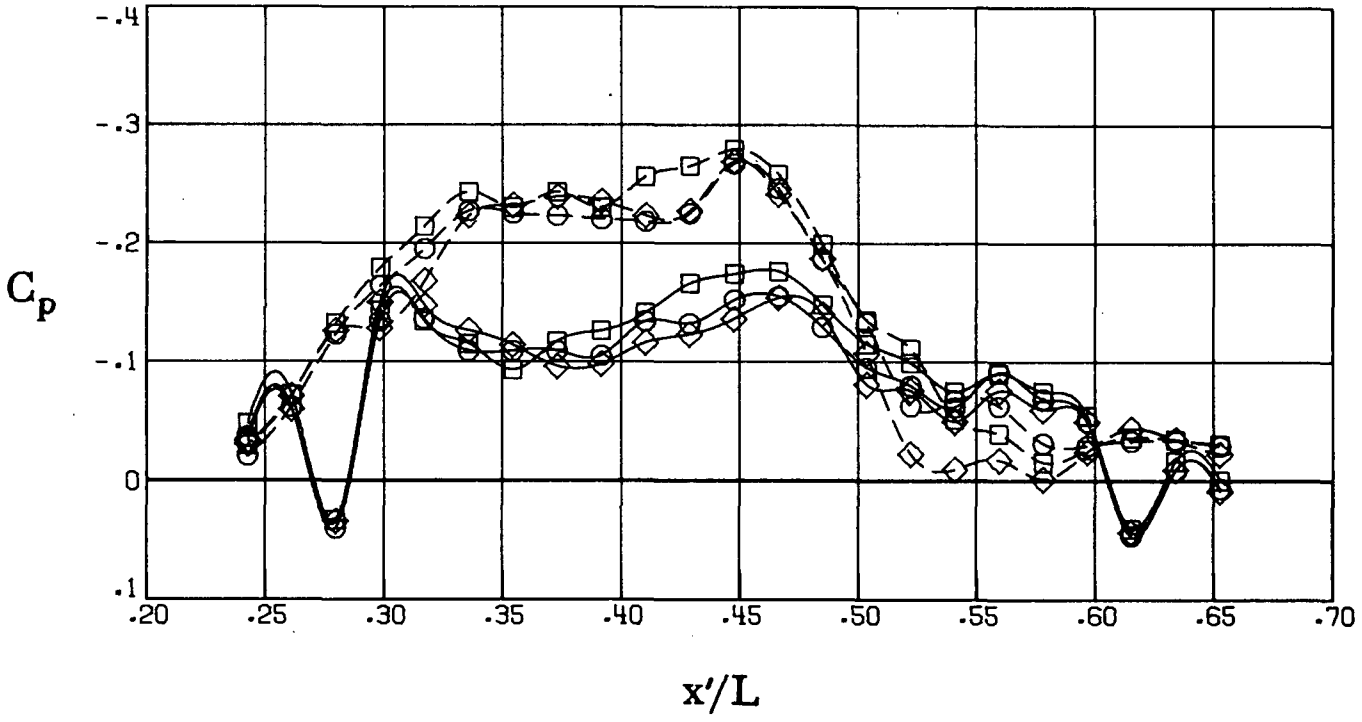
(f) Selected fuselage pressure distributions for control surface deflected 10^{o}.

Figure 46.- Continued.

	δ_{F1}	δ_{F2}	δ_{F3}	δ_{F4}	α
○	0	0	0	-10	3.41
□	0	0	-10	0	3.87
◇	0	-10	0	0	3.95

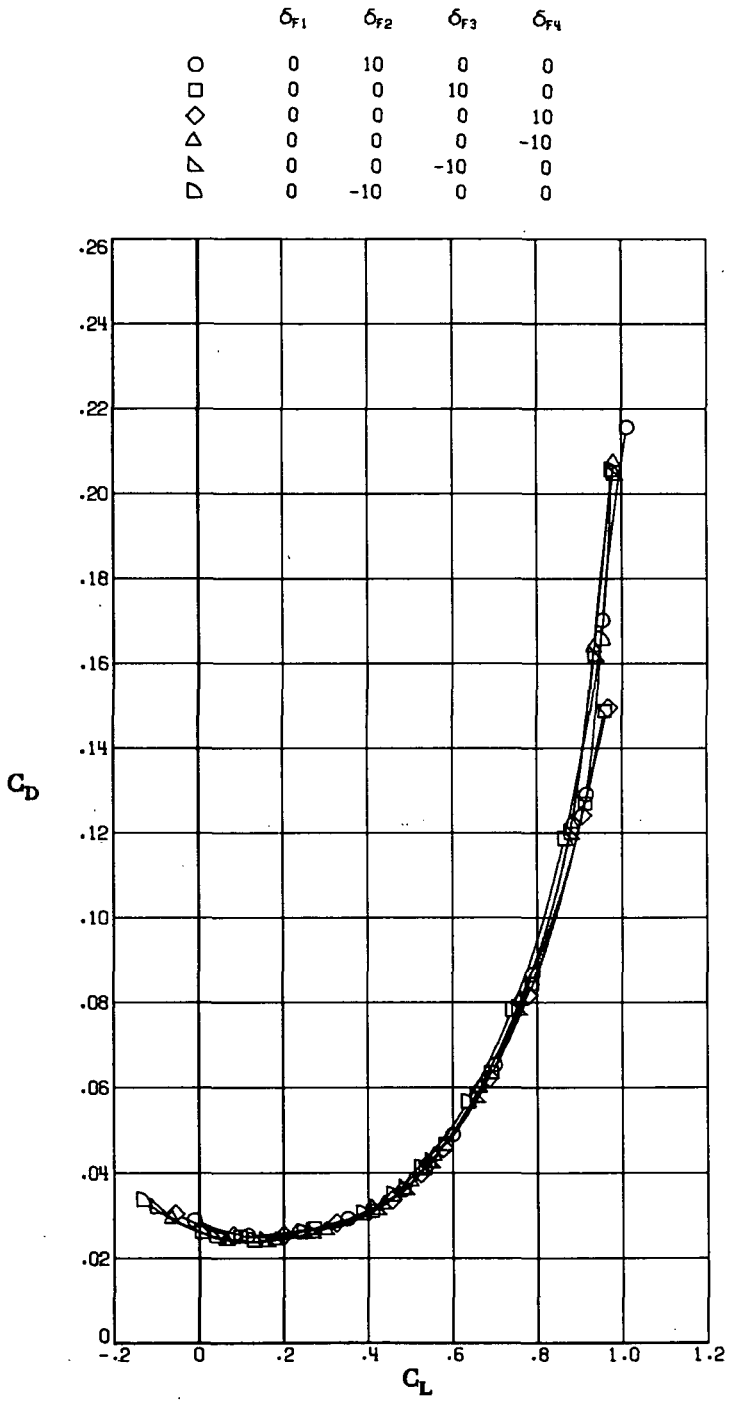
—— Top Centerline

– – Right Side



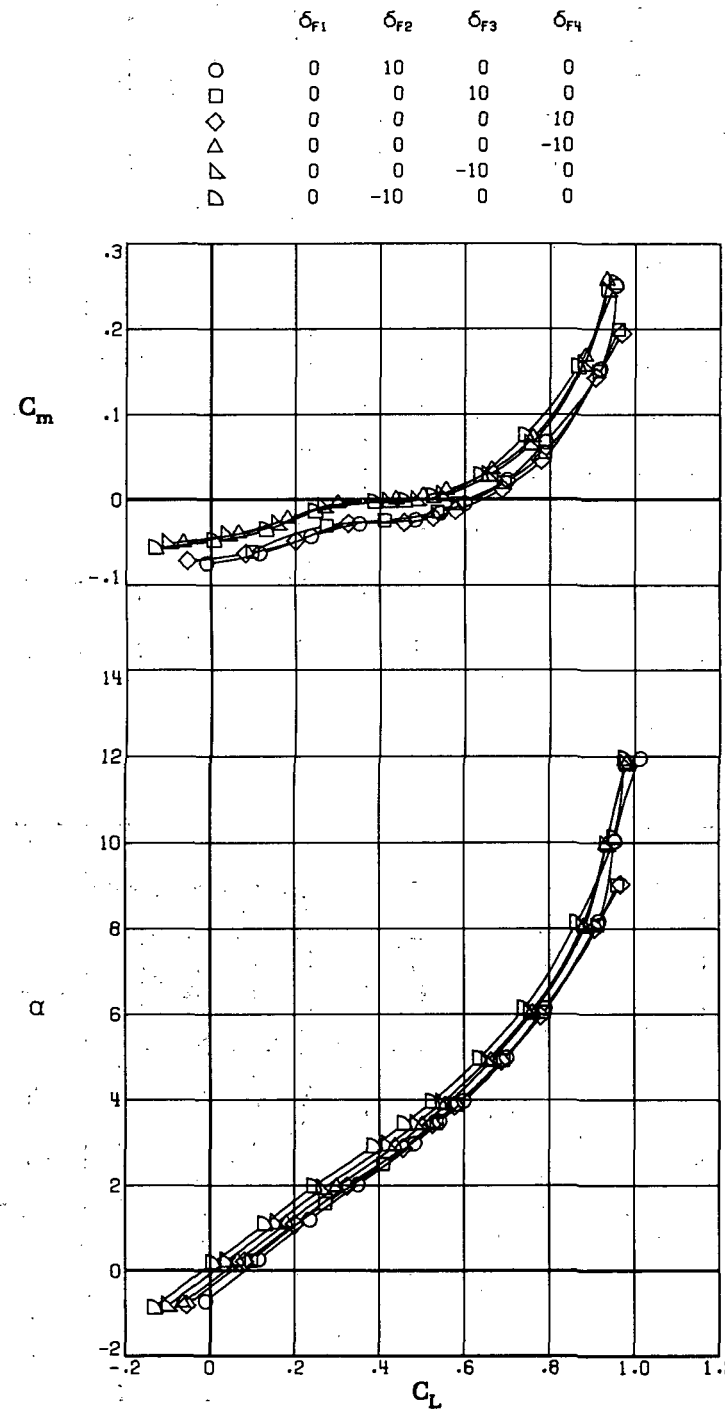
(g) Selected fuselage pressure distributions for control surface deflected -10°.

Figure 46.- Concluded.



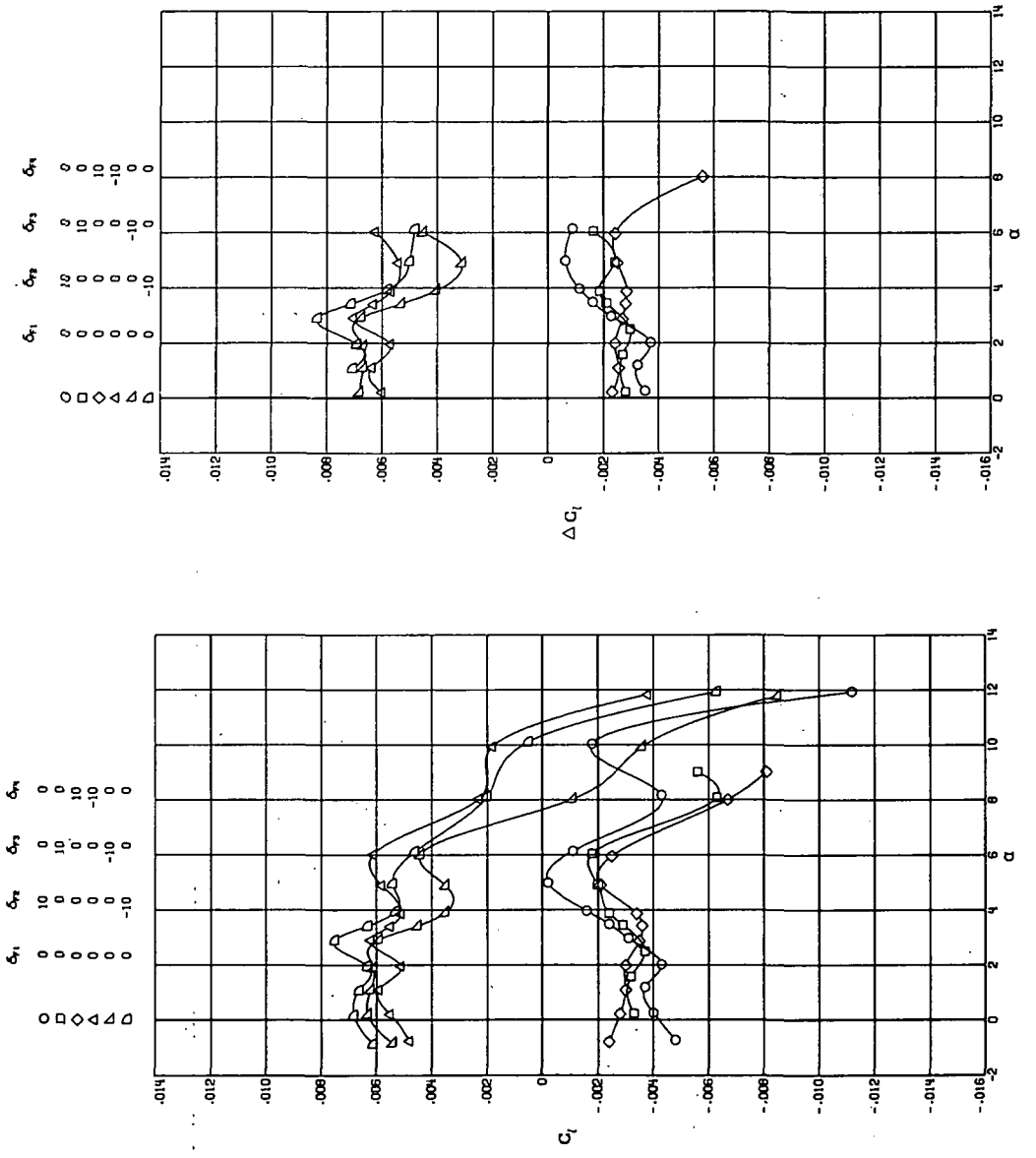
(a) Drag characteristics.

Figure 47.- Effect of spanwise location of trailing-edge control surface deflected $\pm 10^{o}$. Area-ruled fuselage. $M_{\infty} = 0.92$.



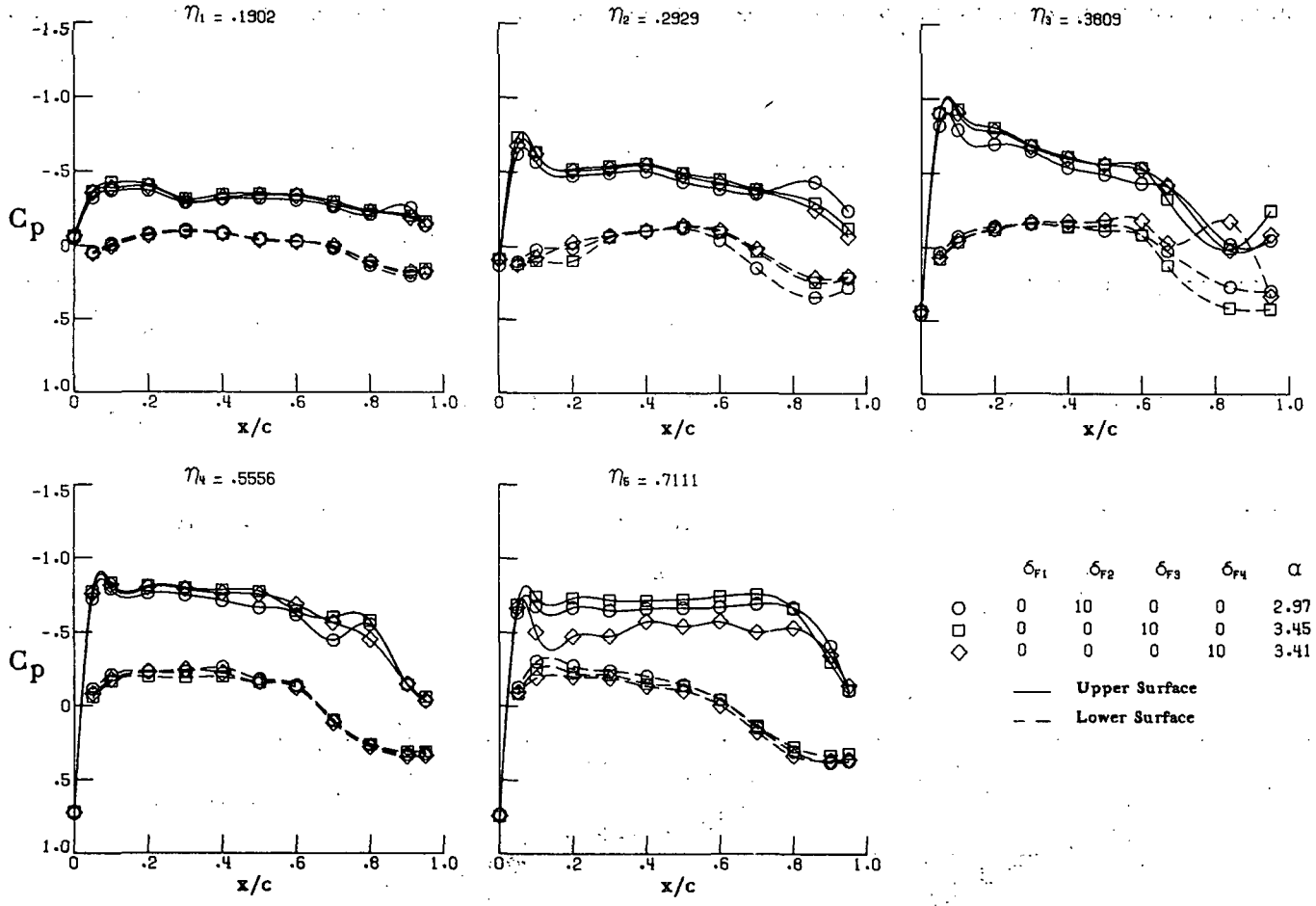
(b) Lift and pitch characteristics.

Figure 47.- Continued.



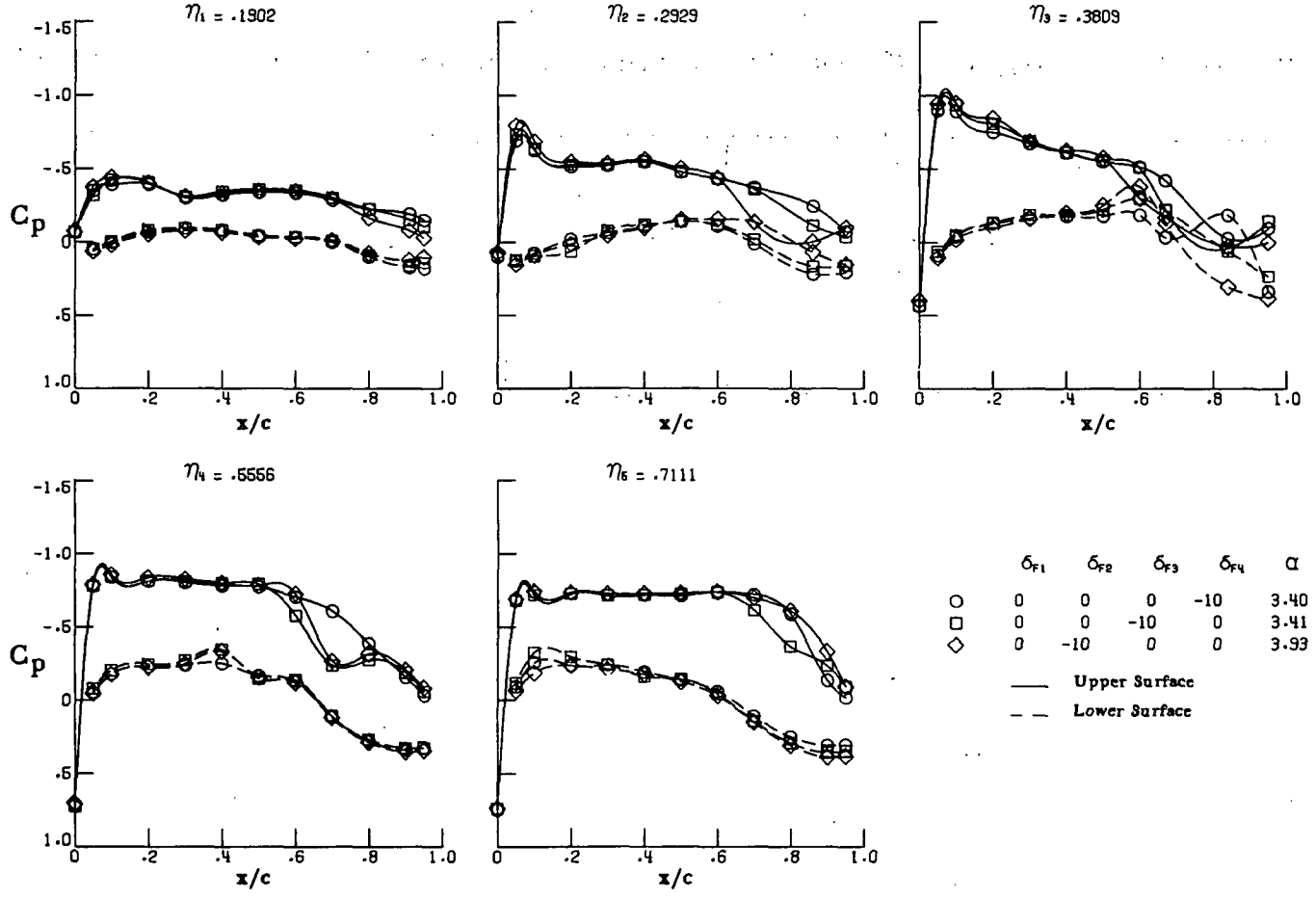
(c) Rolling-moment characteristics.

Figure 47.- Continued.



(d) Selected wing pressure distributions for control surface deflected 10^{o}.

Figure 47.- Continued.



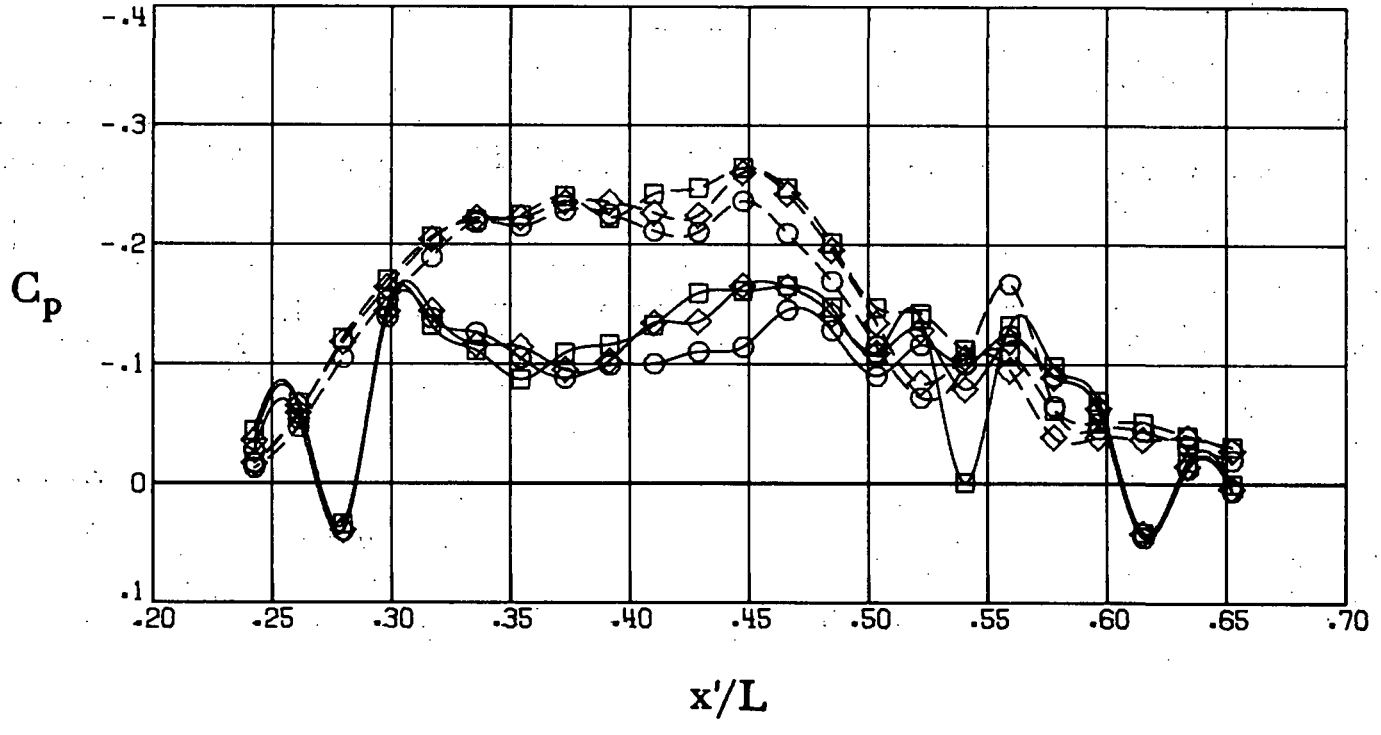
(e) Selected wing pressure distributions for control surface deflected -10°.

Figure 47.- Continued.

	δ_{F1}	δ_{F2}	δ_{F3}	δ_{F4}	α
○	0	10	0	0	2.97
□	0	0	10	0	3.45
◇	0	0	0	10	3.41

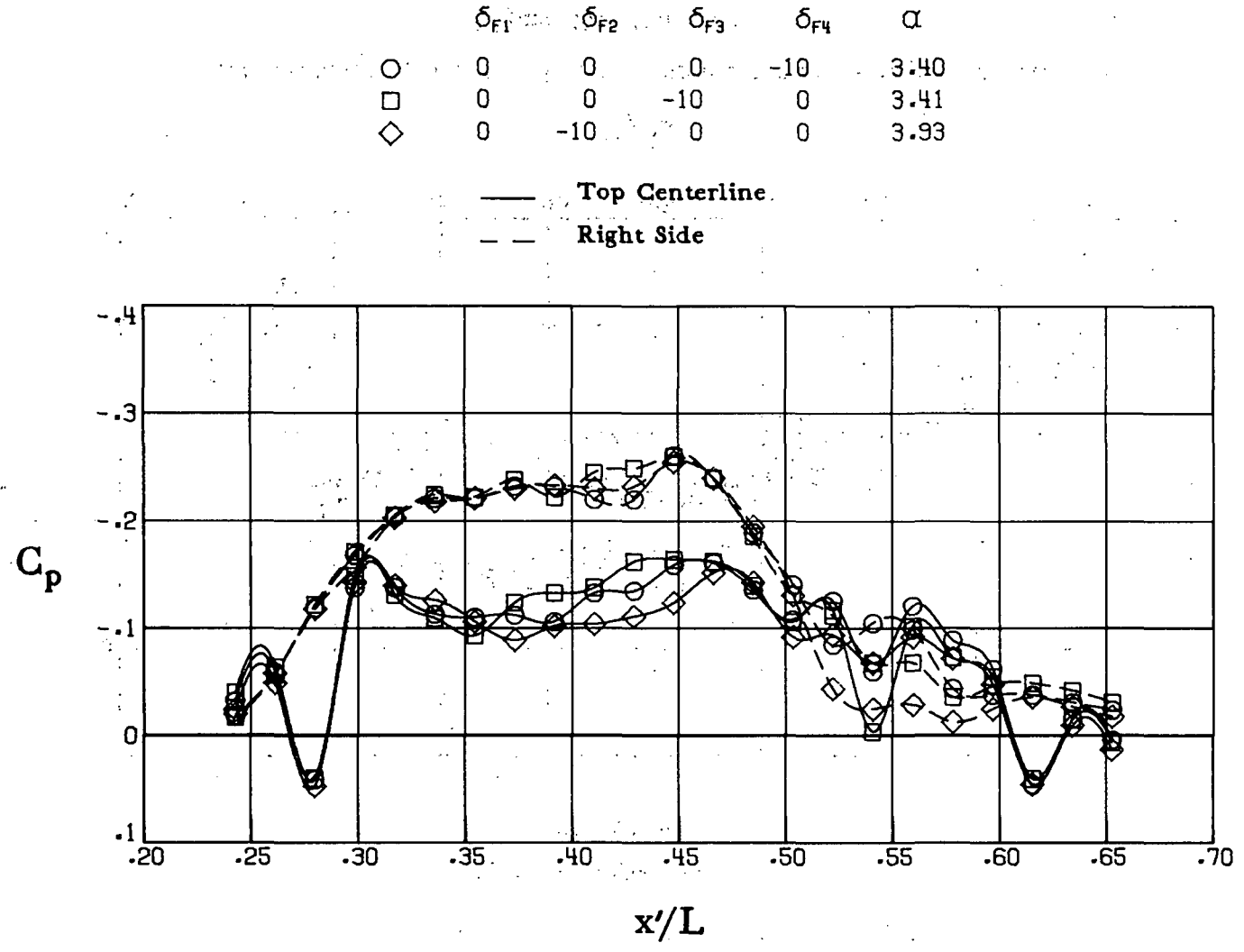
—— Top Centerline

– – Right Side



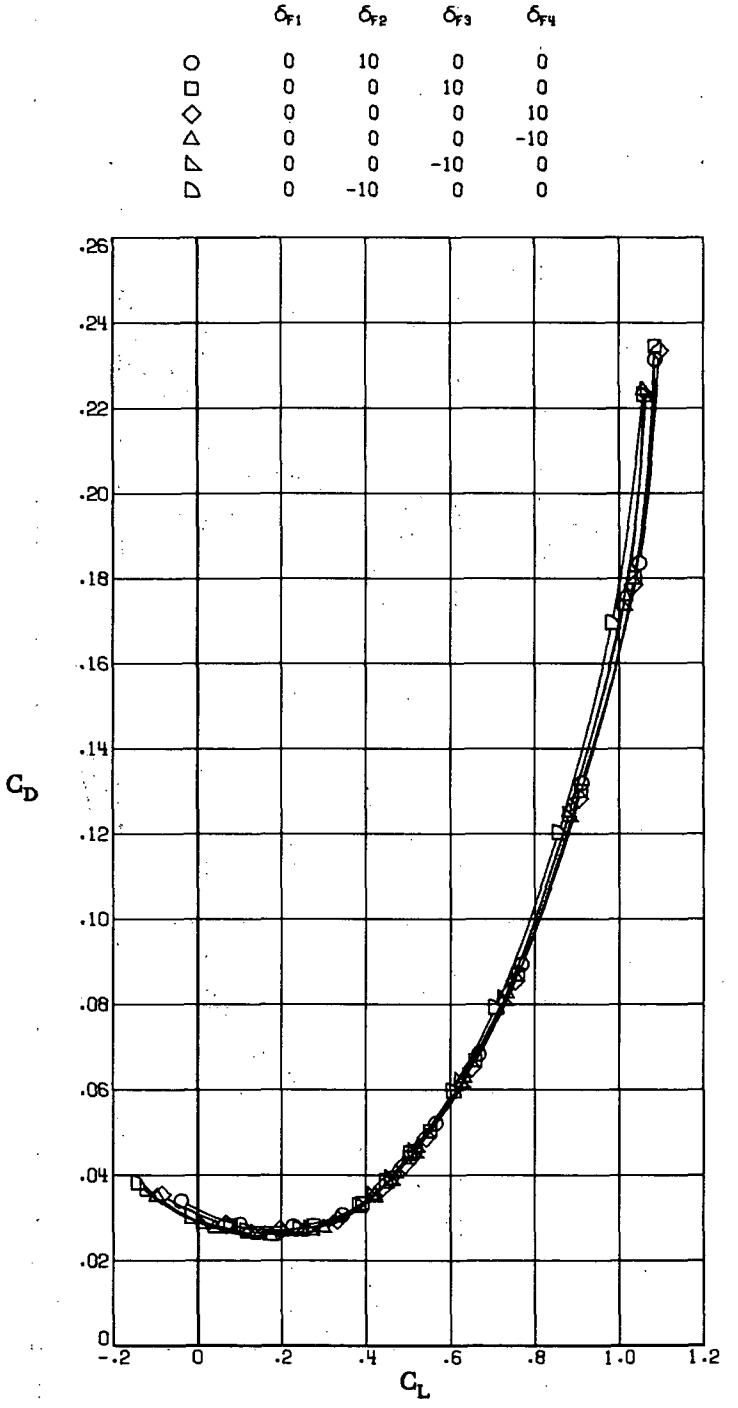
(f) Selected fuselage pressure distributions for control surface deflected 10^{o}.

Figure 47.- Continued.



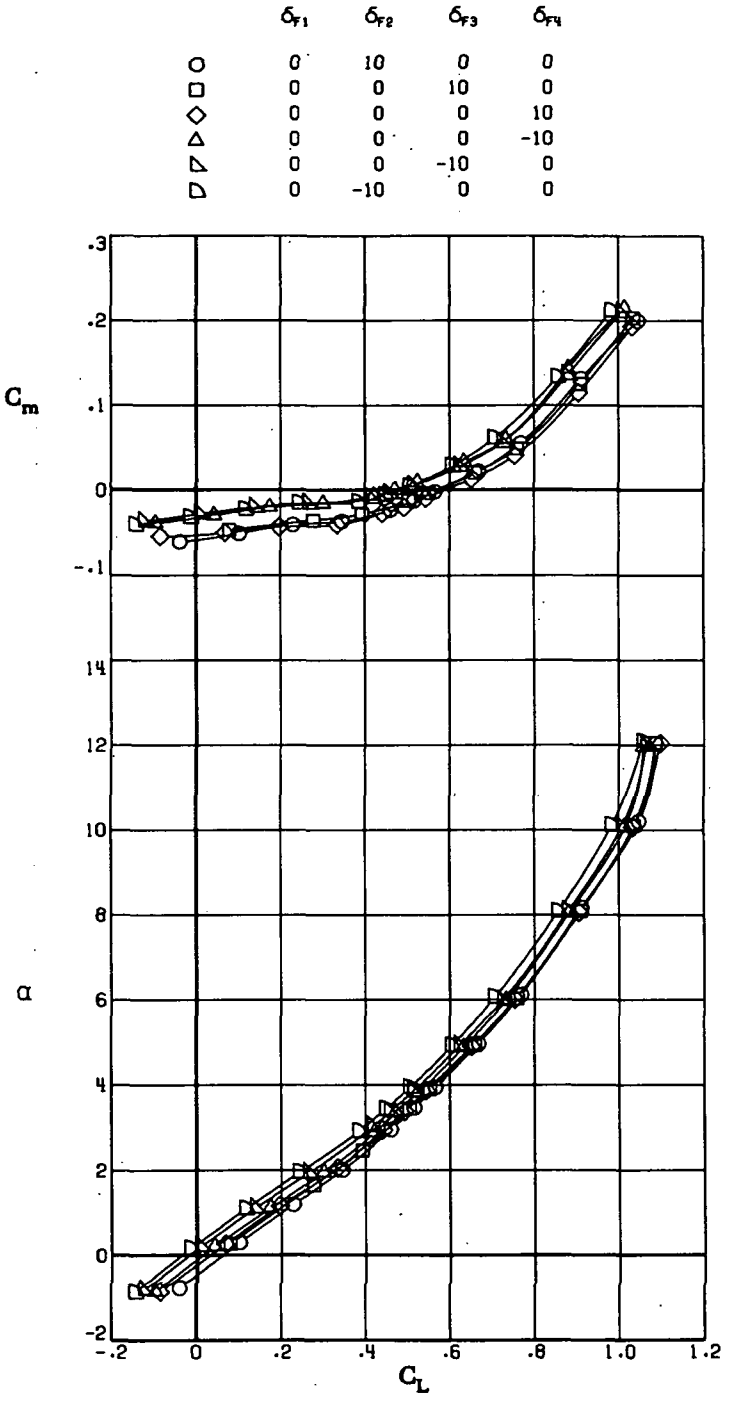
(g) Selected fuselage pressure distributions for control surface deflected -10^{o}.

Figure 47.- Concluded.



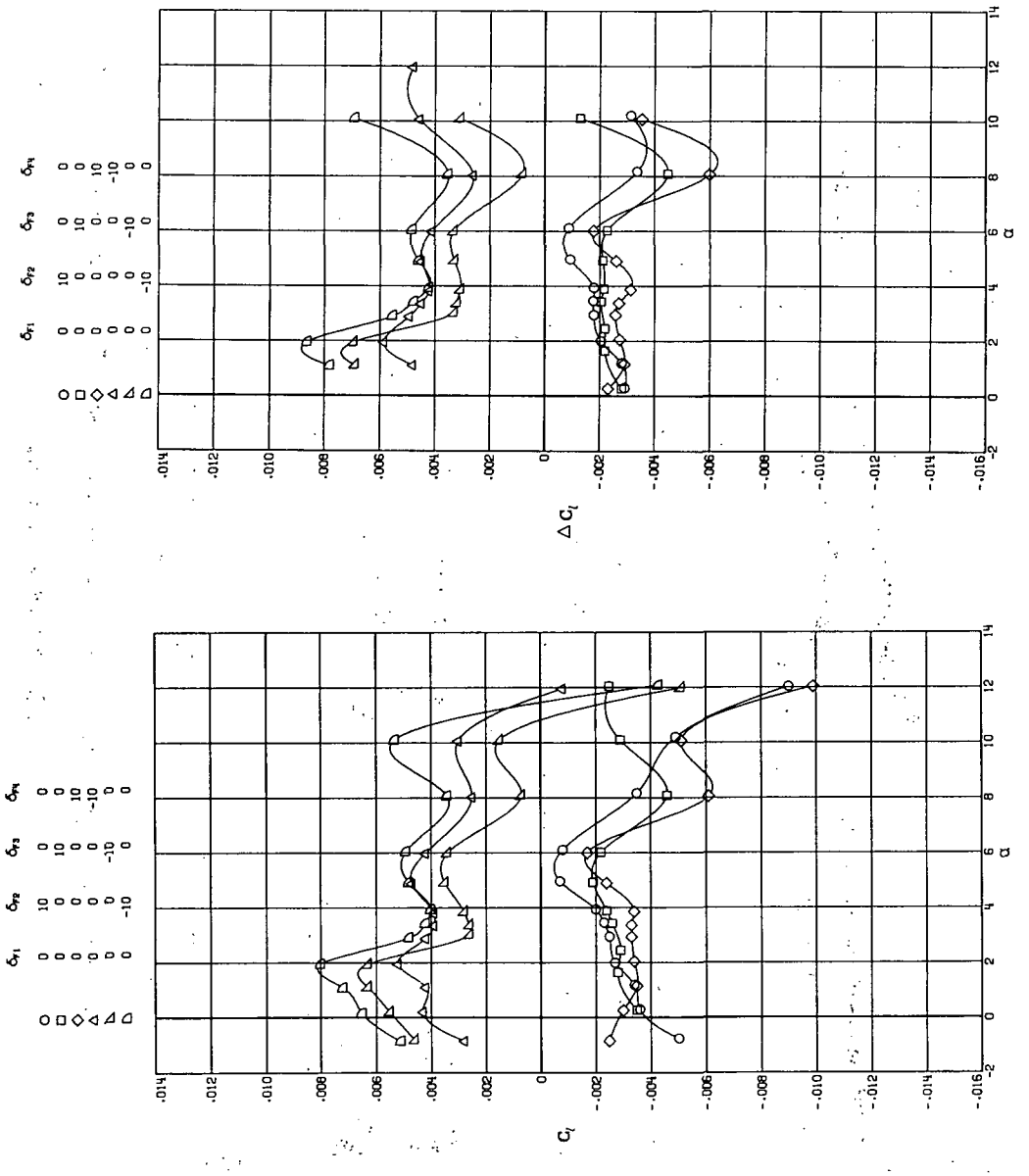
(a) Drag characteristics.

Figure 48.- Effect of spanwise location of trailing-edge control surface deflected $\pm 10^{\circ}$. Area-ruled fuselage. $M_{\infty} = 0.94$.



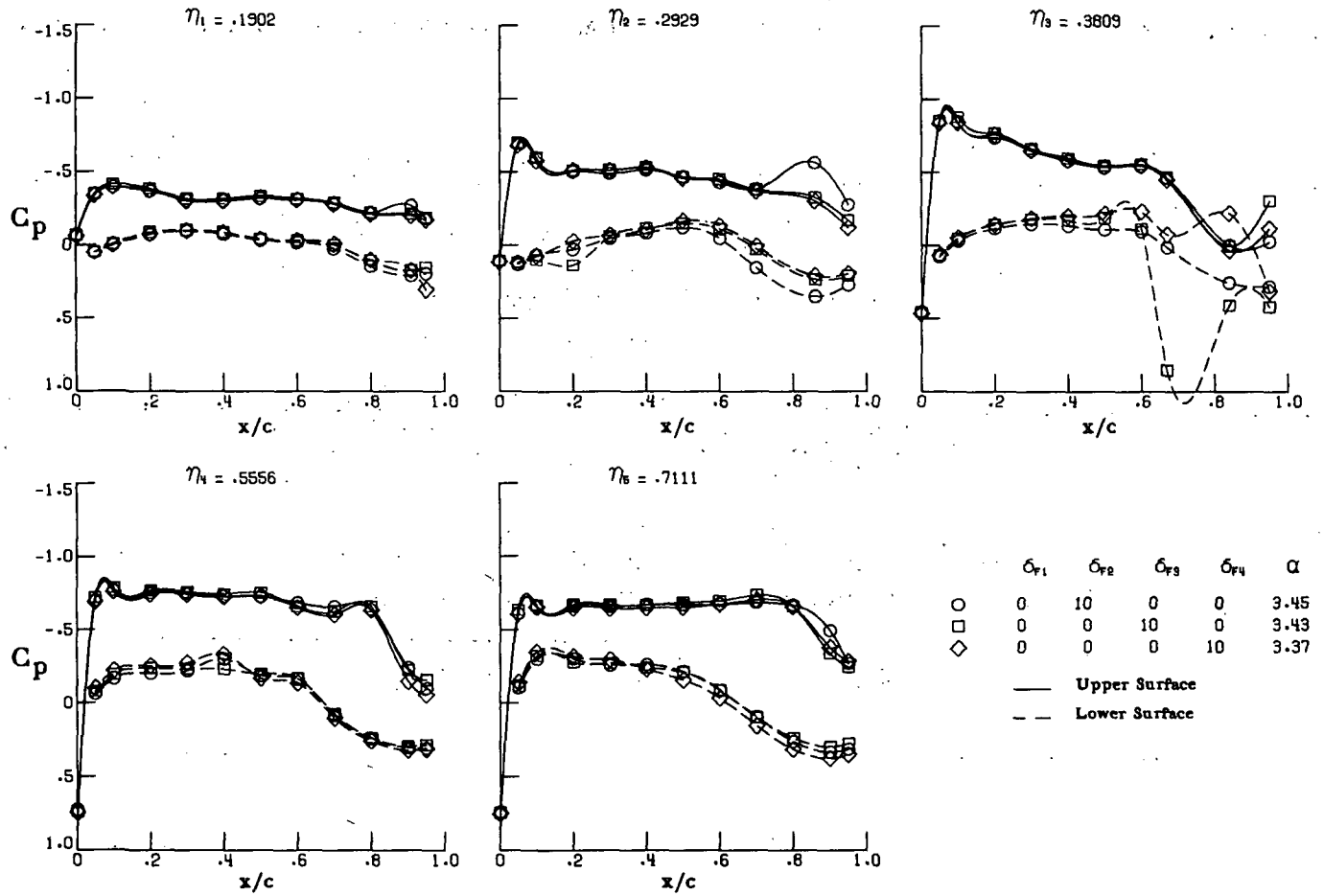
(b) Lift and pitch characteristics.

Figure 48.- Continued.



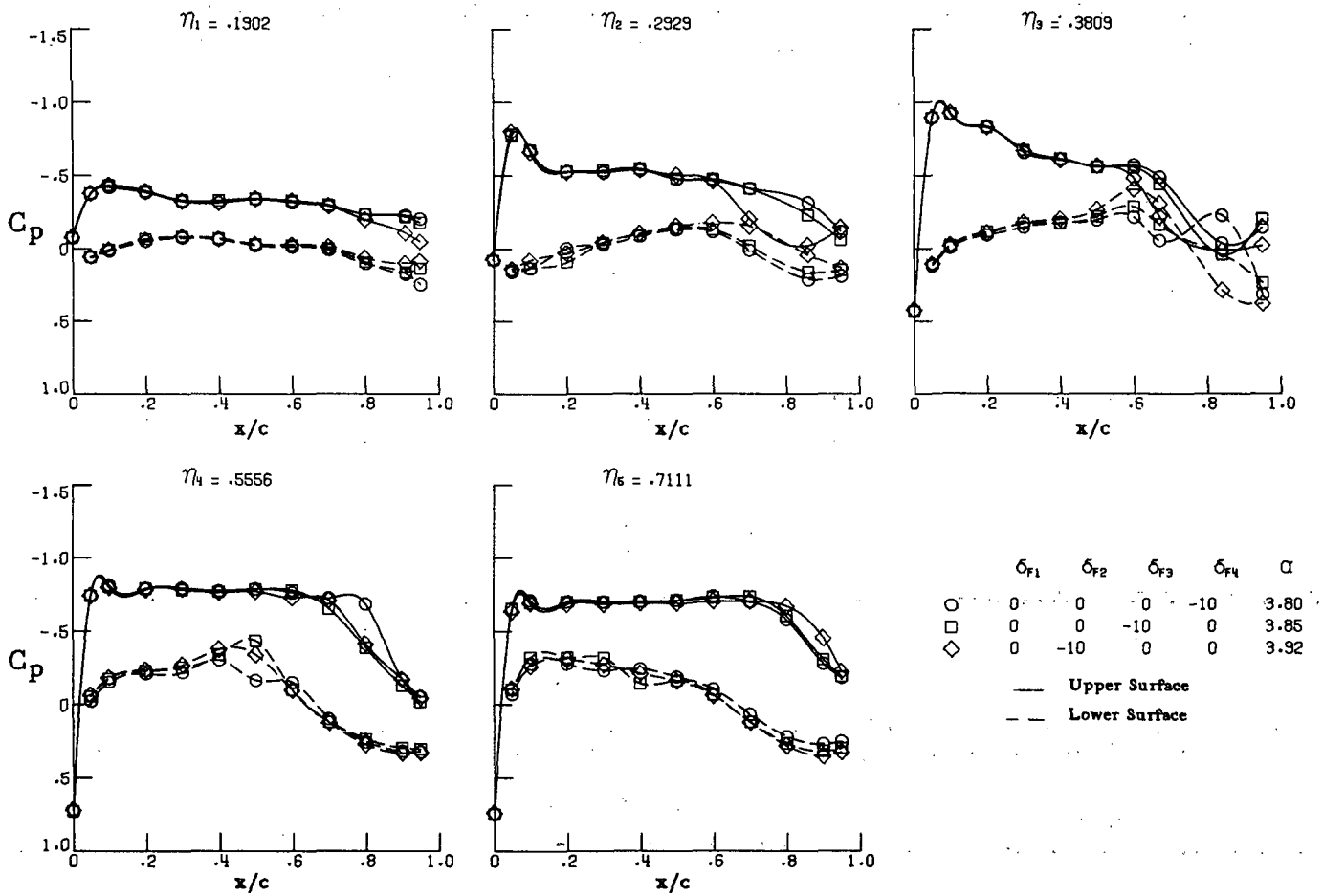
(c) Rolling-moment characteristics.

Figure 48.- Continued.



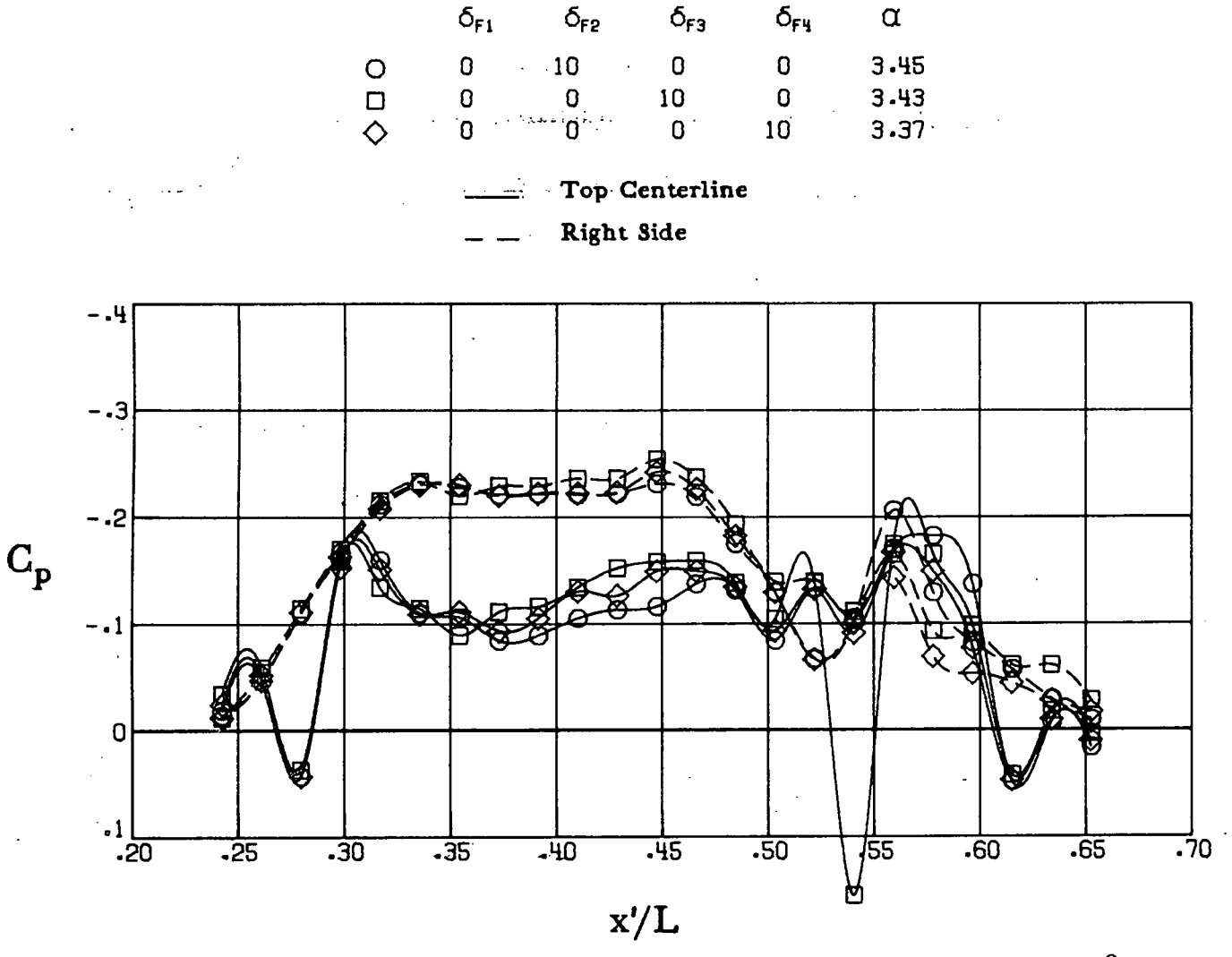
(d) Selected wing pressure distributions for control surface deflected 10^{o}.

Figure 48.- Continued.



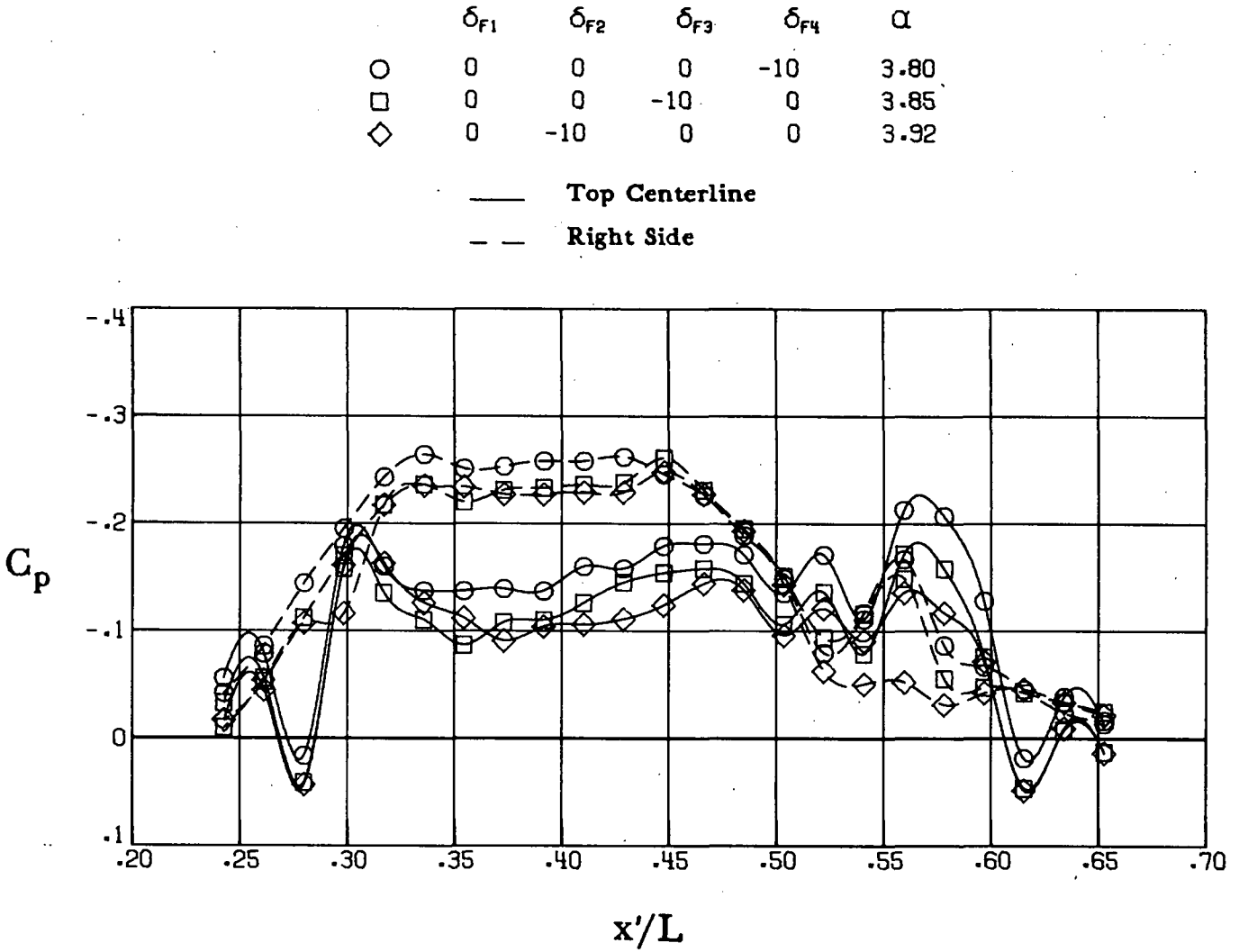
(e) Selected wing pressure distributions for control surface deflected -10^{o}.

Figure 48.- Continued.



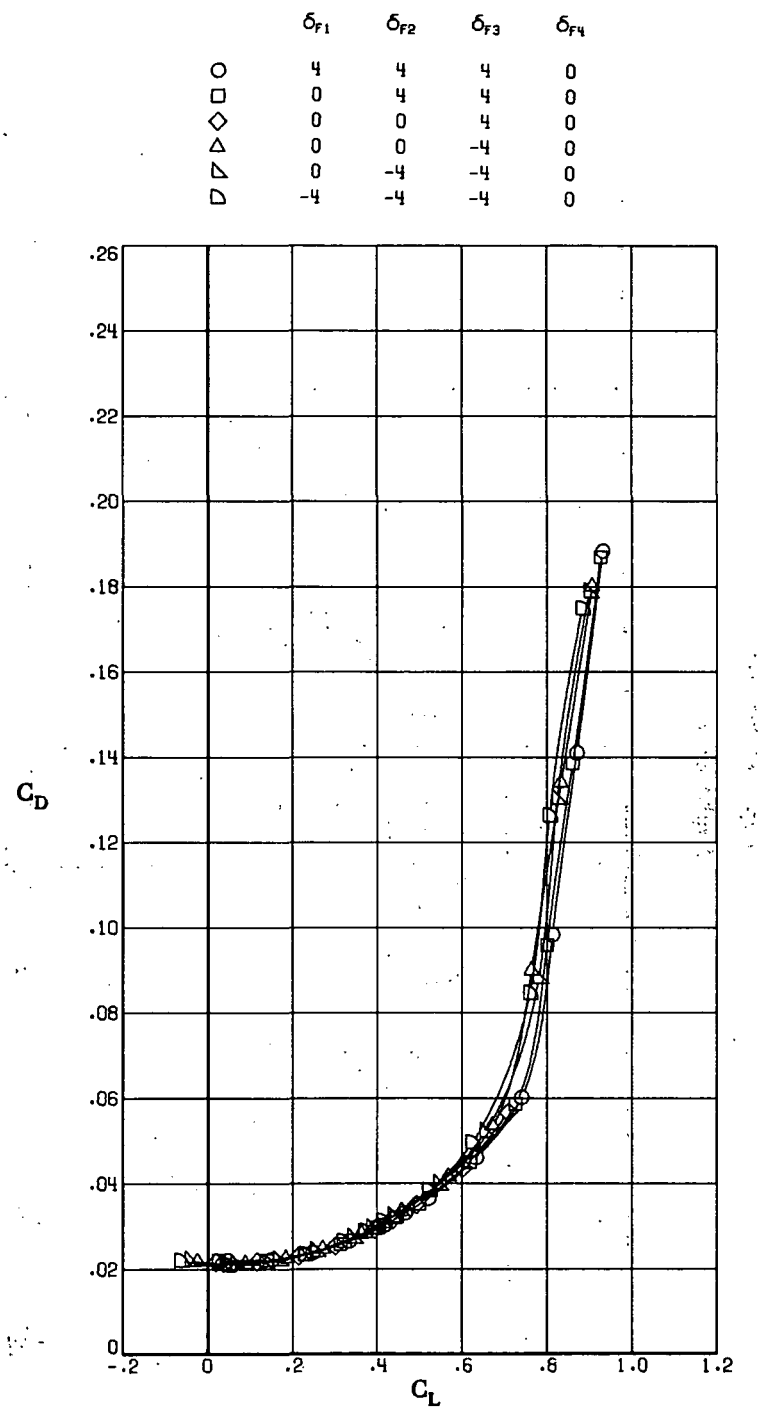
(f) Selected fuselage pressure distributions for control surface deflected 10^{o}.

Figure 48.- Continued.



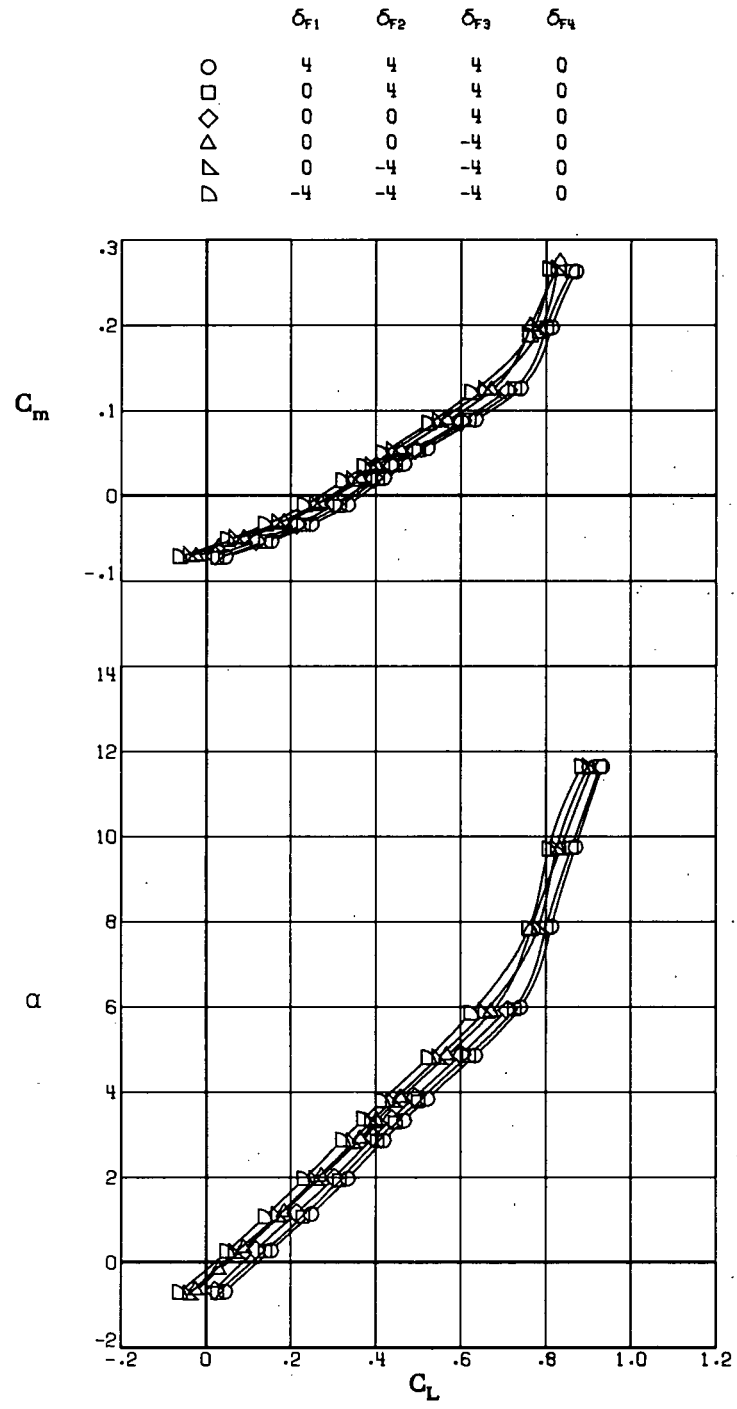
(g) Selected fuselage pressure distributions for control surface deflected -10^{o}.

Figure 48.- Concluded.



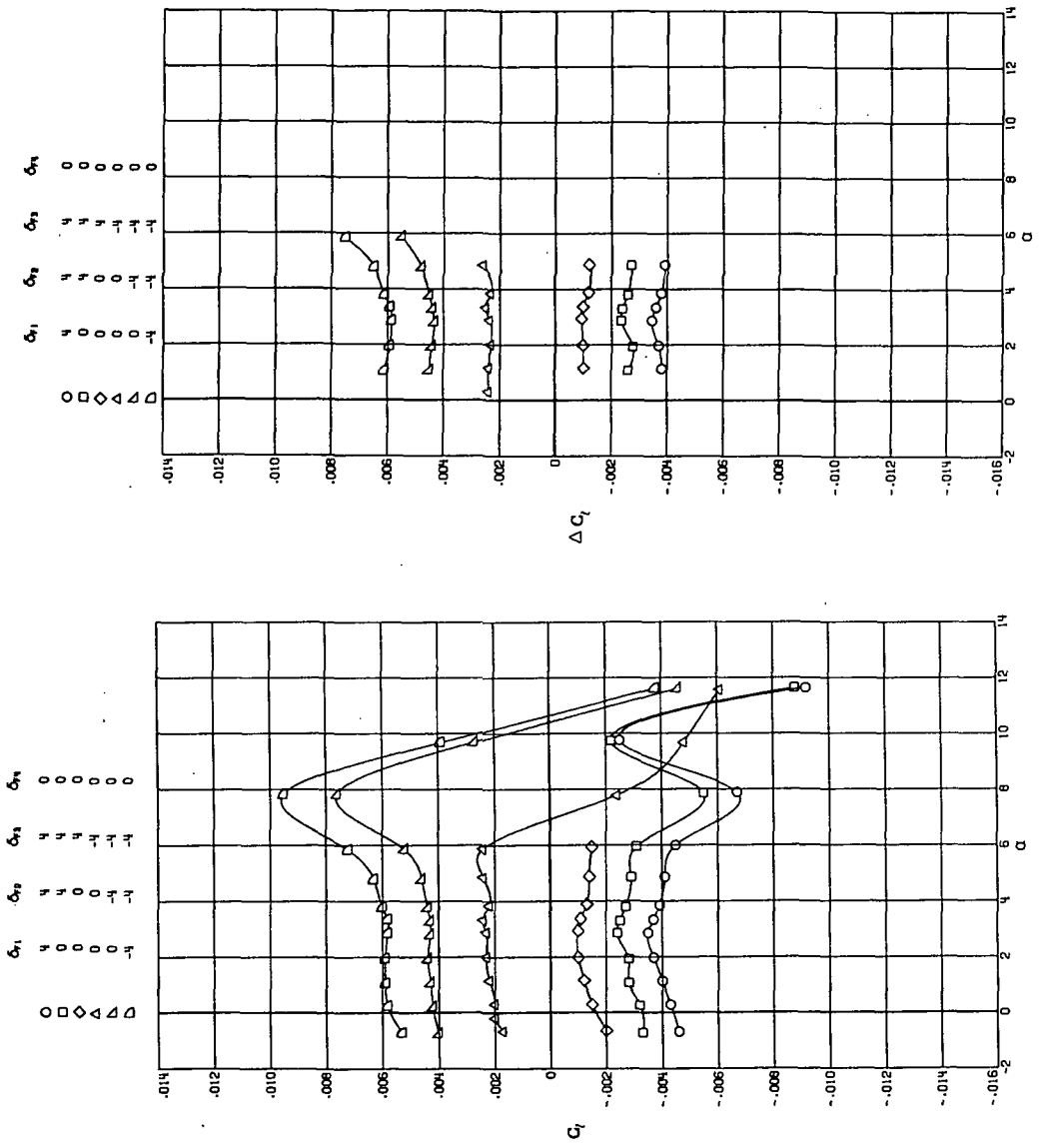
(a) Drag characteristics.

Figure 49.- Effect of spanwise length of trailing-edge control surface deflected $\pm 4^{\circ}$. Area-ruled fuselage. $M_{\infty} = 0.80$.



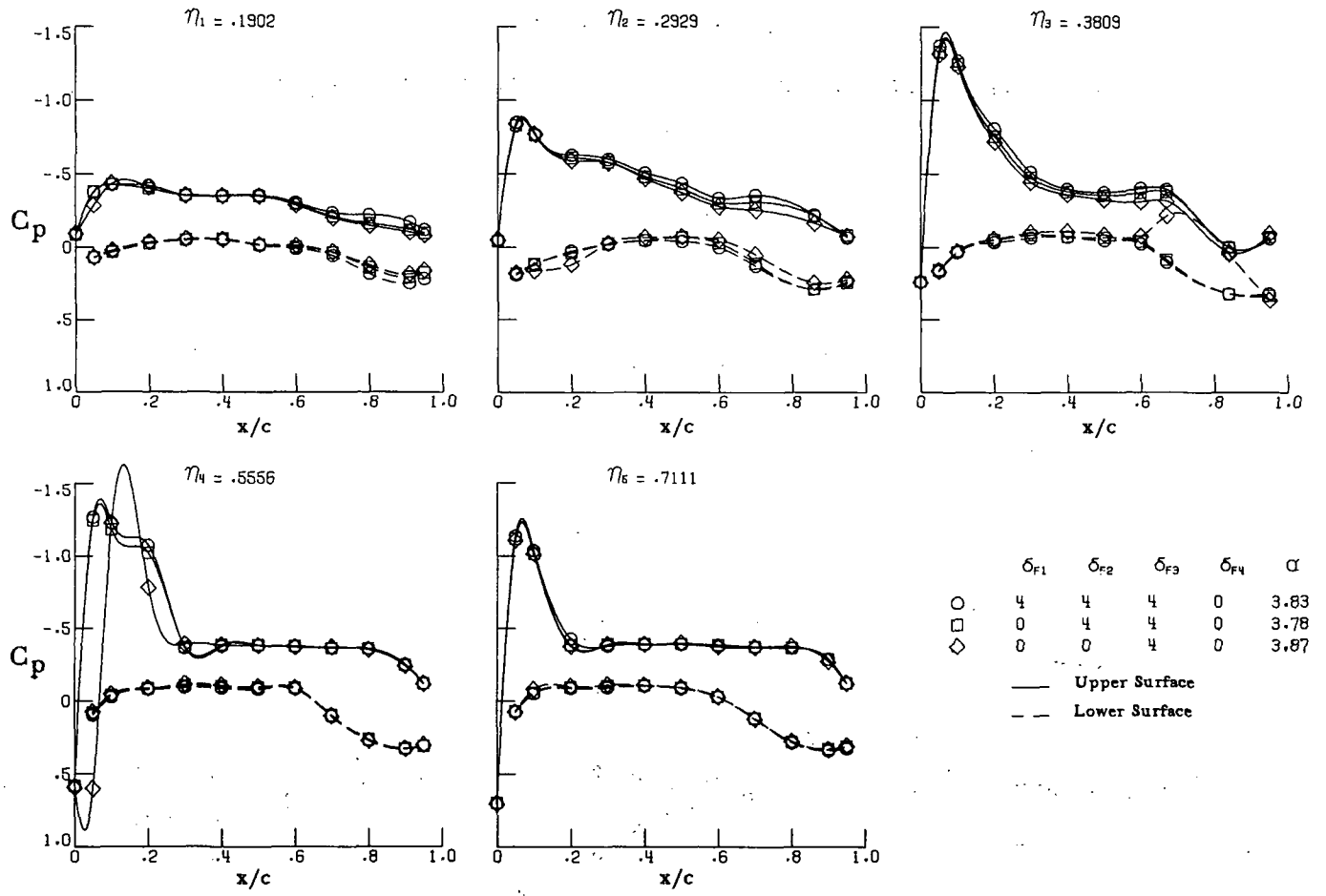
(b) Lift and pitch characteristics.

Figure 49.- Continued.



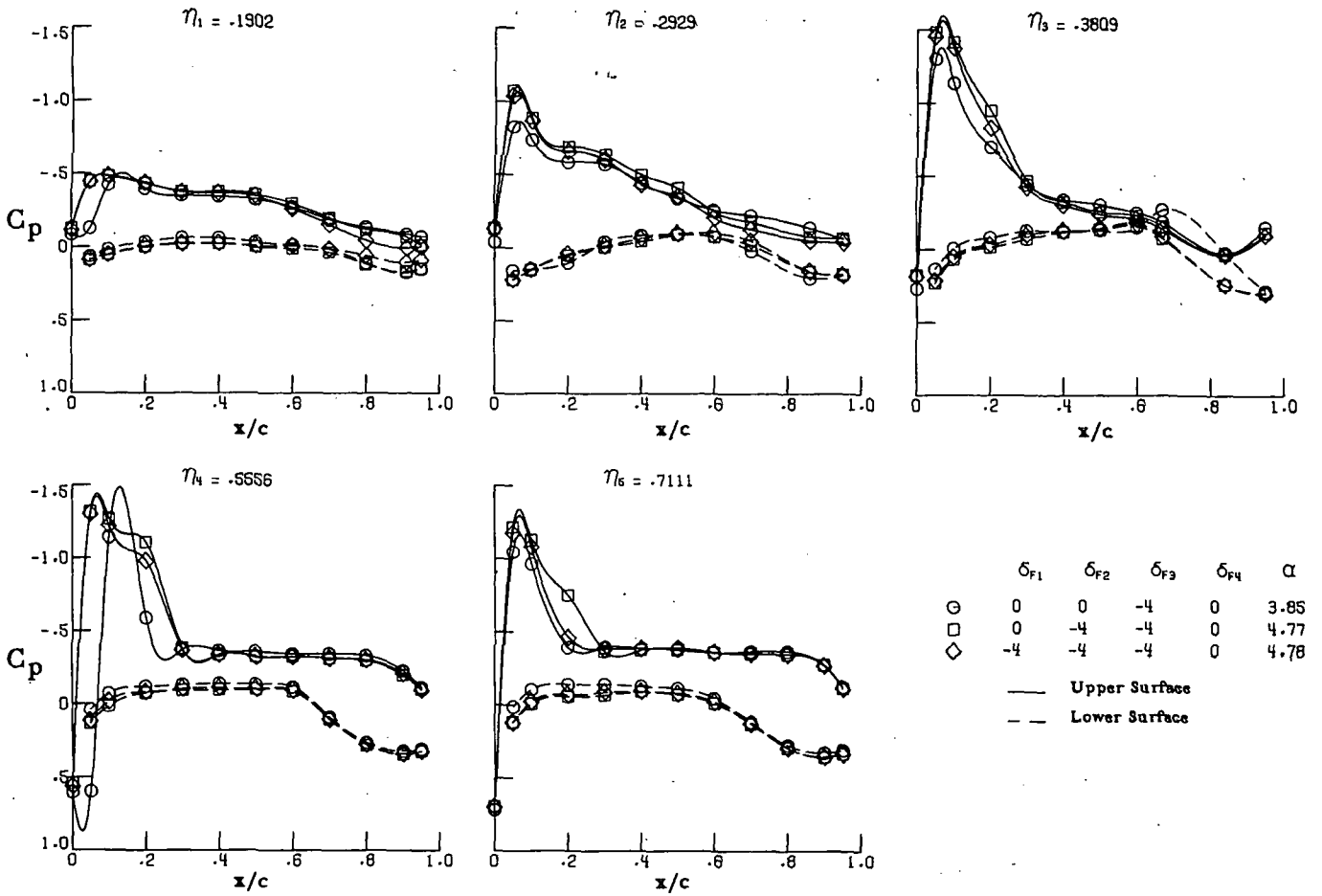
(c) Rolling-moment characteristics.

Figure 49. - Continued.



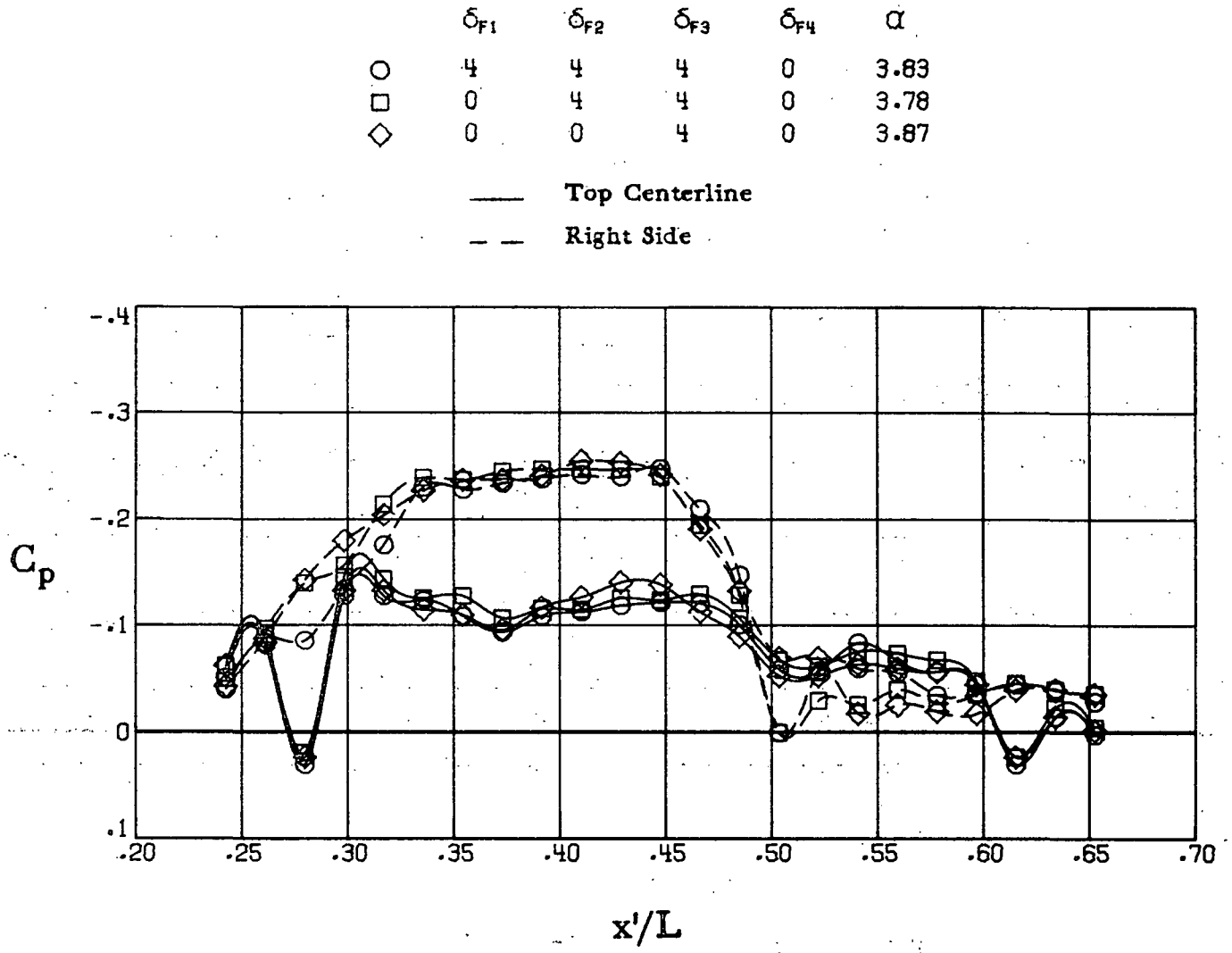
(d) Selected wing pressure distributions for control surface deflected 4^{o}.

Figure 49.- Continued.



(e) Selected wing pressure distributions for control surface deflected -4^{o}.

Figure 49.- Continued.



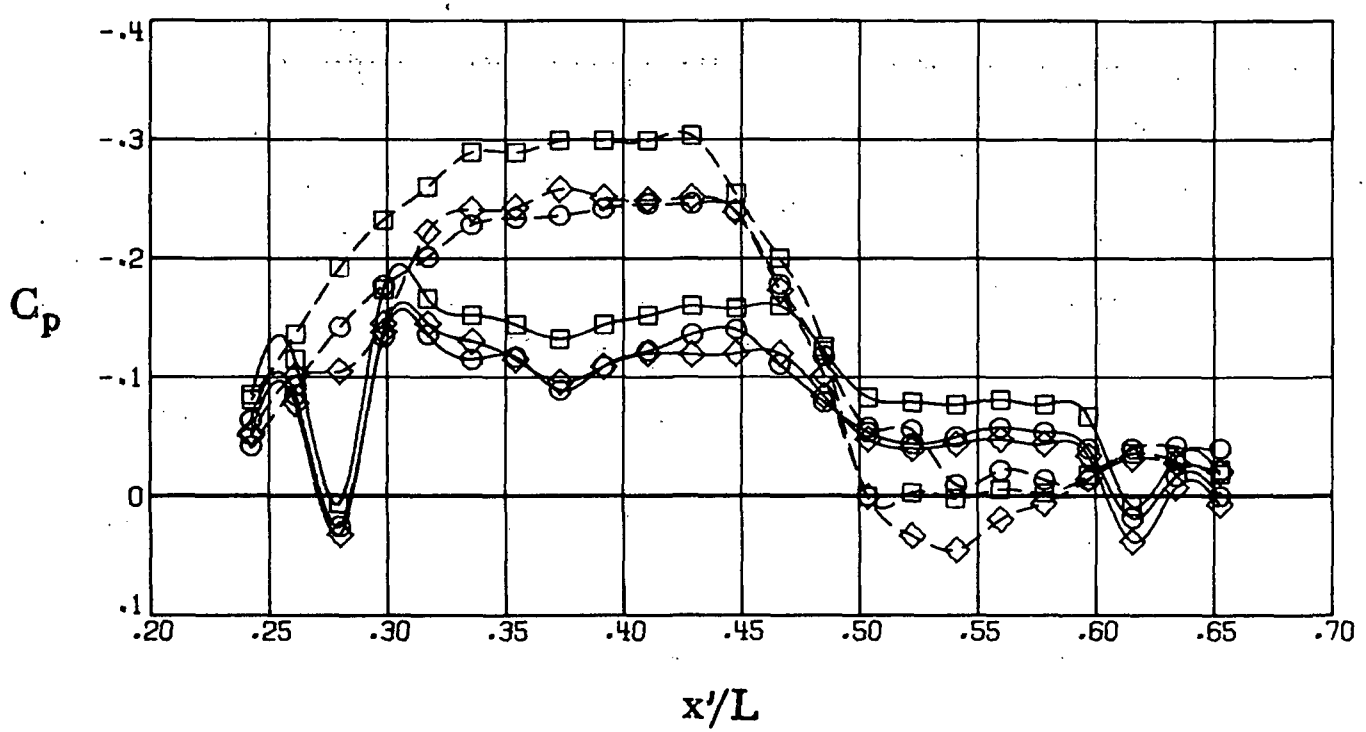
(f) Selected fuselage pressure distributions for control surface deflected 4^{o}.

Figure 49.- Continued.

	δ_{F1}	δ_{F2}	δ_{F3}	δ_{F4}	α
○	0	0	-4	0	3.85
□	0	-4	-4	0	4.77
◇	-4	-4	-4	0	4.78

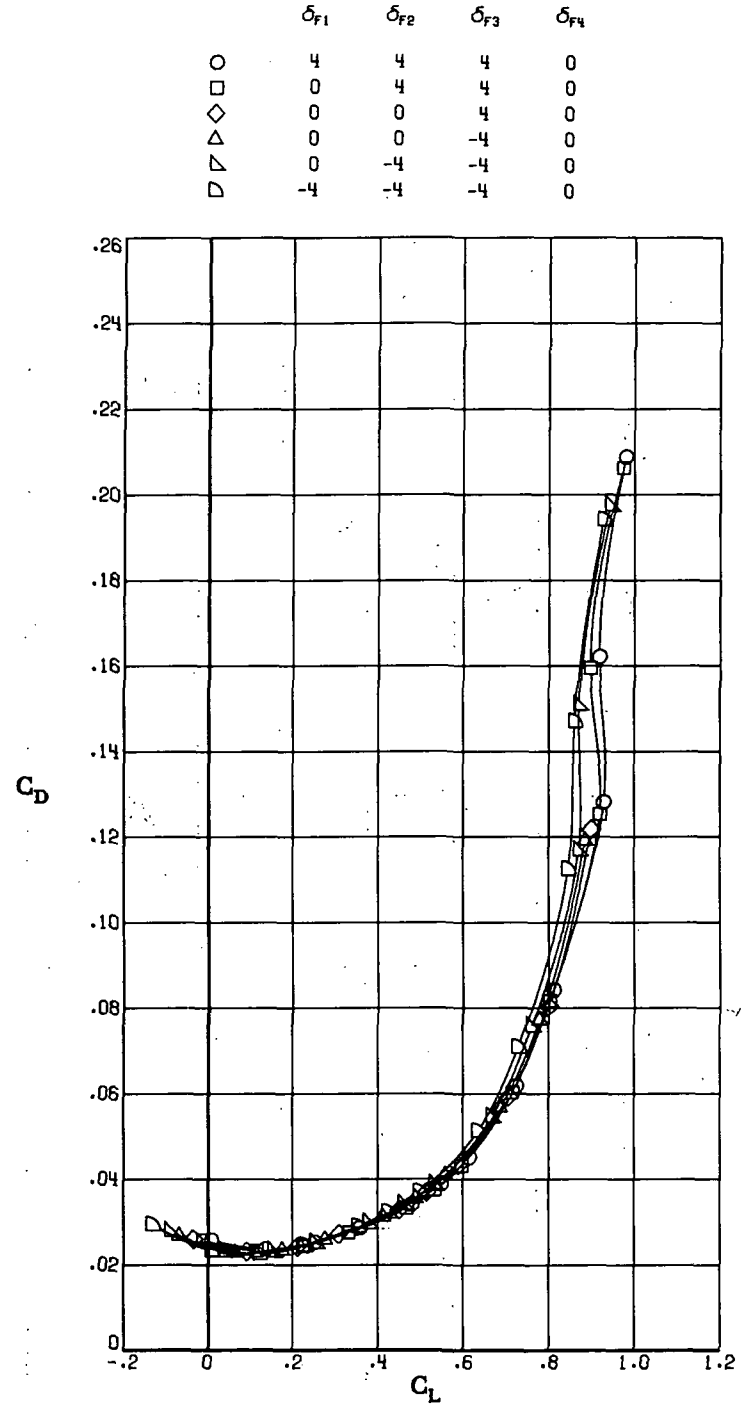
—— Top Centerline

– – Right Side



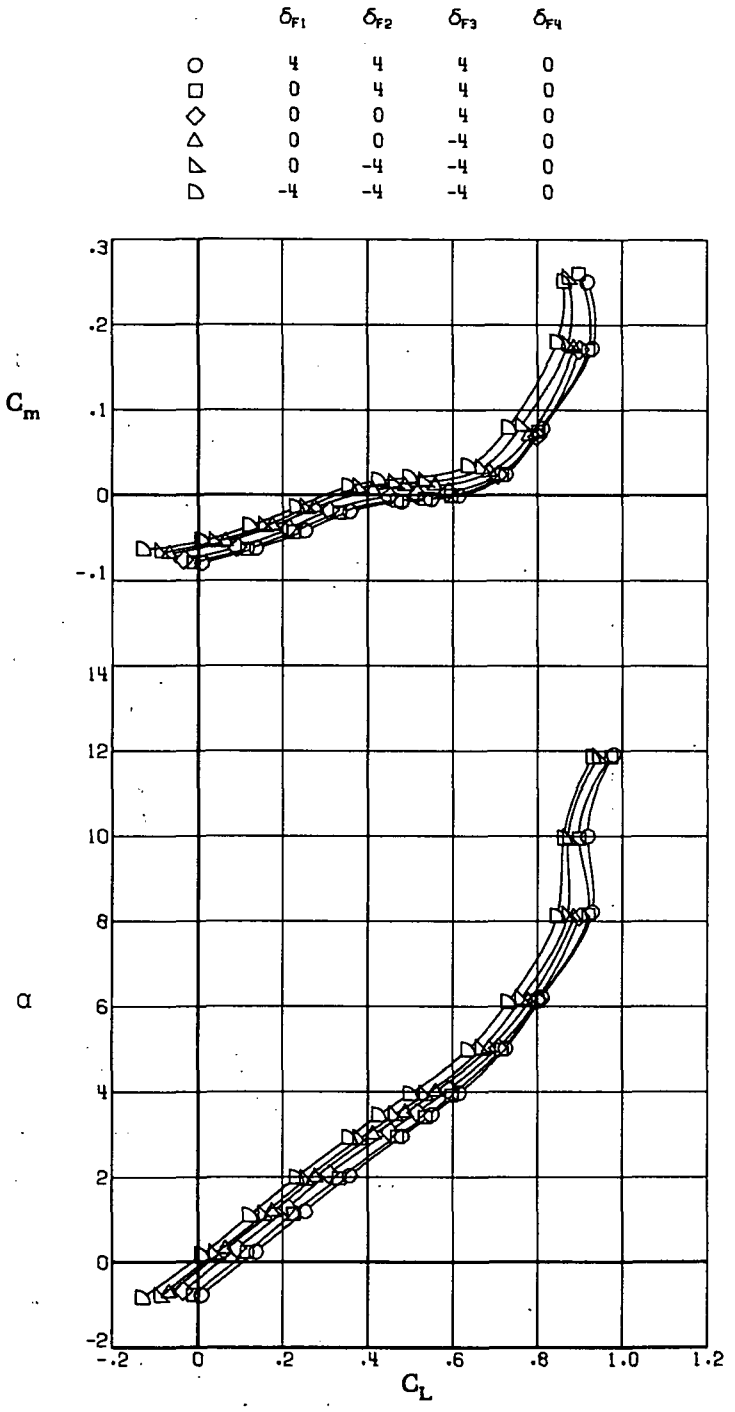
(g) Selected fuselage pressure distributions for control surface deflected -4°.

Figure 49.- Concluded.



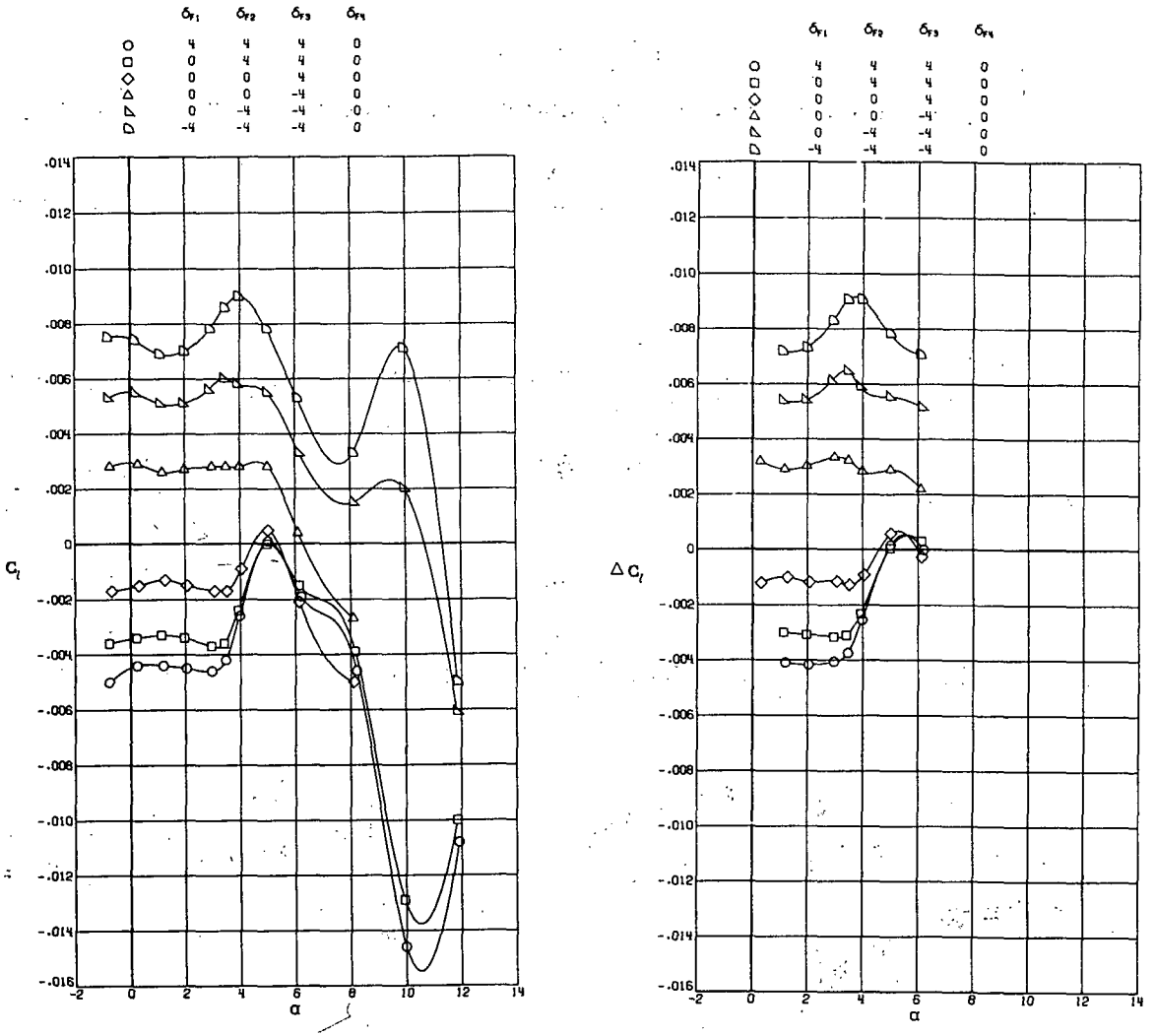
(a) Drag characteristics.

Figure 50.- Effect of spanwise length of trailing-edge control surface deflected $\pm 4^{\circ}$. Area-ruled fuselage. $M_{\infty} = 0.90$.



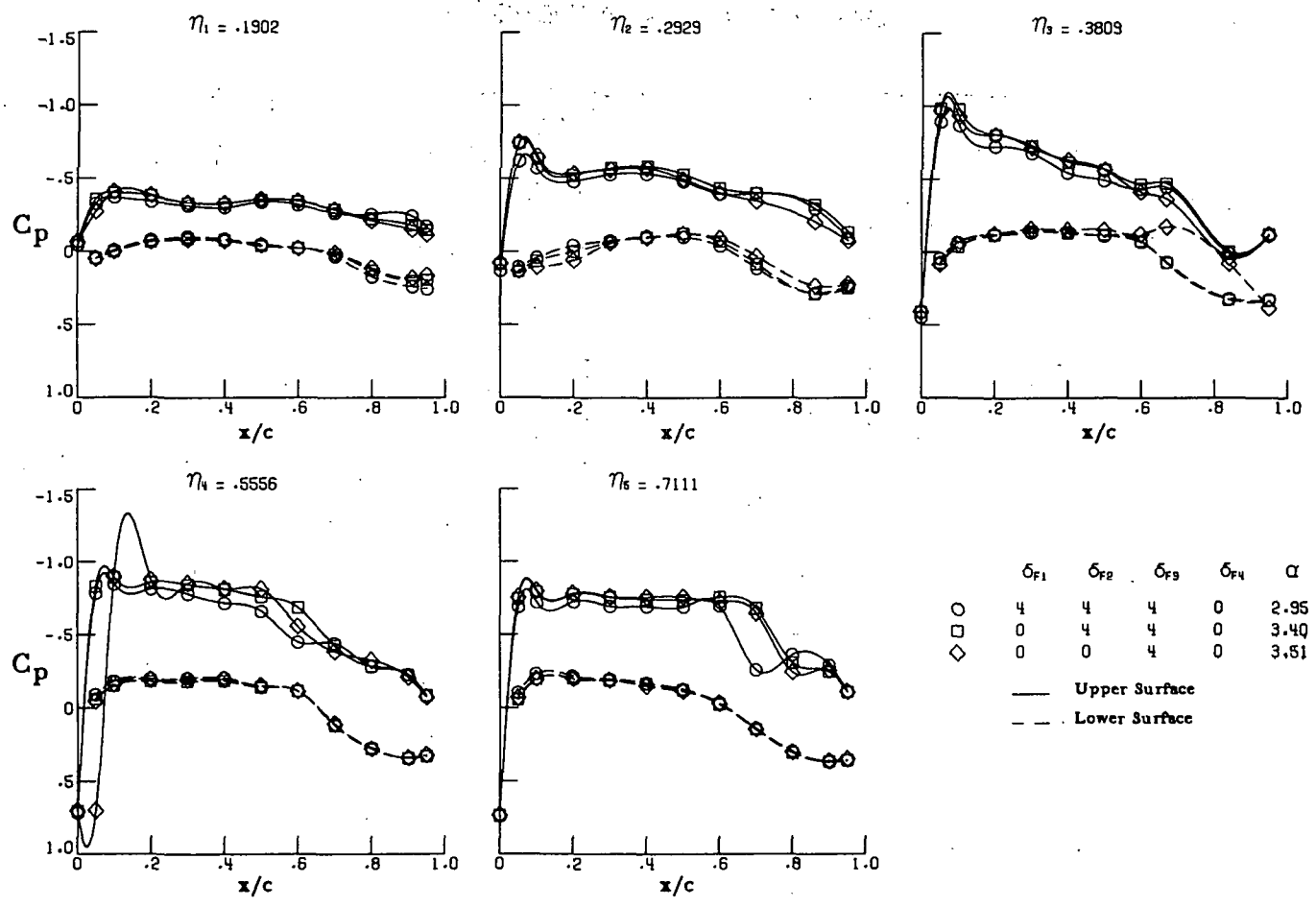
(b) Lift and pitch characteristics.

Figure 50.- Continued.



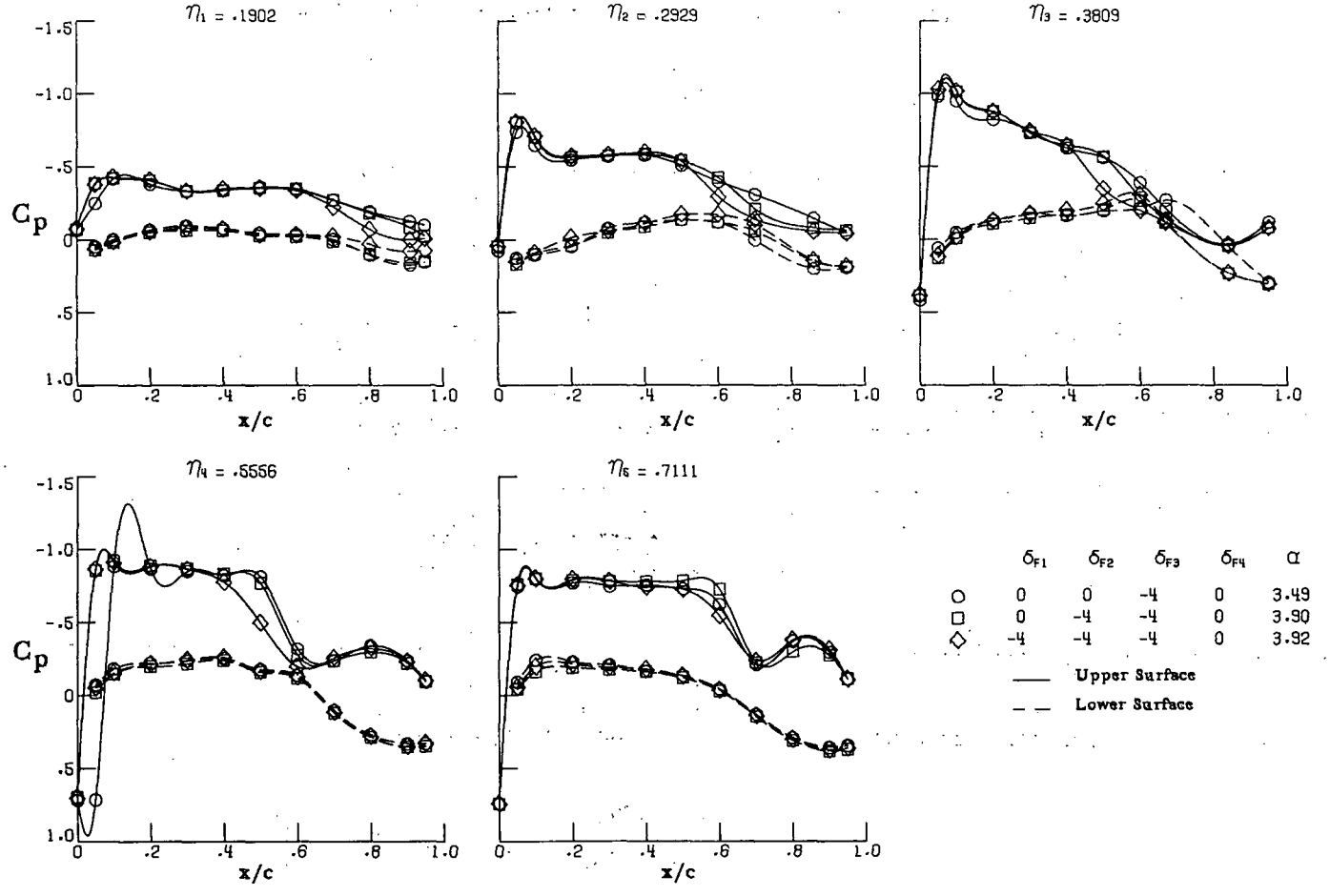
(c) Rolling-moment characteristics.

Figure 50.- Continued.



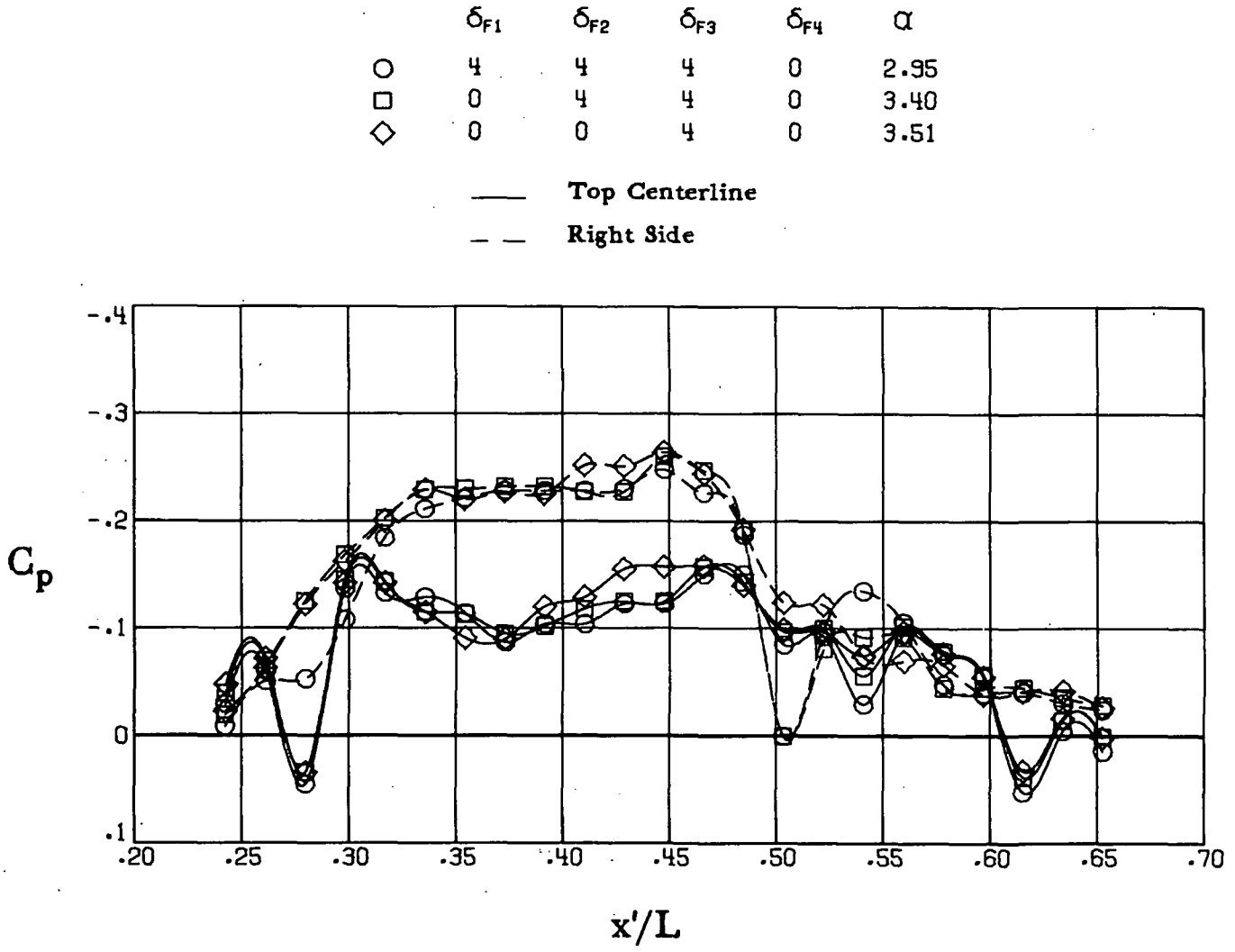
(d) Selected wing pressure distributions for control surface deflected 4^{o}.

Figure 50.- Continued.



(e) Selected wing pressure distributions for control surface deflected -4^{o}.

Figure 50.- Continued.



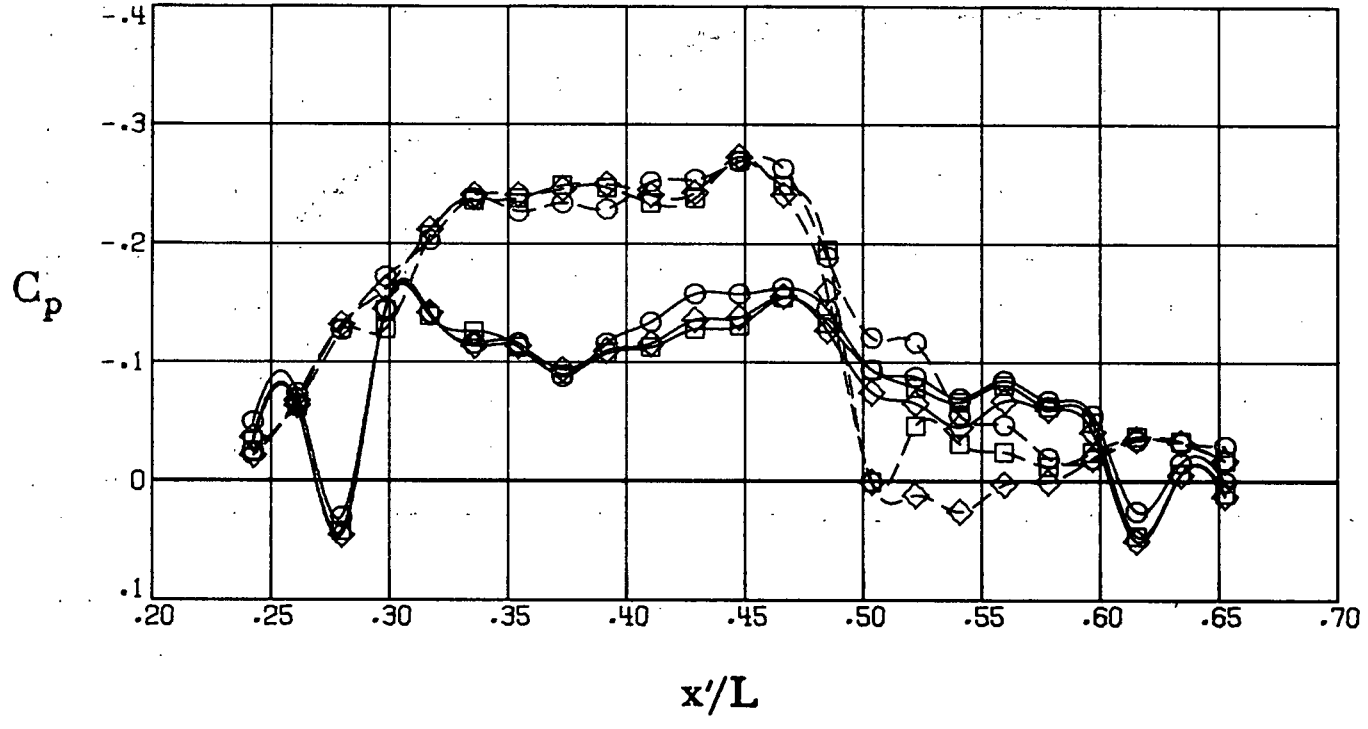
(f) Selected fuselage pressure distributions for control surface deflected 4°.

Figure 50.- Continued.

	δ_{F1}	δ_{F2}	δ_{F3}	δ_{F4}	α
○	0	0	-4	0	3.49
□	0	-4	-4	0	3.90
◇	-4	-4	-4	0	3.92

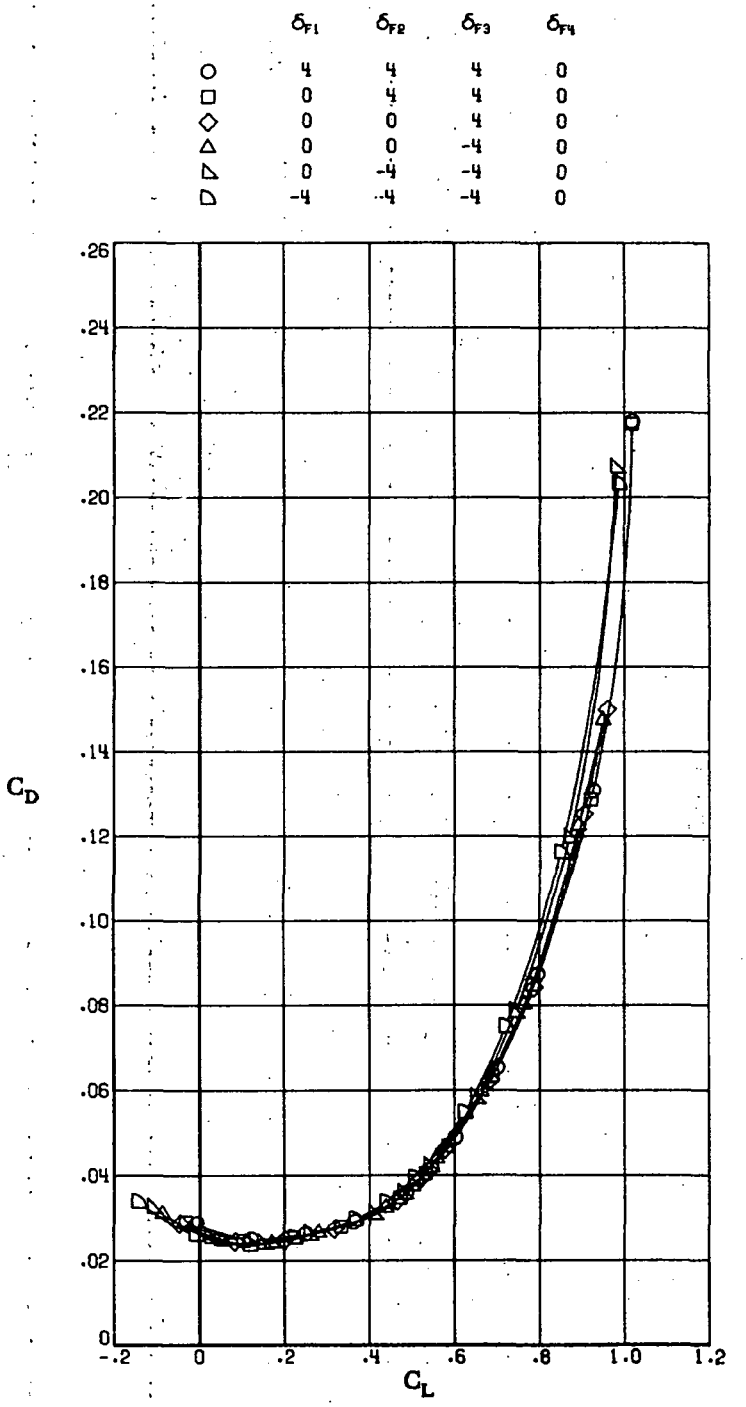
—— Top Centerline

– – Right Side



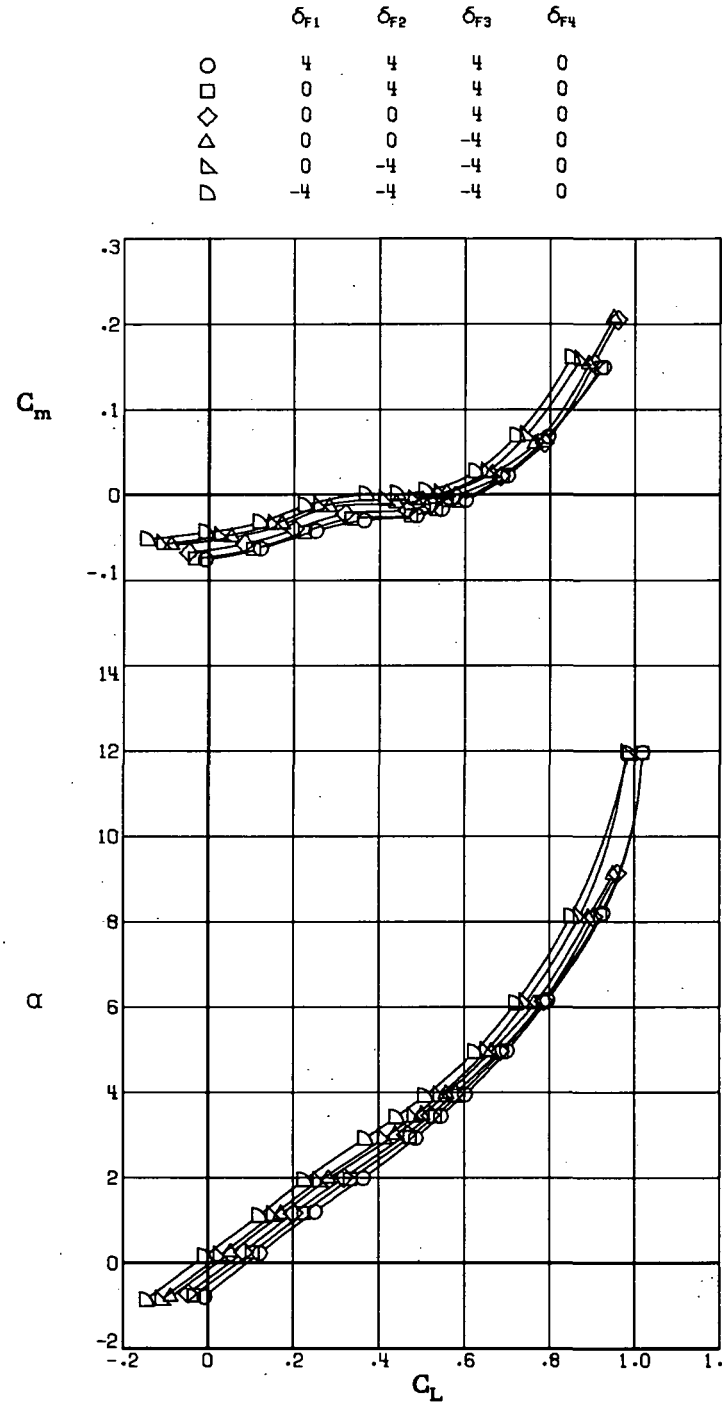
(g) Selected fuselage pressure distributions for control surface deflected -4^{o}.

Figure 50.- Concluded.



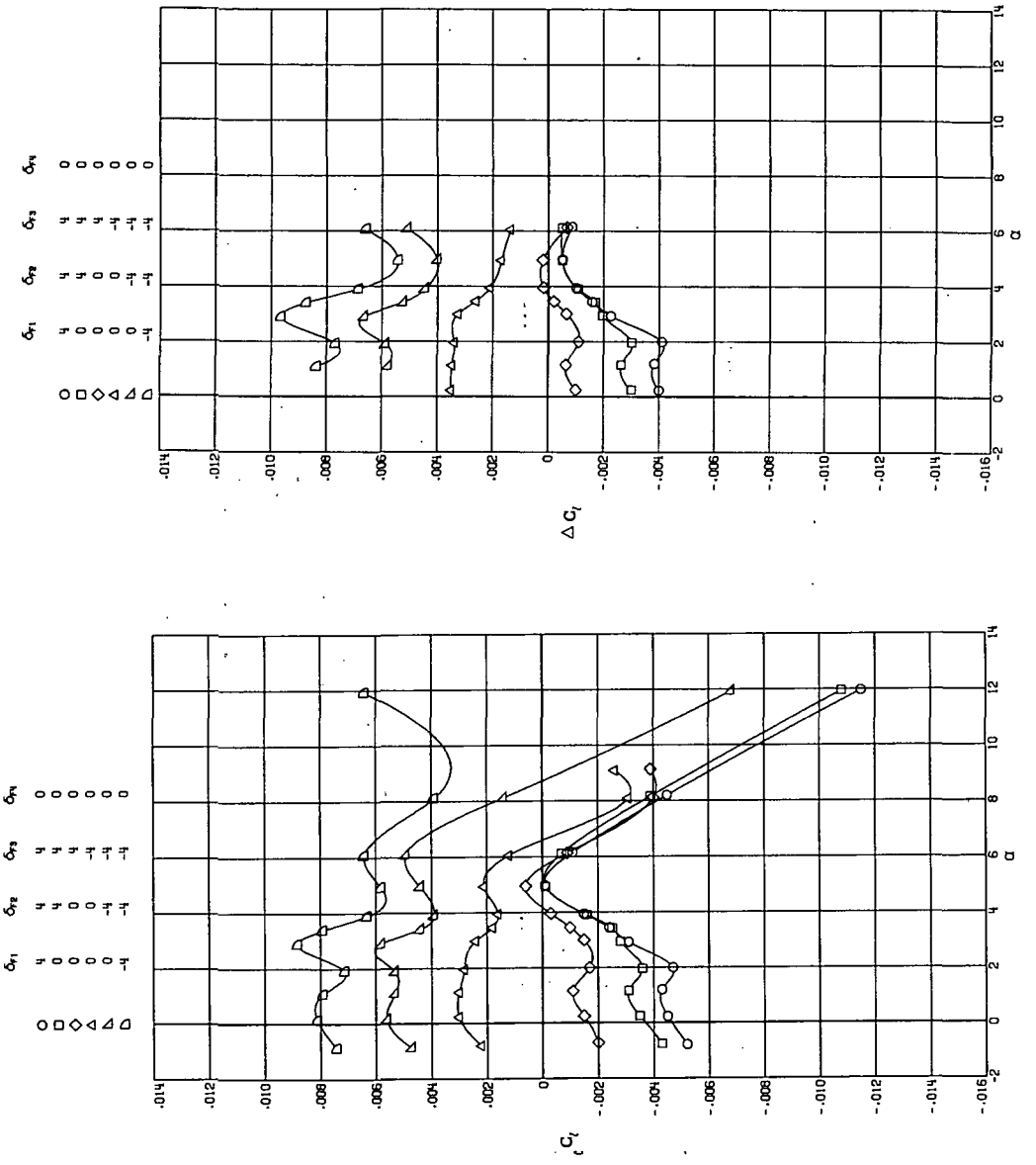
(a) Drag characteristics.

Figure 51.- Effect of spanwise length of trailing-edge control surface deflected $\pm 4^{\circ}$. Area-ruled fuselage. $M_{\infty} = 0.92$.



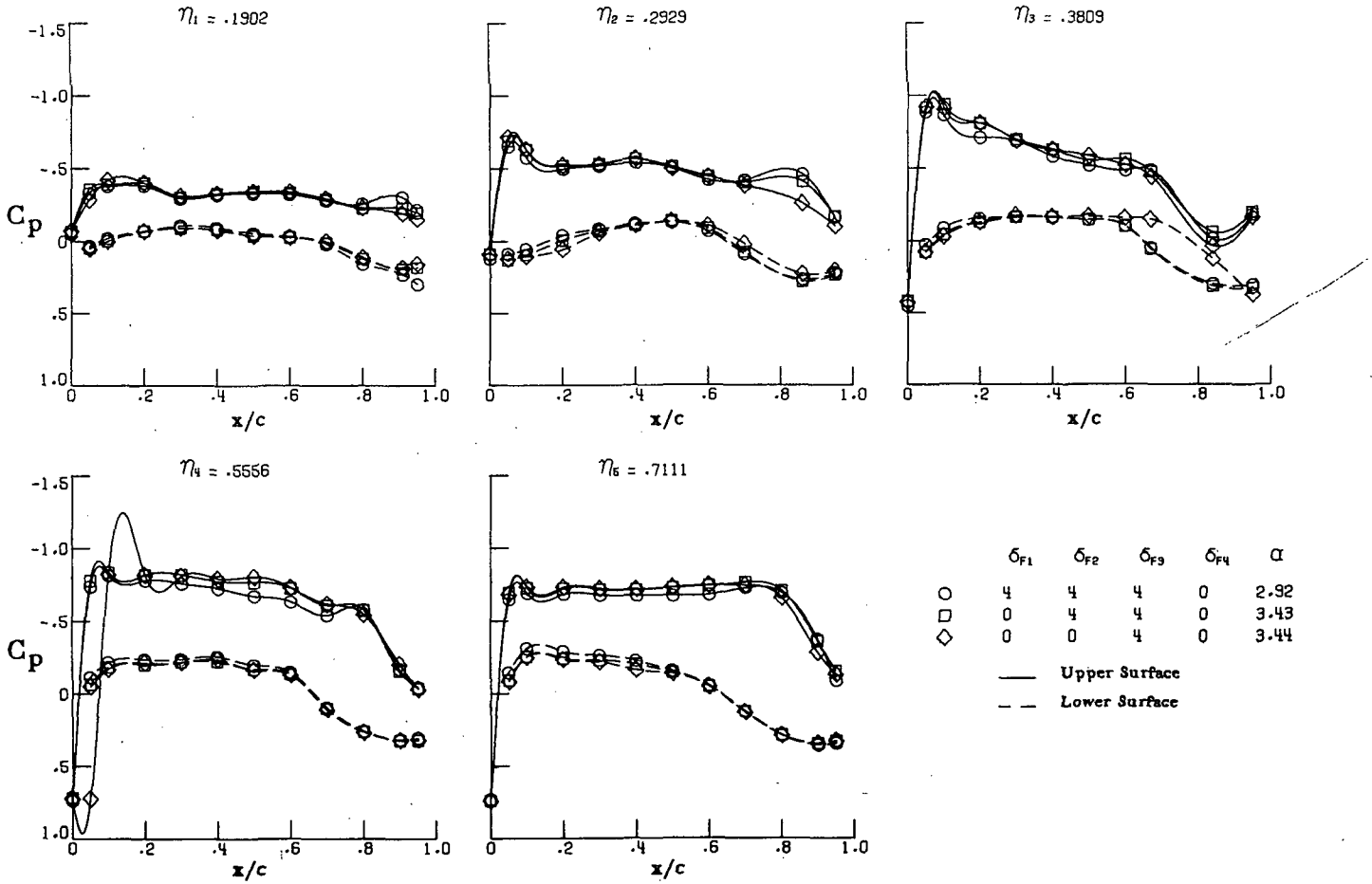
(b) Lift and pitch characteristics.

Figure 51.- Continued.



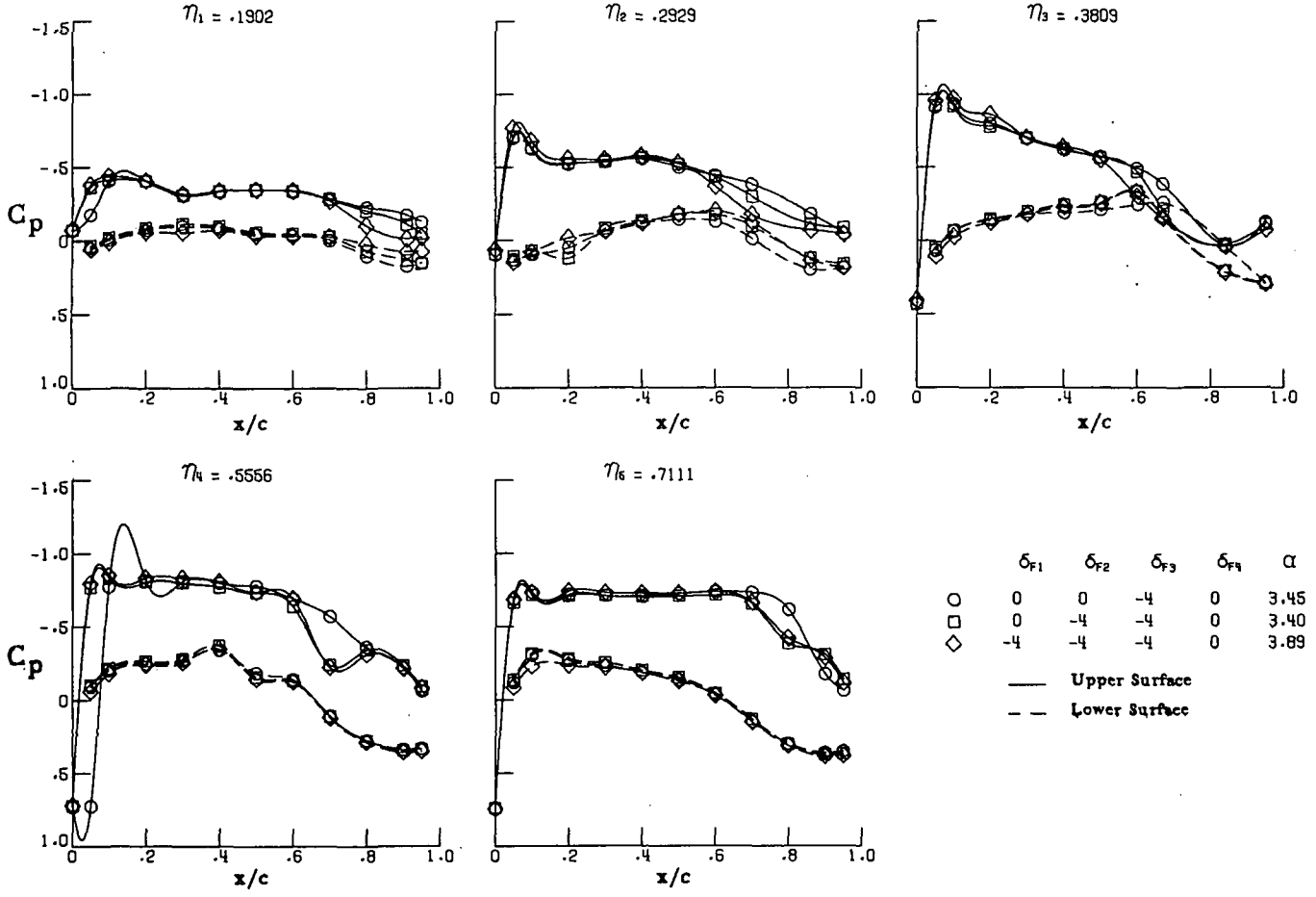
(c) Rolling-moment characteristics.

Figure 51.- Continued.



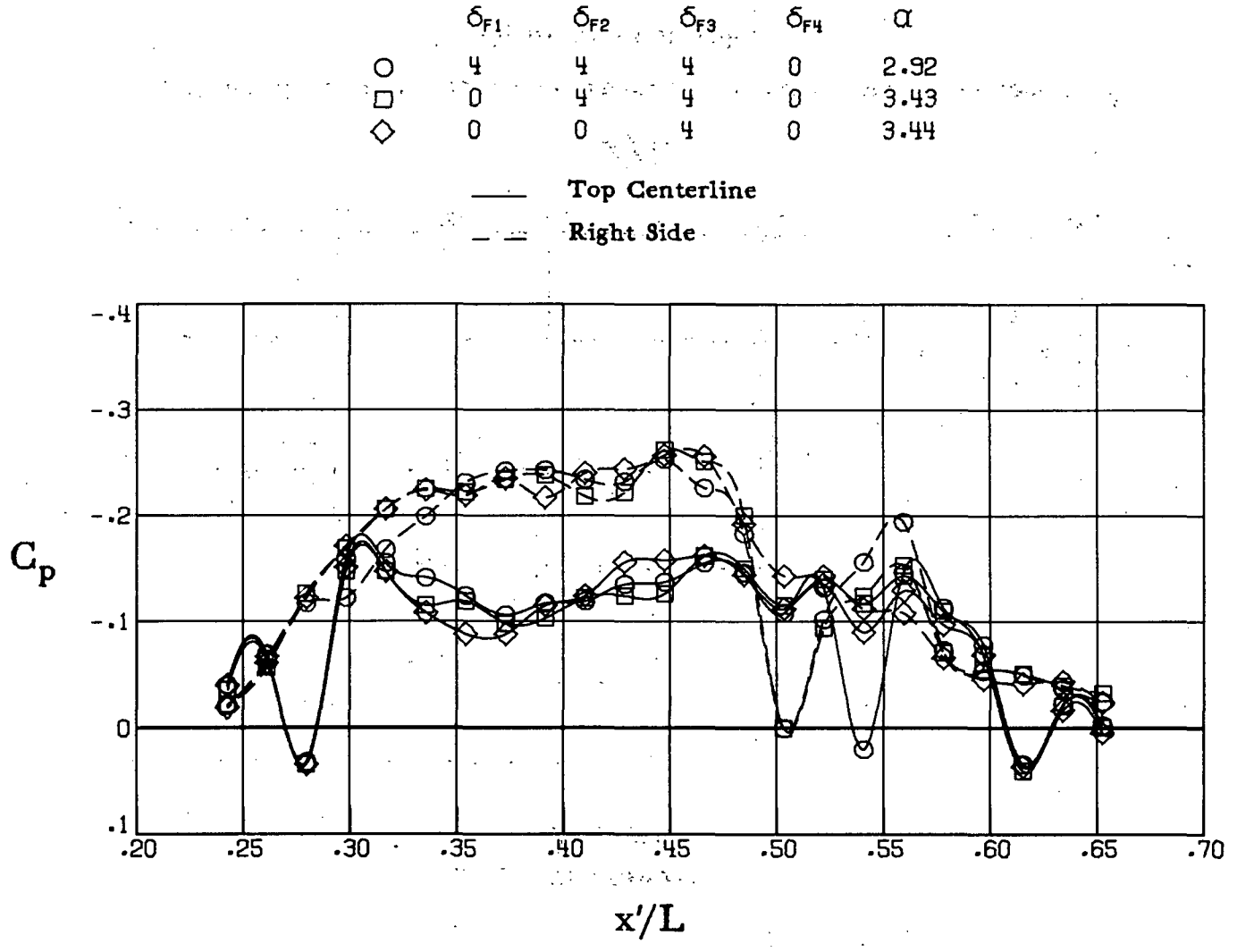
(d) Selected wing pressure distributions for control surface deflected 4^{o}.

Figure 51.- Continued.



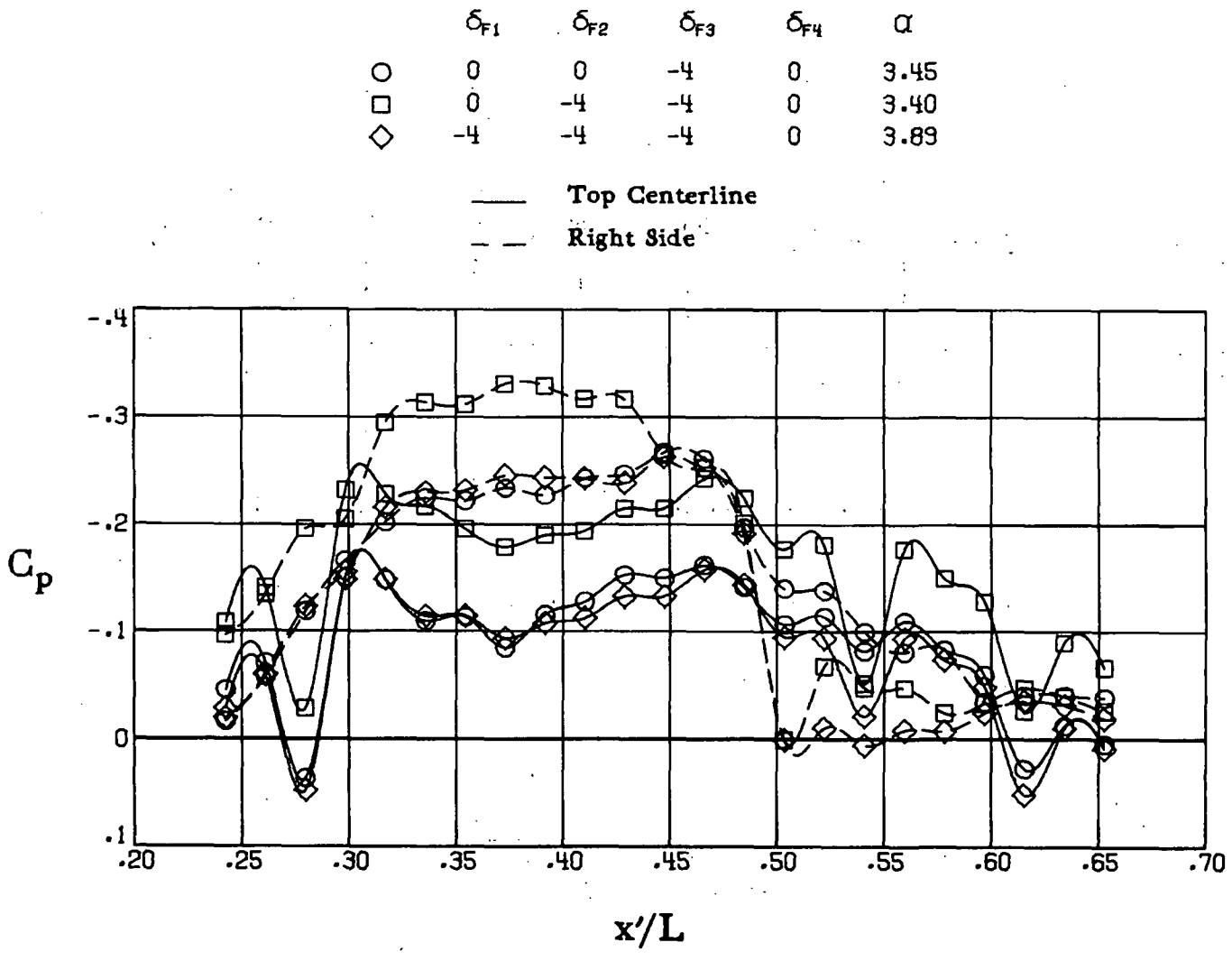
(e) Selected wing pressure distributions for control surface deflected -4°.

Figure 51.- Continued.



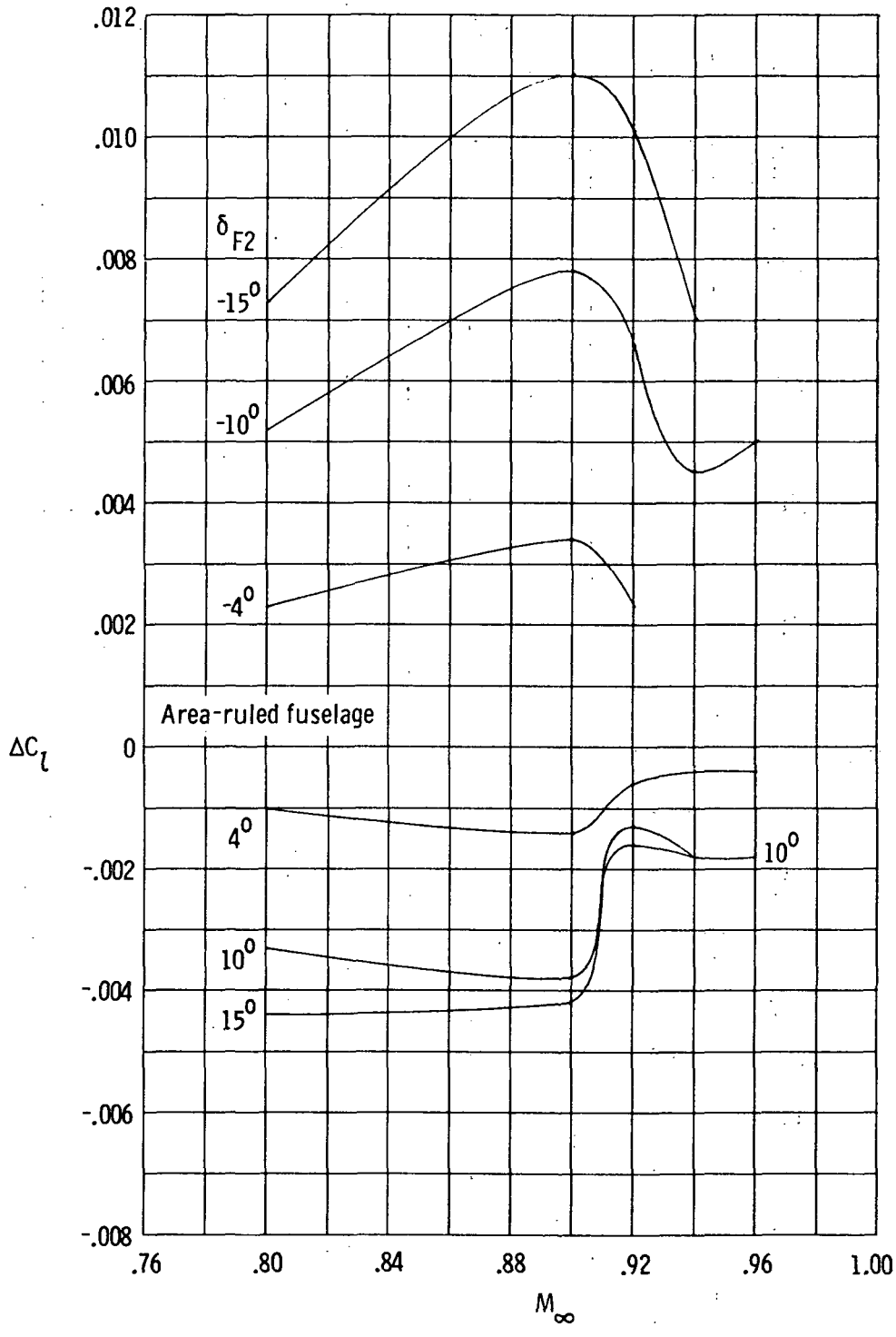
(f) Selected fuselage pressure distributions for control surface deflected 4^{o}.

Figure 51.- Continued.



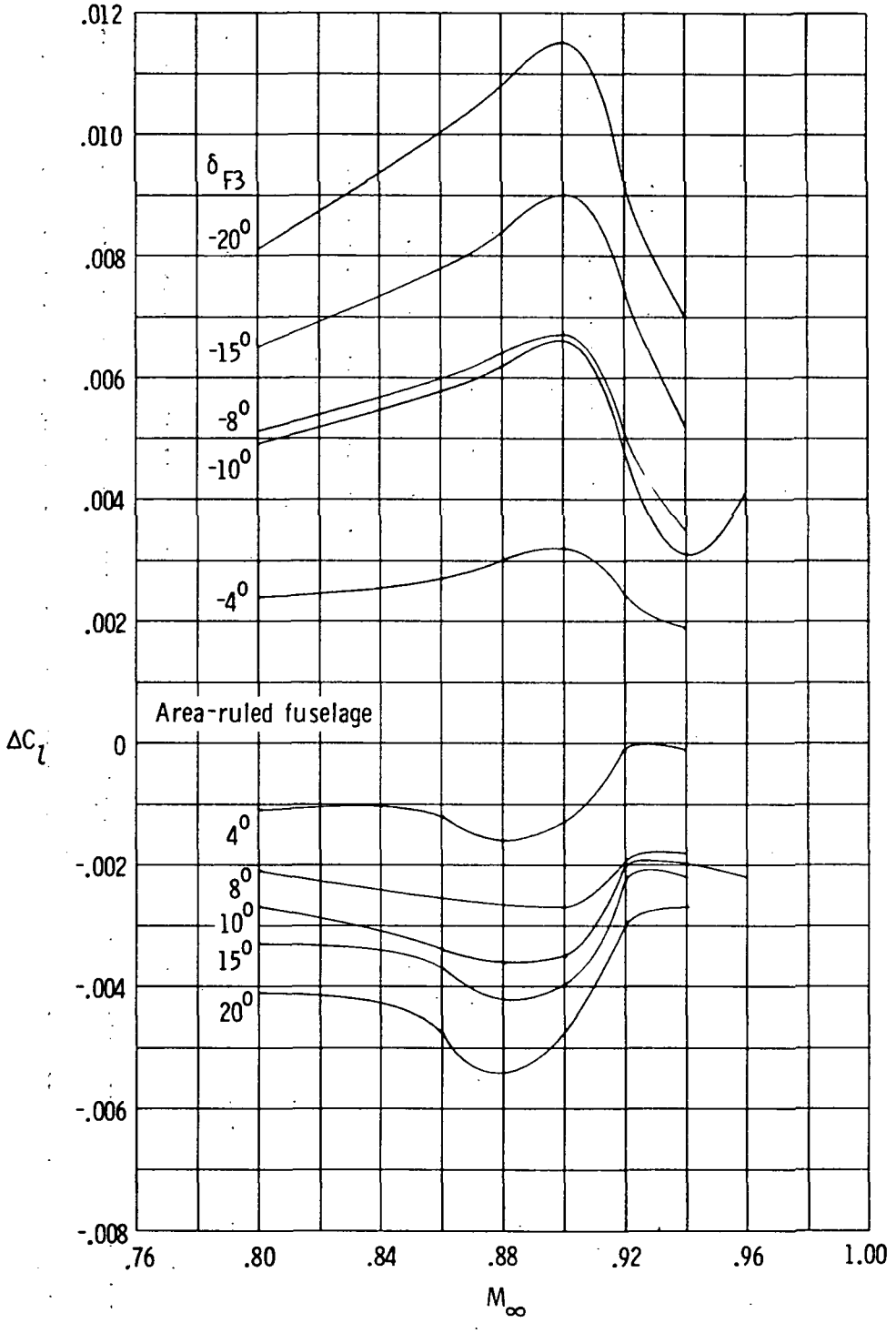
(g) Selected fuselage pressure distributions for control surface deflected -4°.

Figure 51.- Concluded.



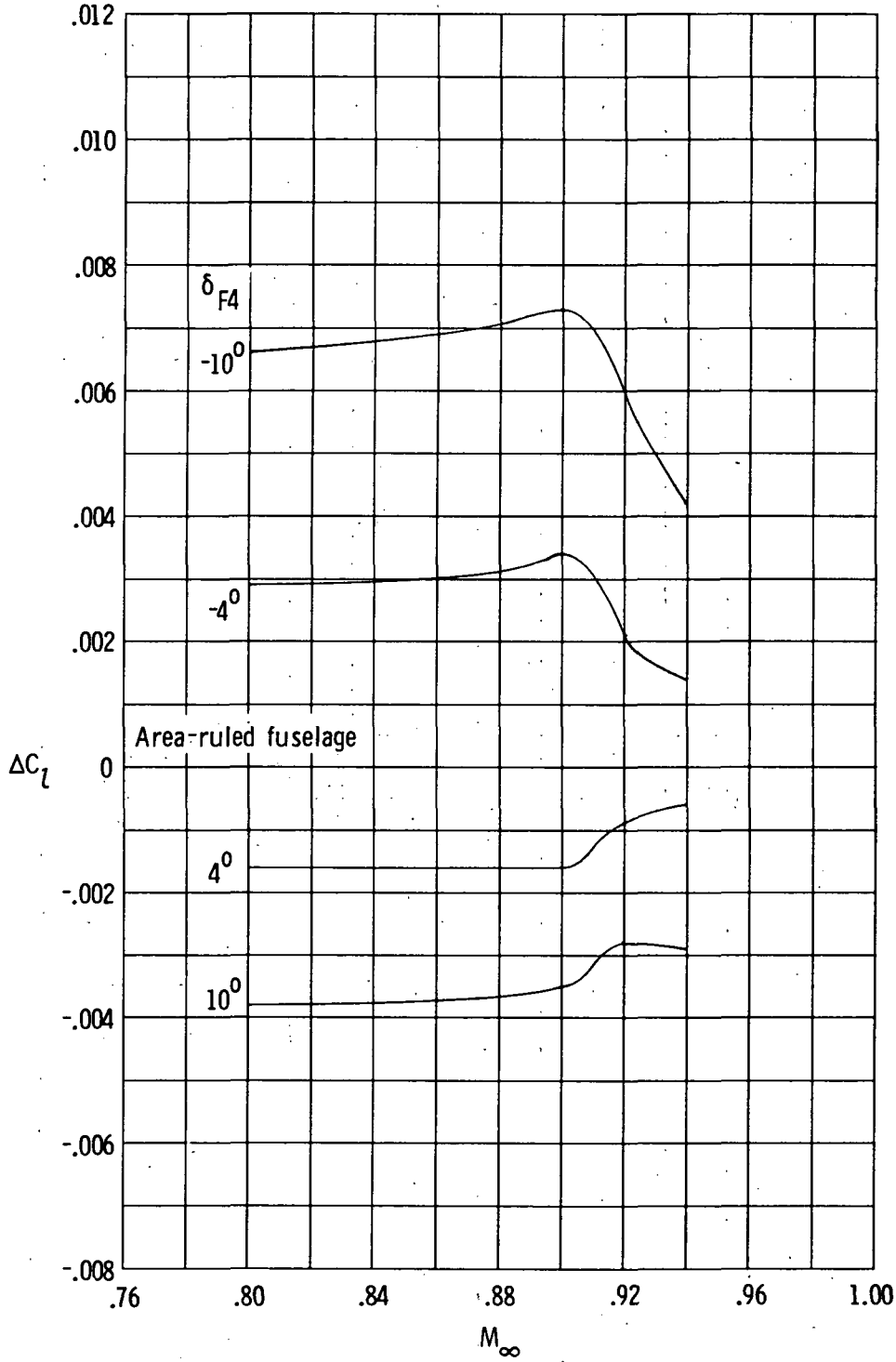
(a) Effect of control surface F_2.

Figure 52.- Summary of rolling moment due to control deflection as a function of Mach number. $\alpha = 3.5^\circ$.



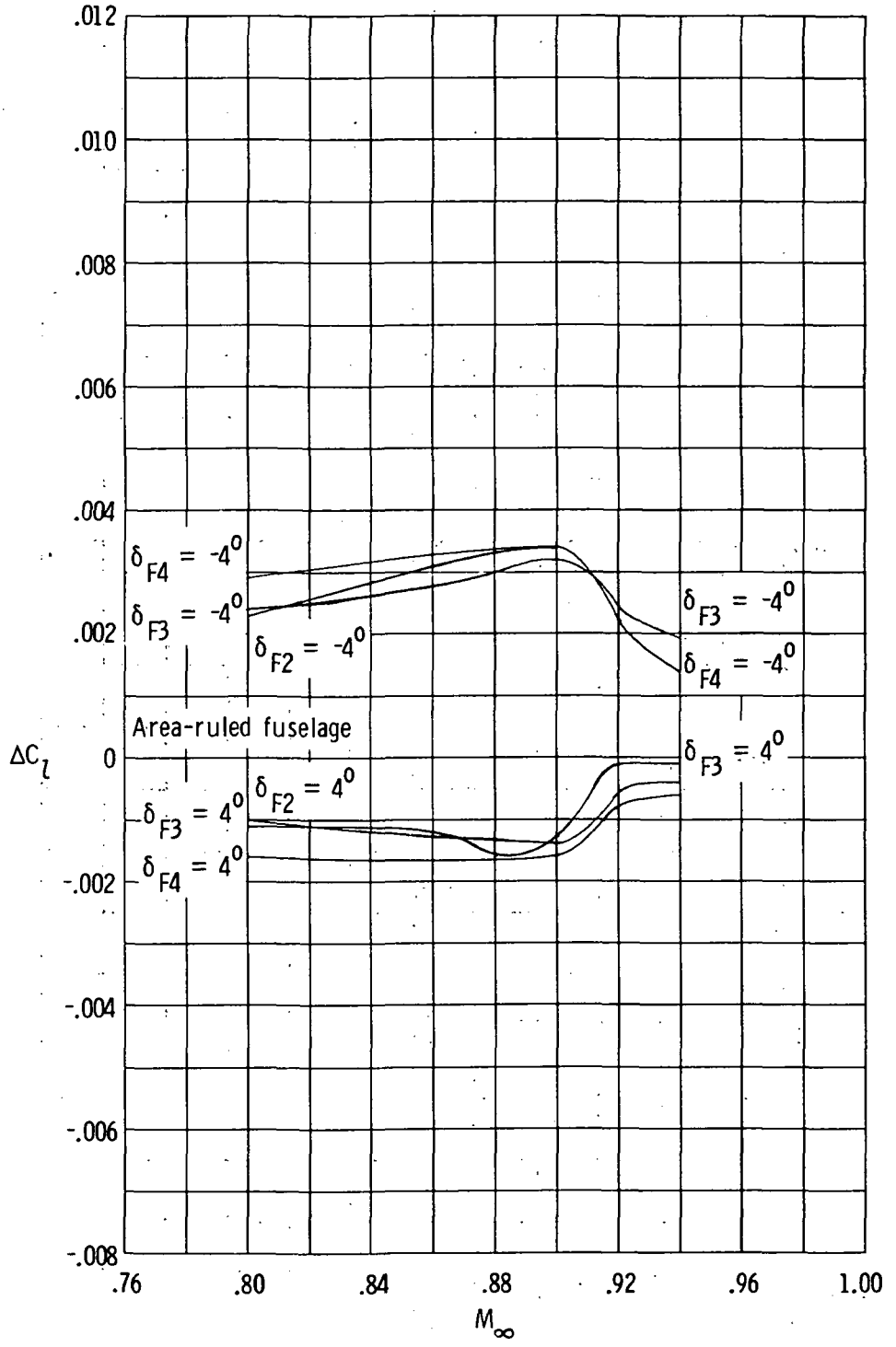
(b) Effect of control surface F_3.

Figure 52.- Continued.



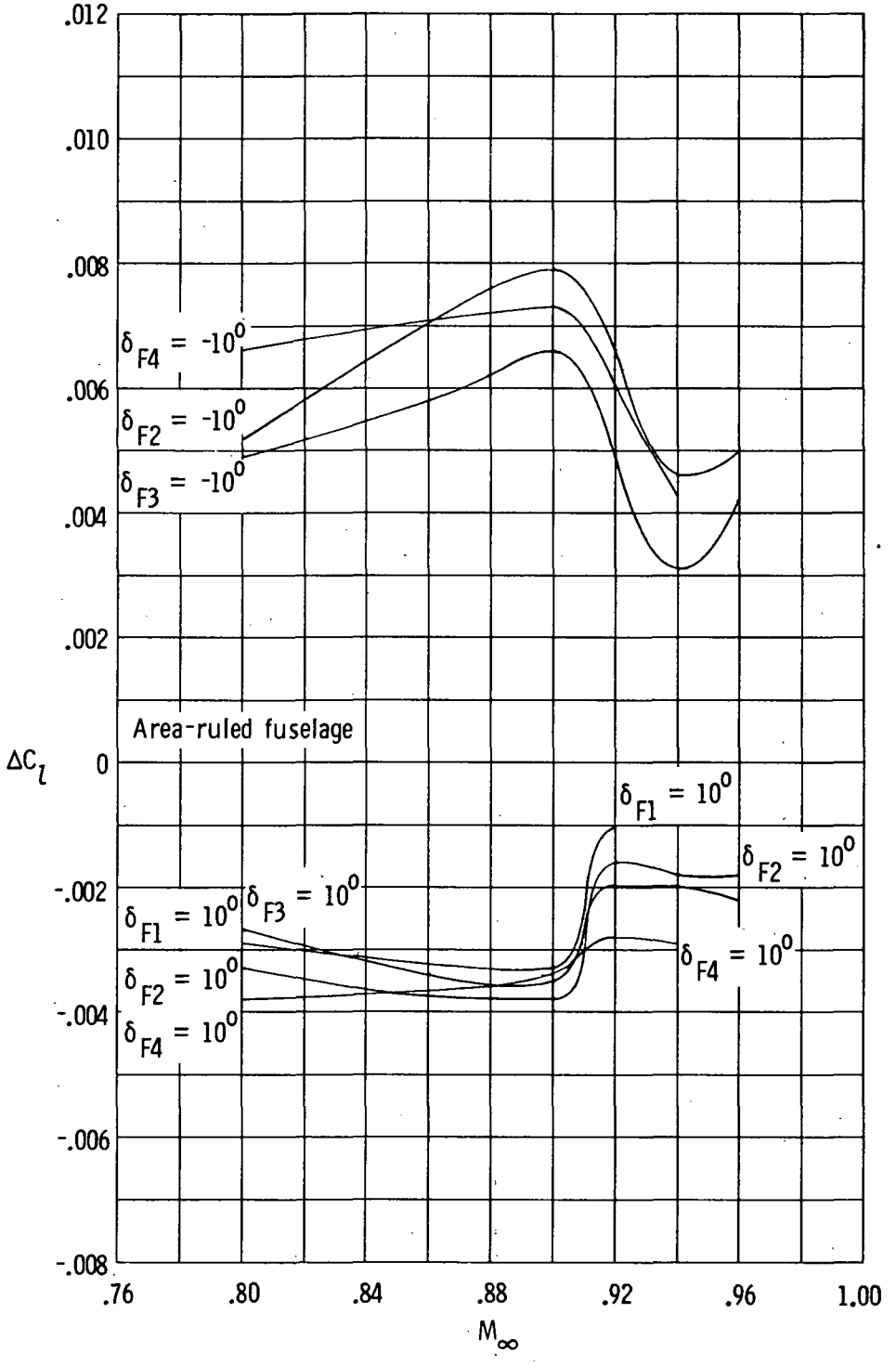
(c) Effect of control surface F_4.

Figure 52.- Continued.



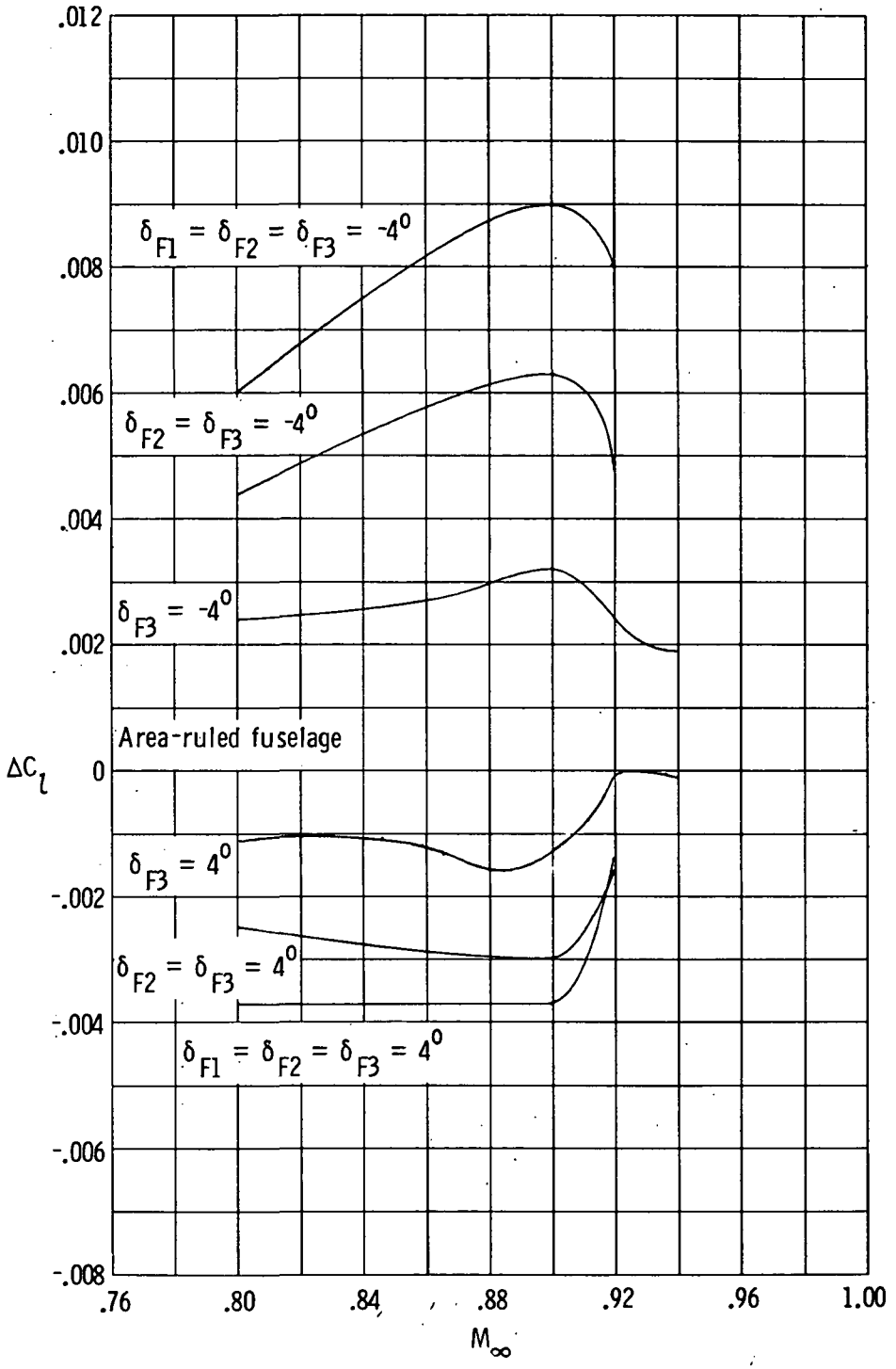
(d) Effect of control-surface spanwise location for $\delta_{Fi} = \pm 4^o$.

Figure 52.- Continued.



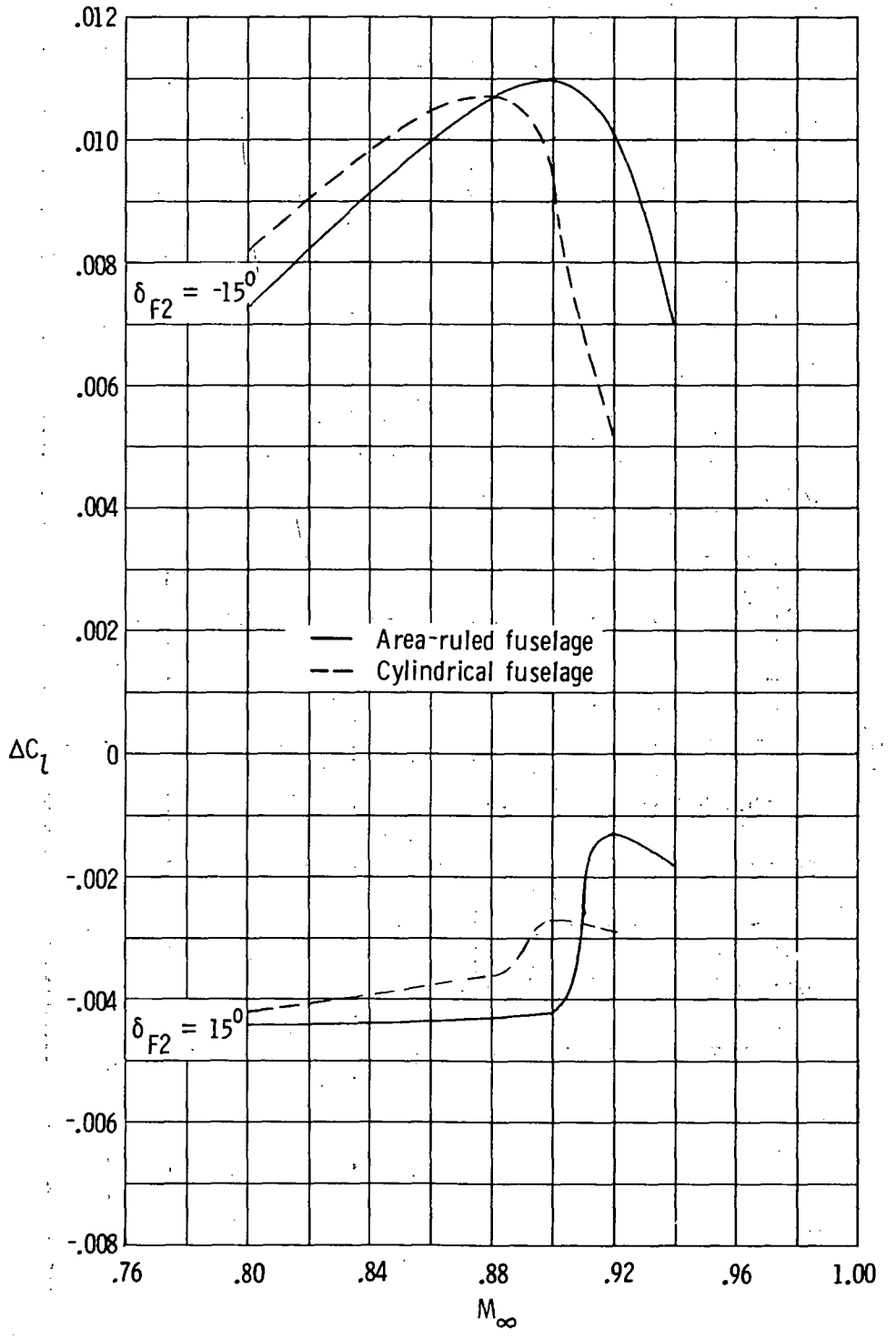
(e) Effect of control-surface spanwise location for $\delta_{Fi} = \pm 10^o$.

Figure 52.- Continued.



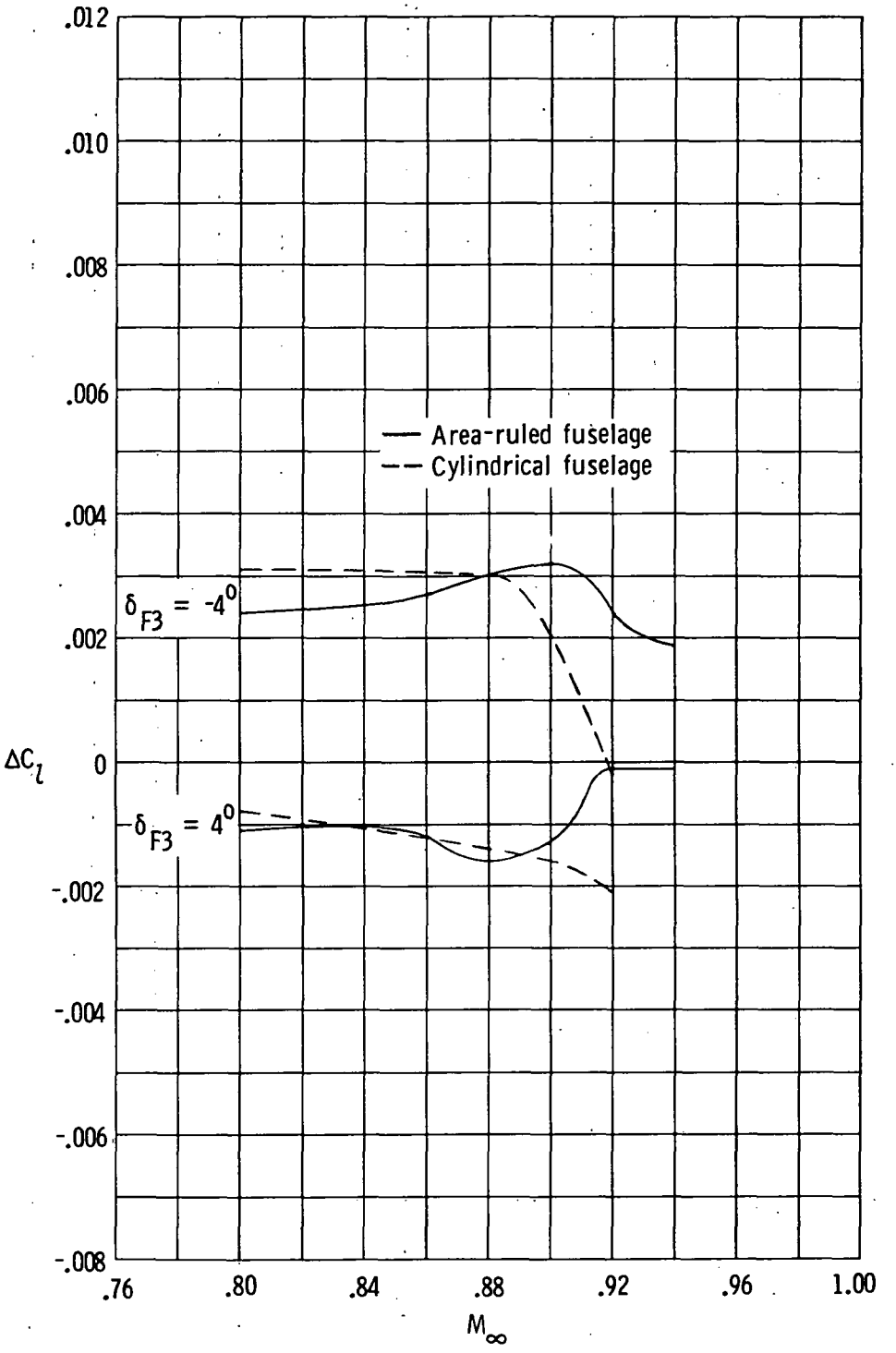
(f) Effect of control-surface span; $\delta_{Fi} = \pm 4^0$.

Figure 52.- Continued.



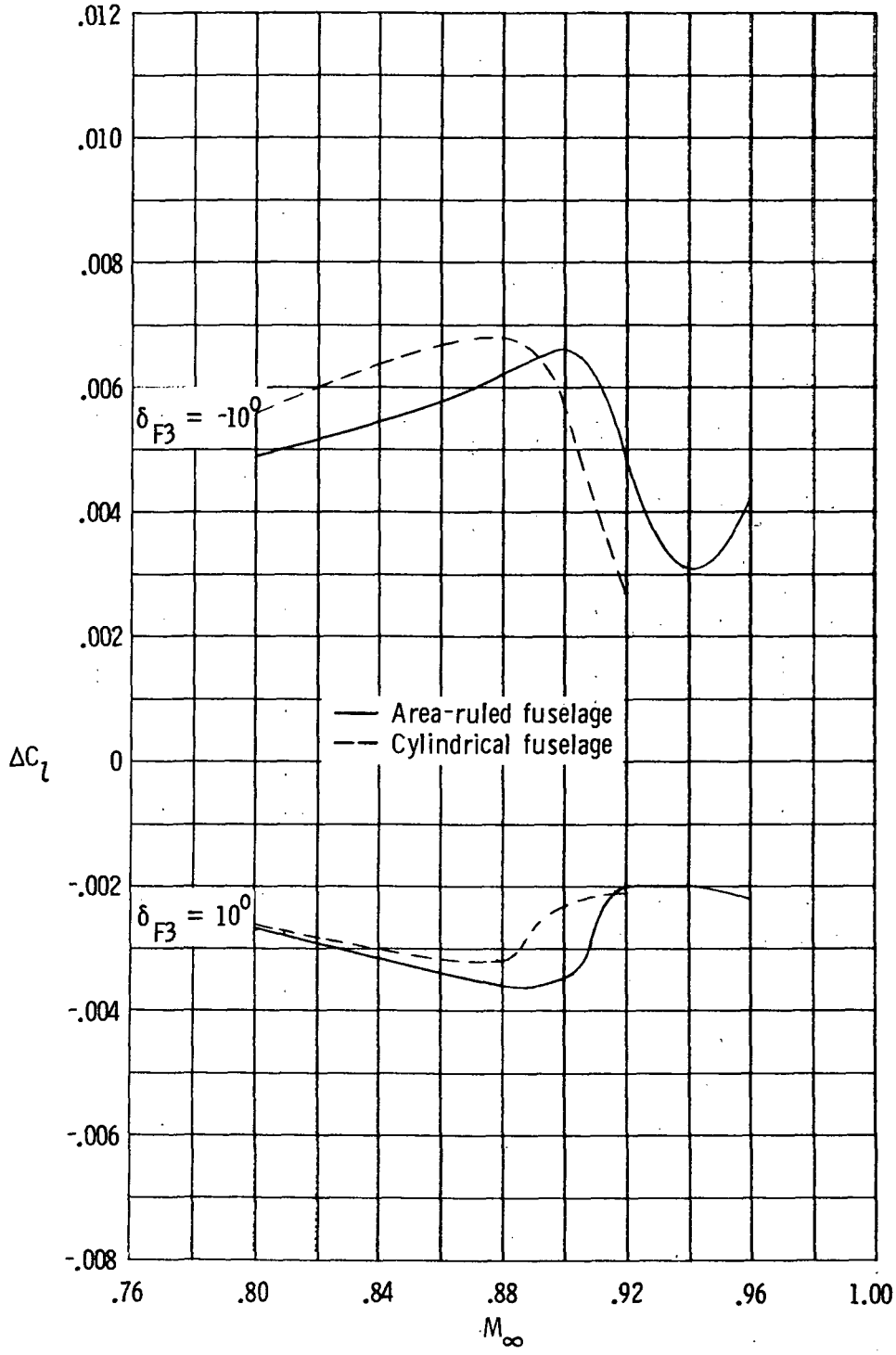
(g) Results for area-ruled and cylindrical fuselages for $\delta_{F2} = \pm 15^0$.

Figure 52.- Continued.



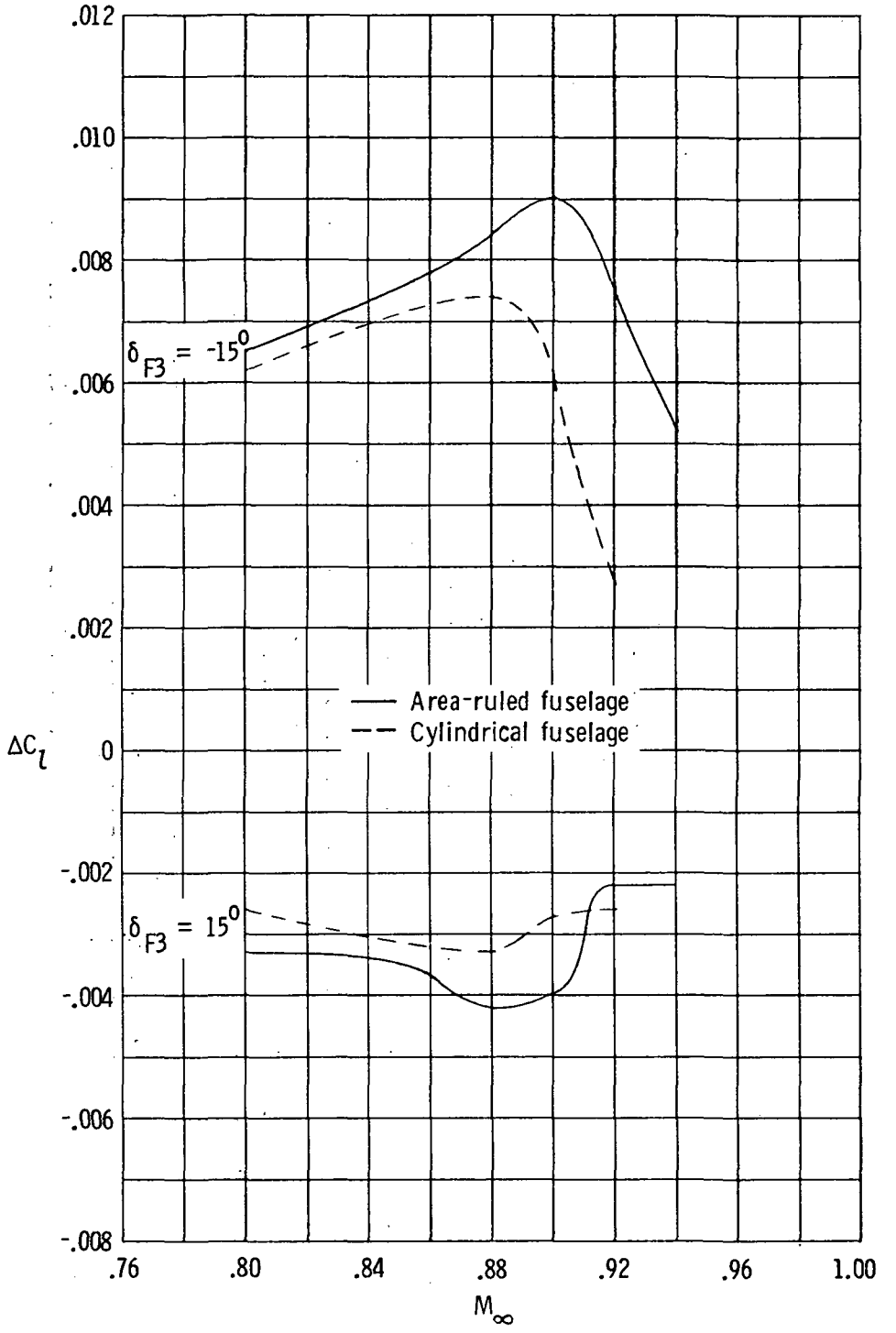
(h) Results for area-ruled and cylindrical fuselages for $\delta_{F3} = \pm 4^o$.

Figure 52.- Continued.



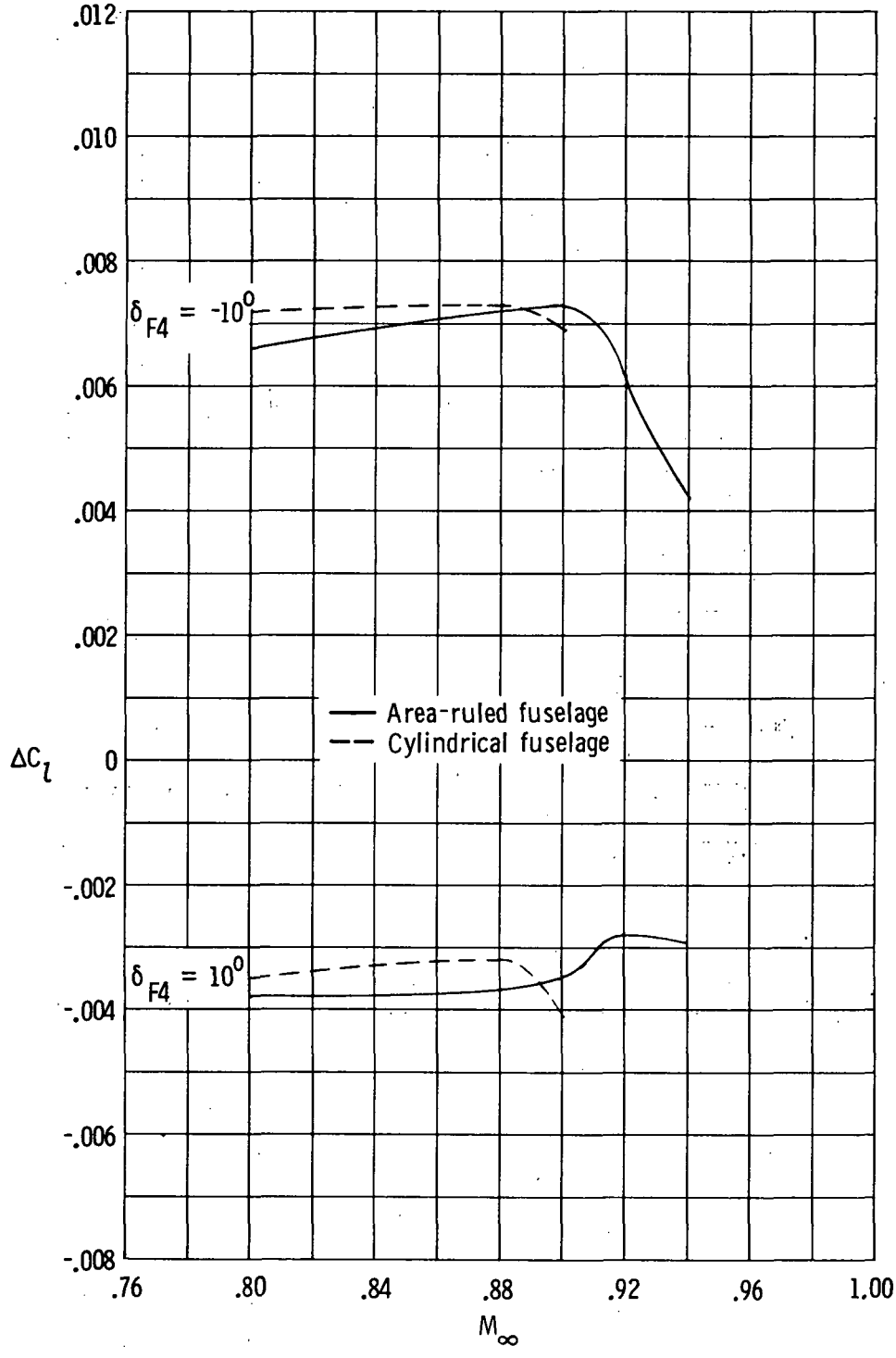
(i) Results for area-ruled and cylindrical fuselages for $\delta_{F3} = \pm 10^o$.

Figure 52.- Continued.



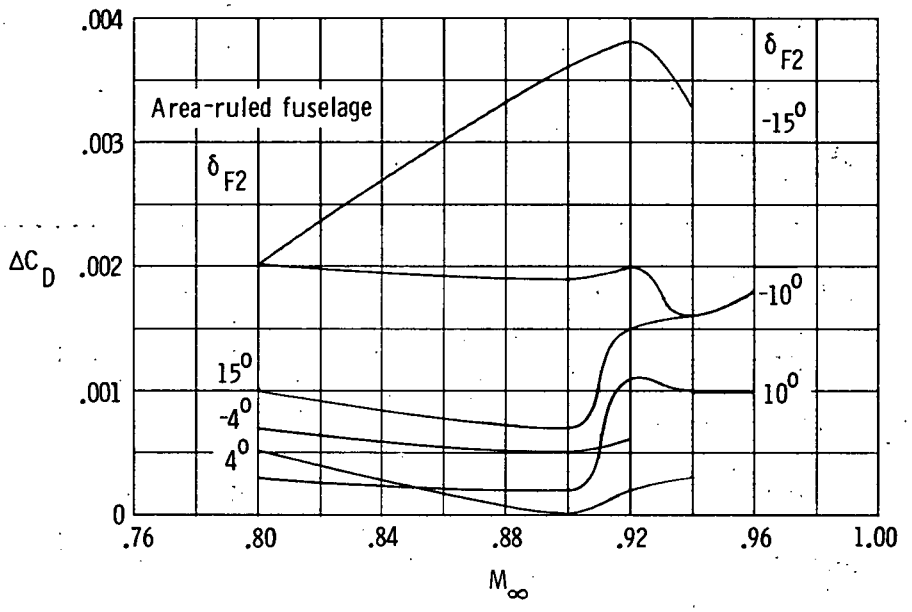
(j) Results for area-ruled and cylindrical fuselages for $\delta_{F3} = \pm 15^o$.

Figure 52.- Continued.



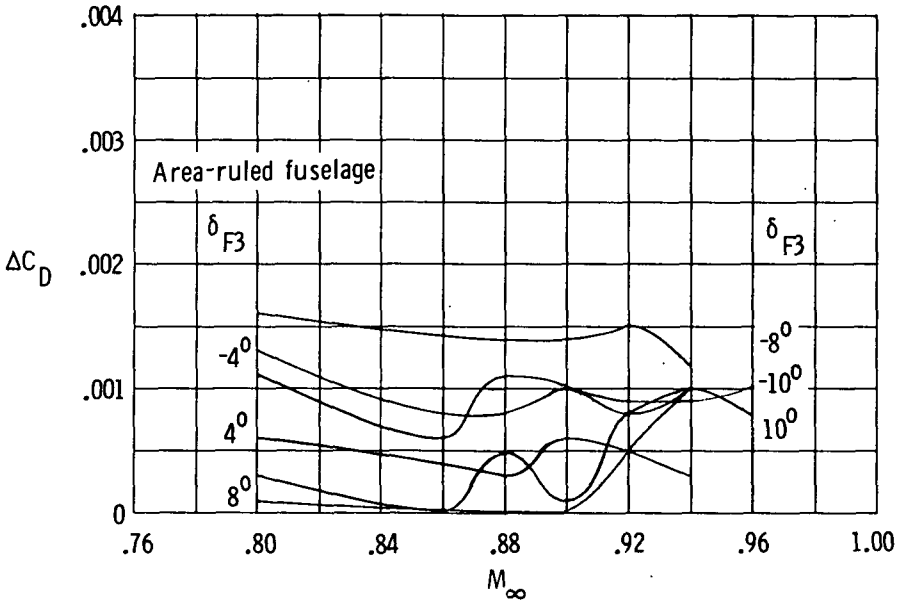
(k) Results for area-ruled and cylindrical fuselages for $\delta_{F4} = \pm 10^o$.

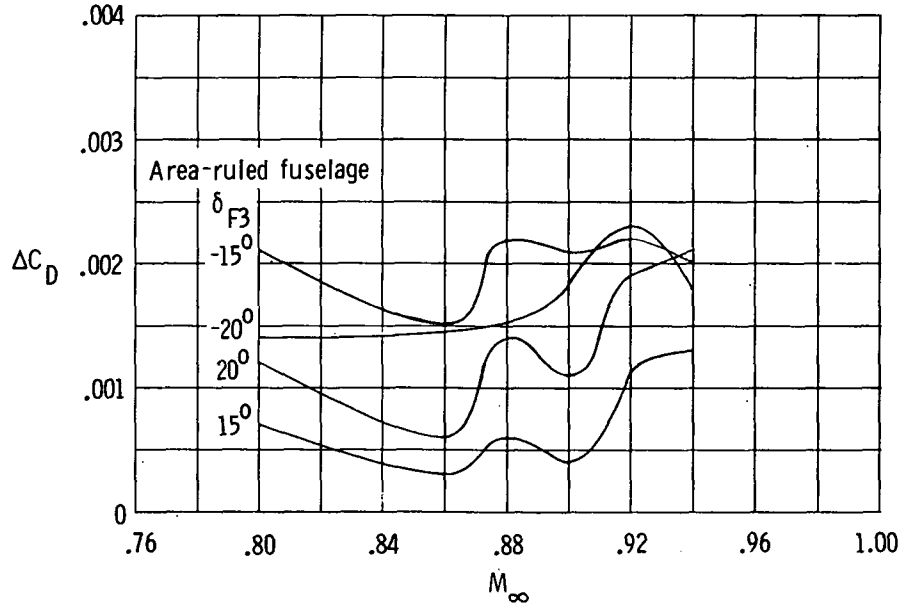
Figure 52.- Concluded.



(a) Effect of control surface F_2.

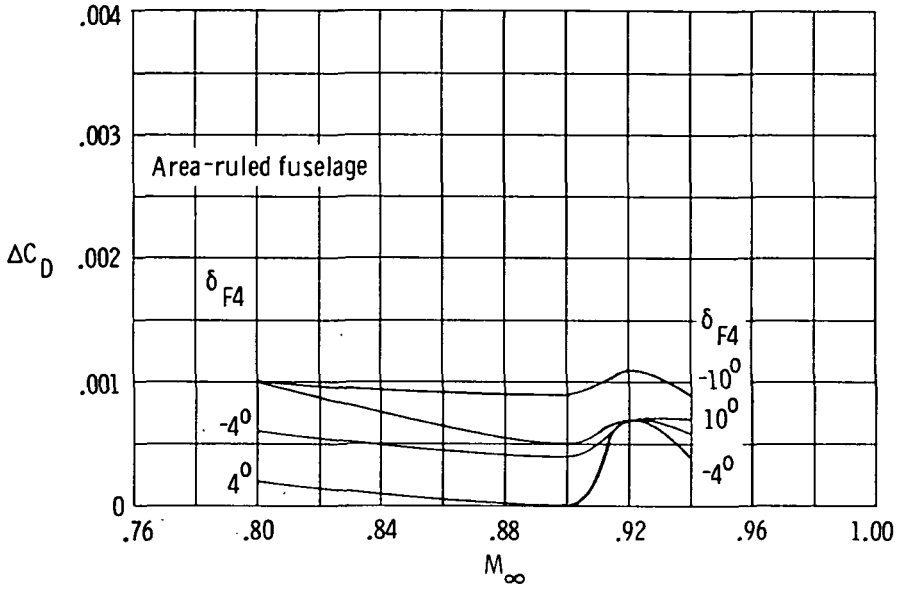
Figure 53.- Summary of drag due to control deflection as a function of Mach number. $C_L = 0.50$.



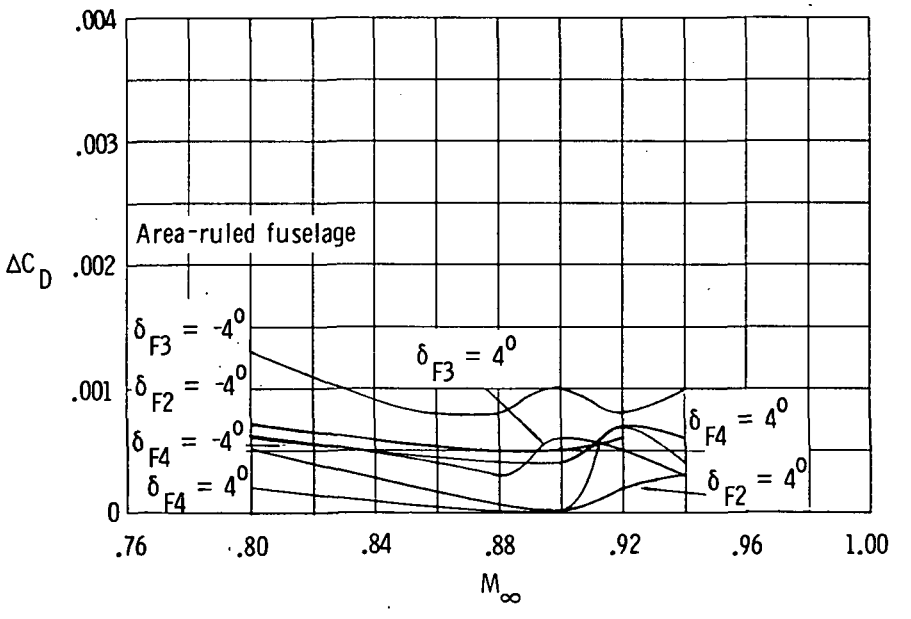


(b) Effect of control surface F_3.

Figure 53.- Continued.

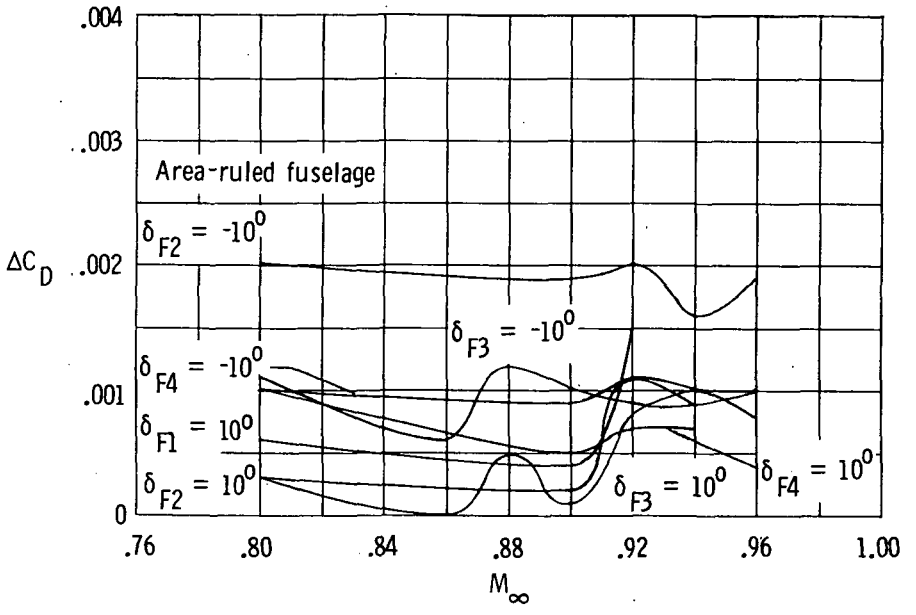


(c) Effect of control surface F_4.

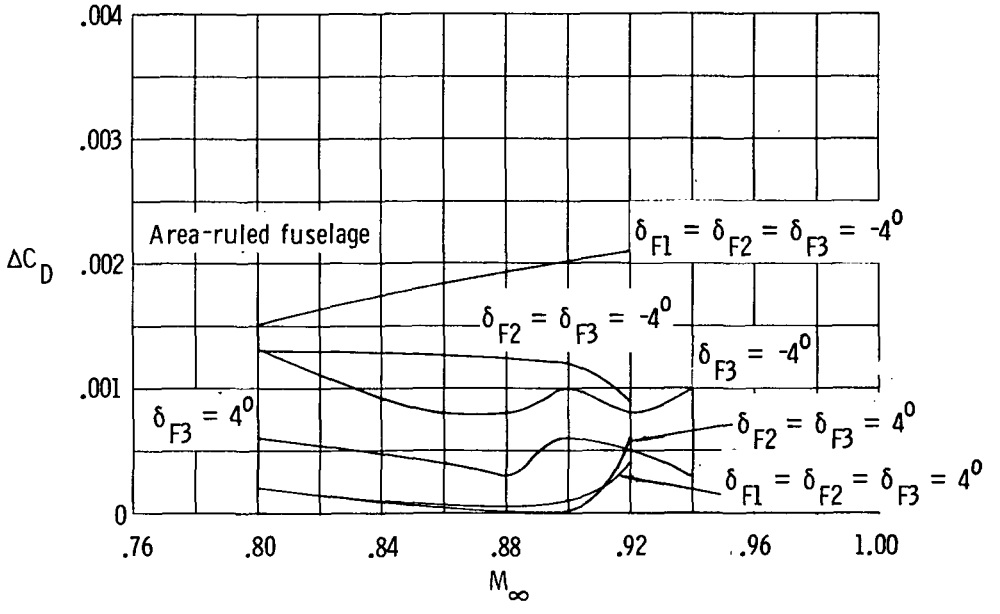


(d) Effect of control-surface spanwise location for $\delta_{Fi} = \pm 4°$.

Figure 53.- Continued.

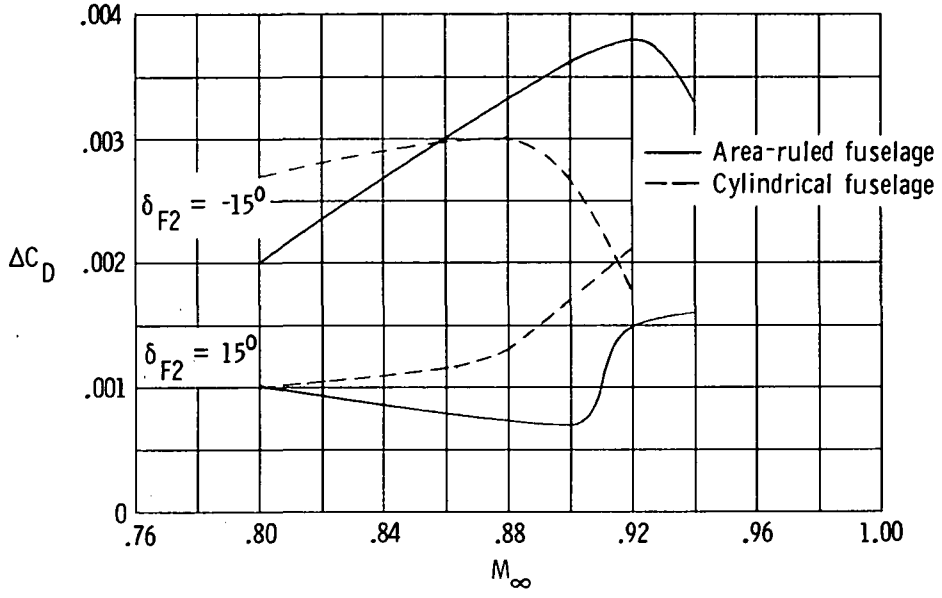


(e) Effect of control-surface spanwise location for $\delta_{Fi} = \pm 10^o$.

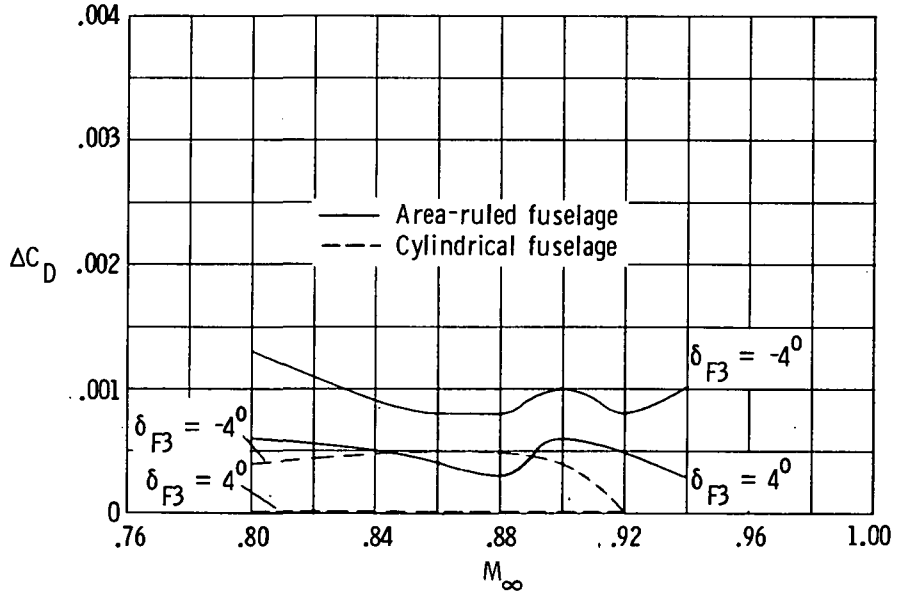


(f) Effect of control-surface span; $\delta_{Fi} = \pm 4^o$.

Figure 53.- Continued.

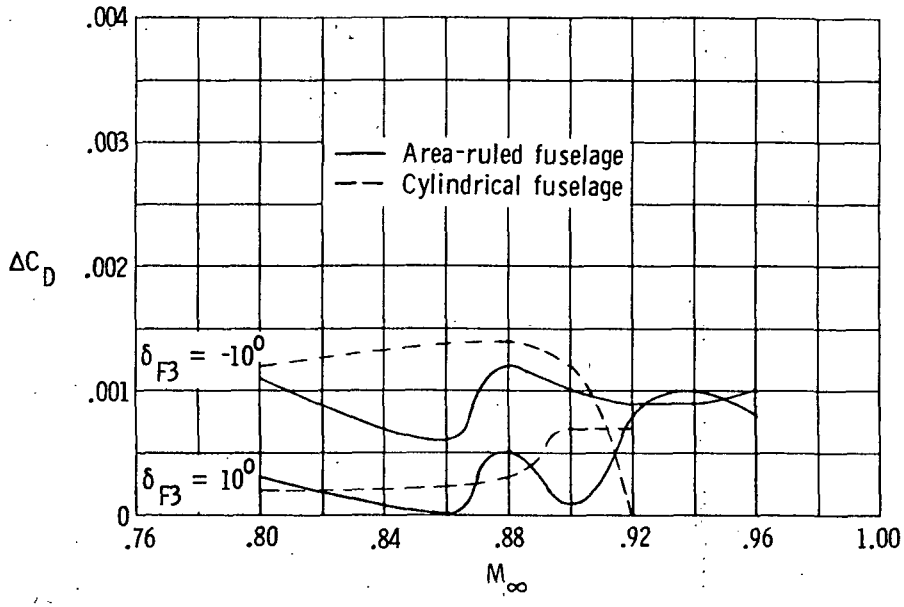


(g) Results for area-ruled and cylindrical fuselages for $\delta_{F2} = \pm 15^o$.

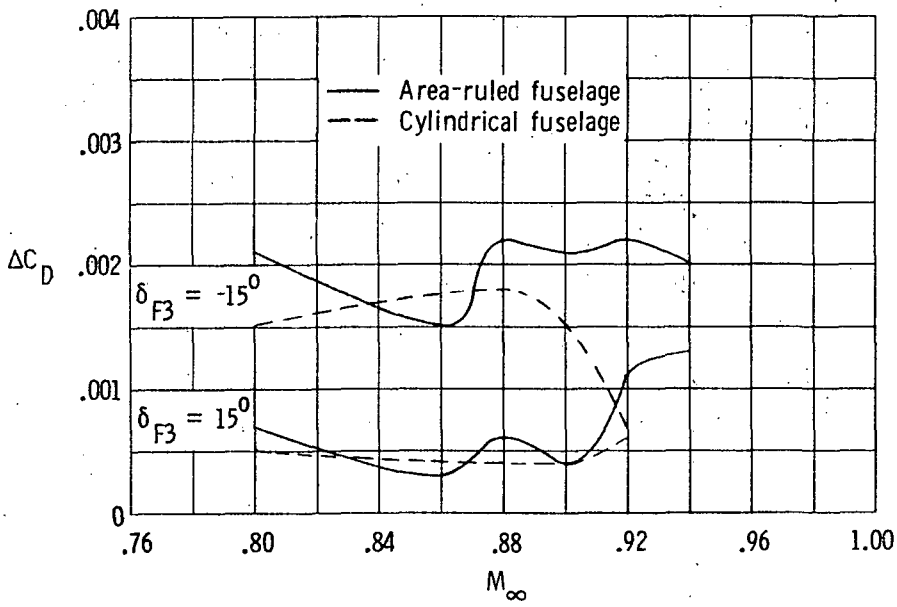


(h) Results for area-ruled and cylindrical fuselages for $\delta_{F3} = \pm 4^o$.

Figure 53.- Continued.

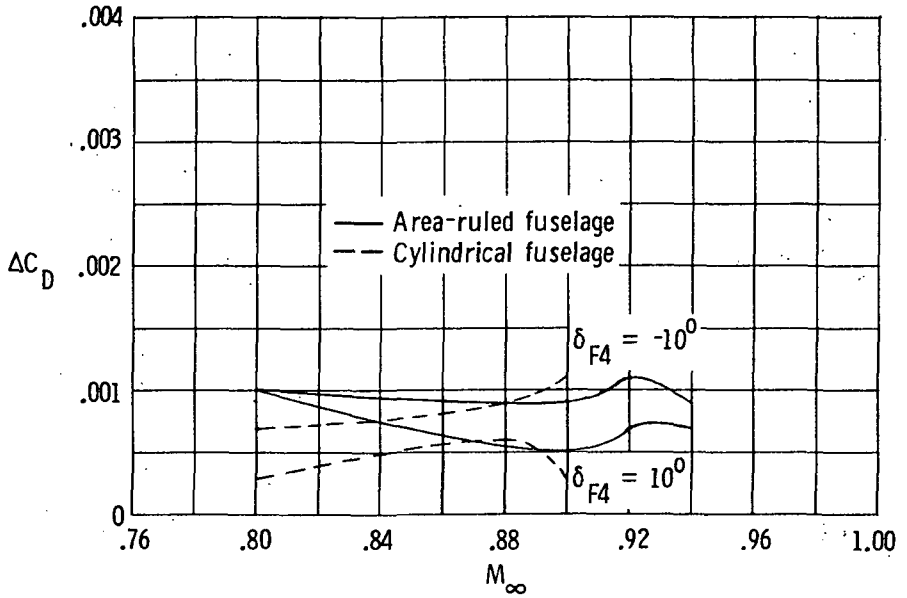


(i) Results for area-ruled and cylindrical fuselages for $\delta_{F3} = \pm 10^o$.



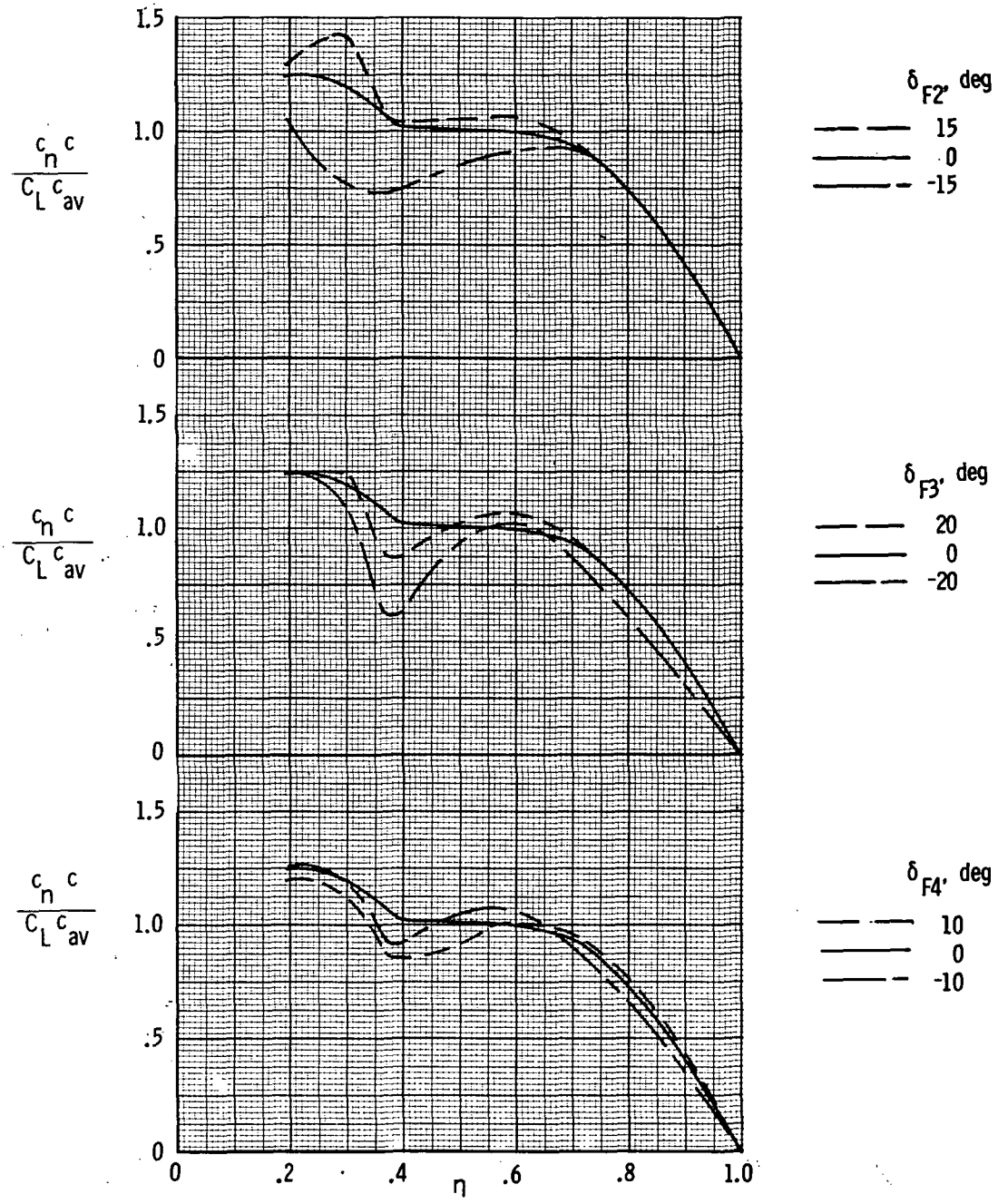
(j) Results for area-ruled and cylindrical fuselages for $\delta_{F3} = \pm 15^o$.

Figure 53.- Continued.



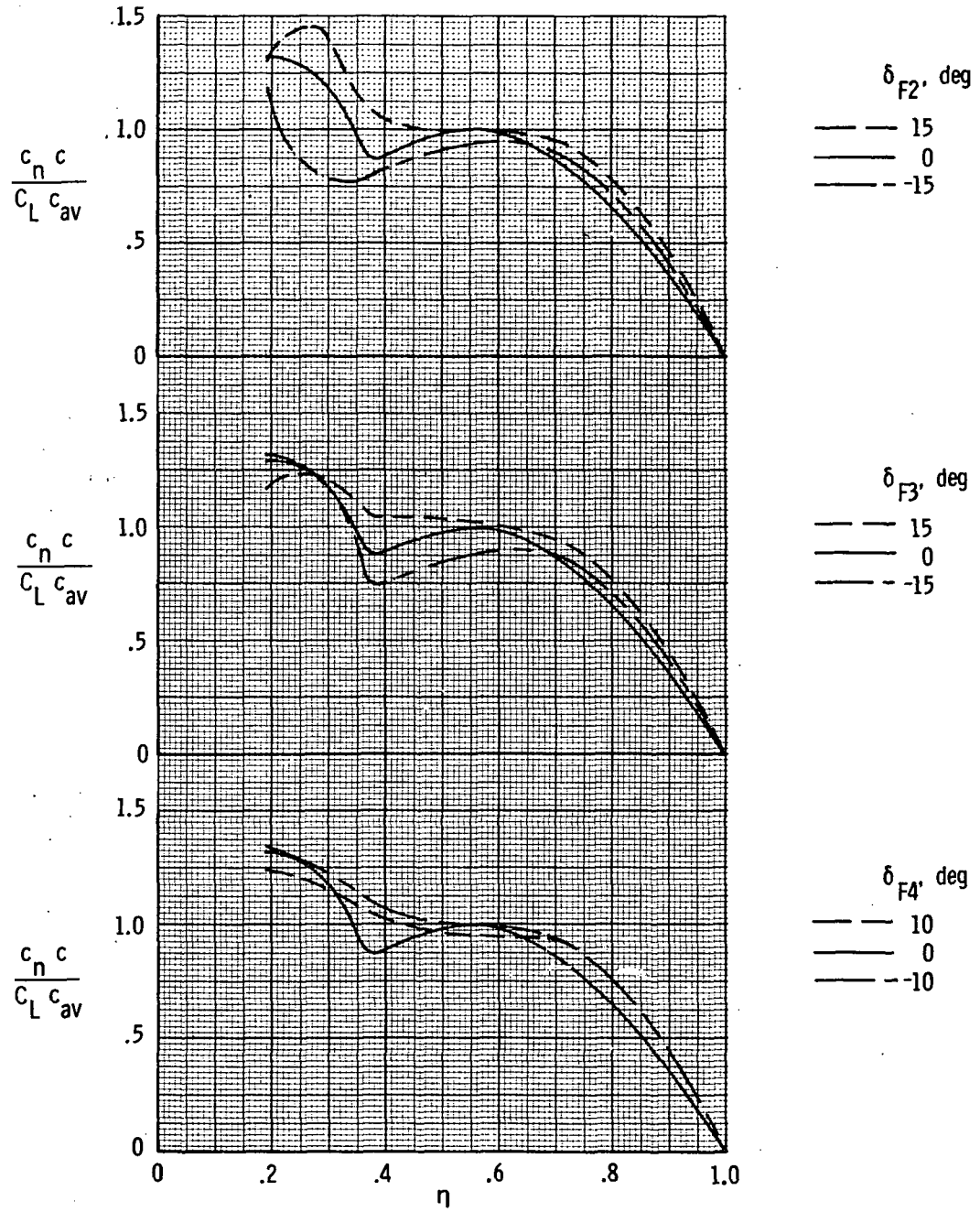
(k) Results for area-ruled and cylindrical fuselages for $\delta_{F4} = \pm 10^o$.

Figure 53.- Concluded.



(a) Area-ruled fuselage.

Figure 54.- Spanwise load distributions near design lift $(C_L \approx 0.50)$ with various control surface deflections. Deflection angles given only for deflected controls (other controls undeflected). $M_\infty = 0.90$.



(b) Cylindrical fuselage.

Figure 54.- Concluded.

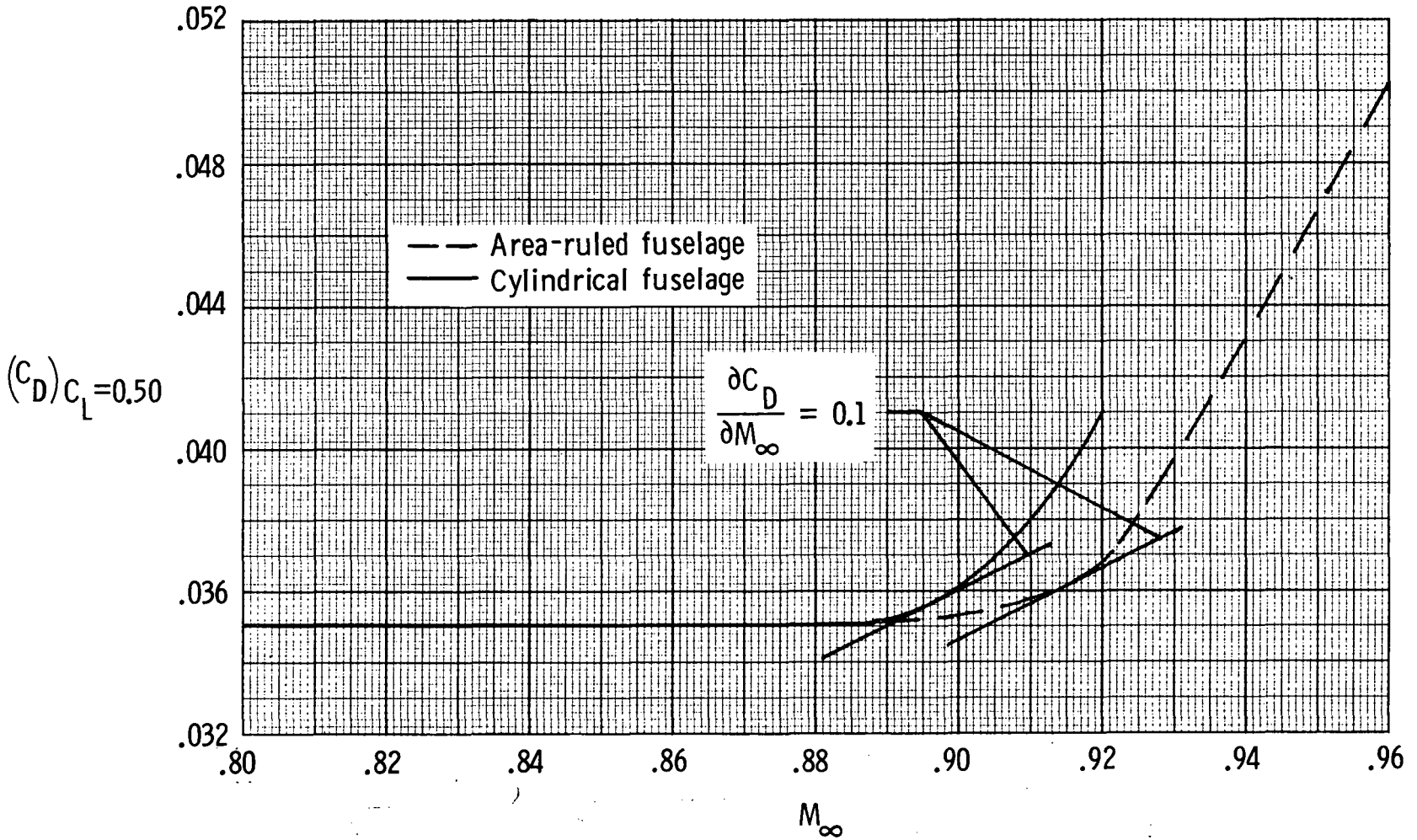
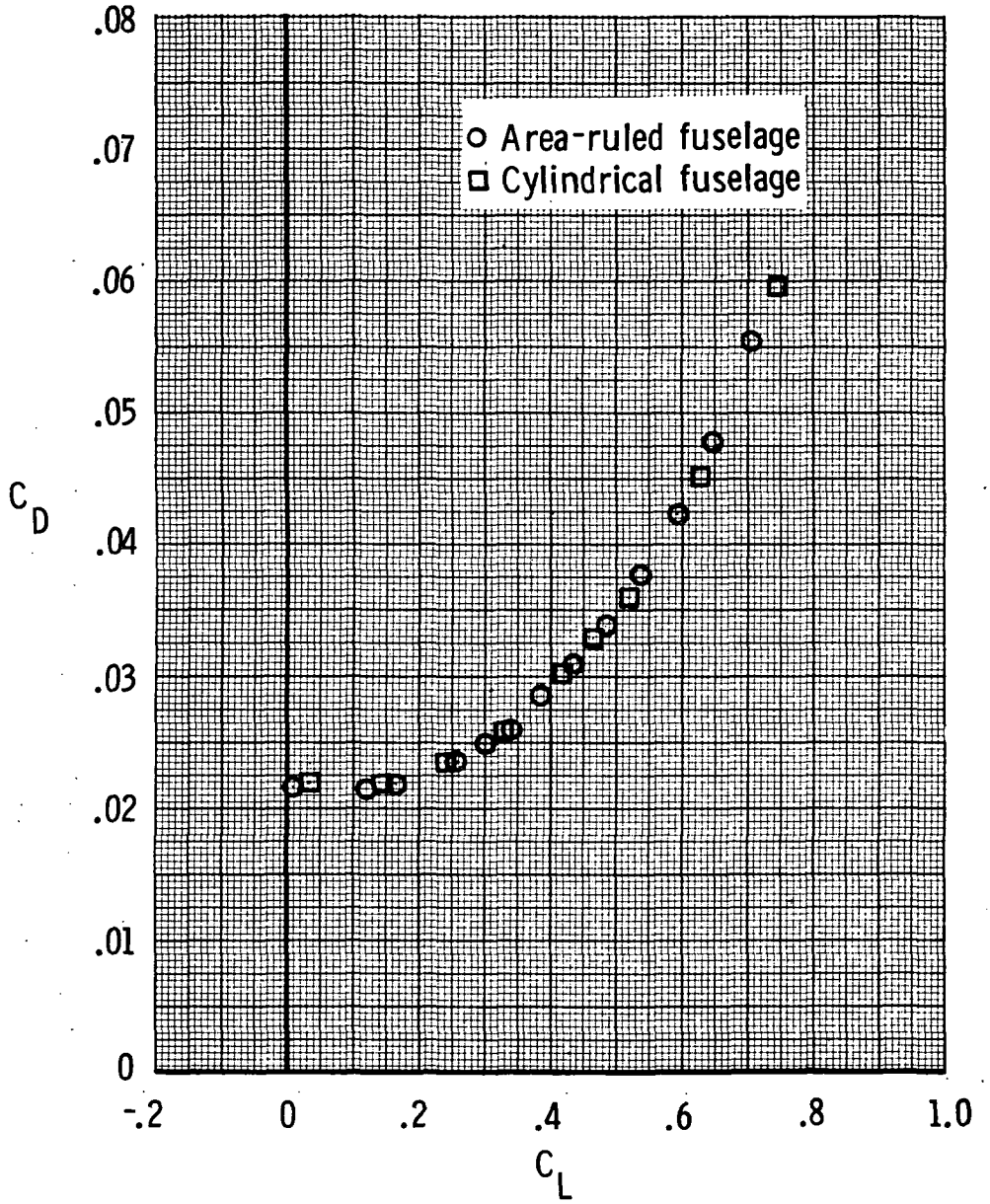
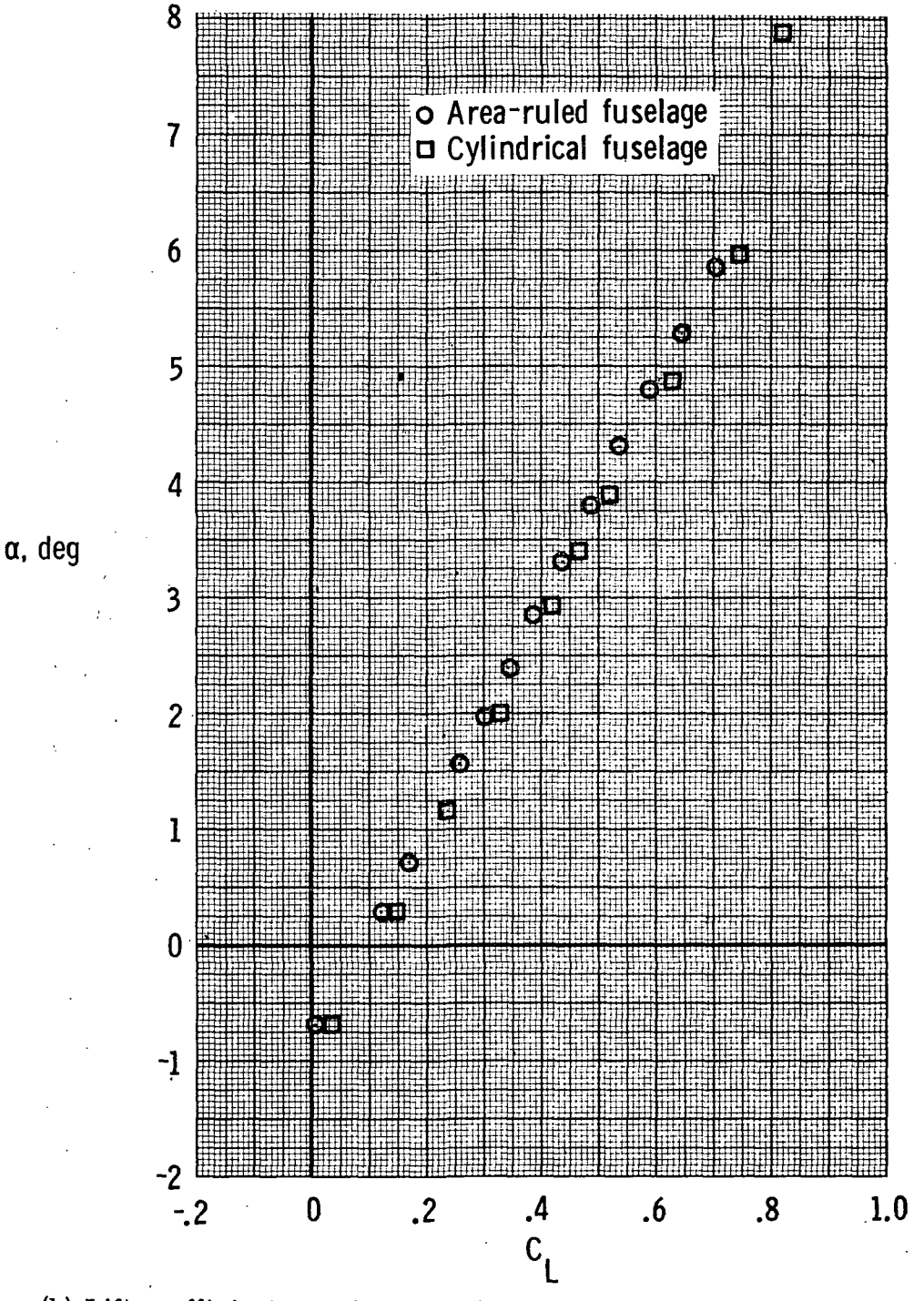


Figure 55.- Variation of drag coefficient with Mach number at $C_L = 0.50$ for area-ruled and cylindrical configurations. Control surfaces undeflected.



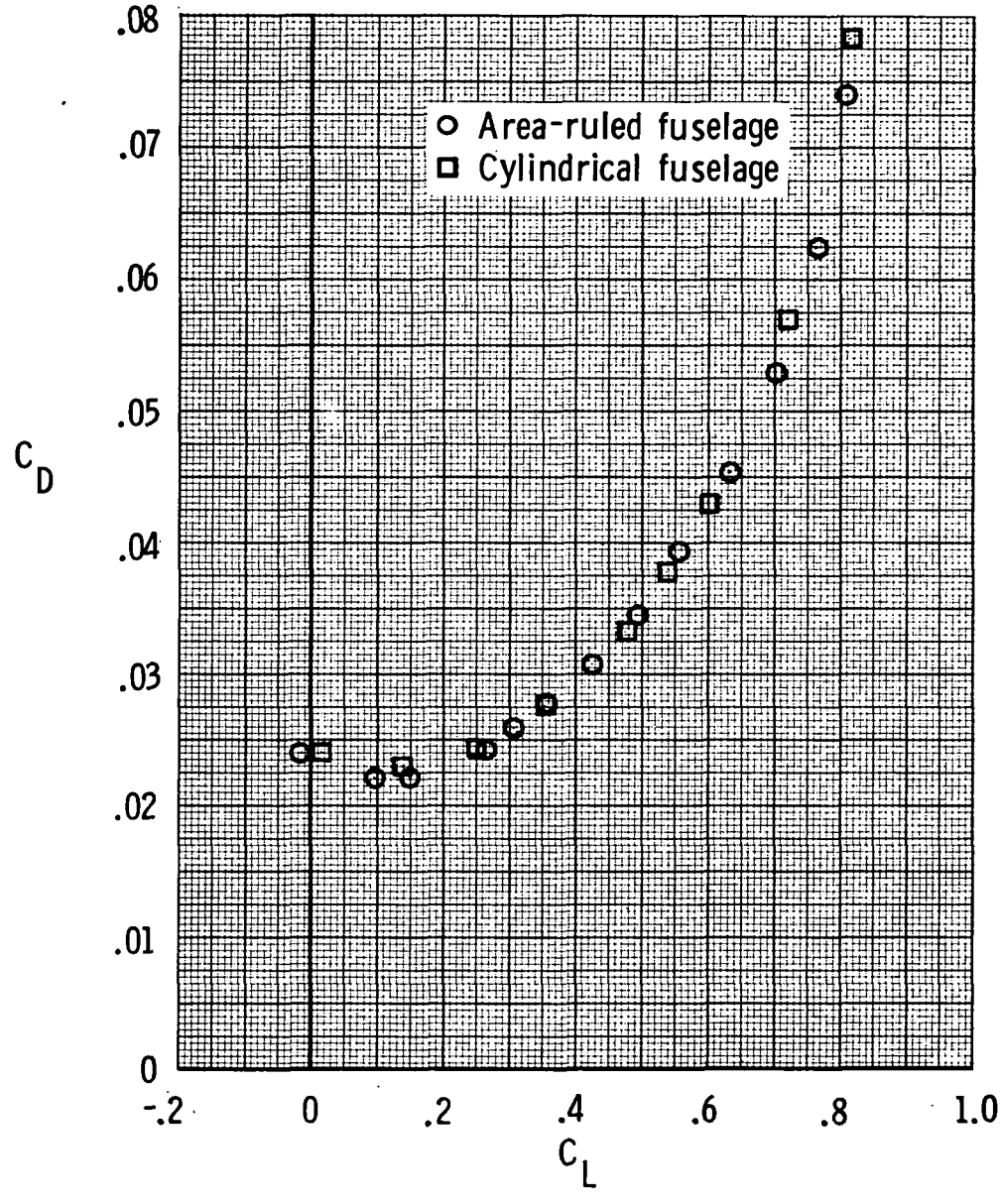
(a) Drag coefficient as a function of lift coefficient at $M_\infty = 0.80$.

Figure 56.- Comparison of longitudinal aerodynamic force characteristics of area-ruled and cylindrical configurations with zero control surface deflections.



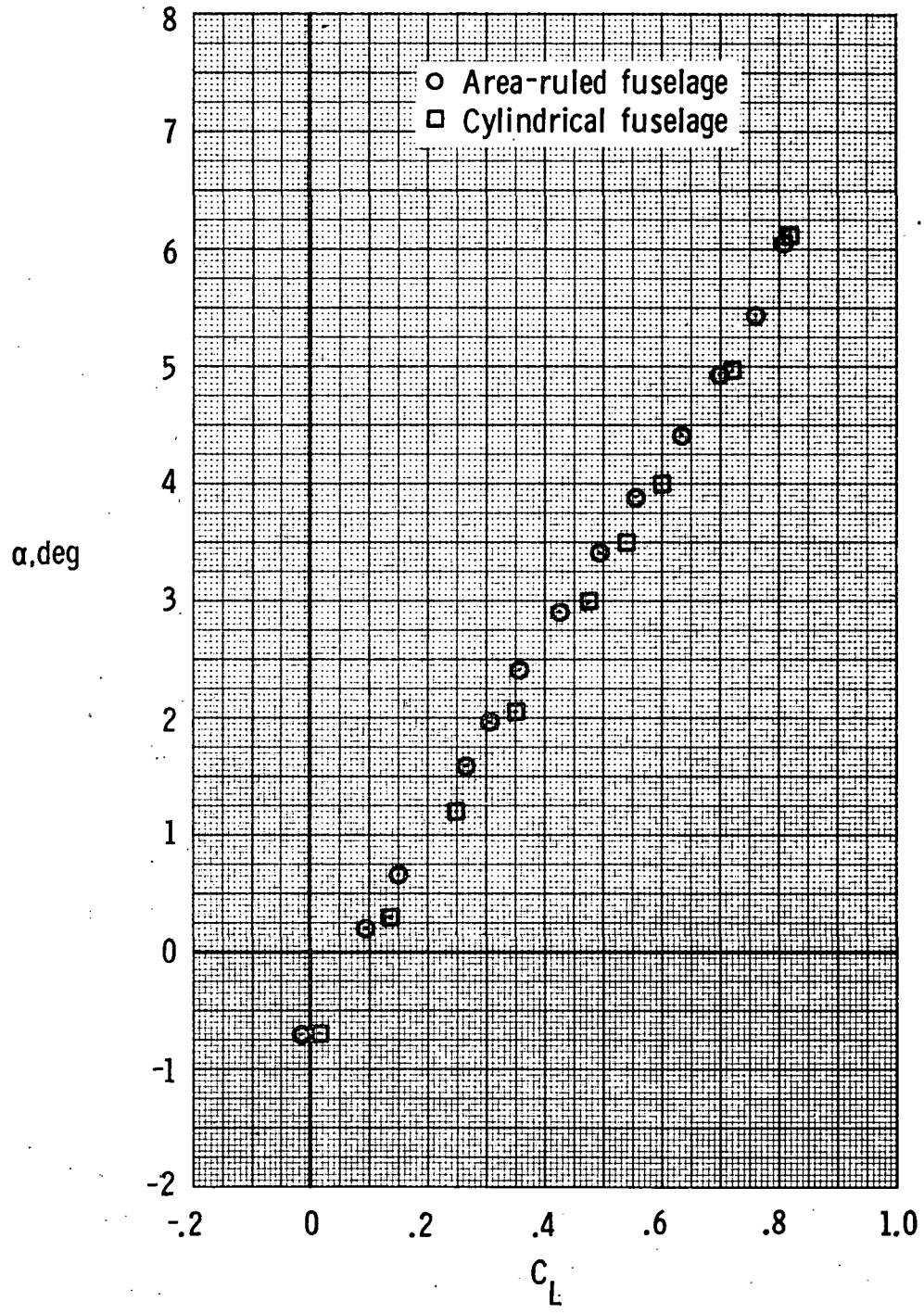
(b) Lift coefficient as a function of angle of attack at $M_\infty = 0.80$.

Figure 56.- Continued.



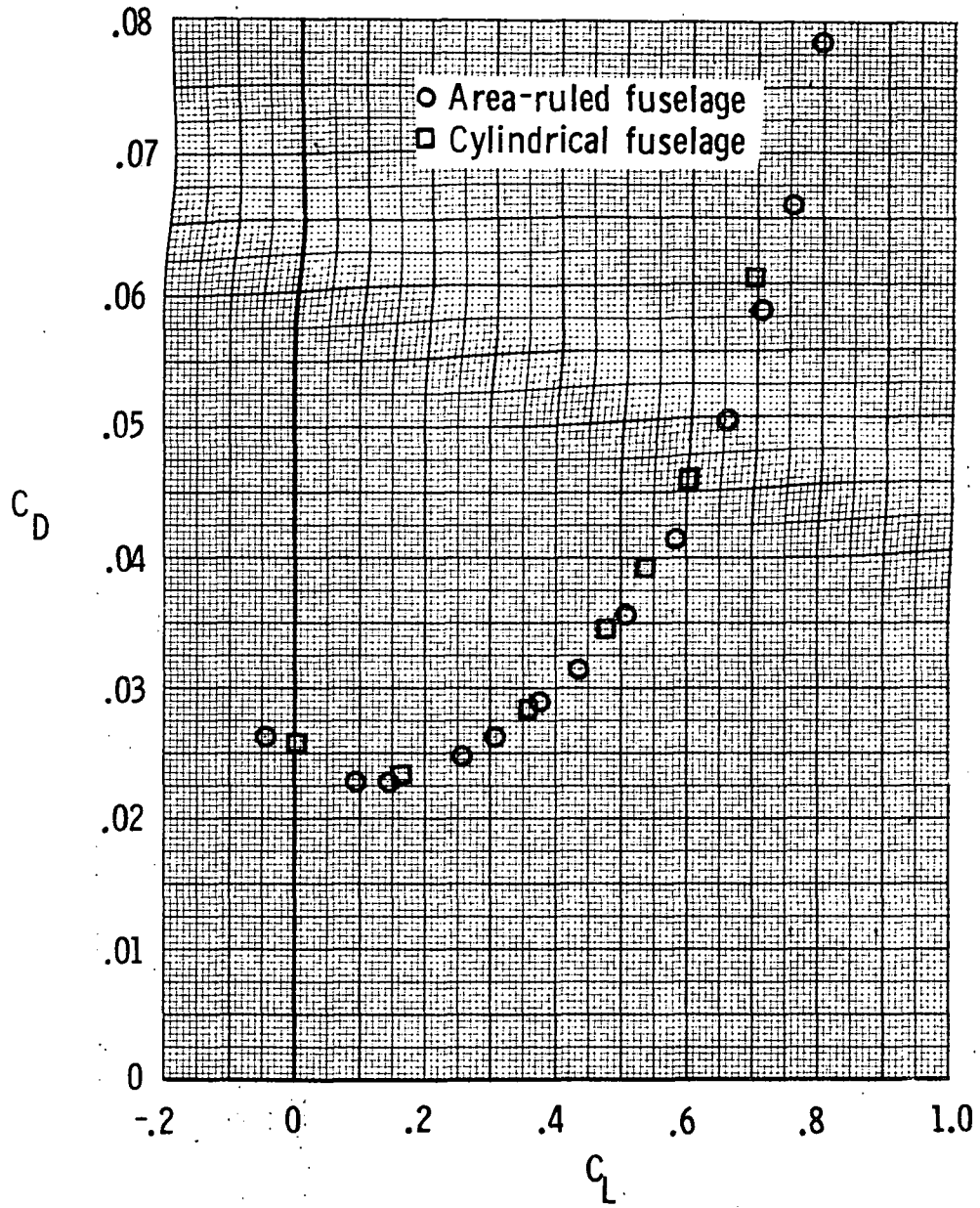
(c) Drag coefficient as a function of lift coefficient at $M_\infty = 0.88$.

Figure 56.- Continued.



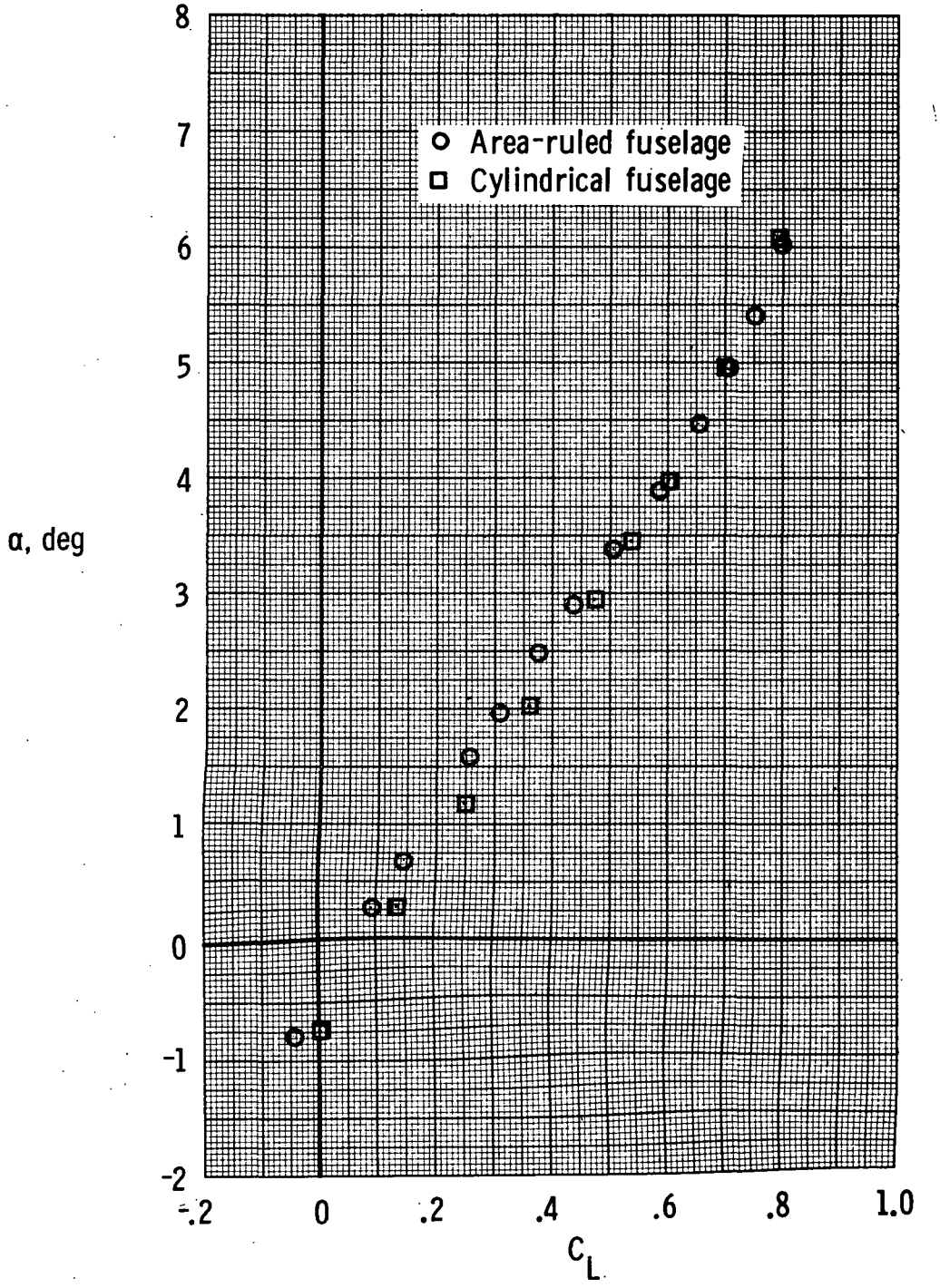
(d) Lift coefficient as a function of angle of attack at $M_\infty = 0.88$.

Figure 56.- Continued.



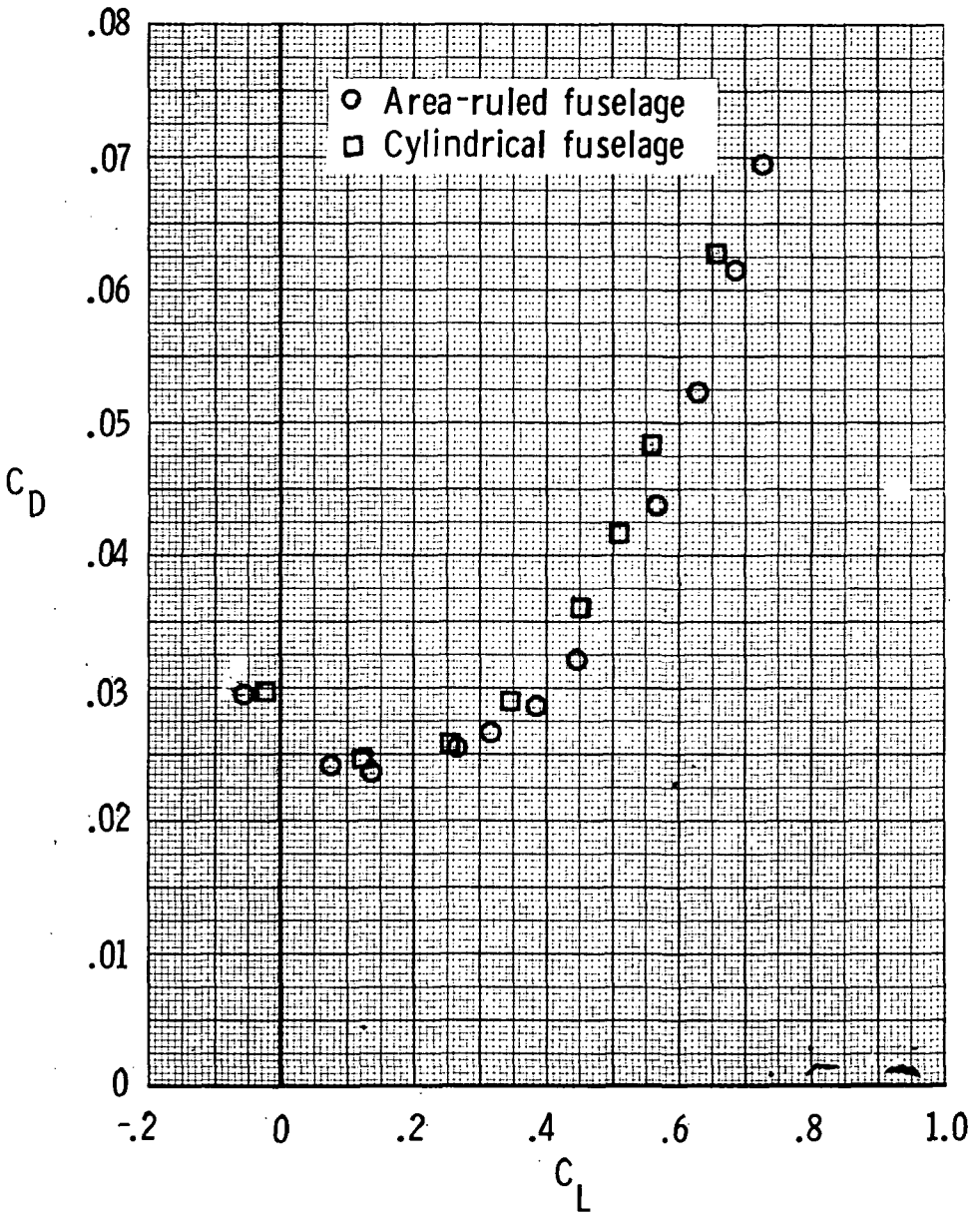
(e) Drag coefficient as a function of lift coefficient at $M_\infty = 0.90$.

Figure 56.- Continued.



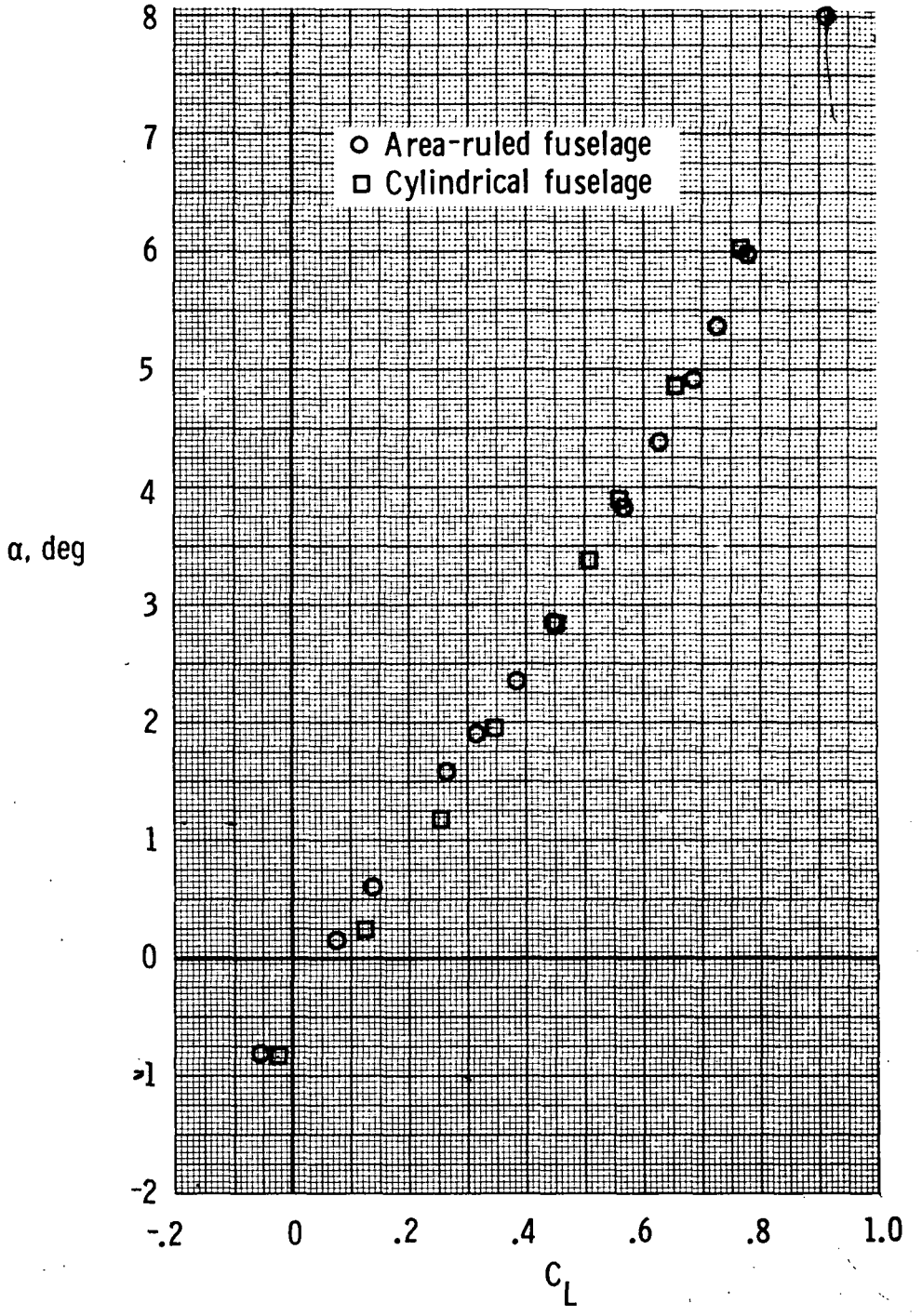
(f) Lift coefficient as a function of angle of attack at $M_\infty = 0.90$.

Figure 56.- Continued.



(g) Drag coefficient as a function of lift coefficient at $M_\infty = 0.92$.

Figure 56.- Continued.



(h) Lift coefficient as a function of angle of attack at $M_\infty = 0.92$.

Figure 56.- Concluded.

*U.S. GOVERNMENT PRINTING OFFICE: 1977 - 735-004/31

Copies of "Supplement (Parts I, II, III, and IV) to NASA TM X-3431" will be furnished upon request.

The supplement consists of tabulations of force data, wing and fuselage pressure data, and free-stream dynamic pressure and oil-flow photographs of the models with zero control deflection.

Requests for "Supplement (Parts I, II, III, and IV) to NASA TM X-3431" should be addressed to:

NASA Scientific and Technical Information Facility
Att: Distribution Control Department
P.O. Box 8757
Baltimore/Washington International Airport, MD 21240

CUT

Date_____

Please forward "Supplement (Parts I, II, III, and IV) to NASA TM X-3431" to

Name of organization

Street number

City and State Zip code

Attention: Mr._____
Title_____

CUT

Place
Stamp
Here

NASA Scientific and Technical Information Facility
Att: Distribution Control Department
P.O. Box 8757
Baltimore/Washington International Airport, MD 21240

National Aeronautics and Space Administration

Washington, D.C.
20546

Official Business
Penalty for Private Use, $300

SPECIAL FOURTH CLASS MAIL
BOOK

Postage and Fees Paid
National Aeronautics and
Space Administration
NASA-451



NASA

POSTMASTER: If Undeliverable (Section 158 Postal Manual) Do Not Return